GRAPHENE POSTERS (269)

GRAPHENE POSTERS (269)

GRAPHENE POSTERS (269)

GRAPHENE POSTERS (269)

GRAPHENE POSTERS (269)

GRAPHENE POSTERS (269)

GRAPHENE POSTERS (269)

GRAPHENE POSTERS (269)

GRAPHENE POSTERS (269)

Wireless NanoSensor Networks using Graphene-based Nanoantennas

Sergi Abadal[1], Josep Miquel Jornet[1,2], Ignacio Llatser[1], Albert Cabellos-Aparicio[1], Eduard Alarcón[1], and Ian F. Akyildiz[1,2]

[1]NaNoNetworking Center in Catalunya (N3Cat)
Universitat Politècnica de Catalunya
Barcelona, Spain
E-mail: {abadal,llatser,acabello,jmjornet,ian}@ac.upc.edu, ealarcon@eel.upc.edu

[2]Broadband Wireless Networking Laboratory
School of Electrical and Computer Engineering
Georgia Institute of Technology, Atlanta, Georgia 30332, USA
E-mail: {jmjornet,ian}@ece.gatech.edu

Nanotechnology is enabling the development of devices in a scale ranging from one to a few hundred nanometers. One of the most promising applications of these nanodevices is in the field of nanosensors. A nanosensor is not just a tiny sensor, but a device that makes use of the novel properties of nanomaterials to detect and measure new types of events in the nanoscale. For example, nanosensors can detect and measure physical characteristics of nanostructures just a few nanometers in size, chemical compounds in concentrations as low as one part per billion, or the presence of biological agents such as virus, bacteria or cancerous cells. However, the sensing range of a single nanosensor is limited to its close nano-environment and thus, many nanosensors are needed to cover significant areas or volumes. Moreover, an external device and the user interaction are necessary to read the measurements from a nanosensor.

Similarly to the way in which communication among computers enabled revolutionary applications such as the Internet, the development of an integrated nanosensor device with communication capabilities will overcome the limitations of individual nanosensors and expand their potential applications. A **Wireless NanoSensor Network (WNSN)** [1] will be able to cover larger areas, to reach unprecedented locations in a non-invasive way, and to perform in-network processing and cooperative actuation. A single nanosensor device detecting or sensing a relevant event will communicate with its neighbors and transmit the information in a multi-hop fashion to a sink or command center, which will connect with the macro-world and the final users. Furthermore, their communication capabilities will allow them to receive commands from other nanosensor devices to change their behavior or actuate, if needed.

WNSNs have a tremendous amount of applications that span diverse fields. In the **biomedical field**, biological WNSNs provide an interface between biological phenomena and electronic nanodevices, and can create novel health monitoring systems and targeted drug delivery systems, amongst others. Second, in the **environmental field**, WNSNs can be used to sense chemical compounds in agriculture fields or protected areas. Finally, in the **industrial field** they can be used to design new consumer goods or enhance existing ones, such as ultrahigh-sensitivity touch surfaces or new haptic interfaces.

However, in order to turn existing nanosensors into autonomous devices, which can create a network, it is necessary to provide them with additional functionalities: a power source, data storage, a processing unit and a communication module. A conceptual nanosensor device, with a size in the order of a few cubic micrometers (comparable to the size of human cells), is illustrated in Fig. 1 [1]. Despite being conceptually similar to a macroscale sensor, it should be taken into account that the solutions in the nanoscale are limited not just in terms of existing manufacturing technologies but also by the physics laws, i.e., we cannot think of a nanosensor as a small and simplified sensor.

To date, several solutions have been proposed for the different components of a nanosensor device. However, although many papers on nanosensor technologies are being published every year, it is still not clear how the communication module of nanosensor devices will operate. In light of the state of the art in small antenna design, a resonant metallic antenna operating for example at the terahertz (THz) band would have a typical dimension in the order of a few hundred micrometers. Scaling them down further to only a few micrometers would make them non-resonant and hence dramatically reduce their antenna efficiency. However, by using materials implicitly lying in the nanoscale, such as graphene, the aforementioned requirements (i.e., small size and reasonable efficiency) can be alleviated.

A few nanoantenna designs based on **carbon nanotubes** or **graphene nanoribbons** can indeed be found in the literature [2,3,4]. The main characteristic of these nanoantennas is that, because of quantum effects, the wave propagation speed in these structures is up to two orders of magnitude below the speed of light in vacuum. As a result, the expected resonant frequency of these antennas is

also two orders of magnitude below that of antennas made with non-carbon materials [2]. Due to the mismatch between these two speeds of propagation, the radiation efficiency of a nanoantenna is also expectedly low, but still expectedly considerably higher than its metallic counterparts. Moreover, nanosensor devices in our envisioned WNSNs will be deployed in a range below one meter, and will incorporate a tiny nanobattery or an energy-harvesting unit. This will enable them to communicate using a very short-range and to fulfill their needs. However, the characteristics of these antennas in the very short range remain unknown.

The targeted breakthrough of our research is to investigate and develop novel graphene-based nanoantennas, which, in our long-term vision, will enable Wireless Nanosensor Networks. These networks are not a mere downscaled version of conventional wireless sensor networks, but there are several properties stemming from the nanoscale nature of nanosensor devices that require a complete rethinking of well-established concepts in conventional networks. We outline the main three of them next.

First of all, a graphene-based nanoantenna is not just a small antenna. Due to the peculiarities of the propagation of electrons and EM waves in graphene, the classical antenna theory needs to be revised. For example, in a graphene-based nanoantenna, the EM wave propagation speed is tightly coupled with the atomic structure of the antenna, its temperature and even on the applied energy. Thus, the dependence of parameters such as the **frequency of operation** and the **radiation efficiency** of a nanoantenna on all these parameters needs to be studied and experimentally validated.

Second, initial results on nanoantenna characterization point to the terahertz band (0.1 – 10 THz). Existing communication channel models on the terahertz band are aimed at its characterization for transmission distances in the order of several meters. Hence, the effects appearing in the terahertz band (such as molecular absorption and molecular noise) in the very short range remain unknown and have not been analyzed yet. Therefore, there is the need to study the different phenomena affecting the **propagation of EM waves in the very short range** and determine the total path-loss, noise, and usable bandwidth affecting the communication among nanosensor devices. This will then allow the development of a **channel model** for short-range communications in the terahertz band.

Finally, the nanosensor devices equipped with a graphene-based nanoantenna will communicate with their neighbors and transmit the sensed information to a sink (representing a gateway with the micro- or macro-world and the users), using a multi-hop protocol. Since nanosensor devices will have a short transmission range, many sensors will be required to create a WNSN. In consequence, each sensor will need to have a low fabrication cost, and thus the architecture of a nanosensor device must be simple. In conclusion, existing modulations, Medium Access Control (MAC) and routing protocols, such as the ones developed for traditional wireless sensor networks, cannot directly be applied to this scenario. A third research challenge is thus to develop a **new network architecture** for WNSNs.

We envisage that Wireless NanoSensor Networks will have a great impact in almost every field of our society, ranging from healthcare to industrial or environmental protection, and we believe that our work will pave the way for the development of this new networking paradigm.

References
[1] I. F. Akyildiz and J. M. Jornet, Nano Communication Networks **1**, (2010) 3-19.
[2] P. Burke, S. Li and Z. Yu, IEEE Transactions on Nanotechnology **5**, (2006) 314-334.
[3] G. Hanson, IEEE Transactions on Antennas and Propagation **53**, (2005) 3426-3435.
[4] J. M. Jornet and I. F. Akyildiz, Proc. European Conference on Antennas and Propagation (2010) 1-5.

Figures
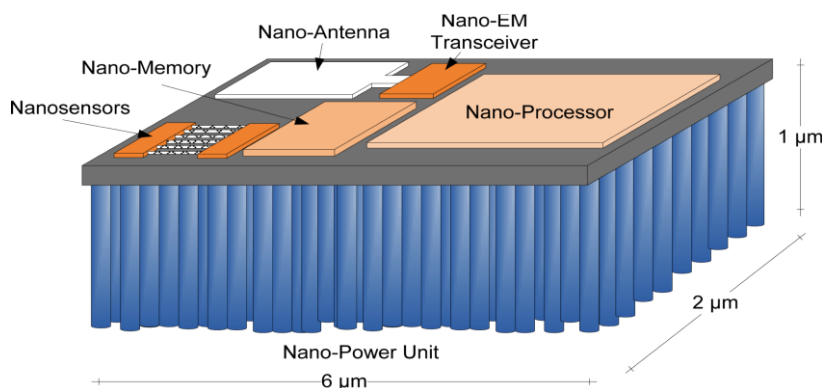
Figure 1: An integrated nanosensor device

Graphene Functionalisation Using Hydrophobin Proteins

J. Ahopelto[1], M. Kainlauri[1], D. Gunnarsson[1], P. Laaksonen[2], H. Jiang[3] and M. Linder[2]

[1]VTT Microsystems and Nanoelectronics, VTT Technical Research Centre of Finland, Tietotie 3, Espoo, Finland
[2]VTT Nanobiomaterials, VTT Technical Research Centre of Finland, Tietotie 2, Espoo, Finland
[3]Nanomaterials, Aalto University, Tietotie 3, Espoo, Finland

jouni.ahopelto@vtt.fi

Since the first experimental realisation of 2D material graphene [1], vast amount of new physics has emerged. Graphene has also been mentioned as a candidate to replace silicon in microelectronics and, because of its optical properties, is a good candidate for transparent electrodes in display technology. Partially the properties are arising from graphene being chemically inert. This is beneficial in many instances but may be disadvantageous, e.g., in sensor applications. One possibility to add functionalities to graphene is to use proteins as linkers. Hydrophobin is a small protein with a hydrophobic patch that attaches to a hydrophobic surface [2]. Hydrophobins form a one-monolayer thick ordered 2-dimensional film that can be used to link biomolecules or nanoparticles onto hydrophobic surfaces. This has been demonstrated with graphite and silicon [3].

2 nm
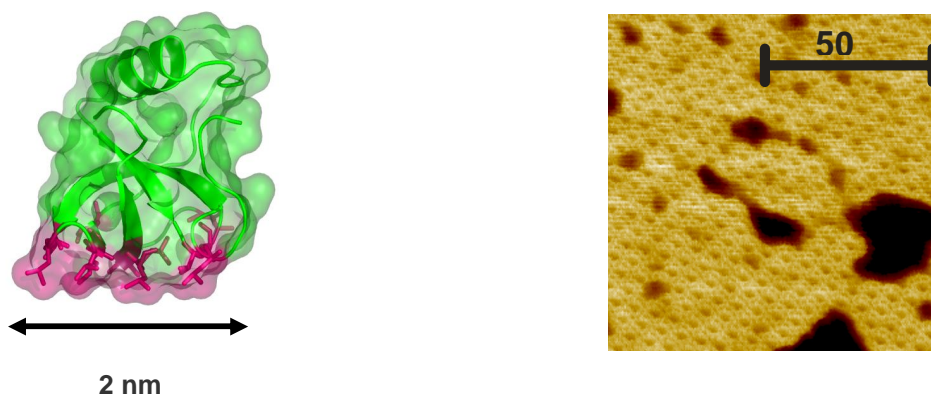
Fig 1. (left) Structure of a hydrophobin HFBI protein. The protein has a hydrophobic patch in the other end of the body, shown red in the picture. (right) Hydrophobins form a one monolayer thick 2-dimensional ordered film that can be transferred onto hydrophobic surfaces, such as graphene. The lattice constant of the hexagonal lattice is about 6 nm.

The aim in this work is to demonstrate that using hydrophobins one can functionalise the otherwise chemically inert graphene surface. In Figure 2 is shown a TEM image of a graphene flake onto which 3 nm Au nanoparticles have been attached using hydrophobins as linkers. The functionalisation is based on an in-situ process. It was found out that hydrophobin solution enhances the exfoliation of graphene from graphite and simultaneously the graphene surface is covered by the proteins [4]. By using engineered hydrophobins that link to gold nanoparticles, the graphene surface can be coated with a monolayer thick and non-agglomerated nanoparticle layer. The same approach can be used to link layers of other proteins or biomolecules for, e.g., sensor applications. The first electrical measurements show that a dry protein film decreases the mobility of a graphene FET about 50 %.
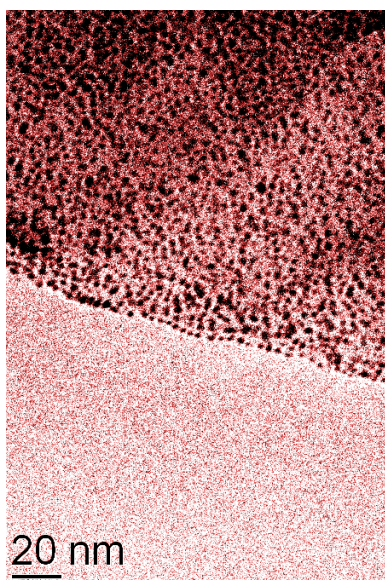
Fig. 2. TEM image of graphene flake covered with a monolayer of hydrophobin proteins to which 3 nm gold nanoparticles have been attached.

References

[1] K. S. Novoselov, et al., Science **306**, 666 (2004).
[2] M. B. Linder, Current Opinion in Colloid & Interface Science **14** (2009) 356–363
[3] P. Laaksonen, J. Kivioja, A. Paananen, M. Kainlauri, K. Kontturi, J. Ahopelto, and M. B. Linder, Langmuir **25**, 2009, 5185–5192.
 [4] P. Laaksonen, M. Kainlauri, T. Laaksonen, A. Shchepetov, H. Jiang, J. Ahopelto, and M. B. Linder, Angew. Chem. Int. Ed. 2010, **49**, 1 – 5.

Graphene on Ru(0001): contact formation and chemical reactivity on the atomic scale

S. J. Altenburg[1], J. Kröger[2], B. Wang[3], M.-L. Bocquet[3], N. Lorente[4] and R. Berndt[1]

[1]Institut für Experimentelle und Angewandte Physik,
Christian-Albrechts-Universität zu Kiel, D-24098 Kiel, Germany
[2]Institut für Physik, Technische Universität Ilmenau, D-98693 Ilmenau, Germany
[3]Université de Lyon, Laboratoire de Chimie, Ecole Normale Supérieure de Lyon,
CNRS, F69007 Lyon, France
[4]Centre d'Investigació en Nanociència i Nanotecnologia (CSIC-ICN),
Campus de la UAB, E-08193 Bellaterra, Spain
altenburg@physik.uni-kiel.de

Graphene layers with a high degree of perfection may be grown on crystal surfaces, where the interaction with the substrate modifies its electronic properties to varying degrees. On most transition metals superstructures occur and lead to periodic modulations of geometric, electronic and bonding properties.

Here, we use a low-temperature scanning tunneling microscope (STM) to probe with atomic precision the conductance $G = I / V$ (I: current, V : sample voltage) of junctions comprising a Au tip and a single graphene layer on Ru(0001). On this substrate graphene forms a hexagonal moiré superstructure with a periodicity of ≈ 30Å, which involves a buckling of the graphene sheet and a strongly inhomogeneous electronic structure. Our STM measurements directly probe the chemical reactivity of graphene during bond formation between tip and sample and reveal its location on the atomic scale. This is possible owing to significant variations of the tip-graphene contact formation process and of the conductance within the moiré unit cell. A smooth transition from tunneling to contact occurs in regions where the graphene layer is buckled away from the substrate, while in the strongly bound parts a jump to contact is observed, similar to point contacts on pristine noble metal surfaces. This behavior can be traced back to the different electronic structure and ultimately to the different chemical reactivity of the graphene layer as revealed by density functional theory. Variations in the conductance at contact formation within the moiré unit cell can be attributed to differing graphene-Ru-distances, as indicated by quantum transport calculations utilizing non-equilibrium Green's functions techniques.
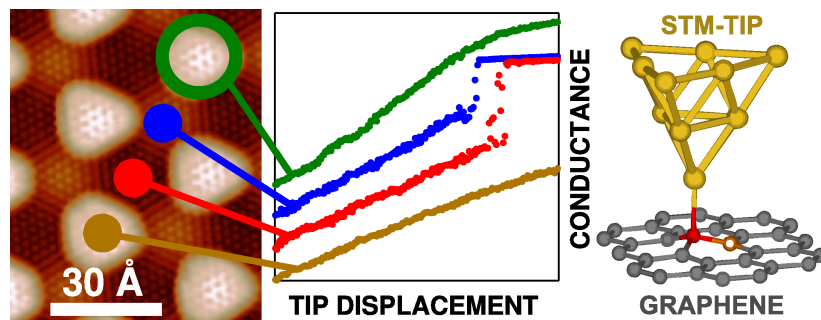
Metal-insulator transitions in graphene.

M. Amado[1,2], E. Diez[1], F. Rossella[3], V. Bellani[3], D. López-Romero[4] and D.K. Maude[5]

[1] Laboratorio de Bajas Temperaturas, Universidad de Salamanca, E-37008 Salamanca, Spain
[2] GISC-QNS, Dpto de Física de Materiales, Universidad Complutense, E-28040 Madrid, Spain
[3] Dipartimento di Fisica "A. Volta" and CNISM, Università degli studi di Pavia, I-27100 Pavia, Italy
[4] CT-ISOM, Universidad Politécnica de Madrid, E-28040 Madrid, Spain
[5] Laboratoire National des Champs Magnétiques Intenses, F-38042 Grenoble, France

marioam@fis.ucm.es

In this work we show the metal-insulator (MI) quantum phase transitions that appear in the quantum Hall effect in graphene, namely the plateau-insulator (PI) and plateau-plateau (PP) transitions. For this purpose we have performed magneto-transport experiments with the magnetic field (up to 28 T) as the driving parameter in the temperature range from 4 K up to 230 K.

The Hall (ρ_{xy}) and longitudinal (ρ_{xx}) resistivities were measured by the standard 4-probe low frequency AC lock-in technique while the graphene sample was obtained by mechanical exfoliation over a Si/SIO$_2$ wafer with subsequent e-Beam lithography and the evaporation of Au/Ti contacts. The charge neutrality point (CNP) appeared at 3.8 V.

When the gate voltage was placed in the vicinity of the charge neutrality point we have observed a transition from the last plateau υ=-2 to an insulating phase. The transient between delocalized to localized states occurs through a T-independent crossing point where, at low temperatures, the isotherms converge as seen the left panel of **Fig.1** where we show ρ_{xx} isotherms as a function of B for V_G = 2 V where a T-independent crossing point appears at a critical magnetic field B_C = 16.05 T. For temperatures above tents of Kelvin, the PI T-independent crossing point disappears, confirming the robustness of the MI transition as pointed out by Zhang *et al.* [1].

For the PI transition we have calculated the associated critical exponent by calculating the value of υ_0 (υ_0 should not be confused with the Landau level filling factor) in from the equation ρ_{xx} = exp[(1/B-1/B$_C$)/ υ_0] applied in the vicinity of the T-independent crossing point [2,3] as shown in the right panel of **Fig.1** Then, extracting υ_0 at every temperature we could calculate the associated critical exponent from $\upsilon_0 {\sim} T^\kappa$. We have obtained a value for κ=0.58±0.01 away from the CNP, in agreement with the expected value for two-dimensional electron gasses (2DEGs) while closer to the CNP the obtained value has been found to match with the one expected in the full percolation limit κ=0.697±0.005. This difference could be attributed to the effect of the disorder present in the sample, dominant the alloy one (Anderson type) for higher densities in contrast with the short-range disorder, that would be dominant at lower densities. What we can firmly question from these results is the universality of the critical exponent associated to the PI transition.

In order to study the PP transition have we tuned the gate voltage tents of volts away from the CNP. We have calculated the critical exponent for the transitions υ = -10→ υ = -6 and υ = -6→ υ = -2 in a range of temperatures from 4.2 to 230 K as seen in **Fig.2**. The PP transition remained clearly observable almost up to the maximum temperature we reached as observed by Giesbers *et al.* [4]. We have extracted the critical exponents both from the temperature dependence of the full width at half maximum (FWHM) of the Shubnikov-de Haas peak in the transition υ = -6→ υ = -2 and from the temperature dependence of the maximum slope for ρ_{xy} between adjacent plateaus in both transitions. The value extracted obtained κ=0.25±0.02 does not match with the expected universal value for 2DEGs κ = 0.42 recently reported also in graphene [4].

With the values obtained for the critical exponents of the MI transitions in graphene we question the universality of such critical exponents in this novel material. We attribute this anomalous behaviour to the effect of the disorder in our samples. Thus, further studies are necessary in order to throw light upon the role of the impurities and disorder in the QPTs in graphene with controlled disordered samples.

References

[1] L. Zhang *et al.*, Phys. Rev. Lett. **105** (2010) 046804.
[2] D. Shahar *et al.*, Sol. St. Comm. **107** (1998) 19.
[3] M. Amado *et al.*, New. J. Phys. **12** (2010) 053004.
[4] A. J. M. Giesbers, *et al.*, Phys. Rev. B **80** (2009) 241411(R).

Figures
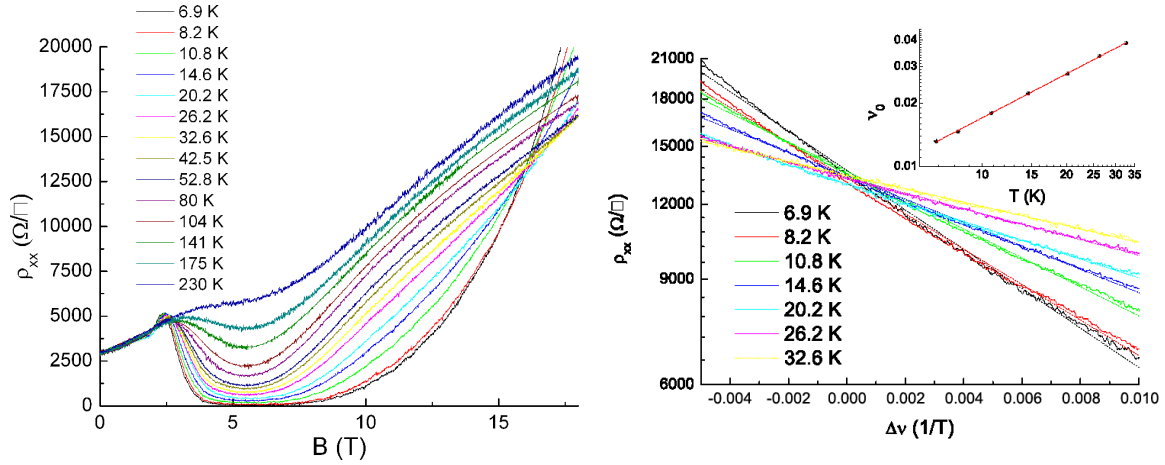
Fig.1.   In the left panel we show ρ_{xx} isotherms as a function of B at V_G = 2 V. The T-independent crossing point disappears when B > 32.6 K that confirms the existence of a possible deactivation temperature of the PI transition. In the right panel we show the renormalization of ρ_{xx} close to the T-independent crossing point following the standard procedure [2,3] for the same density of carriers. The associated critical exponent derived from the fit to $\upsilon_0 T^\kappa$ is κ = 0.697 ± 0.005, in contrast with the expected value 0.58.
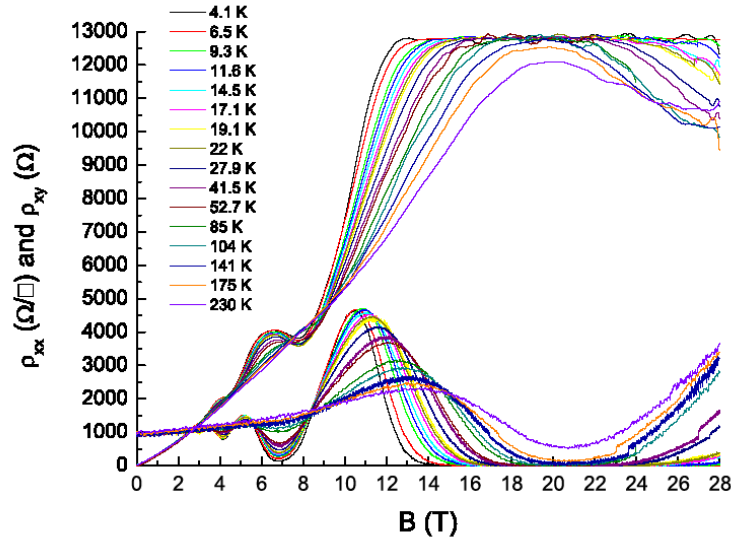
Fig.2. ρ_{xx} and ρ_{xy} isotherms as a function of B for V_G=-8V .Plateaus υ=-10, υ=-6 and υ=-2 and their SdH peaks can be clearly observed up to 230 K.

Plasmonics in Graphene Nanoribbons

David R. Andersen[1,2], Hassan Raza[1]

Department of Electrical and Computer Engineering[1]
Department of Physics and Astrononmy[2]
The University of Iowa
Iowa City IA 52242 USA
k0rx@uiowa.edu

Graphene is a material that has undergone intense study in over the past several years [1,2]. The novel, Dirac-like linear bandstructure near the K points in the Brillioun zone gives rise to a variety of unique phenomena that may have wide applicability in various areas of electronic and optical technology. Specifically, studies of plasmon propagation in graphene and related material have shown that the plasmon dispersion relation persists to very small energies and long wavelengths [3], in distinct contrast to plasmonic propagation in other two-dimensional structures, *e.g.* the metal/dielectric interface [4]. Further, graphene plasmons can exhibit low-loss propagation due to the absence of absorption in the metallic half-space [5].

Recently, the bandstructure of quasi-one-dimensional graphene nanoribbons has been investigated as well [6]. Transverse confinement of the electronic wavefunctions in the nanoribbon causes the bandstructure to split, giving rise to many more bands. This richer electron spectrum modifies the plasmonic dispersion. The new plasmon dispersion characteristics are where we focus our attention now.

In this paper, we discuss our recent calculations of the dielectric function and plasmon dispersion in armchair graphene nanoribbons. Using a 2N-band p_z tight-binding model, where N is the width in atoms of the nanoribbon, we calculate the dielectric function in the Lindhard [7] (random phase) approximation. Details of the plasmon dispersion are then obtained by examining the behavior of the inverse of the dielectric function following the method of Ref. [5].

Several interesting phenomena are observed in armchair nanoribbons of small-integer widths. In particular, for the semimetallic armchair nanoribbons, we find a linear plasmon dispersion for values of the plasmon energy below the onset of the second band absorption threshold. The group velocity for this plasmon is equal to the Fermi velocity in two-dimensional graphene. The dispersion relation calculated for plasmons in N = 8 armchair (acGNR8) nanoribbons is shown in Fig. 1. Semiconducting nanoribbons (*e.g.* acGNR9,10) are found to exhibit near-parabolic plasmon dispersion in the low-energy limit.

The small group velocity of these plasmons, coupled with their localization in the direction normal to the graphene layer suggest the possibility that they may be suitable for inter-device communication in integrated circuit applications.

References

[1] K. S. Novoselov, A. K. Geim, S. V. Morozov, S. Jiang, M. I. Katsnelson, I. V. Grigorieva, S. V. Dubonos, and A. A. Firsov, Nature (London), 438 (2005) 197; Science, 306 (2004) 666.
[2] Y. Zhang, Y. W. Tan, H. L. Stormer, and P. Kim, Nature (London), 438 (2005) 201.
[3] E. W. Hwang and S. Das Sarma, Phys. Rev. B, 75 (2007) 205418.
[4] T. Ando, A. B. Fowler, and F. Stern, Rev. Mod. Phys., 54 (1982) 437.
[5] A. Hill, S. A. Mikhailov, and K. Ziegler, EPL Journal, 87 (2009) 27005.
[6] H. Raza and E. C. Kan, Phys. Rev. B, 77 (2008) 245434.
[7] J. Linhard, Kgl. Danske Videnskab. Selskab, Mat.-Fys. Medd. 28, 8 (1954).

Figure
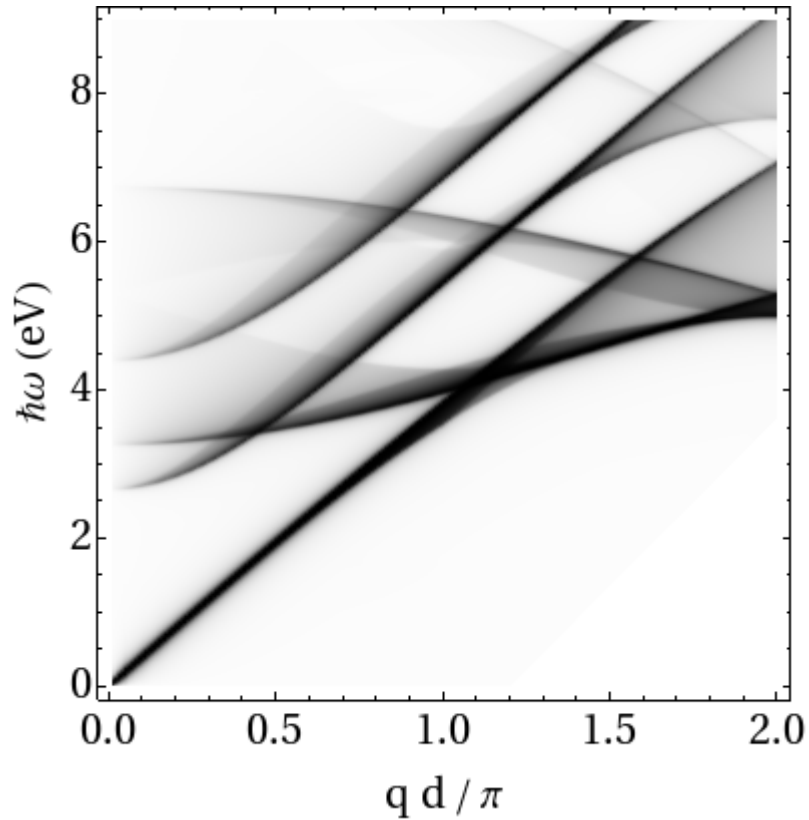
Fig. 1. Plasmon dispersion relation for intrinsic acGNR8 graphene nanoribbon. A linear dispersion characteristic is observed for plasmon energies below ~ 2.6 eV. Above this value, interband scattering of electrons introduces losses into the plasmon propagation, resulting in broadening of the additional branches in the dispersion curve.

Hydrogen adsorption on free-standing and epitaxially grown graphene

Mie Andersen[1], Zeljko Sljivancanin[2], Liv Hornekær[1] and Bjørk Hammer[1]

[1]Interdisciplinary Nanoscience Center, Aarhus University, Ny Munkegade 120, 8000 Aarhus C, Denmark
[2]Vinca Institute of Nuclear Sciences (020), PO Box 522, RS-11001 Belgrade, Serbia

ma06@inano.au.dk

In order to replace silicon-based electronics with new graphene-based devices a tunable band gap needs to be engineered in graphene [1]. Hydrogenation of graphene has turned out to be a promising route towards achieving this goal [2], hence a proper understanding of the interaction of hydrogen with graphene is desirable. Experimentally graphene is often grown epitaxially on metal surfaces, therefore also the role of the substrate in the hydrogenation process is of great importance.

Here is presented density functional theory (DFT) calculations on the structure and stability of small hydrogen clusters on free-standing graphene as well as clusters on graphene grown on the Ir(111) and the hex-reconstructed Pt(100) surfaces. If hydrogen is allowed to adsorb on both sides of a free-standing graphene sheet the energetically favorable clusters have a graphane-like structure, where every other C atom bonds a H atom above and every other bonds a H atom below (the structure of graphane, which is the most stable form of fully hydrogenated graphene, is shown in Figure 1). Furthermore, closed hydrogenated carbon hexagons and a maximal ratio of inside atoms to edge atoms in the cluster are identified as the most important structural motifs causing high cluster stability [3]. This is illustrated in Figure 2.

For graphene adsorbed on Ir(111) and hex-reconstructed Pt(100) the most stable clusters form graphane-like structures as well, but in this case H is adsorbed from above on every second C atom and the metal substrate forms the bonds to every other C atom from below. For Ir(111) such a structure is shown in Figure 3. It turns out that the principle of closed hydrogenated C hexagons holds for these structures as well with half of the bonds to H atoms replaced by bonds to metal atoms below. For the structure in Figure 3 the C atoms in 6 closed hexagons are involved in bonding. Following this principle very favorable clusters are easily identified.

References

[1]   Castro Neto, A.H., et al., Reviews of Modern Physics, **1** (2009) 109-162.
[2]   Balog, R., et al., Nature Materials, **4** (2010) 315-319.
[3]   Sljivancanin, Z., et al., Physical Review B, in print.
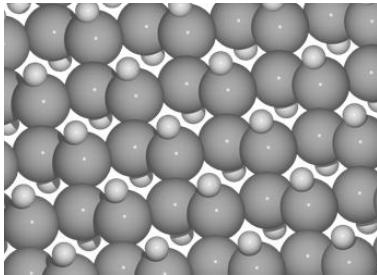
Figure 1. Structure of graphane.
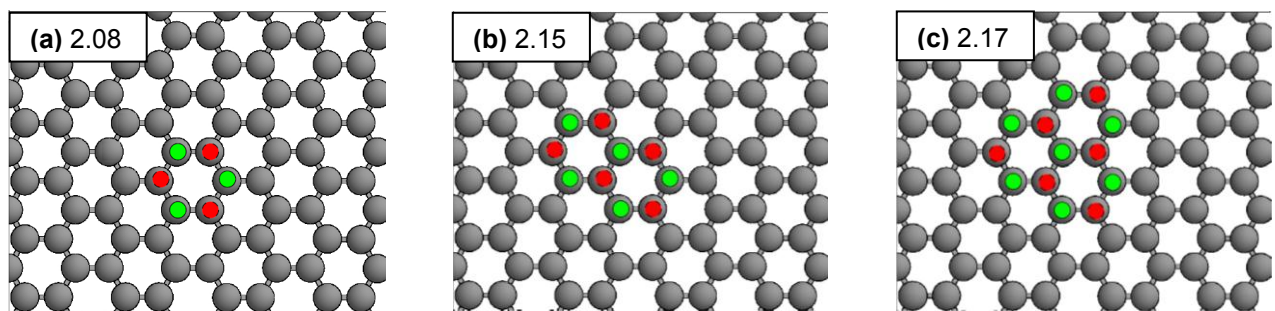
Figure 2. **(a-c)** Schematic structure of graphane-like clusters on free-standing graphene. C atoms are shown in grey, adsorbed H atoms from opposite sides are colored differently. Binding energies are given in eV/H atom. These clusters demonstrate the principle of closed hydrogenated C hexagons for 1, 2 and 3 hexagons. Adapted from [3].
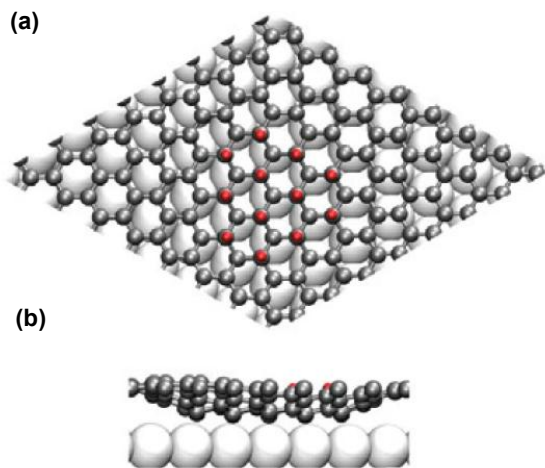
Figure 3. Structure of a graphane-like H cluster on graphene adsorbed on Ir(111). Ir atoms are shown in white, C atoms in grey and H atoms in red. In the cluster every other C atom bonds a H atom above and every other C atom is shifted downwards to bond an Ir atom below. C atoms in 6 closed hexagons are involved in the bonding. **(a)** top view and **(b)** side view. From [2].

Pairing symmetry of superconducting graphene

F. M. D. Pellegrino, **G. G. N. Angilella**, R. Pucci

Dipartimento di Fisica e Astronomia, Università di Catania, Via S. Sofia, 64, I-95123 Catania, Italy
Scuola Superiore di Catania, Via Valdisavoia, 9, I-95123 Catania, Italy
CNISM, UdR Catania, I-95123 Catania, Italy
INFN, Sez. Catania, I-95123 Catania, Italy
giuseppe.angilella@ct.infn.it

The possibility of intrinsic superconductivity in alkali-coated graphene monolayers has been recently suggested theoretically. Here, we derive the possible pairing symmetries of a carbon honeycomb lattice and discuss their phase diagram. We also evaluate the superconducting local density of states (LDOS) around an isolated impurity. This is directly related to scanning tunneling microscopy experiments, and may evidence the occurrence of unconventional superconductivity in graphene.

References

[1] F. M. D. Pellegrino, G. G. N. Angilella, R. Pucci, Eur. Phys. J. B **76**, 469 (2010).

Rapid Thermal CVD of Graphene on Copper

Sanna Arpiainen[1], Olli Svensk[2], Wonjae Kim[2], Markku Kainlauri[1], Hua Jiang[3], and Harri Lipsanen[2]

[1]VTT Microsystems and Nanoelectronics, Micronova, P.O.Box 1000, FI-02044 VTT, Espoo, Finland
[2]Aalto University, Dept. of Micro- and Nanosciences, P.O.Box 3500, FI-00076 AALTO, Espoo, Finland
[3] Aalto University, Dept. of Applied Physics, P.O.Box 15100, FI-00076 AALTO, Espoo, Finland
sanna.arpiainen@vtt.fi

We have studied the chemical vapor deposition (CVD) of graphene in a cold wall reactor designed for rapid thermal processing (RTP) of semiconductors. In addition to the fast operation, the advantages of this reactor type are complete control over the process parameters like temperature gradient which would allow increasing the reactor size up to several meters and compatibility to batch type processing on smaller substrates. The deposition parameters like temperature, methane flow and CH_4/H_2 ratio were optimized at different pressures between 7 and 80 Torr. The composition of the deposited film was characterized with scanning confocal μ-Raman spectroscopy and verified with TEM.

The optimization was performed simultaneously with the process chamber modification. The basis of the process is direct infrared (IR) heating that is provided through a quartz window located at the top of the 8" chamber. Radiation is absorbed by SiC covered graphite susceptor and the heat is transferred into the copper foil attached to it. The temperature is controlled on the basis of the optical pyrometer reading from the susceptor back surface. By increasing the measurement points and control electronics, the IR power could be adjusted *in situ* to provide homogeneous thermal gradient over the chamber, though currently the power profile is calibrated separately. The minimum pressure in the deposition chamber is currently limited to 7 Torr, which is somewhat higher than the optimal 0.5 Torr reported [1].

As expected, the optimal deposition parameters and graphene quality were found to be strongly dependent of the pressure. At high pressures significant amount of hydrogen was required to provide counterbalance to methane pyrolysis that would produce soot or amorphous carbon over all surfaces. Though the deposition parameters could be adjusted to produce graphite, monolayer graphene growth was rare. Under otherwise optimized conditions, the monolayer graphene began to dominate at 16 Torr and the crystalline quality improved with further reduction of the pressure as determined from the decrease of the height of the Raman D peak (1350 cm^{-1}) that has been associated with defect states [2]. When reducing the pressure, the optimal CH_4/H_2 ratio increased from 0.3 to 4, while the deposition temperature was kept close to 1000 ºC. Highest quality graphene was achieved at the lowest achievable pressure, thus further improvement is expected with increased pump capacity.

The Raman spectra (fig. 1) measured from the samples after transfer to a HfO_2 layer indicate continuous graphene, composed of monolayer graphene with about 5 - 10 % coverage of thicker graphene. This is clearly illustrated in SEM images (fig. 2) taken before and after the transfer. The thicker regions are located on large surface corrugations in the copper foil. Electrical analysis of the graphene indicates otherwise good quality; after vacuum cleaning the Dirac point is at zero and the sheet resistivity is close to exfoliated graphene. Mobility measurements are under progress.

The crystalline quality of graphene was further analyzed with HR-TEM (fig. 3). The graphene was transferred with pmma to copper grid with holey carbon support and cleaned with acetone, though all pmma could not be properly removed due to simultaneous etching of the support. TEM imaging revealed continuous graphene lattice extending well beyond the shown 30 nm area, with electron diffraction pattern confirming the monolayer thickness and perfect hexagonal lattice. These results confirm the ability to produce large graphene crystallites at pressures above the UHV conditions.

References

[1] X. Li, C.W. Magnuson, A. Venugopal, J. An, J.W. Suk, B. Han, M. Borysiak, W. Cai, A. Velamakanni, Y. Zhu, L. Fu, E.M. Vogel, E. Voelkl, L. Colombo, and R.S. Ruoff, Nano Letters **10** (2010) 4328.
[2] A.C. Ferrari, Solid State Communications **143** (2007) 47.

Figures
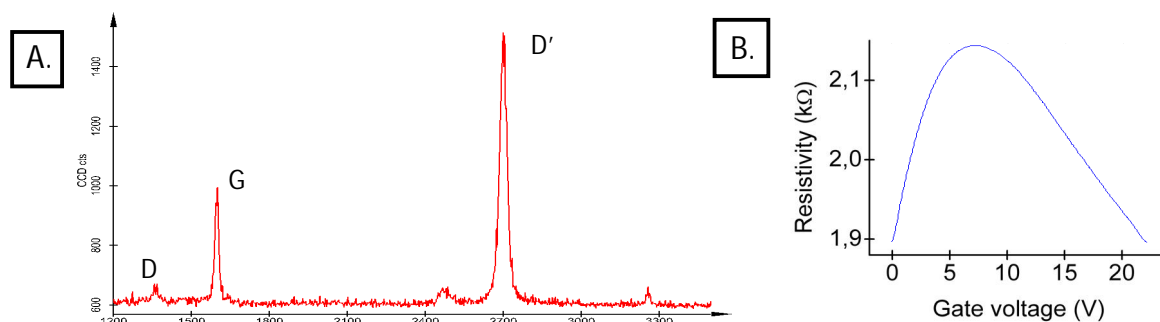
Figure 1 Raman spectrum (a) and resistivity (b) of transferred CVD graphene on 40 nm thick HfO₂. The Raman spectrum is averaged over a 20 x 20 µm² area, excluding the darker multilayer spots shown in figure 2. Measurement was done using WITec alpha 300 R with 532 nm excitation laser. The sheet resistivity as a function of gate voltage shows behavior typical to graphene. Here the Dirac point is still shifted after copper etch induced doping.
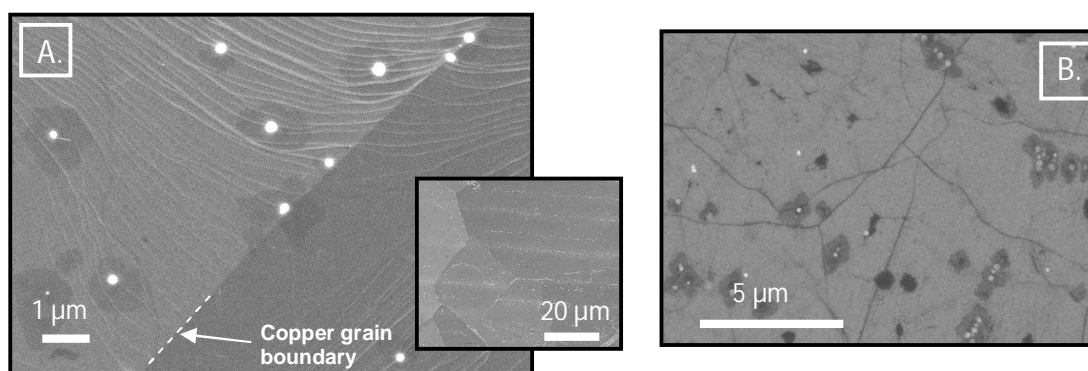
Figure 2 SEM images of continuous graphene deposited on a copper foil. (a) As deposited graphene on copper, showing the atomic terraces and grain boundaries in copper. The spots with thicker graphene (darker areas) are concentrated into the grooves in the foil (inset). (b) Transferred graphene on hafnium oxide, also illustrating the wrinkles caused by the difference in thermal expansion coefficients of copper and graphene.
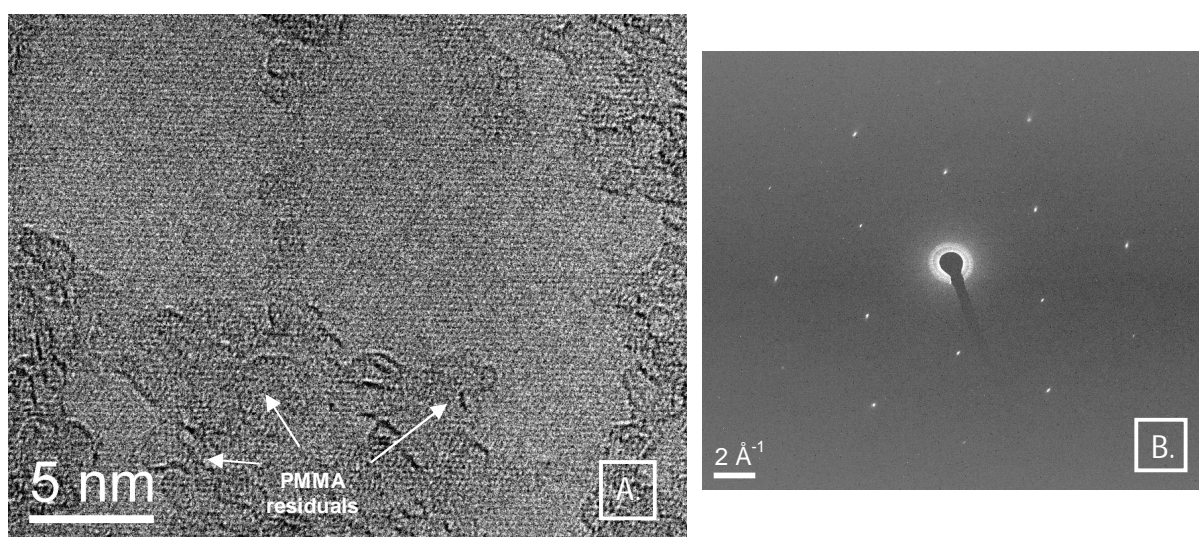
Figure 3 TEM image (a) and diffraction pattern (b) of suspended graphene grown from methane at 7 Torr in a cold wall CVD reactor. The image shows a continuous lattice, though partly under pmma residuals from the transfer process. Diffraction pattern through the whole image area indicates perfect monolayer graphene with single lattice orientation. Similar pattern was measured throughout the sample, also on areas totally under pmma, with no indication of orientational variants related to small misoriented grains. The images were measured using Cs-corrected TEM (JEOL 2200FS) at 80 kV.

Crystallite size effect on the structural modification of graphene oxides by insitu reduction and nitrogen doping.

E. Asedegbega-Nieto[1], M. Pérez-Cadenas[1], B. Bachiller-Baeza[2], E. Gallegos-Suárez[1,2], I. Rodriguez-Ramos[2], A. Guerrero-Ruiz[1]

1. Dpto. Química Inorgánica y Técnica. Facultad de Ciencias UNED. Paseo Senda del Rey nº 9, 28040 Madrid, Spain.
2. Instituto de Catálisis y Petroleoquímica, CSIC, C/ Marie Curie nº 2, Cantoblanco 28049, Spain.
easedegbega@ccia.uned.es

Graphene, the unique two dimensional carbon allotrope [1] of single-atomic thickness, has attracted great interest owing to its interesting physical and chemical properties and there is an increase in its demand in various fields of application involving electronic based devices. The electrical properties of graphene can be modulated by chemical doping. In carbon materials Nitrogen and Boron atoms are appropriate candidates for this tuning process as both elements have almost the same atomic radius and one electron more or less than carbon. Studies involving nitrogen doping of graphene have proven an enhancement in electrical properties of this material [2,3]. In this communication we report the effect of the grain size of the starting graphite material on the structural modification caused by nitrogen doping on the corresponding graphene oxides.

Graphite of three different grain sizes (10, 100 and 200 mesh) were submitted to strong oxidation with nitric acid, obtaining the corresponding graphene oxides (GO10, GO100 and GO200). Thereafter, these materials were heated to 500ºC in a reactive gas mixture composed of NH_3, N_2 and H_2 whose flow rates were 10, 50 and 6 ml/min, respectively. One of the three samples was also nitrogen-dopped at a higher temperature (900ºC) in order to observe any changes in the structural modification. Parallel to these, all three graphene oxides were heated at 500 ºC under inert nitrogen atmosphere (50 ml/min) which served as a reference when comparing with those treated with NH_3. The resulting materials were studied employing various techniques such as TEM, XPS, XRD, etc.

Fig. 1. Shows TEM images of synthesized materials which consists of ultrathin transparent graphene sheets with some wrinkled and folded features (Fig. 1a) proving that graphene oxide was truly exfoliated in the reduction process. Morphological differences can be observed when comparing GO heated under inert atmosphere (Fig. 1b) and that treated with NH_3 (Fig. 1c). In the later, the neatly and parallel lined stack of folded and scrolled edges of graphene layers show certain degree of defects with respect to the former. This effect is further emphasized at higher nitrogen doping temperature (Fig. 1d). Fig. 2 shows the XRD pattern of an original GO sample (before treatment), a GO treated under inert atmosphere and those treated with NH_3 (at 500ºC and at 900ºC). GO has a sharp peak at 16º corresponding to an interlayer distance of 0.67 nm. This peak completely disappears for all reduced GO and a small peak at about 26º is observed owing to the recovery of the graphite crystal structure. A significant difference can be observed when comparing GO of different crystallite sizes as this characteristic peak is smaller and broader for smaller sizes suggesting stacking thickness of resulting reduced GO is greatly dependent on the crystallite size. XPS results confirm the reduction of GO on observing the disappearance of oxygen surface groups on C 1s peak of samples before and after treatment (Fig.3). This technique also gave insights on the amount and type of nitrogen incorporated after the treatment. N 1s spectra of inert treated and NH_3 treated GO is displayed in Fig. 4. The amount of N present in the inert treated GO is insignificant whereas this specie is present in all the others ranging from 3 to 6 % being highest in the GO of larger grain size. At the same time the distribution of N as pyridinic, pyrrolic and quaternary- N is also greatly influenced by the size of the original starting graphite material. GO10 has highest proportion of pyridinic and quaternary-N while in GO200 the formation of pyrrolic- N is favoured.

References

[1] K.S. Novoselov, A.K. Geim, S.V. Morozov, D. Jiang, Y. Zhang, S.V. Dubonos, I.V. Grigoieva and A.A. Firsov, Science **306** (2004), 666.

[2] X. Li, H. Wang, J. T. Robinson, H. Sanchez, G. Diankov, H. Dai, J. Am. Chem. Soc. **131** (2009) 15939.

[3] D-W. Wang, I. R. Gentle, G. Q. Lu, Electrochem. Comm. **12** (2009) 1423.

Figures
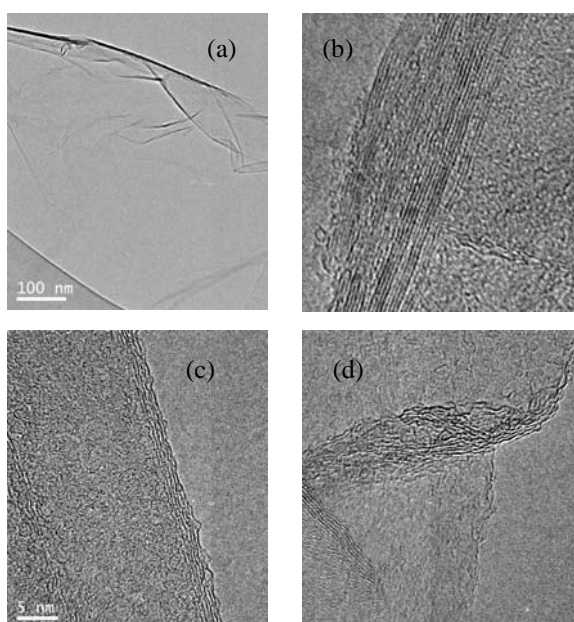
Figure 1. GO10 TEM images
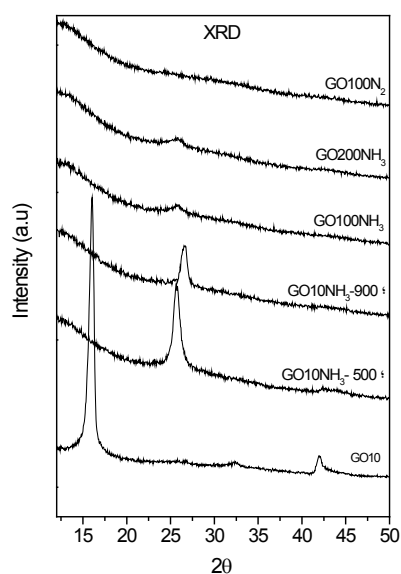
Figure 2. XRD
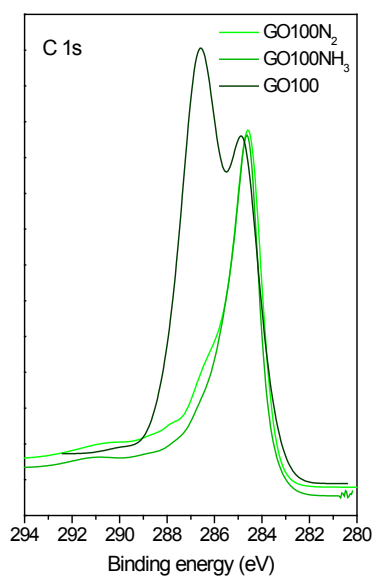
Figure 3. C 1s XPS
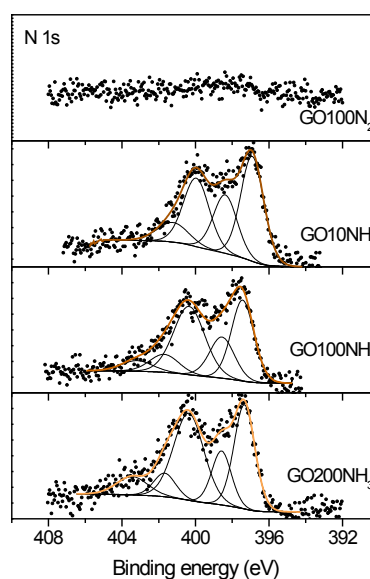
Figure 4. N 1s XPS

A DFT study of the interaction of sodium bisulfate with monolayer graphene

Isabel G. Ayala[1] and Nicolas A. Cordero[1,2]

[1] Physics Department, University of Burgos, C/ Villadiego s/n, E-09001 Burgos, Spain
[2] Department of Materials Science and Engineering, University of Pennsylvania,
3231 Walnut St, Philadelphia PA 19104, USA

isagomez@ubu.es

Large scale production of isolated carbon nanostructures (including graphene sheets) is important for nanotechnology progress. There are basically three approaches to separate carbon nanostructures: chemical functionalization, sonication, and the use of surfactants. Functionalization often changes de properties of the nanostructures and sonication breaks them. So the use of surfactants seems to be the best way to obtain isolated carbon nanostructures in large quantities. Among the best surfactant molecules for dispersing carbon nanostructures are sodium dodecyl sulfate (SDS), sodium dodecylbenzene sulfonate (NaDDBS) and sodium polystyrene sulfonate (NaPSS). All of them have in common a sulfonate head group with a Na atom. Sulfuric acid is itself a good surfactant, but the presence of a Na atom in the sulfuric group seems to enhance the surfactant effect. Our aim is to clarify the role this atom plays for dispersing carbon nanostructures.

We have previously studied the interaction of sulfuric acid with a graphene sheet [1], sulfuric acid, sodium bisulfate and sodium butyl sulfate with a carbon nanotube [2], as well as the behavior of sulfuric acid when in between two graphene sheets [3]. We present now computer simulations of the interaction between $NaHSO_4$ and monolayer graphene. We have used the Density Functional Theory (DFT) in the Local Density Approximation (LDA) as implemented in DACAPO [4]. We have calculated equilibrium geometries, binding energies, charge transfers and densities of states for different concentrations and orientations of both (cis and trans) $NaHSO_4$ isomers. Our results show that there is always protonation of the graphene sheet an that the charge transfer varies with bisulfate concentration and orientation.

References

[1] N.A. Cordero and J.A. Alonso, Nanotechnology, **18**, (2007) 485705.

[2] N.A. Cordero and J.A. Alonso, Journal of Physical Chemistry C, **41**, (2010) 17249.

[3] I.G. Ayala, N.A. Cordero and J.A. Alonso, submitted to Physical Review B (2010).

[4] https://wiki.fysik.dtu.dk/dacapo/Dacapo

Figures
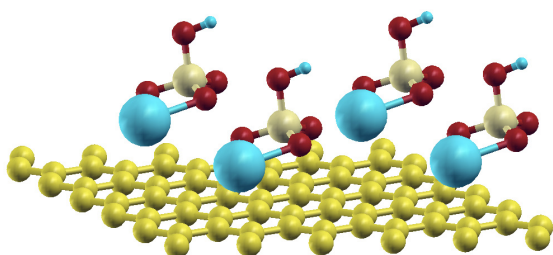
Medium concentration trans-NaHSO4 over a graphene sheet
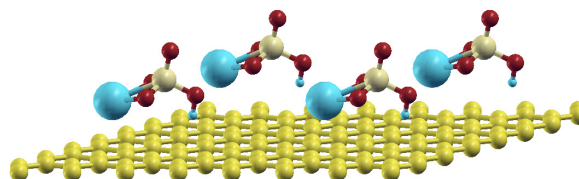
Low concentration cis-NaHSO4 over a graphene sheet

Graphene layers deposited on copper substrate by hot wire CVD

J. Badia-Canal, V.M. Freire, C. Corbella, M. Rubio-Roy, E. Pascual, E. Bertran and J.L. Andújar

FEMAN Group, IN^{2}UB, Department of Applied Physics and Optics, University of Barcelona
c/ Martí i Franquès 1, E-08028 Barcelona, Spain
corberoc@hotmail.com

Graphene layers were grown on copper by chemical vapour deposition (CVD) thermally activated in a hot wire process. The depositions were performed at 250 Pa using CH_4 or C_2H_2 as gas precursors, which were diluted in a hydrogen atmosphere. In order to facilitate the nucleation and growth of the graphene ultrathin layer, a copper film was previously deposited on a polished c-Si wafer by sputtering (PVD) of a pure copper target at 0.5 Pa of argon. To avoid the oxygen contamination, the PVD and CVD processes were performed consecutively in the reactor operating at base pressure of $2 \cdot 10^{-4}$ Pa. A graphite heater kept the substrate temperature at 800ºC and activated the decomposition of the precursor. The other variables considered in this work were the gas flow ratio and the distance between sample and heater. Raman spectroscopy assessed the synthesis of carbon in graphene form by showing the characteristic 2D band. Also, the morphology of the samples was characterized by atomic force microscopy (AFM) and scanning electron microscopy (SEM). These layers were deposited on large area substrates (≈ 5 cm^2). The results, which are discussed in terms of the technological parameters of deposition, suggest the feasibility of hot wire CVD to produce graphene layers on metallic substrates.

Clar Sextet Theory for low-dimensional carbon nanostructures: an efficient approach based on chemical criteria

Matteo Baldoni, Francesco Mercuri, Daniele Selli, Gotthard Seifert

Fachbereich Chemie, Technische Universitaet, Bergstraße 66b, Dresden, Germany
mbaldoni@theory.chm.tu-dresden.de

Recently, the properties of nanostructured carbon materials, like carbon nanotubes (CNTs) and graphene, have been the subject of in-depth investigations in view of their potential use in nanotechnology. Most of the interest concerning nanostructured carbon materials is related to the peculiarities of their electronic structure, which is constituted mainly by a complex network of π-conjugated bonds. Details of the electronic structure play a crucial role in the application of such materials as nanostructured building-blocks for molecular electronics and in functionalization processes, where the CNTs and graphenes undergo chemical reactions. However, the particular structural and electronic features of nanostructured carbon poses significant problems to computational modeling. Relatively recent works indicated the extension of classical organic chemistry concepts, like the "Clar Sextet Theory",[1,2] to the case of low-dimensional nanostructured carbon materials as a successful approach to obtain an accurate and consistent description of the electronic structure of the hexagonal carbon atom network. In this work we apply state-of-the-art numerical techniques to investigations on the stability and on electronic and chemical properties of nanotubes and graphenes and related compounds. Our approach is based on the definition of suitable models of the system under study starting from chemical considerations. Results indicate unprecedented accuracy in the prediction of properties for a large variety of systems, obtained at a relatively cheap computational cost.

References

[1] Baldoni M, Sgamellotti A, Mercuri F, Org. Lett., **9** (2007) 4267.
[2] Baldoni M, Sgamellotti A, Mercuri F, Chem. Phys. Lett., **464** (2008) 202.

Figures
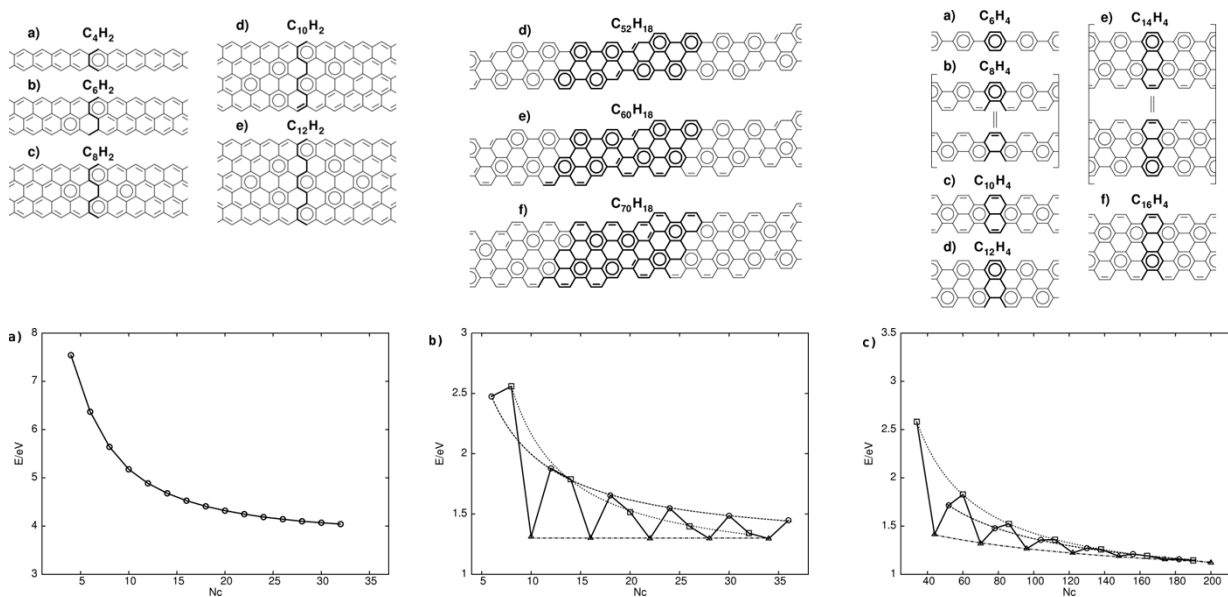
Clar representation for GNRs with different kind of edges. The corresponding trends for the HOMO-LUMO gaps as the width of the ribbon is increased is reported below .

Evidence for Josephson-coupled superconducting regions at the interfaces of highly oriented pyrolytic graphite

A. Ballestar, J. Barzola-Quiquia, P. Esquinazi

Division of Superconductivity and Magnetism, Institute for Experimental Physics II, University of Leipzig, Linnestrasse 5, D-04103, Leipzig, Germany
ana.ballestar@physik.uni-leipzig.de

The first observation of superconductivity in doped graphite goes back to 1965 when it was observed in the potassium graphite intercalated compound C_8K [1]. A considerable amount of studies had reported this phenomenon in intercalated graphite compounds or doped graphite [2-4], however the superconducting properties of pure graphite are still under discussion. Indirect evidences for superconductivity at graphite interfaces have been recently published [5-6]. In order to better understand their properties and confine the path of the input current to go through some of the possible superconducting areas, we prepared micro structured samples (Lamellas) from pure highly oriented pyrolytic graphite. By reducing the dimension in the in-plane configuration to ~ 200nm we can measure the electrical response of graphite interfaces. We obtained evidence for the existence of Josephson-coupled quasi two dimensional superconducting regions (patches) located at internal interfaces of the oriented graphite samples. Temperature dependence of the voltage (Figure 1), as well as I(V) characteristic curves (Figure 2) indicate that superconductivity exists even above 150K. The negative values obtained for the measured voltages can be understood using a simple Wheaston bridge model. The resistor elements of the bridge will correspond to the effective resistances of the inhomogeneous current paths inside the samples. Ambegaokar and Halperin theory [7] is used to describe the I(V) characteristics of the superconducting patches contribution within the model. The results support the view that HOPG is a system with interfaces containing non-percolative superconducting domains immersed in a semiconducting graphene-based matrix.

References

[1] Hannay, N. B. et al., Phys. Rev. Lett., **14**, (1965), 7.

[2] Weller, T. E., et al., Nature Phys., **1**, (2005), 39.

[3] Emery, N. et al., Phys. Rev. Lett., **95**, (2005), 087003.

[4] Kopelevich, Y. et al., Physica C, **408**, (2004), 77.

[5] Esquinazi, P. et al., Physical Review B, **78**, (2008), 134516.

[6] Barzola-Quiquia, J. and Esquinazi, P., J. Supercond. and Novel Magnetism, **23**, (2010), 451.

[7] Ambegakoar, V. and Halperin, B. I., Phys. Rev. Lett., **22**, (1969), 1364.

Figures
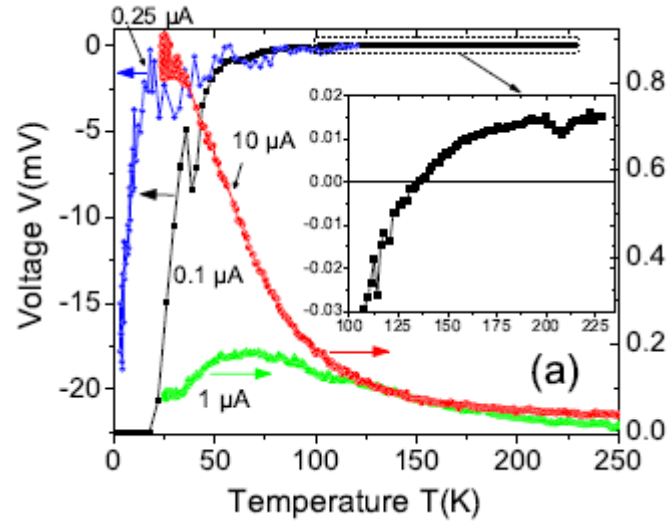
Figure 1. Voltage vs. temperature measured at four different current amplitudes. The right y-axis applies for the results at 1 and 10 µA. The inset shows the results for 100 nA input current in the high temperature region. Note that the change in the voltage is observed even above 150K.
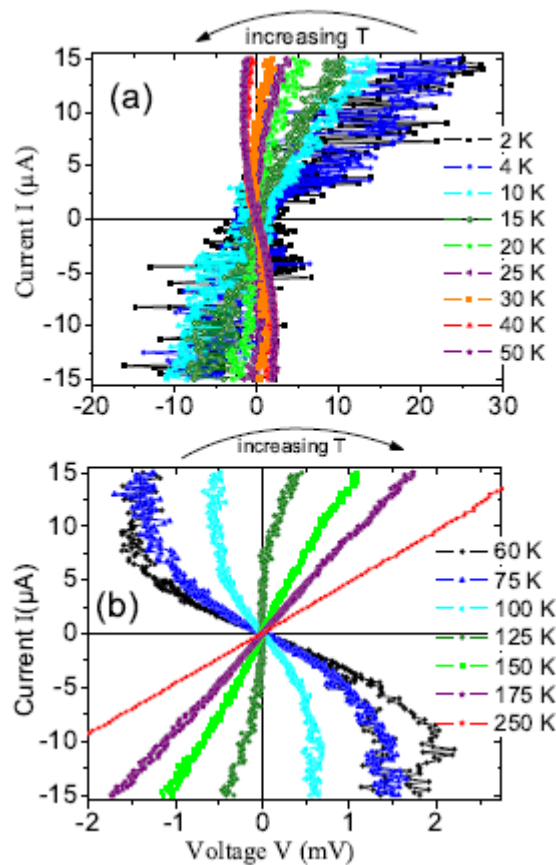
Figure 2. Current-voltage curves at different temperatures. (a) A noisy behavior is found at low temperatures (T≤10K) due to the heterogeneous properties and coupling between the superconducting patches. Above this temperature the noise reduces and the nonlinearity shows a "negative resistance" part that increases up to 60K. (b) Above 60K the nonlinearity gets weaker reaching a linear behavior above 200K.

26

Structured Graphene Devices for Mass Transport

A. Barreiro[1,2], R. Rurali[3], E. R. Hernandez[4], A. Bachtold[1]

[1]CIN2 (ICN-CSIC) Barcelona, Campus UAB, 08193 Bellaterra, Spain
[2]TU Delft, Lorentzweg 1, 2628HJ Delft, The Netherlands
[3]ICMAB-CSIC, Campus UAB, 08193 Bellaterra, Spain
[4]ICMM-CSIC, Campus de Cantoblanco, 28049 Madrid, Spain
a.barreiromegino@tudelft.nl

We report on the achievement of reversible atomic mass transport along graphene devices [1]. The motion of Al and Au in the form of atoms or clusters is driven by applying an electric field (between the metal electrodes that contact the graphene sheet). We show that Al moves in the direction of the applied electric field whereas Au tends to diffuse in all directions. The control of the motion of Al is further demonstrated by achieving a 90 degrees turn, using a graphene device patterned in a crossroad configuration. The controlled motion of Al is attributed to the charge transfer from Al onto the graphene so Al is effectively charged and can be accelerated by the applied electric field. In order to get further insight into the actuation mechanism, we carry out theoretical simulations of individual Al and Au impurities on a perfect graphene sheet. The direct (electrostatic) force is found to be ~1 pN and to be dominant over the wind force. Our findings hold promise for practical use in future mass transport in complex circuits.

References

[1] A. Barreiro, R. Rurali, E. R. Hernandez, A. Bachtold, Small **accepted** (2011)

Figures
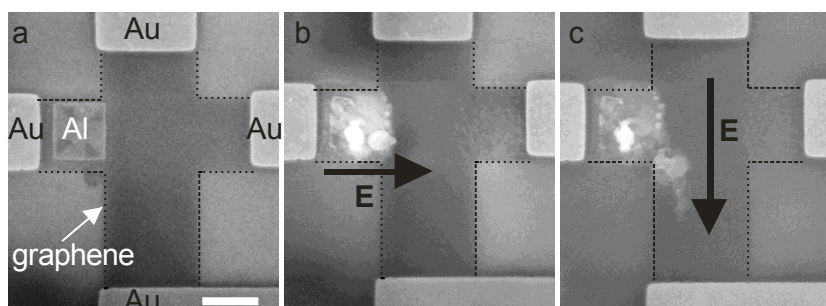
Figure 1 (a) Scanning electron microscopy image of a graphene device structured in a crossroad configuration with one Al plate. The scale bar is 1 μm. (b,c) Motion of the aluminum after having applied an electric field in different directions (indicated by the arrow). In (b) we applied a voltage *V* of 9 V during *t*= 6 minutes and the current *I* was 1.4 mA; in (c) *V* = 12.7 V, *I* = 1.63 mA, *t* = 9 minutes.

From Graphite Oxide to Graphene-like Sheets via Thermal Reduction: Kinetic Mechanisms

Fabienne Barroso-Bujans[1], Ángel Alegría[1,2], Juan Colmenero[1,2,3]

[1]Centro de Física de Materiales-Material Physics Center (CSIC-UPV/EHU), Pº Manuel de Lardizábal 5, 20018 San Sebastián, Spain
[2]Dept. de Física de Materiales, Universidad del País Vasco (UPV/EHU) Apartado 1072, 20080 San Sebastián, Spain
[3]Donostia International Physics Center (DIPC), Paseo Manuel de Lardizábal 4, 20018 San Sebastián, Spain

fbarroso@ehu.es

Introduction

Graphite oxide (GO) has been known since the 19th century but it has recently re-emerged as an intensive research area due to its importance in obtaining large-scale graphene materials, afforded by the chemical or thermal reduction of GO, among others. Chemical reduction involves the use of reducing agents such as hydrazine, hydroquinone and $NaBH_4$ while the thermal treatment at elevated temperatures avoids the use of these hazardous chemicals and provides a rapid and efficient method to produce large amounts of graphene-like sheets. Deoxygenation of GO upon chemical or thermal reduction has been systematically studied in the past, where the restoration of C=C bonds and the decrease in the number of C-OH, C-O-C, COOH groups have been experimentally and theoretically determined [1-3]. However, deoxygenation is not completed after reduction by which residual amounts of oxygen vary depending on the reduction process (temperature, atmosphere, treatment). Studies by molecular dynamics simulations showed that these residual amounts of oxygen in reduced GO are also dependent upon the initial oxygen concentration and the hydroxyl/epoxide ratio [2]. Furthermore, since a great variety of GOs with variable chemical composition and interlayer spaces can be obtained via the synthesis methods that comprises that of Brodie, Hummers and Staudenmaier methods, the composition and, therefore, the chemical-physical properties of reduced GO, can be extensively different.

In spite of repeated efforts, the mechanisms involved in the thermal reduction of GO are far from clear and no predictions can be made on the final properties of the reduced GO. For that reason, intensive studies on the thermal reduction of GO are of great importance, especially when combining different experimental techniques in order to provide structural and compositional information. Following this idea, in the present study, temperature- and time-resolved x-ray diffraction (XRD) and thermogravimetric analysis (TGA) are used to monitor the structural changes of GO upon dynamic (non-isothermal) and static (isothermal) modes. To gain further insight in the reduction reactions taking place, simultaneous TGA/mass spectrometry (MS) experiments are also conducted in both modes. Isothermal TGA is run at various temperatures in the 120-220 ºC range, enabling the establishment of the kinetic mechanisms involved in the thermal reduction of GO. Moreover, the kinetic mechanisms of several GO prepared by the different synthesis methods are compared.

Kinetic experiments

Figure 1 shows the weight loss rate of a Brodie-based GO (from natural graphite) as a function of weight percent. In this representation, it is very apparent that two different mechanisms for weight loss exist, each dominating a particular range. The best fitting for mechanism I was accomplished with a two-dimensional diffusion model whereas for mechanism II an autocatalytic model was found very adequate. These results, although contrast with previously published second order kinetics by both McAllister et al. [1] and Jung et al. [3], are in agreement with a further experiment where GO was obtained from

synthetic graphite (Figure 2a). Notable differences were found in mechanism I for the Brodie-based GO obtained from both synthetic and natural graphite, in which diffusion mechanism occurs in different weight percent ranges. Figure 2 shows the dependence of the reduction kinetic mechanisms on the GO synthesis method. Whereas the weight loss rate for Brodie-GO fitted to both diffusion and autocatalysis, as above mentioned, that for Hummers- and Staudenmaier-GO fitted to n-order kinetics only at highest weight losses. These results account for the importance of both the GO synthesis method and starting graphite in determining the kinetic behavior of thermal reduction.
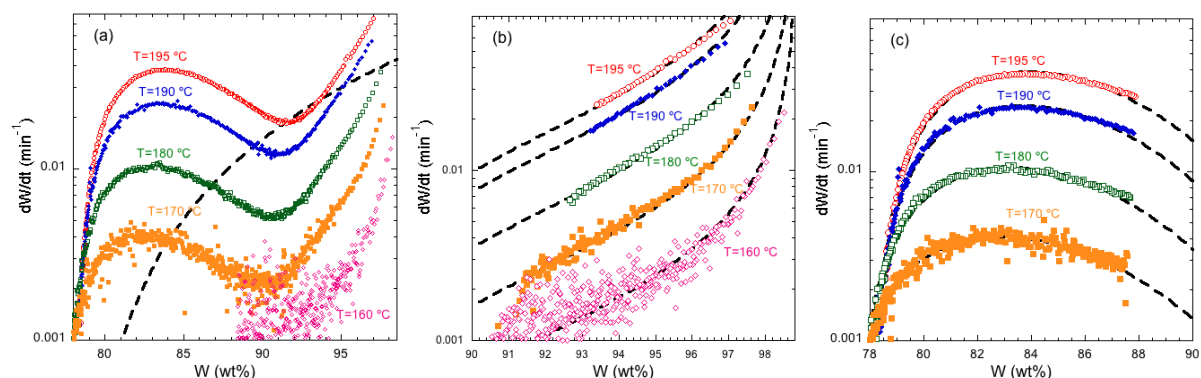
Figure 1. Isothermal TGA experiments. Weight loss rate (dW/dt) of Brodie-based GO (from natural graphite) as a function of the percentage weight loss (W) at different temperatures. a) Whole process. Dashed line depicts a second-order mechanism. b) Mechanism I: fitting curves with a two-dimensional diffusion model and c) Mechanism II: fitting curves with an autocatalytic model. Reported in reference [4].
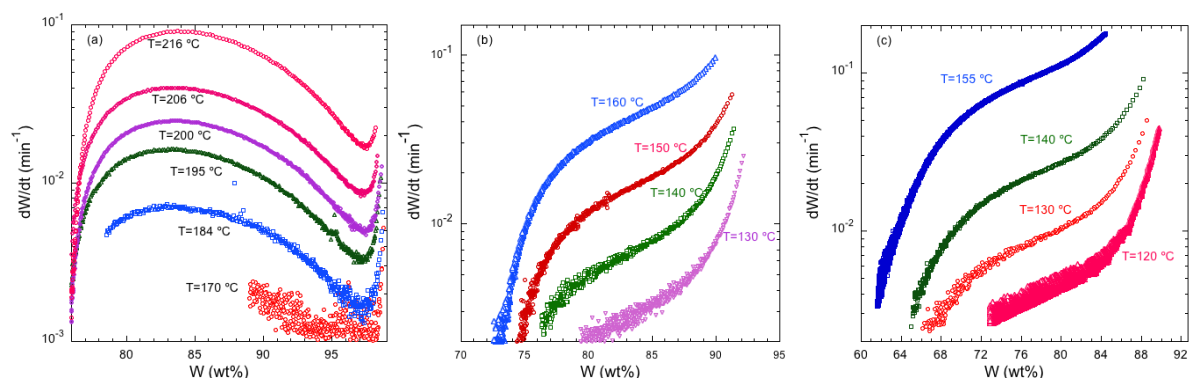
Figure 2. Isothermal TGA experiments. Weight loss rate (dW/dt) of GO (from synthetic graphite) obtained from a) Brodie, b) Staudenmaier c) and Hummers –based methods as a function of the percentage weight loss (W) at different temperatures.

Conclusions

The thermal reduction studies for a series of GO obtained from the Brodie, Staudenmaier and Hummers methods revealed new experimental evidences of the kinetic mechanisms involved. While combined dynamic TGA and temperature-resolved XRD enabled the monitoring of the structural changes taking place in GO during the thermal reduction, isothermal methods were more effective. Combined isothermal-TGA and time-resolved XRD showed that two distinct and well-resolved mechanisms were involved in the thermal reduction of Brodie-based GO, 2D-diffusion and autocatalysis; whereas n-order kinetics were observed for Hummers- and Staudenmaier-based GO.

References

[1] MJ McAllister, J Li, DH Adamson, HC Schniepp, AA Abdala, J Liu, M Herrera-Alonso, DL Milius, R Car, RK Prud'homme, IA Aksay, Chem Mater **19** (2007) 4396.
[2] A Bagri, C Mattevi, M Acik, YJ Chabal, M Chhowalla, V B Shenoy, Nat Chem **2** (2010) 581.
[3] I Jung, DA Field, NJ Clark, Y Zhu, D Yang, RD Piner, S Stankovich, DA Dikin, H Geisler, CA Ventrice, RS Ruoff, J Phys Chem C **113** (2009) 18480.
[4] F Barroso-Bujans, A Alegría, J Colmenero, J Phys Chem C **114** (2010) 21645.

A New Route to Synthesis of Graphene and Graphenol Nanoparticles

Gary W. Beall, Y. Vecherkina, B. Henderson, A. Koshknbayeva

Texas State University, Department of Chemistry and Biochemistry, 601 University Drive, San Marcos, TX, USA

Gb11@txstate.edu

Since the reporting of the discovery of graphene in 2004 a great deal of excitement has been generated in the research community. This interest is due to the fact that graphene exhibits very unique properties including very high electrical and thermal conductivities and the highest tensile strength ever measured. The majority of graphene is currently made by exfoliating graphite with strong acids and oxidizing conditions to first form graphene oxide followed by reduction to graphene. Graphene has also been made by utilizing chemical vapor deposition. These methods result in graphene that is rather expensive. This has been one of the road blocks encountered in commercialization of carbon nanotubes. For both graphene and carbon nanotubes the cost has limited the penetration of them into mass commercial applications. The work reported in this talk should overcome this hurdle to commercialization. A process will be reported that produces graphene and edge functionalized graphene at very low cost. The process starts with carbonaceous material that is very inexpensive and two chemical steps that do not require strong oxidizing acids or strong reductants. The process will be presented in detail. Examples of polymer nanocomposites produced utilizing the graphene or functionalized graphene will also be presented. Commercial quantities utilizing the process are being produced and will also be discussed.

Electron and optical phonon temperatures in electrically biased graphene

Stéphane Berciaud[1,2], Melinda Y. Han[1], Kin Fai Mak[1], Louis E. Brus[1], Philip Kim[1], and Tony F. Heinz[1]

[1]Columbia University, New York, NY 10027, USA

[2]IPCMS (UMR 7504), Université de Strasbourg and CNRS, F-67034 Strasbourg, FRANCE

berciaud@unistra.fr

Graphene is characterized by remarkably large room-temperature carrier mobilities (> 10^5 cm^2Vs^{-1}) [1], as well as by its ability to sustain high current densities (> 10^8 A/cm2) [2, 3, 4, 5]. Recent investigations of high-field transport in graphene indicate a critical role for coupling of energetic carriers with the high-energy optical phonons [4, 5]. The distribution of energy within and among the charge carriers, the strongly coupled optical phonons, and the other phonons in graphene has, however, not yet been established.

Here, we examine the intrinsic energy dissipation steps in electrically biased graphene channels. By combining in-situ measurements of the spontaneous optical emission with a Raman spectroscopy study of the graphene sample under conditions of current flow, we obtain independent information on the energy distribution of the electrons and phonons [6]. The electrons and holes contributing to light emission are found to obey a thermal distribution (see Fig. 1), with temperatures in excess of 1500 K in the regime of current saturation. The zone-center optical phonons are also highly excited and are found to be in equilibrium with the electrons. For a given optical phonon temperature, the anharmonic downshift of the Raman G-mode is smaller than expected under equilibrium conditions, suggesting that the electrons and high-energy optical phonons are not fully equilibrated with all of the phonon modes.
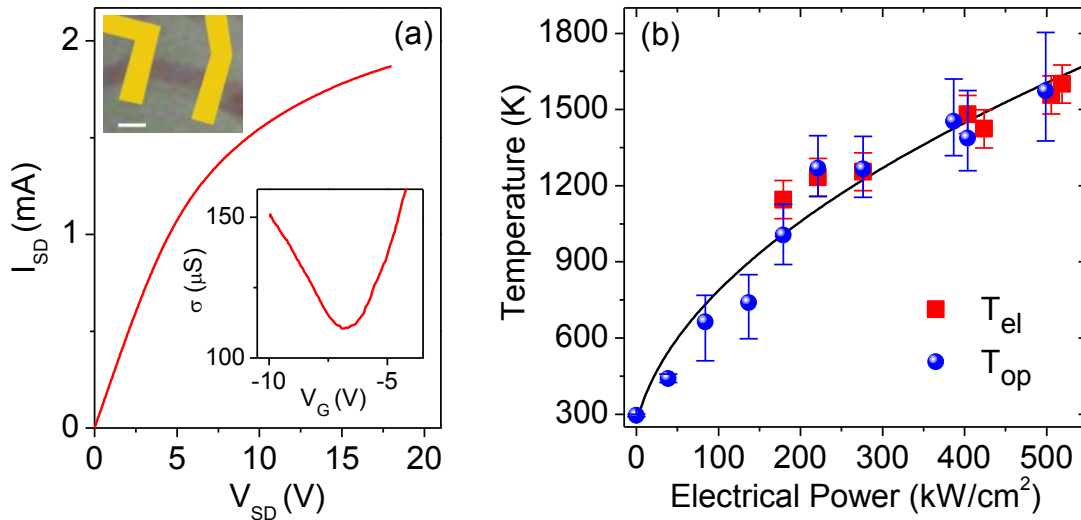
Figure 1: (a) Source-drain current-voltage characteristics at zero gate bias of the 3.6 x 1.6 μm^2 graphene channel shown in the top inset (the scale bar is 2 μm). The lower inset shows the back-gate dependence of the channel conductivity (σ). (b) Electronic (T_{el}, squares, deduced from the spontaneous optical emission spectra) and optical phonon (T_{op}, circles, deduced from Raman measurements) temperatures as a function of the dissipated electrical power. The dashed line is a guide to the eye, based on a scaling of the temperature as $P^{1/2}$.

References

[1] K. I. Bolotin et al., Phys. Rev. Lett., 101, 096802 (2008).

[2] I. Meric et al. Nat. Nanotechnol. 3, 654 (2008).

[3] M. Freitag et al., Nano. Lett. 9, 1883 (2009).

[4] A. Barreiro et al., Phys. Rev. Lett. 103, 076601 (2009).

[5] D-H. Chae et al., Nano Lett. 10, 466 (2010).

[6] S. Berciaud et al., Phys. Rev. Lett. 104, 227401 (2010).

Imaging Coherent Electrons in Graphene

Sagar Bhandari[1], Jesse Berezovsky[1, *], Mario Borunda[2], Eric Heller[2, 3], Robert Westervelt[1]
[1]School of Engineering and Applied Sciences, [2]Department of Physics, [3]Department of Chemistry, Harvard University, Cambridge, MA 02138, U.S.A
sbhandar@fas.harvard.edu
*Jesse Berezovsky, now at the Dept of Physics in Case Western University

Graphene is an exciting new material which provides a test bench for new kinds of experiments. We use a cooled scanning probe microscope (SPM) to probe the motion of electrons in graphene. At low temperatures, the coherent interference of electron waves scattered by disorder leads to universal conductance fluctuations (UCF) and weak localization effects. Using the SPM tip as a local movable scatterer, images of magnetoconductance versus tip position are obtained that show how electron interference is affected by the tip position. The weak localization dip in conductivity at zero magnetic field is obtained by averaging the magnetoconductance traces at different tip positions. The width of the dip yields the coherence length of electrons. For UCF we find conductance images that resemble speckle patterns, that change by $G \sim e^2/h$ when the tip moves by half the Fermi wavelength.

References:

[1] J. Berezovsky et al., Nanotechnology, Vol. 21, Issue 27 (2010), pp. 274014
[2] J. Berezovsky, R.M. Westervelt, Nanotechnology Vol. 21, Issue 27 (2010), pp. 274014

Figures:
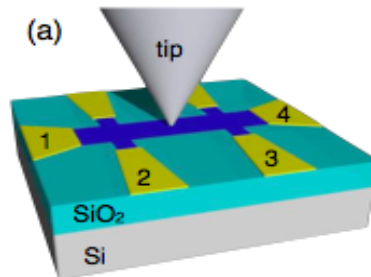
Figure 1: SPM tip as a local scatterer in graphene hall bar sample
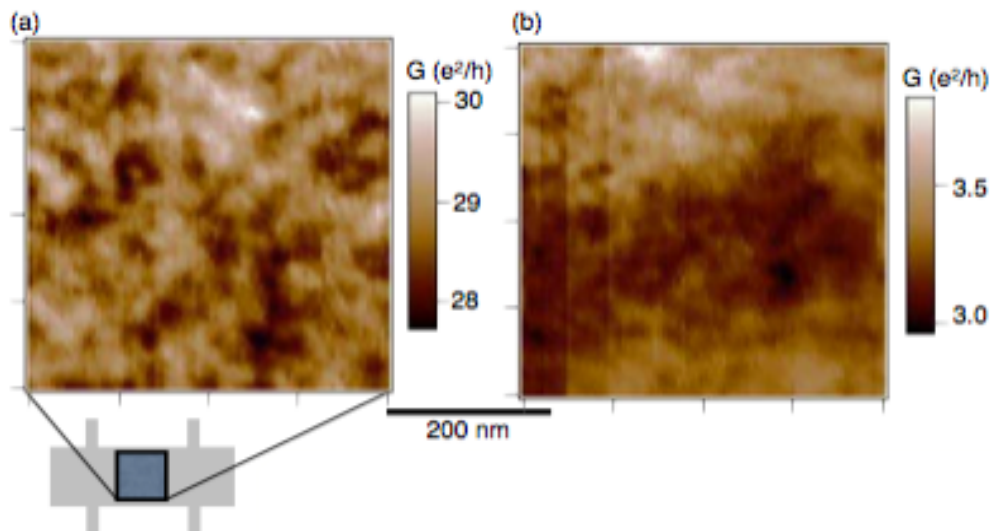
Figure 2: Conductance image vs. tip position: (a) Far from the dirac point , (b) Near the dirac point

(a)

B = 145 mT   139 mT   133 mT   128 mT
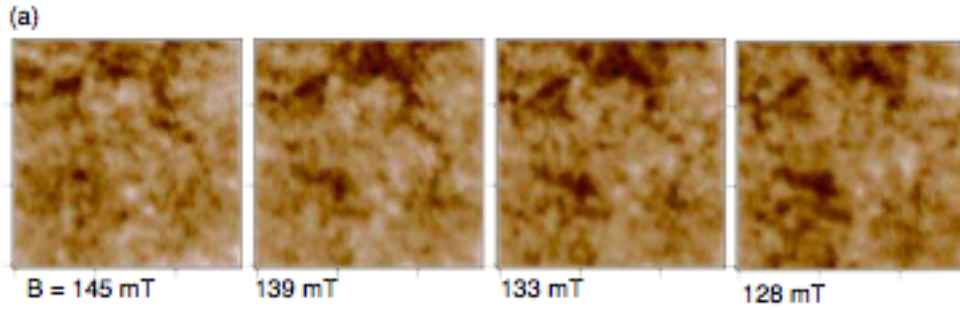
Figure 3: A series of conductance image vs. magnetic field at constant back gate voltage Vg = 0V
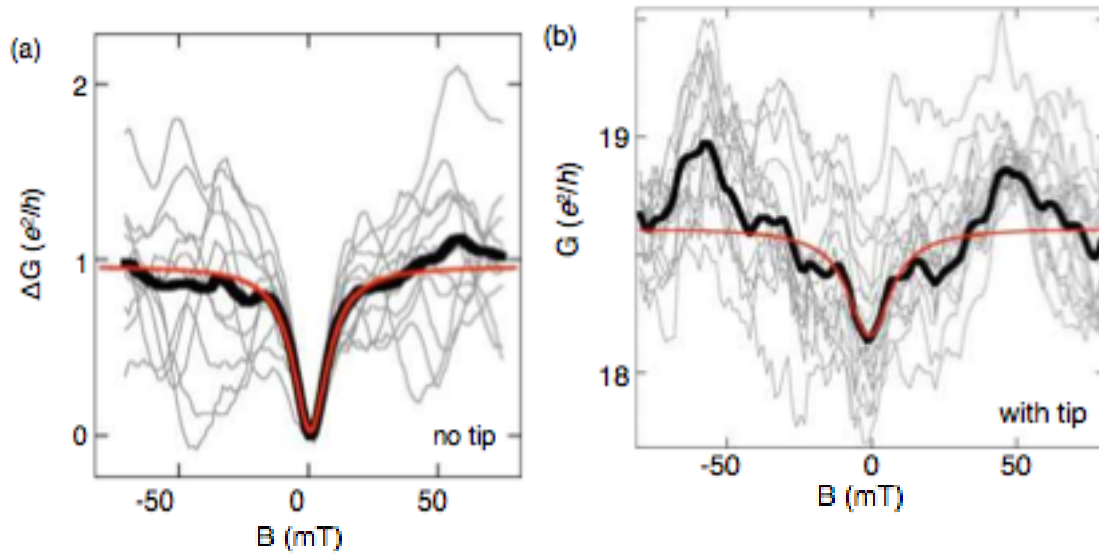
Figure 4 : Weak localization conductance dip in the sample (a) tip far from the sample with different carrier densities, (b) tip close the sample at differen positions but fixed density

Spin Transport and Spin Precession in Bilayer Graphene with Transparent and Tunneling Ferromagnetic Contacts

Bastian Birkner, Jonathan Eroms and Dieter Weiss

Institute for Experimental and Applied Physics, University of Regensburg, Regensburg, Germany
Bastian.Birkner@physik.uni-regensburg.de

We achieved electrical spin injection by employing a DC current from a ferromagnetic contact (Co) into bilayer graphene, both with and without tunneling barrier. The graphene flakes were mechanically exfoliated from natural graphite by using adhesive tape on a SiO_2/p-doped Si substrate where the Si is used as a backgate. The ferromagnetic and normal metal (Pd) electrodes were defined by standard electron beam lithography (Fig. 1). In the case of directly connected ferromagnetic stripes onto bilayer graphene the contact resistance was about 450 Ohm, determined in a three point measurement which indicates that the Co/graphene junctions are transparent [1]. In order to increase the spin injection efficiency and the spin signal ΔR which is defined as the difference of the non-local resistance between parallel and antiparallel magnetization of the ferromagnetic electrodes, tunneling contacts were produced to overcome the conductivity mismatch problem [2]. An approximately 1.4 nm thick AlOx tunneling barrier was produced by depositing Al over the entire sample at 180K and subsequent oxidation at room temperature for 30 minutes. AFM pictures reveal that the Al deposition at low temperature leads to a homogenous barrier. The I-V-characteristics of this Co/AlOx/graphene junction show non-linear behavior suggesting the absence of pinholes. The induced spin accumulation diffuses away from the injection point and is probed in a non-local four terminal scheme where the charge and spin currents are completely separated from each other. For both transparent and tunneling contacts we obtain a clear switching of the non-local resistance whose sign depends on the magnetization orientation (parallel/antiparallel) of the ferromagnetic electrodes (Fig. 2). By applying a perpendicular magnetic field we also detect spin precession (Hanle effect) which confirms that the non-local spin signal originates from spin injection and spin transport. Fitting of these Hanle curves yields the spin relaxation time and length as well as the spin injection efficiency. By comparing the results for transparent and tunneling contacts we find that the tunnel barrier enhances the spin signal by a factor of 30 and the spin injection efficiency increases from 1.7 to 5 percent whereas the spin relaxtion times are in the same range [3].

References

[1] W. Han et al. , Appl. Phys. Lett. **94**, 222 109 (2009)
[2] N. Tombros et al. , Nature (London) **448**, 571 (2007)
[3] W. Han et al. ,Phys. Rev. Lett. **105**, 167 202 (2010)

Figures
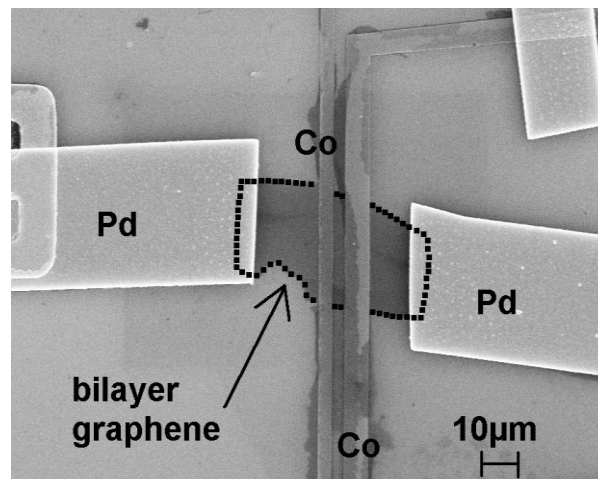
Fig. 1: REM picture of the non-local spin valve structure
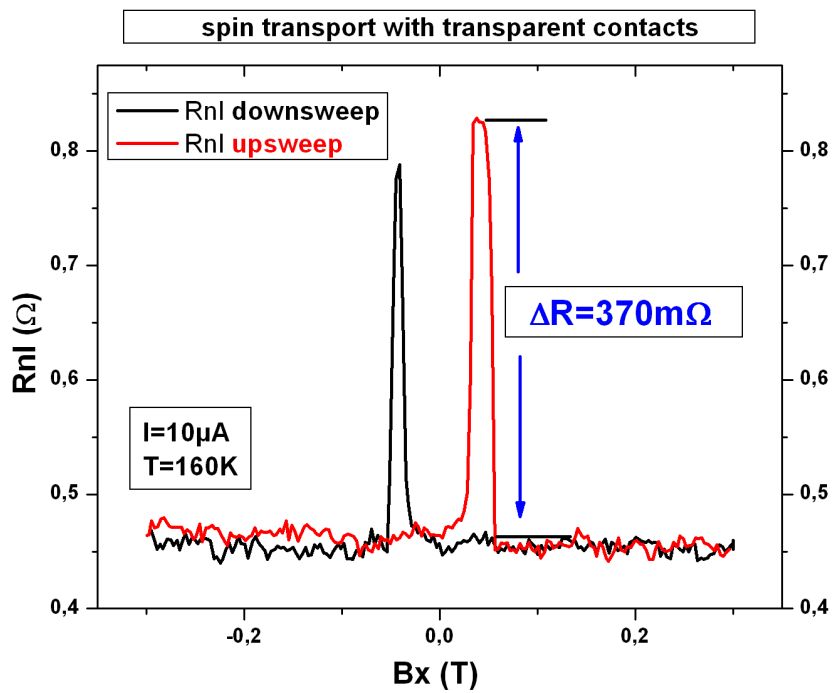
Fig. 2a) : Non-local resistance switching with transparent contacts
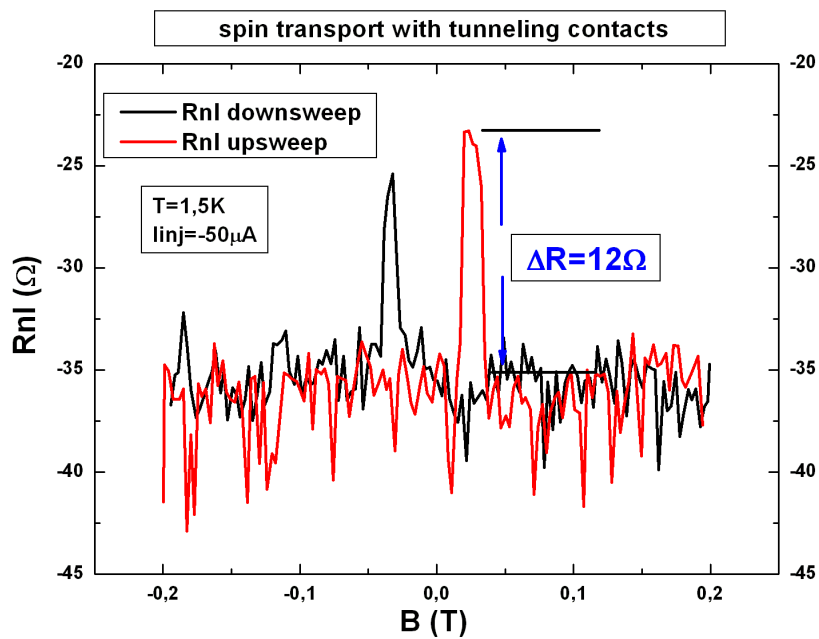
Fig.2b) : Non-local resistance switching with tunneling contacts.

Atomic-Scale Modeling of Carbon Transistors

Anders Blom, Kurt Stokbro

QuantumWise A/S
Lersø Parkalle 107, 2100 Copenhagen, Denmark
Anders.Blom@quantumwise.com

We present atomic-scale simulations which compare the characteristics of transistors made of carbon nanotubes (CNT) [1] and graphene nanoribbons (GNR) [2]. We studied the properties of a semi-conducting CNT attached to metallic electrodes and controlled by a triple back gate. We find that the performance of the device is weakened by quantum tunneling and show that it is related to inefficient control by the back gate. For the GNR transistor we use a structure comprising of two metallic GNRs separated by a semiconducting GNR. We find only weak quantum tunneling and show that the GNR has much better transistor characteristics compared to the CNT.

In addition, we will show that while short graphene nanoribbons operate based on pure ballistic tunneling, the transport properties in longer ribbons exhibit characteristics of thermionic emission.

The calculations were performed with Atomistix ToolKit (ATK) from QuantumWise. ATK is a software package comprising a number of simulation methods for atomic-scale modeling of nanostructures. It collects first-principles, semi-empirical and classical methods in a homogeneous interface, and uses non-equilibrium Greens functions (NEGF) to model the transport properties of nanostructures under an applied bias. Certain features of the software and their relevance for the studied systems will also be discussed in the presentation.

[1]   H. H. B. Sørensen, P.C. Hansen, D.E. Petersen, S. Skelboe and K. Stokbro, *Efficient wave function matching approach for quantum transport calculations*, Phys. Rev. B **79**, 205322 (2009).
[2]   K. Stokbro, D. E. Petersen, S. Smidstrup, M. Ipsen, A. Blom and K. Kaasbjerg, *Semiempirical model for nanoscale device simulations*, Phys. Rev. B **82**, 075420 (2010).
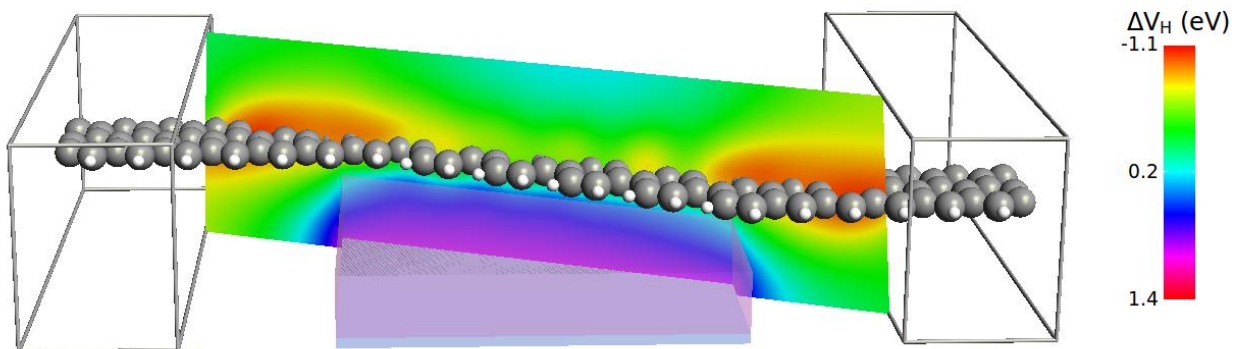
Graphene nanotransistor consisting of two metallic zigzag nanoribbons connected by a semiconducting armchair ribbon. The nanoribbons are passivated with hydrogen, and the width of the ribbons are is 7 Å. The device is sitting on top of a dielectric and the transport is controlled by an electrostatic backgate. The contour plot illustrates the Hartree potential for a gate potential of −1 V.

Conduction properties of graphene as a function of ion irradiation and acid treatment

T. Blom[1], S. H. M. Jafri[1], V. de Cristo[1], K. Carva[2], G. Possnert[2], B. Sanyal[2], H. Grennberg[3], U. Jansson[4], O. Eriksson[2], K. Leifer[1]

[1]Div. of Applied Materials Science, Uppsala University, Box 534, SE-75121, Uppsala, Sweden
[2]Dept. of Physics and Astronomy, Box 516, SE-75120, Uppsala, Sweden
[3]Dept. of Biochemistry and Organic Chemistry
[4]Dept. of Materials Chemistry, Uppsala University, Box 534, SE-75121, Uppsala, Sweden

klaus.leifer@angstrom.uu.se

Materials research has reached impressively and exciting levels with the discovery of graphene. The modification and functionalization of graphene has proved to influence the electrical properties. This strategy is important during the pursuit of a completely tunable material when it comes to physical and electrical properties.

From first-principle simulations of the conductivity of graphene sheets, it has been shown that the insertion of defects in the graphene sheets leads to an increase of the conductivity with more than one order of magnitude [1]. To study this result experimentally, We have introduced defects in the graphene lattices by chemical and physical means, where we have studies of the change in conductivity of graphene with induction of defects.

In the case of acid treatment, graphene-like carbon nanosheets [ref to Jafri, J Phys D] were electrically characterized individually in a focused ion beam / scanning electron microscope (FIB/SEM). This results from this characterization showed that the conductivity increase roughly 50 times upon acid treatment of the nanosheets. This corresponds well to calculations which have showed that a so called metallicity appears around defects (divacancies) in the lattice and this lead to an increased conductivity.

In the case of ion irradiated graphene, electron beam lithography was used for contacting the graphene flakes. A voltage was applied across the contacted flakes giving rise to a current (in the order of nA) which was monitored with respect to time during the ion irradiation. A contacted graphene flake was irradiated with 30 keV Ga^+ ions inside the FIB/SEM, see figure 1. The measured resistivity of the flake increased upon irradiation which is most likely related to the damage (sputtering) of carbon atoms as well as redeposition of the silicon dioxide substrate onto the graphene. The irradiation of 2 MeV protons on contacted graphene resulted in an decreased resistance by two to three times, see figure 2. The red areas and the numbers shows the irradiation periods. The blue areas are just relaxation time. The observed change in resistance is most likely due to charging of the substrate which will act as a gating effect on the measurement.

References

[1] V A Coleman, R Knut, O Karis, H Grennberg, U Jansson, R Quinlan, B C Holloway, B Sanyal, O Eriksson, J. Phys. D: Appl. Phys. **41** (2008) 062001.
[2] S.H.M. Jafri, K. Carva, E. Widenkvist, T. Blom, B. Sanyal, J. Fransson, O. Eriksson, U. Jansson, H. Grennberg, O. Karis, R.A. Quinlan, B.C. Holloway, K. Leifer, J. Phys. D: Appl. Phys. **43** (2010).
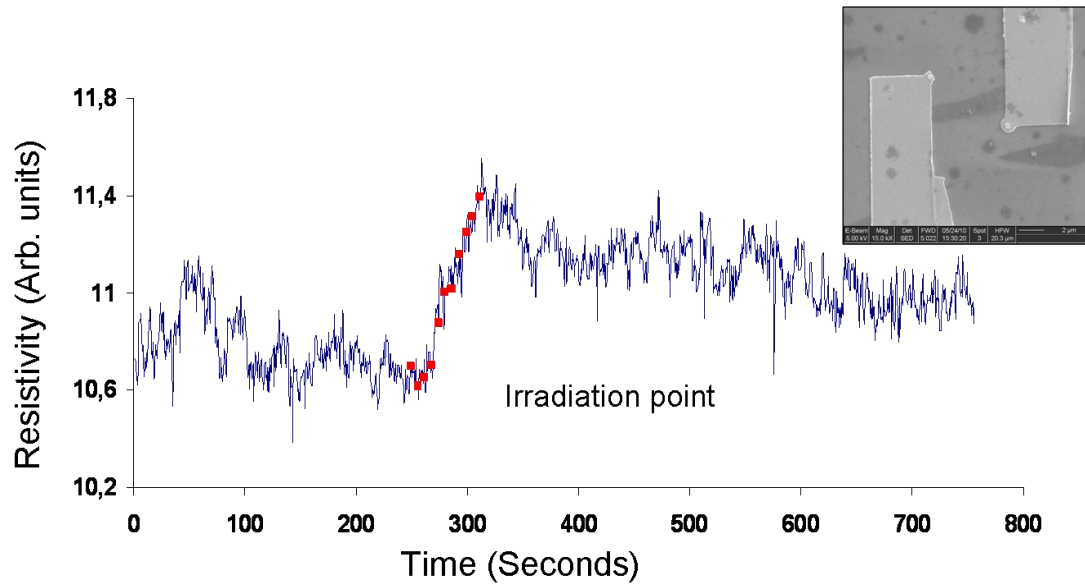
Figure 1. Measured resistivity during irradiation with 30 keV Ga$^+$ ions in the FIB/SEM. The inset to the right is a scanning electron image of the contacted graphene flake.

Figures
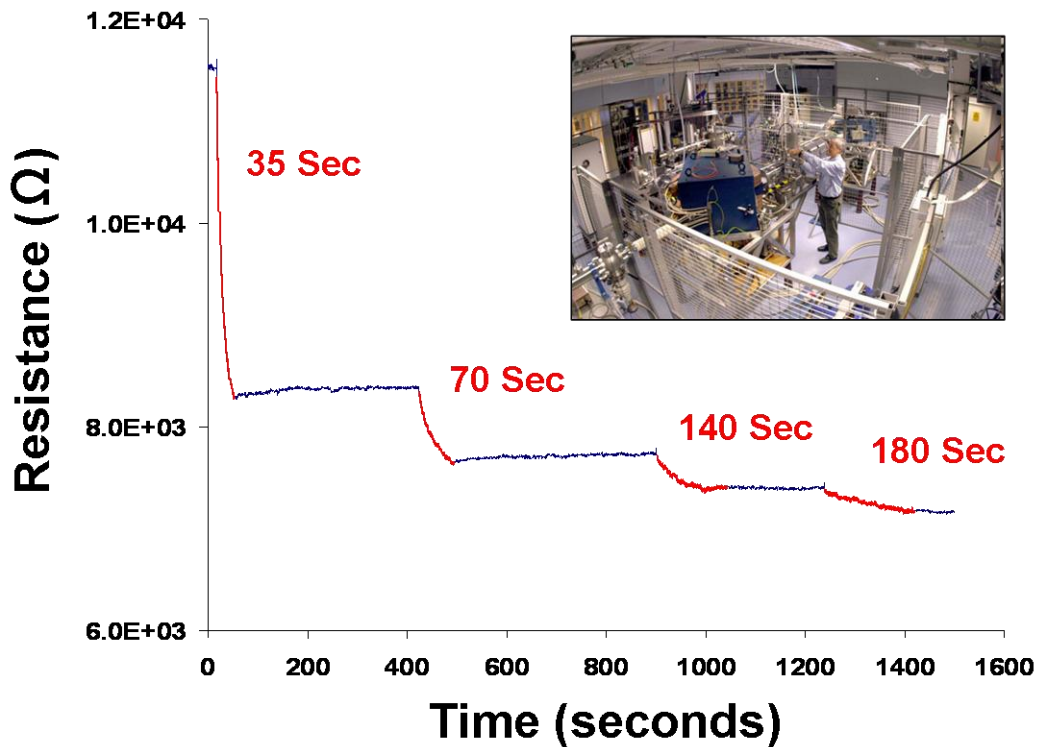
Figure 2. Measured resistance during irradiation with 2 MeV protons with a current of 40 nA/cm^2. The (red) time indications shows the periods of irradiation. The photograph shows a part of the Tandem accelerator at the Angstrom laboratory, used for this experiment.

Excitonic absorption spectra in graphene and carbon nanotubes

Evgeny Bobkin, Andreas Knorr, Ermin Malic

Institut für Theoretische Physik, Technische Universität Berlin, Hardenbergstraße 36, Berlin, Germany
evgeny.bobkin@tu-berlin.de

In this contribution, we propose a theoretical model for calculation of absorption spectra of graphene and carbon nanotubes (CNTs) including excitonic and exciton-phonon features. Our approach is based on the density-matrix formalism combined with tight-binding wave functions. It allows the description of graphene and CNTs of arbitrary chiral angle including many-particle contributions, such as electron-electron and electron-phonon interaction [1, 2]. We derive and numerically solve microscopic graphene- and CNT-Bloch equations describing the temporal evolution of the occupation and transition probabilities of the electronic states [3]. Here, we present results on absorption spectra including the formation of excitons and phonon-induced side-bands.

The free-particle absorption spectrum of graphene is shown in Fig. a (green line). We find a strong impact on the spectrum when taking into account the Coulomb-induced renormalization of the band structure cp. Fig. a (red line). Furthermore, we observe clear excitonic features in graphene and CNTs in agreement with the theoretical studies using density functional theory and recent experiments [4, 5]. We find a significant exciton formation around the M high-symmetry point in the Brillouin zone of graphene. In the immediate vicinity of the K point, however, the excitonic influence is less significant.

Furthermore, in the case of carbon nanotubes we investigate the transfer of the spectral weight induced by exciton-phonon interaction. Here, our approach is extended by introducing an excitonic basis set allowing us to calculate directly the impact of the exciton-phonon dynamics. We observe the formation of a phonon-side band 200 meV away from the zero-phonon line, which we ascribe to the process of phonon emission, illustrated in Fig. b. With the increasing temperature its spectral intensity growths and an additional phonon-side band appears below the zero-phonon line corresponding to a phonon absorption processes. The strong exciton-phonon coupling also leads to a polaron shift of some tens of meV. We investigate the chirality and diameter dependence of the spectral weight transfer to the phonon-side bands as well as of the polaron shift. The description of exciton-phonon induced side-bands in the spectra of graphene is work in progress.

References

[1] E. Malic, et al., Phys. Rev., **B 82** (2010), 035433.
[2] T. Winzer, et al., Nano Lett., **10** (2010), 4839.
[3] E. Bobkin, et al., submitted for publication (2011).
[4] L. Yank, et al., Phys. Rev. Lett., **103** (2009), 186802.
[5] K. F. Mak et al., Phys. Rev. Lett. **101** (2008), 196405.

Figures
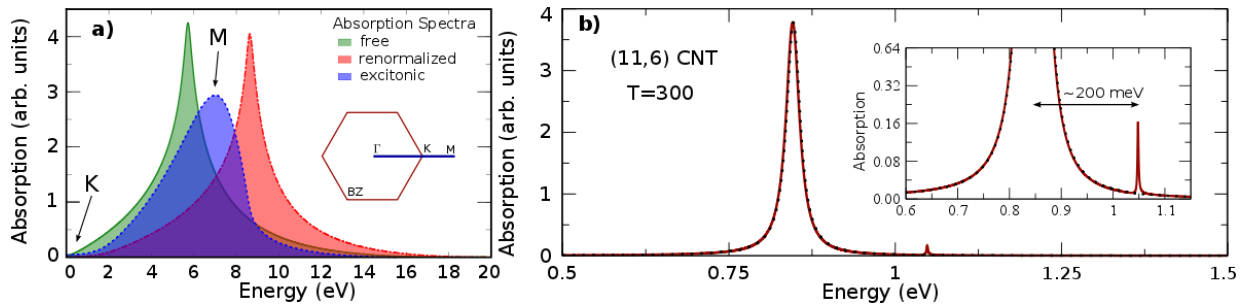
Fig. caption: a) Linear absorption spectra of graphene illustrating the free-particle (green), the renormalized (red), and the excitonic spectrum (blue). The inset figure shows the hexagonal Brillouin zone of graphene within the high symmetry points. b) Excitonic absorption spectrum of the semiconducting (11,6) nanotube including exciton-phonon coupling at room temperature. For comparison, the doted line in the background shows the pure excitonic spectrum. The figure illustrates the formation of a phonon side-band at the higher energy side of the zero-phonon line.

44

Beam-induced damage to graphene in the helium ion microscope

Stuart A. Boden, Zakaria Moktadir, Darren M. Bagnall, Harvey N. Rutt and Hiroshi Mizuta

Electronics and Computer Science, University of Southampton, Highfield, Southampton, SO17 1BJ, UK
sb1@ecs.soton.ac.uk

Graphene is currently attracting massive worldwide interest for its potential to be the foundation of a new generation of nanoscale electronic devices [1, 2]. This is owing to its remarkable properties that include very high carrier mobilities [3] and large current carrying capabilities which could enable the development of faster, less power-hungry devices, pushing the computer industry beyond what is possible with conventional silicon-based CMOS technology. One route for graphene-based electronic integration involves replacing the channel material in field-effect transistors with graphene, shaped into nanoribbons to open up a band gap. Alternatively, quantum dot structures fabricated in graphene could form the architecture for single electron transistor (SET) based electronics [4]. Both approaches require the development of patterning technologies to enable accurate nanoscale fabrication of graphene devices. Currently, the most established graphene device fabrication technique uses electron-beam lithography to pattern resist deposited on top of the graphene, followed by oxygen plasma etching [5,6]. However, the size of the patterns this process is capable of producing is limited by underetching of the resist. Recently, a new patterning technique based on direct milling of graphene using a focused beam of helium ions generated in a helium ion microscope (HIM) has emerged [7,8].

Helium ion microscopy (HIM) is a new surface imaging technique that involves scanning a focused beam of helium ions across a surface to generate an image from the resulting secondary electron (SE) emission, in a similar way to scanning electron microscopy (SEM) [9,10]. An atomically sharp and extremely bright source, combined with the larger momentum (and so smaller de Broglie wavelength) of helium ions compared to electrons, enables a sub-nanometer probe size at the sample surface and so high resolution imaging. Researchers have demonstrated that the tool can also be used to selectively sputter graphene to create intricate nanoscale designs, offering the potential of resist-free patterning of graphene on a finer scale compared to other techniques [11,12].

Patterning of graphene in a HIM involves firstly locating a suitable area on a graphene flake by imaging at a low magnification. The magnification is then increased and control is switched to a pattern generator to scan the beam in the required pattern. It is known that low energy ionic bombardment can cause damage to the graphene lattice [13] so it is important to establish whether HIM imaging to locate a suitable area for patterning can be carried out whilst avoiding damage to the graphene to the extent that the electronic properties are degraded.

Here we present Raman spectroscopy results of a graphene flake before and after exposure to the helium ion beam in a HIM at various ion doses. Damage to the graphene lattice manifests in a Raman peak at around 1350 cm^{-1} and the ratio of this D peak to the G peak, present in pristine and damaged graphene at around 1605 cm^{-1} provides a measure of the extent to which the lattice is damaged. An area of a pristine graphene flake is imaged in the HIM at a field of view (FOV) of 50 μm for 1 min giving a total dose of 1.59×10^{13} ions/cm^2. The FOV is reduced (magnification increased) and the exposure is repeated, resulting in overlaid areas exposed to increasing He ion doses (Figure 1 (a)). We then define a grid of pixels overlaying the exposed flake (b), and collect Raman spectra from each pixel, allowing the mapping of the D and G peak intensities (c). The average D to G ratios can then be plotted as a function He ion dose (d).

We will use this data to quantify the disorder induced in graphene through He ion bombardment which will enable an assessment of the extent to which imaging in the HIM can damage graphene and lead to guidelines on maximum ion doses to avoid substantial damage to graphene devices.

References

[1] K. S. Novoselov, A. K. Geim, S. V. Morozov, D. Jiang, Y. Zhang, S. V. Dubonos, I. V. Grigorieva and A. A. Firsov, Science 306 (2004) 666-669.
[2] A. K. Geim and K. S. Novoselov, Nature Materials, 6, 183-191.
[3] K. I. Bolotin, K. J. Sikes, Z. Jiang, M. Klima, G. Fudenberg, J. Hone, P. Kim and H. L. Stormer, Sol. Stat. Commun. **146** (2008) 351-355.
[4] M. Dragoman and D. Dragoman, Progress in Quantum Electronics **33** (2009) 165-214.
[5] Z. Chen, Y. Lin, M. Rooks and P. Avouris, Physica E **40** (2007) 228-232.
[6] C. Stampfer, J. Güttinger, F. Molitor, D. Graf, T. Ihn and K. Ensslin, Appl. Phys. Lett. **92** (2008) 012102.
[7] D.C. Bell, M. C. Lemme, L. A. Stern, J. R. Williams and C. M. Marcus, Nanotechnology **20** (2009) 455301.
[8] D. Pickard and L. Scipioni, "Graphene Nano-Ribbon Patterning in the Orion Plus", Zeiss application note, Oct 2009.
[9] B. W. Ward, J. A. Notte and N. P. Economou, J. Vac. Sci. Technol. B. 24(6) (2006) 2871-2874.
[10] L. Scipioni, Adv. Mater. Proc. 166 (2008) 27-30.
[11] M. C. Lemme, D. C. Bell, J. R. Williams, L. A. Stern, B. W. H. Baugher, P. Jarillo-Herrero and C. M. Marcus, ACS Nano, 3, **9** (2009) 2674-2676.
[12] S. A Boden, Z. Moktadir, D. M. Bagnall, H. Mizuta and H. N. Rutt, Microelectronic Engineering (2011), in press.
[13] M. M. Lucchese, F. Stavale, E. H. Martins Ferreira, C. Vilani, M. V. O. Moutinho, R. B. Capaz, C. A. Achete and A. Jorio, Carbon 48 (2010) 1592-1597.
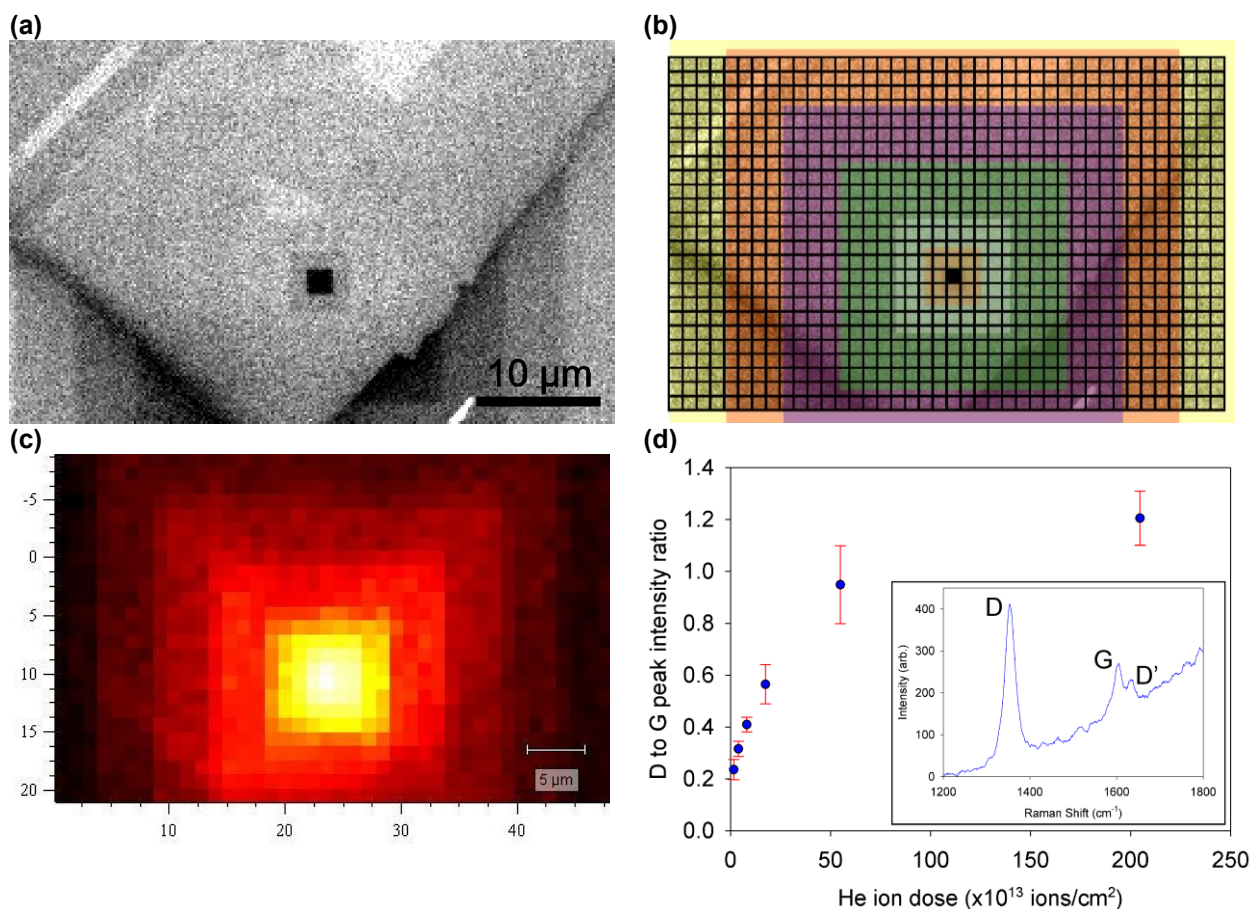
Figure . 1 (a) HIM image of exposed graphene monolayer, (b) overlay of Raman mapping grid and exposure areas, (c) Raman mapping of a region of graphene monolayer showing how the intensity of the D peak at 1353 cm-1 varies after exposure to the helium beam, (d) D to G peak intensity versus dose for exposure of graphene monolayer to 30 kV He ion beam, inset shows Raman spectrum for area exposed at a FOV of 5 μm.

Graphene oxides from graphites of different crystalinity

Cristina Botas, Patricia Alvarez, Clara Blanco, Ricardo Santamaría and Marcos Granda, Rosa Menéndez

Instituto Nacional del Carbón, CSIC, Francisco Pintado Fe, 26, 33011 Oviedo, Spain
rosmenen@incar.csic.es

In the last few years much attention has been devoted to the synthesis of graphenes by different methods (1, 2), and especially to the study oh the electrical behavior of graphene with a view to its potential applications. Graphenes, graphene oxides (GO) and chemically modified graphenes (CMG) or partially reduced graphene oxides (GO-r) are promising materials that offer a wide range of users.

The preparation of graphene by chemical methods offers the possibility of producing high volumes of this product and also of obtaining graphene of different characteristics, depending on the parent graphite and the method used for the oxidation, and the final reduction of graphene oxide to graphene. Moreover, the defects originated during oxidation and/or chemical reduction processes yield a material with a structure in need of further chemical modification.

Despite the huge number of papers published about graphene, there is little information concerning the effect of the graphite precursor used (3). It is generally accepted that there is a need for more experimental work on the properties of isolated carbon crystallites, because polymeric carbons contain a blend of graphite crystalline structures of various sizes, amorphous phases, and high defect populations and, hence, the properties measured represent the global properties of all the constituents taken together.

The objective of this paper is to study the effect of the crystallinity of parent graphite on the reactivity of the material under the oxidation conditions required for graphene oxides preparation by using graphites of a rather different homogeneous crystality (G1- flow domains-, GC – mosaic - and G2 – fine mosaics-) with an increased amount of defects (Figure 1). Microscopy in its different forms (OM, SEM, TEM, AFM) and spectroscopy (Raman, XPS) are the main tools used for the characterization of the graphene oxides and partially reduced graphene oxides.

Graphene oxides were prepared from synthetic graphites by Hummer's method (4), with some modifications. Ultrasonication in water was used to separate the individual graphene oxide sheets. The three oxides are highly hydrophilic, showing good dispersion in water where they remain for along the time of the experiment (Figure 2). According to the XPS results, oxygen is mainly in the form of epoxi groups in the three oxides, with a slightly lower amount in the case of GO-C, which has a larger quantity of hydroxyls and carboxylic functionalities. This is the first indication of the different chemical reactivity of graphites in oxidation conditions. The reduction of the three oxides was performed with hydrazine, as the main feature of the end being that the partially reduced graphene oxide obtained from GO-1 was highly hydrophobic with a greater tendency to associate while those from GO-2 and GO-C showed a good dispersion in water. Under the same conditions the reduction was more effective in GO-1, yielding a partially reduced oxide (GO-1-r) with a C/O ratio of 11 while in the other two the ratio was about 5. Hydroxyl groups were dominant, ranging from 22 % in GO-1-r to 28-29 % in GO-2-r and GO-C-r. Raman spectroscopy results point to the same findings, GO-1 showing a lower ID/IG band with a value of 0.89, whereas GO-2 and GO-C show values of ID/IG, 0.91 and 0.92, respectively. This indicates a larger presence of defects in GO-2, which was obtained from the graphite of lower crystallinity.

SEM was not the best technique for observing the samples but it was of extraordinary help in determining the effectiveness of the cleaning step for removing products from the oxidation reaction and unreacted samples, as these were used in excess. For the same reason and maybe because of the

more extended functionalization, GO-2 was the most difficult to clean, requiring additional washing and ultracentrifugation steps.

In general terms, images obtained by TEM show a wrinkled paper-like structure (Figure 2b) of monolayers and no appreciable differences between the different oxides and partially reduced ones were observed.

AFM characterization confirms the greates presence of monolayers or single sheets in the three oxides. Sheets size distribution was determined, as a certain tendency to lateral association was observed in GO-2r. These results demonstrate that control of the characteristics of the parent graphite made it possible to control the characteristics of the GOs and therefore, of the GO-rs.

References

[1] Sungjin Park and Rodney S. Ruoff, Nature Nanotechnology, **4** (2009) 217-224.
[2] Yanwu Zhu, Shanthi Murali, Weiwei Cai, Xuesong Li, Ji Won Suk, Jeffrey R. Potts, Rodney S. Ruoff, Advanced Materials, 22 (2010) 3906-3924.
[3] Zhong-Shuai Wu, Wencai Ren, Libo Gao, Bilu Liu, Chuanbin Jiang, Hui-Ming Cheng, Carbon, **47** (2009) 493-499.
[4] W. Hummers, R. Offermen, Journal American Chemistry Society, **80** (1958) 1339.
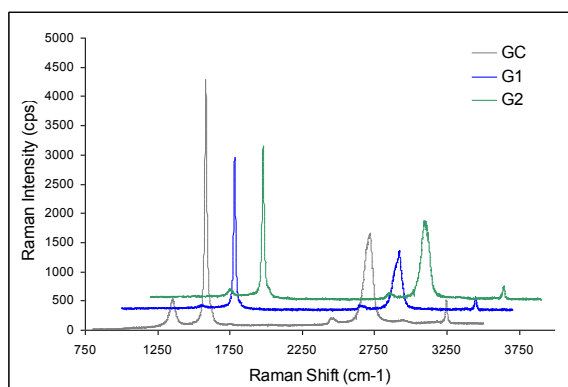
Figures

Figure 1: Raman spectra of graphite G1, GC and G2.
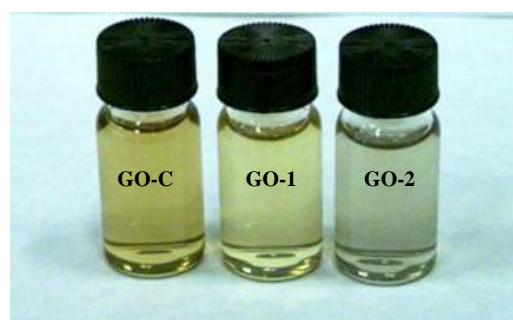
Figure 2: Image of stable dispersions of graphene oxides.
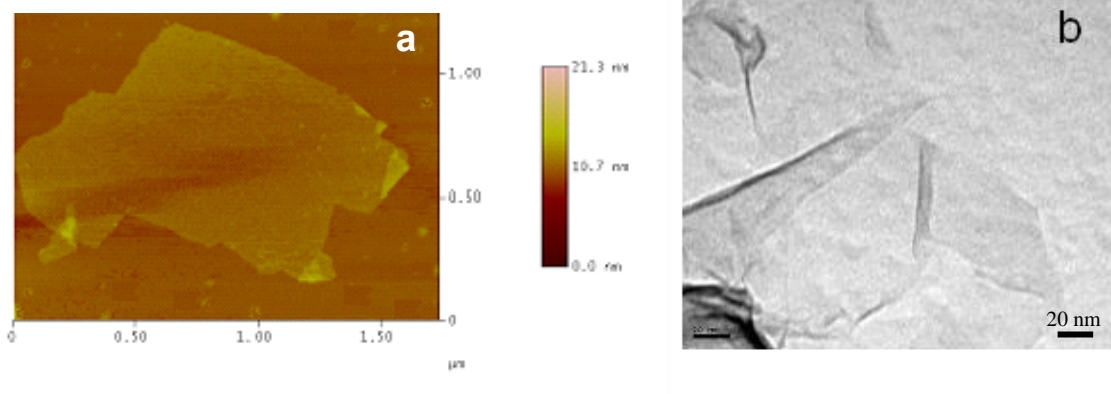
Figure 3. AFM of a single sheet of graphene oxide GO-C (a) and TEM of the same partially reduced oxide (b).

One-dimensional extended lines of defects from di-vacancies in graphene

Andrés R. Botello-Méndez[1], Xavier Declerck[1], Mauricio Terrones[2], Humberto Terrones[1], Jean-Christophe Charlier[1]

[1]Institute of Condensed Matter and Nanosciences, Université Catholique de Louvain, Place Croix du Sud, 1, Louvain-la-Neuve, Belgium
[2]Research Center for Exotic Nanocarbons (JST), Shinshu University, Nagano, Japan
andres.botello@uclouvain.be

Graphene is interesting both as an exceptional system for the study of new quantum phenomena, and as novel material for exciting applications. In particular, the outstanding electronic properties of graphene make it a promising material for the future of nanoelectronics. However, graphene cannot be integrated as a building block for pure carbon-based transistor devices due to the lack of a good I_{ON}/I_{OFF} ratio associated to the absence of a gap. Since the outstanding transport properties of graphene originate from its specific structure, modification at the atomic level of the graphene lattice is needed in order to impact its electronic properties. Thus, topological defects, defined as the introduction of non-hexagonal rings in the carbon lattice preserving the connectivity of the network, play a very important role on graphene and related nanostructures. Indeed, recent experimental observations show that arrays of topological defects exist at the boundary between two domains of graphene grown with different orientations [1]. Such arrays of defects have been studied and are found to have interesting electronic properties [2,3]. However, formation of such lines of defects is difficult to control because it depends on the kinetics at the growth of graphene.

In this work we explore various architectures of extended lines of defects that could arise from the reconstruction of di-vacancies in graphene (Fig.1). Different approaches have been successful for the controlled introduction of single vacancies in graphene under a transmission electron microscope or via scanning tunneling lithography. Furthermore, single vacancies are very mobile, and tend to form di-vacancies, which are more stable and tend to be reconstructed with topological defects. Using a first-principles approach, we study the electronic and quantum transport properties of extended lines of defects that could arise from the reconstruction of di-vacancies. In addition, we present simulated STM images in order to help the identification of these systems experimentally. In particular, we find that some of these systems exhibit conduction channels and localized states which could enhance the chemical reactivity of graphene [4]. Therefore, these extended lines of defects open the possibility of arranging molecules or atoms in a linear fashion, thus behaving as a 1D template.

References

[1] J. Lahiri, Y. Lin, P. Bozkurt, I. I. Oleynki, and M. Batzill. Nat. Nano, **5** (2010), 326.
[2] O. V. Yazyev and S. G. Louie, Nat. Mater., **9** (2010), 806.
[3] O. V. Yazyev and S. G. Louie, Phys. Rev. B, **81** (2010), 195420.
[4] A. R. Botello-Méndez, X. Declerck, M. Terrones, H. Terrones. Nanoscale *(in press)*

Figures
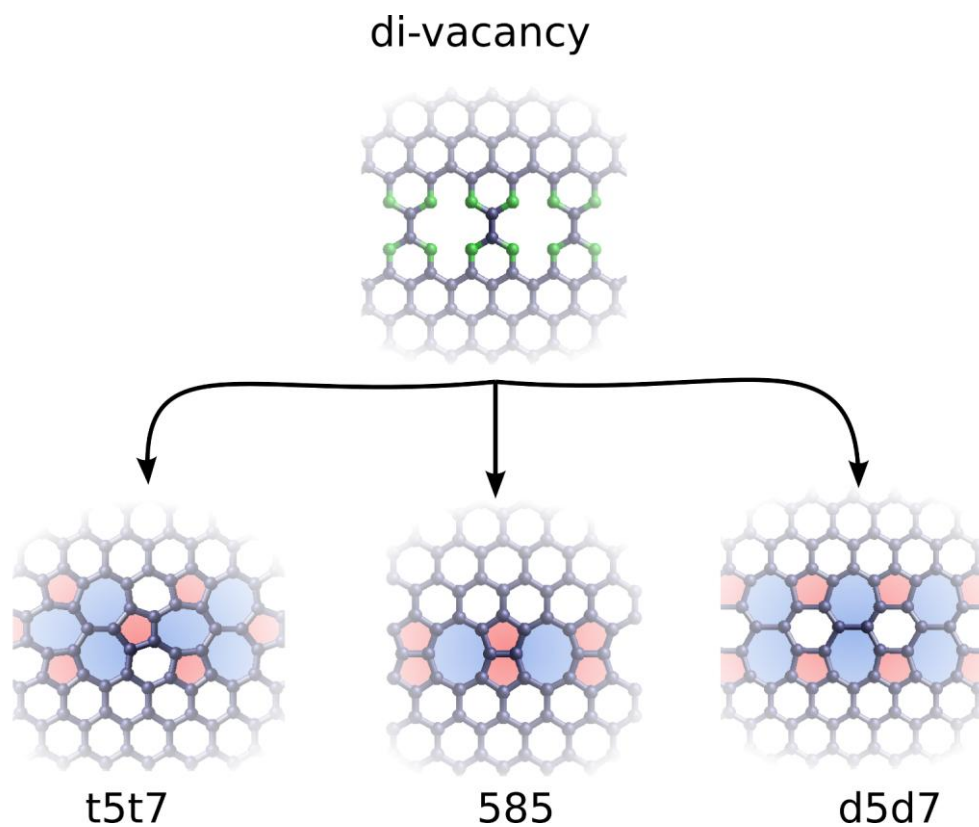
Figure 1. Molecular model of the formation of extended lines of defects in graphene from the reconstruction of divacancies

Electron transport and spin in graphene

Jan Bundesmann[1], Michael Wimmer[2], Klaus Richter[1]

[1]Institut für theoretische Physik, Universität Regensburg, Germany
[2]Instituut Lorentz, TU Leiden, The Netherlands
jan.bundesmann@physik.uni-regensburg

The weak atomic spin-orbit interaction (SOI) in graphene leads to the assumption of large spin relaxation times. Simulations, taking into account spin-scattering from charged impurities in the substrate, yielded spin relaxation times [1] much larger than spin injection experiments in graphene [2,3].

Still assuming that the model of spins scattered at charged impurities is correct, we implemented a tight-binding model for graphene in the presence of SOI.

In our work the focus lies on the effects of SOI on electron transport (i.e. low energy excitations and the role of symmetry classes manifested, e.g., in weak localization) as well as its influence on spin transport in the diffusive regime.

References

[1] Ertler, Konschuh, Gmitra and Fabian, Phys. Rev. B **80**, 041405(R) (2009)

[2] Tombros, Josza, Popinciuc, Jonkman and van Wees, Nature **448**, 571 (2007)

[3] Han, Pi, McCreary, Li, Wong, Swartz and Kawakami, Phys. Rev. Lett. **105**, 167202 (2010)

Ultra Broadband Terahertz Spectroscopy of few-layer graphene films

J. C. D. Buron*†, D.G. Cooke‡*, T. Booth†, P. Bøggild†, P. U. Jepsen*

*DTU Fotonik – Department of Photonics Engineering, Technical University of Denmark, Ørsteds Plads, Bldg. 343
†DTU Nanotech – Department of Micro- and Nanotechnology, Technical University of Denmark, Ørsteds Plads, Bldg. 344
‡Department of Physics, McGill University, Montreal, Quebec, Canada, H3A2T8

jcdb@fotonik.dtu.dk

In addition to being a true 2D material composed of a single sheet of carbon atoms in a hexagonal crystal structure, graphene shows numerous exotic features. Ranging from extraordinary mechanical properties and thermal transport to an unusual optical response and charge carriers behaving like massless Dirac fermions giving rise to ballistic transport over hundreds of nanometers and half-integer quantum hall effect[1] and Klein-tunneling[2] at room temperature, the special properties of graphene continue to draw vast amounts of interest.

Because of graphene's extremely high carrier mobility and the promise of devices with the thinnest possible conducting channels one of the most promising applications is in high speed radiofrequency electronics[3] forecasted to operate in the terahertz(THz) frequency region[4]. Graphene is also anticipated to facilitate THz sources and detectors due to its small and widely tunable bandgap[5]. In particular several proposals of solid state THz lasers based on graphene as the active medium have been made[6,7,8], as well as proposals of graphene photodetectors[9,10] for the THz region. Despite many applications and the obvious relevance of the electrodynamic and optical response in the THz region only a few experimental THz spectroscopy studies[11,12,13] exist, most of them limited to bandwidths from about 0.1 to 3 THz.

In initial experiments we investigate the terahertz response of graphene using time domain spectroscopy. Ultra broadband THz pulses are generated and detected in a laser induced plasma in air (time and frequency representation of the pulses are shown in figures (a) and (b)).

CVD grown graphene films (microscope image shown in figure (c)) and graphene films produced by the Langmuir-Blodgett method from reduced graphene oxide flakes(microscope image shown in figure (d)) are investigated and compared. We report on the recent results of these ultra broadband THz experiments exploring the linear and nonlinear response of single- and few- layer graphene using the air-plasma source.

References

[1] Novoselov K.S. et al, Science, **315** (2007) 1379.
[2] Young, A.F. & Kim, P, Nature Physics, **5** (2009) 222-226.
[3] Schwierz, F., Nature Nanotechnology, **5** (2010) 487-496.
[4] Geim A.K., Science, **324** (2009) 150-1534.
[5] Zhang, Y. et al., Nature, **459** (2009) 820-823.
[6] Dubinov, A.A., Aleshkin, V.Y., Ryzhii, M., Otsuji, T. & Ryzhii, V., Appl. Phys. Express, **2** (2009) 092301.
[7] Aleshkin, V.Y., Dubinov, A.A. & Ryzhii, V., Jetp. Lett., **89** (2009) 63-67.
[8] Ryzhii, V., Dubinov, A.A., Otsuji, T., Mitin, V. & Shur, M.S., J. Appl. Phys., **107** (2010) 054505.
[9] Ryzhii, V., Ryzhii, M., Mitin, V. & Otsuji, T., J. Appl. Phys., **107** (2010) 054512.
[10] Ryzhii, V. & Ryzhii, M., Phys. Rev. B, **79** (2009)
[11] Dawlaty, J.M. et al., Appl. Phys. Lett., **93** (2008) 131905.
[12] Dawlaty, J.M. et al., Appl. Phys. Lett., **92** (2008) 042116.
[13] George, P.A. et al., Nano Lett., **8** (2008) 4248-4251.

Figures

(a)

(b)

(c)

(d)
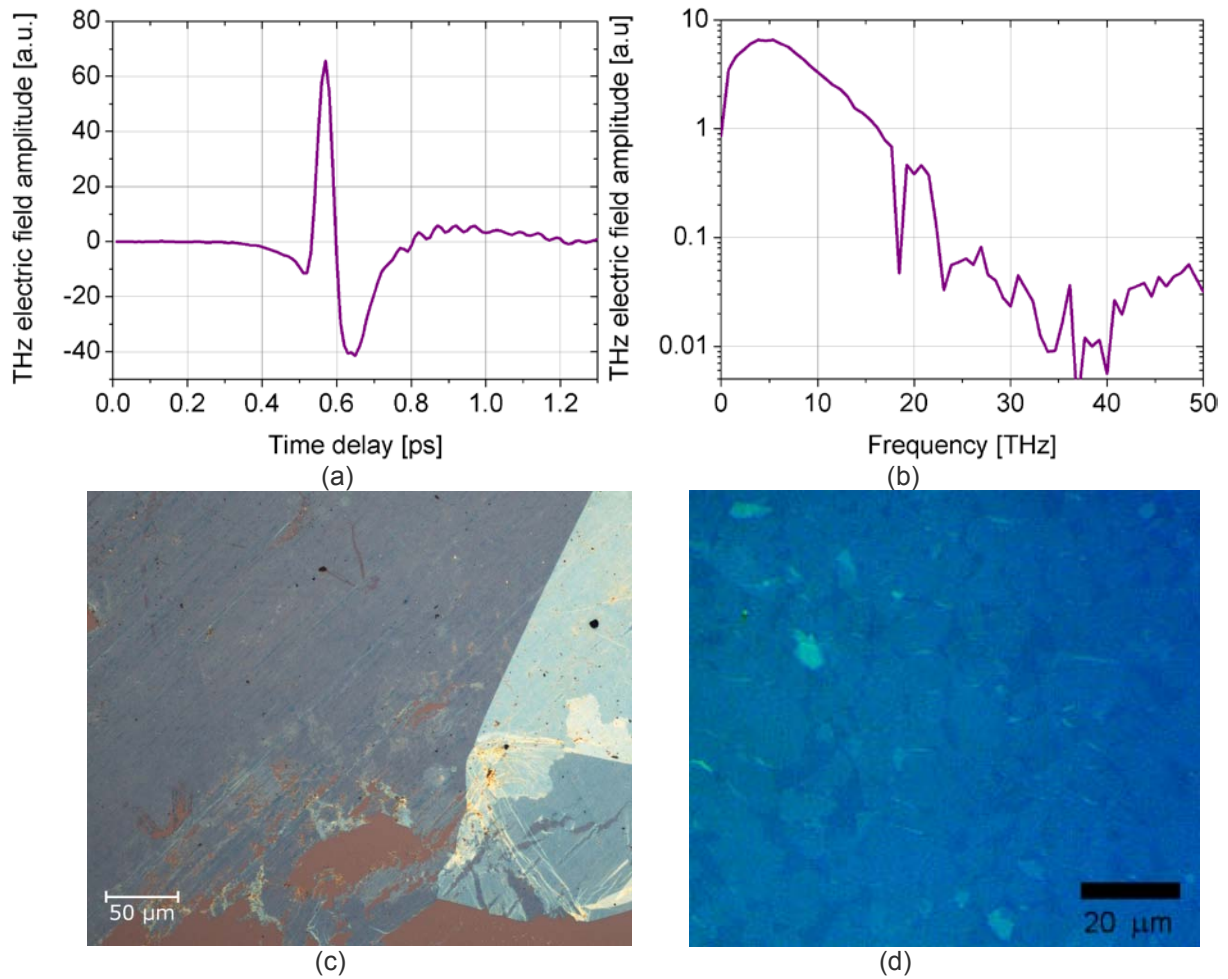
Figure (a) shows the time representation of an ultra broadband THz pulse generated and detected in laser induced plasma in air.

Figure (b) shows the frequency representation of an ultra broadband THz pulse generated and detected in laser induced plasma in air.The shown pulse has a bandwidth of ~30 THz and a peak dynamic ratio of ~100

Figure (c) shows an optical microscope image of few layer CVD graphene transferred to a 90 nm SiO2 on Si substrate. The graphene film was originally grown on copper foil.

Figure (d) shows an optical microscope image of a continuous film made up of graphene flakes, produced by the Langmuir-Blodgett technique.

Fabrication of ultrasensitive graphene nano-biosensors

Gregory Burwell, Guy O.J., Tehrani Z. Castaing A., Doak S.
School of Engineering, Swansea University, Swansea, UK
436734@swansea.ac.uk

Summary

The development of miniaturised systems for detection of disease biomarkers, at clinically relevant concentrations in biological samples, is key in the early diagnosis and monitoring of diseases. This poster presents the development of novel antibody functionalized epitaxial graphene devices for bio-sensing applications. Epitaxial graphene has been grown on silicon carbide (SiC) substrates under high vacuum and high temperature conditions (1200 – 1700°C). A generic electrochemical surface functionalisation chemistry, which can be used to attach a variety of "bio-receptors" to graphitic surfaces, has been developed. The attached bio-receptors are capable of specific and selective interaction with disease biomarkers. When a target biomarker molecule interacts with the "bio-receptor" functionalised surface, the charge density at that surface is affected. This change can be detected as an electrical signal from the biosensor, enabling highly sensitive detection of biomarker analytes.

Motivation

"Bio-chip" sensors, developed using semiconductor devices will enable detection of biomarkers at ultra-low concentrations for early diagnosis and monitoring of diseases. This poster presents novel epitaxial graphene-based devices for bio-sensing applications. Silicon Carbide (SiC) has recently been discovered to be a suitable substrate for graphene growth [1, 13, 2]. During annealing at temperatures of between 1100°C and 1700°C the SiC surface reconstructs itself, with silicon atoms subliming and leaving behind a layer, or multiple layers, of epitaxial graphene [3]. Epitaxial graphene's superb electronic properties (high carrier mobilities), and reported biocompatibility [4], and substrate-inferred processability make it ideal for fabrication of nano-scale electronics and sensors. The biosensors work on the principle of a target disease biomarker, binding with a "bio-receptor" attached to the graphene surface, yielding a change in the surface charge density. This change can be detected as an electrical signal from the biosensor device. The device itself consists of a conductive graphene channel – functionalised with the "bioreceptor". Graphene nano-channel sensors have the potential for much greater sensitivity to biomarkers than traditional bioassays because of their high signal-to-noise ratios (S:N).

Results

This poster presents the growth of multi-layer epitaxial graphene (MEG) on silicon carbide substrates (Fig. 1) and the electrochemical functionalisation of MEG layers with monoclonal antibody bio-receptors. A novel electrochemical method for attachment of antibodies to epitaxial graphene/SiC surfaces using chemical functionalisation of graphene with nitro groups and subsequent reduction to an amine has been monitored using X-ray Photoelectron Spectroscopy (XPS) (Fig. 2). The amino (NH_2) group has been used to bind a fluorescently labeled antibody, in the first known bio-functionalisation of epitaxial graphene on SiC. Strong fluorescence from the quantum dot labeled antibody, bound to the graphene substrate, was detected, indicating good surface attachment (Fig. 3). A control sample , not functionalised with an amine group, showed no fluorescence and thus no binding. Following epitaxial graphene growth, micro and nanochannel graphene devices have been fabricated (Fig 4 and Fig. 5). The results from a specific sensor, fabricated by functionalising a graphene nanochannel surface with an antibody bioreceptor, indicative of oxidative stress and prostate cancer risk, will be presented.

References

[1] O.J. Guy et al. J. Appl. Surf. Sci. 'Investigation of the 4H-SiC surface', Appl. Surf. Sci. 254, p.8098-8105, 2008.

[2] C. Berger et al., Science 312, p.1191, 2006.

[3] A. Castaing, O.J. Guy, M. Lodzinski, S.P. Wilks, "Investigation of Graphene Growth on 4H-SiC", Mater. Sci. Forum 615-617, 223-226, 2009.
[4] X. Sun, Z. Liu, K. Welsher, J.T. Robinson, A. Goodwin, S. Zaric, H. Dai, Nano Res. 1: 203, p.212, 2008.

Figures
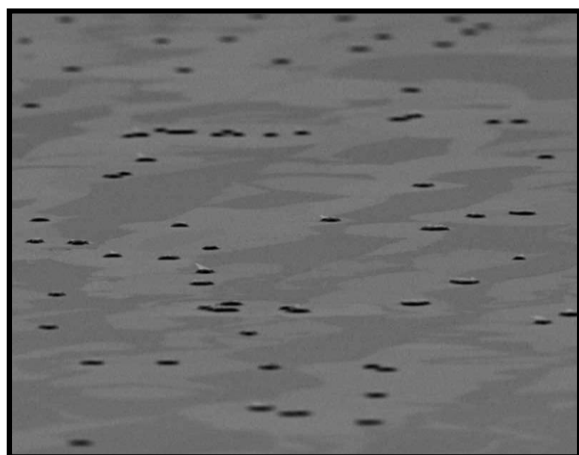
Fig. 1: SEM image of epitaxial graphene grown on a silicon carbide substrate.

Non-functionalised epitaxial Graphene.

Epitaxial Graphene selectively functionalized with a Quantum-dot labeled antibody.
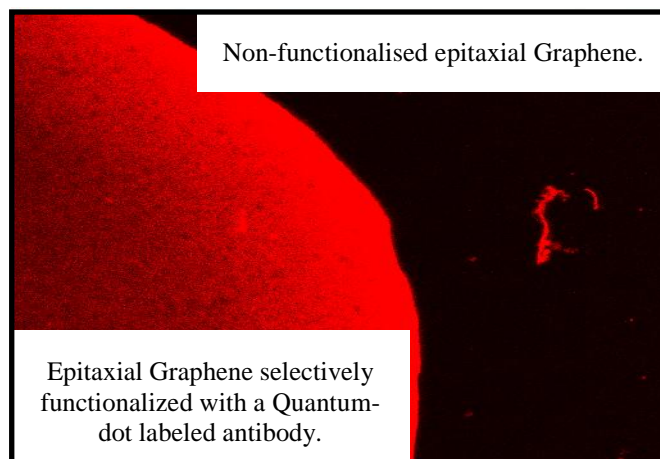
Fig. 2: Laser scanning confocal micrograph of epitaxial Graphene selectively functionalized with a Quantum-dot labeled antibody.
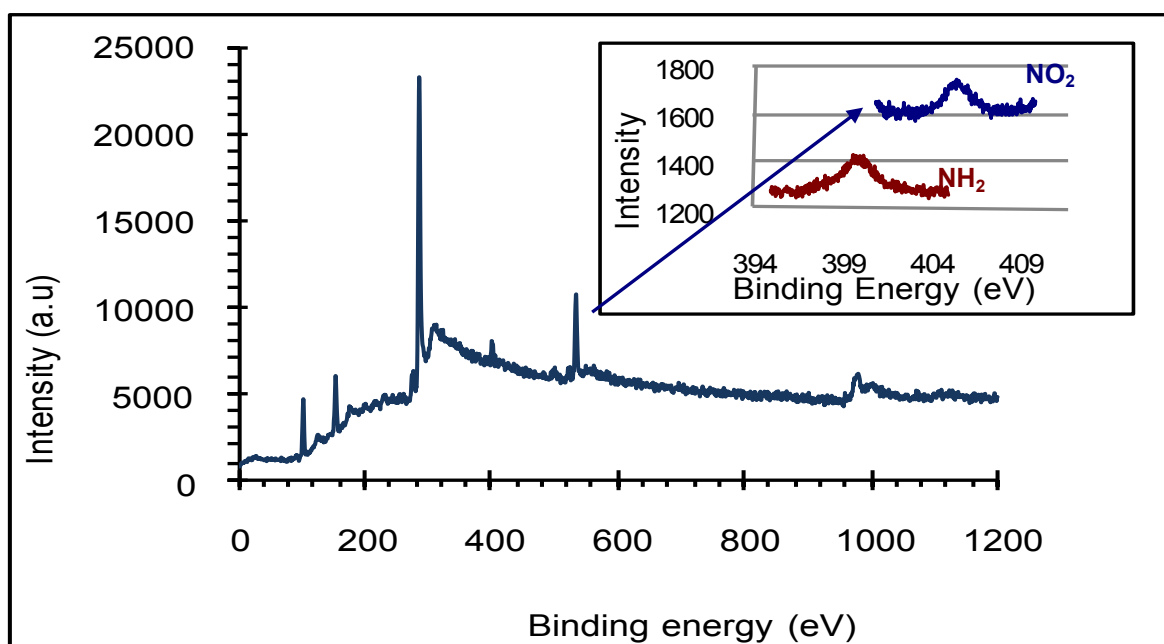
Fig. 3: XPS spectrum of nitrobenzene functionalized graphene surface. Inset: N 1s peak, conversion of nitro to amino group upon subsequent electrochemical reduction to aniline.
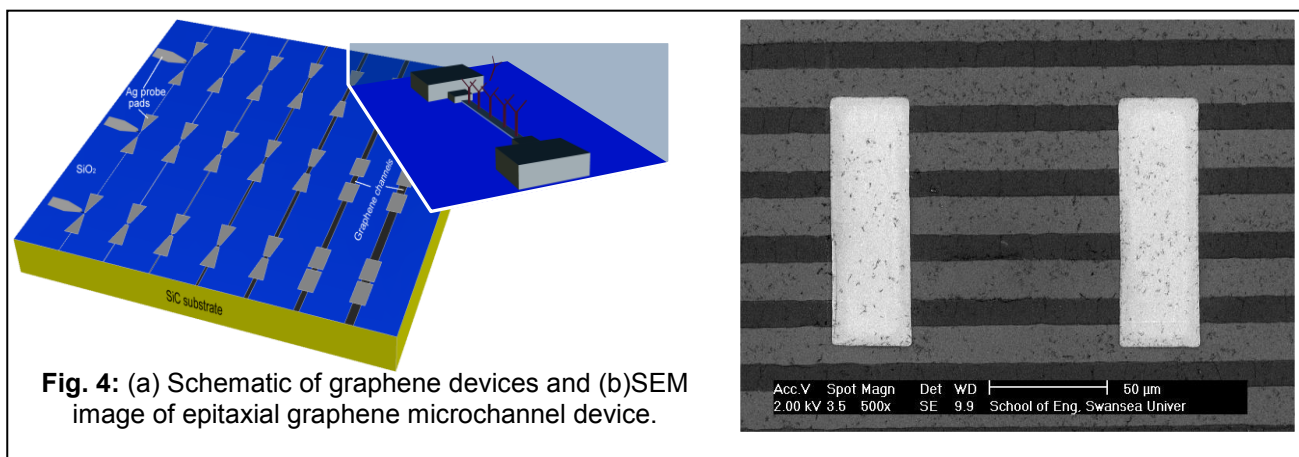
Fig. 4: (a) Schematic of graphene devices and (b)SEM image of epitaxial graphene microchannel device.

Simulations of the Reduction of Graphene Oxide Suspensions by Hydrazine

I. Cabria[1], M. J. López[1], N. A. Cordero[2], J.A. Alonso[1] and J. I. Paredes[3]

[1]Departamento de Física Teórica, Universidad de Valladolid, 47005 Valladolid, Spain
[2]Departamento de Física, Universidad de Burgos, 09001 Burgos, Spain
[3]Instituto Nacional del Carbón, CSIC, 33080 Oviedo, Spain
cabria@fta.uva.es

Simulations of the interaction of hydrazine with graphene oxide have been carried out to understand recent experiments of the reduction of graphene oxide by hydrazine [1]. According to chemical analysis, hydrazine-reduced graphene oxide still contains a certain amount of oxygen functionalities that cannot be removed. Even in the most reduced materials the O/C atomic ratio, 0.08, indicates the presence of a significant amount of residual oxygen. Previous reports on graphene oxide reduction by hydrazine also support the idea that chemical reduction has an intrinsic limit, which is not well understood. A possible explanation of the residual oxygen is the presence of oxygen functionalities in graphene oxide, before the reduction processes, that can not be removed by hydrazine.

We have done DFT calculations of the interaction of hydrazine with several isolated oxygen functionalities on a graphene layer, namely epoxy and hydroxyl groups and a carbonyl pair inside a graphene layer. The results of the calculations indicate that hydrazine could reduce the epoxy groups to hydroxyls and the hydroxyl groups can be reduced to water, which is eliminated from the graphene. In contrast, hydrazine is not able to reduce the carbonyls to form C-O-H groups. We have also done DFT calculations of the interaction of hydrazine with epoxy and hydroxyl groups on a coronene. The results on the coronene differ from those on graphene. This indicates that a finite portion of graphene, the coronene, is not a good model to represent the whole graphene oxide layer, and therefore results on coronenes have to be taken with caution. In summary, our results indicate that a pair of neighbour carbonyls could explain the residual oxygen found experimentally in reduced graphene oxide.

References

[1] M. J. Fernández-Merino, L. Guardia, J. I. Paredes, S. Villar-Rodil, P. Solís-Fernández, A. Martínez-Alonso, and J. M. D. Tascón, J. Phys. Chem. C 114, (2010) 6426–6432

Figures
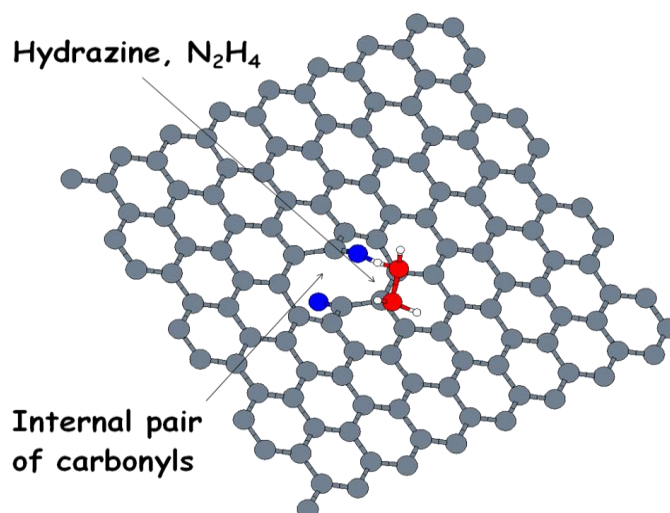
Hydrazine interacting with an internal pair of carbonyls on graphene

Bottom-up fabrication of porous graphene and graphene nanoribbons

Jinming Cai,[a] Pascal Ruffieux,[a] Marco Bieri,[a] Stephan Blankenburg,[a] Carlo Pignedoli,[a] Xinliang Feng,[b] Klaus Müllen,[b] and **Roman Fasel** [a]

[a] *Empa, Swiss Federal Laboratories for Materials Science and Technology, Überlandstrasse 129, 8600 Dübendorf, Switzerland*
[b] *Max Planck Institute for Polymer Research, Ackermannweg 10, 55124 Mainz, Germany*

roman.fasel@empa.ch

Its remarkable properties make graphene attractive for use in nanoscale devices[1]. However, graphene is semimetallic and thus not directly suitable for most electronic or optoelectronic devices, which require a semiconductor with a specific, finite bandgap. This can be overcome by structuring graphene on the nanometer scale, which opens a bandgap suitable for room-temperature applications[2]. Experimentally, nanostructured graphene and graphene-related materials are accessible via lithographic techniques or chemical treatment, but both methods are limited with respect to their ultimate resolution and precision. In this presentation, I will review our recent attempts to overcome these limitations by a bottom-up strategy allowing for the atomically precise fabrication of graphene-related materials[3-7].
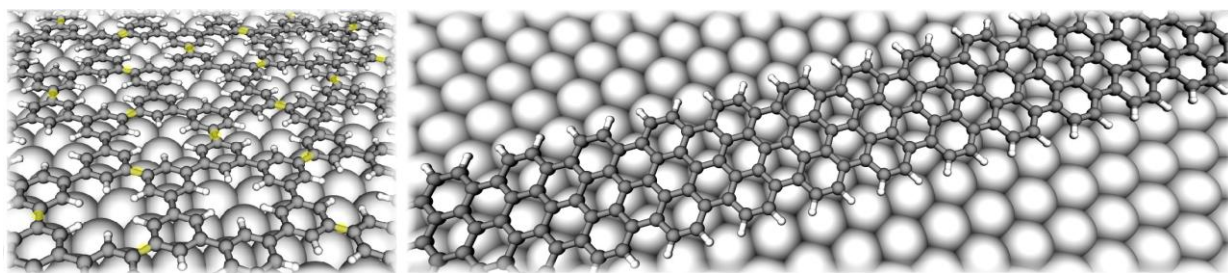
Our surface-chemical method involves the deposition of suitably designed halogen-functionalized molecular precursors onto single crystal metal surfaces under ultrahigh vacuum conditions, and relies on three basic steps: *(i)* surface-catalyzed dehalogenation during adsorption of the precursor monomers, *(ii)* polymer formation by covalent interlinking of the dehalogenated intermediates, and *(iii)* establishment of fully aromatic □-systems by thermally induced cyclodehydrogenation. Using experimental methods such as scanning tunneling microscopy, Raman and photoelectron spectroscopies, which are complemented by density functional theory calculations, we have studied these elementary steps and the resulting graphene-related materials. It will be shown that under suitable conditions the surface-chemical route allows for the fabrication of surface-supported porous graphene or graphene nanoribbons with atomic accuracy. Finally, critical issues such as the balance between mobility and reactivity of the dehalogenated intermediates and the extension of the approach to technologically relevant substrates will be addressed.

References

[1] A. K. Geim, *Science*, **324** (2009) 1530.
[2] V. Barone, O. Hod, G. E. Scuseria, *Nano Lett.*, **6** (2006) 2748.
[3] M. Bieri et al., *Chem. Commun.*, (2009) 6919.
[4] M. Bieri et al., *J. Am. Chem. Soc.*, **132** (2010) 16669.
[5] J. Cai et al., *Nature*, (2010), **466**, 470.
[6] S. Blankenburg et al., *Small*, **6** (2010) 2266.
[7] M. Treier et al., *Nature Chemistry*, **3** (2011) 61.
[8] S. Blankenburg et al., in preparation.

Synthesis of Single-layer Graphene-nanocomposite directly from graphene oxide

Aoneng Cao[1], Zhen Liu[1], Lin Chen[1], Chengwei Fan[1], Sheng Chen[1], Haifang Wang[1], Yuanfang Liu[1,2]

[1]Nanochemistry and Nanobiology, Shanghai University, Shanghai, 200444, China
[2]Beijing National laboratory of Molecular Science, College of Chemistry and Molecular Engineering, Peking University, Beijing, 100871, China
ancao@shu.edu.cn

Assembly of semiconductor nanoparticles, such as quantum dots (QDs), on matrices has been extensively studied for their promising optoelectronic applications [1-7]. To enhance the photocurrent generated by these semiconductor-matrices systems, it is essential to retard the recombination of electron-hole species in the semiconductors by molecular electron-relay semiconductor structures or efficient electron-transport matrices, such as the conductive polymer films or carbon nanotubes (CNT) [3-7]. The superior electrical conductivity and flexible atom-thin two-dimensional feature of graphene would make it an excellent electron-transport matrix. Herein, we report the synthesis of graphene-quantum dots (G-QD) nanocomposite directly from graphene oxide by a facile one-step reaction. Comparing with CNT, the large 2D flexible atom-thin layer of graphene makes it easier to control the distribution of CdS on graphene sheet and to fabricate future optoelectronic devices.

Currently, the yield of single-layer graphene sheets from various mass production methods is quite low, and the major product is usually multiple-layer graphene sheets. An even more serious problem is that single-layer sheets of graphene are not stable in solution and tend to aggregate back to graphite gradually. We developed a one-step method to synthesize G-QD directly from graphene oxide (GO) in dimethyl sulfoxide (DMSO), as illustrated in Figure 1. This approach overcomes the above two problems by synthesizing G-CdS directly from GO in a facile one-pot reaction, where the reduction of GO and the deposition of CdS on graphene occur simultaneously, as evidenced by XPS, FTIR, and Raman measurements.[8] The reduction of GO mainly due to thermal reduction at high reaction temperature (180°C). In addition to the advantage of simplicity and low cost, the high stability of the single-layer GO in solution guarantees the formation of single-layer graphene sheets in the final nanocomposite, hence they possess better structural and optoelectronic properties. Once the reaction was complete, CdS-decoration helps to prevent not only the aggregation of the single-layer graphene sheets, but also the aggregation of CdS QDs. In fact, our G-CdS composite can be stored in the solid state, and the solid product can be re-suspended in different solvents by sonication. The stability of the G-CdS composite against sonication demonstrates the strong binding between the CdS QDs and the graphene sheets. It is also worth mentioning that the CdS QDs are directly decorated on the graphene sheets, and no molecular linkers are needed to bridge the QDs and the graphene matrices. A picoseconds ultrafast electron transfer process from the excited CdS to the graphene sheet has been detected by time-resolved fluorescence spectroscopy, which demonstrates the potential optoelectronic application of this new type of graphene-based semiconductor hybrid system.[8]

Using similar approach, single-layer G-ZnS nanocomposite material has also been prepared from GO. Since the reaction temperature for GO-ZnS nanocomposite is too low to reduce GO to G, an additional reduction step is necessary. This two-step approach might be more popular for the production of graphene-based nanocomposites with varies reaction conditions. The key to this approach is that the deposition step is prior to the reduction step to guarantee single-layer of graphene sheets in the final products.

References

[1] Authors, Journal, **Issue** (Year) page.
[1] S. Banerjee, S. S. Wong, Nano Lett., **2** (2002) 195.
[2] S. Ravindran, S. Chaudhary, B. Colburn, M. Ozkan, C. S. Ozkan, Nano Lett., **3** (2003) 447.
[3] Q. Huang, L. Gao, Nanotechnology, **15** (2004) 1855.
[4] I. Robel, B. A. Bunker, P. V. Kamat, Adv. Mater., **17** (2005) 2458.
[5] L. Sheeney-Haj-Khia, B. Basnar, I. Willner, Angew. Chem. Int. Ed., **44** (2005) 78.
[6] L. Sheeney-Haj-Ichia, J. Wasserman, I. Willner, Adv. Mater., **14** (2002) 1323.
[7] E. Granot, F. Patolsky, I. Willner, J. Phys. Chem. B, **108** (2004) 5875.
[8] A. Cao, Z Liu, S Chu, M Wu, Z Ye, Z Cai, Y Chang, S Wang, Q Gong and Y Liu, Adv. Mater., **22** (2010) 103

Figures
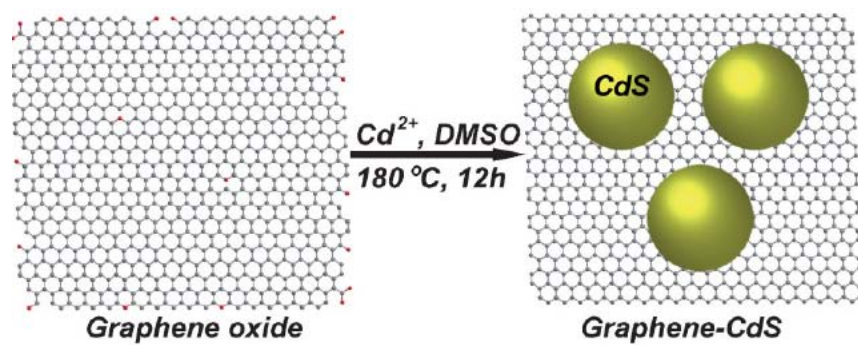
Fig.1 Scheme of the one-step synthesis of G-CdS nanocomposite.
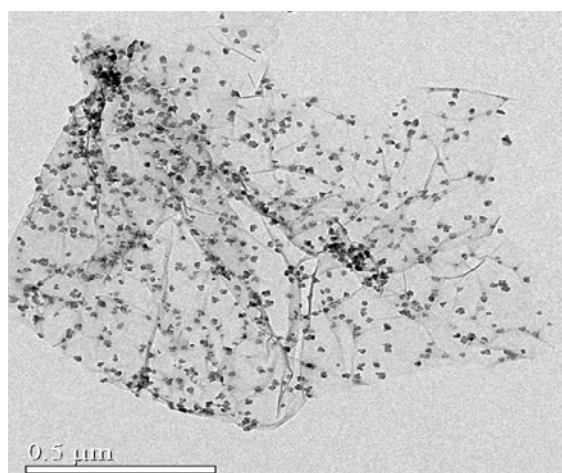
Fig.2 TEM images of Graphene-CdS nanocomposite.
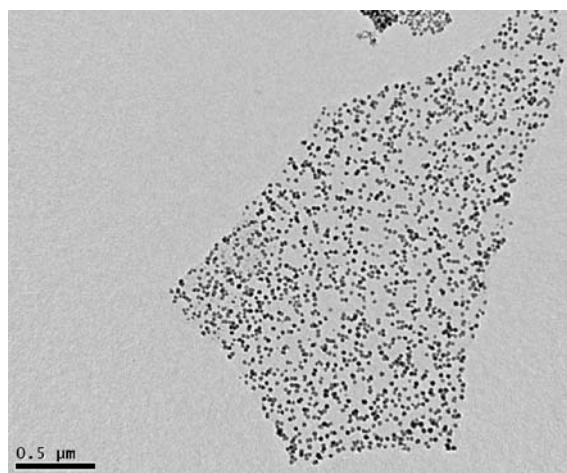
Fig.2 TEM images of Graphene-ZnS nanocomposite.

Graphene mechanical resonators: Direct electrical readout and magnetometry

Changyao Chen, Vikram V. Deshpande, Philip Kim, James Hone

Columbia University, New York, USA
cc2759@columbia.edu

Radio Frequency (RF) nanoelectromechanical systems (NEMSs) are not only widely adapted in practical applications [1], but also powerful tools for exploring fundamental science [2]. Due to its tremendous mechanical strength and outstanding electrical properties, graphene makes a strong candidate for NEMS. Here we demonstrated direct actuation and detection of ultra-clean graphene mechanical resonators, and use them as magnetometer to detect their own magnetization in quantum hall regime.

Recent efforts have realized graphene mechanical resonator with optical interferometry [3] or electrical mixing technique [4], however, neither of these methods is convenient for fast readout and circuit integration. To overcome these drawbacks, we replaced the usual back gate geometry with local gate structure, hence minimizing parasitic capacitance in electrical measurement circuit to enable efficient RF signal transduction [5]. Moreover, by prepared wafers with pre-patterned trenches and electrodes, then deposited graphene by mechanical exfoliation, we approach the clean limit of sample fabrication, allowing us to study the intrinsic properties of graphene.

Figure 1 shows a false-color Scanning Electron Microscopy image of a typical graphene mechanical resonator and measurement scheme. A vector network analyzer (Agilent E5062A) was employed to achieve broadband signal processing, increasing data acquisition speed by two orders of magnitude compared to the mixing method. Figure 2 shows tunable resonant frequencies at different applied local gate voltage, V_g. At low temperatures (below 77K), most of devices showed quality factors, Q, larger than 10,000. This is important for any sensitive detection application, such as magnetometer, as described below.

Additionally, we have developed purely capacitive detection, which enables readout at zero source-drain bias and the absence of transconductance. This is crucial for low temperature experiments such as in quantum hall regime.

With the presence of applied magnetic field $\vec{B}$, there will a $\vec{\mu} \times \vec{B}$ torque exerted on the graphene sample, where $\vec{\mu}$ is the magnetic moment of graphene. This torque changes energy equilibrium hence the resonant frequency f. Performing this experiment in quantum hall regime, we observe saw-tooth-like oscillation of f, which reveals de Haas-van Alphen effect of magnetization. Additionally, frequency spikes showed up on the quantum hall plateaus. This technique provides a bulk measure of quantum hall effect and may be used for probing interacting physics, for instance, in the various symmetry-broken and fractional regime, all of which are accessible in these ultra-clean samples.

References

[1] C. T. C. Nguyen, L. P. B. Katehi, and G. M. Rebeiz, Proc. IEEE **86** (1998), 1756
[2] G. A. Steele, A. K. Hüttel, B. Witkamp, M. Poot, H. B. Meerwaldt, L. P. Kouwenhoven, H. S. J. van der Zant, Science, **325** (2009), 1103.
[3] J. Scott Bunch, Arend M. van der Zande, Scott S. Verbridge, Ian W. Frank, David M. Tanenbaum, Jeevak M. Parpia, Harold G. Craighead, and Paul L. McEuen, Science **315** (2007), 490.
[4] Changyao Chen, Sami Rosenblatt, Kirill I. Bolotin, William Kalb, Philip Kim, Ioannis Kymissis, Horst L. Stormer, Tony F. Heinz, James Hone, Nature Nanotechnology **4** (2009), 861.
[5] Yuehang Xu, Changyao Chen, Vikram V. Deshpande, Frank A. DiRenno, Alexander Gondarenko, David B. Heinz, Shuaimin Liu**,** Philip Kim, and James Hone, Appl. Phys. Lett.*,* **97** (2010) , 243111

Figures

Fig. 1

Fig. 2

Figure caption

Fig. 1. Schematic of measurement circuit. Inset, SEM image of graphene mechanical resonator, scale bar, 1 um.

Fig. 2. Resonant frequency as function of applied gate voltage, V_g.

Electrochemical hydrogen storage of graphene-based materials

Zongping Chen, Wencai Ren*, Zhong-Shuai Wu, Hui-Ming Cheng*

Shenyang National Laboratory for Materials Science, Institute of Metal Research, Chinese Academy of Sciences, Shenyang 110016, P. R. China

Email: wcren@imr.ac.cn, cheng@imr.ac.cn.

Quite recently, graphene, a conceptually new class of two-dimensional atomic crystal material, has attracted increasing interest for its unique structure, various peculiar properties, and a wide range of promising potential applications [1-2]. Efficient storage of hydrogen is not only an important issue of energy and environmental urgencies, but also a great challenge for material science research. C. Ataca et al. [3] theoretically predicted that Li atom covered graphene can serve as a high-capacity hydrogen storage medium with each decorated Li atom absorbing up to four H_2 molecules, amounting to a gravimetric density of 12.8 wt.%, hypothetically supposing that both sides of each graphene sheets are available. However, a small hydrogen adsorption(< 0.4 wt.%) was experimentally obtained for the pristine single-layer graphene sheets at cryogenic and room temperatures, and the authors attributed this small hydrogen adsorption to the serious agglomerates of the graphene sheets and a weak binding to hydrogen for pristine graphene sheets [4]. Therefore, besides keeping the grapheme separated, it is required to create more effective hydrogen absorption sites for graphene in order to further improve their hydrogen storage property.

Here we investigated the electrochemical hydrogen storage of graphene-based materials synthesized by two different methods－thermal expansion/exfoliation of graphite oxide and sonication exfoliation of graphite oxide followed by hydrazine reduction (Fig. 1). The thermal expansion derived graphene sheets show a higher hydrogen storage capacity of 145 mAh g^{-1} than that of sonication derived graphene sheets (125 mAh g^{-1}) due to the higher specific surface area. Further thermal reduction of the graphene samples leads to a decrease in the storage capacity, indicating that the presence of oxygen functional groups is benefit for the hydrogen absorption (Fig. 2). Moreover, we found that the electrocatalytic activity and hydrogen adsorption of the electrode of graphene sheets can be improved by decorating nickel nanoparticles on their surface. The graphene/nickel nanoparticle composite shows a capacity of 300 mAh g^{-1} (Fig. 3). However, a poor charge/discharge cycle performance is also observed, primarily due to the destruction of graphene-nickel interface structure and the anodic oxidation of the metallic nickel nanoparticles during the cycling process. We proposed a strategy to weaken the anodic oxidation of nickel particles and consequently improve the cycle performance of the composite electrode by tuning the discharge cutoff potential.

References:
[1] Novoselov, K. S., Geim, A. K., Morozov, S. V., Jiang, D., Zhang, Y., Dubonos, S. V., Grigorieva, I. V., Firsov, A. A, Science, 306(2004), 666-669.
[2] Geim AK, Science, 324(2009), 1530-1534.
[3] C. Ataca, E. Akturk, S. Ciraci, H. Ustunel, Appl. Phys. Lett. 2008, 93.
[4] L. P. Ma, Z. S. Wu, J. Li, E. D. Wu, W. C. Ren, H. M. Cheng, INT J HYDROGEN ENERG 2009, 34, 2329.
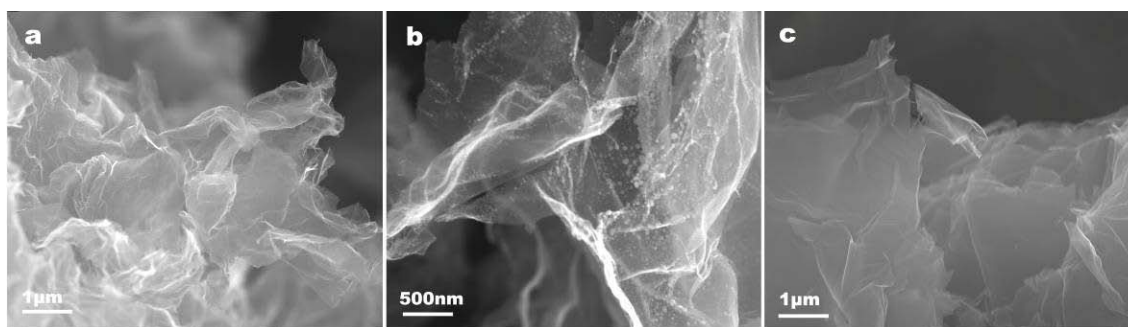
Fig. 1 – SEM images of (a) as-produced thermal expanded graphene sheets (TEGS); (b) graphene sheets decorated with nickel nanoparticles; (c) as-produced chemical reduced graphene sheets (CRGS).
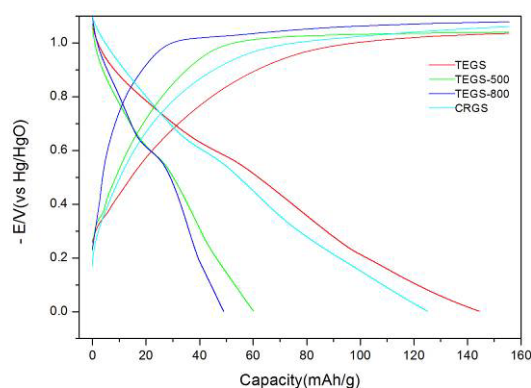
Fig. 2 – The initial charge-discharge curve of the electrode based on (a) as-produced thermal expanded graphene sheets (TEGS); TEGS powder reduced in hydrogen atmosphere at 500 °C (b) and 800 °C (c); (d) as-produced chemical reduced graphene sheets (CRGS).
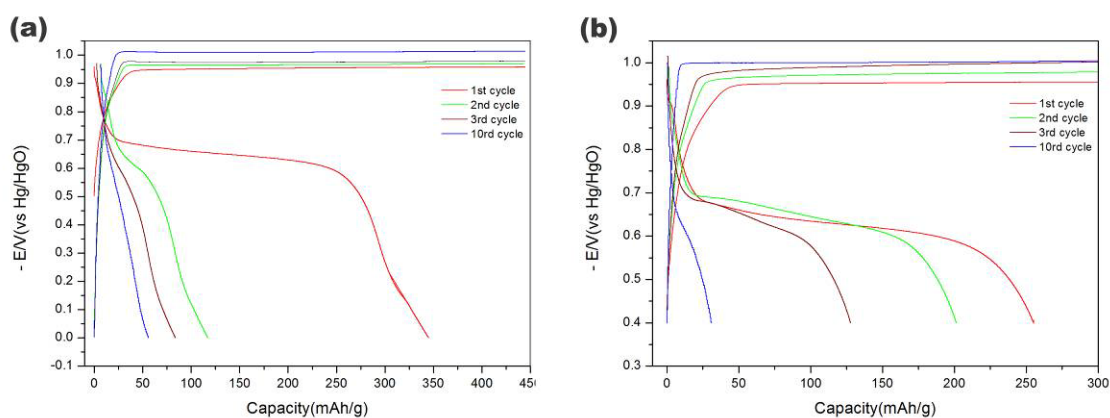
Fig. 3 – Charge–discharge curves of graphene-Ni electrodes at different cutoff potential: (a) 0 V vs. Hg/HgO and (b) -0.4 V vs. Hg/HgO.

66

Magnetic transport in a graphene double quantum dot

Kuei-Lin Chiu, Malcolm Connolly, Jonathan Griffiths, Charles Smith

Semiconductor Group, Cavendish Laboratory, University of Cambridge, J J Thomson Avenue, Cambridge, UK
Eins0728@gmail.com

Owing to its extremely high mobility (>100 m^2 /Vs) and long expected spin relaxation time, graphene is a promising material for making field-effect transistors and quantum computing devices such as spin qubits. Double quantum dots have proved to be model systems for investigating the dynamics of single electrons, and were recently used to measure the spin coherence time in a GaAs based double dot device.[1] In an effort to have equally exquisite access to the dynamics of Dirac quasiparticles in graphene, we have fabricated a graphene double dot device and measured its transport properties at low temperature. Our device consists of two plunger gates for tuning the energy levels in the quantum dots, and three side gates to vary the inter-dot and the dot-lead tunnel barriers (Fig. 1.) At 100mK the conductance of the device as a function of the energy levels in the dots exhibits the honeycomb structure which is typical of a double dot device (Fig. 2.) From the dimensions of the honeycomb we extract the capacitive coupling strength between dots and the gates[2], and examine how this evolves as a function of magnetic field. We will discuss magnetic field dependent changes in the capacitance coupling from the dot to the gate.

References

[1] K. D. Petersson et al, Nano Lett., 2010, 10 (8), pp 2789–2793
[2] Xing Lan Liu et al, Nano Lett., 2010, 10 (8), pp 1623–1627
Figures
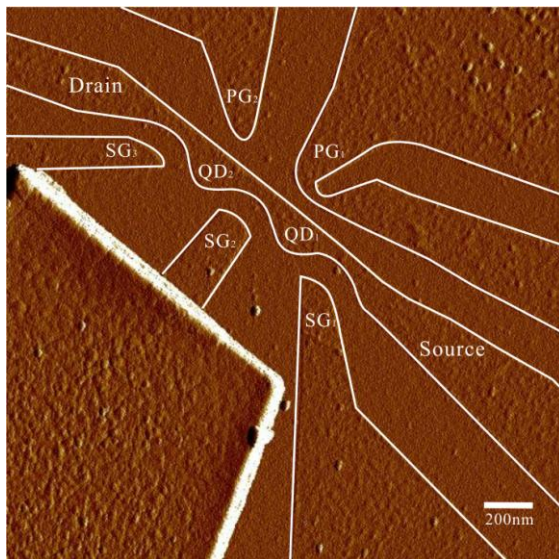
Fig. 1: The AFM image of graphene double quantum dot device that is measured in this work.
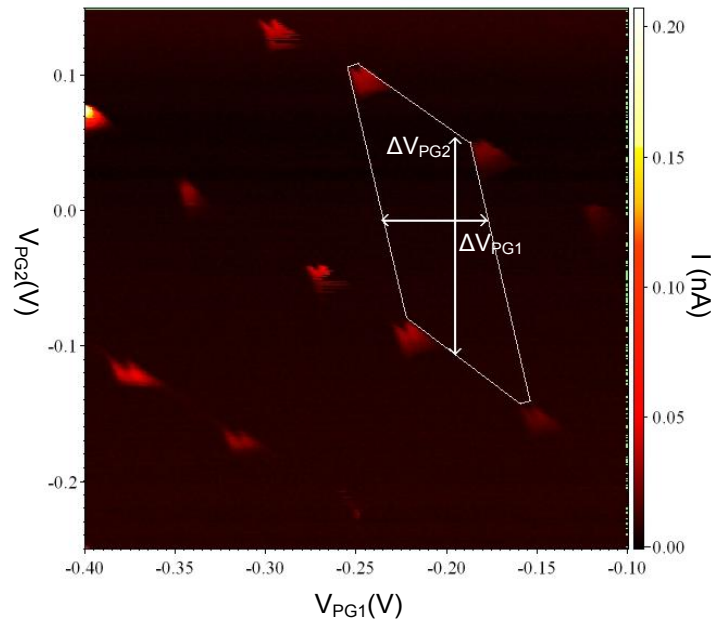
Fig. 2: Current as a function of plunger gate voltages V_{PG1} and V_{PG2} at V_{bias}=-1mV. $\triangle V_{PG1}$ and $\triangle V_{PG2}$ are used to determine the dimension of the honeycomb.

A Graphene-based Hybrid Structure as Flexible, Transparent Field Emitter

Indranil Lahiri[1], Ved Prakash Verma[1], **Mansoo Choi[2]**, Wonbong Choi*[1,2]

[1] Nanomaterials and Device Lab, Department of Mechanical and Materials Engineering, Florida International University, Miami, FL, USA
[2] WCU Department of Energy Engineering, Hanyang University, Seoul, Korea
*choiw@fiu.edu

Graphene is a two-dimensional (2-D) carbon material having unique band structure and outstanding thermal, mechanical and electrical properties [1]. Since the ground-breaking research work of Novoselov et al. in 2004 to propose a simple technique to produce graphene [2] and later through their 'progress article' on the development of this novel 2-D material [3], graphene has received lot of attraction as the most important material for future electronic devices. It is well known that graphene has high mechanical strength (Young's modulus ~1.0 TPa) with flexibility, high transmittance (~97.5%) and high electron mobility (~15,000 cm^2/V.cm). Some of the potential applications of graphene are sensors, transistors, super-capacitors, solar cells, flexible displays etc. One of the future exciting applications is in developing transparent, flexible electrodes. A hybrid of carbon nanotubes over graphene can be considered as an ideal structure for application as flexible and transparent field emission displays. These flexible and transparent displays could have wide application ranges - flexible head-up displays, foldable electronics, lightning tiles etc.

We present here our recent research efforts in developing an all-graphene based cathode and anode structures for flexible and transparent field emission device. Graphene film was grown onto thin Cu foil by thermal chemical vapor deposition and later transferred to a transparent, flexible polymer (PET) substrate through hot press lamination [4]. This transparent and flexible electrode was first used as the anode of a field emission device, in which an interface-controlled multiwall carbon nanotube (MWCNT) structure grown on copper substrate [5] was used as the cathode. This device showed the applicability of graphene-based electrode as a part of field emission devices.

In a further development to this work, we aimed to develop a fully flexible and transparent field emission device, based on graphene. Cathode of this field emission device was developed by spin-coating multiwall carbon nanotubes (MWCNT) onto graphene-PET electrode, as mentioned earlier. A green-phosphor coated graphene-PET film was used as the anode. The device was characterized to understand the field emission response of this graphene-based hybrid field emission device and it offered appreciable emission current. Straight line nature of the Fowler-Nordheim plots guarantee that the electron emission is through tunneling of electrons across the energy barrier. The device also showed good transparency and flexibility [6], which was promising for its application in future flexible and transparent electronic gadgets. The device was also tested for stability of its emission characteristics for 10 hours and has shown appreciable performance. Processing techniques followed to manufacture this novel filed emitter can easily be scaled-up and be tailored for any transparent and flexible substrate. Our results offer exciting applications of graphene in foldable electronics.

References

[1] W. Choi, I. Lahiri, R. Seelaboyina, Y.S. Kang, Critical Reviews in Solid State and Materials Sciences, **35** (2010), 52-71.

[2] K.S. Novoselov, A.K. Geim, S.V. Morozov, D. Jiang, Y. Zhang, S.V. Dubonos, I.V. Grigorieva, A.A. Firsov, Science, **360** (2004) 666-669.

[3] A.K. Geim, K.S. Novoselov, Nature Materials, **6** (2007) 183-191.

[4] V.P. Verma, S. Das, I. Lahiri, W. Choi, Applied Physics Letters, **96** (2010) 203108.

[5] I. Lahiri, R. Seelaboyina, J.Y. Hwang, R. Banerjee, W. Choi, Carbon, **48** (2010) 1531-1538.

[6] I. Lahiri, V.P. Verma, W. Choi, Carbon, DOI: 10.1016/j.carbon.2010.12.044.

Figures
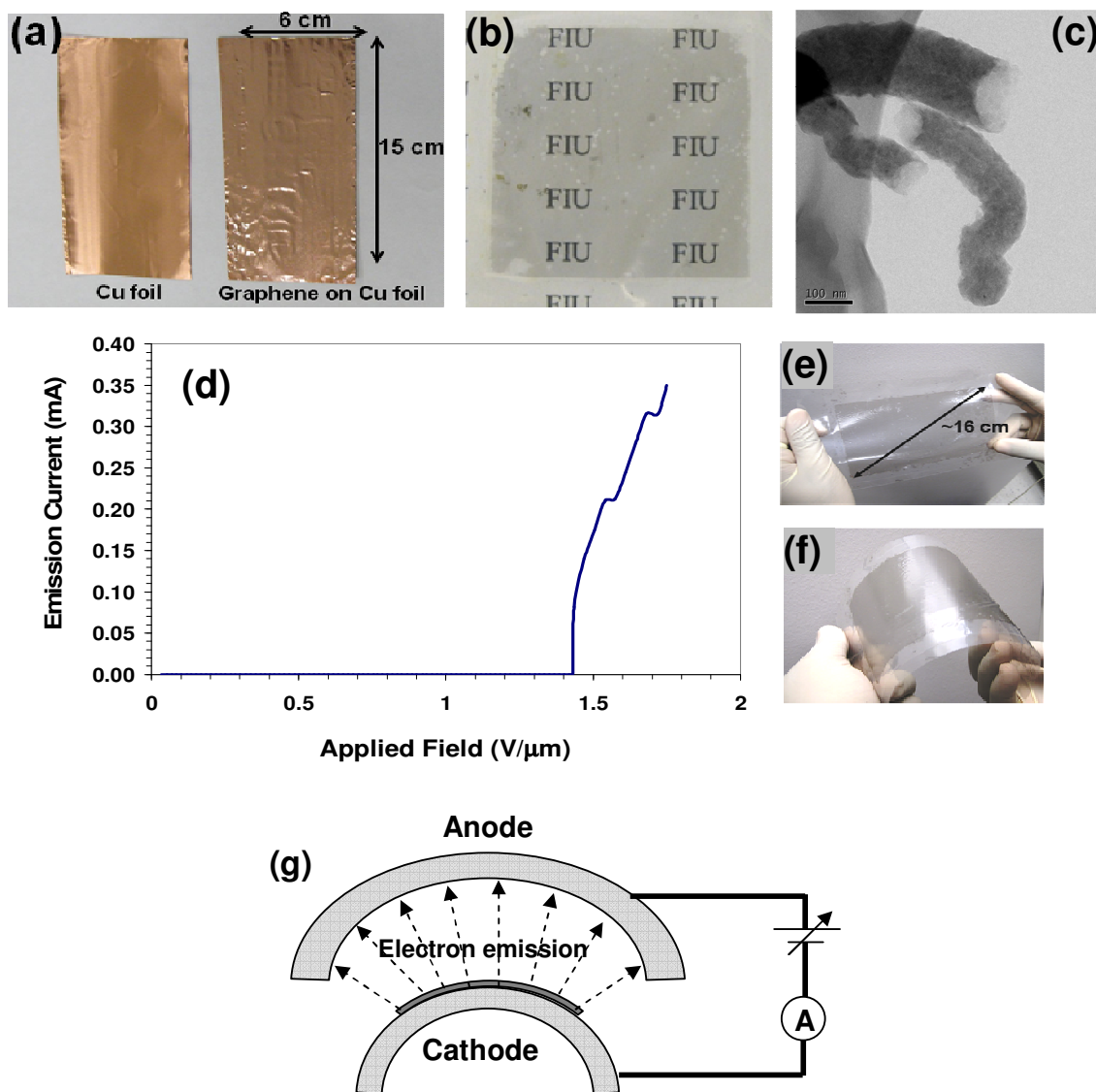
Figure caption

(a) Photos of graphene grown on thin Cu foil, (b) transparency of the graphene film, after transferring onto a PET substrate, (c) TEM image of the MWCNTs embedded on the graphene electrode, (d) field emission response of the graphene-based hybrid field emitter device, (e) graphene transferred to transparent polymer substrate, (f) flexibility of the electrode is demonstrated and (g) schematic of the field emitter device.

Controlling Energy Gap of Bilayer Graphene by Strain

Seon-Myeong Choi[1], Seung-Hoon Jhi[2,3], and Young-Woo Son[1]

[1]Korea Institute for Advanced Study, Seoul 130-722, Korea
[2]Department of Physics, Pohang University of Science and Technology, Pohang 790-784, Korea
[3]Division of Advanced Materials Science, Pohang University of Science and Technology, Pohang 790-784, Korea
sunshine@postech.ac.kr

Using the first principles calculations, we show that mechanically tunable electronic energy gap is realizable in bilayer graphene if different homogeneous strains are applied to the two layers. It is shown that the size of the energy gap can be simply controlled by adjusting the strength and direction of these strains. We also show that the effect originates from the occurrence of strain-induced pseudoscalar potentials in graphene. When homogeneous strains with different strengths are applied to each layer of bilayer graphene, transverse electric fields across the two layers can be generated without any external electronic sources, thereby opening an energy gap. The results demonstrate a simple mechanical method of realizing pseudoelectromagnetism in graphene and suggest a maneuverable approach to fabrication of electromechanical devices based on bilayer graphene.

Graphene on Ru(0001): a combined STM, NC-AFM and FM-KPFM study

Stefan Torbrügge[1], Stefan Schmitt[1], Jörg Rychen[1,2], Oliver Schaff[1]
[1]SPECS GmbH, Voltastrasse 5, 13355 Berlin, Germany
[2]SPECS Zurich GmbH, Technoparkstrasse 1, 8005 Zurich, Switzerland
stefan.torbruegge@specs.com

The possibility of producing single layers of graphene has opened a fascinating new world of physical phenomena in two dimensions and a new route towards all-carbon electronics. Graphene grown on metallic substrates could be important as a source for free-standing graphene samples after dissolving the metallic substrate but it is also of utmost importance from a fundamental point of view. The bonding interaction of the graphene monolayer and the modification of its electronic structure strongly depend on the metallic substrate [1].

In our study graphene was grown by chemical vapor deposition of ethylene on Ru(0001) at elevated temperatures. Recently, we succeeded in monitoring different growth mechanisms of graphene on Ru(0001) by high temperature scanning tunneling microscopy (STM) [2].
To further elucidate the properties of this fascinating material, complementary studies of the electronic and geometrical structure of graphene using STM, noncontact atomic force microscopy (NC-AFM) (see Fig. 1), and frequency-modulation Kelvin probe force microscopy (FM-KPFM) (see Fig. 2) were applied. Combined experiments were carried out with a commercial SPM 150 Aarhus equipped with the piezoelectric KolibriSensor® [3] in ultra-high vacuum. The sensor enables simultaneous STM and NC-AFM experiments [3] beneficial for the study of graphene on Ru(0001).
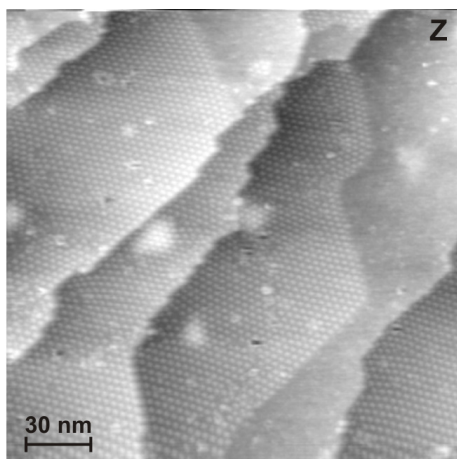
Figure 1: Large scale topographic NC-AFM image of graphene on Ru(0001) at room temperature. The graphene monolayer shows the characteristic buckling resulting in a hexagonal reconstruction.
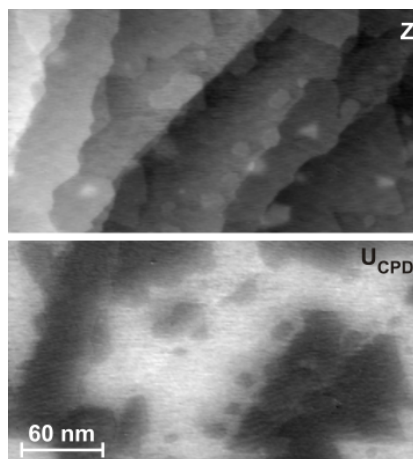
Figure 2: FM-KPFM image of graphene on Ru(0001). Bright areas in the contact potential map U_{CPD} correspond to the metal substrate.

[1] H. Zhang, Q. Fu, Y. Cui, D. Tan, X. Bao, J. Phys. Chem. C, **113**, 8296–8301 (2009)
[2] S. Dänhardt, S. Günther, J. Wintterlin, S. Schmitt, submitted
[3] S. Torbrügge, O. Schaff, J. Rychen, J. Vac. Sci. Technol. B, submitted

Generalization of the Schottky Barrier Postulate at Carbon-Metal Interfaces for Pure, Aligned, Suspended Horizontal Carbon Nanotubes and Hot-press Laminated Graphene Thin Films

M. T. Cole[1], K. Ying[1], S. Haque[2], K. B. K. Teo[3], W. I. Milne[1]

[1] Cambridge University, Centre for Advanced Photonics & Electronics,
9 JJ Thomson Avenue, Cambridge, UK
[2] Nokia Research Centre, Broers Building, 21 JJ Thomson Avenue,
Cambridge, UK
[3] AIXTRON Nanoinstruments Ltd., Swavesey, Cambridge, UK
mtc35@cam.ac.uk

Roll-to-roll, large-area production of flexible transparent metallic and semiconducting thin films is becoming increasingly important in opto-electronic devices. Discrete carbon nanostructured materials, such as carbon nanotube (CNT) and graphene based thin films, offer a potential alternative to the rigid and increasingly expensive industry standard material; indium tin oxide.

In this study, hot-press lamination (HPL) was used to transfer graphene films, synthesised by thermal chemical-vapour-deposition, from their source Cu foil substrates onto polycarbonate (PC) supports (Fig. 1 (a-d)). [1, 2]. Areas in excess of 30 cm^2 have been achieved with typical sheet resistances of ~3 kΩ/□. Multi-Walled carbon nanotube (MWNT) forests (Fig. 2(g)) were also synthesised in the same reactor, and were aligned and suspended across metallic contacts via an extruding technique [3, 4] (Fig. 2 (a-f)).

The HPL-graphene films showed a nominal optical transmittance of 77% (81% substrate transmittance, Fig. 1(f)), and 76% for the freestanding S-MWNT films (Fig.2(h)), comparable values to that achieved through matured ITO processing. Macroscopic investigations into the mechanical robustness of these films showed maximum tensile strains of 35% and >140% for the HPL-graphene and S-MWNTs, respectively; values significantly higher than that of state-of-the-art PC/ITO (1.15%). These exceptionally high strains are attributed to the combined effects of intra-flake/CNT expansion and inter-flake/CNT separation, where this second contribution is significantly enhanced in CNT-based thin-films. The HPL graphene flakes have an exposed area of the order of 400 μm^2 (Fig. 1(e)).

Low temperature *I-V* measurements were undertaken to compare the underlying conduction mechanisms in these discrete nanostructured carbon films. Back and top-gated thin film transistors were also fabricated based on a Si/SiO$_2$ support using a S-MWNT channel and parylene-C dielectric on PC support with a HPL-graphene channel. Al, Pd and Mo source-drain contacts were deposited in each case to investigate the generality of the Schottky barrier postulate, previously identified to explicate the observed electric-field gating effect in SWNTs [5]. Here it was found that the work function of source/drain contact metals played a key role in determining the p-type, n-type or ambipolar behaviour observed.

References

[1]   V. P. Verma, S. Das, I. Lahiri, & W. Choi, *App. Phys. Lett.*, **96**, (2010) 203108.
[2]   I. Lahiri**,** V. P. Verma & W. Choi**,** *Carbon*, (2011).
[3]   M. Zhang, S. L. Fang, A. A. Zakhidov, S. B. Lee, A. E. Aliev, C. D. Williams, & R. H. Baughman, *Science,* **309**, (2005) 1215.
[4]   K. Liu, Y. H. Sun, L. Chen, C. Feng, X. Feng, K. L. Jiang, Y. G. Zhao, S. S. Fan, *Nano Lett.*, **8**, (2008) 700.
[5]   M. H. Yang, K. B. K. Teo, D. G. Hasko, & W. I. Milne, *App. Phys. Lett.*, **87**, (2005) 253116.

Figures
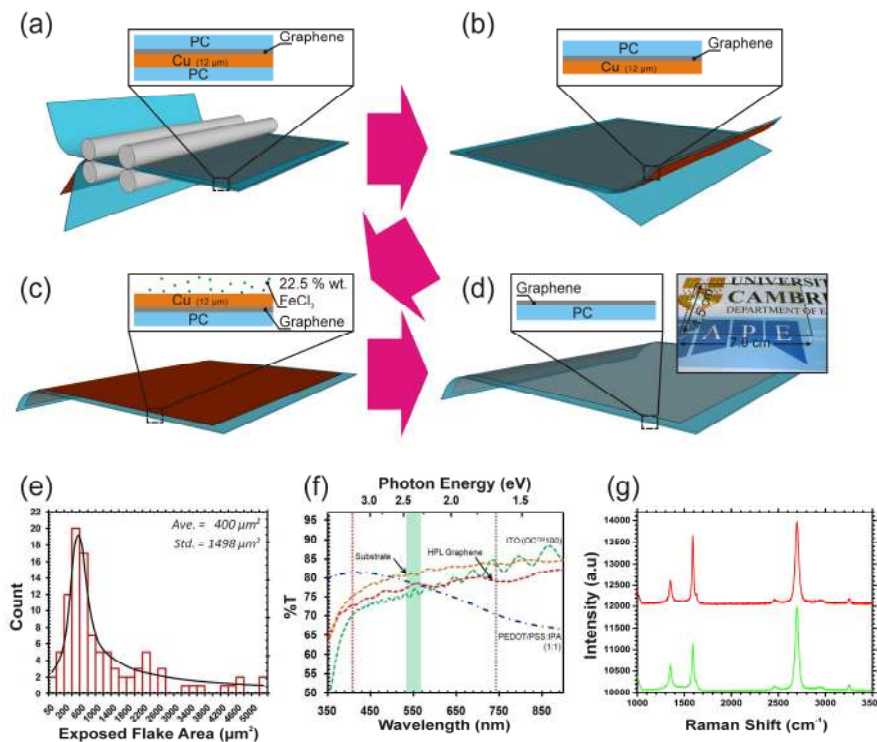
FIG. 1. *Hot-pressed laminated graphene fabrication. (a) Laminating of graphene (synthesized on 12.5 µm Cu foil) at 120 °C on polycarbonate (PC) support. (b) Removal of underside PC laminate. (c) Cu etching using 22.5 % wt. $FeCl_3$. (d) Remaining graphene coated PC substrate. Inset: Optical image of a 4.5 x 7.0 cm graphene/PC sample. (e) Typical histogram of the exposed flake area. Normal distribution fitted (Mean flake area of 400 µm, std. 1498 $µm^2$). (f) UV-Vis transmission spectrum for competing technologies (PEDOT/PSS:IPA, ITO), the bare PC substrate and the graphene/PC platform showing a uniform optical transparency of 77%. (g) Raman spectrum of CVD synthesized graphene transferred to Si/SiO_2 (300 nm).*
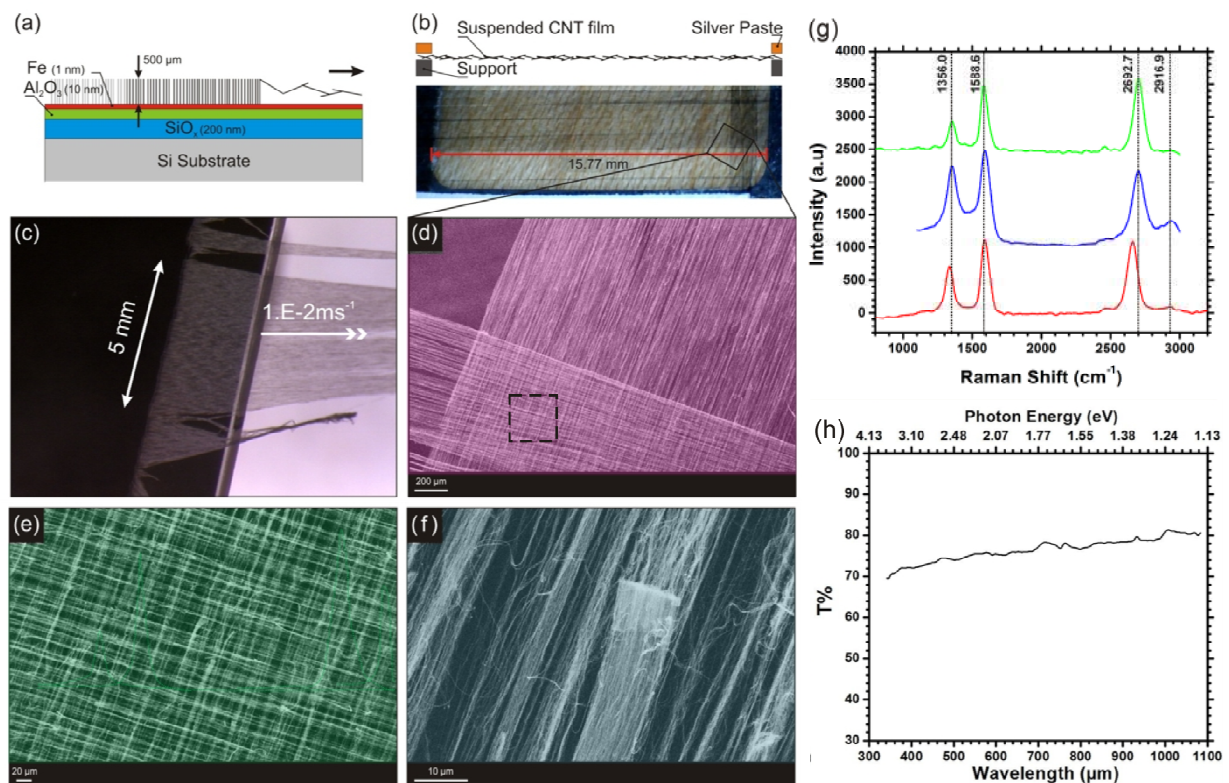
FIG. 2. *(a-f) Suspended MWNT array fabrication process. (g) Typical sample Raman Spectrum. (h) UV-Vis spectrum showing uniform optical transmittance.*

Simple and scalable route for the 'bottom-up' synthesis of few-layer graphene platelets and thin films

Karl S. Coleman, Christopher R. Herron, Rebecca S. Edwards and Budhika G. Mendis

Department of Chemistry, Durham University, South Road, Durham, DH1 3LE, UK
k.s.coleman@durham.ac.uk

Graphene has generated much interest owing to its exceptional electronic properties and high mechanical strength. This has enabled new types of electronic devices and composite materials to be envisaged. The main problem is the availability of the material and the difficulties associated with its synthesis. Here we present a simple, convenient and scalable chemical vapour deposition method involving metal alkoxides in ethanol to produce few-layer graphene platelets. The methodology used has the added flexibility in that it can be used to grow conducting transparent thin films on inert substrates such as silicon wafer and quartz glass. Importantly, no heavy metal catalysts were required to produce the few-layer graphene platelets or graphene films and all non-carbon by-products are soluble in water.

Figures
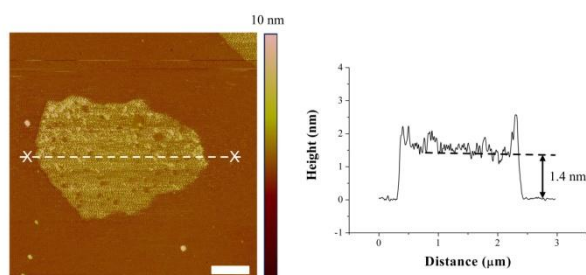
TappingMode AFM height image (3 µm × 3 µm, scale bar 500 nm) of a graphene sheet deposited from an ethanol solution onto a freshly cleaved mica surface. The height profile, following the white line on the image, shows the height of the graphene sheet to be ca. 1.4 nm which is equal to approximately 4 layers.
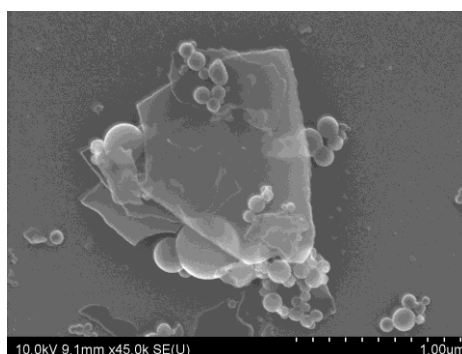
SEM image of graphene platelets stacked on top of one another, scale bar 1 µm.

Probing the potential landscape of a graphene bilayer in the quantum Hall regime

M. R. Connolly[1], R. K. Puddy[1], M. Roy[2], P. Maksym[2], G. A. C Jones[1], C. G. Smith[1]

[1]Cavendish Laboratory, University of Cambridge, JJ Thomson Avenue, Cambridge CB3 0HE, UK
[2]Department of Physics and Astronomy, University of Leicester, University Road, Leicester LEI 7RH, UK

mrc61@cam.ac.uk

Owing to their high mobility and electric field tuneable bandgap, micron-sized sheets of bilayer graphene are emerging as a serious alternative to nanoscale ribbons as the channel material of a graphene field-effect device [1]. While the performance of such bilayer devices potentially competes with that of conventional semiconductors, the "on/off" conductance ratio currently falls short of expectations, probably due to large fluctuations in the local electrostatic potential created by charged impurites [2]. To determine the precise nature of these potential fluctuations, we use the charged tip of a scanning probe microscope to locally perturb the potential landscape in an exfoliated bilayer while measuring its bulk conductance. In a magnetic field we observe a rich texture of ≈ 100 nm "hotspots" where the response to the tip is particularly pronounced. We analyse the evolution of these hotspots as a function of magnetic field, back-gate, and tip voltage, and discuss their origin in terms of tip-enhanced back- and forward-scattering from saddle points in the potential landscape [3].

References

[1] B. N. Szafranek *et al.*, APL, **96** (2010) 3364139.
[2] K. Zou and J. Zhu, PRB, **82** (2010) 081407.
[3] A. Baumgartner *et al.*, PRB **76** (2007)**,** 085316.

Figures
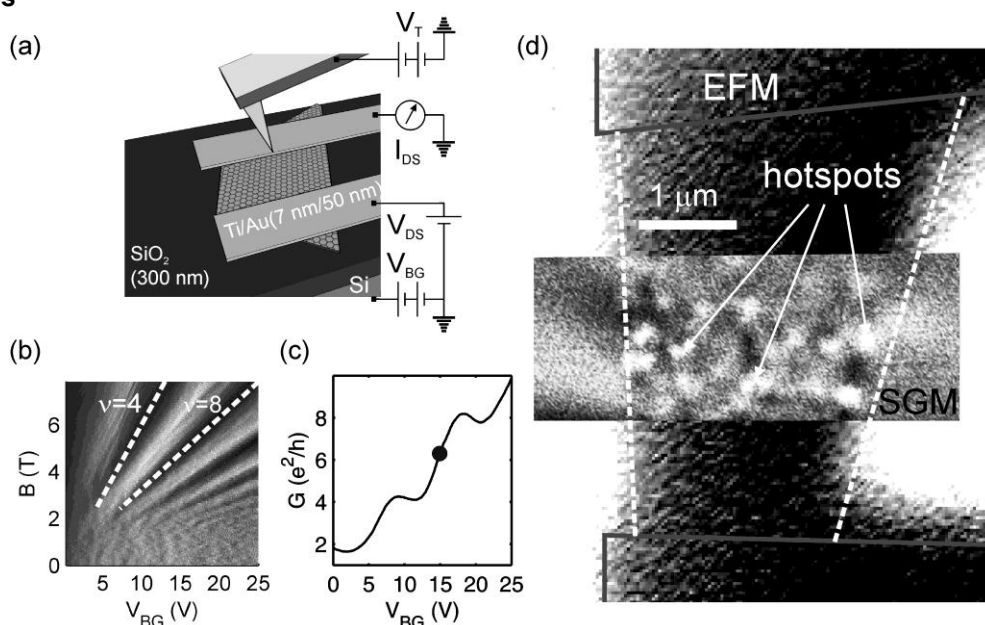
Fig.1. *(a) Schematic of scanning gate microscopy on a graphene flake. The current I_{DS} is recorded as a function of tip position. (b Differential conductance surface of a graphene bilayer as a function of magnetic field and back-gate voltage. Landau levels appearing at filling factors of 4 and 8 confirm that the flake is bilayer. (c) Conductance as a function of magnetic field at B = 6 T. Black circle indicates the back-gate where the SGM image in (d) was captured. (d) Electrostatic force and scanning gate micrograph of a bilayer flake. Dashed outlines indicate the edge of the flake while solid outlines indicate the edge of the contacts.*

Grain coalescence and electronic properties of epitaxial graphene

Graham Creeth,

University of Leeds, UK
g.l.creeth@leeds.ac.uk

Epitaxial growth of graphene on SiC is a candidate system for the growth of graphene on a scale large enough for technological applications [1]. Growth is achieved by annealing at temperatures above 1200C, causing Si to evaporate from the SiC preferentially to C, with the resulting carbon-rich surface forms a graphitic layer, with the structural and electronic properties extremely sensitive to annealing conditions. Crucially, in this system both the supply of carbon and the conditions under which the graphene films coalesce are temperature dependent and therefore closely coupled [2].

We present data from magnetotransport and low energy electron microscopy (LEEM)measurements for (0001) 4H SiC samples annealed under UHV at various temperatures, showing structural and electronic coherence lengths which are in good agreement. The evolution of coherent electronic transport occurs for samples annealed at higher temperatures as the size of individual graphene domains increases from the tens of nm to micron scale under these conditions (shown in figure 1). Using a lower-temperature anneal followed by an additional higher-temperature treatment, we show that the larger grain size is due to a coalescence mechanism, as opposed to faster propagation of single grains. This suggests a means of partially decoupling the carbon supply from the coalescence process: potentially important for integration with large-scale wafer production.

Following lithographic patterning, magnetotransport (MR) data have been taken at various cryogenic temperatures and can be fitted to weak localisation (WL) or weak anti-localisation (WAL) models [3, 4], allowing the various electron scattering rates to be ascertained. Following these fitting procedures, subtraction of the fits from the measured data allows less dominant contributions to magnetotransport to be discerned. For less ordered samples, it is necessary to include an electron-electron interaction term to fit successfully to low-temperature MR data, while the temperatures at which this becomes necessary agree with a deviation from linear temperature dependence of the scattering rate τ_φ.

References

[1] Authors, Journal, **Issue** (Year) page.

[1] C. Berger, Z. Song, T. Li, X. Li, A.Y. Ogbazghi, R. Feng, Z. Dai, A.N. Marchenkov, E.H. Conrad, P.N. First, and W.A. deHeer. Journal of Physical Chemistry B,**108**(2004)19912.

[2] Luxmi, N. Srivastava, Guowei He, R. M. Feenstra, and P. J. Fisher. Phys. Rev. B, **82**(2010) 235406.

[3] Xiaosong Wu, Xuebin Li, Zhimin Song, Claire Berger, and Walt A. de Heer. Phys. Rev. Lett., **98** (2007)136801.

[4] E. McCann, K. Kechedzhi, Vladimir I. Fal'ko, H. Suzuura, T. Ando, and B. L. Altshuler. Weak-localization magnetoresistance and valley symmetry in graphene. Phys. Rev. Lett., **97**(2006)146805.

Figure 1
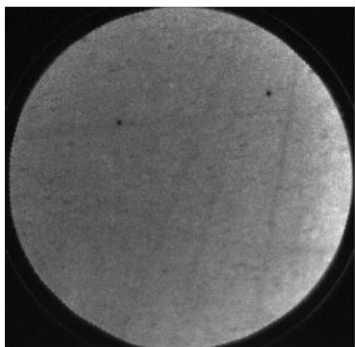
(a) 20 minutes 1300 °C
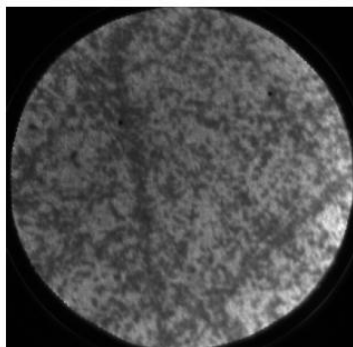
(b) 60 minutes 1300 °C
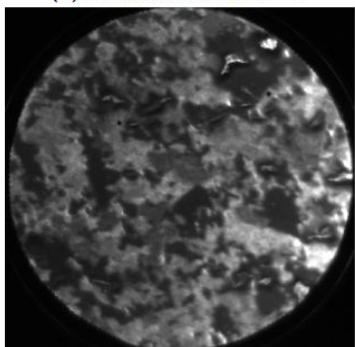
(c) 30 minutes 1400 °C
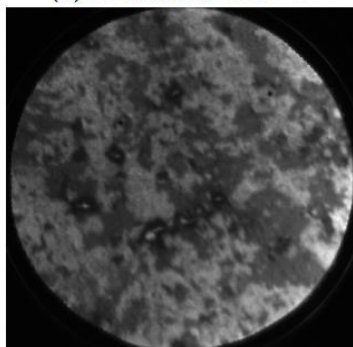
(d) 55 minutes 1400 °C

LEEM images of samples annealed under UHV with varying conditions. Field of view in each case is 10 μm.

Electronic transport in epoxide and methyl functionalized graphene nanoribbons

Alessandro Cresti[1], Stephan Roche[2] and Pablo Ordejón[3]

[1]IMEP-LAHC (UMR CNRS/INPG/UJF 5130), Grenoble INP Minatec, 3 Parvis Louis Néel, BP 257, F-38016 Grenoble, France
crestial@minatec.inpg.fr
[2]CIN2 (ICN-CSIC) and Aniversitat Autonoma de Barcelona, Catalan Institute of Nanotechnology, Campus de la UAB, 08193 Bellaterra (Barcelona), Spain and ICREA, Institucio Catalana de Recerca i Estudis Avançat, 08010 Barcelona, Spain
[3]CIN2 (CSIC-ICN), campus de la UAB, Bellaterra, 08193 Barcelona, Spain

The grafting of chemical groups on the graphene surface strongly modifies the sp^2 hybridization of carbon atoms, thus inducing important modifications on electronic and transport properties, of which the most important is a metal-insulator transition. Possible applications range from carrier mobility engineering to innovative nanolithography techniques. In this context, graphene functionalization has attracted much attention thanks to its reversibility and the possibility of controlling the adsorbate density. However, most of the literature focuses on the functionalization of 2D graphene, without considering the possible role of lateral confinement and edges in nanoribbons.

Here, we present a systematic study of electronic transport in nanoribbons functionalized with two groups of different nature, i.e. epoxide and methyl, see fig.1. We consider ribbons of width W between 5 nm and 20 nm with adsorbate density n between 0.1% and 0.5%. The simulations are based on the Keldysh-Green's function formalism within the tight-binding framework, with Hamiltonians obtained from accurate *ab initio* calculations [1,2]. The results are summarized by fig.2 and fig.3, which show the mean free path ℓ_e as a function of the electron energy E for armchair nanoribbons composed of 41, 83 and 125 dimer lines, corresponding to W=5 nm, 10 nm and 12.5 nm.

As seen from fig.2, methyl functionalization has an almost symmetric impact on the nanoribbon transport properties, which are slightly more degraded for holes (E<0). This trend can be explained in terms of the single defect renormalized Hamiltonian, which is approximately equivalent to that of a vacancy. Conversely, epoxide defects asymmetrically affect ℓ_e, which is markedly reduced for electrons (E>0), see fig3. Again, this originates from the carbon hybridization degree, on whose account the adsorbates are equivalent to divacancies for electrons and to coupled pentagonal rings for holes.

At low methyl density (n=0.1%), for the same number of active conduction modes, ℓ_e decreases with the width of the ribbon, see fig.2(a). For larger ribbons, the dependence of the mean free path on W becomes weaker. Contrariwise, for epoxide functionalization, ℓ_e increases as W increases, see fig.3(a). On the electron side, the mean free path for W=12.5 nm is about 1.5 times that for W=10 nm. This almost linear scaling might be related to the short mean free path (comparable to W), or to the graphene sublattice symmetry preservation. For holes, ℓ_e is almost independent of W. This suggests a more pronounced electron-hole asymmetry in larger ribbons.

When varying the defect density, ℓ_e roughly scales as 1/n for both types of defect if n<0.3%, see fig.2(b) and fig.3(b). However, at higher epoxide densities, ℓ_e scales faster than 1/n for holes, thus indicating possible correlation effects or the rise of bound states.

In conclusion, epoxide and methyl defects have markedly different impact on nanoribbon transport properties. The differences are consequence of carbon hybridization degree and graphene sublattice symmetry breaking or preservation. The electron-hole asymmetry observed for epoxide functionalization suggests applications in mobility gap engineering [3] with prospects for graphene-based logic devices.

References

[1] N. Leconte, J. Moser, P.Ordejón, H. Tao, A. Lherbier, A. Bachtold, F. Alsina, C.M. Sotomayor Torres, J.-C. Charlier and S. Roche, ACS Nano, **4** (2010) 4033

[2] T.O. Wehling, S. Yuan, A.I. Lichtenstein, A.K. Geim and M.I. Katsnelson, Phys. Rev. Lett., **105** (2010) 056802

[3] B. Biel, X. Blase, F. Triozon and S. Roche, Phys. Rev. Lett., **102** (2009) 096803

Figures
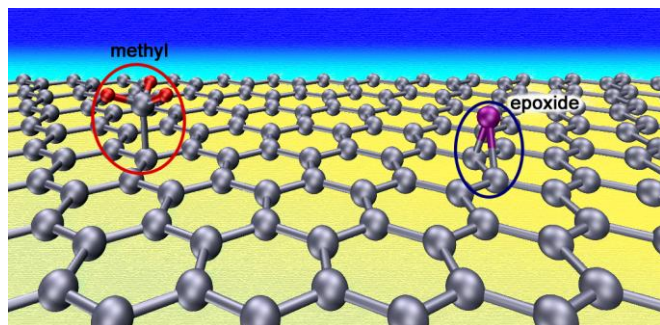
Figure 1: Methyl and epoxide groups on the surface of a graphene nanoribbon.
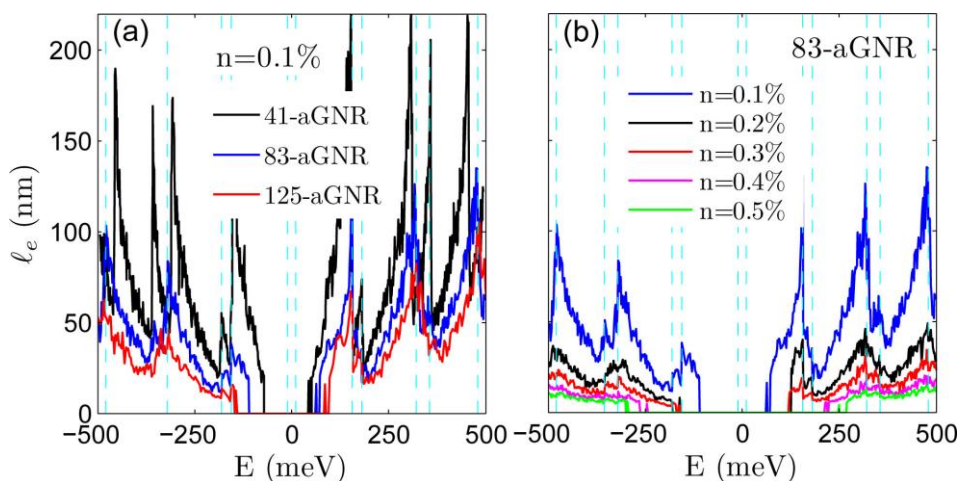
Figure 2: Mean free path for methyl functionalized armchair nanoribbons as a function of the electron energy for (a) impurity density n=0.1% and different ribbon width between 5 nm and 12.5 nm (the energy refers to the 10 nm wide ribbon and it is elsewhere rescaled to make the region with the same number of conduction modes coincide) and (b) for width 10 nm and densities between 0.1% and 5%. Vertical lines indicate the activation of conduction modes.
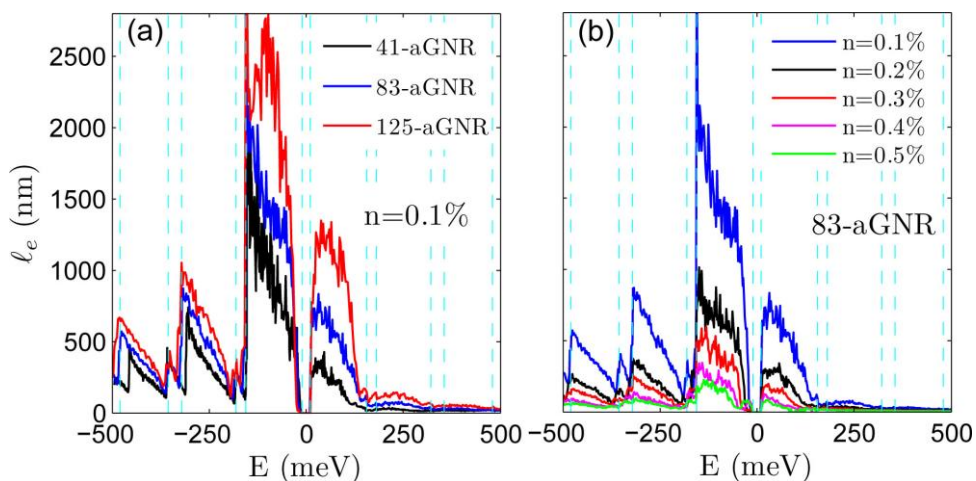
Figure 3: The same as fig.2 but for epoxide functionalized armchair nanoribbons.

Trapping of metal atoms by reconstructed defects in graphene

Ovidiu Cretu[1], Julio Alejandro Rodríguez-Manzo[1], Arkady Krasheninnikov[2,3], Florian Banhart[1]

1. Institut de Physique et Chimie des Matériaux de Strasbourg, 23 rue du Loess, 67034 Strasbourg, France
2. Materials Physics Division, University of Helsinki, P.O. Box 43, FI-00014 Helsinki, Finland
3. Department of Applied Physics, Aalto University, P.O. Box 1100, FI-00076 Aalto, Finland
ovidiu.cretu@ipcms.u-strasbg.fr

We present an in-depth investigation of the interaction between various types of metal atoms and defective graphene. Many of the current growth techniques for graphene produce material that is defective. These defects change the properties of graphene [1], which is why their effects need to be understood but also to take advantage of them in practical applications. Our graphene samples are prepared from HOPG or natural graphite by micromechanical cleavage with regular scotch-tape, which is then dissolved in acetone. The resulting suspension is dropped on standard TEM grids. These are subsequently cleaned by annealing at high temperature (1000-2000°C) under high vacuum, in a furnace. Metal nanoparticles are deposited on top of the sample during or after the annealing process. After these preparation steps, the sample is transferred into the TEM using a special holder, which allows for *in-situ* heating. We correlate our experimental observations with theoretical calculations to obtain a complete image of the observed phenomena.

1. Structuring at the atomic scale with a focused electron beam. The experiments show the possibility of creating sub-nanometer damage in graphene sheets, in a controlled manner, by electron irradiation [2]. We operate our microscope in STEM mode, which focuses the electron beam in a spot of about 1A in diameter. This is made possible by an aberration corrector fitted to the condenser lens system. Placing the beam in a fixed position on the sample yields multiple vacancies whose size varies between less than one and several nanometers and is controlled by the irradiation time. These evolve differently as a function of sample temperature and of the presence of atoms nearby. At lower temperatures, we find that these vacancies have a tendency to either close partially by the trapping of mobile carbon atoms and restructuring of the edges, or remain open. At higher temperatures, these vacancies anneal immediately by trapping atoms diffusing on the surface. We see this for carbon (given for instance by surface contamination) or, more interestingly, for several types of metal atoms. Metal atoms tend to replace carbon atoms in the lattice and lead to new structures which, provided the temperature is lowered and the irradiation stops, are stable. The technique can be extended by programming the beam control software of the microscope to create vacancies in the sample in a pre-defined pattern. Figure 1a shows a region of the graphene sample before irradiation. The large black area in the upper part represents a Mo nanoparticle while smaller black dots throughout the image are individual Mo atoms or small clusters. Figure 1b shows the same area after patterning. A triangular arrangement of Mo clusters is visible below the particle. Subsequent imaging and analysis show that, despite the temperature of 475°C and continued irradiation, some Mo atoms still remain trapped 40 minutes later.

2. Creation of vacancies on a larger area. The second set of experiments provides deeper insight into the trapping of metal atoms by reconstructed defects and the diffusion of metal atoms on the defective graphene surface [3]. We used W atoms, which provide good contrast in the electron microscope because of their high atomic number, and we subjected the sample to uniform and constant electron irradiation. We then acquired videos of the motion of these atoms on the graphitic surface. The atoms did not move as expected – by a standard random walk between adjacent lattice positions – but performed long-distance (1nm) jumps between certain lattice sites. Figure 2 shows the trajectory of an atom during such an experiment. Furthermore, multiple back-and-forth jumping between two defective sites appeared. At temperatures where this type of motion was observed (300-500°C), an interaction energy of about 2 eV between the atom and the lattice site is necessary for the trapping/detrapping behavior and the diffusion with a jump rate that matches the one we see in our experiment. The two extreme cases would be an atom on a perfect surface, which would diffuse too fast for in-situ observation (activation energy 0.5 eV) and an atom trapped in a single vacancy by replacing a carbon atom, making the metal atom immobile (7 eV). By simulating how surface defects reconstruct at these temperatures, we found that the most likely candidates for the structures that trap the W atom are reconstructed 555-777 or 5555-6-7777 defects. These complex structures start as double vacancies (created by the electron beam) and reconstruct at high temperatures. This scenario is further supported by the experimental observation of smaller (0.2 nm) jumps while the atom is trapped at a defective site, between two large jumps. These observations show a long-distance interaction between the metal atom and the defect. We can hence identify the unusual motion of the metal atom as jumps between reconstructed lattice defects in graphene.

References
[1] F Banhart, J Kotakoski, A V Krasheninnikov, ACS Nano, 10.1021/nn102598m, *available online*
[2] J A Rodríguez-Manzo, O Cretu, and F Banhart, ACS Nano **4** (2010) 3422.
[3] O Cretu, A V Krasheninnikov, J A Rodríguez-Manzo, L Sun, R M Nieminen, and F Banhart, Phys. Rev. Lett. **105** (2010) 196102.

Figures
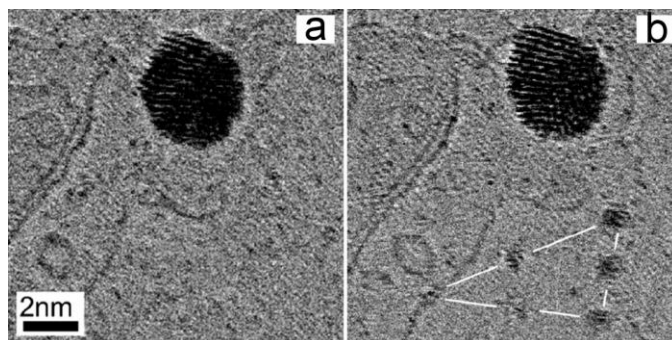
Figure1. Patterning of graphene by trapping Mo atoms at selected locations. The same sample area is shown before (a) and after (b) the patterning with a triangular arrangement of dots. Sample temperature 475°C; patterning time about 5 minutes.
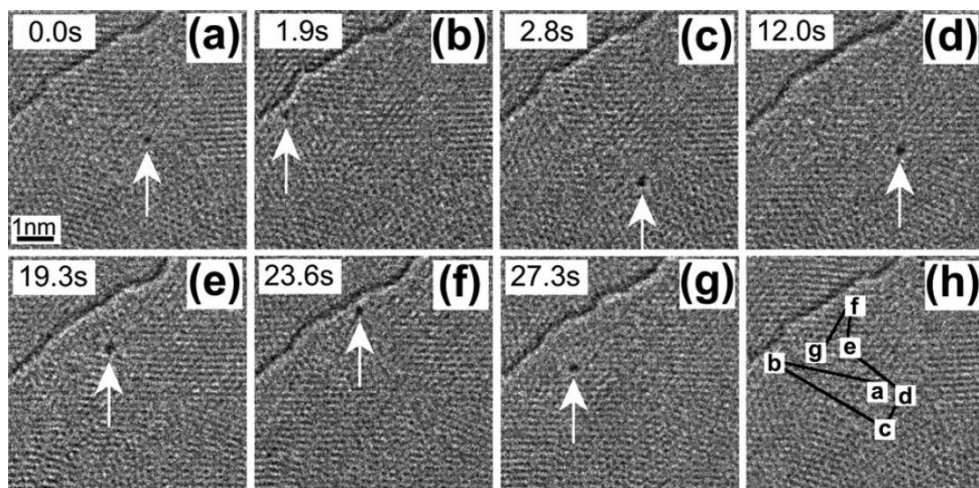
Figure2. Trajectory of a W atom diffusing on a graphene surface. The atom is shown in each of its stable positions on the lattice, marked by a white arrow (a-g); the total trajectory is represented in (h). Sample temperature 470°C; experiment time about 30s.

Spin wave in zigzag graphene and the stability of the edge ferromagnetism

F. J. Culchac, A. Latgé and A. T. Costa

Instituto de Física, Universidade Niterói, RJ, Brazil
latge@if.uff.br

Graphene is being hailed as the big promise for nanoelectronics and spintronics. Its unique transport properties are expected to play a fundamental role in the development of new technologies [1-3]. New physics is also emerging from the interplay between low dimensionality, a bipartite lattice and electron-electron interaction. One of the most striking properties of graphene nanoribbons is the possibility of spontaneous magnetization [4-6]. This, combined with the long spin-coherence times of electrons propagating across graphene, indicates that this system is a strong candidate for future spintronics applications.

The ground state properties of magnetic graphene nanoribbons have been extensively explored by a variety of methods. Recent works have investigated the properties of static excited states based on adiabatic approximations [7, 8]. This approach has been employed to describe the lowest-lying excitations of magnetic metals with relative success. However, it is well known that it misses important features of the excited states, such as its finite lifetime. This arises due to the coupling between spin waves and Stoner excitations, a distinctive feature of itinerant magnets. Moreover, these recent investigations of excited states seem to have disregarded the antiferromagnetic coupling between the magnetizations on opposite edges of graphene nanoribbons. As we shall see, this leads to an incorrect prediction concerning the wave vector dependence of low energy spin excitations. This has already been demonstrated more than a decade ago in the seminal work by Wakabayashi et al. [9]. Those authors used an itinerant model to describe the π electrons in graphene nanoribbons of various widths. They showed clearly the presence of a linear term in the spin wave dispersion relation for small wave vector.

One interesting feature of magnetic graphene nanoribbons is that the spins along each border are ferromagnetically coupled to each other, but there is an antiferromagnetic exchange coupling between the two opposite borders. This coupling is mediated by the conduction electrons, and decreases as the ribbon width is increased Thus, it may appear, at first sight, that this antiferromagnetic. coupling should be unimportant in wide ribbons. It has been shown, however, that this coupling is extremely long ranged in graphene and other related materials [10-14]. Thus, even in rather wide nanoribbons this coupling asserts itself, as we shall see.

We point out that spin wave lifetimes are very long due to the semi-conducting nature of the electrically neutral nanoribbons. However, application of very modest gate voltages causes a discontinuous transition to a regime of finite spin wave lifetime. By further increasing doping the ferromagnetic alignments along the edge become unstable against transverse spin fluctuations. This makes the experimental detection of ferromagnetism is this class of systems very delicate, and poses a difficult challenge to the possible uses of these nanoribbons as basis for spintronic devices.

References

[1] M. Fujita, K. Wakabayashi, K. Nakada, and K. Kusakabe, J. Phys. Soc. Jpn. 65, 1920 (1996).
[2] S. Okada and A. Oshiyama, Phys. Rev. Lett. 87, 146803 (2001).
[3] F. Muñoz-Rojas, J. Fernández-Rossier, and J. J. Palacios,Phys. Rev. Lett. 102, 136810 (2009).
[4] Y.-W. Son, M. L. Cohen, and S. G. Louie, Nature (London) 444, 347 (2006).
[5] Y.-W. Son, M. L. Cohen, and S. G. Louie, Phys. Rev. Lett. 97, 216803 (2006).
[6] L. Pisani, J. A. Chan, B. Montanari, and N. M. Harrison, Phys. Rev. B 75, 064418 (2007).
[7] O. V. Yazyev and M. I. Katsnelson, Phys. Rev. Lett. 100, 047209 (2008).
[8] J. Rhim and K. Moon, Phys. Rev. B 80, 155441 (2009).
[9] K. Wakabayashi, M. Sigrist, and M. Fujita, J. Phys. Soc. Jpn. 67, 2089 (1998).
[10] P. Venezuela, R. B. Muniz, A. T. Costa, D. M. Edwards, S. R. Power, and M. S. Ferreira, Phys. Rev. B80, 241413(R) (2009).
[11] A. T. Costa, D. F. Kirwan, and M. S. Ferreira, Phys. Rev. B 72, 085402 (2005).
[12] A. T. Costa, R. B. Muniz, and M. S. Ferreira, New J. Phys. 10, 063008 (2008).
[13] D. F. Kirwan, C. G. Rocha, A. T. Costa, and M. S. Ferreira, 77, 085432 (2008).
[14] D. F. Kirwan, V. M. de Menezes, C. G. Rocha, A. T. Costa, R. B. Muniz, S. B. Fagan, and M. S. Ferreira, Carbon 47, 2533 (2009).

Atomic Force Microscopy cleaning of graphene deposited on SiO$_2$ substrate

P. Dabrowski [a], I. Wlasny [a], Z. Klusek [a], M. Wojtoniszak [b], E. Borowiak-Paleń [b], A. Sozańska [c], J. Sławińska [d], I. Zasada [a], K. Polański [a], W. Olejniczak [a]

[a] Solid States Physics Department, University of Lodz, Pomorska 149/153, Lodz 90-236, Poland
[b] Institute of Chemical and Environment Engineering, West Pomeranian University of Technology, Pulaskiego 10, Szczecin 70-322, Poland
[c] Renishaw SPD, Old Town, Wotton-under-Edge, Gloucestershire, GL12 7DW, UK
[d] Theoretical Physics Department II, University of Lodz, Pomorska 149/153, Lodz 90-236, Poland
paweldabrowski@std2.phys.uni.lodz.pl

Monolayer graphene (MG) is a new two-dimensional form of carbon material, which possesses unique electronic properties due to mass less Dirac fermion character of carriers derived from the conical dispersion relation close to the Dirac point (E_D). It has been shown that this type of dispersion relation leads to the presence of quantum Hall effect, ballistic transport of electrons, electronic spin transport, micron scale coherence length, single electron tunnelling, evidence of Klein tunnelling and scattering, or for instance existence of the optics-like focusing of electron rays in the p-n graphene junctions.

However it has been demonstrated that the presence of chemical adsorbates on MG leads to the significant modifications of the electronic transport properties of this material. Mainly, these adsorbates left after graphene production processes [1], and electron beam lithography procedures required in the fabrication of MGD [2]. That's way the electronic devices based on graphene require clean and perfect carbon honeycomb layer deposited on different substrates. It seems to be that the experimental controlling of the presence of impurities on the graphene sheet is still far from the understanding and require further theoretical and experimental studies.

Recently, different cleaning methods of graphene have been proposed. The most popular is annealing of graphene in UHV condition or heating with argon/hydrogen atmosphere [3]. Thought, it has been proved that annealing modify graphene surface considerably [4]. It has been also shown that high density of electric current remove contamination adsorbed on the graphene surface [5].

We report on a cleaning method of MG deposited on SiO$_2$ substrate based on repetitive scanning process with atomic force microscope (AFM) and subsequent electron beam irradiation. This process leads to removal of adsorbates and exposing clean graphene layer. In this method contaminations are accumulated at the edges of scanning area and we can immobilize them. In Fig.1 we present AFM topographies showing differences between clean and dirty regions. Measurements show that new cleaning procedure is very effective, and can be used not only for cleaning graphene surface but also in lithography process. This method can lead to production a new type of graphene devices.

References

[1] A. Das, B. Chakraborty, A. K. Sood, Bull. Mater. Sci., 31, 579, (2008)
[2] M. Ishigami, J. H. Chen, W. G. Cullen, M. S. Fuhrer, E. D. Williams, Nano Lett. 7, 1643 (2007).
[3] D. Yang, A. Velamakanni G. Bozoklu, S.Park, M. Stoller, R.D. Piner, S. Stankovich, Inhwa Jung Daniel A. Field Carl A. Ventrice Jr., Rodney S. Ruoff, Carbon 47, 145 (2009).
[4] Z. H. Ni, H. M. Wang, Y. Ma, J. Kasim, Y. H. Wu, Z. X. Shen, ACS Nano 2, 1033 (2008).
[5] J. Moser, A. Barreiro, and A. Bachtold, Appl. Phys. Lett. 91, 163513 (2007).
[1] A. Das, B. Chakraborty, A. K. Sood, Bull. Mater. Sci., 31, 579, (2008)
.

Figures
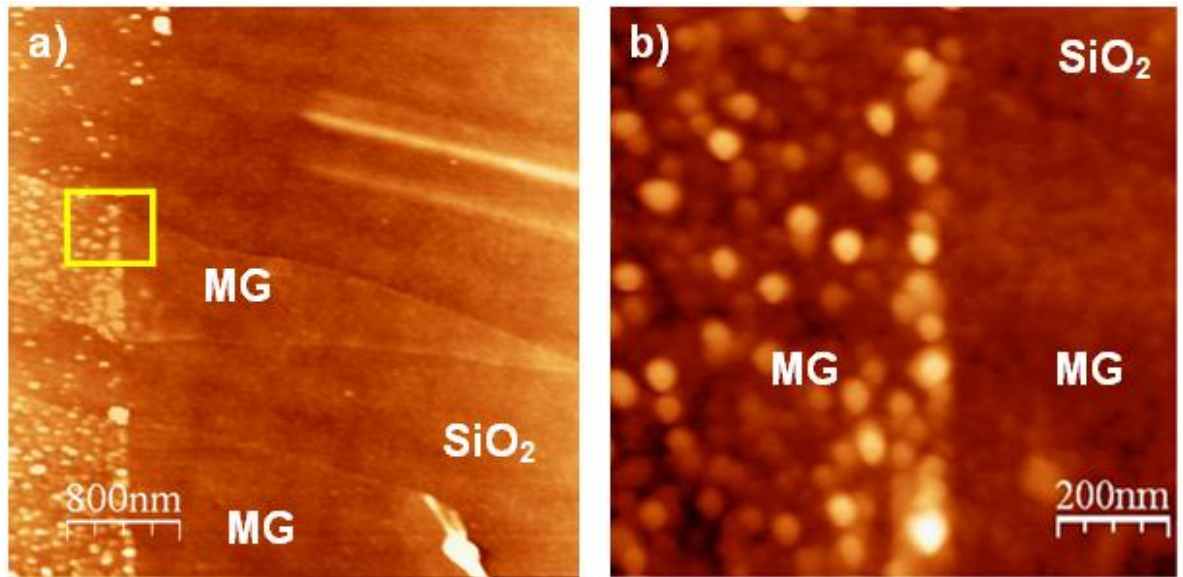
Fig. 1 AFM topography showing SiO$_2$ and MG regions after cleaning procedure. (b) The AFM topography showing the details of the interface between clean and dirty regions

Few-layer graphene as a new 2D support for selective hydrogenation reaction

Cuong PHAM-HUU[a], Kambiz CHIZARI[a], Izabela JANOWSKA[a], Simona M. MOLDOVAN[b], Ovidiu ERSEN[b], Lam D. Nguyen[c], Dominique BEGIN[a], Marc J. LEDOUX[a]

[a] Laboratoire des Matériaux, Surfaces et Procédés pour la Catalyse (LMSPC), UMR 7515 du CNRS, ECPM, Université de Strasbourg, France

[b] Institut de Physique et Chimie des Matériaux de Strasbourg (IPCMS), UMR 7504 du CNRS, Université de Strasbourg, France

[c] Da-Nang University of Technology, University of Da-Nang, 54, Nguyen Luong Bang, Da-Nang, Viet-Nam

cuong.pham-huu@unistra.fr

Catalysis is considered at the core of the success of modern chemistry and industrial development [1]. Indeed, catalysis participates in more than 80 % of the chemical transformations processes to produce food, energy, and commodities for human's day-life. In addition, catalysis also strongly participates to the environmental protection, i.e. off-gas cleaning, automotive exhaust depolution. The development of the new generation of catalysts goes along with the development of new supports which ensure the dispersion and stabilization of the deposited metal active phase [2].

Graphene, a single atomic layer of sp^2-bonded carbon atoms with a honeycomb lattice arrangement has received an over increasing interest [3]. The few-layer graphene (FLG) defines the material constituted by an assembly of graphene layers for which the production and handling are easier than for a single-layer. Graphene and FLG display a relatively high external surface area which allows them to be efficiently employed as catalyst support.

The aim of the present work is to report the use of the FLG as support for palladium in the liquid-phase hydrogenation reaction. The catalytic results will be compared with those obtained on the carbon nanotubes-based catalyst.

The FLG used in this work was obtained by a mechanical exfoliation method of natural graphite following by an ultrasonication step in ethanol medium [4]. TEM micrographs indicate that the FLG is consisted with a relatively large sheet with size ranged between 0.1 to 2 µm (Fig. 1A) and is consisted with a graphene layers ranged from 2 to 15 (Figure 1B). The specific surface area of the FLG, measured by means of the liquid-phase adsorption of the methylene blue, is about 260 m^2. g^{-1}, which is similar to that was obtained with carbon nanotubes material. XPS analysis also indicates the presence of a relatively high number of oxygenated functional groups on the graphene surface which could help the anchorage and dispersion of the palladium active phase on the support surface similarly to that was observed with carbon nanotubes [5, 6]. Representative TEM micrographs of the Pd/FLG catalyst are depicted in Figure 2 and indicate the high dispersion of the palladium metal particles on the graphene surface (Fig. 2A) with an average particle size of around 5 nm (Fig. 2B). In some area of the catalyst few palladium particles with bigger size, i.e. 20 nm, are also observed.

The catalytic performance of the Pd/FLG and Pd/CNT catalysts for the selective hydrogenation of the C=C bond is presented in Figure 3. According to the results the Pd/FLG is more active and selective compared to the Pd/CNT. The high hydrogenation activity of the Pd/FLG could be attributed to the absence of inner channel in the FLG material unlikely to carbon nanotube. In the case of CNT some

metal particles could be localized inside the channel [7] and thus, are less accessible to the reactant leading to a lower activity and selectivity. Cycling tests carried out on the Pd/FLG catalyst confirm the complete absence of any deactivation indicating that no leaching problem has occurred on the catalyst during the test.

In conclusion we have shown that graphene and FLG, 2D material, can be efficiently used as support in the heterogeneous catalysis field. The high amount of the oxygenated functional groups presents on the support surface allows a relatively homogeneous dispersion of the metal particles while the high accessible external surface area of the support significantly increase the exposed metal active surface for performing the reaction.

References

[1] G. Centi, S. Perathoner, Topics Catal. **52** (2009) 948.
[2] C. Pham-Huu, M. J. Ledoux, Catal. Today **102** (2005) 2.
[3] S. Park, R. S. Ruoff, Nat. Nanotechnol. **4** (2009) 217.
[4] I. Janowska, D. Begin, K. Chizari, O. Ersen, P. Bernhardt, Th. Romero, M. J. Ledoux, C. Pham-Huu, PCT/FR2010/000730 (2010).
[5] Ph. Serp, M. Corrias, Ph. Kalck, Appl. Catal. A 253 (2003) 337.
[6] J. P. Tessonnier, O. Ersen, G. Weinberg, C. Pham-Huu, D. S. Su, R. Schlögl, ACS Nano **3** (2009) 2081.
[7] O. Ersen, J. Werckmann, M. Houllé, M. J. Ledoux, C. Pham-Huu, Nano Lett. **7** (2007) 1898.

Figures
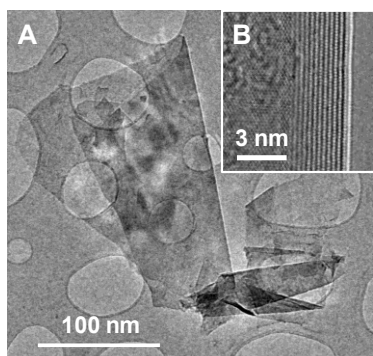
Figure 1. (**A**) TEM micrograph of the FLG. (**B**) HR-TEM of the FLG border containing 12 graphene layers.
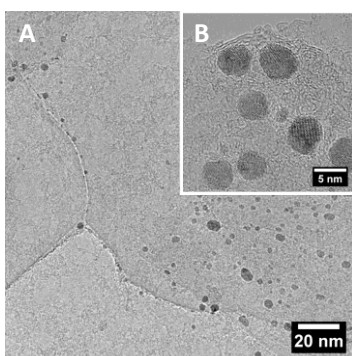
Figure 2. TEM micrographs of the Pd/FLG catalyst with different magnifications.
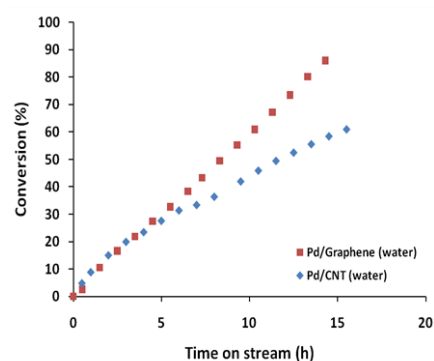
Figure 3. Selective hydrogenation catalytic activity of the Pd/FLG and Pd/CNT.

Chirality of the twisted graphene bilayer

R. de Gail, M. O. Goerbig, F. Guinea, G. Montambaux, and A. H. Castro Neto

Laboratoire de Physique des Solides, UMR 8502, Université de Paris-Sud Bâtiment 510, 91405 Orsay Cedex France

degail@lps.u-psud.fr

The electronic properties of two-dimensional graphitic devices are strongly influenced by the number of graphene layers. Whereas the monolayer band structure is linear at low-energy, the bilayer has a quadratic dispersion. Each system is also associated with a Berry phase of either π (monolayer) or 2π (bilayer) around the degeneracy point of the structure [1].

Graphene bilayer with a twist [2], one layer being slightly misoriented relative to the other, is a new system, which can interpolate between the two situations. For large rotations (misorientations) the two layers are decoupled and the band structure replicates that of the monolayer. On the other hand, for small rotations relative to Bernal stacking, one should recover the bilayer structure. Indeed, band deformations, involving the Dirac cones of each layer, have been observed experimentally [3,4].

We have developed a simple theoretical model [5] based on a previous continuum analysis [2,6], which describes the motion of the cones of different layer, depending on the twist angle. These two cones are separated for a non-zero rotation due to the rotation of the Brillouin zone of the upper layer relative to the lower one and eventually merge to create a quadratic dispersion in case of perfectly AB-stacked bilayer.

This merging is accompanied with peculiar topological properties, since it is derived via symmetry arguments of our Hamiltonian that the two cones each carry the same Berry phase, around the two Dirac points, for a given energy level. This has to be contrasted with previous study of merging of Dirac cones where the Berry phases are opposite [7]. This topological scenario can be tested through the quantum Hall effect where a robust zero-energy Landau level is predicted, which cannot be lifted by relatively strong magnetic field.

References

[1] A. H. Castro Neto, F. Guinea, N. M. R. Peres, K. S. Novoselov and A. K. Geim, Rev. Mod. Phys. **81** (2009) 109.

[2] J. M. B. Lopes dos Santos, N. M. R. Peres, and A. H. Castro Neto, Phys. Rev. Lett. **99**, (2007) 256802.

[3] G. Li, A. Luican, J. M. B. Lopes dos Santos, A. H. Castro Neto, A. Reina, J. Kong, and E. Y. Andrei, Nature
Physics **6** (2010) 109.

[4] A. Luican, Guohong Li, A. Reina, J. Kong, R. R. Nair, K. S. Novoselov, A. K. Geim, E.Y. Andrei arXiv: 1010.4032v1 (2010).

[5] **R. de Gail**, M. O. Goerbig, F. Guinea, G. Montambaux, and A. H. Castro Neto, In preparation

[6] R. Bistritzer and A. H. MacDonald, arXiv:1009.4203 (2010).

[7] G. Montambaux, F. Piéchon, J.-N. Fuchs, and M.O. Goerbig, Phys. Rev. B **80** (2009) 153412; Eur. Phys. J. B **72** (2009) 4.

Influence of the initial stepped SiC surface on epitaxial graphene formation

M.H. Oliveira Jr., T. Schumann, R. Hey, J.M.J. Lopes and H. Riechert

Paul-Drude-Institut für Festkörperelektronik, Hausvogteiplatz 5-7, 10117 Berlin, Germany
oliveira@pdi-berlin.de

Due to its singular properties [1,2], graphene is currently considered to be one of the most promising materials for future electronic applications. Regarding its synthesis, several methods have been employed to prepare graphene layers, from which we can mention mechanical and chemical exfoliation, CVD on catalytic metal surfaces, and epitaxial growth on SiC by surface graphitization. This last approach offers particular potential since it can be realized on wafer size scale [3], without the need of further transferring the graphene layer to another insulating substrate (due to the insulating/semi-insulating nature of the SiC). However, in order to achieve an optimized growth of uniform and high-quality epitaxial graphene on SiC substrates, it is fundamental to understand the phenomena behind the graphene formation and its dependence on the surface step structure of the initial SiC surface. Several details of the nucleation and growth process, including step bunching effects resulting in large and homogeneous graphene terraces, are still under debate. In this work, we will present a study of the formation of epitaxial graphene on stepped SiC surfaces having different surface morphologies obtained as a function of the temperature during H-etching.

The samples investigated in this work were prepared using 6H-SiC(0001) substrates. H-etching and graphene growth were both performed in a cold wall reactor equipped with an induction heating system. The H-etching was carried out in a forming gas (95 % Ar and 5 % H_2) atmosphere at 900 mbar for 15 min. Different temperatures ranging from 1350 ºC to 1550 ºC led to SiC surfaces with different step heights and terrace widths. The step heights observed on the substrate before graphene preparation ranged from about 0.3 nm (non-etched sample) up to about 16 nm for the sample etched at 1550 ºC, while the terrace widths varied from 160 nm up to 5 μm, respectively. After the etching, high-quality epitaxial graphene layers were grown at 1600 ºC in a 900 mbar Ar atmosphere, as proposed by Emtsev *et al.* [4].

Figures 1 shows AFM profiles of a non-etched SiC surface before [1(a)] and after [1(b)] graphene formation, as well as an image of the graphene surface obtained by AFM [1(c)]. It is observed that due to step bunching, even a SiC surface with narrow terraces (~160 nm wide) and very small step heights (~0.3 nm) gives rise to a graphene layer showing macro-terraces (up to 4 μm wide) and large steps (up to 8 nm). The same effect [see figures 1(d),(e), and (f)] is observed for graphene prepared on SiC surfaces offering larger terraces (~0.5 μm wide) and step heights around 0.75 nm (i.e. half of c_{6H-SiC}). However, it is interesting to observe that for a stepped SiC surface with very wide terraces (~5 μm) and even higher steps (16 nm – more than 10 times c_{6H-SiC}), the subsequent graphene growth does not modify the initial surface morphology. As shown in Figs. 2 (a) and (b), there is no significant change on the terrace dimensions before and after graphene growth. Consequently, the profiles in Figs. 2 (c) and (d) reveal that the step heights remain almost unaltered as well. Both findings suggest that the step bunching process is suppressed in this case. Raman spectroscopy analysis reveal that, even though the graphene surface morphology seems to be much more regular for the sample initially etched at 1550 ºC (the case where no additional step bunching is observed during graphene formation), it presents much broader G (29 cm^{-1}) and 2D (61 cm^{-1}) peaks and a 2D peak shift of 42 cm^{-1} compared to the other samples [see Fig 2(e)]. One possible explanation for this is that, due to the absence of step bunching, the multilayer graphene formation at step edges becomes more pronounced. However, this hypothesis

is currently under investigation. Finally, the effects of a graphene growth on SiC with or without step bunching will be also discussed taking into account the resulting transport properties of the layers.

References

[1] K.S. Novoselov et al. Nature, **438** (2005) 197.
[2] Y. Zhang et al. Nature, **438** (2005) 201.
[3] Y.M. Lin et al. Science, **327** (2010) 662.
[4] K.V. Emtsev et al. Nature Materials 8, **3** (2009) 203.

Figures
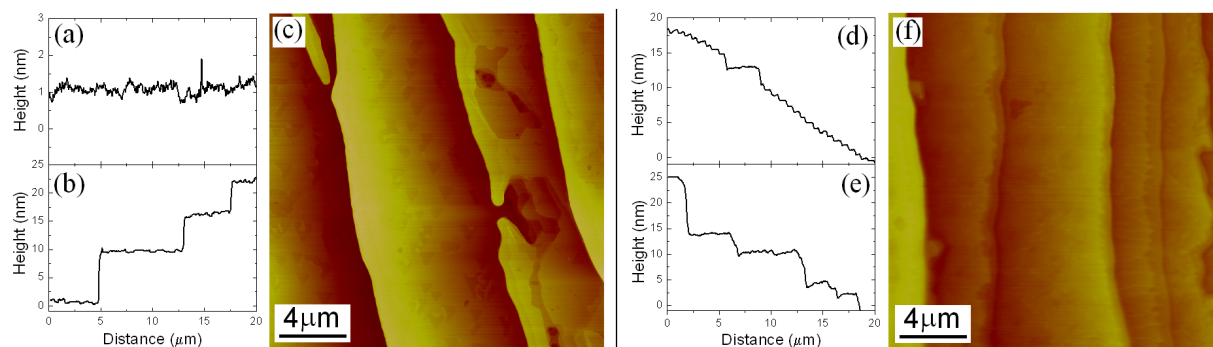
Figure 1
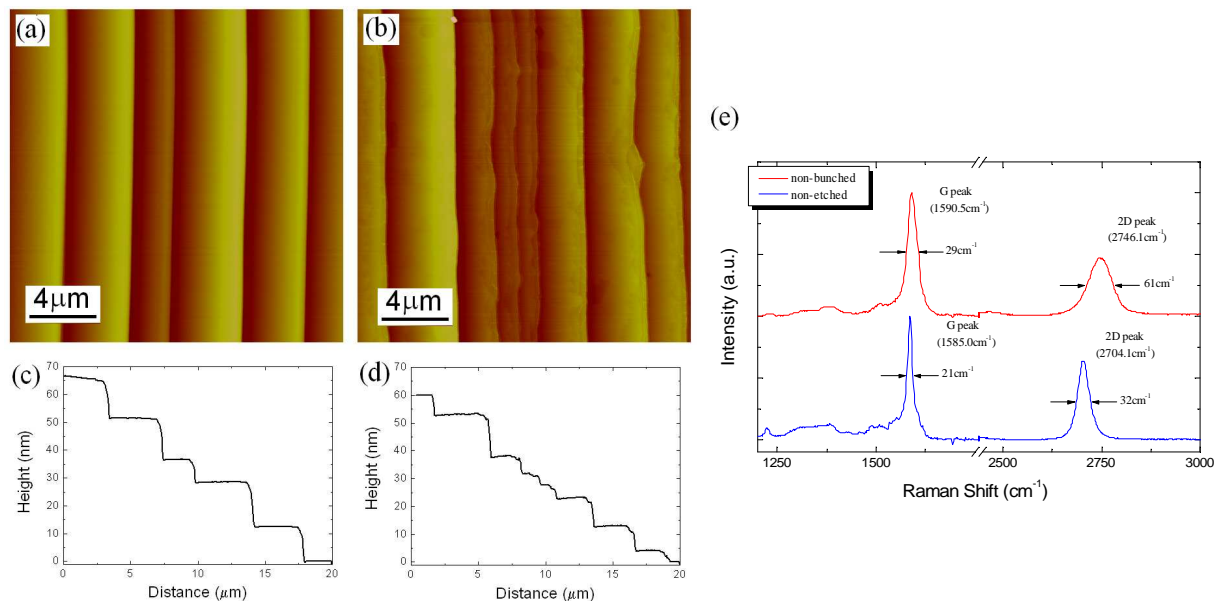
Figure 2

Figure caption

*Figure 1 – Comparison between the profiles for a non-etched SiC sample before **(a)** and after **(b)** the graphene growth, as determined by AFM. AFM image of the surface after graphene formation **(c)**. The same comparison is presented [**(d)** and **(e)**] for a SiC sample etched at 1500 ºC. The respective AFM image of the surface after graphene formation is shown in **(f)**.*

*Figure 2 – Surface image obtained by AFM for the sample etched at 1550 ºC before **(a)** and after **(b)** graphene preparation, and their respective profiles **(c)** and **(d)**. Even though the graphene surface morphology in this case seems to be more regular as compared to the other samples [see Figs. 1 (c) and (f)], its Raman spectrum **(e)** shows broader G and 2D peaks, what may be related to the existence of multilayer graphene on the step edges due to the absence of a step-bunching process.*

Vitamin C as an innocuous and safe reductant for the preparation of graphene suspensions from graphite oxide

M. J. Fernández-Merino, L. Guardia, J. I. Paredes, S. Villar-Rodil, P. Solís-Fernández, A. Martínez-Alonso, and **J. M. D. Tascón.**

Instituto Nacional del Carbón, CSIC, Apartado 73, 33080 Oviedo, Spain
tascon@incar.csic.es

Liquid-phase processing of graphite and its derivatives (particularly graphite oxide) is currently a very attractive option for the high-throughput production of colloidal suspensions of graphene [1, 2]. This preparation typically involves a reduction step using hydrazine [1], but the use of such a reagent in the large-scale implementation of this approach is not desirable due to the high toxicity and potentially explosive character of this compound [3].

In the present work, we compare the deoxygenation efficiency of graphene oxide suspensions by different reductants (sodium borohydride, pyrogallol, and vitamin C, in addition to hidrazine), as well as by heating the suspensions under alkaline conditions [4]. The progress of reaction as a function of time was monitored through UV-vis absorption spectroscopy. It is well-known that the position of the absorption peak of graphene oxide dispersion gradually shifts to red from a value of 231 nm as reduction proceeds [1].

The reduced dispersions were processed into paper-like films, and characterized by TGA, ATR-FTIR and XPS spectroscopy, and also by electrical conductivity measurements.

The spectroscopic techniques showed a decrease in the intensity of the bands associated with oxygen functional groups that depends on the reducing agent used (Figure 1, Figure 2). Thus, Figure 1 shows that the IR bands at 3000-3500 cm^{-1} (O-H stretching vibrations) and 1720 cm^{-1} (C = O stretching vibrations from carbonyl and carboxyl groups) decreased significantly with increasing reducing power. Figure 2 shows that the XPS band at 286.6 eV (attributed to carbons in hydroxyl and epoxy groups and also possibly to C-C bonds in defected structures [5]) virtually disappears when using the most effective reducing agents (ascorbic acid and hydrazine). These data were corroborated by means of TGA and electrical conductivity measurements.

In almost all cases, the degree of deoxygenation attainable and the subsequent restoration of relevant properties (e.g., electrical conductivity) lag significantly behind those achieved with hydrazine. Only vitamin C was found to yield highly reduced suspensions in a way comparable to those provided by hydrazine. Stable suspensions of vitamin C-reduced graphene oxide can be prepared not only in water, but also in common organic solvents, such as N,N-dimethylformamide (DMF) or N-methyl-2-pyrrolidone (NMP). These results open the perspective of replacing hydrazine in the reduction of graphene oxide suspensions by an innocuous and safe reductant of similar efficacy, thus contributing to facilitate the use of graphene-based materials for large-scale applications.

Acknowledgements

References

[1] Li, D., Müller, M.B., Gilje, S., Kaner, R.B., Wallace, G.G. Nature Nanotechnology, **3** (2008) 101.
[2] Park, S., Ruoff, R.S. Nature Nanotechnology, **4** (2009) 217.
[3] Schmidt, E.W. Hydrazine and its Derivatives; Wiley-Interscience: New York, 2001.
[4] Fernández-Merino, M.J., Guardia, L., Paredes,J.I., Villar-Rodil, S., Solís-Fernández, P., Martínez-Alonso, A. and Tascón J.M.D. J Phys Chem C, **114** (2010) 6426.
[5] Paredes,J.I., Villar-Rodil, S., Martínez-Alonso, A. and Tascón, J.M.D. Langmuir, **24** (2008) 10560.

Figures
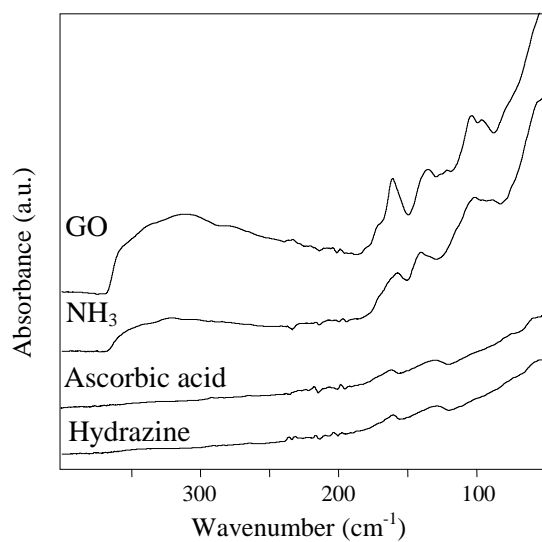
Figure 1. *ATR-FTIR spectra of unreduced graphene oxide and deoxygenated samples.*
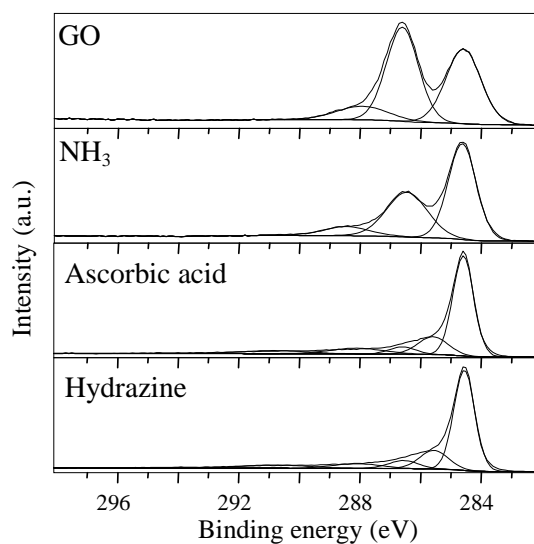
Figure 2. *High resolution C1s X-ray photoelectron spectra for unreduced graphene oxide and deoxygenated samples.*

Large signal graphene spintronics

B. Dlubak[1], P. Seneor[1], A. Anane[1], V. Garcia[1], K. Bouzehouane[1], C. Deranlot[1], B. Servet[2], S. Xavier[2], R. Mattana[1], W. A. De Heer[3], C. Berger[3,4], F. Petroff[1], and A. Fert[1]

[1]*Unité Mixte de Physique CNRS/Thales, 91767 Palaiseau, France and University of Paris-Sud 11, 91405 Orsay, France,*
[2] *Thales Research and Technology, 91767 Palaiseau, France,*
[3] *Georgia Institute of Technology, Atlanta, USA,*
[4] *Institut Néel, Grenoble, France*

In the quest for large signal spintronics, graphitic compounds were already demonstrated as a successful alternative to inorganic semiconductors: long spin diffusion length (50 μm) and large spin signals (80 MΩ) have been achieved for carbon nanotubes [1]. This result awaits now to be extended to wafer scale materials like epitaxial graphene. The high mobility of graphene (up to $10^7 cm^2/Vs$) [2,3] combined with the long predicted spin life-time make it a very promising material for spintronics devices: the spin diffusion length is expected to exceed 100 μm. Successful spin dependent transport has already been demonstrated in micron-sized exfoliated graphene sheets [4,5], with reported spin-diffusion length in the order of 1-4 μm and spin signal of few hundred ohms, more than 4 orders of magnitude lower than for nanotubes. Taking advantage of the full potential of graphene for spintronics will therefore require material and device optimization.

Working on spin injection, transport and detection in graphene, we focused first on the physics involved at the injection. It has been shown since 2000 [6,7] that an interfacial resistance is crucial for efficient spin injection in a semiconductor channel. The most common and efficient tunnel barriers used in the field of spintronics are sputtered Al_2O_3 and MgO. Hence, we chose to study the growth on graphene of these high quality tunnel barriers with thicknesses tuned for efficient spin injection and detection with graphene. To grow 1nm thick layer of Al_2O_3, we first deposit a 0.6nm Al film, and then oxidize it in a pure O_2 atmosphere. In the case of MgO, we directly deposit a 1nm film from a sintered MgO target.

We will present a Raman spectroscopy study quantifying the impact of the barriers growths on the graphene structure followed by spin-dependent transport measurements. Raman spectroscopy point to dramatic effect of sputtered MgO compared to Al_2O_3. When one wants to make use of standard tunnel junctions, Al_2O_3 is shown as definitely more suitable for spin transport together with bilayers (and other multilayers) graphene. The electrical characterization of these Al_2O_3 tunnel barriers reveals their adequacy in order to access high spin signals.

We carried transport measurements on lateral spin valves (Fig. 1.) in exfoliated graphene as well as in epitaxial graphene on SiC. We achieved spin signals in the MΩ range in two terminal geometries. These signals analyzed through an adapted injection/detection model [7] points to a long spin diffusion length in our systems.

References

[1] L. Hueso et al. Nature, 445, 410-413 (2007)
[2] S. Morozov et al., *Phys. Rev. Lett. 100*, 016602 (2008)
[3] P. Neugebauer, *Phys. Rev. Lett. 103*, 136403 (2009)
[4] N. Tombros et al., *Nature 448*, 571-574 (2007)
[5] W. Han et al., *Phys. Rev. Lett. 105, 167202* (2010)
[6] G. Schmidt et al., *Phys. Rev. B 62*, R4790 (2000)
[7] A. Fert & H. Jaffrès, *Phys. Rev. B 64*, 184420 (2001)

`

Combined AFM, Raman and Tip Enhanced Raman studies of graphene with different number of layers

P. Dorozhkin, A. Shchokin, E. Kuznetsov, S. Timofeev and V. Bykov

NT-MDT Co., build. 100, Zelenograd Moscow, 124482 Russia
dorozhkin@ntmdt.com

Graphene flakes (1,2,3 and 4 layers) on gold substrate are investigated by different AFM and spectroscopy techniques. We study in details how the thickness (number of monolayers) in graphene affects its physical properties: surface potential (work function), local friction, elastic modulus, capacitance, conductivity, charge distribution, Raman and Rayleigh light scattering etc. Results for graphene flakes are qualitatively compared to those for carbon nanotubes of different diameters. We show how electrostatic charging of graphene flakes can be effectively measured and modified by AFM cantilever. Studies are performed both in ambient air conditions and in controlled atmosphere and humidity.

We also present graphene measurements by Tip Enhanced Raman Spectroscopy (TERS) or "nano-Raman" mapping realized using integrated AFM-Raman system. We demonstrate near field Raman enhancement effect due to resonant interaction of light with localized surface plasmon at the apex of a metal AFM probe. Plasmonic and near field nature of the Raman enhancement is proven by a number of ways: dependence of the enhancement on the excitation wavelength and polarization, enhancement versus tip-sample distance curves, observation of selective enhancement of Raman signal from thin surface layers of the sample etc. Finally, the ultimate performance of TERS is demonstrated by measuring Raman 2D maps with *subwavelength lateral resolution* – determined not by the wavelength of light, but by the localization area of the surface plasmon electromagnetic field.

Figures
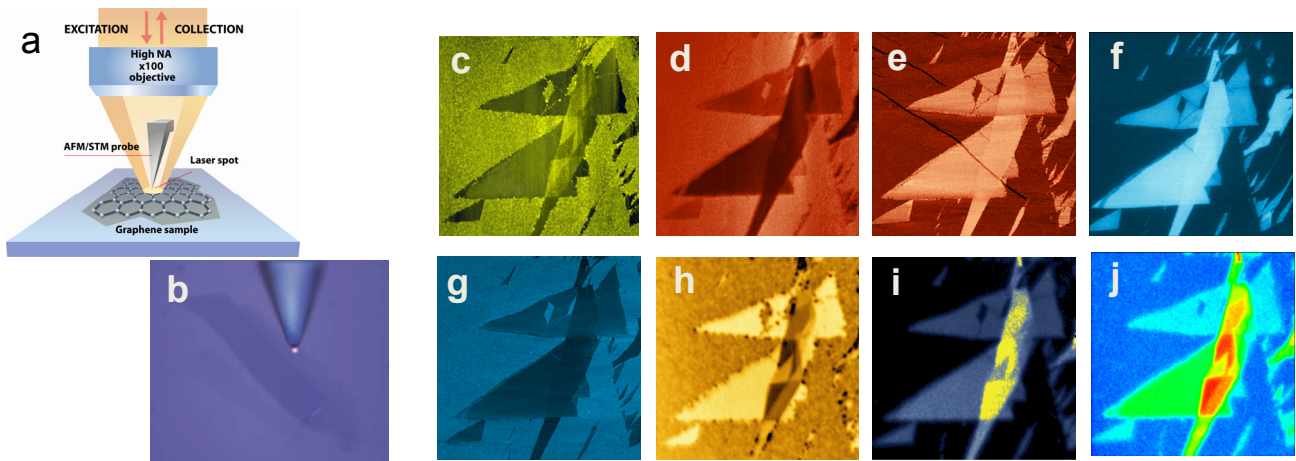
Figure Caption

a), b). AFM – Raman configuration: schematics (a) and white light image (b); Raman laser is tightly (400 nm spot diameter) focused onto the very end of a "nose"- shaped AFM cantilever using 100x objective; Graphene layer is positioned below the cantilever and under the laser spot; while scanning the sample, AFM and Raman data is obtained simultaneously.

c) – g). Various AFM images characterizing different physical properties of the sample - Topography (c), Electrostatic Force (d), Force Modulation (elastic properties) (e), Kelvin Probe (f), Lateral Force (g).

h) – j). Confocal optical images – Rayleigh light (h), Raman 2D band mass center (i), Raman G band intensity (j).

Acoustic phonons and spin coherence in graphene nanoribbons

Matthias Droth and Guido Burkard

Universität Konstanz, 78457 Konstanz, Germany

Electronic mail: matthias.droth@uni-konstanz.de

A spintronics approach to quantum information science is considered promising due to the readily available expertise in solid state physics and possibly long coherence times [1]. We investigate a qubit implementation as real electron spin in graphene nanoribbon quantum dots. This system is particularly interesting because it allows for non-local coupling of qubits [2]. Spin coherence is determined by the coupling to nuclear spins and the lattice and the relaxation time T_1 depends on interaction with phonons. Starting from a continuum model, we derive a full phonon field theory for acoustical phonon modes in a graphene nanoribbon and at the center of the Brillouin zone. We consider fixed boundary conditions at the edges of the quasi-one-dimensional nanoribbon as well as open boundaries. In the latter case, the usual q^2-dependence for out-of-plane modes in bulk is cut off at the zone center (near $q = 0$), where we find a linear dispersion. The transverse and longitudinal sound velocities of the in-plane modes match the literature values for comparable systems [3] and, as expected, all modes approach bulk behavior for wavelengths much smaller than the ribbon width.

[1] D. Loss and D. P. DiVincenzo, Phys. Rev. A **57**, 120-126 (1998).
[2] B. Trauzettel et al., Nature Physics **3**, 192-196 (2007).
[3] L. A. Falkovsky, Phys. Lett. A **372**, 5189-5192 (2008).
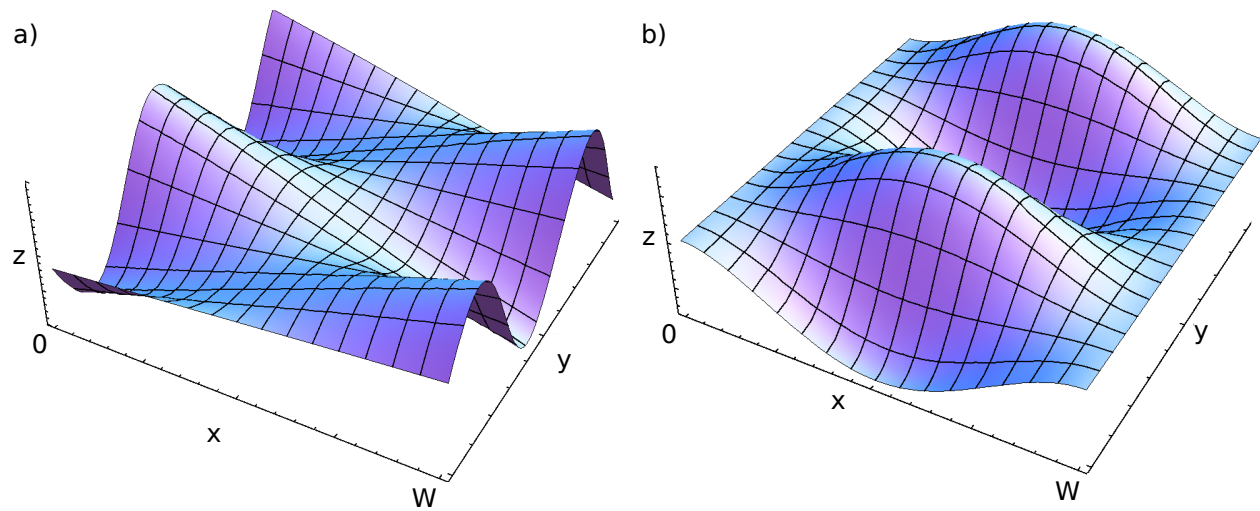
Figure: The graphene nanoribbon lies in the x-y-plane, with free (a) and fixed (b) boundaries at $x = 0, W$. The ribbon length is assumed to be much larger than the ribbon width, thus allowing for periodic boundaries in the y-direction. a) Acoustic out-of-plane mode for free boundaries. b) Acoustic out-of-plane mode for fixed boundaries. We also discuss in-plane modes.

Ballistic transport at room temperature in micrometer size multigraphene

S. Dusari+, J. Barzola-Quiquia+, P. Esquinazi+, N.Garcia*

+Division of Superconductivity and Magnetism, Universität Leipzig,
Faculty of Physics and Earth Sciences, Institute for Experimental Physics II,
Linnéstr. 5, 04103 Leipzig, Germany
*Laboratorio de Física de Sistemas Pequeños y Nanotecnología, Consejo Superior de
Investigaciones Científicas, Serrano 144, E-28006 Madrid, Spain
Contact: srujana@physik.uni-leipzig.de

As an emergent material for electronic applications, graphite and graphene and their electrical transport properties have become a subject of intense focus. The intrinsic values of the carrier mobility and density of the graphene layers inside graphite, the well known structure built on these layers in the Bernal stacking configuration, are not well known mainly because most of the research was done in rather bulk samples where lattice defects hide their intrinsic values. By performing transport measurements through micro and submicro constrictions in ~10 nm thick graphite samples, we observe drastic increase in the resistance decreasing the constriction width. Our experimental observations indicate that electrons behave ballistically even at room temperature and with mean free path of the order of microns. The values obtained for the mobility ($\mu \sim 10^7 \mathrm{cm}^2 \mathrm{v}^{-1} \mathrm{s}^{-1}$) and density of the electrons ($n \sim 10^8 \ \mathrm{cm}^{-2}$) indicates that the graphene layers inside graphite are of higher quality than single ones. The decrease of magneto resistance with decreasing constriction width also indicates that the carrier mean free path is larger than few microns at room temperature. These distinctive transport and ballistic properties have important implications for understanding the values obtained in single graphene and in graphite as well as for implementing in nanoelectronic devices.

The imaging properties of polyoxometalate ions on curved graphene

M.A. Dyson, N. R. Wilson, and J. Sloan

Department of Physics, University of Warwick, Coventry, CV4 7AL, UK,
j.sloan@warwick.ac.uk

Recently we have demonstrated that polyoxometalate (POM) ions, formed from various assemblies of tungsten oxide polyhedra, and of the form $[W_6O_{19}]^{2-}$ or $[\gamma\text{-}SiW_{10}O_{36}]^{8-}$ can be imaged by conventional and aberration corrected transmission electron microscopy (AC-TEM) when supported either within carbon nanotube capillaries[1] or on monolayer graphene oxide.[2,3] These experiments have permitted the observation of small structural distortions within individual anions[1] and have also enabled for the first time the direct visualization of the surface interaction of POMs with hydroxyl functionalities on the surface of graphene oxide.[2] Critical to these studies has been a detailed understanding of the imaging properties of both the respective anions and also the specimen supports which inevitably produce a strong contribution to the composite contrast of both specimen and support.

What is perhaps less well understood is the contribution that the imaging properties of supported molecular scale species supported on ultrathin carbon monolayers (or within nanotubes) can make to the understanding of the local curvature and other morphological features of supporting material. In this, the experimentally imaged polyoxometalates are well-placed to make a significant contribution in that their image contrast both as a function of relative orientation[1,2] and also defocus[1] can readily be simulated. As in certain projections these anions offer either single or pairs of heavy tungsten atoms (Z=74) arranged parallel to the electron beam, the image contrast due to these anions is quantitative and can be used as a measure of local focusing conditions. As the local specimen height and electron microscope objective lens defocus are complementary, the relative focusing properties of individual polyoxometalate anions as a function of relative height can also be simulated and in principle can be used as a local probe for height variation and curvature within a strictly monolayer support film.[4] In this study we therefore assess the imaging properties of individual polyoxometalate ions as a function of the local height of a monolayer support film, in this instance graphene carbon.

For these studies, a version of the transmission electron microscope image simulation code based on the multislice method was implemented in Mathematica 8. This allows the program to take advantage of the recent advances in GPU computing to increase the calculation speed for massively parallel problems and increase the accuracy over previous multislice simulations using the enhanced computing power available. This removes the restrictions inherent in some simulation codes on either the number of atoms that can be simulated or the resolution of the images that can be produced; additionally there are no limits on either the sample size or shape. The simulation can take an input file specifying the positions of all the atoms within the sample and produce a simulated TEM image from the sample with control over aperture size, defocus, spherical aberration, two and three fold astigmatism, accelerating voltage and specimen tilt among others. This is done by splitting the sample into numerous slices perpendicular to the direction of the electron beam, and then calculating the projected atomic potential for each slice. The electron wave can then be successively transmitted through each slice and propagated through a vacuum to the next slice to calculate the wave function upon exiting the sample.

Simulations of individual polyoxometalate anions were then produced for small sections of graphene supporting a single anion (i.e. either the lacunary $[\gamma\text{-}SiW_{10}O_{36}]^{8-}$ Keggin ion or the $[W_6O_{19}]^{2-}$ Linqvist ion) in order to evaluate the effects of objective lens defocus on the anion, the relative orientation of the respective anion (i.e. Figs. 1(a)-(h)) and the coefficient of spherical aberration (set to 0.02 mm in order to reproduce an aberration-corrected TEM). As can be seen, we see that the local imaging characteristics of a given anion in a given orientation vary as a function of defocus. Given the variation in contrast as a function of defocus, we would expect that performing the complementary operation of simulating a graphene film with applied curvature and then varying the local height of the anions would produce a similar progression in contrast and this indeed the case (i.e. Figs. 2(a)-(c)). In this second set of simulations we find a commensurate variation in the image contrast due to both the specified polyoxometalate anions (and the $[W_6O_{19}]^{2-}$ ion in two distinct orientations) as a function of their orientation with respect to the imaging electron beam and also as a function of relative height on the film. Although we have deliberately exaggerated the local curvature of the theoretical graphene monolayer support, we find a sufficient variation in the local contrast of the anions between height differences of 2-5 nm that it ought to be able to image this difference for experimental curved graphene films.

References

[1] J. Sloan, G. Matthewman, C. Dyer-Smith, A-Y. Sung, Z. Liu, K. Suenaga, A. I. Kirkland, E. Flahaut, ACS Nano **2**, (2008) 966.

[2] J. Sloan, Z. Liu, K. Suenaga, N. R. Wilson, P. A. Pandey, L. M. Perkins, J. P. Rourke, and Ian J. Shannon, Nano Lett. **10**, (2010) 4600.

[3] N. R. Wilson, P. A. Pandey, R. Beanland, R. J. Young, I. A. Kinlock, L. Gong, Z. Liu, K. Suenaga, J. P. Rourke, S. York, J. Sloan, ACS Nano, **3**, (2009) 2547.

[4] J. Sloan et al., submitted.

Figures
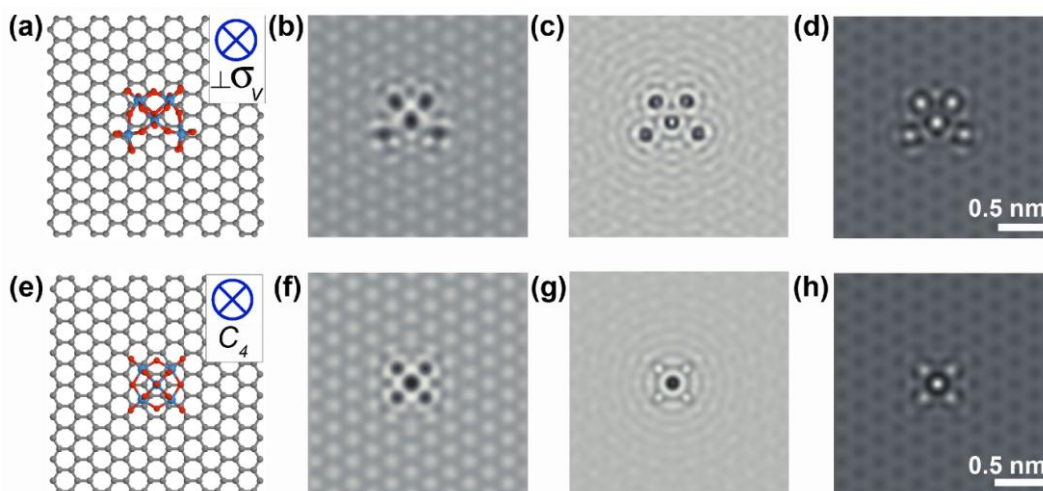
Figure 1. (a) Composite structure model of the $[\gamma\text{-}SiW_{10}O_{36}]^{8-}$ lacunary Keggin ion mounted on graphene projected in a direction orthogonal to its σ_v mirror plane which is arranged parallel to the supporting graphene plane. **(b)** Underfocus image simulation of (a) ($C_s = 0.02$ mm and $\Delta f = -5$ nm). **(c)** At focus image simulation of (a) ($C_s = 0.02$ mm and $\Delta f = 0$ nm). **(d)** Over focus image simulation of (a) (computed with $C_s = 0.02$ mm and $\Delta f = +5$ nm). **(e)** Composite structural model with the $[W_6O_{17}]^{2-}$ Linqvist ion projected along its C_4 rotation axis with the graphene support arranged with its plane orthogonal to the axis and the electron beam direction. **(f)** Underfocus image simulation of (e) ($C_s = 0.02$ mm and $\Delta f = -5$ nm). **(g)** At focus image simulation of (e) ($C_s = 0.02$ mm and $\Delta f = 0$ nm). **(h)** Over focus image simulation of (e) ($C_s = 0.02$ mm and $\Delta f = +5$ nm).
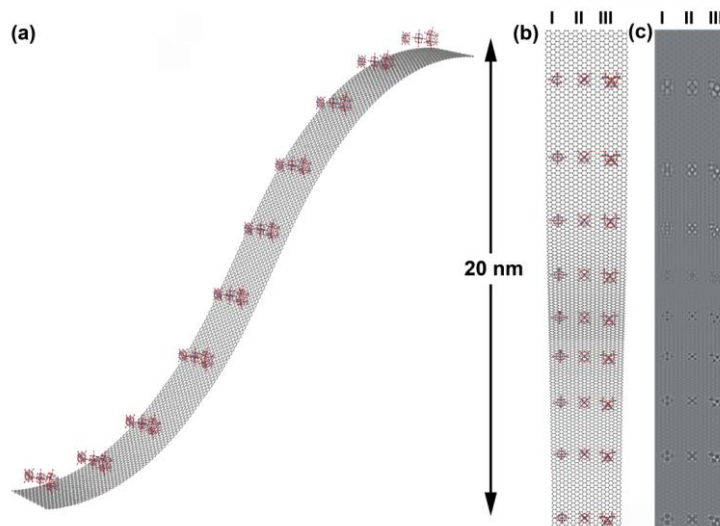
Figure 2(a) Schematic view of a curved graphene sheet with a height of 20 nm with both $[\gamma\text{-}SiW_{10}O_{36}]^{8-}$ lacunary Keggin ions and $[W_6O_{19}]^{2-}$ Linqvist ions arranged at different heights on the curved sheet. **(b)** Top down projection of the sheet in (a) showing effectively columns of $[W_6O_{19}]^{2-}$ Linqvist ions projected along C_2 (i.e.. column **I**) and C_4 (i.e. column **II**) and also the the $[\gamma\text{-}SiW_{10}O_{36}]^{8-}$ lacunary Keggin ion arranged with its σ_v mirror plane arranged orthogonal to the electron beam direction (i.e. column **III**). Because of the deliberately exaggerated curvature of the graphene sheet, the respective orientations of the anions have been adjusted so that the relevant projections are aligned parallel to the electron beam direction (c). Optimum focus image simulation of the model in (b).

Plasmonic-Enhanced Photodetection in Graphene

T.J. Echtermeyer[1], L. Britnell[2], A. Lombardo[1], P.K. Jasnos[1], R. V. Gorbachev[3], A. N. Grigorenko[2], A. K. Geim[3], A. C. Ferrari[1], K. S. Novoselov[2]

1 Department of Engineering, University of Cambridge, Cambridge CB3 0FA, UK
2 School of Physics & Astronomy, University of Manchester, Oxford Road, Manchester M13 9PL, UK
3 Centre for Mesoscience and Nanotechnology, University of Manchester, Oxford Road, Manchester M13 9PL, UK

The electrical and optical properties of graphene make it an ideal material for photonics and optoelectronics [1]. Photodetectors based on graphene with a bandwidth up to 16 GHz have been demonstrated [2]. However, these have low responsivities [2,3].

Graphene-based photodetectors rely on a p-n junction whose electric field at the junction area separates the light generated electron-hole pairs [3]. One of the possible ways to introduce such a junction in graphene is to use a metal contact, where the deposited metal introduces a Fermi-level shift so that a pn-junction forms in the vicinity of the contacts [4].

The interaction of light with a metal particle results in collective oscillations of the free electron gas leading to a strong amplification of the electric field in the vicinity of such metal particles [5,6]

Combining graphene with plasmonic nanostructures allows for field enhancement exactly in the area of the p-n junction. As a result the photovoltage can increase. Also, the plasmonic response of metal nanostructures depends on their geometry and on the wavelength of the incident light [7,8]

Here we fabricate graphene-based photodetectors by mechanical exfoliation of graphene on $Si+SiO_2$ and subsequent contact and nanostructure definition by e-beam lithography, metal deposition and lift-off. Fig. 1 shows an optical micrograph of one of our devices. Nanostructured metal gratings with 300nm pitch are present. The inset shows an AFM micrograph of such a grating. The devices are characterized by photovoltage mapping at different gate voltages, laser powers, light polarization and wavelengths. Fig. 2 shows a photovoltage map of a typical device. At the nanostructure, enhancement of the photovoltage occurs. Depending on wavelength, a photovoltage enhancement of up to 20 times is measured. Further, our detectors show a dependence of the generated photovoltage on light polarization, allowing potential detection of the incoming light polarization.

References

[1] F. Bonaccorso, Z. Sun, T. Hasan, A.C. Ferrari, Nat. Photonics, **4**, 611 (2010).
[2] T. Mueller, F. Xia, P. Avouris, Nat. Photonics, **4**, 297 (2010).
[3] F. Xia, T. Mueller, R. Golizadeh-Mojarad, M. Freitag, Y. Lin, J. Tsang, V. Perebeinos, P. Avouris, Nano Lett., **9**, 1039 (2009).
[4] G. Giovannetti, P. A. Khomyakov, G. Brocks, V. M. Karpan, J. van den Brink, and P. J. Kelly, Phys. Rev. Lett.**101**, 026803 (2008).
[5] S. Nie, S.R. Emory, Science **275**, 1102 (1997).
[6] F. Schedin et. al., ACS Nano **4**, 5617 (2010).
[7] W.L. Barnes, A. Dereux, T.W. Ebbesen, Nature **42**, 824 (2003).
[8] S.A. Meier, *Plasmonics:Fundamentals and Applications*, Springer (2007).

Figures
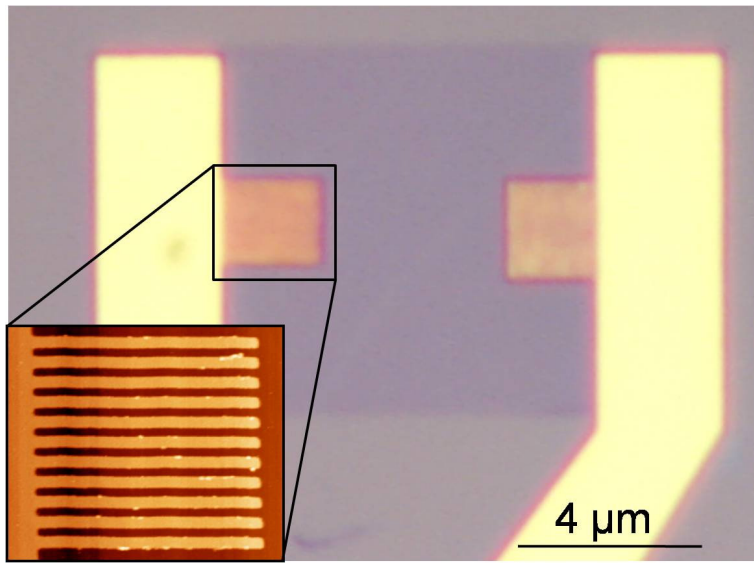
Fig. 1: Optical and AFM micrograph of a graphene-based photodetector with metal nanostructure.
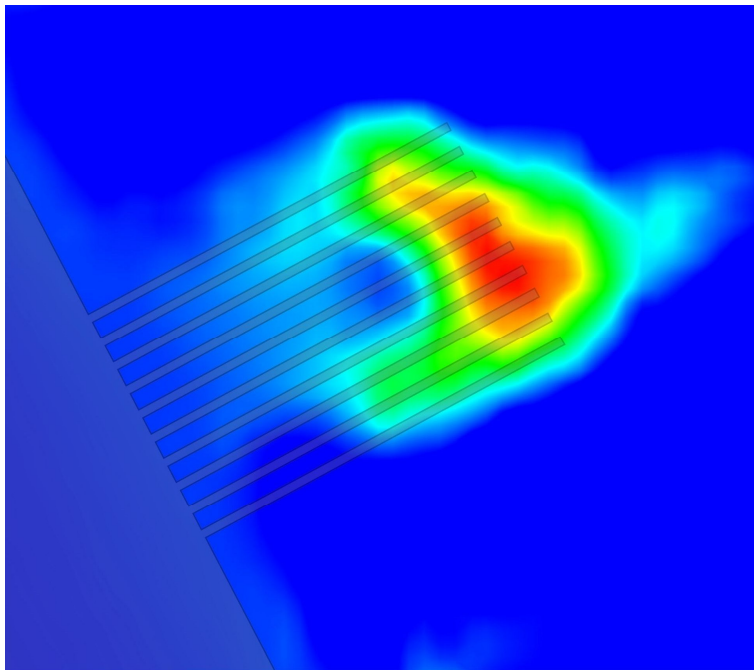
Fig. 2: Photovoltage map of a metal nanostructure enhanced graphene-based photodetector.

Tailoring electrical properties of chemically derived graphene for graphene-based monolithic devices

Goki Eda[1], Paul H. Wöbkenberg[2], James Ball[2], Thomas D. Anthopoulos[2]
Manish Chhowalla[3]

[1]Department of Materials, Imperial College London, Exhibition Road, London, United Kingdom
[2]Department of Physics, Imperial College London, Exhibition Road, London, United Kingdom
[3]Department of Materials Science and Engineering, Rutgers University
607 Taylor Road, Piscataway, NJ 08854, U.S.A.

g.eda@imperial.ac.uk

Chemically derived graphene exhibits a wide range of electrical and optical properties depending on its chemical structure [1]. The versatile properties of this material suggest that graphene-based monolithic electronic devices can be realized by carefully fine-tuning the chemistry and structure of the material and implementing it into device structures [2,3]. In this contribution, we discuss the dielectric properties of graphene oxide (GO) and its implementation into devices as gate dielectric and non-volatile memory elements.

Graphene oxide is an electrical insulator with large in-plane resistivity ($\sim 10^{12}$ Ω/sq) due to strong electronic disorder induced by covalent oxygen functionalization. While many studies have focused on the electrical properties of GO in the in-plane direction, its electrical properties in the out-of-plane direction have received much less attention. Here we show that the out-of-plane electrical properties of GO thin films are highly dependent on film thickness and water adsorption. The dielectric constant was found to vary between 3 and 12 depending on humidity level. The changes in dielectric constant took place immediately when GO was exposed to air from vacuum, reflecting the highly hygroscopic nature of the material. The out-of-plane current-voltage characteristics could be approximated by space-charge-limited conduction and low-bias resistivity increased rapidly with increasing film thickness.

We found that with optimized film thickness, GO thin films exhibit sufficiently high capacitance and low leakage current to be used as a gate dielectric material for field effect devices. We demonstrate operation of monolithic graphene-based top-gated field effect device consisting of partially oxidized graphene (POG) [4] as the channel material and GO as the gate dielectric (Figure 1). We further discuss electrode metal dependence on the electrical behavior of GO thin films and a non-volatile bistable memory effect which we believe arises from electrochemical modification of GO.

Our results demonstrate the viability of using chemically derived graphene as a solution-processable gate dielectric and non-volatile memory material and suggest possibility of further optimization via improved chemical engineering.

References

[1] S. Park and R.S. Ruoff, Nature Nanotech. **4** (2009) 217.
[2] G. Eda and M. Chhowalla, Adv. Mater. **22** (2010) 2392.
[3] P. H. Wöbkenberg, G. Eda, D.-S. Leem, J. C. de Mello, D. D. C. Bradley, M. Chhowalla and T. D. Anthopoulos, Adv. Mater. To appear.
[4] G. Eda, J. Ball, C. Mattevi, Muge Acik, Luca Artiglia, Gaetano Granozzi, Yves Chabal, T. D. Anthopoulos and M. Chhowalla, Under review.

Figures
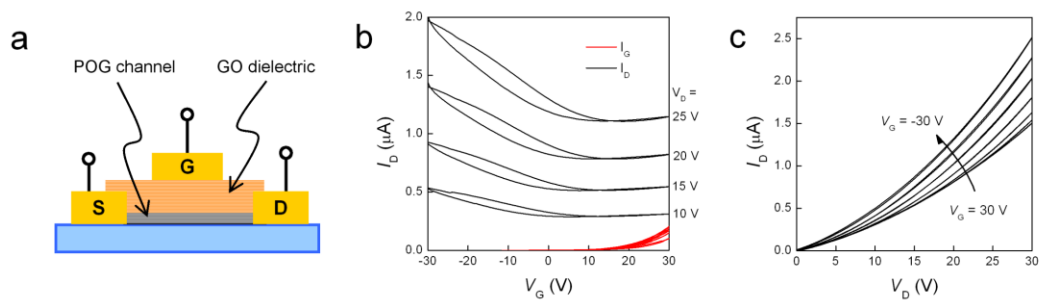
Figure 1 – (a) Structure, (b) transfer and (c) output characteristics of a graphene-based monolithic field effect device consisting of partially oxidized graphene (POG) as the channel and graphene oxide (GO) as the gate dielectric.

Vacancy mediated plastic deformation in graphene

C. P. Ewels[1], C. D. Latham[2], M. I. Heggie[2], U. Bangert[3]

[1] Institute of Materials, CNRS, Université de Nantes, BP32229, F-44322 Nantes, France
[2] Dept. Chemistry and Biochemistry, University of Sussex, Falmer, Brighton, BN1 9QJ, U.K.
[3] School of Materials, The University of Manchester, Manchester, M1 7HS, U. K.
chris.ewels@cnrs-imn.fr

Plasticity and ductile failure in graphene and carbon nanotubes can be mediated through dislocation glide by "Stone Wales" type bond rotations. While the reaction barrier for such bond rearrangements is high, they can be catalysed, for example through the presence of an interstitial carbon atom. We show here that vacancies can act as sources for shuffle dislocations, whose migration barrier is typically four times lower than that of classical glide edge dislocations.

We confirm the existence and structure of shuffle--glide dislocation pairs in graphene via high resolution electron microscopy, supported by density functional calculations.

Vacancies and other dislocation cores can also act as sinks for migrating dislocations. This leads to a new model for ductility and super-plasticity in carbon nanotubes, for example under irradiation, where vacancies emit and absorb rapidly migrating shuffle dislocations. The model is consistent with recent experimental observations of superplasticity in electron irradiated nanotubes under tensile strain. The dislocation pairs induce buckling in the basal plane of the graphene and may represent a very common intrinsic defect species.

Figures
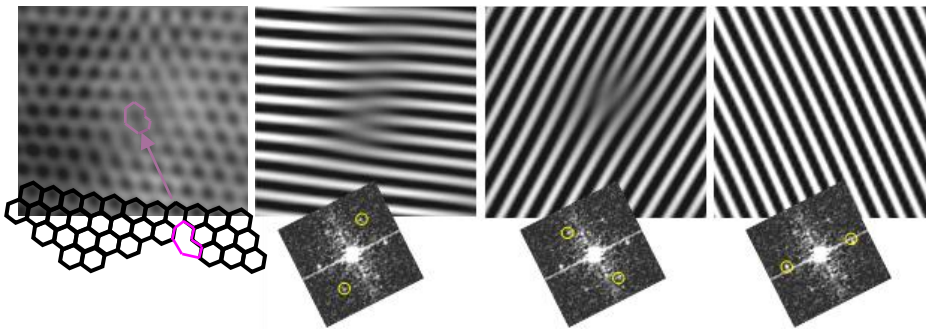
Shuffle dislocation core in graphene viewed using HAADF, with image filtering applied (image construction using only specific points from the electron diffraction).
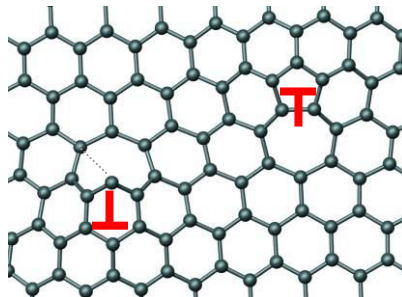
Possible separation of a mono-vacancy into a pair of dislocations (one glide, one shuffle) via motion of the shuffle dislocation core.

Reversible and irreversible deterioration caused by electron- and photo- sensitive resist spin coating on graphene

Jiyu. Fan [a,b], J. M. Michalik [a, b], L. Casado [a], S. Roddaro [c], M. R. Ibarra [a, b, d], J. M. De Teresa [b, d]

[a] Instituto de Nanociencia de Aragón, Universidad de Zaragoza, Zaragoza, 50018, Spain
[b] Departamento de Física de la Materia Condensada, Universidad de Zaragoza, Facultad de Ciencias, Zaragoza, 50009, Spain
[c] NEST, Istituto Nanoscienze-CNR and Scuola Normale Superiore, I56127 Pisa, Italy
[d] Instituto de Ciencia de Materiales de Aragón, Universidad de Zaragoza-CSIC, Facultad de Ciencias, Zaragoza, 50009, Spain

jiyufan@unizar.es

Graphene has recently attracted much attention due to its potential use in nanoelectronics and spintronics applications. [1-3] The correct fabrication of the graphene devices is the key step to obtain the searched functionality. Following our previous work [4], in the present contribution we assess the impact of different lithography process steps in the physical properties of the graphene flakes. In order to produce electrical contacts to the graphene flakes, one can use techniques such as optical lithography and electron-beam lithography. These techniques imply respectively the use of photo-resists and electron-sensitive resists. We have systematically investigated the changes in the Raman spectra of graphene flakes after spin coating photon-sensitive and electron-sensitive resists. Substantial changes in the intensity of D and G Raman peaks are observed after some of these processes related to the generation of disorder and introduction of impurities in the graphene flakes. As shown in Fig. (1), one can find that the deterioration of graphene can be clearly reflected from the nascent D peak after spin coating the PMMA electron-sensitive resist. Furthermore, even after the process of lift-off, the D peak is preserved as well. Therefore, the deterioration of graphene is unavoidable so long as the e-beam lithography is used for pattern design. However, we can find that the D peak has disappeared and the Raman spectra recover to the general shape of the pristine graphene after annealing the sample in argon atmosphere. It implies that this deterioration for the graphene is reversible. On the contrary, as for the graphene with spin coating of a photo-sensitive resist, as shown in the Fig. (2), the amplitude of the G and 2D peaks are not only attenuated but also their shapes obviously deviate from the standard character of graphene exhibiting a behavior typical of amorphization. In fact, we also measured the Raman spectra of the graphite with photo-sensitive resists on its surface, which shows a similar shape of amorphization. Therefore, even after lift-off, the photo-sensitive resists adsorbed on the surface of graphene are not completely removed. In addition, the same annealing condition previously described was performed on the graphene after spin coating photo-sensitive resists. Even though two main peaks of G and 2D can be clearly observed due to the partial elimination of photo-sensitive resists on the top of graphene, the nascent D peak was still present, implying that the deterioration caused by the used photo-sensitive resist is irreversible.

References

[1] A. K. Geim, and K. S. Novoselov, Nature Mater. **6** (2007) 183.
[2] P. Avouris, Z. H. Chen, and V. Perebeinos, Nature Nanotechnol. **2** (2007) 605.
[3] F. Schwierz, Nature Nanotechnol. **5** (2010) 487.
[4] J. M. Michalik, S. Roddaro, L. Casado, M. R. Ibarra and J. M. De Teresa, accepted for publication in Microelectronic Engineering (available online; doi:10.1016/j.mee.2010.12.002)
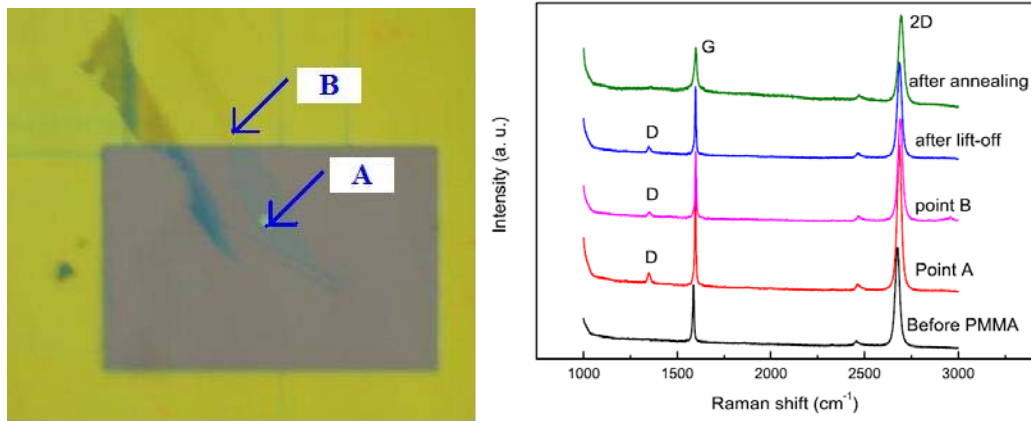
Figures

Figure 1. Left: Optical microscope image of graphene with e-beam lithography. Point A is the exposure part of graphene and point B is unexposure part. Right: Raman spectra for different conditions(1)before spin coating PMMA;(2) measurement of point A; (3) measurement of point B; (4)after lift-off with acetone; (5) after annealing
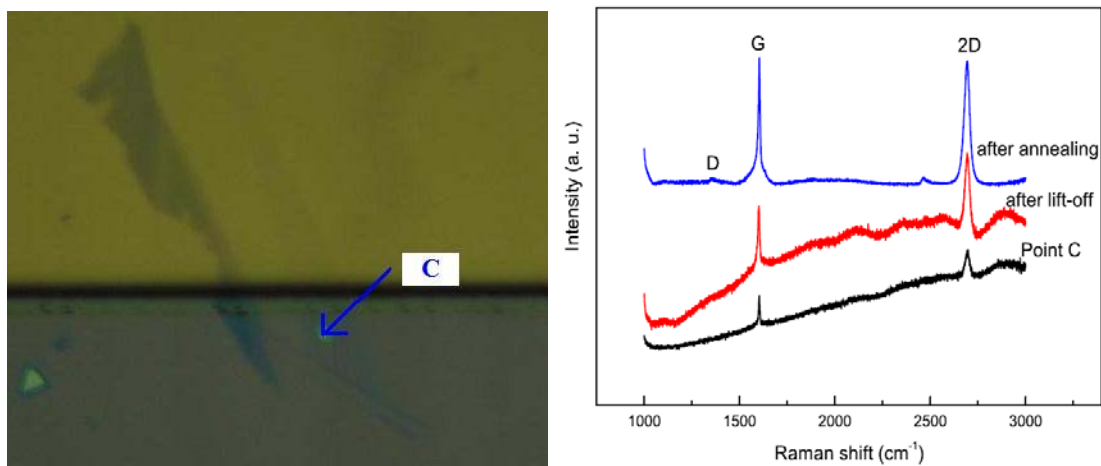
Figure 2. Left: Optical microscope image of graphene with photo lithography, Point C is the exposure part. Right: Raman spectra for different conditions (1) measurement of point C; (2) after lift-off with aceton; (3) after annealing.

Investigation of electron-phonon interaction in hydrogenated graphene through ab-initio calculations

S. Bruzzone, G. Fiori

Dipartimento di Ingegneria dell'Informazione: Elettronica, Informatica, Telecomunicazioni,
Università di Pisa, Via Caruso 16, 56122 Pisa, Italy
samantha.bruzzone@for.unipi.it

The role of electron-phonon interaction is an important issue to be addressed, since it can provide information regarding the ultimate intrinsic mobility limit (μ) of a material. Such an issue is even more relevant, when investigating electrical properties of a new material like hydrogenated graphene. Graphene hydrogenation has been demonstrated [1] to be a viable solution in order to induce an energy gap in graphene, which could path the way to its exploitation in digital electronic applications. However, due to its novelty, many questions still remains unanswered. Simulations based on a multi-scale approach have been recently performed [2], showing that, within the ballistic assumption, 50% and 100% hydrogenated graphene can represent a potential candidate for next-generation nanoscale devices. Such calculations however provide an upper limit for device performance, so that, in order to get a clear understanding of the real potential of such new material, it is of primary importance to take into account source of non-idealities like electron-phonon coupling.

In this work, we address electron-phonon interaction by means of DFT simulations, focusing on 50% and 100% hydrogenated graphene. The electron mobility, which provide a figure of merit of the material under investigation, is computed within the Deformation Potential Approximation, considering longitudinal acoustic phonons, and following the approach described in [3] to compute the deformation potential and the one in [4] to calculate mobility. All the simulations have been performed by means of the Quantum Espresso code [5].

In Fig. 1, we show the atoms position for the 50% and 100% hydrogenated graphene. In the case of 50% hydrogenation, we consider H atoms lying on the top of the pristine graphene, while in the 100% case, H atoms are placed on both sides.

In Figs. 2 and 3, the Phonon Density of States as well the phonon spectra for the 50% and 100% hydrogenated graphene are shown. In both cases, acoustic and optical modes are well separated, especially for the top highest optical branches, and Kohn anomalies are observed in the 100% case, as also shown in [6]. The sound velocity v_s can be extracted from the acoustic branches. In particular, we obtain $v_s=1.7\times10^4$ m/s and $v_s=1.63\times10^4$ m/s for the 100% and 50% case, respectively.

In Table I, we show the computed relative effective masses m^* in the conduction and in the valence band, both in the x and y direction. In the case of 100% hydrogenated graphene, both heavy and ligth holes are reported. As can be seen, the top and the bottom of the conduction band are isotropic, i.e. they show almost the same m^* in both directions.

The deformation potentials for the longitudinal acoustic phonons are also shown, as well as carrier mobilities. As can be seen, mobility in hydrogenated graphene is comparable to mobility expected in graphene (of the order of 10^5 cm^2/Vs as in [7]). Heavy holes in 100% hydrogenated graphene show instead the smallest mobility.

In conclusion, we have investigated electron-phonon interaction through ab-initio simulations, evaluating, for the first time, carrier mobility in hydrogenated graphene. Hydrogenated graphene could represent a viable option for future nanoelectronic devices, since, despite graphene, it presents a large energy gap, while retaining almost the same carrier mobility.

References
[1] D. Elias, T. M. G. M. R. R. Nair, S. V. Morozov, P. Blake, M. P. Halsall, A. C. Ferrari, D. W. Boukhvalov, M. I. Katsnelson, A.Geim, and K. S. Novoselov, Science, **323**, (2009) 610.
[2] G.Fiori, S. Lebegue, A.Betti, P. Michetti, M. Klintenberg, O. Eriksson, G. Iannaccone, Phys. Rev. B, **82**, (2010) 153404.
[3] M.Long, L. Tang, D. Wang, L. Wang, Z. Shuai, J. Am. Chem. Soc., **131**, (2009), 17728.
[4] S. Takagi, A. Toriumi, M. Iwase, H. Tango, IEEE Trans. Electr. Dev., **41**, (1994) 2363.
[5] P. Giannozzi et al., J. Phys. Condens. Matter **21**, (2009) 395502.
[6] G. Savini, A. C. Ferrari, Feliciano Giustino, Phys. Rev. Lett., **105**, (2010) 037002.
[7] K. I. Bolotin, K. J. Sikes, J. Hone, H. L. Stormer, P. Kim, Phys. Rev. Lett., **101**, (2008), 096802.
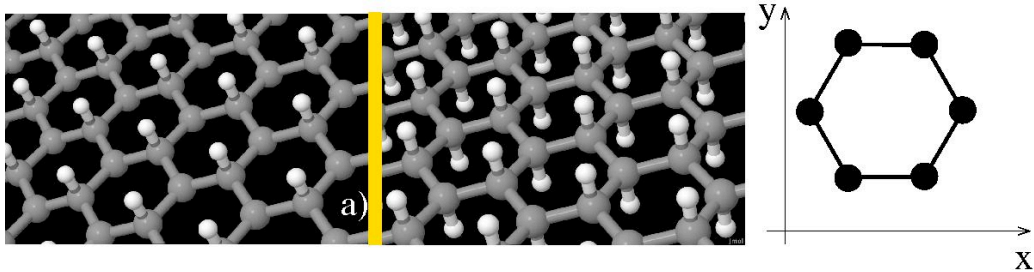
Fig.1: Atoms position in a) 50% and b) 100% hydrogenated graphene
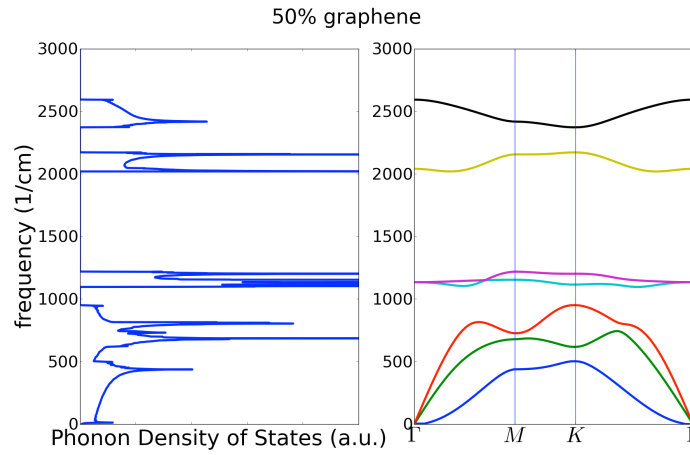
Fig.2: Phonon Density of States and phonon spectra for 50% hydrogenated graphene (spin up)
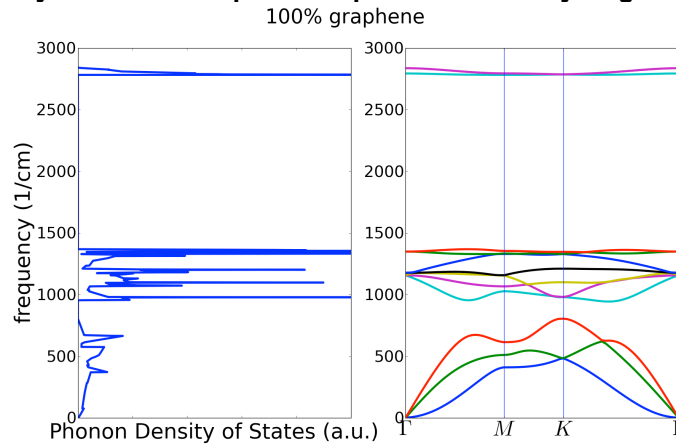
Fig.3: Phonon Density of States and phonon spectra for 100% hydrogenated graphene

Table I

%	$m_{ex}*$	$m_{ey}*$	$m_{hhx}*$	$m_{hhy}*$	$m_{lhx}*$	$m_{lhy}*$	D_{ace} (eV)	D_{achh} (eV)	D_{aclh} (eV)	μ_e (cm^2/Vs)	μ_{hh} (cm^2/Vs)	μ_{lh} (cm^2/Vs)
50	1.315	1.346	1.540	1.478	-	-	2	3.74	-	1.62x10^5	1.189x10^5	-
100	1.029	1.027	0.622	0.641	0.278	0.270	5.228	7.532	7.532	1.09x10^5	5.18x10^4	2.833x10^5

$m_{ex}*$ and $m_{ey}*$ are the relative effective masses of electrons along the *x* and *y* direction, respectively. $m_{hhx}*$, $m_{hhy}*$, $m_{lhx}*$ and $m_{lhy}*$, are the heavy and light hole relative effective masses along the *x* and *y* direction. D_{ace}, D_{achh} and D_{aclh} are the deformation potential for the electrons and the heavy and light holes. μ_e, μ_{hh} and μ_{lh} are the mobility computed for electrons, and heavy and light holes.

Bilayer graphene under uniaxial tension: A Raman study

Otakar Frank[1,2], Georgia Tsoukleri[2,3], John Parthenios[2], Kostas Papagelis[4], Ibtsam Riaz[5], Rashid Jalil[5], Kostya S. Novoselov[5], Ladislav Kavan[1] and Costas Galiotis[2,3,4]

[1]J. Heyrovsky Institute of Physical Chemistry, v.v.i., Academy of Sciences of the Czech Republic, CZ-18223, Prague 8, Czech Republic
[2]Institute of Chemical Engineering and High Temperature Chemical Processes, Foundation for Research and Technology, GR-26504, Patras, Greece
[3]Interdepartmental Programme in Polymer Science and Technology, University of Patras, Greece
[4]Materials Science Department, University of Patras, GR-26500, Greece
[5]School of Physics and Astronomy, University of Manchester, Manchester, M13 9PL, UKO
otakar.frank@jh-inst.cas.cz

With a few notable exceptions, most works dealing with mechanical properties of graphene are of theoretical nature and generally limited to suspended graphene at the atomic scale. Hence, there is a growing demand for experimental data to validate the models and relate them to graphene attached to various substrates. However, up till now, no such experiments on bilayer graphene have been reported. Raman spectroscopy here is a key diagnostic tool to identify the number of layers in a sample and probe physical properties and phenomena [1]. The G band corresponds to the in-plane, zone center, doubly degenerate phonon mode (transverse (TO) and longitudinal (LO) optical) with E_{2g} symmetry. Under tension, the G mode shifts to lower frequencies (phonon softening), while under compression, it shifts to higher frequencies (phonon hardening). On top of that, due to a symmetry break-down induced by the strain, the G mode splits into two sub-bands, denoted G^- and G^+ for the component parallel and perpendicular to strain, resp. Their respective shifts rates were determined to be *ca.* 30 and 10 cm^{-1}/% [2-4]. Their intensities depend on the orientation of the graphene lattice with respect to the strain axis and polarization of the incident light. The D and 2D modes come from a second-order double resonant process between non-equivalent K points in the Brillouin zone (BZ) of graphene, involving two phonons (TO) for the 2D and one phonon and a defect for the D peak. The shift rates for the 2D band are in the range of 50-60 cm^{-1}/%, and very recently its splitting has been reported [5,6]. The origin of the splitting lies in non-equivalent K-K' paths (three for an arbitrary strain orientation) and also depends on the excitation wavelength. For lower excitation energy (like 1.58 eV), inner resonance processes become stronger due to a lesser effect of trigonal warping, and hence all together the 2D band can be composed of six components with different shift rates, which leads to broadening and eventually splitting [5].

In the present work, bilayer graphene flakes have been subjected to a uniaxial tension using the polymer cantilever beam technique. In all cases the mechanical response was monitored by simultaneous Raman measurements using 785 nm (1.58 eV) excitation. The flakes were either laid bare on a polymer substrate or covered by another polymer layer to minimize a possible slippage during loading. For comparison, a monolayer graphene close to the studied bilayer was monitored during the same experiment. Figure 1a shows an example micrograph of embedded mono- and bilayer graphenes. Both of them show the same behavior under tension, with shift rates of 30.5 and 9.5 cm^{-1}/% for G^- and G^+, resp. As can be deduced from Fig.1a as well as from the same G^-/G^+ relative intensities of the respective layers, they belong to the same flake, part of which is composed of a single layer, whereas the other part is overlaid by another layer with Bernal (AB) stacking. Therefore their lattice orientation of 23°, which can be calculated using the G^- and G^+ relative intensities, is the same.

Figure 1b shows the 2D band components evolution under tension for the embedded bilayer. The 4 components come from the splitting of the electronic bands due to interactions between the stacked layers [1,7] with the highest frequency component ($2D_{11}$) originating from resonance processes involving only the "original" π_1 and π_1^* bands belonging to the single layer. The FWHMs were set as

equal for all components and otherwise left unconstrained. The shift rates of the three lower frequency components involving the π_2 and π_2^* electronic bands are all similar - close to 50 cm^{-1}/%. However, the 2D$_{11}$ shifts at a rate of only 30 cm^{-1}/%. The relative intensities of the components evolve differently. The 2D$_{12}$ experiences a double intensity increase in the observed strain range, mainly at the cost of the 2D$_{11}$. It has to be noted, a deconvolution of the 2D band with more than 4 components is very problematic and some of the parameters would need to be constrained – for which there are too few data available at the moment. The evolution of 2D$_{11}$ and 2D$_{12}$ resembles the behavior of the 2D band in a monolayer when excited with the same wavelength. There, the 2D band splits and can be fitted with two Lorentzians (even though there are more, see above) with shift rates of approx. 50 and 30 cm^{-1}/% for the lower and higher frequency component, resp. The evolution of the bilayer 2D band could lead to an assumption that the 2D$_{11}$ splits as does in monolayer and only its higher frequency sub-component can be deconvoluted separately, while the lower frequency sub-component merges with the 2D$_{12}$ and thus contributes to its huge intensity increase. However, more data complemented with first-principles calculations are necessary to fully explain the observed processes.

References

[1] Ferrari A.C., Meyer J. C., Scardaci V., Casiraghi C., Lazzeri M., Mauri F., Piscanec S., Jiang D., Novoselov K.S., Roth S., Geim A.K. Phys.Rev.Lett., **97** (2006) 187401.
[2] Mohiuddin T.M.G., Lombardo A., Nair R.R., Bonetti A., Savini G., Jalil R., Bonini N., Basko D.M., Galiotis C., Marzari N., Novoselov K.S., Geim A.K., Ferrari A.C. Phys.Rev.B, **79** (2009) 2054338.
[3] Tsoukleri G., Parthenios J., Papagelis K., Jalil R., Ferrari A.C., Geim A.K., Novoselov K.S., Galiotis C. Small, **5** (2009) 2397.
[4] Frank O., Tsoukleri G., Parthenios J., Papagelis K., Riaz I., Jalil R., Novoselov K.S., Galiotis C. ACS Nano, **4** (2010) 3131.
[5] Frank O., Mohr M., Maultzsch J., Thomsen C., Riaz I., Jalil R., Novoselov K.S., Tsoukleri G., Parthenios J., Papagelis K., Kavan L. and Galiotis C. Raman 2D-band splitting in graphene: theory and experiment. ACS Nano, submitted.
[6] Huang M., Yan H., Heinz T.F., Hone J. Nano Lett., **10** (2010) 4074.
[7] Cançado L.G., Reina A., Kong J., Dresselhaus M.S. Phys.Rev.B, **77** (2008) 245408.
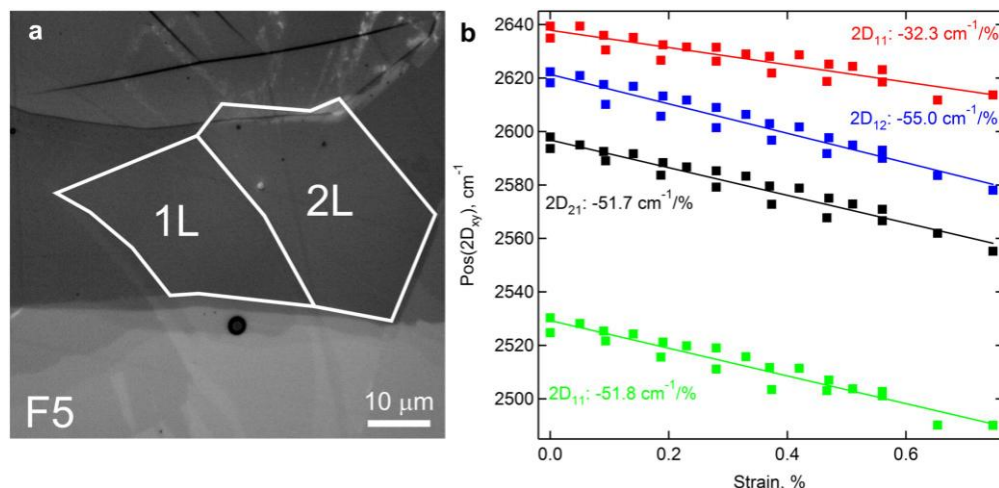
Figure 1. a) optical micrograph of the graphene under study. b) evolution of the Raman 2D band components of the bilayer graphene under tension (excitation wavelength 785 nm).

ELECRTICAL COMPACT MODELLING OF GRAPHENE TRANSISTORS

Sébastien Frégonèse[1], Huu-Nha Nguyen[1], Cristell Maneux[1], Henri Happy[2], Nan Meng[2], Thomas Zimmer[1]

[1]CNRS, UMR 5218, Laboratoire IMS, Université de Bordeaux, France
[2]IEMN – CNRS 8520, Avenue Poincare, 59652 Villeneuve d'ASCQ Cedex, France
sebastien.fregonese@ims-bordeaux.fr

The discovery of single layer graphene has generated much theoretical and experimental interest because of its exceptional properties [1], [2]. The gapless bandstructure in graphene results in good transport properties of carriers such as high mobility and high Fermi velocity. These physical properties are of great interest for electronic application using graphene transistors (GFET and GNRFET). Also, the evaluation of such devices for circuit applications can be performed through appropriate electrical compact models. Moreover, during the graphene synthesis, defects may be created in the graphene sheet which induce trap charges in the channel [3, 7]. This effect must be taken into account for accurate compact modelling. Hence, in this paper we propose a modification of the drift-diffusion compact model for graphene FET devices from Meric et al. [5].

In order to model the drift-diffusive transport, we use the velocity saturation model [4], [5]. The models will be applied to the 2D system of graphene. In the channel, the carrier concentration is calculated using the model in [5, 6]: $n = \sqrt{n_0^2 + \left[C_{top} \left(V_{GS} - V_{DIRAC}^0 \right) / e \right]^2}$, $V^0{}_{DIRAC}$ is the top gate-source voltage at the Dirac point in these regions and n_0 is the minimum 2D carrier concentration which contains the effect of disorder and thermal excitation. The current in the channel is given by $I_d = \frac{W}{L} \int_0^L e.n(x).v_{drift}(x)dx$, where x is the distance along the channel, L and W are the length and the width of the channel. We approximate the carrier drift velocity v_{drift} by a velocity saturation model [6]: $v_{drift}(x) = \frac{\mu E}{1 + \mu E / v_{sat}}$, where the saturated velocity depends on the carrier concentration as $v_{sat} = v_F \left(\hbar\Omega / E_F \right)$ where v_F and E_F is the Fermi velocity and Fermi energy, $\hbar\Omega$ is the surface phonon energy of the substrate.

The GNRFET has been fabricated and characterized by the IEMN laboratory [7, 8]. The transistor is composed of parallel graphene ribbons playing the role of the channel, with a gate length of 150 nm (fig 1). The width of the ribbons is about 50 nm, which is quite large so that the induced band gap may be negligible and the 2D model is applied to model the transistor transport. Its intrinsic cut-off frequency is about 10 GHz. The figure 2 shows I_{DS} versus V_{DS} characteristics for measurement and compact model simulation. A good agreement is observed in DC but doesn't match in AC regime. However, from the measurement, we can observe a strong difference between the transconductance g_M (calculated from measured DC $I_D(V_{GS})$ characteristic) and measured real part of Y_{21} (calculated from measured S-parameters)at medium frequency (10 MHz < f <10 GHz), (see Fig. 3, 4 and 5). We explain this effect by the presence of traps which are active during DC measurement and which are cancelled during the AC ones. To take into account the presence of trap charges in the channel, we modify the formula for the carrier concentration by replacing n_0 (AC regime) by $n_0 + n_{traps}*H(f)$ (DC regime). H(f) is a low frequency band pass filter. Trapped charges are active only in DC regime and at low to moderate frequency. Trapped charges are cancelled in AC regime and modify the Dirac point position. Hence, we modify the $V^0{}_{DIRAC}$ parameter in order to introduce charge dependence. The change in Dirac point voltage is

expressed as: $\Delta V_{DIRAC} = V_{DIRAC}^{traps} - V_{DIRAC}^{AC} = \sqrt{\left[e^2 \left(n_{0AC}^2 - \left(n_{0AC} + n_{TRAPS} \right)^2 \right) / C_{top}^2 \right] + V_{DIRAC}^{AC\,2}} - V_{DIRAC}^{AC}$.

This modification of the compact model improves strongly the accuracy of the model as shown on fig. 4 where the compact model is in agreement with both the transconductance and Y$_{21}$ parameter.

References

[1] Novoselov, K.S., et al., Science, 306 (2004): p. 666-669.

[2] Geim, A.K. and K.S. Novoselov, Nat Mater, 6 (2007): p. 183-191.

[3] Zhu, J., R. Jhaveri, and J.C.S. Woo, Applied Physics Letters, 96 (2010): p. 193503-3

[4] Canali, C.M., G. Minder, R. Ottaviani, G., IEEE Transactions on Electron Devices 22 (1997): p. 1045-1047.

[5] Meric, I., et al., Nat Nano 3 (2008): p. 654-659.

[6] J. L. Xia et al. Applied Physics Letters 96, 162101, 2010.

[7] N. Meng et al, Device Research Conference (DRC), 2010

[8] Meng, N. et al., EuMIC 2010 - Conference Proceedings , art. no. 5613734, pp. 294-297
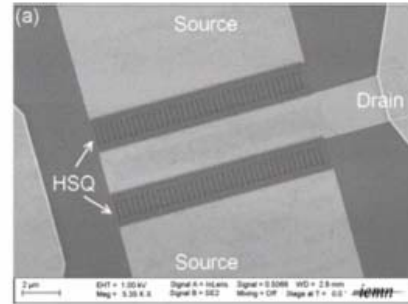
Figure 1. Top gated graphene FET for measurement by the IEMN group.
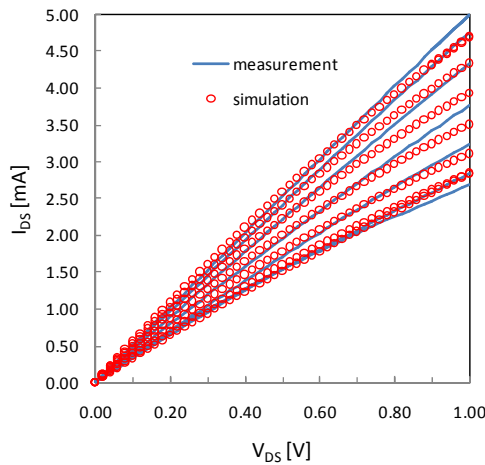
Figure 2. I$_{DS}$-V$_{DS}$ characteristics for V$_{GS}$ = -2 to 1 V (upwards) with the step = 0.5 V. The simulated results are blue lines, the measured ones are red circles
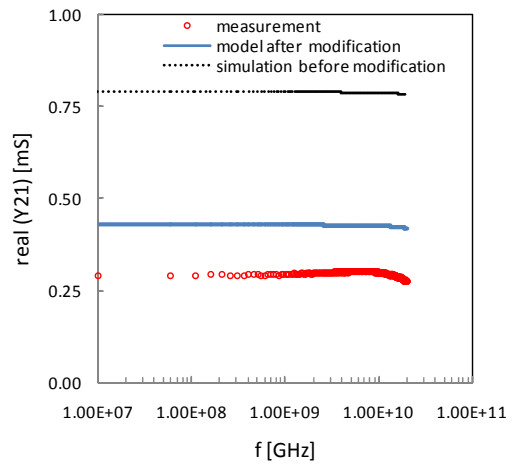
Figure 3. real part of Y$_{21}$ parameter versus frequency for V$_{GS}$ =-0.8V for V$_{DS}$ =1 V.
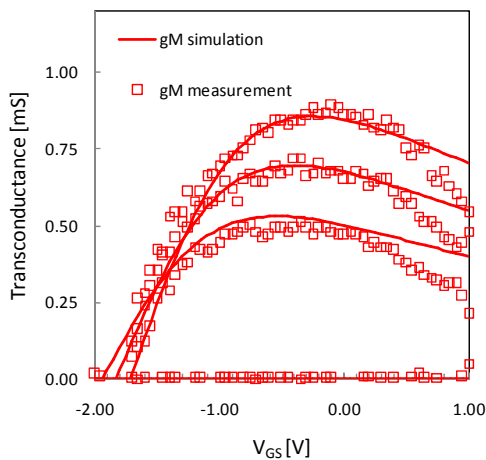
Figure 4. Transconductance g$_M$ as a function of V$_{GS}$ for V$_{DS}$ = 0.6, 0.8, and 1 V.
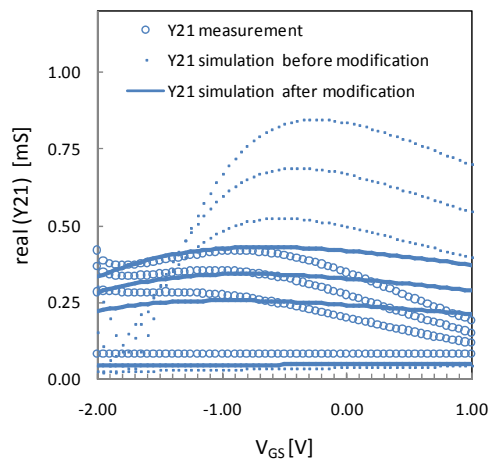
Figure 5. real part of Y$_{21}$ parameter at 3GHz as a function of V$_{GS}$ for V$_{DS}$ = 0.6, 0.8, and 1 V.

Graphene on Polycrystalline Ni Thin Film: Mapping Conductivity by Conducting Atomic Force Microscopy

Yunyi Fu[1], Huabo Zhao[1], Qinqin Wei[1], Zhijun Wei[1], Zhaohui Zhang[2], Zujin Shi[3], Xing Zhu[2], Ru Huang[1]and Xing Zhang[1]

[1]Department of Microelectronics, Peking University, Beijing 100871, People's Republic of China
[2] School of Physics, Peking University, Beijing 100871, China,
[3]College of Chemistry and Molecular Engineering, Peking University, Beijing 100871, People's Republic of China
yyfu@pku.edu.cn

Conducting Atomic Force microscopy (C-AFM) has been used to map the local conductivity of mono- or few-layer graphene grown on polycrystalline Ni thin films on SiO_2/Si substrate. It has been revealed that the local conductivity of graphene depend strongly on the crystal face of underlying Ni crystal. There exists a transition zone between the two adjacent surfaces, where the graphene has unique conductivity properties. Using C-AFM, combining with analysis of the graphene/Ni moiré pattern, we also characterize the graphene morphologies underneath the top graphene sheets, which provide clear evidence for CVD growth of graphene on Ni occurring by carbon segregation. Our findings are important for understanding both the physical properties of graphene sheets and their growth mechanism.

References

[1] P. Sutter, J. T. Sadowski, and E. Sutter, Physical Review B, **80**(2009)245411.

[2] D. Usachov, A. M. Dobrotvorskii, A. Varykhalov, O. Rader, W. Gudat, A. M. Shikin, and V. K. Adamchuk, Physical Review B, **78**(2008)085403.

[3]D. Yu. Usachov, A. M. Dobrotvorskii, A. M. Shikin, V. K. Adamchuk, A. Yu. Varykhalov, O. Rader and W. Gudat, Bulletin of the Russian Academy of Sciences: Physics, **73**(2009)679.

[4] X. S. Li, W. W. Cai, L. G. Colombo, and R. S. Ruoff, Nano Letters*.,* **9**(2009**)**4268

Figures
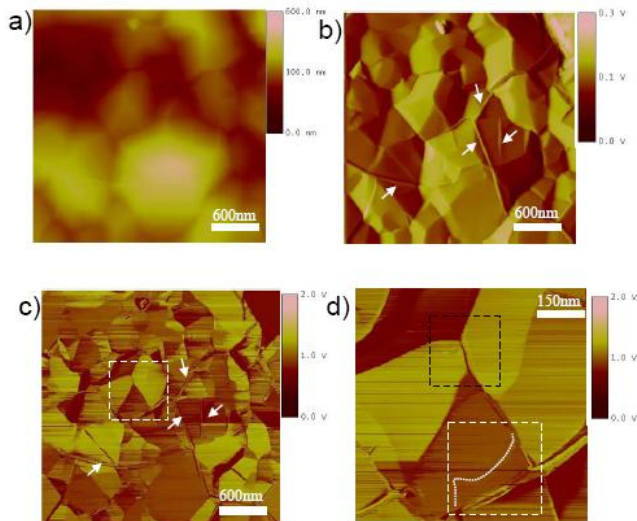
Figure caption

Local conductance maps on the three dimensional Ni crystals:

(a) Lager scale of topography of the graphene on Ni crystals;

(b) Deflection image of the topography;

(c) The conductance map composed of many flat patches with various contrasts corresponding to different facets of the Ni crystals;

(d) The magnified region indicated by the white box in Figure 2c

Photon helicity driven currents in graphene

S. D. Ganichev, J. Karch, P. Olbrich, M. Schmalzbauer, C. Zoth, C. Brinsteiner, M. Fehrenbacher, U. Wurstbauer, M. M. Glazov, S. A. Tarasenko, E. L. Ivchenko, D. Weiss, J. Eroms, R. Yakimova, S. Lara-Avila, and S. Kubatkin

Terahertz Center, University of Regensburg, 93040 Regensburg, Germany

Ioffe Physical-Technical Institute, Russian Academy of Sciences, 194021 St. Petersburg, Russia

Department of Physics, Chemistry and Biology, Linköping University, S-58183 Linköping, Sweden

Department of Microtechnology and Nanoscience, Chalmers University of Technology, S-41296 Göteborg, Sweden

Sergey.Ganichev@physik.uni-regensburg.del

We report on the observation of photon helicity driven currents in graphene. We demonstrate that the illumination of unbiased monolayer graphene samples with terahertz (THz) laser radiation at room temperature under oblique and normal incidence causes directed electric currents. This includes currents which are solely driven by the light's helicity. In this case we observe a net electric current, whose sign reverses upon switching the radiation helicity from left- to right-handed circularly polarized light. The phenomenological and microscopic theories of the observed photocurrents are developed. We demonstrate that under oblique incidence the helicity driven current is caused by the circular ac Hall effect in the bulk of the graphene sheet driven by the crossed ac *E*- and *B*-fields of circularly polarized radiation [1]. Alike the classical dc Hall effect, the voltage is caused by crossed *E*- and *B*-fields which are, however, rotating with the light's frequency. By contrast, the effect observed at normal incidence stems from the sample edges, which reduce the symmetry and result in an asymmetric scattering of carriers driven by the radiation electric field [2]. The observation of a helicity driven photocurrent in graphene demonstrates that this material may be a good candidate for a novel type of detectors of THz radiation. Besides photon helicity dependent currents we also observe photocurrents driven by linearly polarized radiation. The microscopic mechanisms governing this effect are discussed.

References

[1] J. Karch, P. Olbrich, M. Schmalzbauer, C. Zoth, C. Brinsteiner, M. Fehrenbacher, U. Wurstbauer, M. M. Glazov, S. A. Tarasenko, E. L. Ivchenko, D. Weiss, J. Eroms, and S. D. Ganichev, Phys. Rev. Lett. **105** (2010), 227402.

[2] J. Karch, P. Olbrich, M. Schmalzbauer, C. Brinsteiner, U. Wurstbauer, M. M. Glazov, S. A. Tarasenko, E. L. Ivchenko, D. Weiss, J. Eroms, and S. D. Ganichev, arXiv:1002.1047v1 (2010).

Millimeter-Scale Graphene Domains: CVD Growth on Pt and Its Nondestructive Transfer

Libo Gao, Wencai Ren*, Lai-Peng Ma, and Hui-Ming Cheng*

Shenyang National Laboratory for Materials Science, Institute of Metal Research, Chinese Academy of Sciences, 72 Wenhua Road, Shenyang 110016, P. R. China
E-mail: lbgao@imr.ac.cn
*Corresponding authors: wcren@imr.ac.cn, cheng@imr.ac.cn

Graphene, a two-dimensional honeycomb lattice of sp^2-bonded carbon atoms, has attracted the worldwide interests after the experimental isolation from graphite.[1] High-quality graphene can be prepared by micromechanical cleavage method, thermal decomposition of SiC,[2] epitaxial growth and chemical vapor deposition (CVD) on Ru (0001),[3] Pt (111),[4] $Pt_{83}Rh_{17}$ foils,[5] Ni films,[6,7] Cu (111),[8] and Cu foils.[9] Recently, CVD growth of graphene on Cu foils has attracted increasing interests, because of the predominant growth of large area monolayer graphene, easy transfer and cheap substrates. However, the graphene domains grown on Cu foils are small (usually smaller than 10 μm), and no big single crystalline domains were formed even on single crystal Cu substrate. Moreover, the dissolution of Cu during the transfer process unavoidably lead to serious pollution and high cost. Therefore, it still remains great challenges to prepare large area graphene films of high crystalline quality and realize their nondestructive transfer.

Here we present the growth of high quality graphene film with large single crystalline domains on the surface of polycrystalline Pt foils and single crystalline Pt (111) by ambient pressure CVD.[10] Although the solubility of carbon in Pt is high (~ 0.9 at% at 1000 °C), the growth of graphene on Pt follows surface adsorption process, which is similar to that on Cu foils.[11] However, in contrast to Cu foils,[12] a fast graphene growth rate and broad growth window were found for the Pt substrate. The average size of single crystalline graphene domain obtained is up to millimeter size. Its high quality is confirmed by optical microscopy, atomic force microscopy, scanning tunneling microscopy, Raman spectroscopy and transport property measurements. Moreover, we developed a nondestructive method to transfer graphene films from Pt to arbitrary substrates. This unique transfer process does no harm to the graphene films and the metal substrate, which is totally different from the currently used transfer methods for Cu and Ni substrates based on etching, so the Pt foils and single crystalline Pt can be recycled to grow graphene films.

References
[1] Novoselov, K. S.; Geim, A. K.; Morozov, S. V.; Jiang, D.; Zhang, Y.; Dubonos, S. V.; Grigorieva, I. V.; Firsov, A. A. Science, **306** (2004) 666-669.
[2] Berger, C.; Song, Z. M.; Li, X. B.; Wu, X. S.; Brown, N.; Naud, C.; Mayo, D.; Li, T. B.; Hass, J.; Marchenkov, A. N.; Conrad, E. H.; First, P. N.; de Heer, W. A. Science, **312** (2006) 1191-1196.
[3] Sutter, P. W.; Flege, J. I.; Sutter, E. A. Nat. Mater., **7** (2008) 406-411.
[4] Sutter, P.; Sadowski, J. T.; Sutter, E. Phys. Rev. B, **80** (2009) 245411.
[5] Gao, J. H.; Fujita, D.; Xu, M. S.; Onishi, K.; Miyamoto, S. ACS Nano, **4** (2010) 1026-1032.
[6] Kim, K. S.; Zhao, Y.; Jang, H.; Lee, S. Y.; Kim, J. M.; Kim, K. S.; Ahn, J. H.; Kim, P.; Choi, J. Y.; Hong, B. H. Nature, **457** (2009) 706-710.
[7] Reina, A.; Jia, X. T.; Ho, J.; Nezich, D.; Son, H. B.; Bulovic, V.; Dresselhaus, M. S.; Kong, J. Nano Lett., **9** (2009) 3087-3087.
[8] Gao, L.; Guest, J. R.; Guisinger, N. P. Nano Lett., **10** (2010) 3512-3516.
[9] Li, X. S.; Cai, W. W.; An, J. H.; Kim, S.; Nah, J.; Yang, D. X.; Piner, R.; Velamakanni, A.; Jung, I.; Tutuc, E.; Banerjee, S. K.; Colombo, L.; Ruoff, R. S. Science, **324** (2009) 1312-1314.
[10] Gao, L. B.; Ren, W. C.; Cheng, H. M. et al. (in preparation).
[11] Li, X. S.; Cai, W. W.; Colombo, L.; Ruoff, R. S. Nano Lett., **9** (2009) 4268-4272.

[12] Gao, L. B.; Ren, W. C.; Zhao, J. P.; Ma, L. P.; Chen, Z. P.; Cheng, H. M. Appl. Phys. Lett., **96** (2010) 183109.
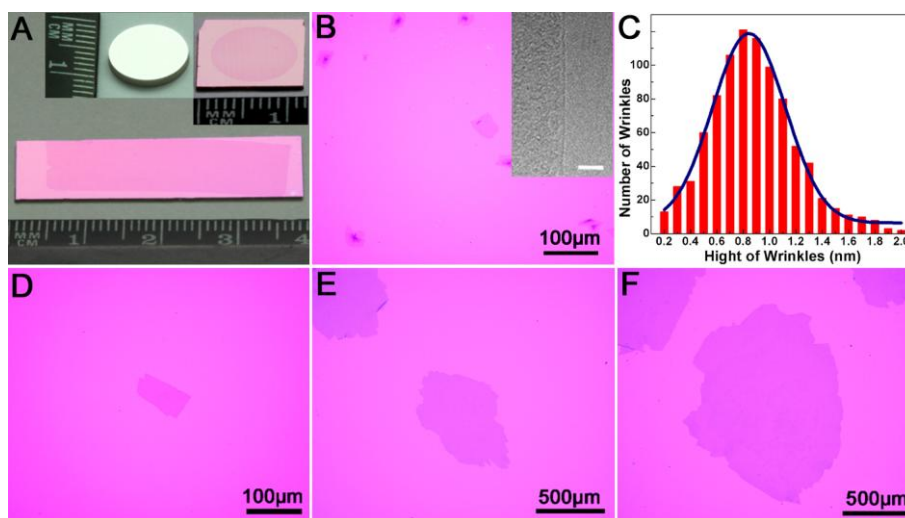
Figure 1. Photograph and optical images of graphene transferred from polycrystalline Pt foils and Pt (111) to Si/SiO$_2$ substrates.

Graphitic carbon molecular beam deposition on dielectric substrates

J. M. García[1,2], U. Wurstbauer[1], R. He[1], L. Zhao[1], A. Rigosi[1], T. Schiros[3], A. S. Plaut[4], P. Kim[1], L. N. Pfeiffer[5], A. Pasupathy[1], and A. Pinczuk[1]

[1] Departments of Physics and Department of Applied Physics and Mathematics, Columbia University
[2] MBE Lab, Instituto de Microelectrónica de Madrid, IMM-CNM, CSIC, Spain
[3] Energy Frontier Research Center, Columbia University
[4] School of Physics, Exeter University, UK
[5] Electrical Engineering Department, Princeton University

jorgem@imm.cnm.csic.es

There has been enormous progress in the synthesis of large area graphene layers, with much of the focus in the use of a catalytic reaction on a metal surface during Chemical Vapor Deposition (CVD) [1-3]. After the graphene is grown on a metal, it must be transferred to a dielectric substrate for its use in transport characterization and in devices. This exfoliation process inevitably induces degradation and contamination of the graphene layers. It would be desirable to be able to grow graphene layers directly on an insulating substrate allowing for high quality, transfer-free graphene devices. We explore a molecular beam epitaxy (MBE) approach to this challenge that could lead, in the future, to further benefits such as the capability to fabricate doped graphene, multilayer heterostructures and high carrier mobility layers.

We present here initial results on the fabrication of ultrathin graphitic layers on several dielectric substrates using a carbon by a molecular beam deposition MBD technique [4]. The samples have been characterized ex situ by: Raman spectroscopy, micro Raman spectroscopy, near-edge x-ray absorption fine structure (NEXAFS), AFM and STM. These results have been obtained on three different dielectric substrates: hexagonal-BN micro flakes (h-BN), SiO_2 and Mica.

The experimental growth set up (Figure 1) has been developed for this purpose that employs a UHV chamber with a carbon cell (figure 1, f) that can deposit sub-monolayer controlled graded amounts of carbon on a heated sample holder (s). The set-up allows in situ post growth high temperature annealing in a furnace as schematically shown in Figure 1.

The micro-Raman spectra (shown in Figure 2) reveal the Raman features D and G that are characteristic of graphitic material. On h-BN (red) an additional sharp and strong resonance is observed at ~1370 cm^{-1} that is from the underlying h-BN substrate. The spectrum taken on SiO_2 (black) shows also some structure around ~2700 cm^{-1}, which in graphene would be associated with a second-order Raman band. Finally, a Mica substrate presents a similar spectrum (blue). Although these Raman features are far away from ideal graphene, they show that it is possible to fabricate graphitic materials directly on dielectric.

NEXAFS measurements confirm the predominant sp^2 bond that confirms the graphitic character of the grown carbon layers. The NEXAFS analysis of a layer of carbon MBE-grown on Mica (figure 3) shows the following graphitic characteristics: an intense C=C π^* resonance at 285 eV (missing for sp^3-like diamond), a C=C σ^* resonance at ~292 eV, and a strong polarization dependence of π^* and σ^* resonances characteristic of an ordered 2-D bonding environment. Finally a fine structure in the σ^* region (photon energy > 290 eV) indicates long-range periodicity in the electronic structure.

References

[1] K.S. Kim, Y. Zhao, H. Jang, S.Y. Lee, J.M. Kim, K.S. Kim, J.-H. Ahn, P. Kim, J.-Y. Choi, B.H. Hong, Large-scale pattern growth of graphene films for stretchable transparent electrodes, Nature 457 (2009) 706.

[2] A. Reina, X. Jia, J. Ho, D. Nezich, H. Son, V. Bulovic, M.S. Dresselhaus, J. Kong, Large Area, Few-Layer Graphene Films on Arbitrary Substrates by Chemical Vapor Deposition, Nano Lett. 9 (2009) 30.

[3] X. S. Li, W. W. Cai, J. H. An, S. Kim, J. Nah, D.X. Yang, R.D. Piner, A. Velamakanni, I. Jung, E. Tutuc, S.K. Banerjee, L. Colombo, R.S. Ruoff, Large-Area Synthesis of High-Quality and Uniform Graphene Films on Copper Foils, Science 2009, 324, 1312-1314.

[4] JM Garcıa, R He, MP Jiang, J Yan, A Pinczuk, YM Zuev. et al. Multilayer graphene films grown by molecular beam deposition, Solid State, Comm. 2010; 150: 17-18

Figures
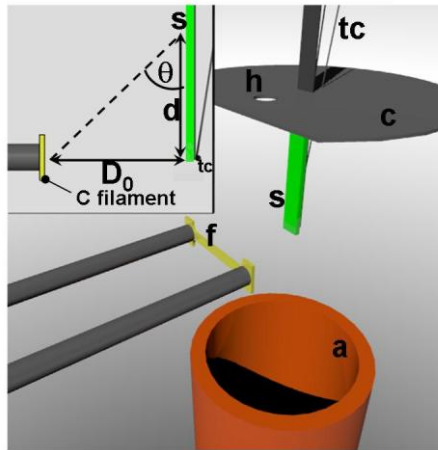
Figure 1: Illustration of the experimental MBE set-up. The carbon is evaporated from the filament (f) onto an elongated arbitrary substrate (s) and further annealed in a furnace (a). The Temperature is measured with the thermocouple (tc). The inset depicts a side view with labels of the geometrical parameters D_0 (13:3 mm), θ and d.
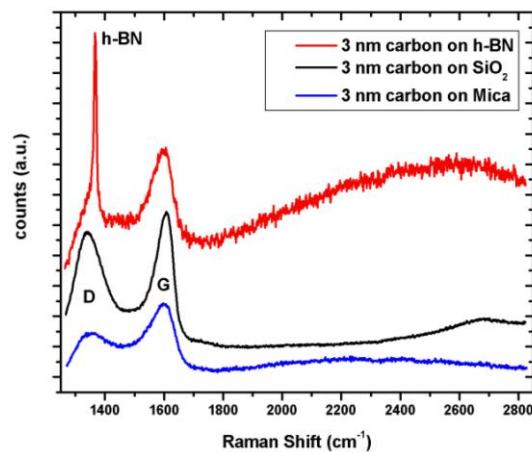
Figure 2: Micro Raman spectroscopy of 3 nm of carbon grown by MBE on hexagonal-BN (red), SiO_2 and Mica substrates.
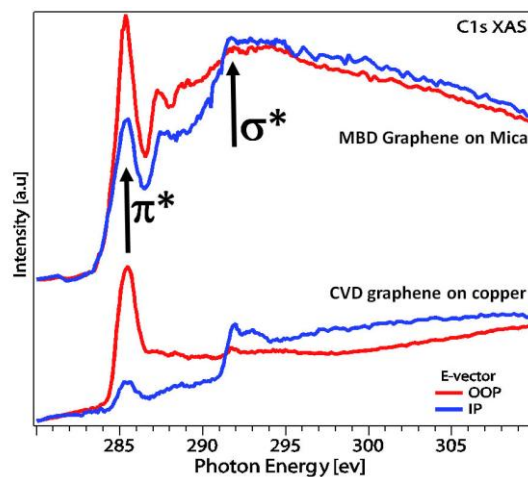
Figure 3: NEXAFS spectra of a MBE grown sample on Mica (top) and, for reference, a CVD grown sample on copper.

130

Lindhard screening in graphene antidot lattices

Marco Haller Schultz[1], Antti-Pekka Jauh**o**[1,2], and Thomas Garm Pedersen[3]

[1]Dept. of Micro and Nanotechnology, DTU Nanotech, DTU, DK-2800 Lyngby, Denmark
[2]Dept. of Applied Physics, Aalto University, P.O. Box 11100, FI-00076 AALTO, Finland
[3]Dept. of Physics and Nanotechnology, Aalborg University, DK-9220 Aalborg East, Denmark
Antti-Pekka.Jauho@nanotech.dtu.dk

Regular perforations of a pristine graphene sheet, i.e., a formation of a graphene antidot lattice (GAL) [1], modify the electronic structure so that a gap may appear in the energy spectrum [2], thus possibly paving the way to nanoelectronic applications. A central concept in the theory of solids is screening, and in many instances an RPA-level theory is sufficient. In the case of graphene, several groups have addressed this issue, initially approximating the electronic spectrum by the linear Dirac cone (see, e.g.,[3,4]), and, more recently, allowing for the full graphene dispersion [5]. Here, we report analogous results for GALs.

The calculations proceed in principle in the same way as discussed in [3-5], however in our case one has to resort to the numerically computed electronic dispersion relations, and one needs to evaluate the matrix elements using the (numerically) known Bloch eigenstates of the antidot lattice. Thus, we must evaluate

$$\chi_0^R(\mathbf{q},\omega) = \frac{2}{(2\pi)^2}\sum_{nn'}\int_{1.\text{BZ}} d\mathbf{k} \left| \sum_{j=1}^{M} \left(c_{n\mathbf{k}}^j\right)^* c_{n'\mathbf{k}+\mathbf{q}}^j e^{-i\mathbf{q}\cdot\mathbf{d}_j} \right|^2 \frac{n_{\text{F}}(\epsilon_{n\mathbf{k}}) - n_{\text{F}}(\epsilon_{n'\mathbf{k}+\mathbf{q}})}{\epsilon_{n\mathbf{k}} - \epsilon_{n'\mathbf{k}+\mathbf{q}} + \omega + i\eta}$$

where the c-coefficients are obtained from the tight-binding wave function,

$$\psi_{n\mathbf{k}}(\mathbf{r}) = \frac{1}{\sqrt{N}}\sum_{\mathbf{R}} e^{i\mathbf{k}\cdot\mathbf{R}} \sum_{j=1}^{M} c_{n\mathbf{k}}^j \varphi(\mathbf{r}-\mathbf{R}-\mathbf{d}_j)$$

It is important to note that the j-sum runs over all the atoms in the unit cell of the antidot lattice (see Fig. 1, left), and that the energies are given by the antidot dispersion ([1], or Fig. 1, right). Thus, in the case of pristine graphene there are only two terms in the j-sum, while for antidot lattices there may be hundreds of terms, implying significant numerical work. Also, the convergence must be carefully tested. In practice, however, we have found that it is often possible to replace the matrix element by a wave-vector and band-index conserving Kronecker symbol, which simplifies the numerical work substantially. In the evaluation of the Brillouin-zone sums we used an improved triangle method [6]. We have benchmarked our numerical algorithm against Ref.[5], and find quantitative agreement for pristine graphene. The full details will be given elsewhere [7].

Figure 2 shows an example of the computed polarizabilities for two different azimuthal angles of the q-vector. Also shown are results for a simplified model, "gapped graphene", where the dispersion is

$$\epsilon_{n\mathbf{k}} = n\sqrt{\Delta^2 + t^2 |\phi_{\mathbf{k}}|^2} \qquad |\phi_{\mathbf{k}}| = \left| e^{i\mathbf{k}\cdot\boldsymbol{\delta}_1} + e^{i\mathbf{k}\cdot\boldsymbol{\delta}_2} + e^{i\mathbf{k}\cdot\boldsymbol{\delta}_3} \right|$$

Here, $n = \pm 1$, and δ_i are the nearest neighbors. The parameter Δ is chosen so that the antidot lattice gap is reproduced. We observe a qualitative agreement, however much of the fine structure is lost in the simple model. We have also computed the plasmon dispersion laws, and find an approximate square-root dependence on the wave-vector (as is the case for pristine graphene), however the dispersion is suppressed as compared to graphene. For plasmon dispersion laws the simple model and the full antidot calculation are in close agreement.

References

[1] T.G. Pedersen, C. Flindt, J. Pedersen, N. A. Mortensen, A. P. Jauho, and K. Pedersen Phys. Rev. Lett. 100, **13** (2008) 136804.

[2] R. Petersen, T. G. Pedersen, and A. P. Jauho, to appear in ACS Nano (available in ASAP papers, December 16).
[3] B. Wunsch, T. Stauber, F. Sols, and F. Guinea, New J. Physics 8, **12** (2006) 318.
[4] E. H.Hwang and S. Das Sarma, Phys. Rev. B 75, **20** (2007) 205418.
[5] T. Stauber, J. Schliemann, and N. M. R. Peres, Phys. Rev. B 81, **8** (2010) 085409.
[6] T.G. Pedersen, C. Flindt, J. Pedersen, A. P. Jauho, N.A. Mortensen, and K. Pedersen.
[7] M. H . Schultz, A. P. Jauho, and T. G. Pedersen, in preparation

Figures
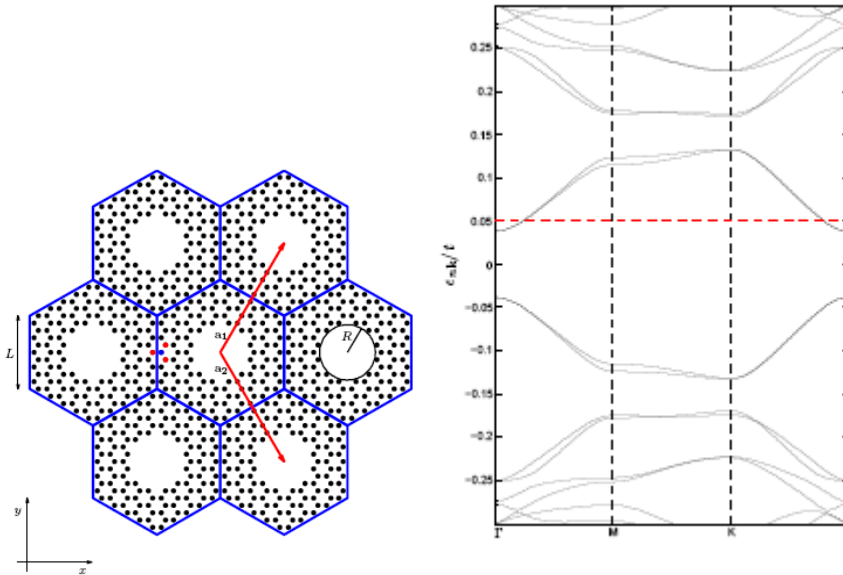
Figure 1. (Left) The geometry of the triangular graphene antidot lattice. The blue hexagons define the unit cell, R is the radius of the area from which carbon atoms have been removed, and the unit vectors $\mathbf{a_{1,2}}$ define the lattice symmetry. (Right) The band dispersion for a {12,3} lattice, used in our calculations. The dashed line indicates value of the chemical potential, for which the polarizability calculations in Fig. 2 are carried out.
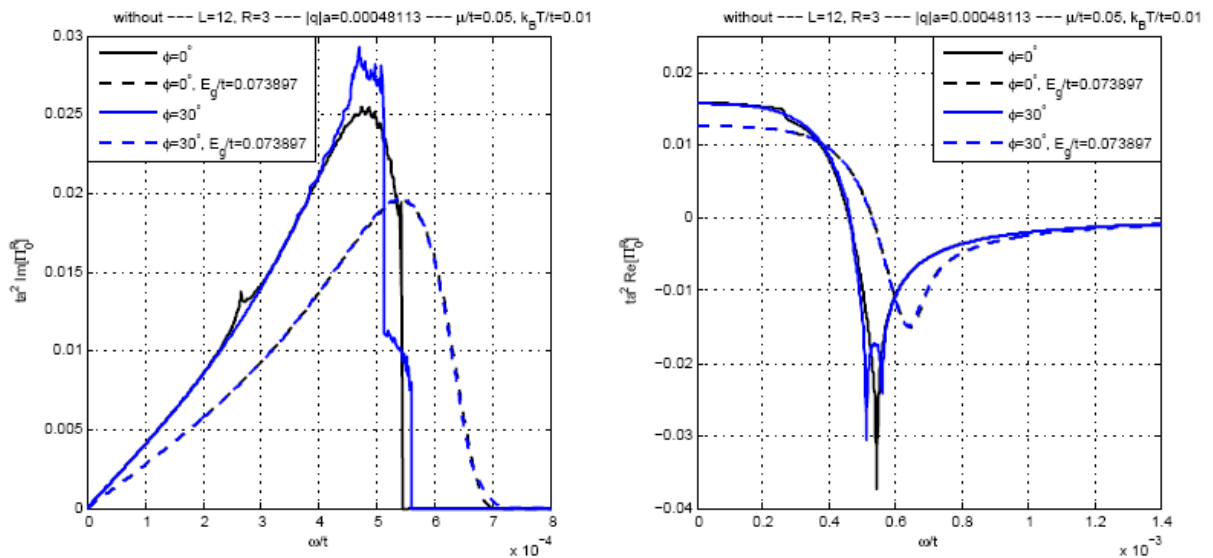
Figure 2. The imaginary (left panel) and the real (right panel) part of the polarization function, shown for two different azimuthal angles of the *q*-vector of length *qa* = 0.00048223, *kT / t = 0.01,* and μ/t 0 0.05. Continuous lines correspond to the full antidot model, while dashed lines correspond to "gapped graphene".

The Role of Threading Screw Dislocations in Graphene Growth on the C- and Si-faces of SiC

D.K. Gaskill, V.D.Wheeler, J.K.Hite, L.O.Nyakiti, J.C.Culbertson, F.J.Bezares, J.D.Caldwell, H.Chun, R.L.Myers-Ward, and C.R.Eddy, Jr.

U.S. Naval Research Laboratory, Washington, DC, USA
gaskill@nrl.navy.mil

Tremendous progress has been achieved in the fabrication of high frequency epitaxial graphene (EG) RF devices. Using SiC substrates for EG growth has enabled this progress as it facilitates large areas of graphene for device processing development. However, controlling the initiation and subsequent growth of graphene on the substrate, which is crucial for improvements in device performance, remains to be addressed. Here we show that threading screw dislocations (TSDs) have a significant impact on graphene growth on C-face 6H-SiC, but a much lesser impact for growth on the Si-face.

For growth on the C-face, conditions during the Si sublimation process (temperature and Ar pressure) were chosen to produce localized graphene formation.[1] These localized graphene areas were determined to lie below the level of the surrounding substrate and are referred to as graphene covered basin (GCBs). This result is consistent with the sublimation of Si from about 3 bilayers of SiC to form a monolayer of graphene.[2] The GCBs showed a range of different morphologies based on size and are thought to represent the early stages of graphene growth. Electron channeling contrast imaging (ECCI) was used to demonstrate the presence of a TSD near the centers of each GCB. Figure 1a shows an example ECCI micrograph of a GCB; note the development of ridges and the hexagonal perimeter. An expanded view of the TSD near the center of the GCB is shown in Fig. 1b. The TSD was confirmed by the change in direction of light-to-dark contrast in the ECCI image as the deviation from the Bragg angle changes sign.[3] By removing the graphene, these dislocations were revealed to lie within the SiC substrate. Optical and Raman spectroscopy showed that island centers were generally thicker than the edges due to the removal of more substrate material. These observations imply that screw dislocations act as nucleation sites for graphene growth on C-face SiC. As a GCB expands laterally, coalescence with other GCBs occur in a stochastic manner. Using the Raman D and G band intensities, we determined the crystallite length scale increases with increasing GCB lateral dimension, from about 100 nm for small GCBs to > 1 μm for macroscopic areas. This implies that the crystallinity of the merged materials improves as the substrate surface is covered.

The case for EG growth on the Si-face is very different. As is well-known, 1 to 2 monolayers of EG lies over the typical terrace and step morphology of the substrate.[4] A wafer was found where ECCI showed evidence for TSDs, but the graphene is relatively unaffected by the dislocation presence. Figure 2 shows a scanning electron micrograph of graphene grown on a region of the Si-face that contains TSDs. The terrace and step morphology is straight between TSDs, but becomes curved near them, similar to the C-face case. The difference is that for the C-face, localized growth continues from the GCBs along the step edge; this is not observed for growth on the Si-face. Using Raman spectroscopy and atomic force microscopy, the thicknesses of the graphene at and near the TSDs were found to be unchanged and there were no obvious morphological changes to the graphene. The fact that there are no gross changes to the substrate in the vicinity of the TSD suggests that the dislocation is probably not a major conduit for Si sublimation during growth (that is, a source of C), in contrast to the case for C-face growth.

References

[1] J.L.Tedesco, *et al.*, Appl. Phys. Lett. 96, 222103 (2010).
[2] P. Lauffer, K.V. Emtsev, R. Graupner, Th. Seyller, L. Ley, S.A. Reshanov, and H.B. Weber, Phys. Rev. B 77 (2008) 155426.
[3] M.E. Twigg and Y.N. Picard, J. Appl. Phys. 105 (2009) 0943250.
[4] J.A.Robinson, *et al.,* Nano Letters 9, 2873 (2009).

Figures
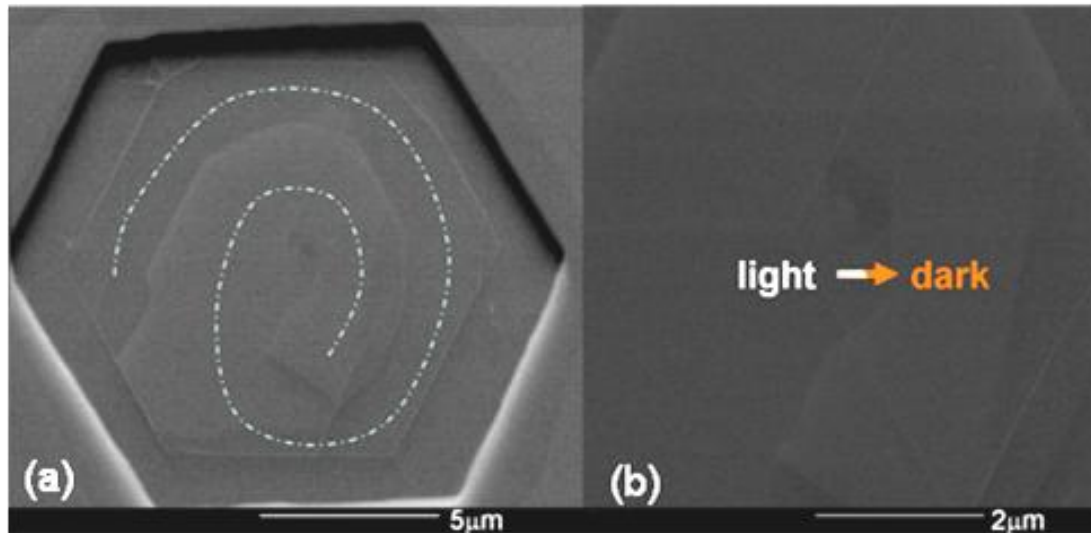
Figure 1. (a) An ECCI image of a small GCB with spiraling growth highlighted by the dotted line. (b) Magnified image of the GCB center, revealing a dislocation, imaged as an area of light/dark contrast. The arrow indicates the direction of the transition of light-to-dark contrast for Bragg angle deviations, consistent with the presence of a threading screw dislocation.
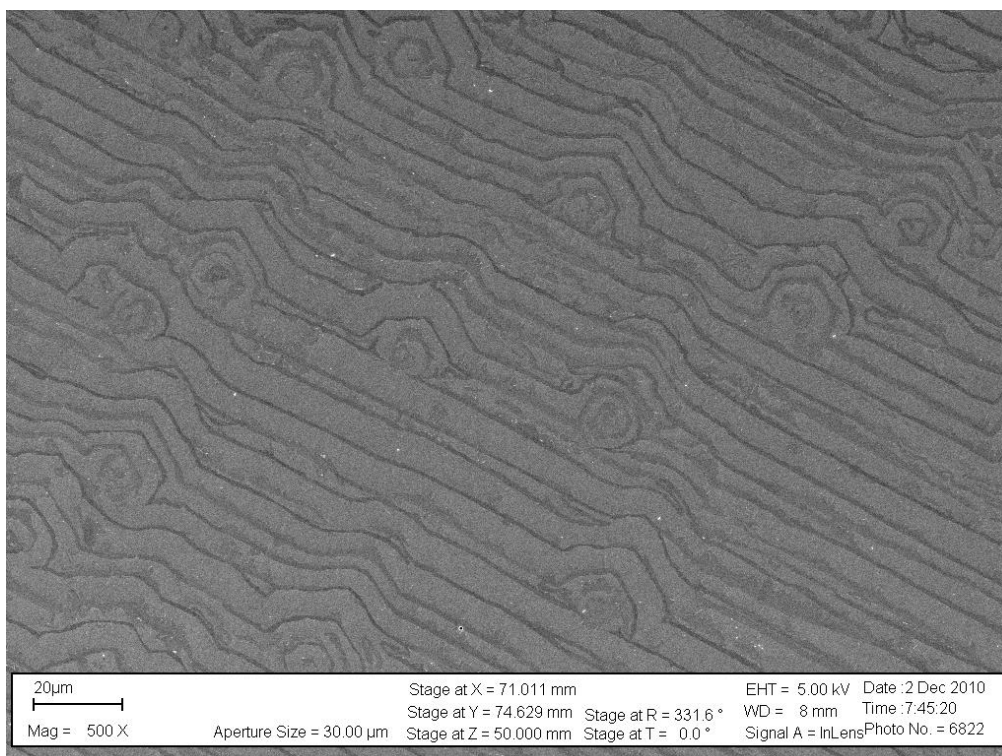
Figure 2. A scanning electron micrograph of graphene grown on the Si-face showing the typical terrace (light gray) and step bunched regions (darker gray). Note how the step bunched regions curve in some locations. ECCI images of those curved regions show the presence of a threading screw dislocation near the center.

Electronic scattering and nanoelectromechanical manipulation of graphene

V. Geringer[1,3], A. Georgi[1,3], D. Subramaniam[1,3], C. Pauly[1,3], T. Mashoff[1,3], M. Pratzer[1,3], B. Szafranek[2], D. Neumaier[2], M. Liebmann[1,3], and M. Morgenstern[1,3]

[1]II. Institute of Physics B, RWTH Aachen University, Otto-Blumenthal-Straße, 52074 Aachen, Germany
[2]Advanced Microelectronic Center Aachen (AMICA), AMO GmbH, Otto-Blumenthal-Straße 25, 52074 Aachen, Germany
[3]Jülich-Aachen Research Alliance: Fundamentals of Future Information Technology (JARA-FIT), Otto-Blumenthal-Straße, 52074 Aachen, Germany

geringer@physik.rwth-aachen.de

Using scanning tunneling microscopy (STM) and spectroscopy (STS), we perform an atomically resolved investigation of the electronic scattering behavior at impurities and a monolayer / bilayer step edge in graphene on SiO_2. Measurements at different tip-sample distances reveal a reversible transition between hexagonal and trigonal symmetry of the atomic corrugation interpreted as a tip-induced buckling, associated with different displacements of the flake.

STM allows a direct observation of microscopic scattering, which could possibly affect the electrical properties of this system. Our measurements reveal intense interference patterns with a wavelength of 0.37 nm. This $\sqrt{3} \times \sqrt{3}$R30° superstructure is only observed in the vicinity of strong scatterers, such as edges or adsorbates (Fig. 1), and is induced by intervalley scattering of electrons. The interference effect shows an energy dependence which corresponds to the conical band structure of graphene. Moreover, a simultaneous imaging of the electronic scattering pattern and the atomic structure enables the determination of the impurity position with respect to the crystal lattice.

Employing tip-graphene interactions, we move parts of the flake under the tip vertically [1]. Thereby, we also modify the atomic lattice of graphene, observing a phase transition between a hexagonal and a buckled, threefold symmetry phase. Different models, including mechanical compression and modifications of the local density of states, are discussed.
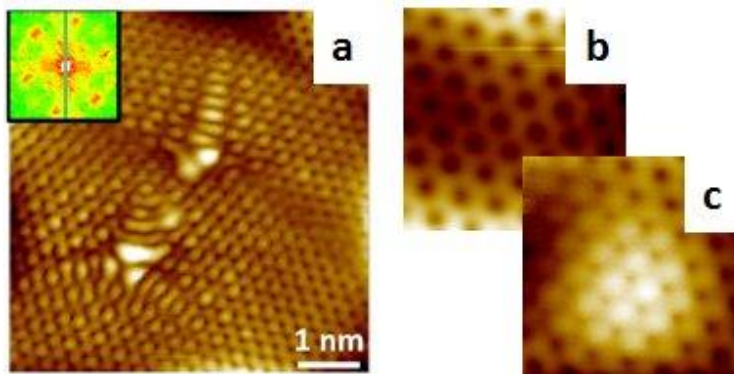
Fig. 1: STM constant current images of (a) scattering patterns at an adsorbate, (b) hexagonal contrast at 0.5 V, 0.1 nA (larger tip-sample distance), (c) trigonal contrast at 0.5 V, 5 nA (smaller distance).

References

[1] T. Mashoff, M. Pratzer, V. Geringer, T. J. Echtermeyer, M. C. Lemme, M. Liebmann, and M. Morgenstern: *Bistability and Oscillatory Motion of Natural Nanomembranes Appearing within Monolayer Graphene on Silicon Dioxide.* Nano Lett. **10**, 461 (2010).

Electrical conductivity of carbon nanopowders.

Marcos Ghislandi[a], Bernardo Marinho[a,b], Evgeniy Tkalya[c], Cor Koning[c], Joachim Loos[a], Gijsbertus de With[a].

[a]Laboratory of Materials and Interface Chemistry, Eindhoven University of Technology, 5600 MB Eindhoven, The Netherlands
[b] Department of Chemical Engineering, Federal University of Minas Gerais, Av. Antônio Carlos 6627, 31270-901, Belo Horizonte, Brazil
[c] Laboratory of Polymer Chemistry, Eindhoven University of Technology, 5600 MB Eindhoven, The Netherlands.

m.g.ghislandi@tue.nl

The discovery of graphitic nanoparticles with exceptional electrical transport properties, like high conductivity and high charge mobility, has incredibly broadened the range of potential applications of this class of materials, thus unleashing a revolution in electronic devices industry. Two of the most important members of this new generation of materials are undoubtedly carbon nanotubes and graphene. Perhaps the biggest challenge to be faced is how to manipulate these nanoparticles in order to bring effectively their remarkable electrical properties onto the macroscopic level. Since the conductive performance of the composites is directly related to the formation of a conductive network through the polymer matrix, its understanding depends, at least partly, on the knowledge of the electrical behavior of the nanoparticles agglomerates, here called bulk powder.

The electrical conductive behavior of different carbon materials (multi-walled carbon nanotubes, graphene, carbon black and graphite), widely used as fillers in polymeric matrices, was studied using compacts produced by the buckypaper preparation process and powder compression [1-7]. Powder pressing assays show that the bulk conductivity depends not only on the intrinsic material properties but is also strongly affected by the number of particle contacts and the packing density. For nanotube, graphene and graphite particles, the conductive behavior during compaction is governed by mechanical particle arrangement/deformation mechanisms. The buckypaper preparation process induces a high in-plane preferred orientation for the large surface area nanotube and graphene particles, thereby yielding largely the single particle intrinsic conductivity for the in-plane direction. The relevance of the results for composite processing is discussed.

References

[1] Noda T, Kato H, Takasu T, Okura A, Inagaki M., Bull. Chem. Soc. Jpn., **39** (1966), 829-833.
[2] Euler KJ, Kirchhof R, Metzendorf H., Mater. Chem., **4(4)** (1979), 611-629.
[3] Espinola A, Mourente M, Salles M, Pinto A., Carbon, **24** (1986), 337-341.
[4] Kendall, K., J. Phys. D: Appl. Phys., **23** (1990), 1329-1331.
[5] Celzard A, Marêche JF, Payot, F, Furdin, G., Carbon, **40** (2002), 2801-2815.
[6] Pantea D, Darmstadt H, Kaliaguine S, Roy C., Appl. Surf. Sci., **217** (2003), 181-193
[7] Mamunya YP, Zois H, Apekis L, Lebedev EV., Powder Technol., **140** (2004), 49-55.
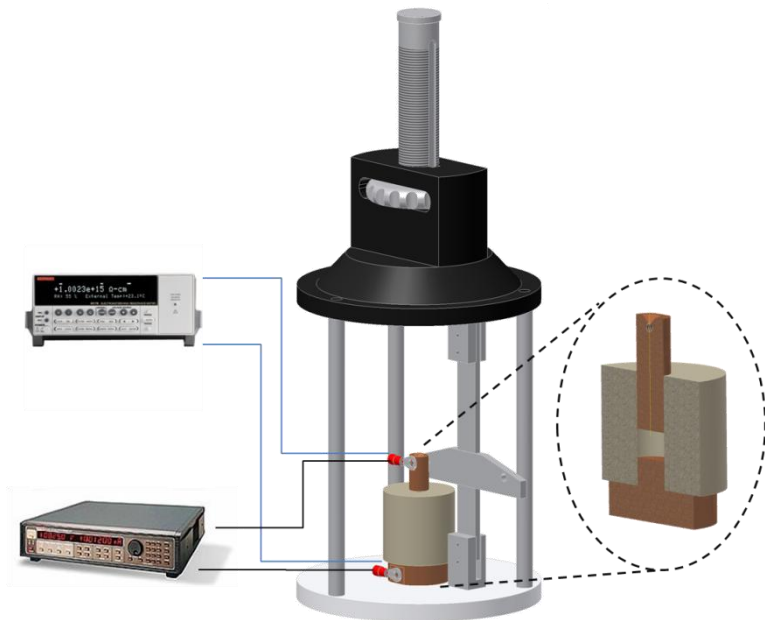
Figure 1. *Schematic representation of the experimental set-up involved in the measurement of the powder conductivity.*
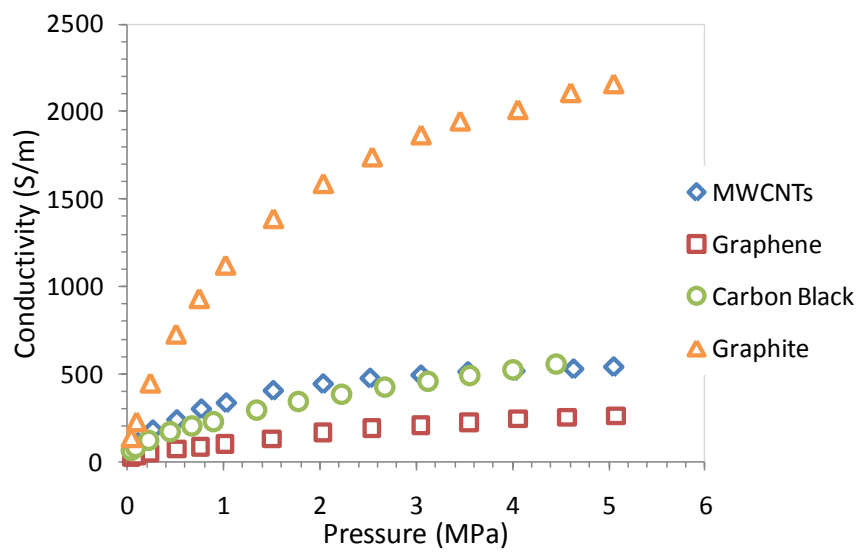
Figure 2. *Electrical conductivity behavior of the different carbon powders as a function of pressure. For each material the data points represent an average of at least 3 identical assays differing not more than 3%..*

Effect of graphene/substrate interface on the electronic transport properties

F. Giannazzo, S. Sonde, C. Vecchio, E. Rimini, V. Raineri

CNR-IMM, Strada VIII, 5   95121 Catania, Italy
filippo.giannazzo@imm.cnr.it

Graphene is currently the object of many research interests especially for its remarkable electronic transport properties, making this material a promising candidate for future "post-Si" electronics. In a free standing graphene sheet without defects and adsorbed impurities, charge carriers can exhibit a giant intrinsic mobility [1] and can travel for micrometers without scattering even at room temperature. So far, very high values of mobility ($>2\times10^5$ cm^{2}V^{-1}s^{-1}) and electron mean free path have been observed in vacuum and at low temperature (5K) in "suspended" graphene after a current-induced cleaning [2]. However, graphene for electronics applications is commonly supported by a dielectric substrate or by semi-insulating SiC, and the values of the electron mean free path (l) and mobility (μ) measured in supported graphene are usually significantly lower than in suspended ones.

In the present work, l and μ have been comparatively evaluated in graphene sheets mechanically exfoliated from highly oriented pyrolytic graphite and deposited on substrates with different relative dielectric permittivities, SiO$_2$ (k_{SiO2}=3.9), Si$_3$N$_4$ (k_{Si3N4}=7.5), 4H-SiC (0001) (k_{SiC}=9.7) and strontium titanate, STO (k_{STO}=330), and in single layer graphene epitaxially grown by thermal decomposition of 4H-SiC (0001). The transport properties have been measured at room temperature both on micrometer size test patterns in graphene, using conventional electrical characterization (sheet resistance and Hall effect measurements on Van der Pauw structures) and, locally, by using a recently demonstrated scanning probe method based on localized capacitance measurements [3,4]. From the experimentally found dependence of l on the carrier density (n), three main scattering mechanisms affecting electronic transport in supported graphene sheets have been identified, i.e. (i) Coulomb scattering by charged impurities, either adsorbed on graphene or located at the interface with the substrate, (ii) scattering by point defects [5], working as resonant scatterers [6] and (iii) scattering by the substrate surface polar phonons (SPP) [7]. Scattering by charged impurities is reduced in graphene sheets on substrates with higher permittivity, due to a more efficient dielectric screening of Coulomb potential. Hence, the role played by SPP and by defects becomes increasingly important in graphene on high-k dielectrics and ultimately limits its transport properties. As an example, both in the case of graphene deposited on SiO$_2$ and on 4H-SiC(0001), scattering by charged impurities is still the main scattering mechanism. However, a higher electron mean free path is measured in graphene on SiC, due both to the three-times higher dielectric permittivity than SiO$_2$ and to the higher SPP phonon frequency (see Fig.1). In the case of graphene on the high-k substrate STO, a mean free path significantly lower than that expected by charged impurities scattering is measured, indicating that the scattering by SPP and defects become the mechanisms limiting transport properties.

Finally, comparing the mean free path locally measured on several surface positions in deposited graphene on 4H-SiC (0001) and in epitaxial graphene grown on the same substrate, it was worth noting, in the latter case, an average value ~0.4 times than in deposited graphene and a much broader distribution of the locally measured values. These differences have been explained in terms of the peculiar interface structure of epitaxial graphene on the Si face of hexagonal SiC, in particular as a consequence of the presence of a large density of dangling bonds between the C buffer layer (the precursor of epitaxial graphene formation) and the substrate [8,9].

References

[1] Chen J H, Jang C, Xiao S, Ishigami M and Fuhrer M S, Nat. Nanotechnol. **3**, 206 (2008).

[2] Bolotin K I, Sikes K J, Jiang Z, Klima M, Fudenberg G, Hone J, Kim P and Stormer H L, Solid State Commun. **146**, (2008) 351.

[3] F. Giannazzo, S. Sonde, V. Raineri, E. Rimini, Nano Lett., **9**, (2009) 23.

[4] F. Giannazzo, S. Sonde, V. Raineri, E. Rimini, Appl. Phy. Lett., **97**, (2010) 132101.

[5] F. Giannazzo, S. Sonde, V. Raineri, E. Rimini, Appl. Phy. Lett., **95**, (2009) 263109.

[6] Z. H. Ni, L. A. Ponomarenko, R. R. Nair, R. Yang, S. Anissimova, I. V. Grigorieva, F. Schedin, P. Blake, Z. X. Shen, E. H. Hill, K. S. Novoselov, A. K. Geim, Nano Lett.**, 10**, *(*2010) 3868.

[7] S. Fratini, F. Guinea, Phys. Rev. B **77**, (2008) 195415.

[8] Th. Seyller, A. Bostwick, K. V. Emtsev, K. Horn, L. Ley, J. L. McChesney, T. Ohta, J. D. Riley, E. Rotenberg, F. Speck, Phys. Stat. Sol. (b) **245**, (2008) 1436.

[9] S. Sonde, F. Giannazzo, V. Raineri, R. Yakimova, J.-R. Huntzinger, A. Tiberj, and J. Camassel, Phy. Rev. B **80**, 241406(R) (2009).

Figures
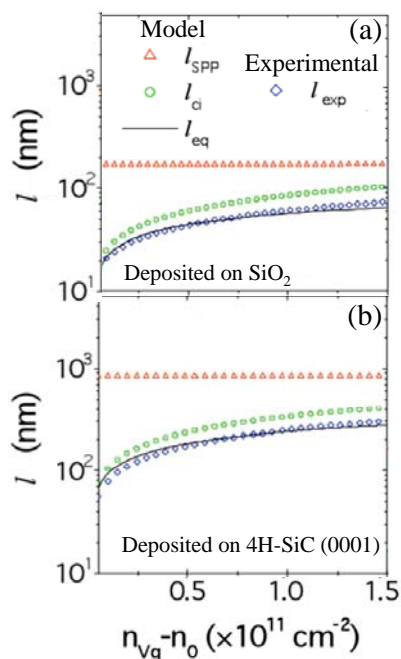
Fig.1 Electron mean free path versus carrier density in graphene exfoliated from HOPG and deposited on SiO₂ (a) and on the Si face of 4H-SiC (b). The fit of the experimental data is reported, as well as the calculated electron mean free path limited by charged impurities and surface polar phonons scattering.
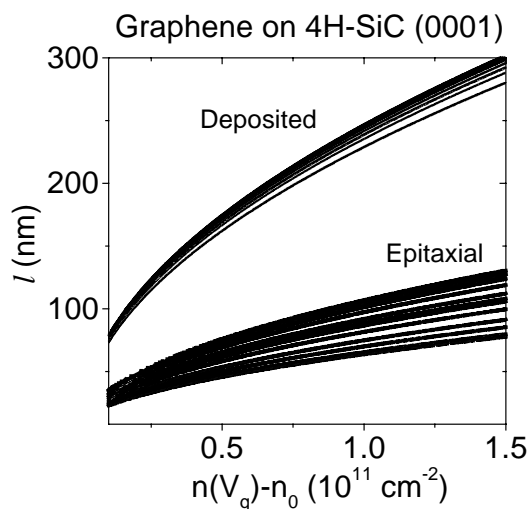
Fig.2 Locally measured electron mean free path versus carrier density on several surface positions in graphene exfoliated from HOPG and deposited on 4H-SiC (0001) and in epitaxial graphene grown on the same substrate.

Fabrication of Graphene Layers by Means of Chemical Vapor Deposition for Field Effect Device Fabrication

Pia Juliane Ginsel, Frank Wessely, Udo Schwalke

Institute for Semiconductor Technology and Nanoelectronics (ISTN)
Darmstadt University of Technology
Schlossgartenstrasse 8
64289 Darmstadt, Germany
e-mail: ginsel@iht.tu-darmstadt.de

Abstract - In this paper we report on the fabrication and characterization of graphene layers for graphene field effect devices, which is a modified and advanced approach already developed at ISTN for the in situ fabrication of single walled carbon nanotubes [1]. After the graphene layers are generated by means of chemical vapor deposition using a methane feedstock, the band gap is engineered constricting the lateral dimensions of graphene obtaining graphene nanoribbons. The graphene nanoribbons (GNRs) are contacted by selected metals to form field effect devices with various applications.

I.   Fabrication

As substrate highly p-doped silicon wafers are used, which are oxidized in dry ambient at 1000°C to form an oxide of 60 nm. In the following the oxide is patterned by several lithography steps. Subsequently a structured photoresist remains on the wafer surface and a thin aluminum and nickel layer is evaporated on the whole wafer surface and structured via liftoff. After annealing at high temperature (900 °C) in hydrogen atmosphere the Al-Ni layer forms the catalyst. The so called sacrificial catalyst Al transforms itself into an insulator aluminum oxide which is covered with nickel nanoclusters [1]. By means of chemical vapor deposition (CVD) with a methane feedstock, a thin graphene layer grows near catalytic aluminum/nickel areas (see Fig 1).

II.   Analysis

The first analysis of the graphene layer by atomic force microscopy AFM (see Fig. 2) shows a layer thickness of around 2.5 nm, which corresponds to five to seven stacked graphene sheets. The conductive AFM (C-AFM) measurement shows that the ultra-thin layer around Al/Ni regions is made of a conductive material (see Fig. 3), as expected for graphene. The scanning electron microscopy image of the probe at the catalyst graphene junction points at a higher resolution of the composition (see Fig. 4), some carbon nanotubes growing from the nickel cluster can be seen, as they are supposed to be [3],[4]. To proof whether the carbon has an amorphous or a lattice structure, the probe was mould in epoxy resin for the structural transmission electron microscopy examination (TEM). Figure 5 shows the TEM examination of a graphene layer on a silicon dioxide surface with fourier analysis. The interplanar spacing of 3.5Å is a strong evidence for the existence of graphene grown by means of CVD.

III.   Conclusion and Outlook

The analysis of the produced layer yields several stacked graphene sheets. By constricting the lateral dimensions of graphene to obtain designable band gaps, graphene becomes a viable material for transistor applications, for example as GNR field effect devices. At ISTN, graphene layers produced by means of CVD will be patterned into GNRs using electron-beam lithography followed by reactive-ion etching allowing lateral downscaling in the sub-100 nm range, as already achieved for silicon nanowires [2]. The physical characterization of the GNRs will be prepared by means of AFM while the electrical characterization will be done by Keithley measuring station, already used for the characterization of carbon nanotube field effect devices (CNTFETs).

IV.   Acknowledgement

This research is part of the ELOGRAPH project within the ESF EuroGRAPHENE EUROCORES programme.

V.   References

[1]   L. Rispal, P. J. Ginsel, U. Schwalke, ECS Trans., **"In Situ Growth of Carbon for Nanoelectronics: From Nanotubes to Graphene"**, (2010) 33, 13
[2]   F. Wessely, T. Krauss, U. Schwalke, ESSDERC, **"Dopant-Independent and Voltage-Selectable Silicon-Nanowire-CMOS Technology for Reconfigurable Logic Applications"**, 2010
[3]   L. Rispal, T. Tschischke, H. Yang and U. Schwalke, ECS Trans., **"Mass-Production of Passivated CNTFETs: Statistics and Gate-Field Dependence of Hysteresis Effect"** ,(2008), 13, 65
[4]   L. Rispal and U. Schwalke, IEEE Electron Device Lett., **"Large-Scale In Situ Fabrication of Voltage-Programmable Dual-Layer High-k Dielectric Carbon Nanotube Memory Devices With High On/Off Ratio"**, (2008), 29, 1349

VI.   Figures
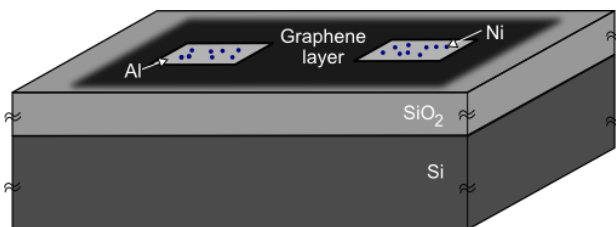
Figure 1. Schematic of silicon substrate covered by silicon dioxide. The graphene layer on top is grown by means of CVD with a methane feedstock near catalytic aluminum/nickel areas.
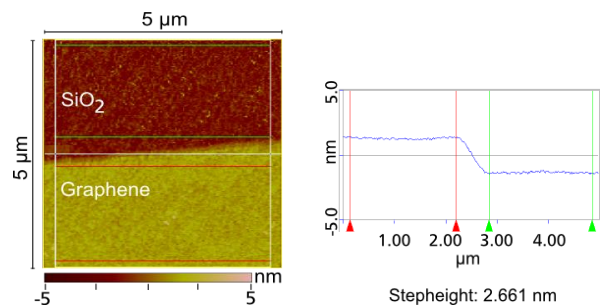
Figure 2. AFM Measurement (left) of the graphene layer on a silicon dioxide surface, (right) corresponding stepheight analysis by average heigth value calculated at the red and green lines.
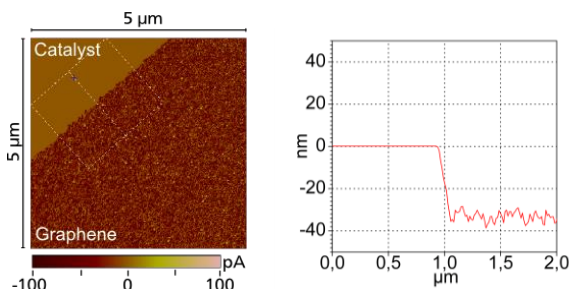
Figure 3. (left) AFM current scan of the graphene layer and the corresponding cross-section within the white square (right).
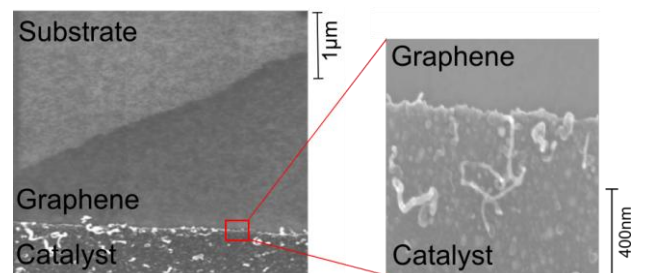
Figure 4. Scanning electron microscopy image of the probe at the catalyst graphene interface.
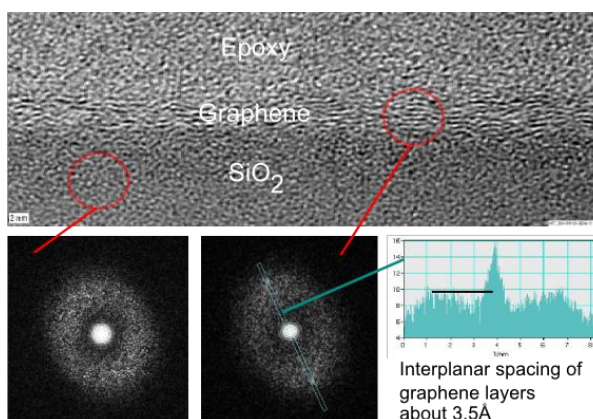
Figure 5. Structural transmission electron microscopy examination of a graphene layer on a silicon dioxide surface with fourier analysis.

One-Pot Greener Reduction and Magnetization of Graphene Oxide Sandwich structures for Trapping Toxic Chromium (VI) Contaminants

Ganesh Gollavelli[a] and Yong-Chien Ling[a*]

[a]Department of Chemistry, National Tsing Hua University, Hsinchu, Taiwan 30013

Contact @ E-mail: ganesgollavelli@gmail.com

In recent years, Graphene has explored versatile applications in nano electronics, sensors and biomedical diagnosis etc. Several synthetic strategies were developed to obtain reduced and magnetic graphene oxide (rMGO). Many of them, however, are either time-consuming, multi-step or require the use of highly toxic or environmentally unfriendly reagents. It is necessary to develop a simple, rapid and green synthetic process to achieve reduction and magnetization of graphene oxide. In this report, a facile in-situ solid-state microwave induced process was developed to facilitate the reduction and magnetization in one pot. The obtained rMGO sandwich structures were well characterized by the spectroscopic and microscopic techniques. The bare rMGO possess excellent magnetic property and efficient binding capacity for Cr (VI), whose presence was considered to be the most toxic and carcinogenic in the ecological system. Through the comprehensive exploration of adsorption experiments, it has proven possible to create the first example of reduced magnetic graphene oxide based adsorbant for trapping chromium metal contaminants with almost 99.9% removal efficiencies. The discovery of simple, rapid, facile and green synthesis of rMGO will provide new opportunities for research that exploits the blend and synergism of graphene oxide for environmental applications.

References

[1] Vimlesh Chandra, Jaesung Park, Young Chun, Jung Woo Lee, In-Chul Hwang,* and Kwang S. Kim*, ACS Nano, **4** (2010) 3979.
[2] Di Zhang, Suying Wei, Chandana Kaila, Xin Su, Ji Wu, Amar B. Karki, David P. Young and Zhanhu Guo, Nanoscale, **2** (2010) 917.
[3] Yanwu Zhu, Shanthi Murali, Meryl D. Stoller, Aruna Velamakanni, Richard D. Piner, Rodney S. Ruoff, Carbon, **48** (2010) 2106.

Figure
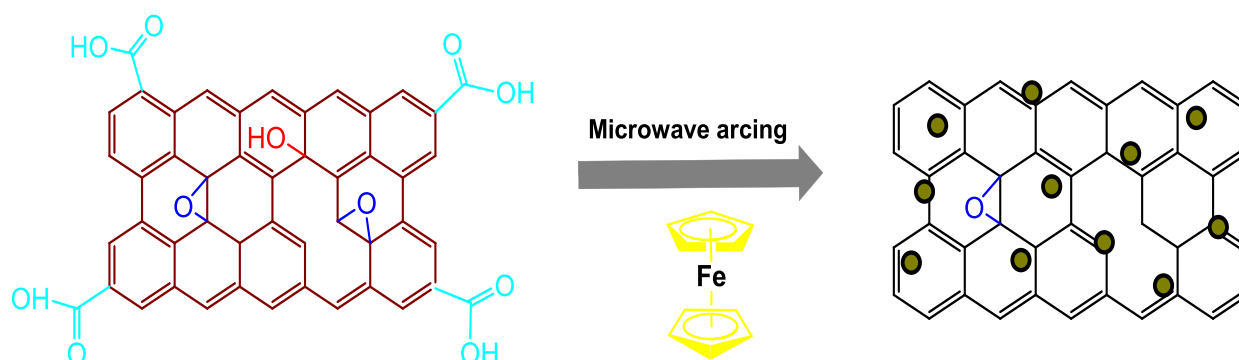
Schematic procedure for the synthesis of reduced magnetic graphene oxide (rMGO) via microwave arcing

Functionalization of Carbon Nanostructures with Inorganic Nanoparticles

Neus G. Bastus[1,2,*], Miriam Varon[2], Michaela Meyns[1], Christian Klinke[1], Horst Weller[1] and Victor F. Puntes[1,3]

1- Institute of Physical Chemistry; University of Hamburg, Grindelallee 117, 20146 Hamburg, Germany.
2- Institut Català de Nanotecnologia, Campus UAB Bellaterra,,08193 Barcelona, Spain
3- Institut de Recerca i Estudis Avançats (ICREA)

Email*: neus.bastus@chemie.uni-hamburg.de*

Inorganic nanoparticles (NPs) have emerged as a new class of materials particularly interesting due to their unique size and shape-dependent electronic, optical, magnetic and catalytical properties. On the other hand, carbon nanostructures (CNS) presents a high surface area, high thermal and electrical conductivity and chemical inertness. On this regard, the combination of these two components in an hybrid nanostructure (HNS) may lead to a new class of functional materials that integrate the properties of both components. These HNS present important features for catalysis, nanotechnology and materials science applications [1] while electronic communication between both structures open new frontiers in the design of photoelectronic of light-energy conversion devices. Additionally, CNS can be used as a scaffolds to build 1D or 2D self-assembled nanowires or nanosheets of inorganic NPs.

The most important and crucial point for the future expansion of these new class of materials for technological applications is to find power synthetic methodologies to produce HNS with reproducible properties and performances. Up to date, all used methods are either based on the direct growth of NPs onto CNS or the attachment of pre-synthesized NPs to CNSs via their covalent linking through organic molecules. While the direct growth is usually a simple and effective synthetic method, it does not allow the easy control of the final NPs morphology. Alternatively, the attachment of pre-formed NPs to CNT leads to better size and shape selection, although it involves a multi-reaction process in order to modify the inert facets of the CNS. In this context, we developed a protocol for the functionalization of CNS with inorganic NPs based on the use of CNS as ligands. Under the appropriate conditions, this method allows i) the destabilization of the original surfactant layer of the NP and ii) the further use of CNS facets as additional ligands. This technique leads to CNS selectively decorated with metal NPs, avoiding tedious surface modification[2-4].
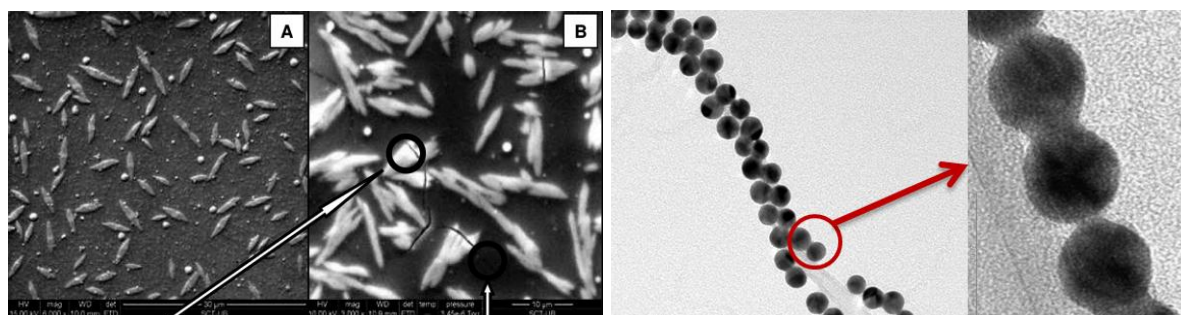
Functionalization of CNS with Inorganic Nanoparticles: (Left) Co-CNS hybrid nanostructures (4-8 µmCo rice-grain like structures). **(Right)** Au-CNT HNCs dispersed in toluene (Au NPs are 12 nm in diameter)**.**

References:

1. Wildgoose, G., C. Banks, and R. Compton, Metal Nanoparticles and Related Materials Supported on Carbon Nanotubes: Methods and Applications. Small, 2006. 2(2): p. 182-193.
2. Juarez, B.H., et al., Quantum Dot Attachment and Morphology Control by Carbon Nanotubes. Nano Letters, 2007. 7(12): p. 3564-3568.
3. Ritz, B., et al., Reversible Attachment of Platinum Alloy Nanoparticles to Nonfunctionalized Carbon Nanotubes. ACS Nano. 4(4): p. 2438-2444.
4. Varon, M., et al., Dipolar Driven Spontaneous Self Assembly of Superparamagnetic Co Nanoparticles into Micrometric Rice-Grain like Structures. Langmuir, 2010. 26(1): p. 109-116.

Chemically derived graphene: electronic and mechanical properties

C. Gómez-Navarro[1,2*], R.S. Sundaram[2], V. López[1], F. Zamora[1], J. Gómez-Herrero[1], M. Burghard[2], K. Kern[2]

[1]*Universidad Autonoma de Madrid, Spain*
[2] *Max Planck Institute for Solid State Research, Stuttgart, Germany*

[*]e-mail address: *cristina.gomez@uam.es*

The promising electronic, mechanical and thermal properties of graphene for high demanding applications call for the need of approaches that provide access to large amounts of graphene monolayers.

Here we report on the electronic and mechanical properties of single graphene sheets obtained via chemical reduction of graphite oxide, a promising route for the large scale production of graphene layers that offers the possibility to assemble them on insulating technological relevant substrates.

Chemically reduced single graphene oxide layers exhibit moderate conductivities due to the presence of defects or residual functional groups remaining after reduction[1]. This moderate electrical performance can be extraordinarily improved by a CVD process to heal defects contained within the monolayers. In this manner, sheets with two orders of magnitude conductivity enhancement can be obtained[2], reaching mobilities that exceed those of the molecular semiconductors currently used in organic electronics.

From the mechanical point of view, AFM indentation experiments on suspended chemically derived layers reveal a Young modulus closely approaching that of pristine graphene[3], with their electrical conductivity scaling inversely with the elastic modulus.

References

1.   Gomez-Navarro, C.; Weitz, R. T.; Bittner, A. M.; Scolari, M.; Mews, A.; Burghard, M.; Kern, K. **Nano Letters** 2007**,** 7, (11), 3499-3503.
2.   López, V.; Sundaram, R. S.; Gómez-Navarro, C.; Olea, D.; Burghard, M.; Gómez-Herrero, J.; Zamora, F.; Kern, K. Advanced Materials 2009, 21 , 46
3.   Gomez-Navarro, C.; Burghard, M.; Kern, K. **Nano Letters** 2008**,** 8, (7), 2045-2049.

Electronic and Optical Properties of Graphene Antidot Lattices

Jesper Goor Pedersen, Thomas Garm Pedersen

Department of Physics and Nanotechnology, Aalborg University, DK-9220 Aalborg Ø, Denmark
jgp@nano.aau.dk

While pristine graphene has presented a wealth of intriguing electronic properties, the lack of a sizable band gap is a significant drawback for possible applications in the field of electronics. We have shown how a periodic modulation of a graphene sheet, in the form of a regular array of holes, introduces a band gap around the Fermi level, the size of which depends on the size and periodicity of the holes [1]. While we have originally focused on perforations as the source of the modulation, several experiments have presented alternate methods of realizing such graphene antidot lattices, such as e.g. patterned hydrogen adsorption [2]. The crucial ingredient is the breaking of the symmetry between the two sublattices of graphene.

We present results of band structure calculations using three computational methods of increasing complexity; (i) finite-element solutions of the Dirac equation (DE) with an infinite mass term in the location of the antidots, (ii) nearest-neighbor tight-binding (TB) calculations, and (iii) full-fledged density functional theory (DFT) calculations. We find good agreement between DFT and TB calculations, while the DE method consistently reports larger band gaps. The discrepancies of the DE results are linked to the lack of an adiabatic transition between the perfect graphene sheet and a graphene antidot lattice with vanishing hole radius [3]. A simple correction of the DE results leads to much better agreement between all three methods.

The lower conduction and upper valence band of graphene antidot lattices can be described qualitatively in a simple continuum model, by introducing a mass term in the Dirac equation of pristine graphene. We present closed-form expressions of the optical conductivity predicted from such a model [4] and compare with results obtained from atomistic modelling [5]. The model admits analytical solutions, also with a magnetic field perpendicular to the graphene plane. Using these analytical solutions, we present preliminary results on the influence of magnetic fields on the optical properties of gapped graphene, with an emphasis on the off-diagonal conductivity. We compare these results to calculations using a tight-binding model with a staggered potential, where the magnetic field is introduced via a Peierls substitution.

References

[1] T. G. Pedersen *et al.*, Physical Review Letters, **100** (2008) 136804.
[2] R. Balog *et al.*, Nature Materials, **9** (2010) 315.
[3] J. Fürst *et al.*, New Journal of Physics, **11** (2009) 095020.
[4] T. G. Pedersen *et al.*, Physical Review B **79** (2009) 113406.
[5] T. G. Pedersen *et al.*, Physical Review B **77** (2008) 245431.

Figures
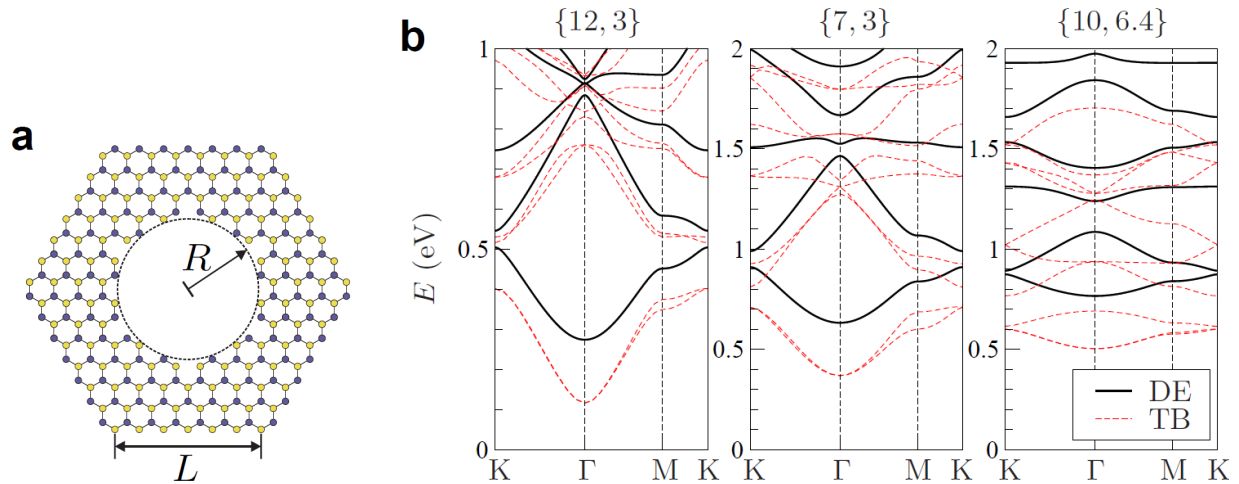
(a) Unit cell of the {L,R}={7,3} graphene antidot lattice, with L and R given in units of the graphene lattice constant. (b) Band structure calculated for three different antidot lattices, comparing results obtained using the Dirac equation to those obtained using a nearest-neighbor tight-binding approach. Only positive energies are shown, as both methods exhibit perfect electron-hole symmetry. Note that while the methods are in qualitative agreement on the shape of the bands, the DE results consistently show larger band gaps.
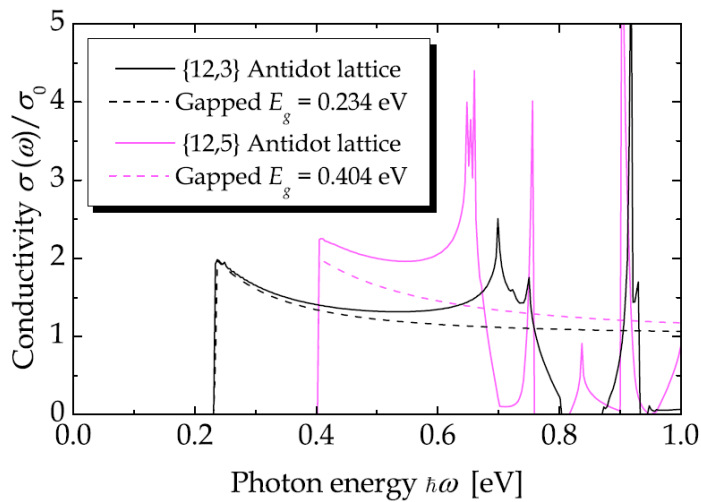
Optical conductivity calculated for gapped graphene compared to results obtained using atomistic modelling of graphene antidot lattices. The mass term of the gapped graphene has been adjusted to fit the band gap of the chosen antidot lattices. Note the qualitative agreement at low energies.

Quantum pumping in graphene nanoribbons at resonant transmission

E. Grichuk[1], E. Manykin[2]

[1]National Research Nuclear University "MEPhI", 115409, Kashirskoe sh., 31, Moscow, Russia
[2]Russian Research Centre "Kurchatov Institute", 123182, pl. Kurchatova, 1, Moscow, Russia
evgeny.sg@gmail.com

In recent years graphene has been the subject of intense theoretical and experimental research mainly due to its very peculiar electronic structure and electronic properties, resulting in numerous unusual effects: Klein tunnelling "paradox", half-integer quantum Hall effect, and other effects [1]. Many authors consider graphene as a good candidate for spintronics and for future replacement of silicon-based electronics. A graphene sheet can be cut to form graphene nanoribbons (GNR) with different orientations of edges relative to the graphene crystal structure. If two (or more) independent parameters (e.g., gate voltages) of a mesoscopic system are adiabatically modulated in time, finite dc current through the device can be generated. This phenomenon is known as adiabatic quantum pump effect. Quantum pump effect in graphene was previously studied by E.Prada et al. using Dirac approximation [2]. They argued that the Klein tunnelling effect has a great impact on the properties of graphene-based pumping devices due to the unusual (in comparison with normal devices) contribution of evanescent modes. Pumping with two potential barriers, separated by a finite unbiased central region, was considered in ref. [3]. It was demonstrated that due to the high anisotropy of transmission through a potential barrier in graphene both directions of pumping can be realized for a fixed pumping contour in contrast to normal devices. Pumping with a series of barriers was considered in a recent paper by Z.Wu et al. [4].

We consider adiabatic quantum charge pumping in graphene nanoribbon double barrier structures with armchair (AGNR) and zigzag (ZGNR) edges in the resonant transmission regime [5]. The geometry of the setup is depicted in fig. 1(a). The Hamiltonian of the device is expressed using orthogonal nearest-neighbour tight-binding approximation. Pumping is achieved by periodic variation of two external gate voltages which are modelled by adding on-site energies U_1 and U_2 to the diagonal terms of the Hamiltonian. Electron-electron interactions are neglected and the spin degeneracy factor of 2 is omitted for clarity. In the adiabatic approximation the charge pumped through the device can be calculated within scattering matrix formalism using Brouwer's formula [6]. Alternatively, Green's function formalism can be used [7].

In the case of AGNR the whole resonance line of conductance contributes to the pumping of a single electron per cycle through the device. This picture is reminiscent of that of a simple 1D double barrier structure (a quantum dot separated from the leads by two point contacts with variable conductances). In fig. 2(a) the dependence of the pumped charge Q on the Fermi energy E_F in the leads is plotted. The transmission amplitude is peaked when E_F becomes equal to the energy of some quasi-bound state in the device region. When the Fermi level is far from any such state, no resonance is observed. One can see from fig. 2(a) that for some values of E_F the pumped charge tends to the electron charge value. This happens each time when the pumping contour encloses a large part of the resonance line. This charge quantization behaviour is in agreement with charge loading/unloading picture discussed in ref. [8]. The pumping contour crosses the resonance line in two resonance points A and B (see fig. 1(b)). When the point A is crossed, the quasi-bound level inside the device moves below the Fermi level in the leads and an electron tunnels from the left lead into the central region. At the point B the quasi-bound level moves up and an electron tunnels into the right lead.

The situation is qualitatively different for ZGNR due to zero-conductance resonances (dips) inherent to locally gated ZGNRs and associated with the formation of discrete quantum levels in the barrier region. [9]. In fig. 2(b) we plot the dependence of the pumped charge on the Fermi energy. The pumped charge is also quantized, but in contrast to AGNR, both directions of current are now possible for fixed direction of the pumping contour. Such behaviour can be explained within charge loading/unloading picture [8] taking into account the zero-conductance resonances. In the AGNR case at point A (fig. 1(b)) the probability of tunnelling through the right barrier is much lower than the probability of tunnelling through the left one because the right barrier is much higher. At the point B the situation is reversed. The parameters can be adjusted such that the tunnelling through the left (right) barrier at point A (B) is blocked by the zero-conductance resonance. This results in the backward direction of current. These conductance dips separate the whole resonance line into several parts, each of which corresponds to the pumping of a single electron through the device, and in contrast to AGNR, one electron can be pumped from the left lead to the right one or backwards.

References

[1] Katsnelson M. I., Novoselov K. S. and Geim A. K., Nature Physics, **2** (2006) 620; Ando T., Physica E, **40** (2007) 213; Castro Neto A. H. et al., Guinea F., Peres N. M. R., Novoselov K. S. and Geim A. K., Rev. Mod. Phys., **81** (2009) 109.

[2] Prada E., San-Jose P. and Schomerus H., Phys. Rev. B, **80** (2009) 245414.

[3] Zhu R. and Chen H., Appl. Phys. Lett., **95** (2009) 122111.

[4] Wu Z., Chang K. and Chan K. S., arXiv:1008.0463, preprint (2010).

[5] Grichuk E., Manykin E., EPL, **92** (2010) 47010.

[6] Brouwer P. W., Phys. Rev. B, **58** (1998) R10135; Buttiker M., Thomas H. and Pretre A., Z. Phys. B, **94** (1994) 133.

[7] Wei Y. and Wang J., Phys. Rev. B, **66** (2002) 195419.

[8] Levinson Y., Entin-Wohlman O. and Wolfle P., Physica A, **302** (2001) 335; Entin-Wohlman O. and Aharony A., Phys. Rev. B, **66** (2002) 035329; Kashcheyevs V., Aharony A. and Entin-Wohlman O., Phys. Rev. B, **69** (2004) 195301.

[9] Wakabayashi K. and Sigrist M., Phys. Rev. Lett., **84** (2000) 3390; Wakabayashi K., Phys. Rev. B, **64** (2001) 125428; Wakabayashi K. and Aoki T., Int. J. of Mod. Phys. B, **16** (2002) 4897.

Figures
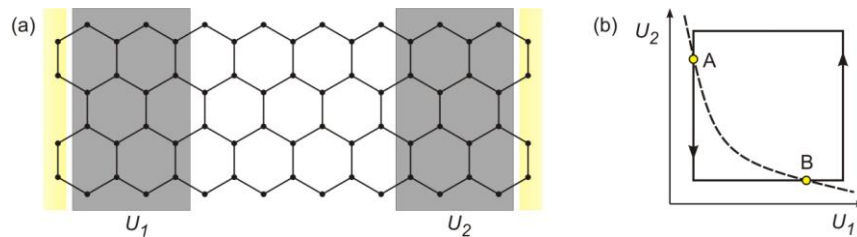
Fig. 1. (a) Schematic of the quantum pump ZGNR-based device (AGNR case is similar and not shown). Pumping is achieved by periodical variation of potentials U_1 and U_2. (b) Typical pumping contour, schematic resonance line of conductance and two resonance points A and B.
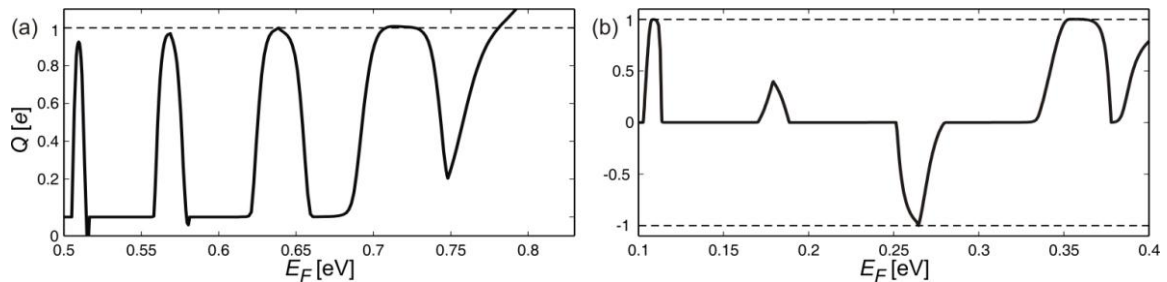
Fig 2. (a) The pumped charge per cycle Q for 10-AGNR as a function of the Fermi energy E_F in the leads for a fixed pumping contour. (b) The pumped charge per cycle Q for 10-ZGNR as a function of the Fermi energy E_F in the leads for a fixed pumping contour. See ref. [5] for the details.

Probing the strain in epitaxial graphene grown by different methods with Raman spectroscopy

K.Grodecki [1,2], W.Strupinski[1], A.Wysmołek[2], R.Stępniewski[2], and J.M.Baranowski [1,2]

[1]Institute of Electronic Materials Technology, Wolczynska 133, 01-919 Warsaw, Poland

[2]Faculty of Physics, University of Warsaw, Hoza 69, 00-681 Warsaw, Poland

<kacper.grodecki@fuw.edu.pl>

The difference between epitaxial graphene layers on 4H-SiC(0001) obtained by two different growing techniques have been investigated with micro Raman spectroscopy. The first one, commonly used is based on sublimation of Si from SiC(0001) surface at high temperature (S-EG). The second method has been developed by chemical vapor deposition technique (CVD-EG). This new technique involves controlling the dynamic flow of argon in the reactor, which stops Si sublimation and uses propane gas as the carbon precursor.

The micro Raman maps have been created with 3μm light spot using 530 points measured on 2,3 x 2,3 mm area in the center of the sample. The wavelength of the light used was 532nm. Micro Raman maps allowed to make histograms, on which number of points with the same 2D line frequency $v \pm 1 cm^{-1}$ were plotted against frequency v. It was found that there are two main differences between maps obtained on the S-EG and CVD-EG layers. The histogram for typical S-EG sample has shown that the mean position of the 2D line is located at frequency $2743 cm^{-1}$(Fig 1). Such a shift of the 2D line (blue shift up to $63 cm^{-1}$) in comparison to free unstrained graphene, in which the 2D line is at frequency $2680 cm^{-1}$, indicates that the S-EG layer is under strong compressive strain. On the other hand, histograms for the CVD-EG have shown that mean position of the 2D line is at frequency $2708 cm^{-1}$ (Fig 1). This reveals that CVD growth of graphene produces much less strained layers (blue shift up to $28 cm^{-1}$). The effect is dramatic – the compressive strain in the CVD-EG is two times smaller than in the S-EG. Similar effect observed for the position of the G line confirmed the results for 2D line. Another important difference between Raman spectra of samples produced by this two growth modes is that the layers grown by CVD are much more uniform in comparison to the S-EG ones. This is noticeable from the half-width of histograms shown in Fig.1: the one for CVD-EG is much more narrow than the one for the S-EG. This proves that the quality of graphene layers grown by CVD-EG technique is significantly higher.

Discussion on the unexpected different compressive strain obtained for the S-EG and CVD-EG layers has also been presented. It has often been argued, that the origin of compressive strain in S-EG comes from the different thermal expansion coefficients for graphene and SiC. In the case of S-EG growth, the origin of Si sublimation from SiC surface is probably connected with atomic steps and also with all kind of defects present on the SiC surface, in particular with dislocations. Thus, the graphene layer can be pinned to the SiC surface at many randomly distributed points. This will inevitably lead to much larger strain in the S-EG layers and eventually to their poorer quality. In the case of CVD-EG the nucleation sites of graphene layer are probably connected only with atomic steps of SiC surface and will be much less sensitive to surface defects. Subsequently grown layers will weakly interact with the ones already grown, and may more easily relax the strain. It may explains superior quality of the CVD-EG layers.
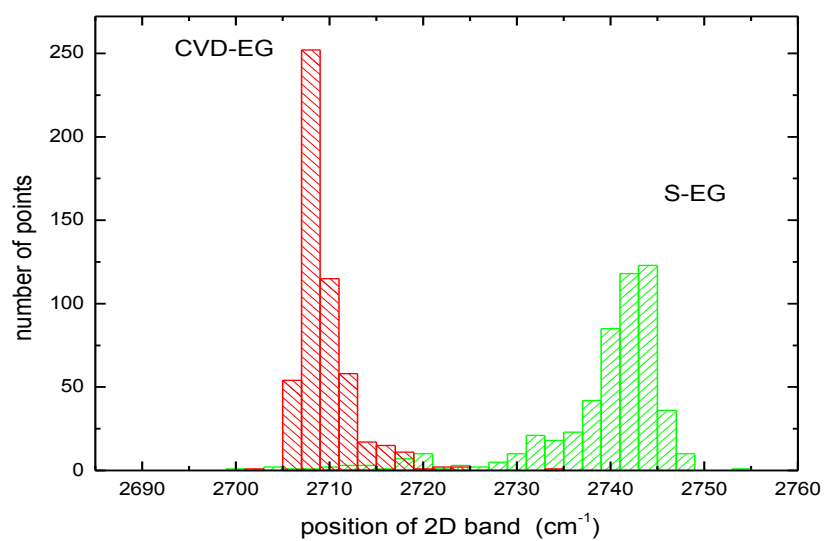
Fig1. Typical histograms obtained from micro Raman maps for epitaxial graphene layers grown on 4H-on axis SiC(0001) by chemical vapor deposition (CVD-EG) – red area, and by conventional Si sublimation (S-EG) – green one.

Substrates, electron-phonon interactions and the modification of graphene band gaps

J.P. Hague

The Open University, Walton Hall, Milton Keynes, MK7 6AA, United Kingdom
J.P.Hague@open.ac.uk

While the zero bandgap in graphene leads to exceptional electronic properties, it hampers attempts to make transistors for digital applications. This presentation describes how the presence of substrates might be used to solve this problem. Recent experimental work has shown that there may be bandgaps in graphene on certain substrates: There has been significant debate regarding whether a gap is present in monolayer graphene on silicon carbide [1,2] and ARPES measurements have found a gap in graphene on a monolayer of intercalculated gold on ruthenium [3]. While there is significant controversy about the origin of the gap seen in Ref. [1] and the nature of the reconstruction of the surface of the SiC system (see e.g. [4]), the authors of Ref. [3] have found evidence for the opening of the gap in the ruthenium system due to a breaking of the symmetry of the two carbon sub-lattices in graphene. Given this surprise gap opening, there are likely to be many other systems in which gaps can be generated by a substrate.

The existence of substrates that can modify the electronic structure of graphene raises the interesting possibility of using the substrate to induce interactions between the electrons in the monolayer. In a two dimensional material, effective electron-electron interactions can be induced via a strong interaction between the electrons in the layer and phonons in a strongly polarizable substrate because of limited out of plane screening [5]. I calculate the effects of electron phonon interaction on electrons in both a linear chain (1D analogue) and a honeycomb lattice (graphene) where a gap has been opened with a modulated potential. I present results for both systems, computed using the numerically exact diagrammatic quantum Monte Carlo technique. The results show an increase in the gap on increased electron-phonon coupling, until the gap becomes filled when polaron side bands form. This demonstrates the potential to use substrate (or superstrate) induced electronic correlations to engineer the electronic properties of graphene.

References

[1] S. Y. Zhou, G.-H. Gweon, A. V. Fedorov, P. N. First, W. A. De Heer, D.-H. Lee, F. Guinea, A. H. Castro Neto and A. Lanzara Nature Materials **6** (2007) 770

[2] A. Bostwick, T. Ohta, T. Seyller, K. Horn and E. Rotenberg. Nature Physics **3** (2007) 36

[3] C. Enderlein, Y. S. Kim, A. Bostwick, E. Rotenberg and K. Horn. New J. Phys. **12** (2010) 033014.

[4] Y. Qi, S. H. Rhim, G. F. Sun, M. Weinert and L. Li. Phys. Rev. Lett. **105** (2010) 085502

[5] A. S. Alexandrov and P. E. Kornilovitch. J. Phys.: Condens. Matter **14** (2002) 5337

Figures
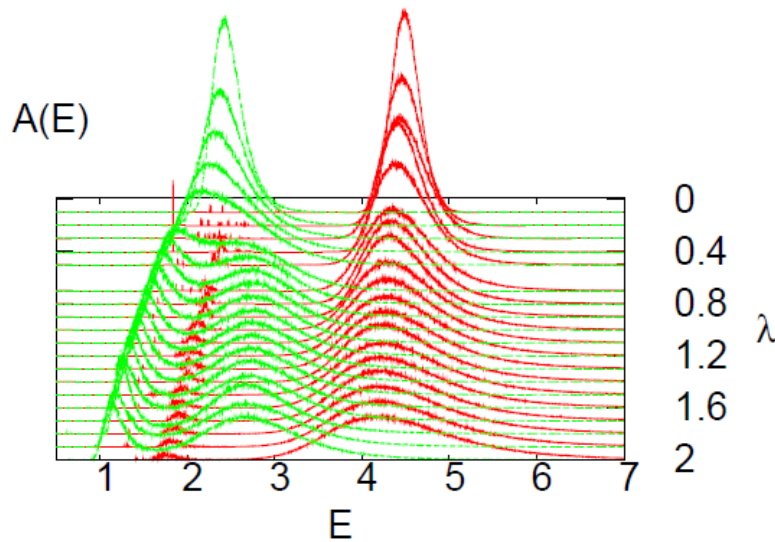
Spectral functions A(E) of A and B type electrons at the edge of the Brillouin zone on a chain with modulated potential used as a 1D analogue of the graphene substrate system. Note the increase in the band gap as the electron-phonon coupling (λ) is increased, and the polaron side band which forms in the gap at large coupling.

Single-atom sensitive imaging of two-dimensional MoS$_2$ nanoparticles

Lars P. Hansen[1,2], Christian Kisielowski[3], Quentin M. Ramasse[4], Michael Brorson[1], Erik Johnson[2], and Stig Helveg[1]

[1]Haldor Topsøe A/S, Nymøllevej 55, DK-2800 Kgs. Lyngby, Denmark
[2]Nano-Science Center, Niels Bohr Institute, Universitetsparken 5, 2100 København Ø.,Denmark
[3]National Center for Electron Microscopy & Helios SERC, Lawrence Berkeley National Laboratory, 1 Cyclotron Road, Berkeley, CA 94708, USA
[4]SuperSTEM Laboratory, STFC Daresbury, Keckwick Lane, Daresbury WA4 4AD, UK
lpha@topsoe.dk

The anisotropic, layered structure of graphite is encountered in a variety of complex compound materials such as the transition metal disulfides MS$_2$ (M=Mo, W). These compounds consist of S-M-S layers with covalent intralayer bonds and with a weak van der Waals interlayer interaction. Like graphene, such S-M-S layers have within the last two decades been found to form numerous of nanoscale polymorfs (including fullerene-like structures, nanotubes/wires and platelets), each with unique physico-chemical properties significantly different from the corresponding bulk materials [1]. Here, we focus on planar, single-layer MoS$_2$ nanoparticles, which is of broad, current interest as catalyst for the industrial oil refining, hydrogen evolution and photo-oxidation.

It is well-known that the catalytic reactivity of MoS$_2$ is associated with the edges of its 2-dimensional S-Mo-S layers. Detailed edge structure information is thus essential in order to understand the nature of the catalytic active sites [2]. Previously, unprecedented insight into the atomic structure of single-layer MoS$_2$ nanoparticles prepared under ultra high-vacuum conditions on planar model substrates have been obtained from scanning tunneling microscopy (STM) and from density functional theory (DFT) calculations [2]. However, the information from the model systems is difficult to relate to catalyst particles synthesized by industrial-style methods because the precise structure and distribution of the edge sites are sensitive to the preparation conditions, edge-attached promoter atoms, and interactions with support media [2]. For long, it has therefore been a key goal to obtain high-resolution electron microscopy images of industrial-style, supported MoS$_2$ catalysts, viewed in the (001) projection, but the lack of sufficient contrast and resolution has prevented such images to be obtained [3].

Recent advances in high-resolution transmission electron microscopy (HRTEM) have now made it possible to obtain images of unsupported graphene-type structures with single-atom sensitivity [4]. In this contribution, we demonstrate how this HRTEM approach also provides atomically resolved information of MoS$_2$ nanoparticles dispersed on a high-surface-area graphite support [5]. Figure 1 shows the HRTEM reconstructed phase image of a hexagonal MoS$_2$ nanocrystal supported on a few graphene-layers thick flake. A detailed contrast analysis of the image provides an unambiguous identification of the single- and double-layer domains in the MoS$_2$ nanocrystal and thus information about the types and concentration of the edge sites. It will be discussed how this atomic-scale information about the industrial-style catalysts may be related to catalytic reactivity and assist new, improved structure-functionality relationships to be established.

References

[1] Tenne, R., Nat. Nanotechnol., **1** (2006) 103.
[2] Besenbacher, F. et al., Catal. Today, **130** (2008) 86.
[3] Brorson, M. et al., Catal. Today, **123** (2007) 31.
[4] Girit, C. et al., Science **323** (2009) 1705.
[5] Kisielowski, C. et al., Angew. Chem. Int. Ed., **49** (2010) 2708.

Figures
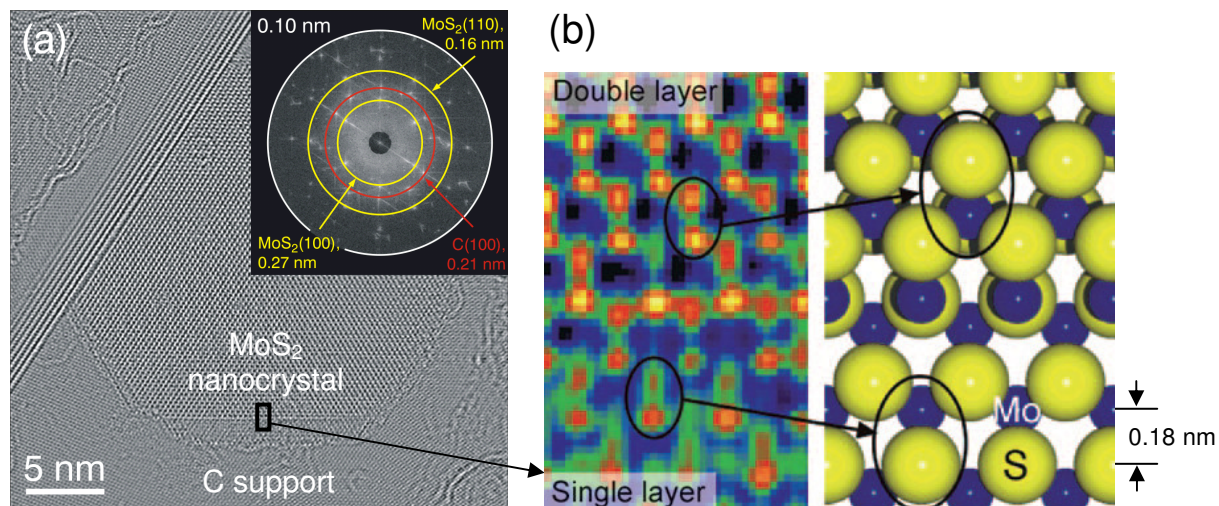
Figure 1: (a) Reconstructed aberration corrected HRTEM phase image of a MoS_2 nanocatalyst supported on graphite recorded in MoS_2 (001) projection as revealed from the Fourier transform (inset). (b) Close-up of region near the edge of the MoS_2 particle illustrating the atomic arrangement of single- and double layer MoS_2 structure [5].

Interlayer Hopping Effects on Energy Bands in Bilayer Graphene
(Boron-Carbon-Nitride) Nanoribbons with Zigzag Edges

Kikuo Harigaya, Hiroshi Imamura

Nanosystem Research Institute, AIST, Tsukuba 305-8568, Japan
E-mail: k.harigaya@aist.go.jp

The graphite, multi-layer, and single-layer graphene materials have been studied intensively, since the electric field effect has been found in atomically thin graphene films [1]. These materials can be regarded as bulk systems. On the other hand, nanographenes with controlled edge structures have been predicted to have localized states along the zigzag edges [2]. The presence of the edge states has been observed by experiments of scanning tunneling spectroscopy [3,4]. Thus, the studies of the edge states are one of the interesting topics of the field. The recent atomic bottom-up fabrication of nanoribbons really promotes experimental and theoretical investigations [5].

In this paper, bilayer graphene (and boron-carbon-nitride) nanoribbon with zigzag edge is investigated with the tight binding model. Two stacking structures, α and β, are considered. Their structures are shown in Fig. 1. In the α structure, the upper layer is shift by the bond length downward to the position of the lower layer. In the β structure, the lower layer is shift to the right-down direction. In the boron-carbon-nitride nanoribbons, the upper edge atoms are replaced with borons, and the lower edge atoms are substituted with nitrogens. The band splitting is seen in the α structure, while the splitting in the wave number direction is found in the β structure (Fig. 2). The local density of states in the β structure tends to avoid the sites where interlayer hopping interactions are present. The dependence of the number of states on energy reflects the band structures, and this will appear in quantization of conductance experimentally.

In detail, the energy band structures of the systems with the zigzag line number 10 are displayed in Fig. 2, for the single layer (a), the α structure (b), and the β structure (c). The interlayer interaction strength is t_1=0.1t. In Fig. 2 (b), the split of the energy bands is seen compared with Fig. 2 (a). In contrast, split in the perpendicular direction is negligibly small in Fig. 2 (c). The nearly flat band due to the edge state in $2\pi/3 < |kd| < \pi$ is present at the energy E~0 in Figs. 2 (a-c), where d is the unit cell length of the one dimensional direction of Figs. 1 (a) and (b). The energy bands starts at E=1.0t at $|kd|=\pi$, typical to the graphene structure. Comparing Fig. 2 (b) with Fig. 2 (c), the energy split is not seen in Fig. 2 (c), and split in the wave number direction is found.

References

[1] K. S. Novoselov, A. K. Geim, S. V. Morozov, D. Jiang, Y. Zhang, S. V. Dubonos, I. V. Grigorieva, and A. A. Firsovet, Science **306**, 666 (2004).

[2] M. Fujita, K. Wakabayashi, K. Nakada, and K. Kusakabe, J. Phys. Soc. Jpn. **65**, 1920 (1996).

[3] Y. Kobayashi, K. Fukui, T. Enoki, and K. Kusakabe, Phys. Rev. B **73**, 125415 (2006).

[4] Y. Niimi, T. Matsui, H. Kambara, K. Tagami, M. Tsukada, and H. Fukuyama, Phys. Rev. B **73**, 085421 (2006).

[5] J. Cai et al., Nature **466**, 470 (2010).

Figure 1
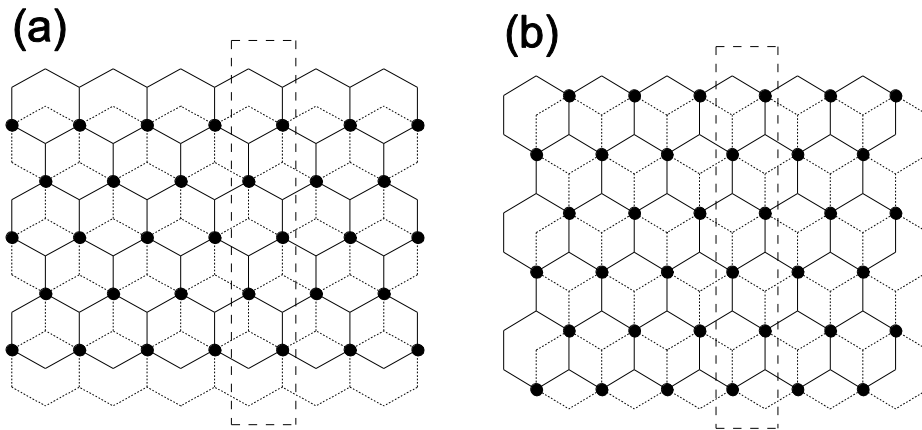
A-B stacked bilayer graphene nanoribbon with zigzag edges. The upper layer is shown by the solid lines, and the lower layer by dotted lines. In the α structure (a), the upper layer is shift by the bond length downward to the position of the lower layer. The region surrounded by the dashed line is the unit cell in the direction of the one dimensional direction. At the circles, two carbon atoms of the upper and lower layers overlap completely, and there is the weak hopping interaction t_1 here. In (b), the β structure is shown, where the lower layer is shift to the right-down direction so the stacking pattern is different from that of the α structure.

Figure 2
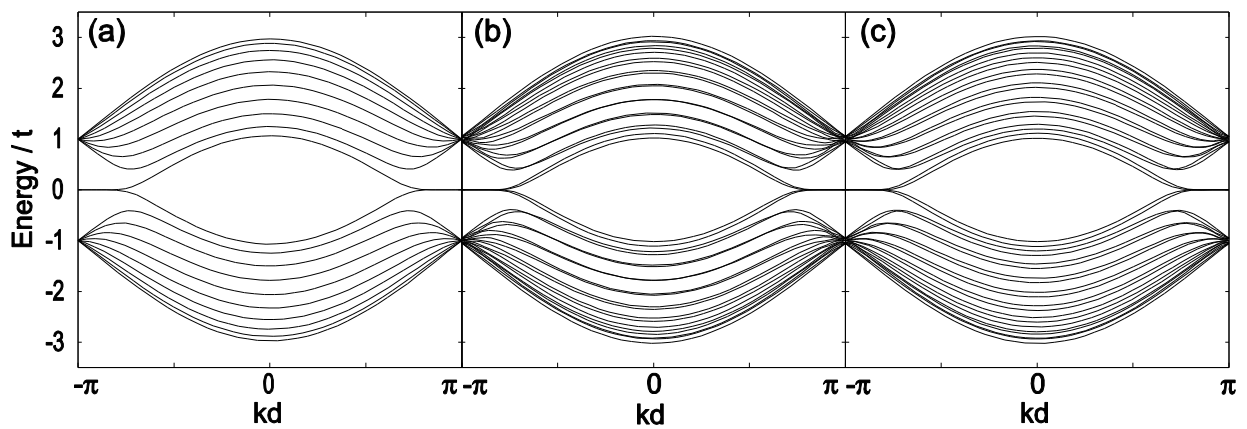
Energy band structures in the single layer (a), α structure (b), and β structure (c).

160

Graphene-Graphane ribbons on substrate

Ari Harju[1], Mari Ijäs[1], Paula Havu[1], Pirjo Pasanen[2]

[1]Aalto University School of Science, Espoo, Finland
[2]Nokia Research Center, Helsinki, Finland
ari.harju@aalto.fi

Ever since the first experimental discovery of graphene and its extraordinary electronic properties [1], the search for practical applications for this new material has been intense. As the lack of a band gap is a hindrance for applications, various methods have been suggested to induce a gap, among them cutting the material into thin stripes, graphene nanoribbons (GNRs). Confinement induces a width- and edge- dependent gap [2], but manufacturing these experimentally with atomic precision is challenging. An interesting possibility to generate graphene nanoribbons is by selective dehydrogenation of graphane [3], the fully hydrogenated graphene.

We have theoretically studied the stability of the one-side hydrogenated graphane on the oxygen-terminated silicon dioxide surface. Scanning and relaxing around 500 initial configurations, we have found the two most stable graphane configurations shown in Fig. 1. Both configurations are insulators but their band gaps differ considerably. The quarter-hydrogenated configuration has only a small band gap of 0.46 eV, and for the half-hydrogenated graphane the magnitude is 3.7 eV. Whereas our simulations show that graphene binds to the silicon dioxide via the van der Waals forces, graphane binds to the surface covalently.

We have formed graphene ribbons on graphane by removing hydrogens from the half-hydrogenated configuration, see Fig. 2. In experiments, this can be done using STM tip [4]. For the electronic structure of the resulting ribbons, both antiferromagnetic and ferromagnetic spin order were found, the antiferromagnetic ones being lower in energy. In addition, the coupling of the graphane to the substrate leads to an interesting electronic structure: As the substrate is not symmetric on the two edges, see Fig. 2, and because the edge atoms in the ground state have opposite spins, the spin symmetry of the ribbons is broken by the substrate and the two spin channels turn out to have gaps of different magnitude. As a result, the system shows a half-semiconducting band structure. The gaps in ribbons typically get smaller as the ribbons get wider, and in this case the electronic structure might change to half-metallicity.

References

[1] K.S. Novoselov *et al.*, Science, **306** (2004) 666.
[2] M.Y. Han,B. Özyilmaz,Y. Zhang,and P. Kim, Physical Review Letters, **98** (2007) 206805.
[3] J. O. Sofo, A. S. Chaudhari, and G. D. Barber, Physical Review B, **75** (2007) 153401.
[4] P. Sessi, J. R. Guest, M. Bode, and N. P. Guisinger, Nano Letters, **9**, (2009) 4343.

Figures
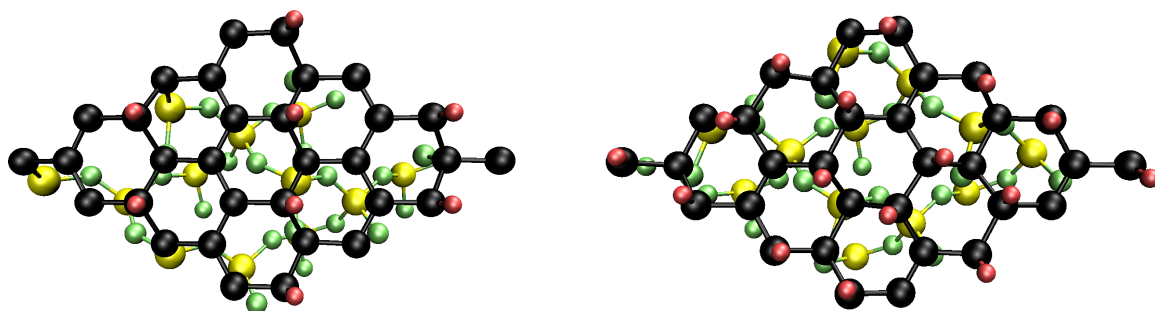
Figure 1: *Quarter- (left) and half-hydrogenated (right) graphanes on substrate.*
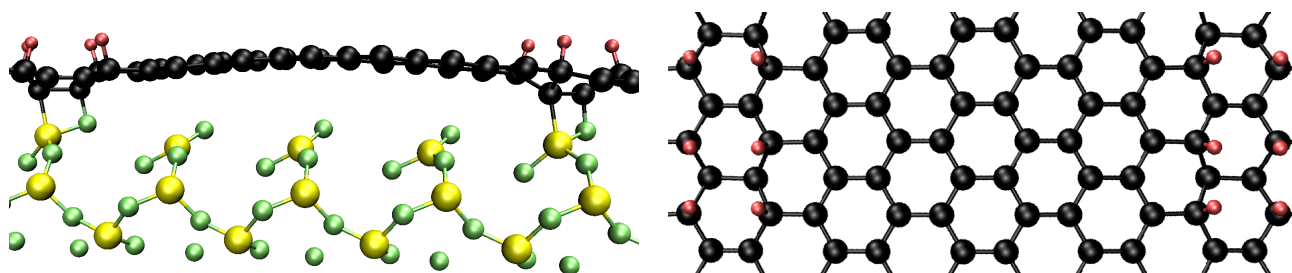
Figure 2: *Graphene ribbon created by removing rows of hydrogen.*

162

All-carbon ferromagnetism derived from edge states in graphene nano-pore arrays

K. Tada[1], S. Kamikawa[1], Y. Yagi[1], J. Haruyama[1*], T. Matsui[2], H. Fukuyama[2]

[1]Faculty of Science and Engineering, Aoyama Gakuin University, 5-10-1 Fuchinobe, Sagamihara, Kanagawa 252-5258, JAPAN

[2]Department of Physics, University of Tokyo, 7-3-1 Hongo, Bunkyo-ku, Tokyo 113-8656, JAPAN

Ferromagnetism in carbon-based materials is unique as compared to conventional ferromagnets arisen from 3d or 4f electrons, because only s and p orbital electrons form it. Many theoretical works have predicted the appearance of ferromagnetism in carbon-based systems from viewpoints of edge-localized electrons[1-7]. However, few independent observations have reported the existence of ferromagnetism in controllable systems with high reproducibility, such as poor reproducibility in uncontrollable graphite-related systems[8-10]. On the other hand, the edge structures of graphene are of particular interest[11-22]. Theoretically, the so-called zigzag edge has strongly localized electrons due to the presence of flat bands near the Fermi level[1]. The localized electron spins are also strongly polarized, resulting in the emergence of ferromagnetism[3,5,13,14]. However, no study thus far has experimentally reported ferromagnetism. Here, in the present work, we fabricate honeycomb-like array of nano-sized pores on graphenes (antidot-lattice graphene) with a large ensemble of hydrogen-terminated nano-pore edges by a non-lithographic and low-damage method using nanoporous alumina templates[3]. We observe room-temperature ferromagnetism derived from the polarized electron spins at the nano-pore edges. This promises the realization of all-carbon magnets and spintronic devices based on a spin Hall effect[22,24-27].

Ferromagnetism in graphite-related systems has been poorly demonstrated such as in highly oriented pyrolytic graphite (HOPG) detected specifically at defects[8] and activated carbon fibers (ACFs)[9]. The origin of ferromagnetism has been interpreted in terms of high electronic density of states (EDOS, i.e., edge states), which exists at the zigzag edges of a two-dimensional (2D) array of point defects at HOPG grain boundaries and the 3D disordered network of nano-graphite domains in ACFs. However, the origin of ferromagnetism remains ambiguous because of those complicated and uncontrolled structures. Only edge states have been possibly observed in graphite using scanning tunnel microscopy (STM)[10].

On the other hand, the zigzag edge of graphene has theoretically high EDOSs owing to its strongly localized electrons (edge states), which have been introduced by presence of flat bands near the Fermi level (E_F)[1]. The localized electron spins are strongly polarized depending on the spin interaction between two edge lines (e.g., in graphene nanoribbons (GNRs) that are 1D restriction of graphene with edges on both longitudinal sides) and become responsible for magnetic behaviour such as ferromagnetism or antiferromagnetism[3,5-7,13,14]. This is because the nonbonding states of carbon atoms (i.e., dangling bonds) at the zigzag edge are half filled and behave like the outer shell of a ferromagnetic atom, which is not stable when spin is taken into account. The exchange interaction requires the spin in these orbitals to be maximized, similar to Hund's rule for atoms. It determines whether either ferromagnetism or antiferromagnetism appears in GNRs, which in turn strongly depends on the termination of edge carbon atoms by foreign atoms (e.g., hydrogen or oxygen).

Many works have theoretically predicted the appearance of ferromagnetism in graphene-related systems such as GNRs[1-7], antidot-lattice graphenes (ADLGs) with honeycomb-shaped antidots[13], and graphene nano-flakes (nano-islands) with triangular and hexagonal shapes[14]. However, there have been no reports of the experimental observation of ferromagnetism, although experiments to observe and control graphene edge structures have been conducted using approaches such as Joule heating with an STM probe[15], fabrication of GNRs[17-19], and formation of ADLGs with edges around the antidots[20,21].

Figure 1a shows the top view of a scanning electron microscopy (SEM) image of a nanoporous alumina template[23] (Al_2O_3; NPAT) that was then used as an etching mask to form the antidot lattice (ADL) on the graphene (Supplementary information (1)). Atomic force microscopy (AFM) images of ADLG and one antidot formed by optimized low-power Ar gas etching using the NPAT are shown in Fig. 1b. The inset of Fig. 1b proves the hexagonal shape of the antidote (Supplementary information (2) - (4)). Figure 1c shows an STM image obtained in a ~10-layer ADLG with hydrogen termination (Supplementary information (5)). It demonstrates the possible presence of high EDOS (white regions) at the antidot edges on the surface graphene layer, although the high EDOSs are smeared due to the blurred tip of top of the STM probe.

Figure 2a shows a magnetization curve of the hydrogen-terminated monolayer ADLG at $T = 2$ K (Supplementary information (5)). A ferromagnetic-like hysteresis loop is clearly observed. In contrast, this feature

1
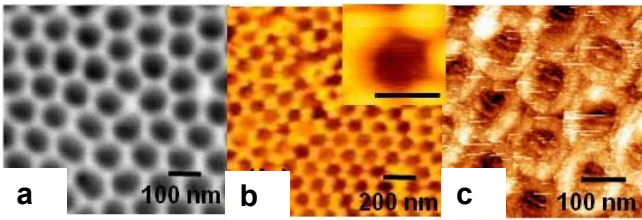
Figure 1. Top view images of samples. a, SEM of a nanoporous alumina template (NPAT) with antidot diameter φ ~ 80 nm and antidot spacing L_s ~ 20 nm (i.e., corresponding to the width of GNRs); **b,** AFM of an ADLG formed by using **a** as an etching mask; **inset of b,** one antidot in main panel proving its hexagonal shape (the scale bar is 100nm); and **c,** STM of the ~10-layer ADLG obtained at a temperature of 80 K in a constant-current mode. Lighter regions at antidot edges denote higher EDOSs. In the present ADLG, the narrow space between two antidots can be a GNR (Fig.4b). Consequently, the ADLG can provide a large volume of GNRs and edge structures, which result in a large signal of magnetism.

becomes an antimagnetism-like weak hysteresis loop in oxygen-terminated ADLGs (Fig.2b) (Supplementary information (5)). Bulk graphene without antidots show no such features (Fig. 2(c)). These results suggest that ferromagnetism observed in Fig. 2a is strongly associated with the hydrogen-terminated ADL, because this non-lithographic method gives less damage to the antidot edges (Supplementary information (3)) and there are no damage and impurities in bulk graphene regions covered by the NPAT with a thickness over 5 μm. The structure is quite simple and highly reproducible compared with previous graphite-related systems to observe ferromagnetism. To date, 5 samples of the measured 11 samples have shown ferromagnetism like Fig.2a (Supplementary information (5))

Moreover, we find the features observed at T = 2K appear even at room temperature with a larger magnitude of hysteresis loops (Figs. 2d – 2f), although the amplitude of magnetization decreases.

In Fig. 3, magnetizations of the hydrogen-terminated ADL-graphite with the same ADL structure parameters are shown at T = 2K and room temperature. Although ferromagnetic-like hysteresis loops still remain at both temperatures, the magnitude of loops decreases drastically.

The saturation magnetization (M_s) value corresponds to a magnetic moment of ~1.2×10^2 μ$_B$ per edge carbon atom (Fig. 2d; μ$_B$ is the Bohr magneton), based on the origin of ferromagnetism discussed later. This value is mostly 100 times larger than those reported in theory[5] and indicates that other carbon atoms possessing weakly localized π-electrons also contribute to magnetization. Assuming that all carbon atoms within 7 nm from the zigzag edge (estimated as ~10^{15}) equally contribute to magnetization, a magnetic moment of ~1.2 μ$_B$ per edge carbon atom is estimated. This value is in good agreement with theory[5].

As mentioned in a latter part, spin interference, caused by
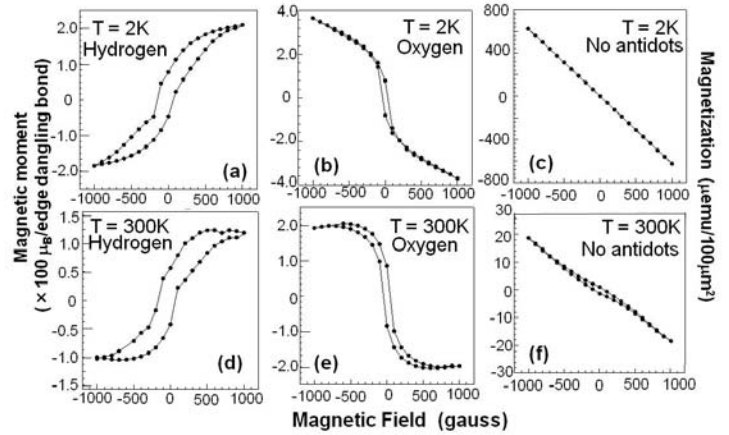
Figure 2. Magnetization of monolayer ADLGs (Supplementary information (5)) with φ ~ 80 nm and L_s ~ 20 nm for **a, d** hydrogen-terminated and **b, e** oxygen-terminated antidot edges, and **c, f** bulk graphene without ADL, measured by a superconducting quantum interference device (SQUID; Quantum design) at T= 2K and room temperature, respectively. Magnetic fields were applied perpendicular to the ADLG. Y axis's for a, b, d, and e are noted for magnetic moment per edge carbon atom at dangling bonds of hexagonal antidots, assuming that only the carbon atoms ((estimated as ~10^{13} using two lengths (Fig.4a) and number of carbon atoms of 166/(40 nm length of one boundary of a hexagonal antidot)) have magnetic moment. Those for c and d are just for magnetization per unit area.
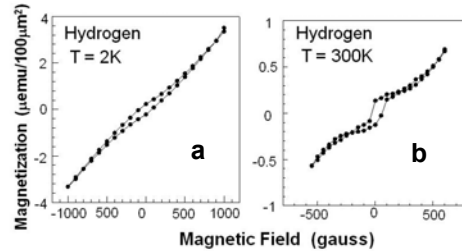
Figure 3. Magnetization of ADL-Graphite with the same ADL structure parameters as those for Fig.2 (with hydrogen-terminated antidot edge), measured at **a** T = 2K and **b** room temperature. Y axis is noted for magnetization per unit area because of unknown layer number and stuck structures of Kish graphite.

both zigzag edges of a GNR, at every carbon site in a GNR determines the appearance of either ferromagnetism or antiferromagnetism (Fig. 4a), depending on termination by foreign atoms and the width of the GNR. The width of space between the present two antidots (i.e., GNR width) of ~20 nm (Fig. 4b) is narrow enough for this spin interference. This implies that carbon atoms located notonly at the zigzag edge but also away from the zigzag edge can actually contribute to magnetization, although carbon atoms located at the dangling bond of the zigzag edge should have magnetic moment larger than ~1.2 μ$_B$.

The disappearance of the antimagnetism of bulk graphene in ADLGs (Figs. 2c and 2f) is attributed to the formation of ADL, because it drastically reduces the area of bulk graphene sufficient for the presence of loop currents to produce antimagnetism at the presently applied magnetic-field range (i.e., only GNRs with W = ~20 nm

2

between antidots can correspond to this space (Fig. 4b). The radius of cyclotron motion electrons is given by $R_c = (\pi n_S)^{1/2}(h/2\pi)/eB$. From observing magnetoresistance (i.e., commensurability peak), we estimate $n_S \sim 4 \times 10^{11}$ cm^{-2} in the present ADLGs. Based on this n_s value, R_c is estimated to be as large as ~400 nm even for the presently applied largest magnetic field of 1000 gauss in Fig. 2. Indeed, this R_c value is 20 times larger than W = ~20 nm between the present antidots and prohibits the emergence of loop currents for diamagnetism.

We discuss the origin of the observed ferromagnetism. It is theoretically known that the chemical modification of zigzag-edges GNRs with foreign atoms produces various types of magnetism[3,5-7,9](Supplementary information (6)). In particular, the band structure of mono-hydrogenated and di-hydrogenated GNRs with a large width were shown by tight-binding calculations in Ref. 5 in detail. There are three types for hydrogen terminated edge structures as following. (1) Mono-hydrogenated both edges with a flat band and localized π-orbital edge states at $2\pi/3 \leq k \leq \pi$. (2) Di-hydrogenated edges on both ends with a flat band and localized edge states at $0 \leq k \leq 2\pi/3$. (3) Both types of edges present (i.e., GNRs with mono-hydrogenated one side and di-hydrogenated the other side) with a flat band in the whole range of band structures at $0 \leq k \leq \pi$. Electrons strongly localize at any k values. This case is consistent with Refs. 3 and 4, and the most suitable for the observed ferromagnetism here (Figs.2a and 2d)

The localized electron spins at each edges are ferromagnetically (FM) polarized due to maximizing of exchange energy gain[5]. When the width of a GNR is smaller, two different edge states in different edges for case (3) can be misconceived as an intrinsic property of GNRs. Two different spin configurations are theoretically considered on both edges (Fig. 4a). Under absent hydrogen terminations, antiferromagnetical (AFM) state is stable due to the magnetic tails' interaction which maximizes exchange energy gain (Fig. 4a), while FM state becomes stable when the abovementioned case (2) is realized[5].

From the calculated band structures of the majority and minority spins of the FM configuration and the up- and down-spins of the AFM configuration under case (3)[5], it was found that the FM configuration had a lower energy than the AFM configuration by 4.9 meV per edge atom. Therefore, ferromagnetism can stably emerge in GNRs for case (3). This was also consistent with Ref. 3, which showed that the flat band for up-spins were below E_F and entirely filled, resulting in the appearance of ferromagnetism. The ferromagnetism observed in Figs. 2a and 2d reflects this FM edge configuration.

Here, the regions between the antidots in the present ADLGs behave as GNRs with a width of ~20 nm (Fig. 4b).
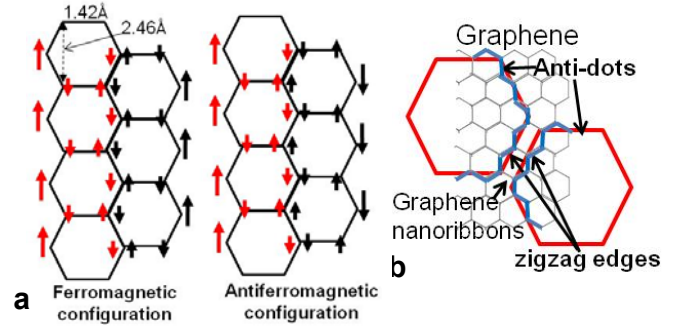
Figure 4. Shematic views of spin configurations of GNRs. a, Spin configuration for ferromagnetic and antiferromagnetic ordering in GNRs without hydrogen termination. Arrows mean electron spins on each sites. The dangling bond states localized at the edge contribute significantly to the total magnetic moment with a large exchange splitting, which in turn enhances the exchange splitting of the π-orbital states localized at the edge. Due to the lattice symmetry, the tails of the π-orbital wave function extend into the inner sites of the GNR. The exchange interaction requires the spin ordering on each carbon site to be maximized, similar to Hund's rule for atoms. **b,** Schematic view of graphene masked by an NPAT with hexagonal-shape antidots, showing the alignment of the antidot boundaries with the zigzag edge structure. The space between two antidots corresponds to a GNR with a width of ~20 nm.

Therefore, the ferromagnetism observed in Figs. 2a and 2d correspond qualitatively to case (3). This also suggests presence of zigzag edge at hexagonal antidot edges (Supplementary information (7)). This is consistent with STM observation (Fig.1c).

On the other hand, Ref. 6 reported that the formation of a spin-paired carbon-oxide (C–O) bond drastically reduced the local atomic magnetic moment of carbon at the zigzag edge of GNRs and suppressed the emergence of ferromagnetism. The disappearance of ferromagnetism in Figs. 2b and 2e can be qualitatively consistent with this configuration.

Moreover, Ref. 7 showed that regardless of the stacking sequences, either AB or AA, the magnetic moment caused by the localized orbital states disappears upon the interlayer stacking of graphite with hydrogen-terminated edges. This also qualitatively explains the reduced ferromagnetic-like loops in Fig. 3.

Although an atomic-scale observation of the edge structures (Supplementary information (7)) is indispensable to confirm this discussion, all the present results are qualitatively consistent with theories. Apart from the edge effect, Ref. 13 also predicted the appearance of ferromagnetism in ADLGs with honeycomb-shaped antidots from a group-theoretical consideration based on the tight-binding model. Although the study did not mention edge termination by foreign atoms, the structures directly correspond to the present ADLGs with honeycomb-shaped antidots (Fig. 1b) and might explain the present ferromagnetism.

Here, three reasons are considered about why evident

3

ferromagnetism can be observed in the present system as following. Approximately 50% of the fabricated hydrogen-annealed ADLG samples (number of 5/11; Supplementary information (5)) have exhibited ferromagnetism to date.

(1) The benefit of the non-lithographic fabrication method, which exploits NPAT in conjunction with low-power gas etching and high-temperature annealing. This process ensures only slight damage to the graphene edges. (2) The lattices of the hexagonal-shaped antidots can result in the formation of a large number of GNRs with sufficient length (e.g., 40 nm in the present case) due to the presence of six boundaries among the neighbouring six antidots for each one antidot in comparison with lattices of the square- and round-shaped antidots. In the actual ADLG, it is speculated that zigzag- and arm-chair edges exist with mixed states in one GNR (one boundary), as in the STM observation in Ref. 9. Nevertheless, the large number of GNRs in the present ADLGs can yield a large area of assembled zigzag-edge GNRs. (3) The hexagonal-shaped antidot transferred from the pore of the NPAT. When a hexagonal-shaped antidot is fabricated on graphene consisting of hexagonal carbon lattices, the six boundaries (edges) of an antidot tend to have the same atomic structure (Fig. 4b). Once an NPAT mask is placed onto the graphene so that one boundary of the antidot coincides with the zigzag edge, all the antidot edges acquire a zigzag structure.

These three factors have an equal probability for antidots with a zigzag, arm-chair, or mixed structure (Supplementary information (7)). However, if only the zigzag edge is likely to be formed with low damage by Ar gas etching as it is the most stable, these advantages will effectively contribute to the observed ferromagnetism.

Recently, the possibility of a spin filtering effect[22] and a (quantum) spin Hall effect (QSHE)[25-27] utilizing edge spin current of graphene has been predicted, assuming enhanced spin-orbit interaction. SHE is expected to realize novel spintronic devices[24], because electron spins are controlled by electric fields and are carried without energy dissipation even in paramagnetic materials. The ferromagnetism observed here turned out spin polarization at the graphene zigzag edge and promises the appearance of a large-magnitude spin current. This must open a new door to a 2-D (Q)SHE and carbon spintronic devices by modulating flat bands.

1. Nakada, K., Fujita, M., Dresselhaus, G. and Dresselhaus, M. S., Edge state in graphene ribbons: nanometer size effect and edge shape dependence. *Phys. Rev. B* **54**, 17954–17961 (1996).

2. Fujita, M. et al. Peculiar localized state at zigzag graphite edge. *J. Phys. Soc. Jpn.* **65**, 1920–1923 (1996).

3. Kusakabe, K. and Maruyama, M., Magnetic nanographite. *Phys. Rev. B* **67**, 092406 (2003).

4. Okada, S. and Oshiyama, A., Magnetic Ordering in Hexagonally Bonded Sheets with First-Row Elements. *Phys. Rev. Lett.* **87**, 146803 (2001).

5. Lee, H. et al., Magnetic ordering at the edges of graphitic fragments: Magnetic tail interactions between the edge-localized states. *Phys. Rev. B* **72**, 174431 (2005)

6. Veiga, R. G. A. et al., Quenching of local magnetic moment in oxygen adsorbed graphene nanoribbons. *J. Chem. Phys.* **128**, 201101 (2008).

7. Lee, H. et al., Ferromagnetism at the edges of the stacked graphitic fragments: an ab initio study. *Chem. Phys. Lett.* **398** 207–211 (2004).

8. Cervenka, J. et al., Room-temperature ferromagnetism in graphite driven by two-dimensional networks of point defects. *Nature Phys.* **5**, 840–844 (2009).

9. Enoki, T. et al., The edge state of nanographene and the magnetism of the edge-state spins. *Sol. Stat. Comm.* **149**, 1144–1150 (2009).

10. Niimi, Y. et al., Scanning tunneling microscopy and spectroscopy of the electronic local density of states of graphite surface near monoatomic step edges. *Phys. Rev. B* **73**, 085421 (2006).

11. Son, Y-W., Cohen, M. L. and Louie, S. G., Energy gaps in graphene nanoribbons. *Phys. Rev. Lett.* **97**, 216803 (2006).

12. Yang, L. Louie, S. G., et al., Quasiparticle energies and band gaps in graphene nanoribbons *Phys. Rev. Lett.* **99**, 186801 (2007).

13. Shima, N. and Aoki. H., Electronic structure of superhoneycomb systems. *Phys. Rev. Lett.* **71**, 4389–4392 (1993).

14. Rosser, J. F. and Palacios, J. J., Magnetism in graphene nanoislands. *Phys. Rev. Lett.* **99**, 177204 (2007).

15. Jia, X. M. et al., Controlled formation of sharp zigzag and armchair edges in graphitic nanoribbons. *Science* **323**, 1701–1705 (2009).

16. Girit, C. O. et al., Graphene at the edge: stability and dynamics. *Science* **323**, 1705–1708 (2009).

17. Shimizu, T., Haruyama, J., et al., Large intrinsic energy bandgaps in annealed nanotube-derived graphene nanoribbons. *Nature Nanotech*. Advance online publication (19th December 2010).

18. Han, M. Y., et al., Electron transport in disordered graphene nanoribbons. *Phys. Rev. Lett.* **104**, 056801 (2010).

19. Wang, X., et al., Room-temperature all-semiconducting sub-10-nm graphene nanoribbon field-effect transistors. *Phys. Rev. Lett.* **100**, 206803 (2008).

20. Bai,J., Zhong, X. et al., Graphene nanomesh. *Nature Nanotech.* **5**, 190-194 (2010).

21. Russo, S., et al., Observation of Aharonov-Bohm conductance oscillations in a graphene ring. *Phys. Rev. B* **77**, 085413 (2008).

22. Son, Y-W., Cohen, M. L. and Louie, S. G., Half-metallic graphene nanoribbons. *Nature* **444**, 347–349 (2006).

23. Takesue, I., et al., Superconductivity in entirely end-bonded

multiwalled carbon nanotubes. *Phys. Rev. Lett.* **96**, 057001 (2006).

24. Murakami, S., Nagaosa, N., and Zhang, S. C., Dissipationless quantum spin current at room temperature. *Science* **301**, 1348–1351 (2003).

25. Kane, C. L. and Mele, E. J., Quantum spin Hall effect in graphene. *Phys. Rev. Lett*. **95**, 226801 (2005).

26. Kane, C. L., Graphene and quantum spin Hall effect. *J. Modern Phys. B* 21, 1155–1164 (2007).

27. Schmidt, M. J. and Loss, D., Edge states and enhanced spin-orbit interaction at graphene/graphane interfaces. *Phys. Rev. B* **81**, 165439 (2010).

Author contributions

J.H. conceived and designed the experiments. K.T., S.K., and Y.Y. performed the experiments. J.H. analyzed the data and wrote the paper. T.M. and H.F. contributed to the STM observations.

Additional information

Correspondence and requests for materials should be addressed to J.H. (J-haru@ee.aoyama.ac.jp).

Thermal fluctuation of graphene: origin of ripples

Nils Hasselmann[1,2], Fabio L. Braghin[2,3]

[1]Max-Planck-Institute for Solid State Research, Heisenbergstr. 1, D-70569 Stuttgart, Germany
[2]International Institute of Physics ,Univ. Fed. RN, 59072-970, Natal, RN, Brazil
[3]Instituto de Fisica, Univ. Fed. de Goias, P.B.131, Campus II, 74001-970, Goiania, GO, Brazil

n.hasselmann@fkf.mpg.de

We use nonperturbative renormalization group techniques to calculate the momentum dependence of thermal fluctuations of graphene, based on a self-consistent calculation of the momentum-dependent elastic constants of a tethered membrane [1,2]. In the infrared limit, such tethered membranes are known to exhibit highly unusual properties, such as anomalous fluctuations with a large anomalous exponent, a negative Poisson's ration and non-linear stress-strain relations. We analyse the membrane fluctuations and find a sharp crossover from the perturbative to the anomalous regime. Our results are for all momenta in excellent agreement with Monte Carlo results [3] for the out-of-plane fluctuations of graphene, and we give an accurate value for the crossover scale. Our work is the first renormalization group analysis to compute the membrane fluctuations at finite momenta and strongly supports the notion that graphene is well described as a tethered membrane. We find a simple and natural interpretation of ripples in free standing graphene. The characteristic scale of the ripples coincides with the Ginzburg scale of the non-linear elasticity of the membrane.

References

[1] F. L. Braghin and N. Hasselmann, Phys.Rev. B, **82** (2010) 035407.
[2] N. Hasselmann and F. L. Braghin, arXiv:1012.0313 (2010).
[3] A. Fasolino, J. H. Los, and M. I. Katsnelson, Nature Mater. 6 (2007) 858; J. H. Los, M. I. Katsnelson, O. Yazyev, K.V. Zakharchenko, and A. Fasolino, Phys.Rev. B, 80 (2009) 021405(R).

Pressure-Dependent Nucleation and Growth of Graphene Islands on Cu by Chemical Vapor Deposition

Kenjiro Hayashi, Shintaro Sato, Daiyu Kondo, Katsunori Yagi, Ayaka Yamada,
Naoki Harada, Naoki Yokoyama

Green Nanoelectronics Collaborative Research Center (GNC), AIST
West 7A, Onogawa 16-1, Tsukuba, Ibaraki, Japan
hayashi.kenjiro@aist.go.jp

We observed the initial stages of graphene growth on Cu catalyst films by thermal chemical vapor deposition (CVD) under various growth conditions. It was revealed that the graphene growth mode, represented by the shape and spatial density of graphene islands, sensitively depends on the partial pressure of the source gas (P_{source}). Our results also suggest that the morphology of the Cu surface, such as grain boundaries and steps, can play a crucial role in the nucleation and growth of graphene islands under a relatively-high P_{source} condition.

Since the discovery of extraordinary electronic properties of single-layer graphene, a number of efforts have been made toward the preparation of graphene and its device applications. Recently, high-quality graphene has been synthesized on metal catalysts, such as Ni, Co, Ru, by means of the thermal CVD method. Especially, Li and co-workers found that single-layer graphene with good uniformity can be formed on the surface of Cu foil [1]. Since it is difficult to synthesize single-layer graphene uniformly with other catalysts, graphene growth using Cu is a promising way to prepare graphene for various applications. Initial stages of graphene growth on Cu surface have also been investigated by several groups [2, 3]; however, many questions still remain to be solved, which include the nucleation and growth mechanisms, and their dependence on the growth condition and Cu-surface morphology. Understanding these issues is essential to control the domain size and the number of graphene layers. We investigated graphene islands on Cu films formed by the thermal CVD method, and found that the graphene growth mode sensitively depends on experimental conditions such as P_{source}, growth time and the nature of the Cu catalyst surface.

In our experiments, graphene was synthesized on a sputtered Cu film on Si/SiO$_2$ wafer placed in a cold-wall type high-vacuum chamber using C$_2$H$_4$ or CH$_4$ diluted by Ar and H$_2$ as the carbon source. After H$_2$ / Ar annealing, graphene growth was performed at temperatures ranged from 700 to 1000 $^{\circ}$C. P_{source} was 0.1, 0.7, or 4.5 Pa, while the total pressure was kept at 1 kPa. The growth time was varied from several seconds to 60 min.

Graphene islands grown at P_{source} of 0.1 Pa yielded mottled patterns (dark regions) on the Cu surface where some islands stepped over the Cu grain boundaries as seen in scanning electron microscopy (SEM) images in Fig. 1. As P_{source} increases, while the total amount of source gas supply [$P_{source} \times$ growth time] is kept constant, the island size becomes smaller and the islands' density becomes higher as shown in Fig. 2 (P_{source} = 0.7 Pa). In addition, the islands form into a scale-like shape and they tend to be aligned along steps on the Cu surface. This result indicates that the surface morphology such as grain boundaries and surface steps strongly influences the graphene growth mode under this condition. The graphene islands grown at P_{source} of 4.5 Pa (Fig. 3) can be seen to be elongated along the steps. This kind of island shape is different from those reported in previous papers [2, 3]. It was also reported that the shape of islands depended on the total gas pressure [4], but our results clearly indicate that the shape also depends on P_{source} .

We then made back-gate field-effect transistors using graphene grown at P_{source} of 0.7 Pa. For transistor fabrication, graphene was transferred to an SiO$_2$/Si substrate and patterned by the conventional photolithography technique. The fabricated transistors were successfully modulated by the gate voltage,

and exhibited ambipolar behavior. The transistors were found to have fileld effect mobilities exceeding 1000 cm^2 / Vs.

References

[1] X. Li, W. Cai, J. An, S. Kim, J. Nah, D. Yang, R. Piner, A. Velamakanni, I. Jung, E. Tutuc, S. K. Banerjee, L. Colombo, R. S. Ruoff, Science **324** (2009) 1312.

[2] X. Li, W. Cai, L. Colombo, R. S. Ruoff, Nano Lett. **9** (2009) 4268

[3] J. M. Wofford, S. Nie, K. F. McCarty, N. C. Bartelt, O. D. Dubon, Nano Lett. **10** (2010) 4890

[4] Qingkai Yu, L. A. Jauregui, W. Wu, R. Colby, J. Tian, Z. Su, H. Cao, Z. Liu, D. Pandey, D. Wei, T. F. Chung, P. Peng, N. Guisinger, E. A. Stach, J. Bao, S-S. Pei, Y. P. Chen, arXiv:1011.4690v1 (2010)

Figures
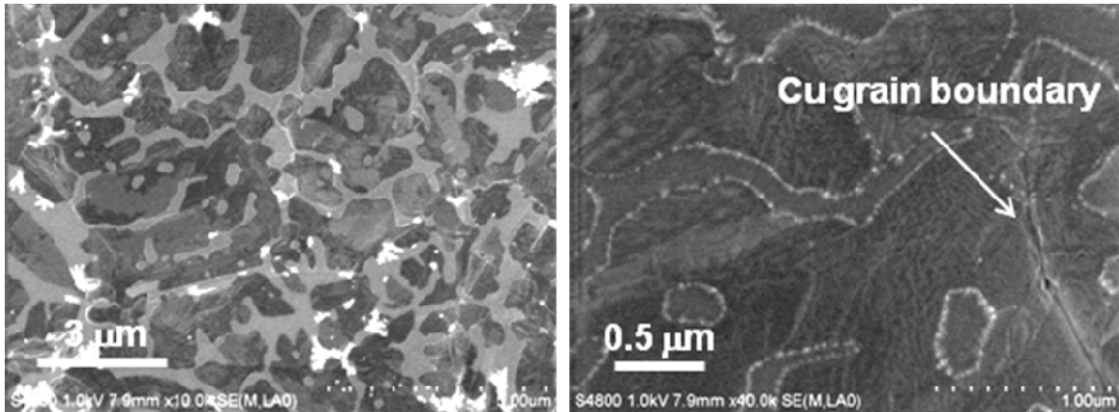
Figure 1
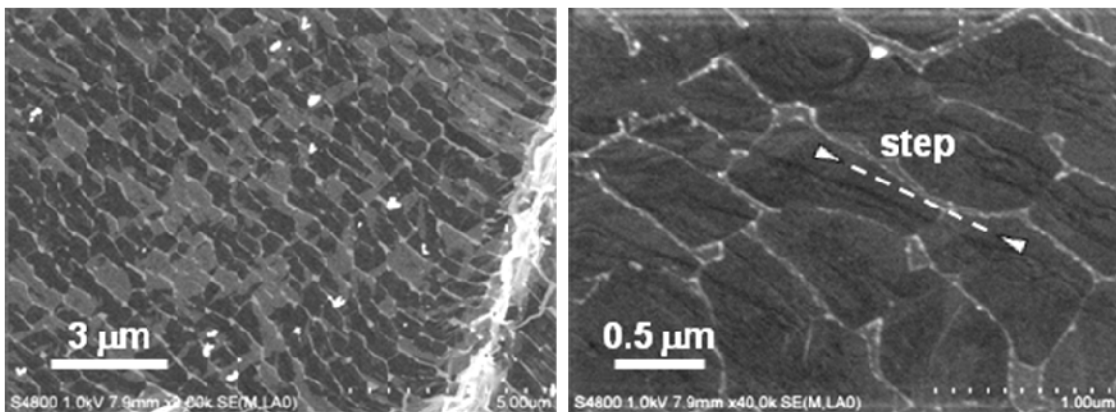
Figure 2
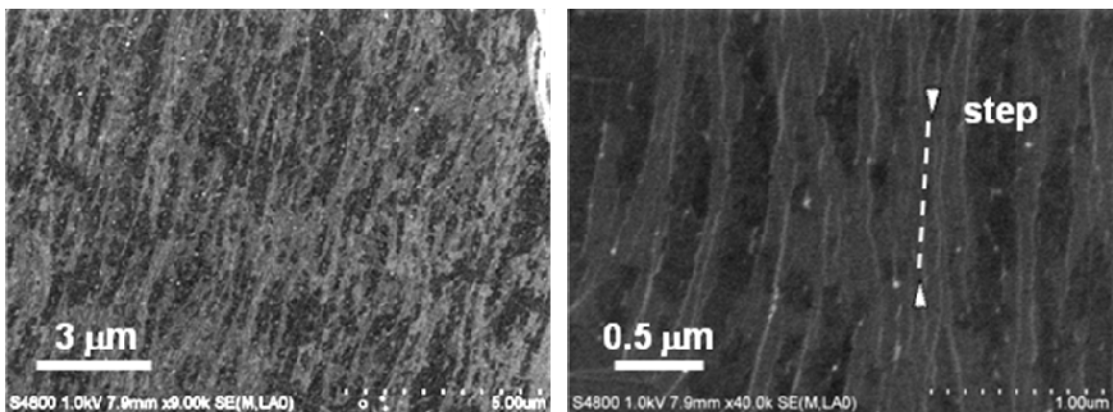
Figure 3

Figure caption
SEM images of graphene islands grown at lower (Fig.1), at medium (Fig.2) and at higher (Fig.3) P$_{source}$ *conditions.*

Scanning Tunneling Microscopy Studies of CVD Graphene on Mica

Kevin T. He, Joshua D. Wood, Eric Pop, and Joseph W. Lyding

University of Illinois at Urbana-Champaign, Beckman Institute, 405 N. Mathews Ave., Urbana, IL, USA
lyding@illinois.edu

Research in graphene has skyrocketed in recent years due to its unique electronic and mechanical properties [1]. Graphene has become not only a sandbox for scientists to study rare physical phenomena [2], but also a potential material for use in future semiconductor devices [3]. However, many issues still need to be resolved before graphene can be commercially viable. For instance, depending on the substrate on which graphene is deposited, there is a major shift in measured carrier mobility [4]. It was recently shown that the ultraflat, insulating boron nitride substrate helps to preserve many of the electronic properties normally seen only in suspended graphene [5]. However, sheets of single-crystal boron nitride can be difficult to obtain, leading to the investigation of other flat, insulating substrates on which graphene can be incorporated.

One widely available mineral which satisfies these conditions is mica. Muscovite ($KAl_2(Si_3Al)O_{10}(OH,F)_2$) is the most common form of mica, with a perfect cleavage plane along the [100] direction, resulting in easily obtainable, atomically flat surfaces. Mica is already used as an insulator in the electronics industry due to its high electronic band gap (~7.8 eV), making it a good candidate for a substrate in graphene-based devices.

Recent atomic force microscopy (AFM) studies of graphene deposited onto mica surfaces have yielded some very interesting results in terms of surface topology [6] and the effect of water adlayers [7]. We present the next logical progression of that work, which is using scanning tunneling microscopy (STM) to characterize the surface with atomic resolution. We transfer graphene grown via chemical vapor deposition (CVD) of methane on copper onto a cleaved mica surface. From the wet transfer process, one or more adlayers of water are adsorbed to the mica surface and become trapped between the mica and graphene after deposition. The graphene acts as a protective covering over the water, preventing evaporation during insertion into ultra-high vacuum (UHV) and subsequent high-temperature degas. Raman spectroscopic analysis confirms the presence of monolayer graphene. The D and G bands on the graphene have large intensities, suggesting locally defective graphene regions or the presence of ice [7].

An STM image of the graphene-water-mica surface can be seen in figure 1. A very interesting spider-web structure appears on the surface, most likely caused by a layer of adsorbed water. We believe that this spider-web structure appears from the high wettability of water on mica [8]. The height of the layer is ~4 Å, closely matching the height of the water layer reported by Xu *et al* [9]. The entire surface is covered in a layer of graphene, and the honeycomb graphene lattice is easily resolved, as seen in the inset. The top water layer appears fairly rough, with a non-periodic structure permeating over the entire surface. As of yet, it is still unclear whether the depression is graphene over bare mica, or graphene over a bottom water layer. The measured roughness of the areas in the depression is much lower than that of the top water layer; whatever it may be has a non-amorphous crystal structure.

Figure 2 shows a 3D image rendered from an STM topograph containing a graphene grain boundary. A hexagonal Moiré pattern with period ~2.8 Å can be seen over the left grain. The cause of this Moiré pattern is unknown. The structure suggests that it could be due to two misaligned graphene lattices, but we observe areas where the Moiré pattern is imperfect, which would not occur with stacked graphene.

References

[1] A.K. Geim and K.S. Novoselov, Nature Materials, **6** (2007) 183.
[2] Y. Zhang, Y.T. Tan, H.L. Stormer, and P. Kim, Nature, **438** (2005) 201.
[3] P. Avouris, Z. Chen, and V. Perebeinos, Nature Nanotechnology **2**, (2007) 605.
[4] X, Du, I. Skachko, A. Barker, and E.Y. Andrei, Nature Nanotechnology **3**, (2008) 491.
[5] C.R. Dean, A.F. Young, I. Meric, C. Lee, L. Wang, S. Sorgenfrei, K Watanabe, T. Taniguchi, P. Kim, K.L Shepard, and J. Hone, Nature Nanotechnology, **5**, (2010) 722.
[6] C.H. Lui, L. Liu, K.F. Mak, G.W. Flynn, and T.F. Heinz, Nature, **462** (2009) 339.
[7] J.R. Scherer and R.G. Snyder, J. Chem. Phys. **67**, (1977) 4794.
[8] L. Xu, A. Lio, J. Hu, D.F. Ogletree, and M. Salmeron, J. Phys. Chem. B, **102** (1998) 540.
[9] K. Xu, P. Cao, and J.R. Heath, Science, **329** (2010) 1188.

Figures
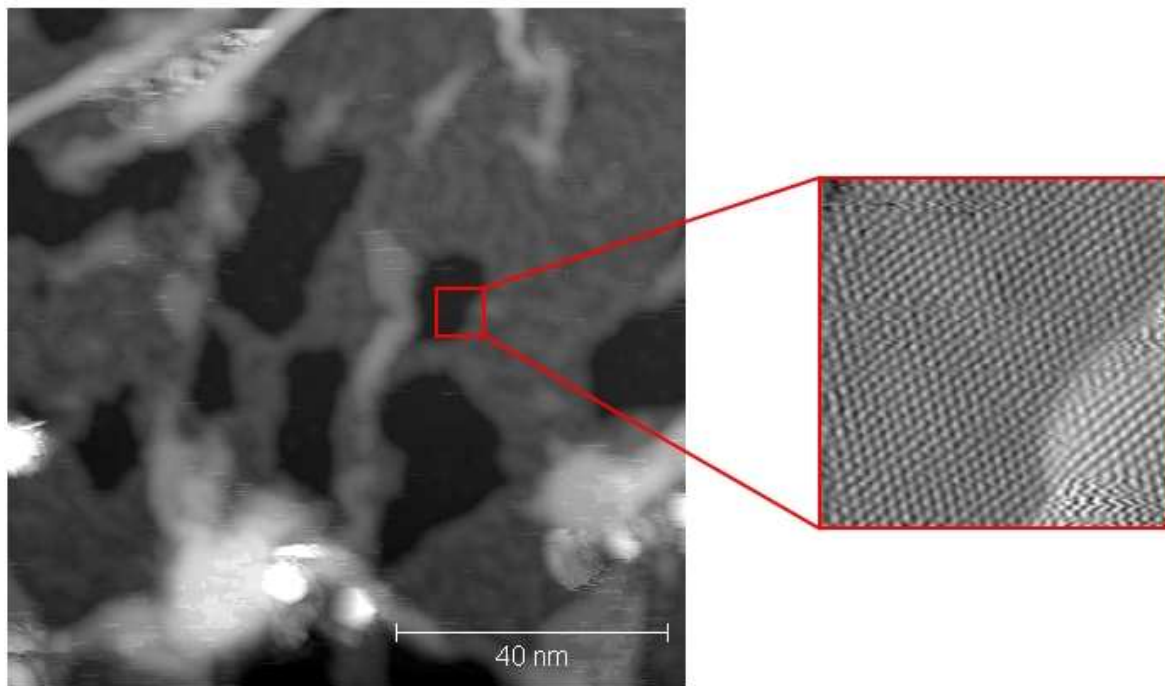
Figure 1*:Scanning tunneling microscope topograph of graphene deposited onto the mica surface.*
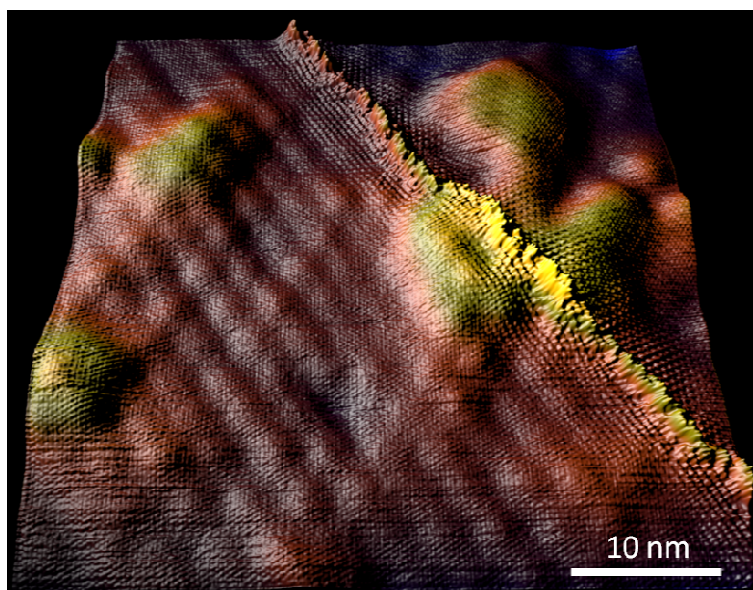
Figure 2: *3D rendering of an STM topograph showing a graphene grain boundary and Moiré pattern.*

Scanning Tunneling Microscopy Simulations of Nitrogen- and Boron Doped single layer and bi-layer graphene

Luc Henrard, Stéphane-Olivier Guillaume, Bing Zheng(*)

PMR, University of Namur (Belgium)
(*) Present Address : PCPM & ETSF, Université Catholique de Louvain (Belgium)
luc.henrard@fundp.ac.be

The control of the doping of few layer graphene and carbon nanotubes represents a challenge that could lead to a production of carbon nanosystems with precise structural and electronic properties or chemical reactivity. Nowadays however, the first experimental data on chemical modification of carbon nanosystems with boron and nitrogen raise fundamental questions on the atomic configurations of the 'defect sites'. What are the most stable chemical modification atomic configurations ? Does the final configuration depends on the production method ? What are the chemical and physical properties of those configurations ? In this contribution, we present density-functional theory based simulations on the electronic properties and on the scanning tunneling microscopy (STM) signature of single layer and bi-layer graphene.

For monolayer graphene [1], the shift of the Fermi level away from the Dirac point and the position of the localized states associated with the defect is studied for several atomic configurations (substitution, pyridine like systems, adsorption, …). The associated STM patterns and STS spectra are deduced within the Tersoff-Hamman approach. For example, for metallic nanotubes, a shift of the Fermi level together with a localized donor (acceptor) states are observed for nitrogen (boron) substitution. Semiconducting tubes tend to become metallic under n and p substitutional doping. Finally, STM fingerprints of the localized states have been computed. We compare also our data with the few available experimental works.

Bi-layer (and multilayer) graphene are known to present electronic properties close the Fermi level dependent on the number of layer and their stacking [2]. For example, the well described massless fermion behavior of single layer graphene is destroyed by the interaction with a second layer, except in the case of rotationally disordered stacking. As a consequence the symmetry of the STM pattern depends on the layer stacking. Here, we show that the substitutional doping on bilayer graphene could also lead to a modification of the STM pattern symmetry, as a result of the asymmetry of the charge on the layer of the doped systems.

References

[1] B. Zheng, P. Hermet, L. Henrard. ACS Nano, **7** (2010) 54165
[2] S. Latil, L. Henrard. Phys. Rev. Lett., **97** (2006) 036803
    S. Latil, V. Meunier, M. Henrard. Phys. Rev. B **76** (2007) 201402
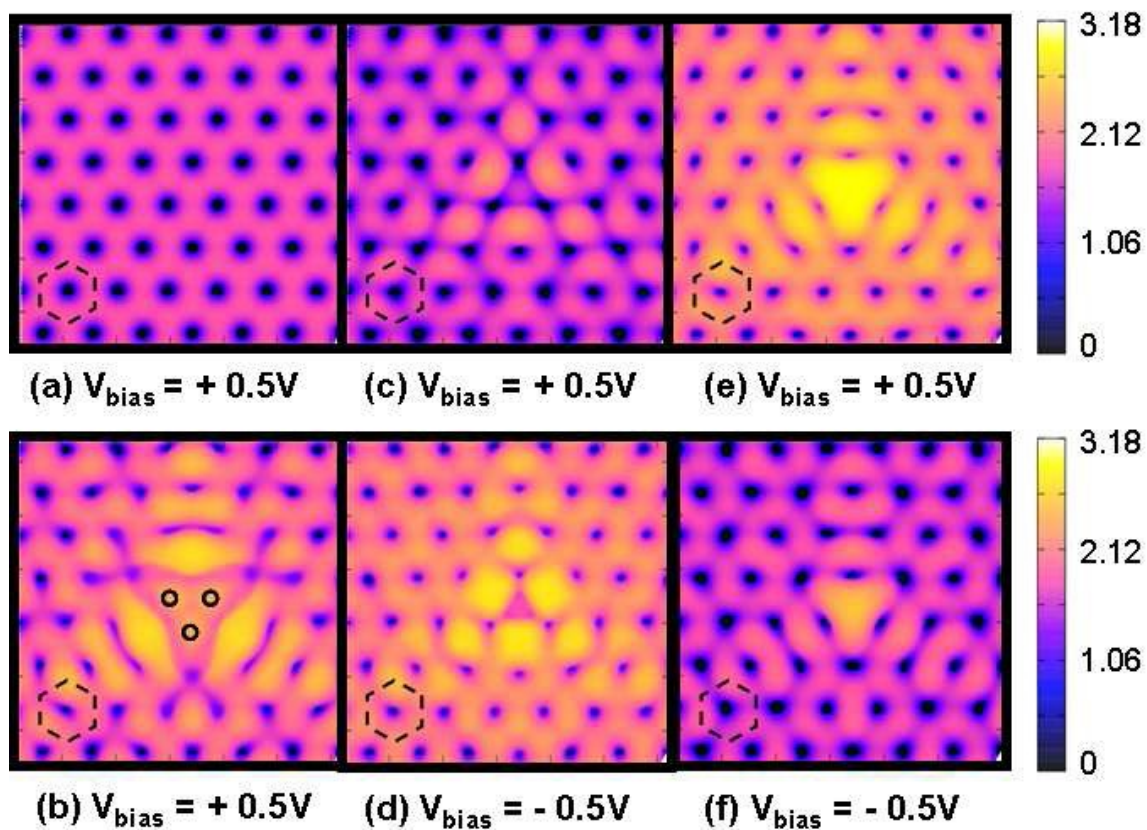
Computed STM images of pristine and doped graphene: (a) pristine, (b) pyridine (locations of 3N are denoted by black circles), (c,d) N-substitution, (e,f) B-substitution. One dashed hexagon is represented on the different images to highlight the atomic network. The color scales for height are in Angstroem. (From Ref 1)

Transmission and conductance across a square barrier potential in monolayer graphene

C. Hdez. Fuentevilla, J.D. Lejarreta, E. Diez,

Universidad de Salamanca, Facultad de Ciencias, 37008 Salamanca, Spain
chernan@usal.es

The transport properties and the tunneling resonant in graphene have attracted very attention [1], [2]. We have studied the transmission coefficient (T) and the conductance across a square barrier in monolayer graphene.

We obtain an analytical expression for the transmission coefficient of a square barrier in graphene which depends on the one hand, of the energy (E) and the angle (ϕ) of the carrier incident, and on the other hand of the barrier potential (V_0) and of the barrier length (D):

$$T(E, V_0, D, \phi) = \left[1 + \frac{V_0^2 \sin^2\left(\frac{1}{658.2} D \sqrt{(V_0 - E)^2 - E^2 \sin^2 \phi} \right) \cdot \tan^2 \phi}{(V_0 - E)^2 - E^2 \sin^2 \phi} \right]^{-1}.$$

We study the T versus the incident angle for different values of the energy, the height of potential, and the barrier length. The T is an even function of the incident angle, and T is always the unity when the incidence is perpendicular to the barrier due to the *Klein paradox* [3], but we also found there are others incident angles that make the T to achieve the unity.

Afterwards we calculate the conductance in the scope of the Landauer-Büttiker formalism [4]

$$G = \frac{2e^2}{h} \int M(E) T(E) \left(-\frac{\partial f_0}{\partial E} \right) dE$$

We define the *effective conductance* like the conductance by the unit of width W in a sheet of graphene on fundamental units e^2/h. By using the previous expression of the T, we have obtained the effective conductance across a square barrier in monolayer graphene

$$G_{ef}(E_F, V_0, D, \phi) = \frac{4E_F}{658.2 \cdot \pi} \left[1 + \frac{V_0^2 \sin^2\left(\frac{1}{658.2} D \sqrt{(V_0 - E_F)^2 - E_F^2 \sin^2 \phi} \right) \cdot \tan^2 \phi}{(V_0 - E_F)^2 - E_F^2 \sin^2 \phi} \right]^{-1}$$

We note that this expression depends on the Fermi energy (E_F), because has been obtained for the case of very low temperatures. We represent in Fig. 1 the effective conductance versus the incident angle for a particular value of the Fermi energy and the barrier length and for three different values of the potential barrier (V_0). We observed that increasing the potential barrier the conductance takes relevant values for a wider set of incident angles.

Finally we consider that in a experiment of electronic transport across a barrier in a graphene sheet the carriers will arrive with different angles and therefore could have sense to calculate a *weighted conductance* in accordance with a certain probability distribution to the incidence angles on the barrier. Two typical cases are considered by using a delta function (only one angle is possible) and the arithmetical average function (all angles have equal probability).

In a standard configuration with the barrier perfectly perpendicular to the current, without considering any scattering mechanism, we can expect all carriers will achieve the barrier with angle $\phi=0$. In this particular case ($\phi=0$) the transmission coefficient is the unity and therefore the effective conductance is maxima, and only depend on the Fermi energy. We can prepare a different set-up as proposed in [5] just preparing the barrier with a particular angle ϕ_0 with the electrical current direction then all carriers will achieve the barrier with this particular angle, again in the absence of any scattering. Nevertheless in this situation the T will not need to be the unity and will depends also of the rest of parameters.

In the case of high scattering we could expect that all angles will have the same probability and then by using an arithmetical average function we can study such a situation showed in Fig 2 as a function of both the Fermi energy and the barrier potential.

References

[1] N.M.R. Peres, J. Phys.: Condens. Matter., **21** (2009) 323201.
[2] H.C. Nguyen, V.L. Nguyen, J. Phys.: Condens. Matter., **21** (2009) 045305.
[3] M.I. Katsnelson, K.S. Novoselov, A.K. Geim, Nature Phys., **2** (2006) 620.
[4] S. Datta, *Electronic transport in mesoscopic systems*, Cambridge University Press (2006).
[5] T. Low, J. Apenzeller, Phys. Rev. B, **80** (2009) 155406.

Figures
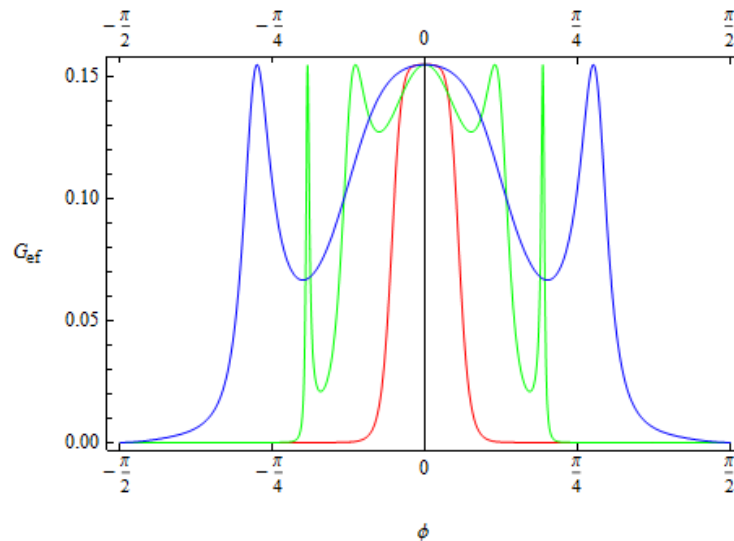
Figure 1 : Conductance effective for E_F = 80 meV, V_0 = 100(red), 130(green), 200(blue) and D = 100 nm
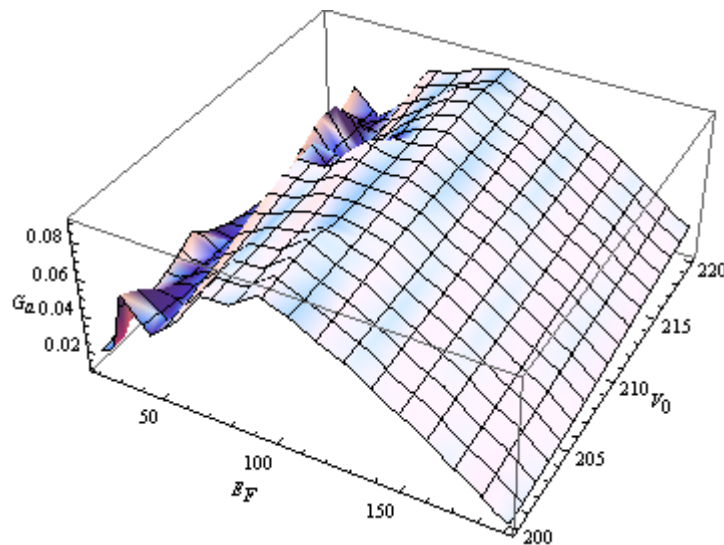
Figure 2 : Conductance with arithmetical average function for D = 100 nm with E_F in meV and V_0 in mV

Orbital magnetism in ballistic graphene nanostructures

L. Hesse, J. Wurm, I. Adagideli, K. Richter

Universität Regensburg

Institut I - Theoretische Physik / Universitätsstraße 31, Regensburg (Germany)

We study the effect of small external magnetic fields on quasiparticles in graphene nanostructures within a semiclassical approach. Therefore we are focusing on magnetic susceptibilities of billiard-systems arising from the orbital motion of the charge carriers To this end we derive the semiclassical expression for the density of states which is closely related to the magnetic susceptibility, starting from an exact expansion for the Green function of a graphene flake. The results depend sensitively on the geometry of the billiard and the types of edges and differ from those of comparable 2DEG systems.

Scanning Raman spectroscopy of graphene antidot lattices: Evidence for p-type doping

S. Heydrich, M. Hirmer, C. Preis, T. Korn, J. Eroms, D. Weiss, and C. Schüller

Institut für Experimentelle und Angewandte Physik, Universität Regensburg, D-93040 Regensburg, Germany
stefanie.heydrich@physik.uni-regensburg.de

Since the first report about the preparation of graphene single layers via mechanical exfoliation technique, the interest in this seemingly ideal two-dimensional system has grown enormously. For the most part, this is motivated by the vision that the two-dimensional carbon system is potentially a promising candidate for future electronic devices. Scanning Raman spectroscopy has proven to be a powerful technique for the characterization and investigation of graphene samples. It enables a fast and nondestructive investigation of the electronic and structural properties of layered and laterally-structured samples with micron or even submicron spatial resolution.

We have investigated antidot lattices, which were prepared on exfoliated graphene single layers via electron-beam lithography and ion etching, by means of scanning Raman spectroscopy. The peak positions, peak widths and intensities of the characteristic phonon modes of the carbon lattice have been studied systematically in a series of samples. In the patterned samples, we found a systematic stiffening of the G band mode, accompanied with a line narrowing, while the 2D mode energies are found to be linearly correlated with the G mode energies. We interpret this as evidence for p-type doping of the graphene antidot lattices [1].

References

[1] S. Heydrich, M. Hirmer, C. Preis, et. al, Appl. Phys. Lett., **97** (2010) 043113.

Figures
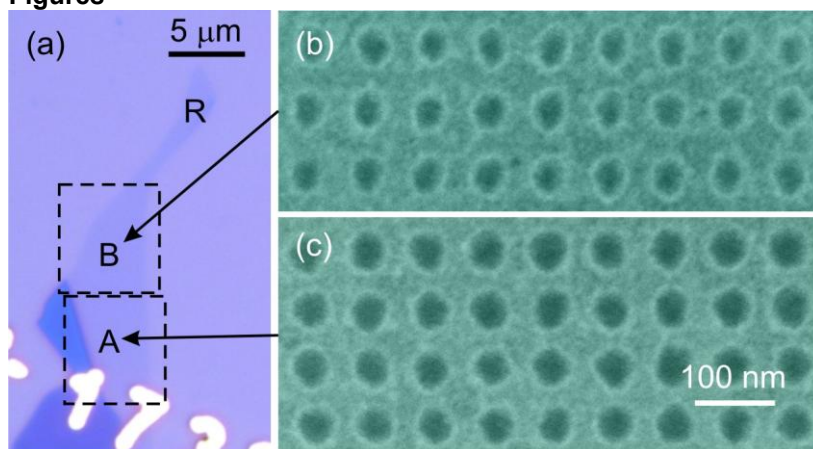
Fig. 1 (a) Microscope image of a single-layer graphene flake, patterned with antidots in areas A and B. Distance of the etched holes is 80nm in both sections. The diameter of the antidots is about 60nm in area A and about 50nm in area B. Region R was left unpatterned as reference section. (b) and (c) SEM images of parts of regions A and B. from Ref. [1].
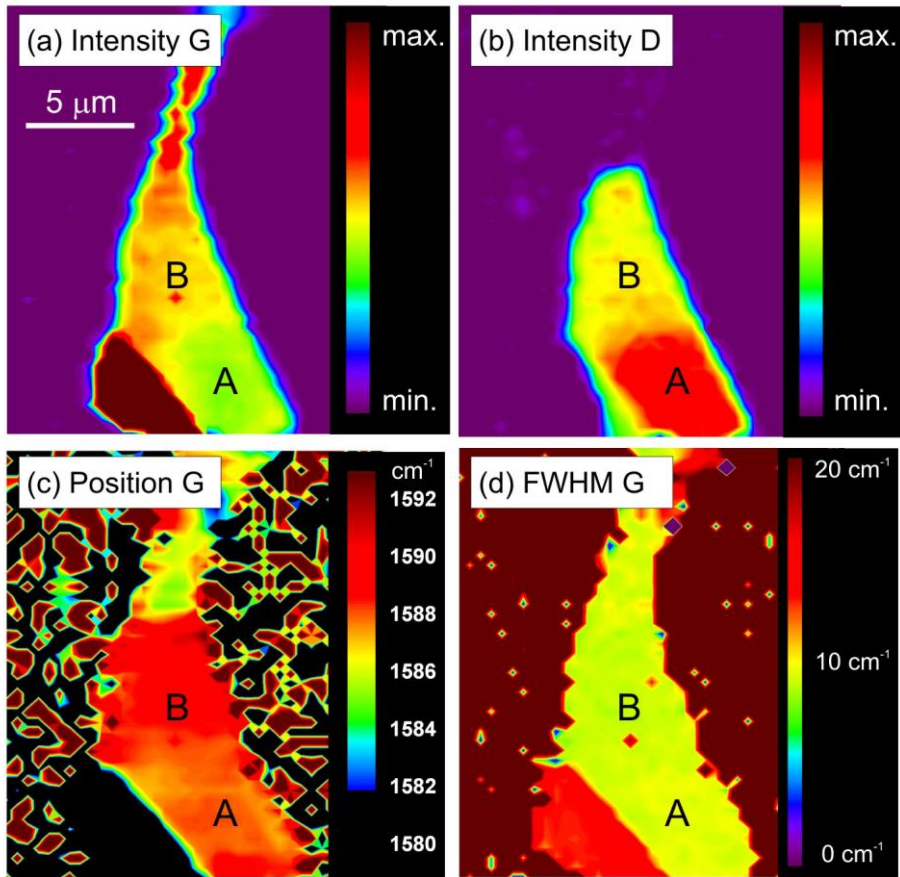
Fig. 2: Raman scan of single-layer graphene flake depicted in fig. 1. (a) shows the intensity of the G peak, (b) the intensity of the D peak. (c) and (d) show the position (energy) and FWHM (full width half maximum) of the G peak. The G peak is stiffened on the patterned areas and appears sharp everywhere on the flake. from Ref. [1].

Grains and Grain Boundaries in Single-Layer CVD Graphene: An Atomic Patchwork Quilt

Pinshane Y. Huang, A.M. van der Zande, C.S. Ruiz-Vargas, W. S. Whitney, M.P. Levendorf, J. W. Kevek, Y. Zhu, J. Park, P. L. McEuen, D.A. Muller

Cornell University, Ithaca, NY, USA
ph269@cornell.edu

Single-layer graphene can be produced by chemical vapor deposition (CVD) on copper substrates on up to meter scales(*1, 2*), making their polycrystallinity(*3, 4*) almost unavoidable. Understanding the grain structure of CVD graphene is critical because graphene grain boundaries have been predicted to significantly alter the electronic(*5-8*), magnetic(*9*), chemical(*10*), and mechanical(*11-13*) properties of graphene monolayers. By combining aberration-corrected scanning transmission electron microscopy (ADF-STEM) and dark-field transmission electron microscopy (DF-TEM), we image graphene grains and grain boundaries across six orders of magnitude in CVD graphene grown on copper. Combining these images with scanned probe and transport measurements, we probe the electrical and mechanical properties of the grain boundaries. These results, reported in Reference (4), will enable studies on the structure, properties, and control of graphene grains and grain boundaries.

To characterize graphene membranes at all length scales, we first approached the atomic-scale using ADF-STEM imaging at 60 kV. The resulting atomic-resolution images of graphene grain boundaries reveal that different grains stitch together predominantly via pentagon-heptagon pairs (Figure 1b). We next used diffraction-filtered imaging to map the shape and orientation of several hundred grains and boundaries on the scale of tens of nanometers to tens of microns. These images reveal an intricate patchwork of grains connected by tilt boundaries, with average grain sizes ranging from 250 nm up to 2-4 microns (Figure1a). We used these DF-TEM methods to directly correlate grain size with growth condition and demonstrate that the graphene grain size can be increased by over an order of magnitude with only slight changes to the growth conditions.

By correlating grain imaging with scanned probe and transport measurements, we show that grain boundaries dramatically weaken the mechanical strength of graphene membranes, but do not as dramatically alter their electrical properties. We first examined the failure strength of the polycrystalline CVD graphene membranes using atomic force microscopy (AFM). We used AFM phase imaging to locate grains and then pressed downward with the AFM tip to test the mechanical strength of the membranes. We next probed the electrical properties of polycrystalline graphene by fabricating electrically-contacted devices using graphene from graphene grown with three different growth methods on copper. By comparing these measurements against corresponding DF-TEM images from each growth, we find that surprisingly, while mobility is clearly affected by growth conditions, high mobility does not directly correlate with large grain size. These methods will be crucial both for exploring synthesis strategies to optimize grain properties and for further studies on the microscopic and macroscopic impact of grain structure on graphene membranes.

References

[1]   X. Li et al., Science **324** (2009) 1312.
[2]   S. Bae et al., Nature Nanotechnol. **5** (2010) 574.
[3]   J. M. Wofford, S. Nie, K. F. McCarty, N. C. Bartlet, O. D. Dubon, Nano Lett., **10** (2010) 4890–4896.
[4].   P.Y. Huang, C.S. Ruiz-Vargas, A. M. van der Zande, W. S. Whitney, M. P. Levendorf, J.W. Kevek, S.Garg, J.S. Alden, C. J. Hustedt, Ye Zhu, J. Park, P. L. McEuen, D. A. Muller., Nature, **doi:10.1038/nature09718** (2011) .
[5]   J. Cervenka, C. F. J. Flipse, Phys. Rev. B **79**, (2009) 195429.
[6]   N. M. R. Peres, F. Guinea, A. H. Castro-Neto, Phys. Rev. B **73**, (2006).
[7]   O. V. Yazyev, S. G. Louie, Nature Mater., **9** (2010) 806-809.
[8]   A. Mesaros, S. Papanikolaou, C. F. J. Flipse, D. Sadri, J. Zaanen, Phys. Rev. B, **82** (2010) 205119.
[9]   J. Cervenka, M. I. Katsnelson, C. F. J. Flipse, Nature Phys. **5** (2009) 840.
[10]   S. Malola, H. Hakkinen, P. Koskinen, Phys. Rev. B **81** (2010) 165447.
[11]   R. Grantab, V. B. Shenoy, R. S. Ruoff, Science **330** (2010) 946.
[12]   Y. Liu, B. I. Yakobson, Nano Lett. **10** (2010) 2178.
[13]   O. V. Yazyev, S. G. Louie, Phys. Rev. B **81** (2010) 195420.

Figures
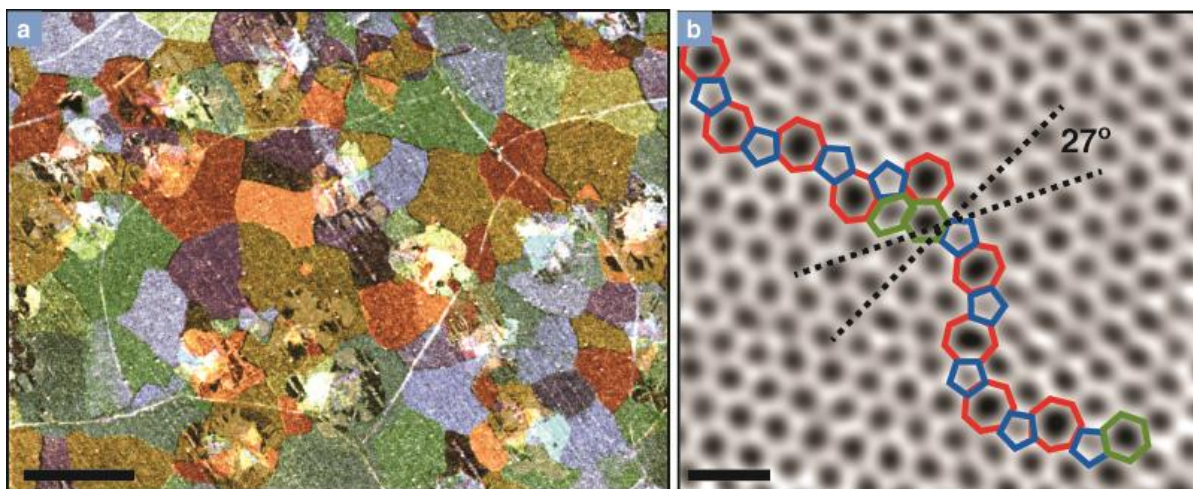
Figure 1: Images of the grain structure of CVD graphene grown on copper. (a), Composite, colored DF-TEM image of graphene grains. Each color represents graphene of a small (~5 degrees) range of in-plane crystallographic orientations. Scale bar 2 microns. (b) ADF-STEM image of the atomic structure of a grain boundary in which the two grains meet with a relative crystallographic rotation of 27 degrees. Pentagons (blue), heptagons (red), and disordered hexagons (green) make up the meandering, aperiodic structure at the grain boundary. Reproduced from Reference 4, scale bar 5 angstroms

Immobilization of E2 protein and its supramolecular complexes, and activity retention on graphene

Abeer Al-Shammari[1], Mareike Posner[2], Abhishek Upadhyay[2], Gavin Jones[1], Stefan Bagby[2], Pedro Estrela[3], and Adelina Ilie[1]

[1]Department of Physics and Centre for Graphene Science, [2]Department of Biology and Biochemistry, [3]Department of Electronic Engineering, University of Bath, Bath, BA2 7AY, UK
a.ilie@bath.ac.uk

Protein immobilization is central to the development of new bio-assays or sensing platforms as it is directly linked to such issues as protein conformation and subsequently to whether they remain active or not after immobilization. Immobilized enzymes are routinely used in the biotechnology industry but there are numerous problems with their immobilization for industrial usage [1]. Here we are exploring graphene as a surface for enzyme immobilization and activity detection. Graphene has shown extreme (down to single-molecule) sensitivity to environmental changes [2] and progress in its synthesis now allows its growth on large areas [3], thus making it a potentially superior candidate for the bio/inorganic interface.

The 2-oxo acid dehydrogenase protein complex (OADHC) (Figure 1c) is one of the largest enzyme complexes, which is central to energy metabolism [4]. It consists of a dihydrolipoyl acyl-transferase (E2) protein core, on which 2-oxo acid decarboxylase (E1) and dihydrolipoamide dehydrogenase (E3) proteins bind non-covalently, but specifically [4]. In this work we first succeeded in immobilizing the E2 monomer *directly* onto the graphene surface and then investigated the supramolecular assembly of the E2 core as well as of the whole 2-OADHC complex. Finally, the retention of activity of the whole complex is tested through its redox electron transfer to a Field-Effect graphene sensor.

Our approach is different to those taken in prior studies of protein binding on graphene, where only small proteins, simple in structure and with single function have been used (see for example [5]). Contrary to them, our thermostable E2 protein offers extensive flexibility for tailoring protein-protein interactions and resulting functions, and with its enhanced thermostability, constitutes a model system for scaffolding of complex, multidomain protein systems.

References

[1] Fang Y, Huang X, Chen P, Xu Z, *BMB reports*, **44** ,87,(2011).
[2] Guo S, Dong S, *Chem Soc Rev*., **3** (2011) Advance article
[3] Zhang S, Shao Y, Liao H, Engelhard MH, Yin G, Lin Y, *ACS Nano*, 1 March (2011)
[4] Perham RN, *Ann. Rev. Biochem.,* **69,** 961, (2000).
[5] Changsheng S, Huafeng Y, Jiangfeng S, Dongxue H, Ari I, Li N, *Anal Chem*, **81**, 2378 (2009); Ping Wua, Qian Shaoa, Yaojuan Hua, Juan Jina, Yajing Yina, Hui Zhanga and Chenxin Cai, *Electrochimica Acta*, **55**, 8606 (2010); Wang K, Liu Q, Guan QM, Wu J, Li HN, Yan JJ., *Biosens Bioelectron*. **26**, 2252 (2011).
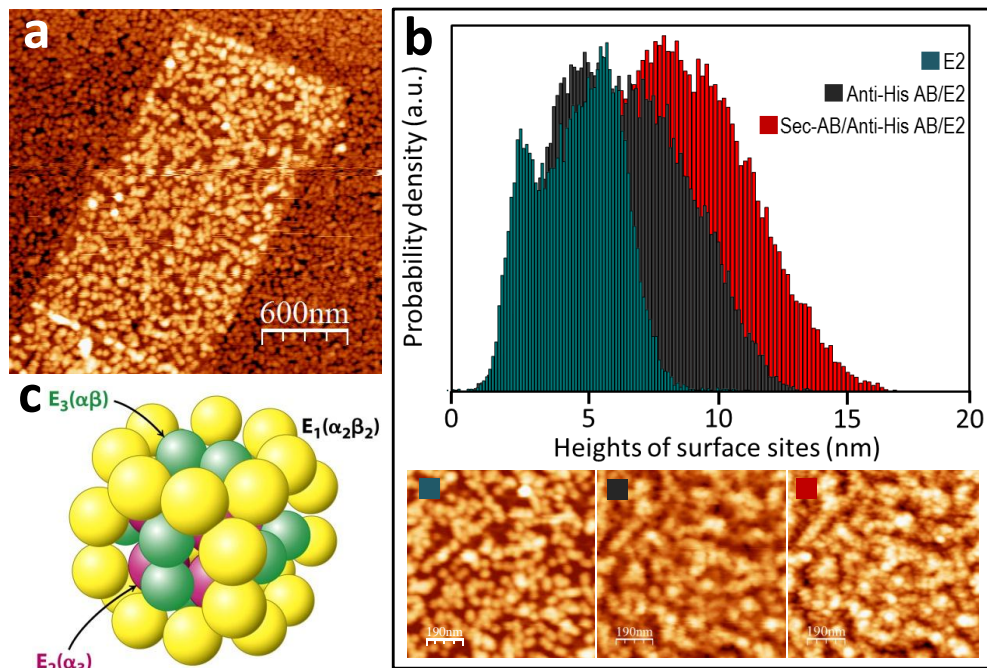
Figure 1: (a) E2 has attached non-covalently onto graphene (thus preserving graphene electronic properties); (b) shows that the His-tag of the E2 protein is accessible for specific binding, tested here with an Anti-His Antibody (Anti-His AB), whose presence is then confirmed by the attachment of a complementary, secondary antibody (Sec-AB).The build-up of this scaffolding system is shown through topographic changes obtained through Atomic Force Microscopy, directly in images as well as in changes in the distribution of surface site heights; (c) the full 2-OADHC complex.

Large Area Graphene Field Effect Devices with Sputtered Nitride and Oxide Top-Dielectrics

S.A. Imam[1], A. Guermoune[2], M. Siaj[2], T. Szkopek[1]

McGill University, 3480 University Street, Montréal, Québec, Canada
Université du Québec à Montréal, 405 rue Sainte-Catherine Est, Montréal, Québec, Canada
shahriar.imam@mcgill.ca, thomas.szkopek@mcgil.ca

Realizing high-speed (high f_t) graphene transistors requires the high capacitance of a thin top-gated dielectric structure. The deposition of a top-gate dielectric can significantly reduce mobility due an increased density of trapped charges [1] and damage to the graphene during the deposition process. However, high-κ dielectrics such as ionic liquids have been observed to enhance mobility [2], explained by dielectric screening of charged impurities. The effect of a dielectric on mobility remains not fully understood [3,4]. Moreover, a graphene field effect device is doped by adsorbates according to the chemical nature of the dielectric surface in contact with the graphene [5]. We report an experimental study on the field effect mobility and doping of large area graphene field effect devices encapsulated by two top-layer dielectrics: SiO_2 ($\varepsilon_r \sim 3.9$) and Si_3N_4 ($\varepsilon_r \sim 3.9$) grown by magnetron sputter deposition.

Graphene was grown on Cu foils in a tube furnace with a methane/hydrogen gas mixture at a growth temperature of 900°C. The graphene was transferred to insulating substrates using a poly(methyl methacrylate) (PMMA) handle and sacrificial etch of the Cu in ammonium persulfate (0.1M). Further details of the growth and transfer process are described elsewhere [6,7]. Heavily doped Si (n-doped, 8-20 mΩ-cm) with 300 nm of dry, chlorinated thermal SiO_2, was chosen as the substrate for back-gated electrical measurements. Standard photolithography, electron beam evaporation and lift-off techniques were used to define Ohmic contacts (10nm Ti/100nm Au). Subsequent photolithography and oxygen plasma treatment was used to isolate graphene sheets in a 4-point van der Pauw geometry (Fig. 1).

Raman spectroscopy at a 514.5nm pump wavelength was used to characterize the graphene before and after deposition of a top-side dielectric. The sheet resistance R_S was measured by the van der Pauw technique as a function of back gate voltage V_{GS}. All electrical measurements were performed in a variable environment probe station following a 400K, 10^{-5}Torr anneal over a minimum of 12 hours. Sheet resistance measurements were taken before and after deposition of a top-side dielectric. Magnetron sputtering with a Si target and RF plasma source was used to deposit 10nm of SiO_2 (20sccm of Ar and O_2 gas at 5mbar, 20nm/min growth rate) or 10nm of Si_3N_4 (25sccm of Ar and N_2 gas at 5mbar, 3.3nm/min growth rate).

Raman spectroscopy reveals an increase in D-peak ($\sim 1350cm^{-1}$) intensity following deposition of either dielectric, as well as an increase in background fluorescence (Fig. 2). The origin of the fluorescence is possibly due to plasma induced damage of graphene during sputtering [8]. Sheet resistance R_S versus back gate voltage V_{GS} measurements (Fig. 3) reveal that both SiO_2 and Si_3N_4 top-dielectric layers significantly reduce the doping of the field effect transistors, presumably due to the reduced presence of water [5]. The carrier mobility, $\mu = [CR_S(V_{GS} - V_{NP})]^{-1}$ where $C = 11.8nF/cm^2$ is the back-gate capacitance and V_{NP} is the neutrality point back-gate voltage, was compared at an electron density $n = 10^{12}/cm^2$ for a series of devices before and after deposition of top-gate dielectrics (Fig. 4). Carrier mobilities as high as $\sim 2000cm^2/Vs$ were achieved with a top-dielectric. Our results are comparable to that of microscopic exfoliated graphene samples encapsulated with nitride by chemical vapour deposition [9]. In several devices, a minimal change in mobility was observed before and after Si_3N_4 deposition. Future work to incorporate top-gated large-area graphene devices in high-frequency compatible structures is underway.

References

[1] M.C. Lemme et al., Solid State Electron. **52** (2008) 514-518.
[2] F. Chen, J. Xia, and N. Tao, Nano Lett. **9**, (2009) 1621-1625.
[3] L.A. Ponomarenko et al., Phys. Rev. Lett. **102**, (2009) 206603.
[4] C.R. Dean et al., Nature Nanotech. **5**, (2010) 722-726.
[5] P.L. Levesque et al., Nano Lett. **11**, (2011) 132-137.
[6] A. Guermoune et al., under review.
[7] X. Li et al., Science **324** (2009) 1312-1314.
[8] T. Gokus et al., ACS Nano **3** (2009) 3963-3968.
[9] W. Zhu, D. Neumayer, V Perebeinos and P. Avouris, Nano Lett. **10** (2010) 3572-3576.

Figures
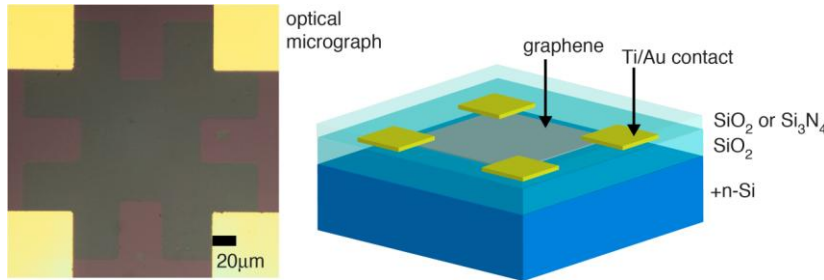
Fig. 1 : Graphene is transferred, etched and contacted into a van der Pauw sample on a SiO$_2$/Si substrate for back gating. A dielectric top layer of 10nm SiO$_2$ or 10nm Si$_3$N$_4$ is sputtered for encapsulation.
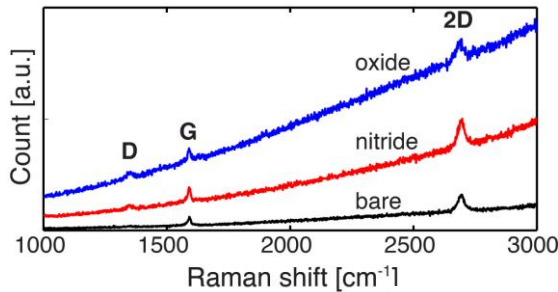
Fig. 2 : Raman spectra (λ=514.5nm) of large area graphene as transferred to SiO$_2$/Si. Following deposition of a Si$_3$N$_4$ dielectric top layer, an increase in D-peak (~1350cm^{-1}) scattering and background fluorescence is observed. A more intense D-peak and greater background fluorescence is observed with SiO$_2$ deposited as a dielectric top layer.
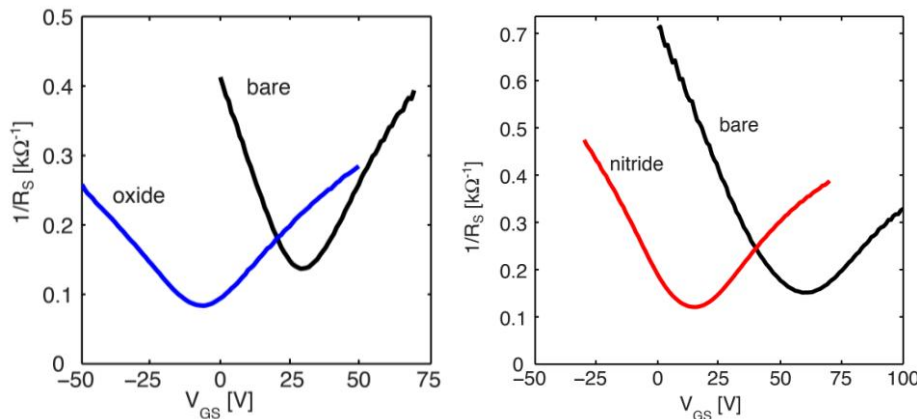
Fig. 3 : Sheet resistance R_S measured by van der Pauw technique versus back-gate voltage V_{GS}. A device before and after SiO$_2$ top-dielectric deposition (left) shows a reduction in doping and a reduction in mobility. A device before and after Si$_3$N$_4$ deposition (right) shows a reduction in doping and a negligible change in mobility.
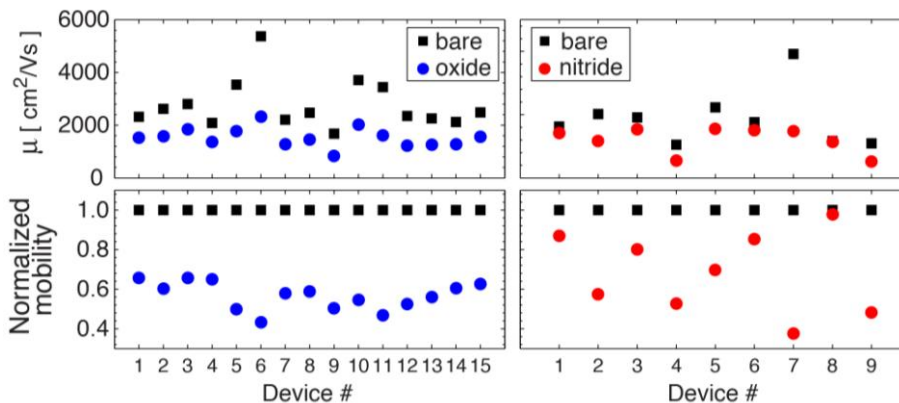
Fig. 4 : Carrier mobility μ at electron density n = 10^{12}/cm^2 inferred from R_S versus V_{GS}. The mobility is compared before and after dielectric deposition. The mobility normalized to that of the bare device before deposition is also compared. In several cases, a minimal change in mobility is observed.

Repair for Process-induced Defects of Transferred Graphene

T. Ishida[1)], Y. Shimotsuji[1)], R. Kajiwara[2)], S. Tanaka[2)] and A. Hashimoto[1)]

[1)] Graduate School of Electrical & Electronics Engineering, University of Fukui,
Bunkyo 3-9-1, Fukui 910-8507, Japan
[2)] Department of Applied Quantum Physics & Nuclear Engineering, Kyushu University,
744 Motooka, Nishi-ku, Fukuoka 819-0395, Japan
fe070049@fuee.u-fukui.ac.jp

Formation of few layer epitaxial graphene on SiC substrate by Si sublimation is one of the most important issues to obtain the high quality and large area graphene with controlled layer numbers.[1] From the various application viewpoints, we think that it is necessary for the epitaxial graphene with large area to transfer from the SiC original surface onto the arbitrary insulator layers such as SiO_2 layer formed on Si substrates. We have already reported that such transfer process of the large area epitaxial graphene from the Si-face SiC substrate onto the SiO_2 layer can be successfully established using the Ti intermediate layer deposited on the graphene and we have successfully achieved to obtain the large area (4mm × 7mm) mono- and bi-layer transferred graphene on the SiO_2/Si substrate.[2] However, there is one serious problem in this transfer process, that is, some defects are induced in the final stage of the transfer process. Therefore, the repair technique for the defects of the transferred graphene on the SiO_2/Si substrate should be necessary to obtain the high quality transferred graphene on the SiO_2 layer. In this work, we have investigated that a new repair technique for the defects by carbon MBE are very effective to improvement the quality for the process-induced defects of the large area transferred epitaxial graphene.

We have investigated about the thermal stability of the defective transferred graphene at 800℃, 900℃, and 1000℃ under the ultra high vacuum (UHV) better than 1.0×10^{-9} Torr, before the investigation of the repair technique of the defects. The carbon MBE onto the defective transferred graphene surface was performed at 900℃ under the ultra high vacuum better than 1.0×10^{-9} Torr to explore a possibility of the repair of process-induced defects. We used carbon heater as a carbon beam source for MBE to supply carbon atoms onto the transferred graphene surface. The quality of the transferred graphene before and after the repair by the carbon MBE was characterized by the microscopic laser Raman spectroscopy.

Figure 1 shows Raman spectra from the two points of A and B with the different quality on the transferred graphene before and after the UHV annealing. All Raman peaks from both points of A and B shifted to the high energy side by annealing. The increase of Raman intensity between the D and the G peaks indicates that the defective transferred graphene net easily changed to the amorphous carbon by the UHV annealing. Figure 2 shows the typical Raman spectra from the transferred graphene before and after the repair process by the carbon MBE. We can easily observe the drastically decrease of the defect originated D- and the D'-band peak intensities after the carbon MBE and the result strongly indicate that the repair of the defects by the carbon MBE is expected to improve the quality of the transferred graphene.

References

[1] K. Hayashi, S. Mizuno, S. Tanaka, H. Toyoda, H. Tochihara and I. Suemune, Jpn. J. Appl. Phys. Express Lett, **44** (2005) L803.
[2] A. Hashimoto, H. Terasaki, K. Morita, H. Hibino and S. Tanaka, International Conference On Silicon Carbide And Related Materials, (2009) Tu-P-86.
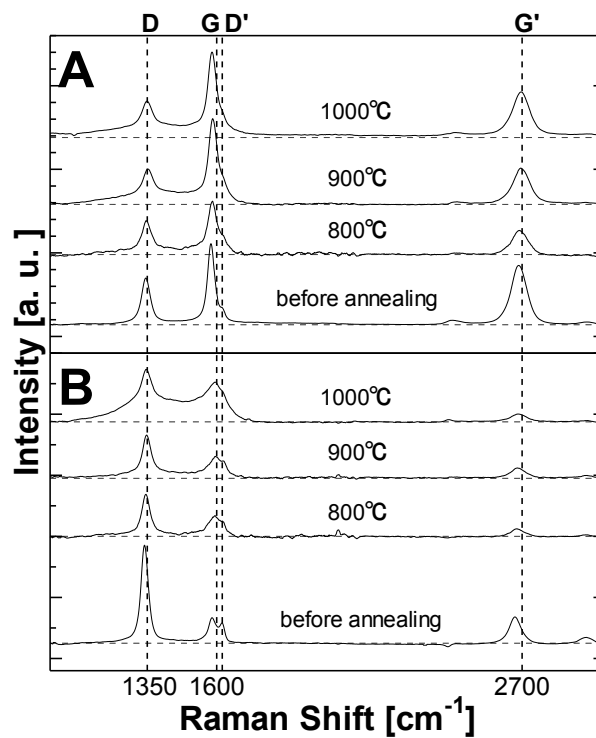
Fig. 1 Raman spectra from transferred graphene by UHV annealing
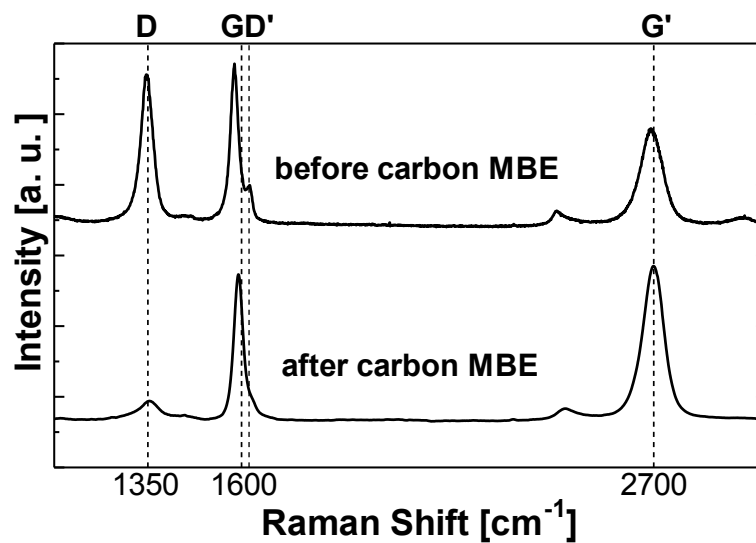
Fig. 2 typical Raman spectra from transferred graphene before and after repair process by carbon MBE

Unconventional Plasmon-Phonon coupling in Graphene

Marinko Jablan[1], Marin Soljacic[2], and Hrvoje Buljan[1]

[1]Department of Physics, University of Zagreb, Bijenicka c. 32, 10000 Zagreb, Croatia
[2]Physics Department, Massachusetts Institute of Technology, 77 Massachusetts Avenue, Cambridge MA 02139, USA
mjablan@phy.hr

The interaction of collective vibrations of crystal lattice (phonons) and electrons has fundamental implications on properties of materials. This interaction takes an unusual form in graphene [1] leading to breakdown of Born-Oppenheimer approximation [2] or the anomaly of the optical phonon [3]. In light of this peculiar electron-phonon interaction, and recent interest in collective excitations of electrons in graphene – plasmons (e.g., see [4] and Refs. therein), here we consider plasmon-phonon coupling in graphene. We predict [4] that plasmon-phonon coupling occurs with a peculiar crossing of polarizations: longitudinal plasmons couple exclusively to transverse optical phonons, whereas graphene's transverse plasmons couple only to longitudinal optical phonons. This is calculated within the framework of the self-consistent linear response formalism.

To understand physical mechanism behind this unusual crossing of polarizations, let us look at the band structure of graphene. Near high symmetry K point (shown in Fig. 1b.) electrons are described by Dirac cones with effective Hamiltonian given by the tight-binding approximation [1]:

$$H_e = \hbar v_F \vec{\sigma} \cdot \vec{k} \quad (1).$$

If we now imagine a collective oscillation of electrons, i.e. a plasmon, we can describe it with a mean field vector potential $\vec{A}$ (scalar potential is gauged to zero) which acts on the electrons in a self-consistent way. To quantify this interaction we use a general substitution $\hbar \vec{k} \rightarrow \hbar \vec{k} + e\vec{A}$ in Eq. (1), so that electron-plasmon interaction can be written as:

$$H_{e-pl} = e v_F \vec{\sigma} \cdot \vec{A} \quad (2).$$

Turning our attention to phonons let us first assume that $\vec{u} = (\vec{u}_A - \vec{u}_B)/\sqrt{2}$ denotes a small displacement of the atoms A and B in the basis as shown in Fig. 1c. Within tight-biding approximation this results in the interaction Hamiltonian given by (see [3] and Refs. therein):

$$H_{e-ph} = -\sqrt{2}\frac{\beta\gamma}{b^2}\vec{\sigma} \times \vec{u} = e v_F \vec{\sigma} \cdot \vec{A}_{eff} \quad (3).$$

When comparing this to Eq. (2) one can see that Eq. (3) is equivalent to the presence of an effective vector potential $\left|\vec{A}_{eff}\right| \propto \left|\vec{u}\right|$ which simply shifts original Dirac cone to a new position as show in Fig. 1d.

The peculiar property of graphene is that vector $\vec{A}_{eff}$ is perpendicular to the displacement vector $\vec{u}$ so that the oscillation of logitudinal (transverse) optical phonons creates an effective vector potential, and thereby an effective electric field, in the transverse (longitudinal) direction. On the other hand, since longitudinal (transverse) plasmons are accompanied by longitudinal (transverse) electric field this will lead to the mentioned crossing of polarization of the two collective excitations. The plasmon-phonon coupling will be greatest when phonon energy and momentum match that of the appropriate plasmon mode since then the effective electric field created by phonon will have a huge response due to collective motion of electrons. These points are clearly shown in Fig. 2.

Finally we note that the frequency shift of the transverse optical phonon due to interaction with collective electron excitations (Fig. 2a.) is much larger than the one where phonon interacts with single particle excitations which was recently measured in the Raman experiment [2]. In this context plasmon-phonon coupling can serve as a magnifier for exploring the electron-phonon interaction in graphene, while it also offers novel electronical control over phonon frequencies. To point out the technological implications we note that there has been an increased interest for plasmons in graphene in the context of plasmonics and metamaterials and we have shown in another paper [5] that plasmon-phonon interaction plays an important role there.

References

[1] A. H. Castro Neto, F. Guinea, N. M. R. Peres, K. S. Novoselov, and A. K. Geim, Rev. Mod. Phys. **81** (2009) 109.

[2] S. Pisana, M. Lazzeri, C. Casiraghi, K. S. Novoselov, A. K. Geim, A. C. Ferrari, and F. Mauri, Nature Materials **6** (2007) 198.

[3] T. Ando, J. Phy. Soc. Jpn. **75** (2006) 124701.

[4] M. Jablan, M. Soljacic, and H. Buljan, arXiv:1010.4871.

[5] M. Jablan, H. Buljan, and M. Soljacic, Phys. Rev. B. **80** (2009) 245435
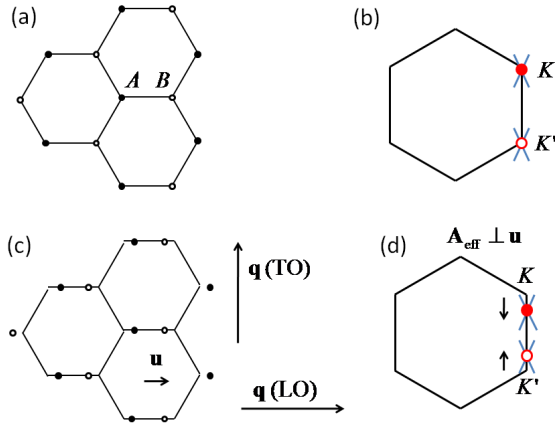
Fig. 1. (a) Bravais lattice of graphene with two atoms *A* and *B* in the basis. (b) Brillouin zone with Dirac cones at *K* and *K'* points. (c) displacement of basis atoms corresponding to the profile of optical phonon mode and (d) the resulting movement of the Dirac cones which can be described trough the action of effective vector potential $\vec{A}_{eff} \perp \vec{u}$. We also show in figure (c) the orientation of wave vector $\vec{q}$ for different polarizations of phonon modes.
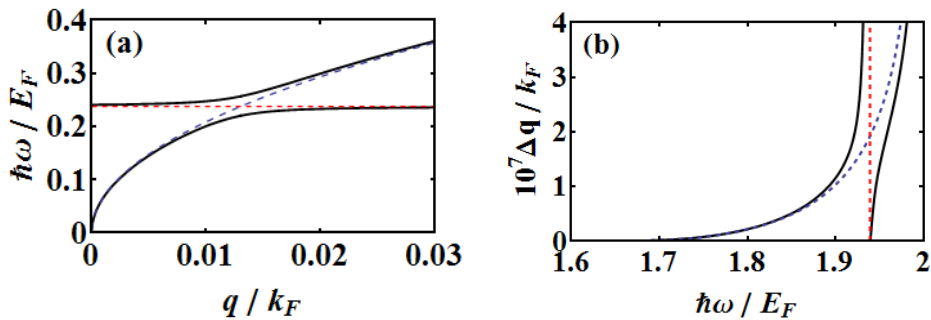
Fig. 2. Dispersion relation for coupled: (a) longitudinal plasmon-transverse optical phonon mode at doping value $E_F = 0.82eV$, and (b) transverse plasmon-longitudinal optical phonon mode for doping value $E_F = 0.1eV$. The coupled (uncoupled) modes are depicted by solid (dashed) lines and note that phonons are effectively dispersion-less for these wave vectors. Finally note that, since dispersion relation of transverse plasmons is very close to the light line, we plot $\Delta q = q - \omega / c$ on ordinate axis in figure (b).

Graphene and few layer graphene (FLG) synthesis methods

Izabela Janowska[a], Ovidiu Ersen[b], Kambiz Chizari[a], Spyridon Zafeiratos[a], Dominique Bégin[a], Marc-Jacques Ledoux[a], Cuong Pham-Huu[a]

[a] Laboratoire des Matériaux, Surface et Procédés pour la catalyse (LMSPC),
UMR 7515 CNRS-Université de Strasbourg, France
[b] Institut de Physique et Chimie des Matériaux de Strasbourg (IPCMS)
UMR 7504 CNRS- Université de Strasbourg, France
janowskai@unistra.fr

Three new different synthesis methods of graphene and few layer graphene (FLG) materials were developed.

Two of them were based on the use of the microwaves irradiation, the first one: to induce the catalytic unzipping of the carbon nanotubes and an exfoliation of the expanded graphite in the second one [1, 2]. The last method, very recently developed, was based on the use of the mechanical thinning of graphite based materials [3]. All methods have different advantages: unzipping of the carbon nanotubes allows the control of the number of the graphene sheets in the final products, the FLG obtained from the expanded graphite consist of big size (up to few tenth micrometers) sheets and finally the third method results in high yield (up to 60%), low cost and process simplicity which make it very promising for the industrial scale applications. The obtained graphene and FLG were characterized by different microscopic and spectroscopic techniques such as TEM, TEM-SAED, TEM-DF-SAED AFM, XPS, IR. The theoretical simulations using Reactive Forcefields show that the presence of the catalyst nanoclusters and oxygen at the carbon nanotubes decreases the energy barrier during their unzipping process. An example of the TEM of few micrometer size graphene sheets and TEM-DF-SAED are presented on the figure below.

References

[1] I. Janowska, O. Ersen, T. Jacob, P. Vennégues, D. Bégin, M.-J. Ledoux, C. Pham-Huu, App. Catal.A, **371** (2009) 22.
[2] I. Janowska, K. Chizari, O. Ersen, S. Zafeiratos, D. Soubane, V. Da Costa, V. Speisser, Ch.

Boeglin, M. Houllé, D. Bégin, D. Plee, M.-J. Ledoux, C. Pham-Huu, Nano Research, **3** (2010) 126-137.

[3] Préparation de graphène par amincissement mécanique de matériaux graphitiques.
   Janowska I., Bégin D., Chizari K., Ersen O., Bernhardt P., Romero Th., Ledoux M. J., Pham-Huu C. PCT/FR2010/000730 (2010).
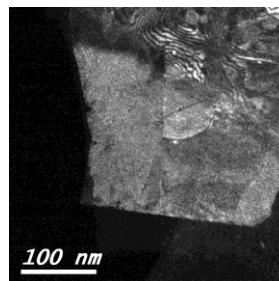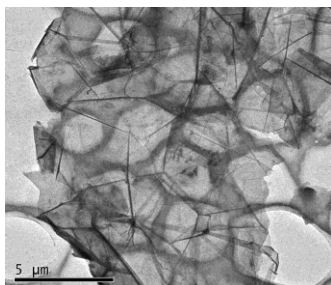
Figure: TEM (left) and TEM-DF-SAED (right) images of the graphene materials obtained by exfoliation of the expanded graphite under microwaves irradiation.

Atomistic effects in graphene antidot lattices: influence of lattice symmetry and hole edges on electronic structure and transport properties

Antti-Pekka Jauho[1,2], Tue Gunst[1], Rene Petersen[3], Troels Markussen[4], Mads Brandbyge[1], and Thomas Garm Pedersen[3]

[1]Dept. of Micro and Nanotechnology, DTU Nanotech, DTU, DK-2800 Lyngby, Denmark
[2]Dept. of Applied Physics, Aalto University, P.O. Box 11100, FI-00076 AALTO, Finland
[3]Dept. of Physics and Nanotechnology, Aalborg University, DK-9220 Aalborg East, Denmark
[4]Dept. of Physics, DTU Fysik, CAMD, DK-2800 Lyngby, Denmark
Antti-Pekka.Jauho@nanotech.dtu.dk

Antidot lattices defined on graphene (GAL) have been promoted as a flexible platform for creating a tunable band gap thereby possibly allowing the realization of a number of technological applications [1]. The antidot lattice can be viewed as a regular nanoperforation of the pristine graphene sheet. Theoretically the properties of triangular GALs have been examined already quite substantially (e.g., optical properties [2], excitons [3], electronic properties [4,5], electron-phonon coupling [6], detection of edge states [7], or details of band gap scaling [8]). Most importantly, the experimental techniques for fabricating GALs have evolved rapidly [9-11], presently reaching lattice constants of a few tens of nanometers, where many of the interesting quantum mechanical effects predicted by theory should become visible.

GALs may be designed in many different ways, as far as their microscopic structure is concerned. Here we report results for two specific aspects: (i) the effect of the symmetry of the antidot lattice, and (ii) the effect of the atomic arrangement at the edge of the etched holes.

(i) The block-copolymer technique for fabricating GALs [10,11] may yield many different lattice symmetries. Our calculations show, perhaps surprisingly, that only one-third of the rotated triangular or rectangular lattices lead to sizable band gaps (Figure (A), middle and bottom panels) while all triangular lattices display a gap (Figure (A), top). An explanation of these regular patterns of the gap formation can be given based on *Clar structures* [13]: structures allowing a full benzenoid structure are most stable (triangular structures belong to this class, while only one-third of rotated triangular or rectangular lattices do so), and therefore display a sizable gap. A full discussion will be given soon [12].

(ii) In view of possible thermoelectric applications, it is of interest to examine how the electronic and phonon transmission properties of graphene samples are affected by embedded GALs, and, in particular, whether the details of the hole edges have a significant effect. In Figs. (B) and (C) we report such a study; full details will be discussed soon [14]. Remarkably, the structure where the holes have a zigzag edge displays an additional splitting up of the GAL minibands (top panel in (B), inset), while a similar armchair structure does not (bottom panel in (B), inset). This can be traced to the much more pronounced structural relaxation that takes place in the structure with zigzag holes [14]. The GAL suppresses both electronic transmission and the phonon transmission ((B) and (C); respectively), however for phonons the reduction in transmission is much stronger which in turn leads to an enhancement in ZT, the thermoelectric figure of merit. In some of our simulations we have recorded ZT's approaching one-half – rather remarkable for graphene-based structures which usually have an exceedingly low ZT due to the high intrinsic heat conductivity.

References

[1] T.G. Pedersen, C. Flindt, J. Pedersen, N. A. Mortensen, A. P. Jauho, and K. Pedersen Phys. Rev. Lett. 100, **13** (2008) 136804.
[2] T.G. Pedersen, C. Flindt, J. Pedersen, N. A. Mortensen, A. P. Jauho, and K. Pedersen Phys. Rev. B 77, **24** (2008) 245431.

[3] T.G. Pedersen, A. P. Jauho, and K. Pedersen Phys. Rev. B 79, **11** (2009) 113406.

[4] J. A. Fürst, J. Pedersen, J. G. Pedersen, C. Flindt, N. A. Mortensen, M. Brandbyge, T. G. Pedersen, and A. P. Jauho, New J. Phys. 11 (2009) 095020.

[5] M. Vanevic, V. M. Stojanovic, and M. Kindermann, Phys. Rev. B 80, **4** (2009) 045410.

[6] V. M. Stojanovic, N. Vukmirovic, and C. Bruder, Phys. Rev. B 82, **16** (2010) 165410.

[7] M. Wimmer, A. R. Akmherov, and F. Guinea, Phys. Rev. B 82, **4** (2010) 045409.

[8] W. Liu, Z. F. Wang, Q. W. Shi, J. Yang, and F. Liu, Phys. Rev. B 80, **23** (2009) 233405.

[9] J. Eroms and D. Weiss, New J. Phys. 11 (2009) 095021

[10] J.W. Bai, X. Zhong, S. Jiang, Y. Huang, and X. Duan, Nat. Nanotechnol. 5, **3** (2010) 190

[11] M. Kim, N. Safron, E. Han, M. S. Arnold, and P. Gopalan, Nano Lett. 10, **4** (2010) 1125

[12] R. Petersen, T. G. Pedersen, and A. P. Jauho, to appear in ACS Nano (available in ASAP papers, December 16)

[13] E. Clar, *The aromatic sextet*, Wiley: New York (1972)

[14] T. Gunst, T. Markussen, M. Brandbyge, and A. P. Jauho, in preparation

Figures

(A) (B) (C)
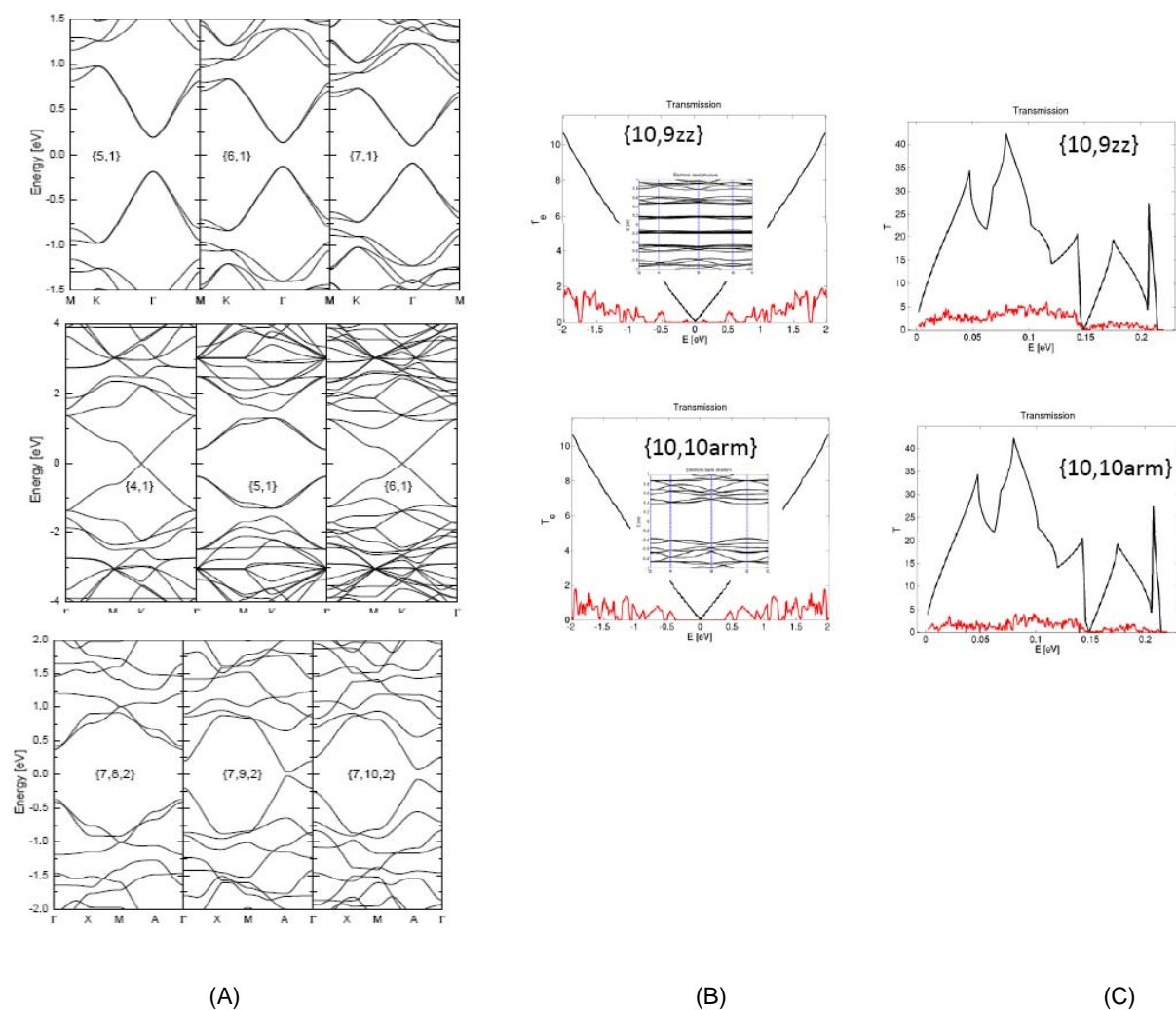
Figure caption. (A) Band structures for triangular (top), rotated triangular (middle), and rectangular (bottom) GALs. The insets define the details of the respective lattice structures [12]. (B) Electronic transmission for graphene samples with zigzag (top) and armchair (bottom) holes, red curve. The insets show the electronic bandstructures. (C) Phonon transmission for the geometries in (B). The black curves in (B) and (C) give the pristine electronic and phonon transmissions, respectively.

Angle-resolved photoemission spectroscopy study of epitaxial graphene on Cu(111)

Cheolho Jeon,[1] Han-nah Hwang,[2] Chong-Yun Park,[1,*] Chan-Cuk Hwang[2,†]

[1]Department of Physics and Center for Nanotubes and Nanostructured Composites, Suwon, Republic of Korea,
[2]Beamline Research Division, POSTECH, Pohang Accelerator Laboratory, Pohang, Republic of Korea
cypark@skku.edu, cchwang@postech.ac.kr

Interactions between a substrate and graphene have been a major interest in graphene research field, because it could alter the electronic properties of graphene, such as carrier concentration, band gap, and mobility. The interactions are induced by a bonding or stacking between them. Especially, the substrates used for graphene growth by chemical vapor deposition (CVD) have received huge attention to investigate the role of catalytic behavior. Ni substrate was firstly used for CVD graphene growth, but it showed difficulties in layer thickness control. Cu foil was suggested as a substrate for the growth of monolayer graphene with the self-limiting process, since it has lower carbon solubility than those of Ni and Fe.[1] Recently, scanning tunneling microscopy study revealed the multi-domain graphene growth on Cu(111) surface,[2] which is in contrast to the graphene growth on Ni(111). The various domain formations on Cu foil by CVD growth were also reported, in which the domain width can be varied by growth condition.[3] However, the band structure of multi-domain graphene on Cu substrate has not been yet reported despite its importance.

In this study, we investigated the band structure of epitaxial graphene on Cu(111) surface using angle-resolved photoemission spectroscopy (ARPES). The experiment was performed at the beamline 3A2 of the Pohang Light Source in Korea. Graphene was grown on Cu(111) surface in an ultra-high vacuum chamber connected to the ARPES chamber equipped with R4000 analyzer (VG-Scienta) by introducing C_2H_2 at 1250 K. The band structure of graphene was observed at the K point after C_2H_2 dosing of 10 L (1 L = 1×10^{-6} Torr for 1 sec.). At the same time, the Shockley surface state of Cu(111) at Γ was split into two states. The one appeared at the lower binding energy side exhibited the charge transfer from Cu surface to graphene, resulting in the band structure of graphene with n-type doping. As increasing the dose of C_2H_2, several linear bands of graphene were observed as expected from STM results.[2] Every graphene band showed a similar n-type doping character regardless their orientations, and the band images were not changed except their intensity until the Shockley state was emerged by one with p-type doping character, which implies the formation of monolayer graphene on Cu(111) surface. We would like to discuss more detail about the results on site.

References

[1] X. Li, W. Cai, J. An, S. Kim, J. Nah, D. Yang, R. Piner, A. Velamakanni, U. Jung, E. Tutuc, S. K. Banerjee, L. Colombo, R. S. Ruoff, Science, **324** (2009) 1312.
[2] Li Gao, J. R. Guest, and N. P. Guisinger, Nano Lett., **10** (2010) 3512.
[3] P. Y. Huang, C. S. Ruiz-Vargas, A. M. Van der Zande, W. s. Whitney, M. P. Levendorf, J. W. Kevek, S. Garg, J. S. Alden, C. J. Hustedt, Y. Zhu, J. Park, P. L. McEuen, D. A. Muller, Nature, **469** (2011) 389.

Figure
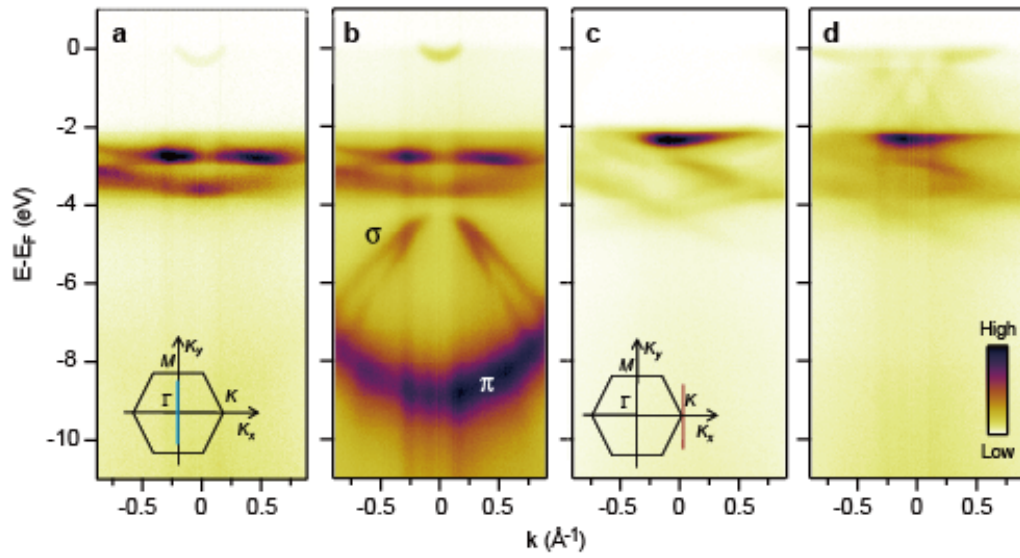
Fig. 1: Band structures of Cu(111) surface around the (a, b) Γ and (c, d) K points before and after graphene growth, respectively.

High Performance Transparent Conductive Films using Rheologically-Derived Reduced Graphene Oxide

Hee Jin Jeong, Seung Yol Jeong, Sung Hun Kim, Joong Tark Han, Sunhye Yang, and Geon-Woong Lee

Nano Carbon Materials Research Group, Korea Electrotechnology Research Institute, Changwon, 641-120, Republic of Korea
wavicle11@keri.re.kr

We produced large area graphene oxide (GO) sheets with fewer defects on the basal plane by application of shear stress in solution to obtain high quality reduced graphene oxide (RGO) sheets without the need for post annealing processes. This is described as rheologically-derived RGO which is shown in Figure 1a. The large area GO sheets were generated using a homogenizer in aqueous solution, which induced slippage of the GO in the in-plane direction during the exfoliation process, in contrast with the conventional sonication method. The effects of chemical reduction under mild conditions demonstrated that the formation of structural defects during the exfoliation process affected the RGO properties. In the Raman spectra, the I_D/I_G ratio of the homogenized-RGO (HRGO) increased more than that of the sonicated-RGO (SRGO) due to the large number of ordered sixfold rings on the basal plane. The enhanced sheet resistance of the HRGO thin film was found to be 2.2 kohms/sq at 80% transmittance as shown in Figure 1b. This result is comparable to the values reported by others in studies of the optoelectrical properties of RGO using hydrazine reduction.[1-5] The effective exfoliation method has great potential for application to high performance RGO-transparent conducting films.

References

[1] G. Eda, G. Fanchini, M. Chhowalla, Nat. Nanotechnol., **3** (2008) 270.
[2] X. Li, G. Zhang, X. Bai, X. Sun, X. Wang, E. Wang, H. Dai, Nat. Nanotechnol., **3** (2008) 538.
[3] C. Su, Y. Xu, W. Zhang, J. Zhao, X. Tang, C. Tsai, L. Li, Chem. Mater., **21** (2009) 5647.
[4] A. A. Green, M. C. Hersam, Nano Lett., **9** (2009) 4031.
[5] H. Yamaguchi, G. Eda, C. Mattevi, H. Kim, M. Chhowalla, ACS Nano, **4** (2010) 524.

Figures
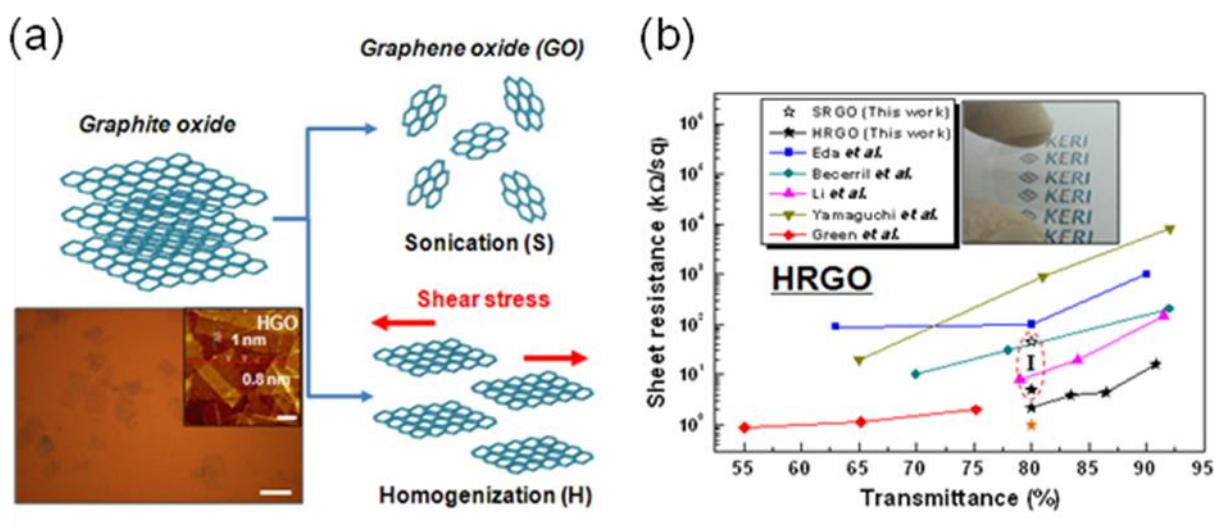
(a) Schematic diagram for the exfoliation mechanism of GO via sonication (S) or homogenization (H), and optical and AFM image of the homogenized GO samples. (b) Sheet resistance *vs.* transmittance plot of RGO-TCFs fabricated from previously reported results and our work.

Analytic drain-current model of Graphene Field-Effect Transistors targeting analog/radiofrequency applications

David Jiménez, Oana Moldovan

Departament d'Enginyeria Electrònica, Escola d'Enginyeria,
Universitat Autònoma de Barcelona, Spain

david.jimenez@uab.es

Graphene has emerged as a candidate material for future nanoelectronic devices. Aside the impressive mechanical properties, graphene exhibits very high mobility ($\sim 10^5$ cm^2/V-s) and saturation velocity ($\sim 10^8$ cm/s), together with a promising ability to scale to short gate lengths and high speeds by virtue of its thinness. The main problem is the absence of a gap, therefore limiting the usefulness of graphene in digital applications. Several approaches have appeared in the last years to open a gap. For instance, graphene nanoribbons providing quantum confinement, bilayer graphene, or strained graphene have been suggested. However, zero gap graphene could still be very useful in analog and radiofrequency (RF) applications where high ON/OFF current ratios are not required [1]. For instance, for small signal amplifiers, the transistor is operated in the ON-state and small RF signals that are to be amplified are superimposed onto the DC gate-source voltage. Instead, what is needed to push the limits of analog/RF performance is an operation region where high transconductance together with a small output conductance is accomplished. This situation is realized for state-of-the-art graphene field-effect transistors (GFETs). Specifically, for large-area GFETs, the output characteristic shows a weak saturation that could be exploited for analog/RF applications. Recently, cutoff frequencies in the range of hundreds GHz [2] have been demonstrated and operation in the THz range is envisioned.

At this stage of development of GFET technology, modeling is a key aspect for device design optimization, projection of performance, and exploration of circuit designs providing new functionalities. We have done this modeling effort in the framework of the drift-difussion theory. This theory has proved to be successful in explaining the electrical behavior of GFETS [3,4]. In this work we present a fully analytic physics-based electrical model of the useful for analog/RF research community. Explicit close-form expressions for the drain current have been derived and benchmarked with experimental results [5].

References

[1] F. Schwierz, Nature Nanotechnology, **5** (2010) 487.
[2] Y.-M. Lin et al., Science, **327** (2010) 662.
[3] I. Meric et al., Nature Nanotechnology, **3** (2008) 654.
[4] S. Thiele et al., Journal of Applied Physics, **107** (2010) 094505
[5] Kedzierski et al., IEEE Electron Device Lett., **30** 745 (2009).
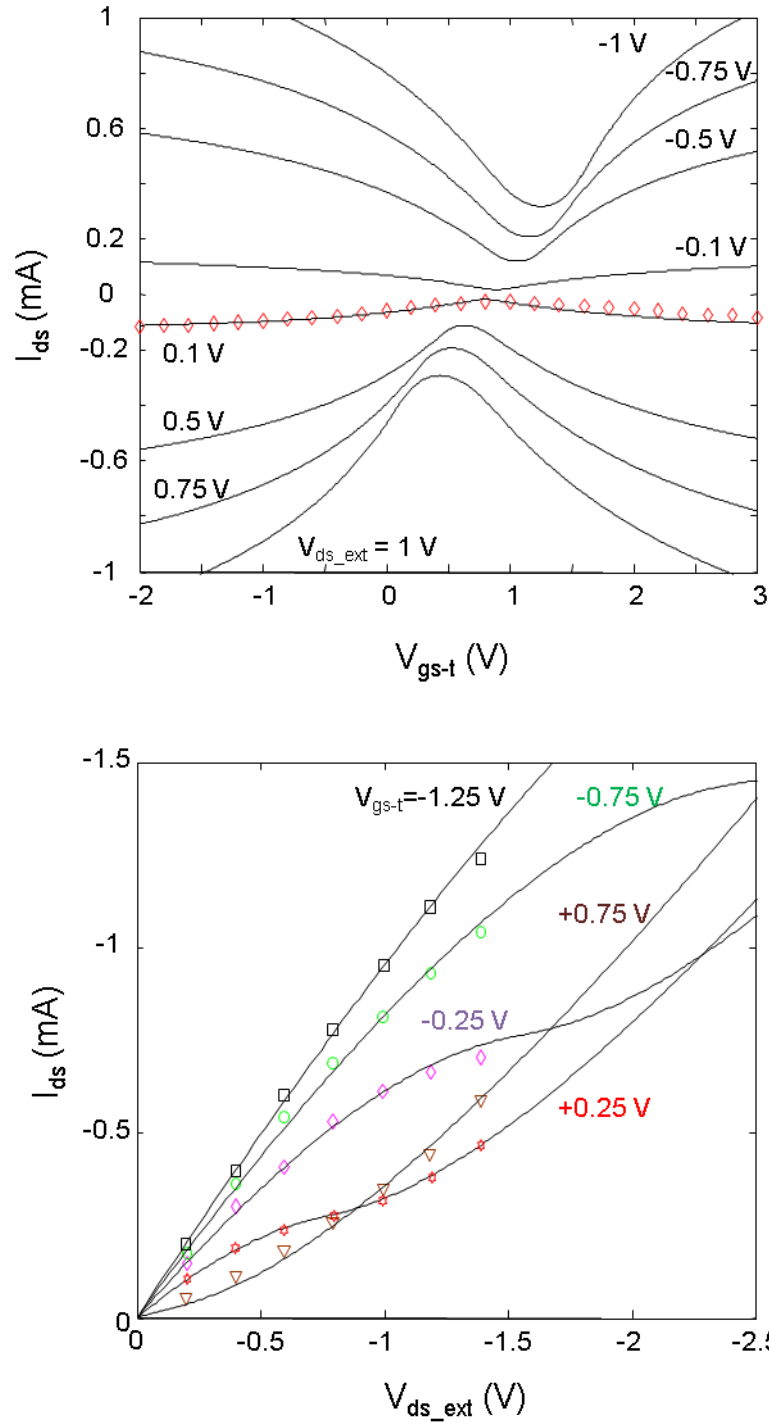
Figure 1. *Transfer and output characteristics of a prototype GFET* as computed with the analytical model benchmarked with experimental results reported by Kedzierski et al., IEEE Electron Device Lett. 30, 745 (2009). The device under test is a top-gate GFET with channel length of 10 μm, gate width of 5 μm, top dielectric is hafnium oxide with thickness of 40 nm and permittivity $\sim$ 16. The flat-band voltage was tuned to 0.85 V according to the location of Dirac point from the transfer characteristics. A low-field mobility of 7500 cm^2/V-s for both electrons and holes, source/drain resistances of 300 Ω, and phonon effective energy $\sim$ 100 meV was considered. These values are consistent with the extracted values from measurements. As input parameter a sheet carrier density =3·10^{11} cm^{-2} was used for the final fine tuning. Symbols: experimental results. Solid line: model results.

Substrate enhanced stability of hydrogen adsorption complexes on graphene on Ir(111)

Bjarke Jørgensen, *John Thrower, Saoud Baouche, Richard Balog, Louis Nilsson, Emil Enderup Friis, Arnd Baurichter, Thomas Zecho, Alan Luntz, Flemming Besenbacher, and Liv Hornekær*

Dept. Physics and Astronomy and Interdisciplinary Nanoscience Center (iNANO), Aarhus University, Denmark.

inabj@inano.dk

We present temperature programmed desorption (TPD) measurements investigating the interaction of hydrogen with graphene supported on an Ir(111) substrate. These experiments demonstrate how the substrate influences the reactivity of graphene towards atomic hydrogen, as well as the stability of the resulting hydrogenated graphene compounds. The presented data reveal a distinctively different behavior for hydrogenated graphene on an Ir(111) substrate as compared to hydrogenated graphite.

Figure 1 shows a TPD spectra for D_2 desorbing from graphene on an Ir(111) substrate for a series of relative D coverages with respect to that at saturation. A distinct asymmetric peak is evident in the spectra. Analysis of the spectra revealed that the barrier to D_2 desorption is significantly larger than what is found for the desorption of D_2 from graphite [1]. It has previously been suggested that hydrogen chemisorbed on graphene on an Ir(111) substrate form a graphane-like structure [2]. Such a graphane model can successfully explain the observed enhanced stability of the hydrogen adsorbates.

It was also found that the absolute coverage of D adsorbed on graphene on an Ir(111) substrate at saturation is independent of the kinetic energy of the impinging D atoms. This is in contrast to the behavior observed for HOPG, where the absolute coverage at saturation is reduced for lower D beam temperatures. Such a temperature dependence is directly related to the existence of adsorption barriers, which are a consequence of surface reconstruction during the C-H bond formation [3]. These adsorption barriers are most likely modified by the presence of the underlying Ir(111) substrate resulting in different kinetics for hydrogenation than those observed for HOPG. Hence, even though graphene on Ir(111) exhibits electronic properties that are essentially unchanged from those for free standing graphene, the chemical properties of graphene are observed to be severely modified by the underlying substrate.
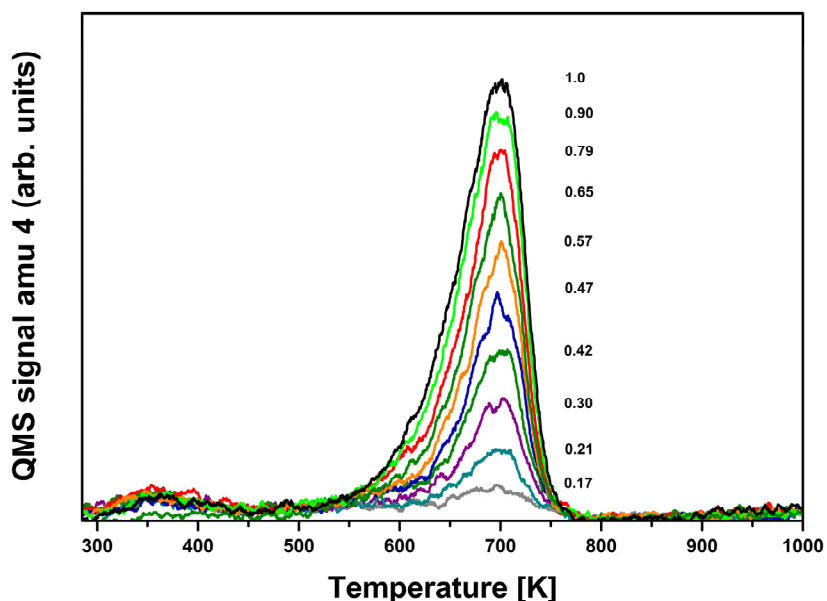
Figure 1 TPD spectra of D_2 desorbing from graphene on an Ir(111) substrate following exposure to atomic D. The employed temperature ramp was 1 K/s. The individual traces are labeled with coverage relative to that achieved at saturation.

References:

1.	Zecho, T., et al., *Adsorption of hydrogen and deuterium atoms on the (0001) graphite surface.* Journal of Chemical Physics, 2002. **117**(18): p. 8486-8492.
2.	Balog, R., et al., *Bandgap opening in graphene induced by patterned hydrogen adsorption.* Nature Materials, 2010. **9**(4): p. 315-319.
3.	Sha, X.W. and B. Jackson, *First-principles study of the structural and energetic properties of H atoms on a graphite (0001) surface.* Surface Science, 2002. **496**(3): p. 318-330.

Doping graphene with Nitrogen: an STM study

Frédéric Joucken, Jacques Dumont, Bing Zheng(*), Luc Henrard, Damien Cabosart and Robert Sporken

Research Center in Physics of Matter and Radiation (PMR), University of Namur (FUNDP), rue de Bruxelles 61, 5000 Namur, Belgium
(*) Present Address : PCPM & ETSF, Université Catholique de Louvain, Place Croix du Sud, 1 B-1348 Louvain-la-Neuve, Belgique

Contact: frederic.joucken@fundp.ac.be

Tuning the electronic properties of graphene is necessary in order to broaden its possible field of applications. In microelectronic devices, such as field transistors, the active material for the transport layer needs the presence of an energy gap by which the conducting behavior of electrons or holes as charge carriers can be controlled with the voltage [1].

In this context, theoretical studies ([2,3]) have shown that different doping configurations of graphene with nitrogen would shift the Fermi level away from the Dirac point and induce a valence-conduction bands asymmetry. STM images have been simulated for various kinds of doping (substitution, pyridine like bonding,...) [3].

According to literature [4-7], graphene can be obtained by annealing a 6H SiC (000-1) single crystal. In our work, we exposed SiC at 850 °C to a Si flux, followed by annealing at 950 °C to produce a 3x3 reconstruction. Finally, annealing at 1080°C resulted in the graphene formation. STM operating at room temperature showed Moiré patterns as reported in [5,6] and atomic resolution was achieved revealing the typical honeycomb structure (figure 1).

The sample was then exposed to a flux of atomic nitrogen produced by a remote plasma source. After nitrogen exposure, several defects were created on the originally defect-free graphene surface. As shown on figure 2, the overall shape of a single typical defect presents a localized triangular pattern of 1 nm size. Variations of the pattern with bias voltage have been observed (figure 2).

With the support of Density-Functional Theory, we tentatively attributed the observed pattern to pyridine-like doping (figure 3). Similarities and differences between experimental data and more theoretical simulations are to be discussed during the talk.

References:

[1] M. S. Fuhrer, C. N. Lau, and A. H. MacDonald, MRS Bulletin **35**, 289 (2010)
[2] A. Lherbier, X. Blase, Y.-M. Niquet, F. Triozon, S. Roche, Phys. Rev. Lett. **101**, 036808 (2008)
[3] B. Zheng, P. Hermet and L. Henrard. ACS Nano **7**, 4165 (2010)
[4] I. Forbeaux, J.-M. Themlin, and J.-M. Debever, Surf. Sci. **442**, 9 (1999)
[5] F. Varchon, P. Mallet, L. Magaud and J.-Y. Veuillen, Physical Review B **77**, 165415 (2008)
[6] F. Hiebel, P. Mallet, F. Varchon, L. Magaud, and J-Y. Veuillen, Physical Review B **78**, 153412 (2008)
[7] U. Starke and C. Riedl, J. Phys.: Condens. Matter **21** 134016 (2009)

Figures:
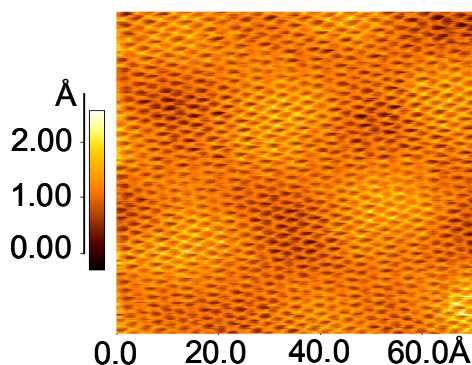
Figure 1: Graphene (V_s = -0.5V; I = 3nA)
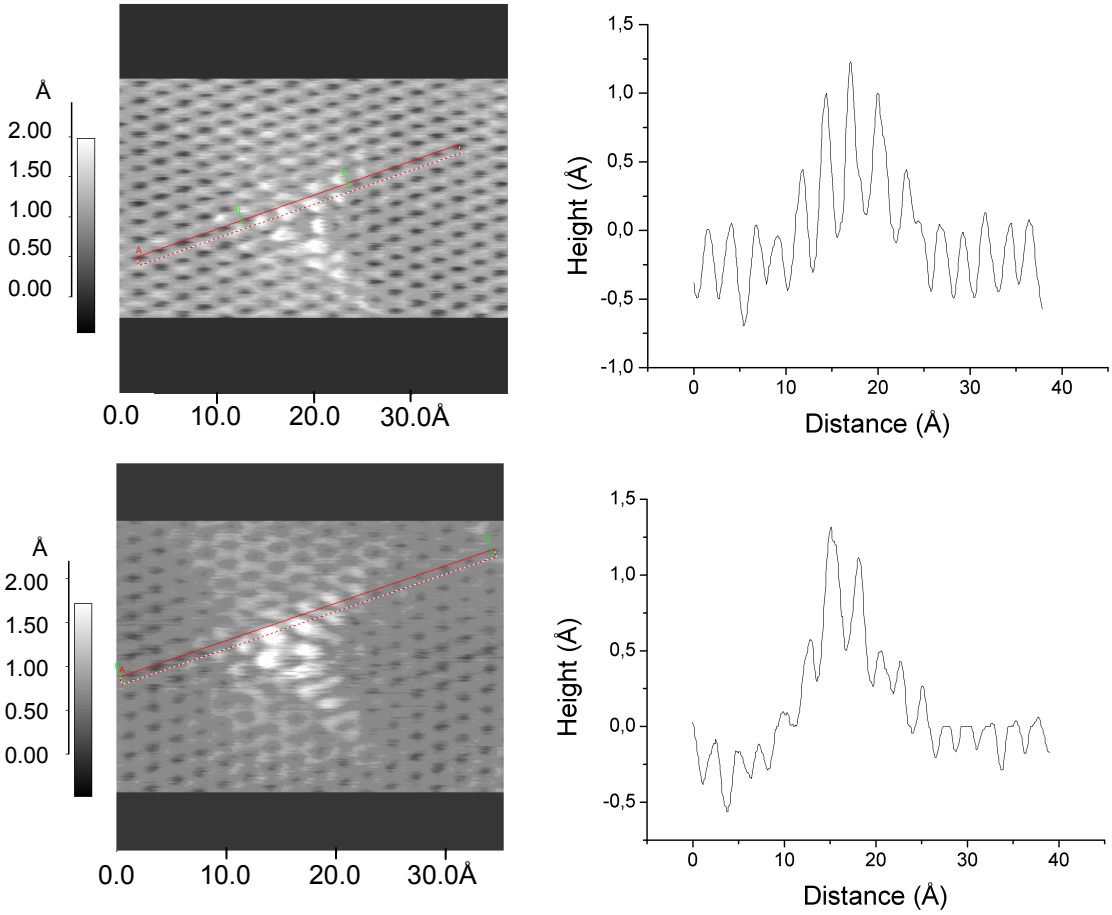
Figure 2: I=8nA. Above: V_s=+0.5V; below: V_s=-0.5V

(units: a_0)
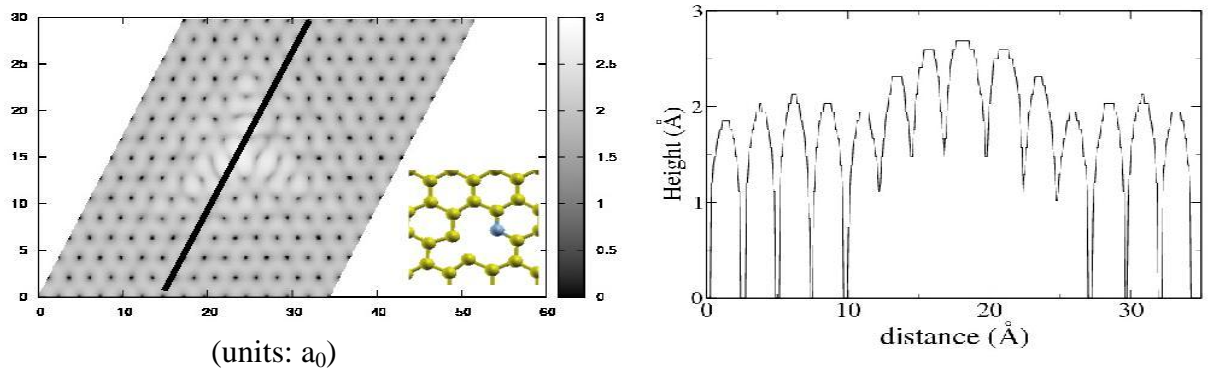
Figure 3: STM simulation of a pyridine-like N-doping (V_s = + 0.5 V)

Robust, High-Performance of Flexible, Transparent Conducting Films from Graphene and their Shape Memory Polymer Nanocomposites

Yong Chae Jung[1], Yoong Ahm Kim[1], Hiroyuki Muramatsu[2], Takuya Hayashi[1], Morinobu Endo[1,2]

[1]Faculty of Engineering, Shinshu University 4-17-1 Wakasato, Nagano-shi, 380-8553, Japan
[2]Institute of Carbon Science and Technology, Shinshu University 4-17-1 Wakasato, Nagano-shi, 380-8553, Japan
ycjung@endomoribu.shinshu-u.ac.jp

The graphene discovered in 2004 from Dr. Geim et al., it has been touted as a "next generation materials" because of its remarkable optical, electronic, and thermal properties, chemical and mechanical stability, and large surface area for applications in emerging field such as transistors, sensors, polymer nanocompoistes, energy devices.

In general, shape memory polymers are very usefully materials in bio and medical research area. Specially, polyurethane block copolymers are able to recover the original shape almost completely at appropriate conditions when they are deformed. These materials have the advantages of light weight, and excellent processability. For this reason, polyurethane block copolymer may play an important role in thin area. Consequently, the combination of shape memory polyurethane with graphenes allows to creating new polymeric materials with unique high performance properties.

In this study, we have used highly quality graphenes, prepared by the solvent exfoliation process from expended graphite (EG). To understand the effects of the exfoliation quality of graphenes and dispersion property of graphenes within the PU, graphene solution in NMP were prepared under strong sonication and centrifuge. Finally, graphene/PU composite films were evaluated in terms of their optical, mechanical and thermal properties as well as electrical conductivity.

References

[1] X. K. Lu, M. F. Yu, H. Huang, R. S. Ruoff, Nanotechnology **10** (1999) 269
[2] K. S. Novoselov, A. K. Geim, S. V. Morozov, D. Jiang, Y. Zhang, S. V. Dubonos, I. V. Grigorieva, A. A. Firsov, Science **306** (2004) 666.
[3] J. C. Meyer, A. K. Geim, M. I. Katsnelson, K.S. Novoselov, T. J. Booth, S. Roth, Nature **446** (2007) 60.
[4] K. I. Bolotin, K.J. Sikes, Z. Jiang, M. Klima, G. Fudenberg, J. Hone, P. Kim, H. L. Stormer, Solid State Commun. **146** (2008) 351.
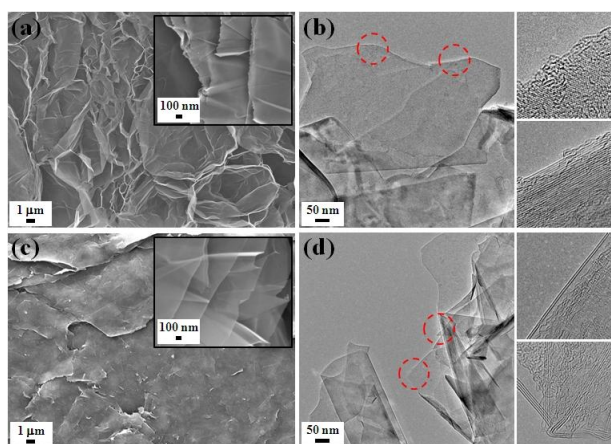
Figure 1. SEM and TEM images of pristine expanded graphite (a,b), and exfoliated graphene (c,d)

Acknowledgment

Electrochemical doping of CVD Graphene

Martin Kalbac[a,c], Alfonso Reina-Cecco, [b] Hootan Farhat, [b] Jing Kong,[c] Ladislav Kavan,[a] and Mildred S. Dresselhaus [c,d]

[a] *J. Heyrovský Institute of Physical Chemistry, Academy of Sciences of the Czech Republic, v.v.i., Dolejškova 3, CZ-18223 Prague 8, Czech Republic. Tel: 420 2 6605 3804; Fax: 420 2 8658 2307; E-mail: kalbac@jh-inst.cas.cz*
[b] *Department of Materials Science and Engineering, MIT, Cambridge, Massachusetts 02139, USA*
[c] *Department of Electrical Engineering and Computer Science, MIT, Cambridge, Massachusetts 02139, USA*
[d] *Department of Physics, MIT, Cambridge, Massachusetts 02139, USA*

Recent advances in chemical vapor deposition (CVD) synthesis have now allowed the preparation of large and uniform monolayer graphene flakes. The CVD prepared graphene thus significantly simplifies the materials processing and more detailed studies with such samples can be readily performed. The successful application of graphene requires a detailed understanding of its electronic properties, including both its neutral and doped states. The doping of graphene leads to a shift of the Fermi level and for this reason doping provides a simple way to control the transport and optical properties. In our study the electrochemical charging has been applied to study the influence of doping on the intensity of the various Raman features of chemical vapor deposition –grown graphene. Three different laser excitation energies have been used to probe the influence of the excitation energy on the behavior of both the G and G' modes regarding their dependence on doping. The intensities of both the G and G' modes exhibit a significant but different dependence on doping. While the intensity of the G' band monotonically decreases with increasing magnitude of the electrode potential (positive or negative), for the G band a more complex behavior has been found. The striking feature is an increase of the Raman intensity of the G mode at a high value of the positive electrode potential. Furthermore, the observed increase of the Raman intensity of the G mode is found to be a function of laser excitation energy.

Ballistic transport in step edge aligned cross junctions on epitaxial graphene

Epaminondas Karaissaridis[1], Sonja Weingart[1], Claudia Bock[1], Ulrich Kunze[1], Florian Speck[2], Thomas Seyller[2]

[1]Werkstoffe und Nanoelektronik, Ruhr-Universität Bochum, Universitätsstraße 150, 44801 Bochum, Germany

[2]Lehrstuhl für Technische Physik, Friedrich-Alexander-Universität Erlangen-Nürnberg, Erwin-Rommel-Strasse 1, 91058 Erlangen, Germany

epaminondas.karaissaridis@ruhr-uni-bochum.de

We studied ballistic transport in nanoscale orthogonal cross junctions fabricated from epitaxial monolayer graphene grown on the Si-face of SiC. Measurements were performed on conventionally grown [1] and hydrogen intercalated graphene films [2, 3]. The devices were aligned parallel to the step edges of the SiC substrate. Using ac and dc measuring techniques, we obtained a negative bend resistance for low temperatures, which indicates electronic transport in the ballistic regime. As temperature is increased, a transition to the diffusive regime is observed.

Sample A is prepared by thermal decomposition of SiC(0001) under Ar atmosphere [1]. Sample B was additionally hydrogen intercalated after film growth, resulting in a quasi-freestanding monolayer graphene film [2, 3]. Hall bar structures (600 nm wide and 3 µm long) for film characterization and cross junctions with four identical leads of 50 nm width and 400 nm length are prepared using a mix-and-match process [4].

First of all samples A and B are characterized by Hall measurements in a temperature range of $1.5\,K \leq T \leq 300\,K$. At $T = 4.2\,K$ for sample A a mobility of $\mu_A = 4180\ cm^2V^{-1}s^{-1}$ and an electron density of $n_{2D,A} = 2.6 \cdot 10^{12}\ cm^{-2}$ are determined, which is equivalent to a mean free path of $l_e = 78\ nm$. As temperature is increased to $T = 300\,K$ the mobility decreases nearly linearly to $\mu_A = 1470\ cm^2V^{-1}s^{-1}$. For sample B we obtain a mobility and hole density of about $\mu_B = 1920\ cm^2V^{-1}s^{-1}$ and $p_{2D,B} = 5.1 \cdot 10^{12}\ cm^{-2}$, respectively. These values are constant in the whole temperature range and correspond to a mean free path of $l_e = 50\ nm$.

For sample A the cross junctions are studied in bend resistance geometry by dc transfer measurements [Fig. 1, (b)]. A bend resistance of $R_{12,43} = -175$ indicates ballistic transport [Fig. 1 (a)]. The negative slope is nearly the same for all four measurement configurations due to the geometrical symmetry of an orthogonal cross junction. Corresponding measurements for unaligned devices on another sample demonstrated a strong dependence of the bend resistance on the measurement configuration [5], which indicates that scattering at step edges destroys ballistic transport. Since the mean free path of sample B is close to the device dimensions, the bend resistance of the device is close to zero in the absence of magnetic field. Therefore we used lock-in technique to study the differential bend resistance $r_{12,43}$ as a function of a perpendicular magnetic field B [Fig. 2 (b)]. Figure 2 (a) shows $r_{12,43}$ for sample B as a function of B at $T = 4.2\,K$. The magnetic field dependent negative peaks indicate ballistic transport. The maximum value $r_{12,43} = -147$ at $B = 200\ mT$ is comparable to the results of sample A and former ballistic transport measurements [5]. As temperature is increased to $T = 50\,K$ the signatures of ballistic transport disappear which indicates a transition from the ballistic into the diffusive transport regime. These results point out that in contrast to 2D measurements, which yield a mean free path l_e independent of T, and surface spectroscopy measurements [3], which promise epitaxial graphene-based ballistic devices even at room temperature, additional scattering in 1D systems plays an important role and must be studied in detail.

Low-frequency noise in graphene

A. A. Kaverzin, A. S. Mayorov, A. K. Savchenko, A. V. Shytov and D. W. Horsell

School of Physics, University of Exeter, Stocker Road, Exeter, EX4 4QL, UK

ak328@exeter.ac.uk

The most common source of low-frequency *1/f* noise in transistor structures is the tunneling of carriers between a conductive channel and surrounding impurities [1]. The scattering of carriers is highly sensitive to the distribution of these impurities. As a result, *1/f* noise can be used as a tool to investigate the mechanisms of scattering.

Carrier scattering in graphene is unusual and not fully understood. We have studied *1/f* noise in monolayer graphene structures on Si/SiO_2 substrates in the frequency range from 10 to 400Hz at room temperature. In conventional Si MOSFET structures the normalised noise power S_R/R^2 diverges at the conductance threshold. In contrast, *1/f* noise in graphene is seen to exhibit a pronounced dip at the Dirac point where a maximum in resistance occurs (Figure, a) [2].

The *1/f* noise in graphene has been observed to change in the presence of water. We show that water acts as an acceptor of electrons. The normalised noise power increases after doping, indicating that water molecules are a significant source of scattering (Figure, b). The mechanism of scattering by water can be understood from the change in the shape of the noise dependence on gate voltage.

We discuss possible reasons for the suppression of *1/f* noise at the Dirac point in monolayer graphene, and the origin of *1/f* noise in the presence of water molecules.

References

[1] S. Kogan, Electronic Noise and Fluctuations in Solids (Cambridge University Press, 1996)

[2] Y.-M. Lin and P. Avouris, Nano Letters **8**, (2008) 2119.

Figures
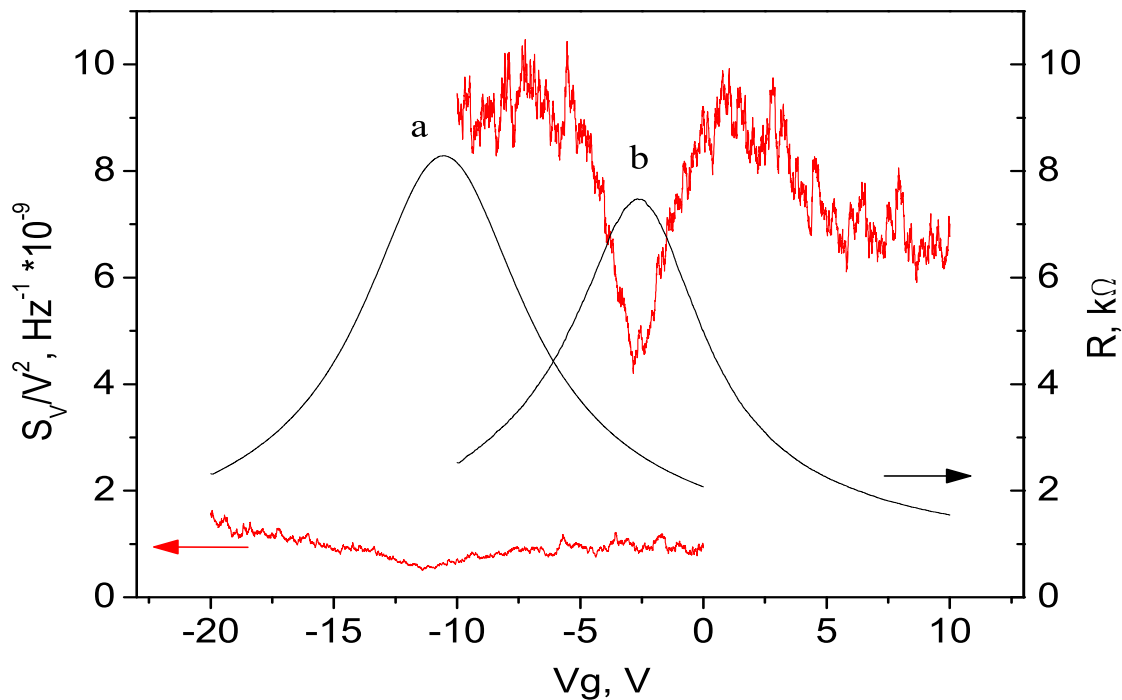
Figure. Peak in the resistance as a function of V_g accompanied by a dip in the noise power: a) before doping and b) after doping with H_2O.

Adhesion and frictional characteristics of CVD-grown graphene

Kwang-Seop Kim[1], Hee-Jung Lee[1], Changgu Lee[2], Seoung-Ki Lee[3], Houk Jang[3], Jong-Hyun Ahn[3], Jae-Hyun Kim[1], Hak-Joo Lee[1]

[1] Department of Nano Mechanics, Nano Convergence and Manufacturing Systems Research Division, Korea Institute of Machinery & Materials, 104 Sinseongno, Yuseong, Daejeon, 305-343, Republic of Korea

[2] School of Mechanical Engineering, Sungkyunkwan University, 300 Cheoncheon, Jangan, Suwon, Gyeonggi, 440-746, Republic of Korea

[3] School of Advanced Materials Science & Engineering, Sungkyunkwan University, 300 Cheoncheon, Jangan, Suwon, Gyeonggi, 440-746, Republic of Korea

kskim08@kimm.re.kr

Surface forces such as adhesion and friction forces are crucial in the fabrication and operation of microelectromechanical systems (MEMS) and nanoelectromechanical systems (NEMS) as well as in the nanofabrication processes such as nanoimprint lithography and contact printing process [1]. Various lubricant materials, patterns, and surface treatment processes have been developed for control of the interfacial forces and lubrication between contacting surfaces. We think that graphene can be one of good candidates for lubrication in the small scale because graphene is very thin as a few nanometers and is expected to have good properties of graphite for lubrication. Large-area graphene grown by CVD process can be transferred easily onto various substrates and the transferred graphene would be used as a solid lubricant for contacting surfaces. Recently, it was reported that the surface properties of graphene can be altered [2], and graphene sheets more than five layers show friction forces as small as for bulk graphite [3]. Graphene plates were added to oil in order to increase the lubrication performance of oil [4].

In this study, we characterized the adhesion and frictional properties of CVD-grown graphene to investigate the feasibility of graphene as a thin solid lubricant. CVD-grown graphene has a great merit as a surface coating because of its excellent scalability and transferability. The graphene was synthesized on Cu foil and Ni film by chemical vapor deposition (CVD) process and transferred on SiO2/Si substrate by a wet transfer method [5,6]. Adhesion and friction tests were performed by a home-built microtribometer to investigate the adhesion and frictional characteristics of the graphene in microscale.

Figure 1 shows optical images of Cu-grown graphene and Ni-grown graphene on SiO_2/Si substrate. The optical image of each graphene film shows clear contrast between areas with different numbers of graphene layers. To investigate the adhesion properties of the graphene, the adhesion test was performed using microtribometer. Figure 2 shows the pull-off force measured by microtribometer. In microscale contacts, the graphene reduce the pull-off force significantly. Figure 3 shows the frictional characteristics of graphene films. The results show that the graphene effectively reduced friction force. The Ni-grown graphene on SiO_2 shows relatively durable and low friction coefficient compared to the Cu-grown graphene on SiO_2, In summary, the CVD-grown graphene is so effective to reduce the adhesion and friction forces, and have strong potential to be used as a thin solid lubricant.

References

[1] B. Bhushan., Nanotribology and nanomechanics: an introduction, Springer Verlag (2005).
[2] Y. J. Shin, Y. Wang, H. Huang, G. Kalon, A. T. S. Wee, Z. Shen, C. S. Bhatia, H. Yang, Langmuir, **26** (2010), 3798.
[3] C. Lee, Q. Li, W. Kalb, X.-Z. Liu, H. Berger, R. W. Carpick, J. Hone, Science, **328** (2010), 76.
[4] J. Lin, L. Wang, G. Chen, Tribology Letters, **41** (2011), 209.

[5] K. S. Kim, Y. Zhao, H. Jang, S. Y. Lee, J. M. Kim, K. S. Kim, J. H. Ahn, P. Kim, J. Y. Choi, B. H. Hong, Nature, **457** (2009), 706.
[6] S. Bae, H. Kim, Y. Lee, X. Xu, J - S. Park, Y. Zheng, J. Balakrishnan, T. Lei, H. R. Kim, Y. I. Song, Y.-J. Kim, K. S. Kim, B. Özyilmaz, J.-H. Ahn, B. H. Hong, S. Iijima, Nat. Nanotechnol., **5** (2010), 574.

Figures

(a)   (b)
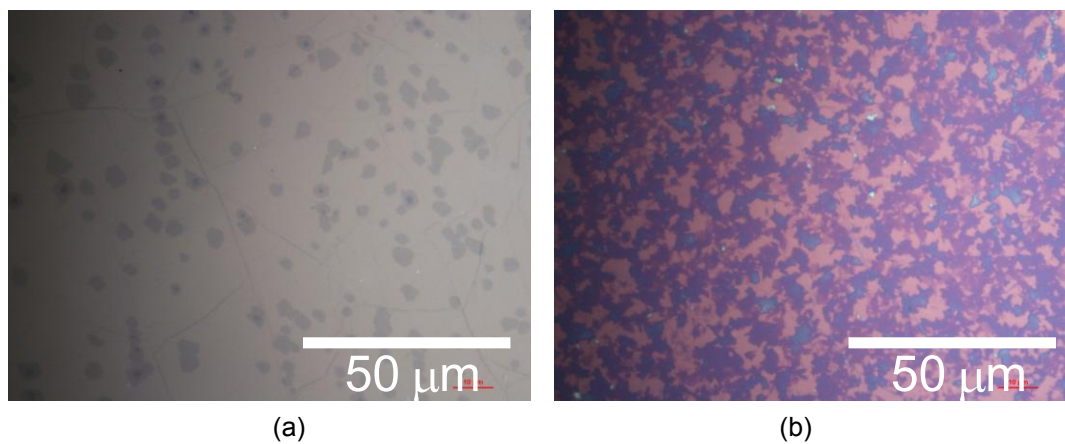
Figure 1. Optical micrograph of the graphene films transferred on SiO2/Si substrate.
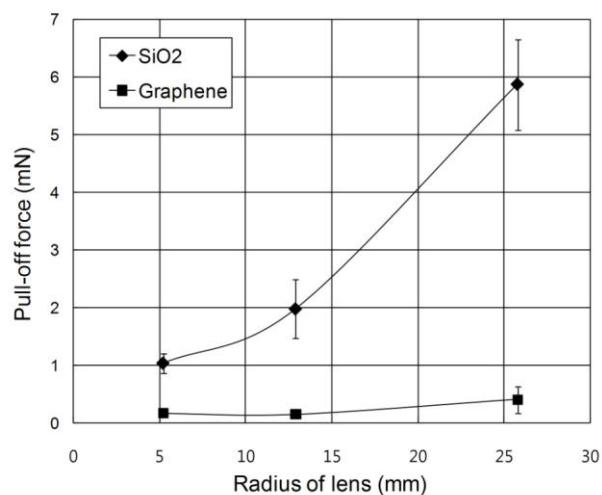
Figure 2. Pull-off force on the graphene samples measured by microtribometer.
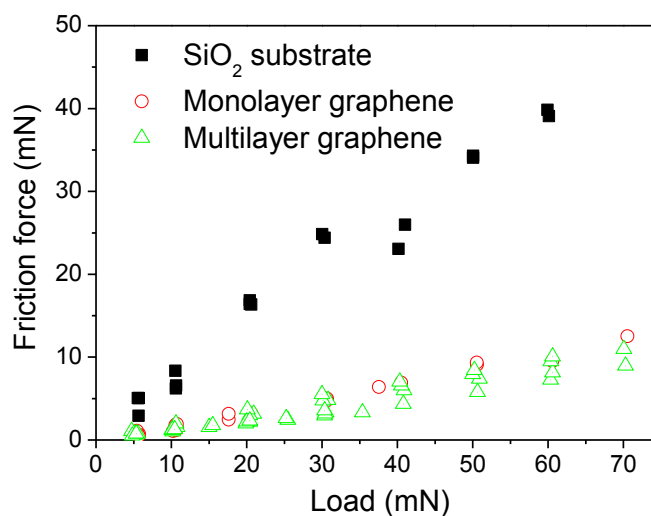
Figure 3. Friction force as a function of load for graphene films.

216

Orbital diamagnetism and broken symmetries in strained induced graphene quantum dot

Kang-Hun Ahn[1,2] and Kyung-Joong Kim[1]

[1]Department of Physics, Chungnam National University, Daejeon 305-764, Republic of Korea
[2]Department of Physics, University of Bath, Bath BA2 7AY, United Kingdom
ahnkh@cnu.ac.kr

Recently, the successful preparation of grapheme [1,2]- has provided the opportunity of theoretical and experimental research of one-atom layer nanoelectronics. Naturally, quantum dot, which confines quasi-particles in zero dimensional states, is an important building block for nanoelectronic application. In graphene where the quasi-particles are described by massless Dirac Fermions, confinement is nontrivial issue since the quasi-particles can penetrate large and wide electrostatic barrier through Klein tunneling[3]. To overcome the obstacle of the confinement, it has been suggested to confine quasiparticles via electrostatic potential in graphene stripes[4,5,6], or via magnetic barrier[7]. In principles, graphene dots can be realized by a spatially inhomogeneous magnetic field[8,9]. The required magnetic field strength, however, is too big for nanoelectronics application.

Here, we will show that graphene quantum dot can be formed via experimentally accessible size of strain due to its unique topology and strength of the pseudo-magnetic field formed in graphene. More

interestingly, the orbital magnetic response of the strained graphene will be very sensitive to the applied strain, which might be useful for sensor application. The pseudo magnetic field appears when lattice defects, the intrinsic and extrinsic curvature of the graphene sheets and the variation of hopping energies by elastic strains enter into the Dirac equation [10,11,12,13]. It will be demonstrated here that the strained graphene breaks its mirror reflection symmetry (MRS) and time reversal symmetry (TRS) by application of `real' magnetic field, which originated from the particular symmetry of the pseudo-magnetic field. It will be shown that the interplay between the real and pseudo magnetic field manifests by the orbital diamagnetism of the localized state in graphene quantum dot.

References

[1] K.S. Novoselov et.al., Science **306**, 666 (2004);Nature(London) **438**, 197 (2005).
[2] Y. Zhang, Y.W. Tan, H. Stormer, and P. Kim, Nature(London) **438**, 201 (2005).
[3] M. I. Katsnelson, K. S. Novoselov and A. K. Geim, Nature physics **2**, 620 (2006)
[4] P. G. Silvestrov and K. B. Efetov, Phys. Rev.Lett**. 98**, 016802 (2007).
[5] A. Matulis and F. M. Peeters, Phys. Rev. B, **77**, 115423 (2008).
[6] P. Recher et. al., Phys. Rev. B **79**, 085407 (2009).
[7] A. De Martino, L. Dell'Anna, and R. Egger, Phys. Rev. Lett. **98**, 066802 (2007).
[8] G.Giavaras, P. A. Maksym and M. Roy, J. Phys. Condes. Matter **21** 102201 (2009)
[9] D. Wang, G. Jin, Phys Lett. A, **373**, 4082, (2009).
[10] Vitor M. Pereira et. al., Phys. Rev. Lett., **96**, 036801 (2006)
[11] Alberto Cortijo, M.A.H. Vozmediano, Nucl. Phys. B **763**, 293 (2007)
[12] Eun-Ah Kim and A. H. Castro Neto, Europhys. Lett., **84**, 57007, (2008)
[13] N. M. R. Peres, F. Guinea, and A. H. Castro Neto, Phys. Rev. B, **73**, 125411, (2006).

Non-linear behavior of three terminal graphene junctions at room temperature

Wonjae Kim[1], Pirjo Pasanen[2], Juha Riikonen[1], Markku Rouvala[2], and Harri Lipsanen[1]

[1]Aalto University, Micronova, P.O. Box 13500, FI-00076 Aalto, Espoo, Finland
[2]Nokia Research Center, P.O. Box 407, FI-00045 Nokia, Helsinki, Finland

wonjae.kim@tkk.fi

Graphene is an attractive material for device applications due to its high carrier mobility in two dimensional charge carrier transport [1]. The transport behavior of two dimensional electron gas has been studied using three terminal ballistic junctions based on III-V semiconductors [2-8]. Recent study has also demonstrated non-linear electrical properties at low temperature on graphene using three terminal junctions fabricated by etching three trenches on a graphene flake [9]. Here we have further investigated electrical properties of the graphene device with three terminal T-branch structure at room temperature and shown that the rectified effect is around 10% at room temperature.

T-branch devices were patterned on exfoliated single layer graphene prepared on a 300-nm-thick silicon dioxide using O_2 plasma etching (Fig. 1a). The width and length of the channel from the left to right is 200 nm and 600 nm, respectively. The center branch is around 100 nm wide and 300 nm long. The metal contact is formed with Ti/Au (5 nm/40 nm) by e-beam evaporation.

In the measurements anti-symmetric voltage sources, so-called push-pull configuration ($V_L=-V_R$), are applied to the left and right terminals simultaneously and the output voltage is measured at the center branch with various the backgate voltages. The substrate of highly doped silicon is used as a global back gate electrode. All measurements were carried out at room temperature.

As shown in Fig. 2(b), when the left and right terminals are biased by push-pull manner with a backgate voltage, the output voltage at the center branch is dominantly negative or positive regardless of the sign of input voltage. Moreover, the output voltage becomes almost zero when the backgate voltage reaches the carrier neutrality point as expected. The Dirac point is found around 20 V of the backgate voltage (Fig. 1c). Also, the curvature of rectification becomes stronger when the Fermi level is increased by the backgate voltage. This implies that the curvature of rectification is dependent on the carrier density. Furthermore, the sign of the rectified curve is altered by changing the carrier (hole or electron) type. Positive rectification occurs at electron transport region and negative rectification at the hole transport region.

We assume that the inhomogeneous charge carrier distribution can result in non-linear rectification of the electric potential along the channel [11-12]. The carriers can be also affected by the impurities and space charge on the graphene surface. It is important to understand this type of effect since they can have a large impact on how circuits made of graphene will behave.

References

[1] K.S. Novoselov *et al*., Science, **306** (2004) 666.
[2] Katharina Hieke *et a*l., Physical Review B, **62** (2000) 16727.
[3] H. Q. Xu, Applied Physics Letters, **78** (2001) 2064.
[4] I. Shorubalko *et al*., Applied Physics Letters, **79** (2001) 1384.
[5] J. Mateos *et al*., Nanotechnology, **14** (2003) 117.
[6] Javier Mateos *et al*., IEEE Electronic Device Letters, **25** (2004) 235.
[7] D. Wallin *et al*., Applied Physics Letters, **89** (2006) 092124.
[8] M. Koyama *et al*., Physica Status Solidi (c) 5, **1** (2008) 107.
[9] A. Jacobsen *et al*., Applied Physics Letters, **97** (2010) 032110.
[10] Fantao Meng *et al*., Applied Physics Letters, **97** (2010) 242106.
[11] V. Ryzhii *et al*., Journal of Applied Physics, **103** (2008) 094510.
[12] Brett W. Scott *et al*., [cond-mat.mes-hall] arXiv:1010.4037v1, (2010)

Figures
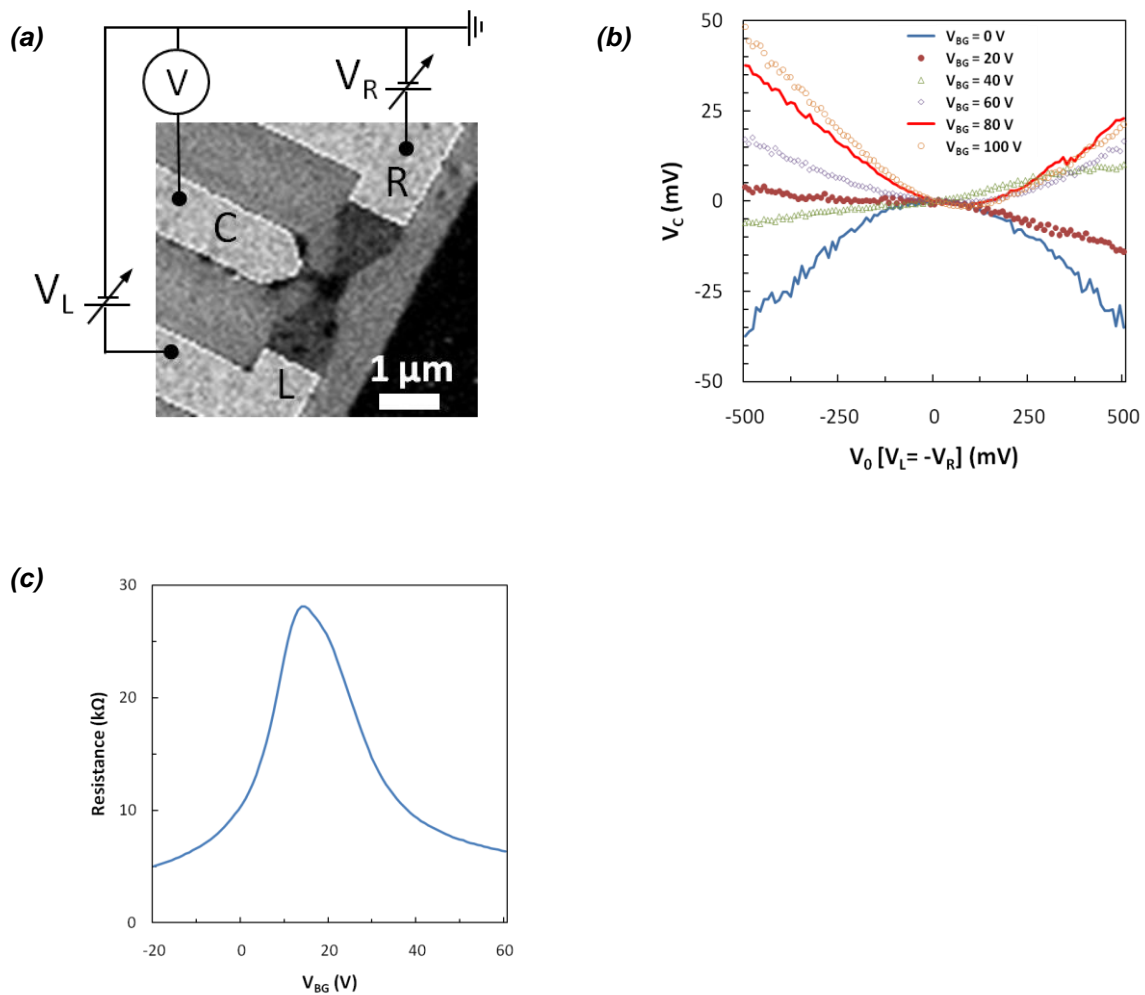
Figure. 1. (a) SEM image of T-branch structure and schematic of measurement configuration. (b) Measured output voltages at the center terminal **C** as a function of anti-symmetric bias voltage **V_0** (push-pull, V_L = -V_R) with various backgate voltages at room temperature. (c) Resistance of the channel between the left and right terminals as a function of the backgate voltage when the left terminal is biased and others are grounded.

Photocurrent of arrayed CdSe nanoparticles on Graphene by mesoporous silica templates

Yong-Tae Kim, Young-Seon Ko, Byung Hee Hong*, and Young-Uk Kwon*

[*] Prof. B. H. Hong, Prof. Y. -U. Kwon
Department of Chemistry, BK-21 School of Chemical Materials Science
SKKU Advanced Institute of Nanotechnology, Sungkyunkwon University, Swon, Korea
Y.-S. Ko, Y.-T. Kim
Department of Chemistry, BK-21 School of Chemical Materials Science,
Sungkyunkwon University, Swon, Korea
tanatos@skku.edu

Semiconductor quantum dots (QDs) of group II–VI compounds have been one of the most prominent research topic in the past two decades. QDs show great promises for uses in various applications, such as photovoltaic devices, solar cells and organic/inorganic light emitting devices because II–VI QDs have relatively small band gaps and thus are capable of harvesting photons in the visible and infrared regions. In photon harvesting devices, one of the important aspects to realize is fast electron transfer to the substrates such as indium tin oxide (ITO), fluorine-doped SnO_2 transparent conducting oxide (FTO), and carbon support materials. However, almost all of the researches show problems of inefficient electron transfer. One of the possible reasons for this problem arises from the interface between QDs and the substrate. In this regard the interface between QDs and substrate is a very important factor in improving the solar cells efficiency [1-3].

Recently, hybrid materials based of semiconductor QDs and graphene have motivated active optoelectronic devices studies. Graphene has several unique electronic properties such as high carrier mobility, high transparency, and enhance charge transfer. Therefore, this line of researches may lead to multifunctional materials or even materials with completely new properties. However, at present, the study of QDs/graphene hybrid materials is very limited. Xiumei Geng et al. reported that the flexible and transparent optoelectronic films fabricated from chemically converted graphene (CCG) and QD composites showed improved photosensity with the loading of QDs increasing. However, due to the indirect contact between CCG and CdSe QDs capped with Pyridine, the transfer efficiency of the photoinduced carriers is still limited. Probably, it is because of the difficulty in forming junctions between QDs and graphene [4-6].

In our previous work [7], we synthesized CdSe QDs arrays on the graphene basal plane by using electrochemical synthesis method and a mesoporous silica thin film template. This approach produced 8 nm–sized CdSe QDs ordered into a hexagonal array on graphene. The electron diffraction (ED) pattern taken from the top of the graphene plane shows that the (001) planes of the hexagonal CdSe QDs are missing. This suggests that the CdSe QDs are grown epitaxially to the graphene layer, which, in turn, indicate that the interface between the CdSe QDs and the graphene surface has some chemical interaction, desirable for fast electron transfer. In order to prove this possibility and also to develop photon harvesting devices based on our CdSe QDs/graphene hybrid materials, we investigated its photocurrent properties.

References

[1] C. B. Murray, D. J. Norris, and M. G. Bawendi, *J. Am. Chem. Soc.*, **115** (1993), 8706.
[2] A. Kongkanand, K. Tvrdy, K. Takechi, M. K. Kuno, and P. V. Kamat, *J. Am. Chem. Soc.*, **130** (2008), 4007.
[3] Y. Lin, K. Zhang, W. Chen, Y. Liu, Z. Geng, J. Zeng, N. Pan, L. Yan, X. Wang, and J. G. Hou, *ACS Nano* **4** (2010), 3033.
[4] K. S. Kim, Y. Zhao, H. Jang, S. Y. Lee, J. M. Kim, K. S. Kim, J.-H. Ahn, P. Kim, J.-Y. Choi, B. H. Hong, *Nature* **457** (2009), 706.
[5] X. Geng, L. Niu, Z. Xing, R. Song, G. Liu, M. Sun, G. Cheng, H. Zhong, Z. Liu, Z. Zhang, L. Sun, H. Xu, L. Lu, and L. Liu, *Adv. Mater.* **22** (2010), 638.
[6] Z. Chen, S. Berciaud, C. Nuckolls, T. F. Heinz, and L. E. Brus, *ACS Nano* **4** (2010), 2964.
[7] Y. T. Kim*, J. H. Han*, B. H. Hong*, and Y. U. Kwon, *Adv. Mater.* **22** (2010), 515.

Figures
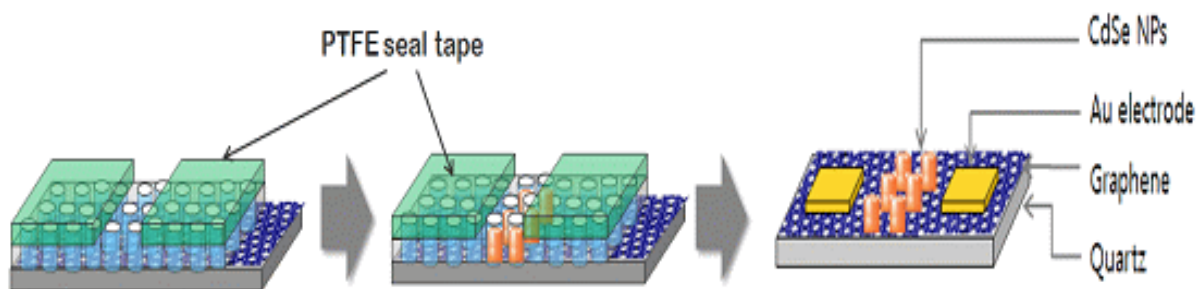
Figure 1. Scheme of the photo-device by CdSe QDs arrays on graphene sheet.
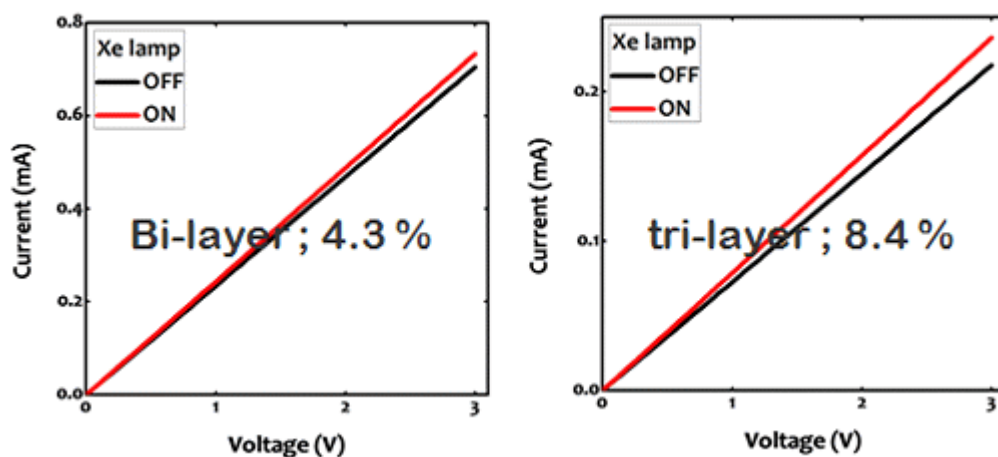
Figure 2. Current-voltage characteristics of the CdSe QDs (240s)/graphene/quartz with and without the irradiation under a 100 mW/cm^2 light illumination condition. The amount of electrodeposited CdSe QDs on graphene is the same each other, but the number of layers of grephene is controlled as follows: bi-layer and tri-layer graphene.

Quantum Nanoelectromechanics of Graphene Membranes

Aurora Voje, Andreas Isacsson and Jari Kinaret

Department of Applied Physics, Chalmers University of Technology, Gothenburg, Sweden
aurora@chalmers.se

Suspended graphene films can be used as mechanical resonators with applications in, e.g., radio technology and mass sensing. In this theoretical study we consider nanomechanical graphene resonators operating in the quantum limit where the mechanical motion exhibits quantum effects. Compared to one-dimensional beam resonators, using graphene literally adds another dimension to quantum nanomechanical systems. For instance, symmetric graphene structures exhibit degeneracies in their vibration spectra and nonlinearities become important already at very small amplitudes. This naturally limits excitation amplitudes and facilitate mode coupling. Here we propose to use asymmetrically applied gate voltages to achieve a controlled breaking of the degeneracies as well as tuning of the nonlinearities. This opens many possibilities for studying mechanical effects in the quantum regime.

Graphene-Metal Interactions
The case of mono- bi- and tri- graphene layers deposited on gold substrate studied by Scanning Tunneling Spectroscopy (STS) and Density Functional Theory (DFT)

Z. Klusek [a], P. Dabrowski [a], J. Slawinska [b], I. Wlasny [a],
M. Wojtoniszak [d], E. Borowiak-Palen [d], I. Zasada [c]

[a] Division of Physics and Technology of Nanometer Structures, Solid States Physics Department, University of Lodz, Pomorska 149/153, Lodz 90-236, Poland
[b] Theoretical Physics Department II, University of Lodz, Pomorska 149/153, Lodz 90-236, Poland
[c] Solid States Physics Department, University of Lodz, Pomorska 149/153, Lodz 90-236, Poland
[d] Centre of Knowledge Based Nanomaterials and Technologies, Institute of Chemical and Environment Engineering, West Pomeranian University of Technology,ul. Pulaskiego 10, 70-322 Szczecin, Poland

zbklusek@mvii.uni.lodz.pl

It is crucial for the future applications to understand the nanoscale electronic properties of graphene considered in terms of the electron local density of states (LDOS) on different substrates. This is because a substrate or deposited coating can considerably affect nanoscale electronic properties of graphene. Particularly, it has been proved theoretically using density functional theory (DFT) and van der Waals density functional (vdW-DF) calculations that the unique conical dispersion relation around K/K' points in graphene is preserved on (111) surfaces of Al, Cu, Ag, Pt, and Au [1-3]. However, this is accompanied with the change of position of the Dirac point (E_D) relative to the Fermi level (E_F) due to the presence of substrate (doping effect). This is especially important in the case of Au which is widely used in fabrication of metal-graphene contacts in graphene devices.

In the presentation we will show detailed scanning tunneling microscopy and spectroscopy (STM/STS) studies of graphene interactions with gold substrate. The obtained experimental results will be discussed in the frame of theoretical models. Mono-, bi- and tri- graphene layers (MG, BG, TG) were deposited on 8 nm of Au, with 0.5 nm Cr adhesion layer sputtered onto 100 nm SiO_2 (Graphene Industries, UK). This type of substrate enables to create a setup suitable for the STM/STS experiments without micro fabrication processes and studies of LDOS on multilayer graphene systems [4]. Identification of MG, BG and TG were carried out using optical microscopy (OM), Raman spectroscopy (RS) – (Renishaw InVia) and scanning electron microscopy (SEM) - (Vega Tescan). All the STM/STS experiments were carried out at room temperature in UHV condition using VT-STM/AFM microscope integrated with the XPS/UPS/AES/LEED/MULTIPROBE P system (Omicron GmbH).

The STM results show that the height of MG relative to Au substrate is close to 0.5 nm, the height of BG relative to MG varies from 0.30 nm up to 0.50 nm, while TG relative to BG gives the value 0.35-0.50 nm. The detailed STM topography of MG/Au border structure is presented in Fig.1a.The STM topographies for MG/BG/TG on Au at atomic resolution present triangular structure typical for graphite with the distance between atoms equals about 0.25 nm. We would like to emphasize that honeycomb lattice typical for unperturbed MG with the distance between atoms equal to 0.142 nm has never been observed.

The STS results prove that holes are donated by Au substrate to graphene which becomes p-type doped i.e. E_F is located below E_D. Particularly, E_D for MG is located in the range of 0.35 - 0.43 eV; for BG varies from 0.22 eV up to 0.30 eV, and for TG is close to 0.1- 0.15 eV. Estimated positions of the Dirac point show that the higher number of graphene layers the lower Fermi level shift is observed. Typical STS results for MG and TG are presented in Fig.1b,d and Fig.2b,c,d,e. Additionally the STS results show presence of energetic heterogeneity considered in terms of changes LDOS measured at different places on the surface. This is particularly well seen in the case of TG on Au – see Fig.2a,d.

Finally, graphene-gold interactions were studied using both local density approximation and van der Waals density functionals. In the LDOS profiles the Dirac points were clearly identified and compared with the positions of Dirac cones in the bandstructure. The theoretical results will be compared with experimental STM/STS data.

References

[1] G. Giovannetti, P. A. Khomyakov, G. Brocks, V. M. Karpan, J.van den Brink, J.P. Kelly, Physical Review Letters **101** (2008) 026803.

[2] P. A. Khomyakov, G. Giovannetti, P. C. Rusu, G. Brocks, J. van den Brink, P. J. Kelly, Physical Review B **79** (2009) 195425.

[3] M. Vanin, J. J. Mortensen, A. K. Kelkkanen, J. M. Garcia-Lastra, K. Thygesen, W. Jacobsen, Physical Review B **81** (2010) 81408.

[4] Z. Klusek, P. Dabrowski, P. Kowalczyk, W. Kozlowski, W. Olejniczak, P. Blake, M. Szybowicz, T. Runka, Applied Physics Letters **95** (2009) 113114.

Figures
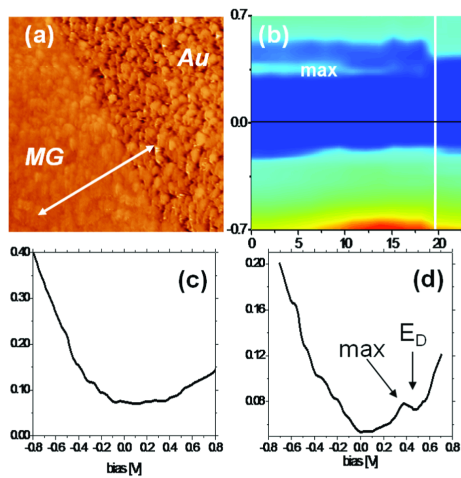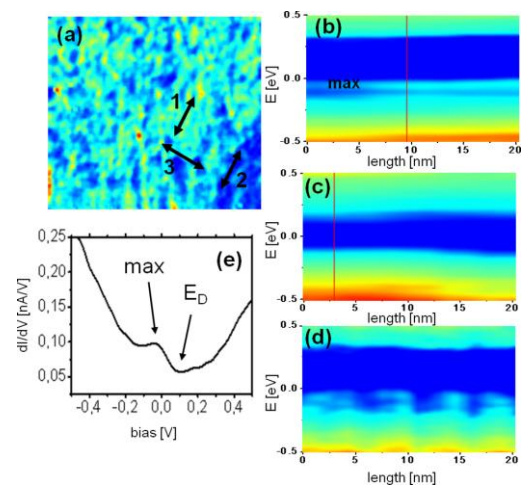
Fig.1

Fig.2

Fig.1 (a) 450 nm x 450 nm STM topography showing the details of MG and Au border line. (b) dI/dV (E, line) map recorded on MG/Au along arrow in figure (a). Colors: blue, green, red - low, intermediate, and high value of the LDOS, respectively. (c) dI/dV profile of Au. (d) Typical dI/dV profile of MG/Au.

Fig.2 (a) 200 nm x 200 nm dI/dV (E, x, y) map recorded at 0.05 eV on TG/Au. Colors: blue, green, red - low, intermediate, and high value of the LDOS, respectively.(b, c, d) dI/dV (E, line) maps recorded on different TG/Au regions denoted by #1, #2 and #3 lines on figure (a). (e) Typical dI/dV profile of TG/Au showing Dirac point.

Atomic Scale Electronic Characterization of Grain Boundaries in Graphene Grown by Chemical Vapor Deposition on Copper Foil

Justin C. Koepke, Joshua D. Wood, David Estrada, Eric Pop, Joseph W. Lyding

Beckman Institute, Micro and Nanotechnology Laboratory, Dept. of Electrical and Computer Engineering, Univ. of Illinois at Urbana-Champaign, 405 North Mathews Ave., Urbana, IL 61801, USA
jkoepke@illinois.edu

Wafer-scale growth of monolayer graphene is a critical step to allow integration of graphene into future nanoelectronic devices. Chemical vapor deposition (CVD) growth of graphene on copper is an area of focused research efforts due to the ability to grow predominantly monolayer graphene with the right growth conditions [1]. Recent experimental work elucidated the graphene grain boundary topology [2,3], and recent theoretical calculations simulated the electrical transport properties of ideal boundaries [4,5]. Nonetheless, to date there have been few scanning tunneling microscopy (STM) studies of graphene grown by CVD on Cu and no studies of the electronic properties of the films' grain boundaries on the atomic scale. To address this gap, we study grain boundaries in graphene grown by CVD on Cu foil using ultrahigh vacuum scanning tunneling microscopy (UHV-STM) and spectroscopy (STS).

The graphene was grown on 1.4 mil copper foil using methane in an Atomate CVD system at 1000 °C for 30 min. and transferred onto a SiO_2/n+ Si substrate after growth. Figure 1(a) shows an optical image of the graphene after the post-growth transfer to the SiO_2/Si. The dots indicate the location of the Raman spectra shown in Fig. 1(b). The G'/G ratios for these spectra suggest that the transferred graphene was indeed one monolayer. The D' band in the green spectra suggests that there was more local disorder. We degassed the sample in the UHV-STM system by direct current heating through the Si substrate at a temperature of 600–700 °C for 24 hours. Figure 1(c) shows a small STM topograph from a clean area of the sample, clearly showing the monolayer graphene lattice.

We have studied grain boundaries with misorientation angles between the grains of approximately 6°, 9°, 20°, 22°, 26°, 30°, and 32°. These grain boundaries were continuous across large protrusions and wrinkles in the graphene and other surface topography. Figure 2(a) shows the spatial derivative of an STM topograph of the meeting point of three grain boundaries. The misorientation angles between the lower-left and top grains, top and lower-right grains, and lower-left and lower-right grains approximately 9°, 22°, and 30°, respectively. Figure 2(b) shows a map of the tunneling conductance (dI/dV) recorded along the dashed green line shown in Fig. 2(a) with the color map to the right and the purple line indicating the approximate location of the grain boundary. The bottom of the dashed green line corresponds to the left side of the spectra map, and the top of the line corresponds to the right side of the spectra map. The map clearly shows larger dI/dV in empty states on the grain boundary than for spectra taken on the graphene away from the boundary. Figure 2(c) shows a comparison of the density of states (DOS), (dI/dV)/(I/V), and the dI/dV for a spectrum taken on the same grain boundary as data in Fig. 2(b) and a spectrum taken in the lower-right grain away from the boundary. These two individual specta show enhanced dI/dV in empty states and also a somewhat higher density of states in empty states at the grain boundary.

Depending on the misorientation angle between the graphene grains, we observe strong standing wave patterns adjacent to the actual grain boundaries. Figure 3(a) shows a grain boundary between two grains with a relative misorientation angle of approximately 32°. There is a clearly visible standing wave pattern on both sides of the grain boundary. Figures 3(b) and 3(c) show the fast Fourier transform (FFT) for the left and right grains, respectively, with the graphene lattice filtered out. This leaves standing waves, from which we extract their spatial extent in Fig. 3(e). Based on the misorientation angle and theory [4,5], we determine a possible grain boundary geometry, which has heptagons and pentagons as shown in Fig. 3(d). Consequently, standing waves originate from interference [6] with that particular geometry. The standing waves possess decay lengths of ~2 nm (left) and ~1.3 nm (right).

For the first time, we probe the atomic-scale electronic and topographical nature of graphene grain boundaries using STM and STS, complementing previous experimental [2,3] and theoretical work [4,5] in the field. We find that standing waves arise for scattering off particular grain boundary geometries and misorientation angles. Hence, the grain boundaries with standing waves will be deleterious for transport.

References

[1] X. Li, Science **324** (2009) 1312.
[2] P.Y. Huang, Nature AOP (2011) nature09718.
[3] J. An, arXiv: 1010.3905v1 (2010).
[4] O.V. Yazyev, Nature Materials **9** (2010) 806.
[5] O.V. Yazyev, Phys. Rev. B **81** (2010) 195420.
[6] H. Yang, Nano Letters **10** (2010) 943.

Figures
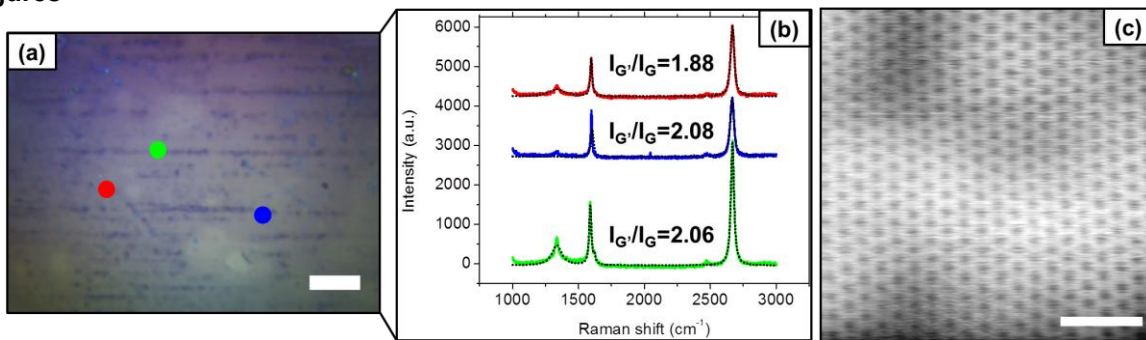
Figure 1. (a) Optical image of transferred monolayer graphene on 80 nm of SiO_2. Raman spectroscopy taken at spots indicated. Scale bar is 20 µm. (b) Raman spectroscopy of graphene, showing G', G, and D bands and Lorentzian fits in black. The green spectra has a D' band, indicating higher order disorder. All spectra have high $I_{G'}/I_G$ ratios, indicating monolayer coverage. (c) STM topograph of a clean area of the graphene. Scale bar is 1 nm.
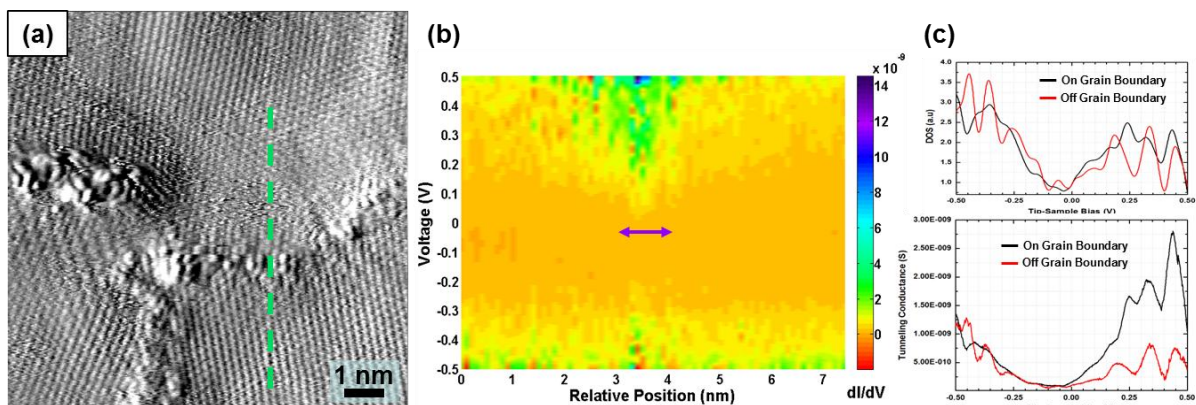
Figure 2. (a) Spatial derivative of an STM topograph of a meeting point of three grain boundaries. The misorientation angles between the graphene grains are ~22° between the top and lower-right grains, ~30° between the lower-left and lower-right grains, and ~9° between the lower-left and top grains. (b) Tunneling conductance map of calculated dI/dV spectra taken along the green dashed line from (a). The map shows a very clear enhancement of the tunneling conductance in the vicinity of the grain boundary, as indicated by the purple line on the map. (c) Comparison of tunneling conductance and normalized tunneling conductance (DOS) for a point on the grain boundary between the top and the right grains and a point away from the grain boundary in the right grain. The plots show the larger empty states dI/dV and somewhat higher empty states DOS for the spectra point on grain boundary compared to the spectra point taken away from the grain boundary.
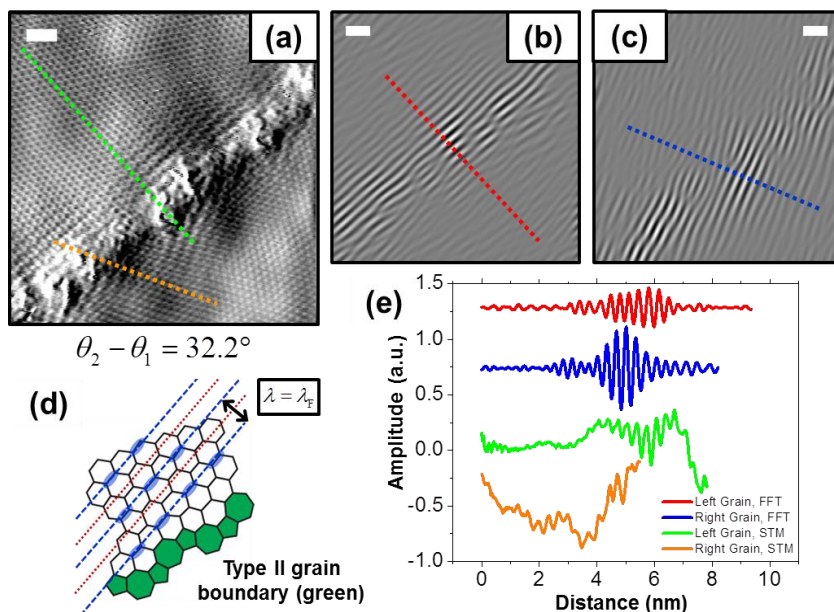
Figure 3. (a) Spatial derivative of an STM topograph of a type II grain boundary with standing waves; the misorientation angle between the two graphene lattices is ~32°. Fast Fourier transforms for the left (b) and right (c) graphene grains, with the graphene lattice filtered out, showing standing waves. (d) Schematic diagram of left graphene lattice near the heptagon-pentagon grain boundary. Light blue regions indicate interference localization along C-C bonds, giving a backscattering standing wave of wavelength λ_F (blue line, Fermi wavelength). (e) Spatial extent of standing waves, where line sections correspond to (a-c). Left grain standing wave extends ~2 nm, and right grain extends ~1.3 nm. All scale bars are 1 nm.

Optimizing the identification of graphene mono- and bilayers on multi-layered-systems

Christopher Kontis, Marcel Müller and Joachim Knoch

TU Dortmund University, Emil-Figge Strasse 68, 44227 Dortmund, Germany
Christopher.Kontis@udo.edu

Graphene has recently attracted a great deal of interest as material for future nanoelectronic devices due to its excellent electronic transport properties. However, to date most investigations of graphene imply the deposition of graphene flakes on a substrate, necessitating an unambiguous identification of mono- and bilayers with optical microscopy. While it is well known that e.g. a 90 nm SiO_2 [1] or 72 nm Al_2O_3 [2] layer on top of a silicon substrate provides sufficient contrast to observe a monolayer of graphene this fact limits at the same time experiments to be done on a single layer substrate. However, the deposition of graphene on a multi-layer system providing for instance buried gates is desirable as well as the incorporation of alternative materials such as high-k gate dielectrics.

This work presents an investigation and optimization of the identification of graphene mono- and bilayers on various multi-layer substrates. Instead of the mere contrast between substrate and substrate/mono/bilayer systems [1], the luminance differences are used to obtain optimum visibility, based on the work presented in Ref. [2]. Our approach uses a genetic algorithm is employed that not only allows optimizing the visibility of graphene on a single layer substrate but also enables finding the most appropriate composition of a multi-layer systems in terms of materials in use and their thicknesses. In addition, a major benefit of our approach is the possibility to qualify appropriate layer systems with respect to their manufacturability.

The reflection spectra of a multi-layer system with and without graphene layer are computed using the Fresnel-equations and a transfer matrix formalism [3] as illustrated in Fig. 1. From these spectra colors can be extracted using the CIE-Lab color space [4] which includes the color perception of the human eye. Eventually, three so called color-luminance-difference values (CLD) are obtained where CLD_1 describes the luminance difference between the colors of a monolayer graphene and the top of the multi-layer system, CLD_2 between a mono- and a bilayer graphene and CLD_3 describes the luminance difference between a bilayer and the multi-layer system's surface. A genetic algorithm is then used to optimize the multi-layer system with respect to obtaining maximum differences between the three CLD-values, i.e. obtaining the best visibility and possibility to distinguish between graphene mono- and bi-layers.

Fig. 2 presents a number of multi-layer systems generated automatically with the genetic algorithm. Obviously, which allow a clear colored identification of graphene. The calculated colors for substrate/mono/bilayer graphene are illustrated in row calculated colors. The substrate's color surrounds the monolayer (top) and the one of the bilayer (bottom). All presented systems provide a rather large tolerance in terms of the visibility of grapheme even with thickness variations of each layer of up to +/- 10 nm. Fig. 3 illustrates the visibility of graphene for the multi-layer system 10 (cf. Fig. 2) as a function of the thickness of the three respective layers. All three layer can even vary more then +/- 10 nm, while graphene will still be visibile with optical microscopy.

In summary, by using a genetic algorithm to generate multi-layered-systems, it is possible to achieve an arbitrary multi-layered-system, allowing a clear visibility and identification of mono- and a bilayer of graphene including a large tolerance of layer thickness variations during manufacturing.

References

[1] P.Blake, K. S. Novoselov, A. H. Castro Neto, D. Jiang, R. Yang, T .J. Booth, A. K. Geim, E. W. Hill, Appl. Phys. Lett. 91, 063124, **Making graphene visible** (2007)
[2] Libo Gao, Wencai Ren, Feng Li, Hui-Ming Cheng, ACS Nano, **Total Color Difference for Rapid and Accurate Identification of Graphene** (2008) 1625 - 1633
[3] M. V. Klein, T. E. Furtak, Springer, **Optics** (1988) 230 - 234
[4] M. Richter, Gruyter, **Einfuehrung in die Farbmetrik** (1981)

Figures
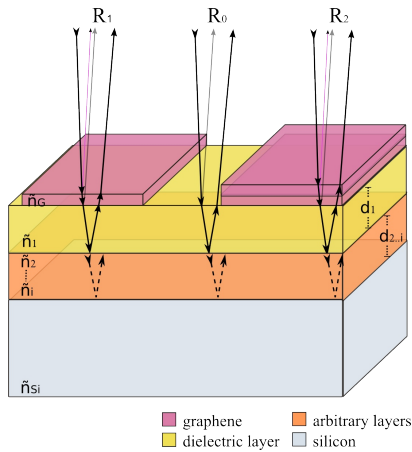
Fig. 1. Fresnel-law-based multi-layered system to achieve the reflection spectra R_0, R_1 and R_2, which are functions of the layer's thicknesses $d_1, d_2...d_n$ and of the refractive indexes $ñ_1, ñ_2....ñ_n$.
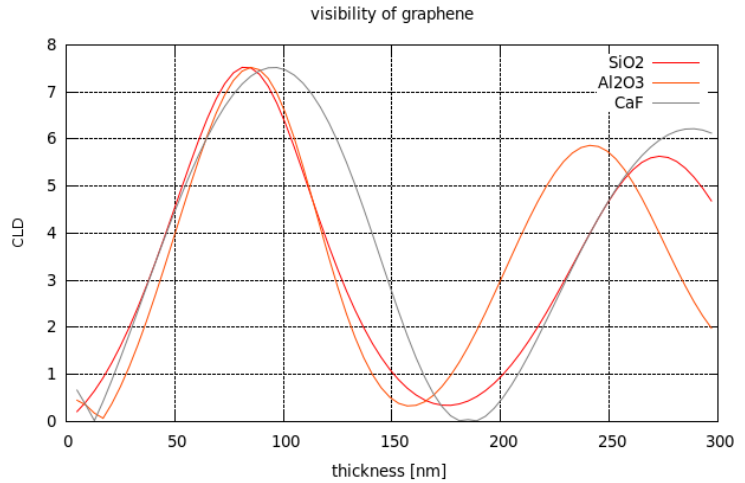
Fig. 3. Visibility of graphene depending on the three layers's thicknesses for stack 10 in Fig. 2.

substance	stack1	stack2	stack3	stack4	stack5	stack6	stack7	stack8	stack9	stack10	stack11	stack12
Graphene												
SiO_2	300 nm	90 nm				65 nm	61 nm	37 nm		81 nm	83 nm	85 nm
Al_2O_3				72 nm			25 nm			85 nm	221 nm	131 nm
Si_3N_4			55 nm									
HfO_2						25 nm			45 nm		25 nm	10 nm
CaF					90 nm			242 nm		95 nm		
Ag									20 nm			20 nm
Si												
Calculated colors:												
CLD1	1.2	2.2	0.5	1.8	2.3	2.1	2.2	2.2	2.3	1.9	2.1	1.4
CLD2	1.1	2.2	0.4	1.8	2.2	2.1	2.2	2.2	2.3	1.9	2	1.4
CLD3	2.2	4.4	1	3.6	4.5	4.3	4.3	4.5	4.6	3.8	4.1	2.8
Σ CLD	**4.5**	**8.8**	**1.9**	**7.2**	**9**	**8.5**	**8.7**	**8.9**	**9.2**	**7.6**	**8.2**	**5.6**

Fig. 2. Multi-layered-systems generated using a genetic algorithm, which offer a clear visibility and identification of graphene and at least +/- 10 nm fault-tolerance by layer-manufacturings (cf Fig. 3).

Tailoring the Atomic and Electronic Structure of Two-Dimensional Carbon and Boron-Nitride Systems with Electron and Ion Beams

A.V. Krasheninnikov,[1,2] J. Kotakoski,[1] O. Lehtinen,[1] N. Berseneva,[2] and R.M. Nieminen[2]

[1]Department of Physics, University of Helsinki, Finland
[2] Department of Applied Physics, Aalto University, Finland
akrashen@acclab.helsinki.fi

Recent experiments (see Refs. [1,2] for an overview) on ion and electron bombardment of nanostructures demonstrate that irradiation can have beneficial effects on such targets and that electron or ion beams can serve as tools to change the morphology and tailor mechanical, electronic and even magnetic properties of various nanostructured materials.

We systematically study irradiation effects in nanomaterilas, including two-dimensional (2D) systems like graphene and hexagonal boron-nitride (h-BN) sheets. By employing various atomistic models ranging from empirical potentials to time-dependent density functional theory we simulate collisions of energetic particles with 2D nanostructures and calculate the properties of the systems with the irradiation-induced defect. In this talk, our latest theoretical results on the response of graphene and h-BN to irradiation will be presented, combined with the experimental results obtained in collaboration with several groups [3,4]. The electronic structure of defected graphene sheets with adsorbed transition metal atoms will be discussed [5], and possible avenues for tailoring the electronic and magnetic structure of graphene by irradiation-induced defects and impurities will be introduced [4,6]. The effects of ion and electron irradiation on boron-nitride sheets and nanotubes will also be touched upon. Finally, we will discuss how electron irradiation and electron beam-assisted deposition can be used for engineering hybrid BN-C nanosystems by substituting B and N atoms with carbon with high spatial resolution.

References

[1] Krasheninnikov A. V. and Banhart F., Nature Materials, 6, 723 (2007).

[2] Krasheninnikov A. V. and Nordlund K., J. Appl. Phys. (Appl. Phys. Reviews), 107, 071301 (2010).

[3] J. Kotakoski, C. H. Jin, O. Lehtinen, K. Suenaga, and A. V. Krasheninnikov, Phys. Rev. B 82 (2010) 113404.

[4] O. Cretu, A.V. Krasheninnikov, J. A. Rodriguez-Manzo, L.Sun, R.M. Nieminen, and F.Banhart. Phys. Rev. Lett. 105 (2010) 196102.

[5] A. V. Krasheninnikov, P.O. Lehtinen, A.S. Foster, P. Pyykko, and R. M. Nieminen, Phys. Rev. Lett. 102 (2009) 126807.

[6] F. Banhart, J. Kotakoski and A. V. Krasheninnikov, ACS Nano, (2011) in press.

Microwave experiments beyond pure Graphene using dielectric discs

U. Kuhl, S. Barkhofen, F. Mortessagne

Organization: LPMC - UMR 6622, Université de Nice-Sophia Antipolis
Address: Ulrich Kuhl, LPMC - UMR 6222, Université de Nice-Sophia
Antipolis, Parc Valrose, 06108 Nice, France
City: Nice
Country: France
Contact@E-mail: ulrich.kuhl@unice.fr

Abstract:
Experiments on hexagonal graphene-like structures using microwave measuring techniques are presented [1]. Employing dielectric discs between two metallic plates and a TE-antenna we establish a tight-binding configuration baring a lot of opportunities realizing different lattice structures. In measurements on graphene-like sheets the vanishing density of states at the Dirac point is observed as well as the linear slope close to it as is shown in the figure below.
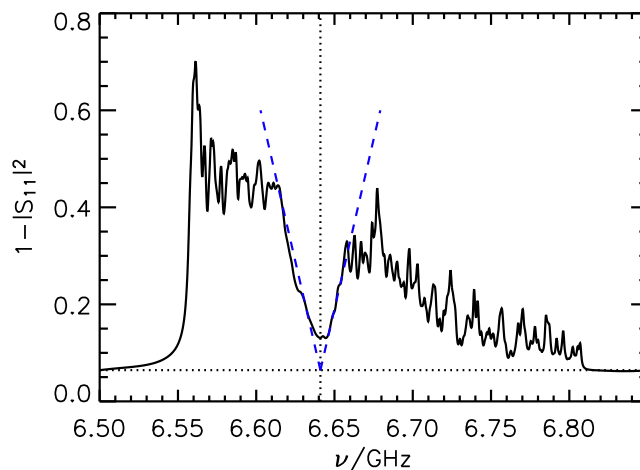
Taking advantage of the high flexibility of the setup we move the antenna to zigzag edges of the lattice and find edge states that can not be found in the interior of the sheet or at an armchair edge in agreement with theoretical predictions. The consequences of introduced disorder are investigated and an imitation of boron-nitride- a hexagonal crystal consisting of two different sorts of atoms- is implemented. The experimental results are confirmed by numerical simulation assuming the tight-binding model.

[1] U. Kuhl, S. Barkhofen, T. Tudorovskiy, H.-J. Stöckmann, T. Hossain, L. de Forges de Parny, and F. Mortessagne. Dirac point and edge states in a microwave realization of tight-binding graphene-like structures. Phys. Rev. B **100**, 094308 (2010).

Large area CVD Graphene TEM supports

Shishir Kumar, Ehsan Rezvani, Nikos Peltekis, Anne Weidlich, Georg S. Duesberg

School of Chemistry and Centre for Research on Adaptive Nanostructures and Nanodevices (CRANN),
Trinity College, Dublin, Ireland.
duesberg@tcd.ie

We present a process for fabricating large area TEM support using CVD graphene grown on copper foils. The thinness of graphene and low atomic number of carbon facilitates imaging of nanoparticles and biomaterials. The TEM supports are composed of graphene held sandwiched between two sets of perpendicular exposed and annealed photoresist lines, whose dimensions can be varied as needed. Unlike other methods, graphene is strongly adhered to this mesh structure, providing it mechanical stability. The mesh is mechanically strong enough to be handled by tweezers. We display large area structures covering whole TEM grids (3 mm). Further, the whole structure is carbonaceous and therefore, can undergo harsh chemical treatments and is biocompatible. The characterisation of graphene available on these samples was done using STEM, TEM and Raman spectroscopy, showing good quality monolayer graphene. Small amount of organic contaminants, leftover from fabrication, can be cleaned using a process developed in our group. Finally, we use these grids for imaging nanoparticles and show their advantages compared to normal TEM grids.

Figures:
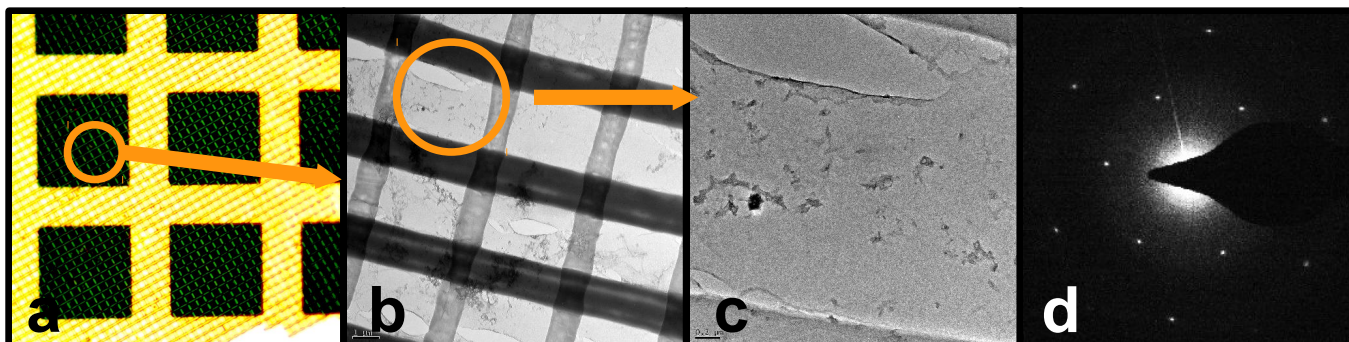
a) Optical image of copper TEM grid covered with carbon mesh. b) STEM of carbon mesh made of photoresist lines and graphene. c) TEM image and d) ED pattern of graphene in mesh. The width of photoresist lines in (b) is about 1 μm.

Graphene edge magnetism for spintronics applications: Dream or Reality?

Jens Kunstmann (1), Cem Özdo?an (2), Alexander Quandt (3,4), Holger Fehske (3), Hâldun Sevinçli (1), Gianaurelio Cuniberti (1)

(1) Institute for Materials Science, TU Dresden, 01062 Dresden, Germany
(2) Department of Materials Science and Engineering, Cankaya University, Ankara, Turkey
(3) Institut für Physik, Ernst-Moritz-Arndt-Universität Greifswald, Germany
(4) School of Physics and DST/NRF Centre of Excellence In Strong Materials, University of the Witwatersrand, South Africa
jens.kunstmann@tu-dresden.de

We critically discuss the stability of edge states and edge magnetism in zigzag edge graphene nanoribbons (ZGNRs). We point out that magnetic edge states might not exist in real systems, and show that there are at least three very natural mechanisms - edge reconstruction, edge passivation, and edge closure - which dramatically reduce the effect of edge states in ZGNRs or even totally eliminate them. Even if systems with magnetic edge states could be made, the intrinsic magnetism would not be stable at room temperature. Charge doping and the presence of edge defects further destabilize the intrinsic magnetism of such systems. We conclude that edge magnetism within graphenes ZGNRs is much too weak to be of practical significance, in particular for spintronics applications. We further discuss the influence of nonmagnetic edges on the electron transport through ZGNRs.

References

[1] J. Kunstmann, C. Özdo?an , A. Quandt, H. Fehske, arXiv:1007.2602 (2010).

Spin-splitting in graphene

E.V. Kurganova[1], H.J. van Elferen[1], A. McCollam[1], K.S. Novoselov[2], B.J. van Wees[3], J.C. Maan[1], U. Zeitler[1]

[1]High Field Magnet Laboratory, Institute for Molecules and Materials, Radboud University Nijmegen, Toernooiveld 7, 6525 ED Nijmegen, The Netherlands
[2]School of Physics and Astronomy, University of Manchester, M13 9PL, Manchester, United Kingdom
[3]Physics of Nanodevices, Zernike Institute for Advanced Materials, University of Groningen, Nijenborgh 4, 9747 AG Groningen, The Netherlands

e.kurganova@science.ru.nl

The Landau levels in graphene are spin and valley degenerate. In order to lift the spin degeneracy completely, fields of a few hundred Tesla are necessary. However, even in fields of 30 T spin splitting already becomes visible as a reduction of Shubnikov-de Haas (SdH) oscillations. We present recent results exploring the spin-splitting by means of tilted-field magnetotransport experiments at magnetic fields up to 30 T.

The Landau level splitting in a graphene flake increases with a magnetic field B_n perpendicular to the flake. It follows a square root dependence in single layer graphene (SLG) [1] and an almost linear dependence in bilayer graphene (BLG) [2,3]. Spin-splitting of each Landau level increases linearly with the total magnetic field B. Therefore, tilting a sample in a magnetic field increases the ratio between the Zeeman splitting and the Landau level splitting and, as a consequence, reduces the amplitude of the SdH oscillations.

To observe the spin-splitting we have measured the longitudinal resistance as a function of charge carrier concentration in SLG and BLG in tilted magnetic fields. Our measurements show that increasing the total magnetic field B at a constant perpendicular field B_n leads to a damping of the SdH oscillation amplitudes (Fig.1). We fitted the experimental dependences by the Lifshitz-Kosevich formula and determined the SdH oscillation amplitudes, reduced by the Zeeman splitting with an added in-plane field. The amplitudes found for BLG are plotted in Fig.2 as a function of total field B for a constant perpendicular field $B_n = 8$ T and for different Landau level indices N. The reduction of the SdH amplitude can be quantitatively described by a factor $cos\left(\dfrac{\pi \ g^* m^* B}{2 m_e B_n}\right)$ [4] for particles with an effective g-factor g^* and a cyclotron mass $m^* = \dfrac{\hbar^2}{2\pi} \dfrac{dS(E)}{dE}$, where $S(E) = \pi k^2$ is the area in k-space of the Landau orbits at the Fermi energy. This allows us to extract $g^* m^*$ from our measurements.

Assuming a parabolic dispersion at low magnetic fields for BLG and using a constant effective mass $m^* = 0.032 \ m_e$ [5] results in the effective g-factors g^* plotted in the inset of Fig.2. The experimental g^* are enhanced compared to the free electron g-factor with increasing enhancement for the higher Landau levels. We note that such an enhancement can also be caused by increasing the cyclotron mass with carrier concentration [6]. For SLG preliminary results suggest that g^* is comparable to free electron g-factor for low Landau levels ($N = \pm 1$), though we cannot yet exclude an enhancement for the higher levels as seen in BLG.

References

[1] K.S. Novoselov *et al.*, Nature **438** (2005) 197

[2] E. McCann, V.I. Fal'ko, Phys. Rev. Lett. **96** (2006) 086805

[3] J.M. Pereira Jr., F.M. Peeters, P. Vasilopoulos, Phys. Rev. B **76** (2007) 115419

[4] A.E. Stephens, D.G. Seiler, J.R. Sybert, HJ. Mackey, Phys. Rev. B **11** (1975) 4999

[5] E.V. Kurganova *et al.*, Solid State Communications, 150 (2010) 2209

[6] E.V.Castro et al., Phys. Rev. Lett, 99 (2007) 216802

Figures
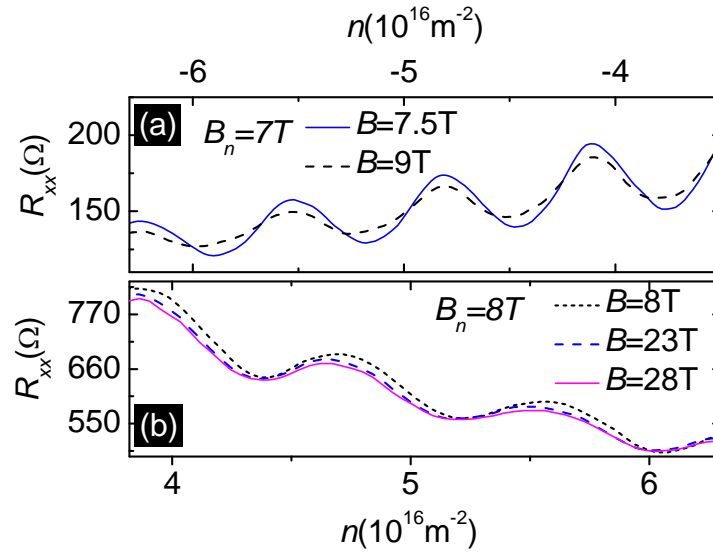
Figure 1: *(color online) SdH oscillations of longitudinal resistance as a function of carrier concentration in SLG (a) and BLG (b). The traces are recorded for different tilt angle/total field and a constant perpendicular field B_n at T=0.4 K*
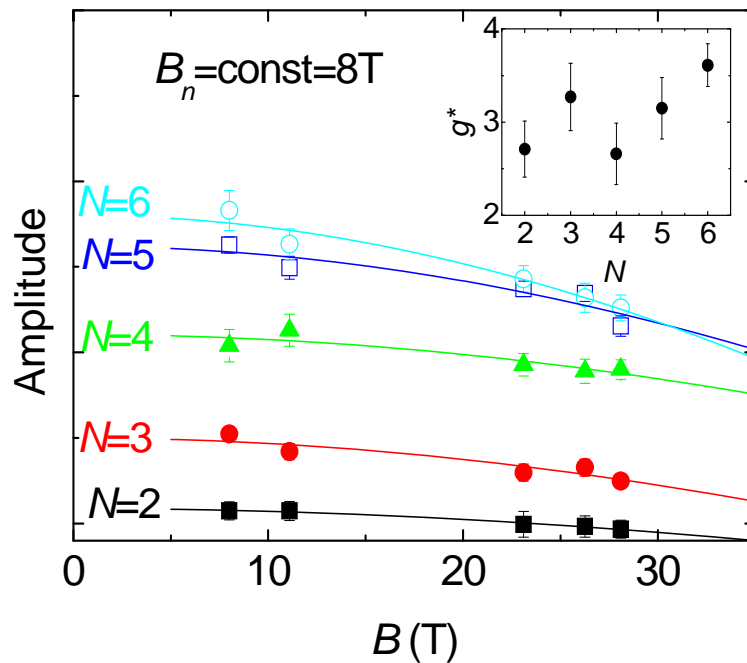
Figure 2: *(color online) Oscillation amplitude as a function of total field B at a constant perpendicular field B_n=8 T in BLG. Solid lines are fits by $cos\left(\dfrac{\pi \, g^* m^* B}{2 m_e B_n}\right)$, the g^* extracted from this is shown in the inset as a function of Landau level index N*

240

The Role of a Bifunctional Matrix Protein in a Biomimetic Graphene/Nanocellulose Composite

[1]**Päivi Laaksonen**, [1,2]Jani-Markus Malho, [3]Markku Kainlauri, [2]Andreas Walther, [2]Olli Ikkala, [1]Markus, B. Linder

[1]VTT Nanobiomaterials, VTT Technical Research Centre of Finland, Tietotie 2 P.O. Box 1000, FI-02044 VTT, Espoo, Finland, [2]Molecular materials, Aalto University, P.O. Box 15100, FI-00076 AALTO Finland, [3]VTT Micro and Nanoelectronics, VTT Technical Research Centre of Finland, Tietotie 2 P.O. Box 1000, FI-02044 VTT, Espoo, Finland,

paivi.laaksonen@vtt.fi

We present a truly biomimetic approach for building nanocomposites by using engineered biomolecules, nanocellulose and graphene flakes. Biomimetics is used as a tool for understanding how high performance materials can be built by the means of specifically binding matrix molecules. A significant reinforcement of cellulose film could be obtained when graphene, interfaced with a novel bi-functional protein HFBI-DCBD, was embedded in it. HFBI-DCBD is a recombinant protein where an amphiphilic hydrophobin molecule (HFBI) has been fused with two cellulose binding domains (CBD) as presented in Scheme 1. Due to the strong interactions that the proteins create between the components, nanocomposites prepared by this method showed excellent values for toughness (20.2 GPa), strength (278 MPa) and work-of-fracture (5.8 J/m^2). The method uses sustainable materials and is readily up-scalable.
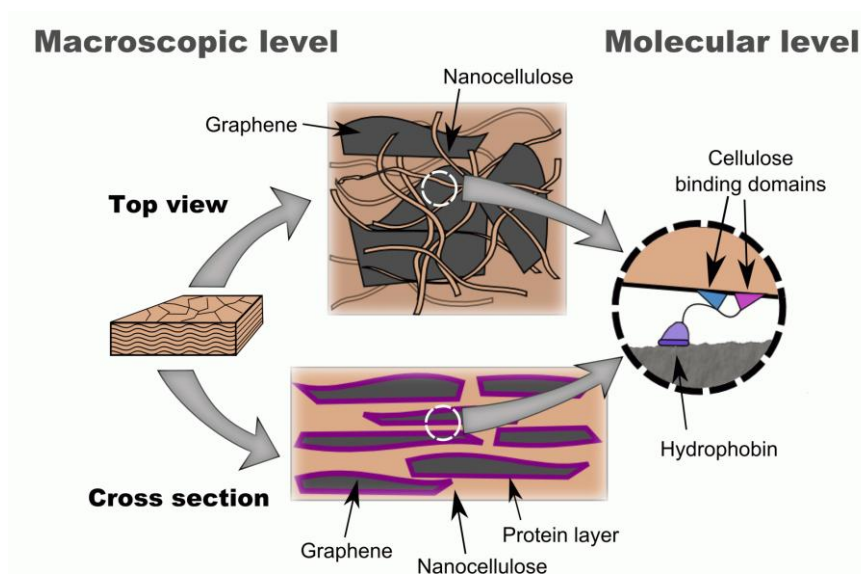
Scheme 1. *A schematic presentation of the structure of the composite from macroscopic to molecular level. Top view: Graphene flakes are interlocked in the percolating network of cellulose, which provides structural rigidity. Cross section: Cellulose fibrils and protein-coated graphene form a layered structure where protein is facing both graphene and cellulose. The scheme on molecular level shows how the fusion protein HFBI-DCBD is oriented at the interface between cellulose and graphene. The violet part represents the amphiphilic hydrophobin (HFBI) which attaches to graphene. Blue and purple parts are two the cellulose-binding domains (CBDs).*

The studied composite matrix was formed from cellulose and graphene flakes [1], which were coated with a layer of fusion protein HFBI-DCBD. The two functional parts of the fusion protein appear in nature for totally different purposes compared to what we are now using them. Instead of breaking down

materials, which is how the host organism (*Trichoderma reesei*) of these proteins operates, we use these molecules for building new materials. Hydrophobins are amphiphilic and assemble at interfaces [2], thus forming monolayers at surfaces of hydrophobic materials, such as graphene.[3] The second part of the molecule, CBD, originates from a cellulase,[4] which uses it for anchoring to cellulose surfaces. Functionalizing of nanofibrillar cellulose (NFC)[5] with CBD-containing molecules provides a soft non-destructive way to add function and to modify its properties. It was shown that exfoliation of graphene in a mixture of HFBI-DCBD and NFC resulted in suspension of graphene flakes attached to the cellulose nanofibrils. This suspension was then vacuum filtrated into films whose mechanical properties were characterized. The composite has excellent mechanical properties (See Figure 1), is light-weight and all its components are from sustainable sources.
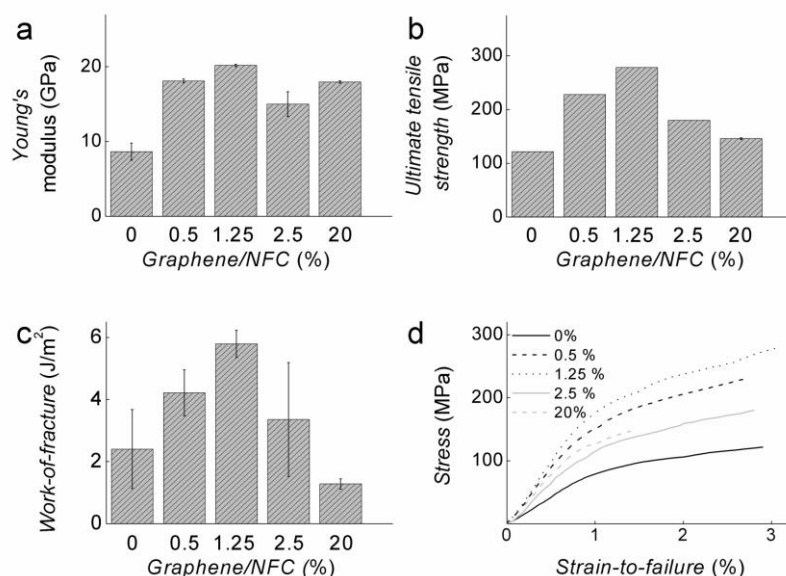
Figure 1. *Mechanical properties of composites consisting a varying amount of graphene. Amount of graphene is given as a w-% of graphene to nanocellulose. Stiffness (a) and ultimate tensile strength (b) and toughness (c) of the composite significantly increased when graphene content was increased and reached a maximum level at graphene content 1.25 %. d: Example stress vs. strain curves from samples containing different amounts of graphene. Graphene fraction is given as percentage to the mass of NFC.*

References

[1] A. K. Geim, K. S. Novoselov, *Nat. Mater. 6* (2007) 183-191.

[2] M. B. Linder, *Curr. Opin. Colloid Interface Sci.,***14** (2009) 356-363.

[3] P. Laaksonen, M. Kainlauri, T. Laaksonen, A. Shchepetov, H. Jiang, J. Ahopelto and M.B. Linder, *Angew. Chem. Int. Ed.* **49** (2010) 4946–4949.

[4] M. Linder and T. T. Teeri, *J. Biotechnol.,* **57** (1997) 15-28.

[5] S. J. Eichhorn, A. Dufresne, M. Aranguren, N. E. Marcovich, J. R. Capadona, S. J. Rowan, C. Weder, W. Thielemans, M. Toman, S. Renneckar, W. Gindl, S. Veigel, J. Keckes, H. Yano, K. Abe, M. Nogi, A. N. Nakagaito, A. Mangalam, J. Simonsen, A. S. Benight, A. Bismarck, L. A. Berglund and T. Peijs, *J. Mater. Sci.,* **45** (2010), 1-33.

Chemically tunable transport phenomena of functionalized graphene

Nicolas Leconte[1], D. Soriano[2,3], P. Ordejon[4], A. Lherbier[1], J.J. Palacios[5], J.-C. Charlier[1], S. Roche[4,6]

[1]IMCN, Université Catholique de Louvain, Place Croix du Sud 1, (NAPS-ETSF), B -1348, Louvain-la-Neuve, Belgium
[2]Departamento de Física Aplicada, Universidad de Alicante, San Vicente del Raspeig, Alicante 03690, Spain
[3]Instituto de Ciencia de Materiales de Madrid (CSIC), Cantoblanco, Madrid, 28049, Spain
[4]CIN2 (ICN-CSIC) Barcelona, Campus UAB, E08193 Bellaterra, Spain
[5]Departamento de Física de la Materia Condensada, Universidad Autónoma de Madrid, Cantoblanco, Madrid 28049, Spain
[6]ICREA, Institucio Catalana de Recerca i Estudis Avançats, 08010 Barcelona, Spain

nicolas.leconte@uclouvain.be

We present an *ab initio* multiscale study and quantum transport simulations using the Kubo formalism [1] of chemically modified graphene based materials, whose properties are tuned by changing the density and nature of grafted molecular units. Depending on the nature of the introduced molecular bonding different conduction mechanism are obtained, including transition from weak to strong Anderson localization [2,3], as well as spin-dependent phenomena[4]. Experimental results[5] supporting the interpretation as a metal-insulator in the case of ozone treatment are also provided.

References

[1] H. Ishii, F. Triozon, N. Kobayashi, K. Hirose, and S. Roche, C. R. Physique **10**, 283 (2009)
[2] N. Leconte, J. Moser, P. Ordejon, H. Tao, A. Lherbier, A. Bachtold, F. Alsina, C.M. Sotomayor Torres, J.-C. Charlier, and S. Roche, ACS Nano **4**, 7, 4033-4038 (2010)
[3] N. Leconte, P. Ordejon, A. Lherbier, J.-C. Charlier, and S. Roche (in preparation)
[4] N. Leconte, D. Soriano, P. Ordejon, J.J. Palacios, J.-C. Charlier, and S. Roche (submitted)
[5] J. Moser, H. Tao, S. Roche, F. Alsina, C.M. Sotomayor Torres, and A. Bachtold, Phys. Rev. B **81,** 205445 (2010)

Figures
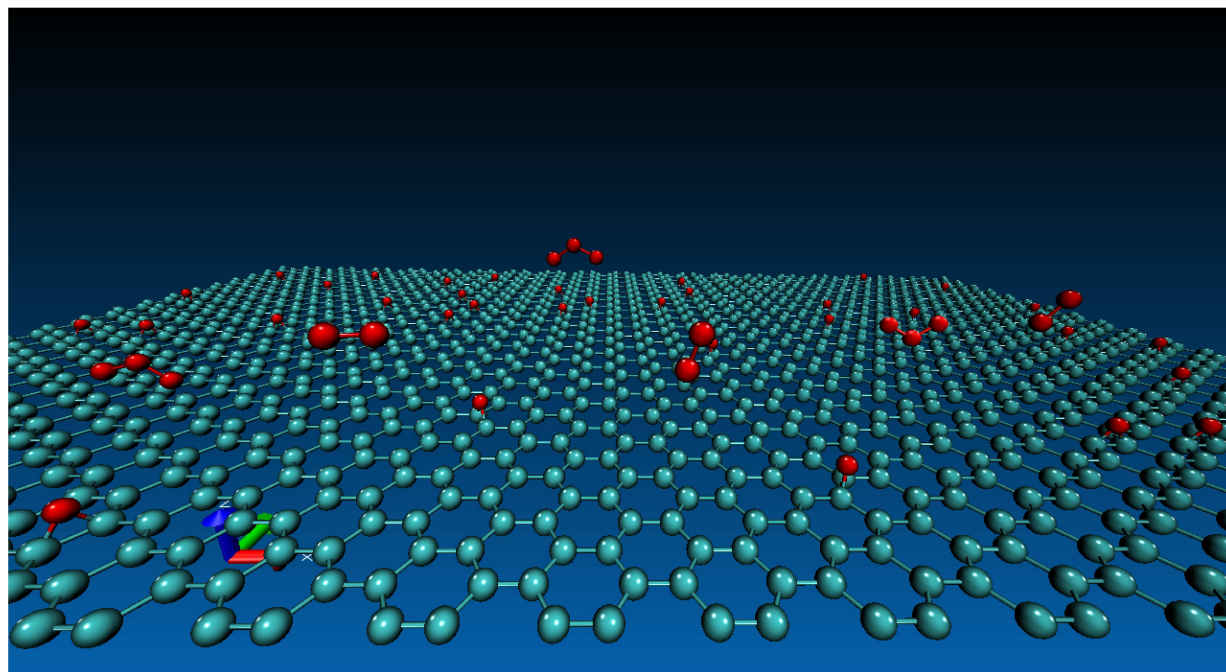
Functionalization of graphene due to ozone treatment

Thermal conductivity of suspended single-layer graphene measured by Raman spectroscopy

Jae-Ung Lee,[1] Duhee Yoon,[1] Hakseong Kim,[2] Sang Wook Lee,[2] and Hyeonsik Cheong[1,*]

[1]*Department of Physics, Sogang University, Seoul 121-742, Korea,*
[2]*Division of Quantum Phases and Devices, School of Physics, Konkuk University, Seoul 143-701, Korea*
hcheong@sogang.ac.kr

Since Balandin et al. first reported an extremely large value for the thermal conductivity of ~5,000 $Wm^{-1}K^{-1}$ for single layer graphene [1], the superior thermal properties of graphene has attracted much interest. Several groups since have measured thermal conductivity of mechanically exfoliated [1-3] or chemical vapor deposition (CVD)-grown [4,5] graphene using different methods. For suspended, exfoliated single-layer graphene, the reported values range between 660 and 5,300 $Wm^{-1}K^{-1}$ [1,2]. Given the importance of this key parameter for device applications, an accurate measurement is crucial. In this work, we present the measurement of the thermal conductivity for suspended single-layer graphene at temperatures between 300 K and 500 K using Raman spectroscopy on a clean sample prepared directly on a patterned substrate without involving a transfer process.

The substrates with round holes with various diameters were prepared by photolithography and dry etching of Si substrates covered with a 300 nm-thick SiO_2 layer. The depth of the holes is ~1.7 µm, deep enough to prevent interference from laser light reflected and scattered from the bottom of the holes [6]. The diameters were 2.6, 3.6, 4.6, and 6.6 µm. The samples were prepared directly on the cleaned substrate by mechanical exfoliation from natural graphite flakes. No chemical treatment of the sample was involved in the preparation process. This ensures that the sample surface is free from chemical contaminants that may affect the measured thermal conductivity values. The sample used was a single-layer graphene flake of 35×60 µm^2 dimensions identified by the Raman spectrum [7,8]. The 514.5-nm (2.41 eV) beam of an Ar ion laser was focused onto the graphene sample by a 50× microscope objective lens (N.A. 0.8), and the scattered light was collected and collimated by the same objective. The laser spot size was measured using the modified knife-edge method [5], and the beam spot size was approximately 0.29 µm in radius. The scattered signal was dispersed with a Jobin-Yvon Triax 550 spectrometer (1800 grooves/mm) and detected with a liquid-nitrogen-cooled charge-coupled-device detector. The spectral resolution was about 0.7 cm^{-1}.

The light absorption induces local heating that raises the temperature in the vicinity of the laser spot. In a steady state, there exists a temperature gradient that depends on the total power supplied by the laser beam, thermal conductivity, and the boundary conditions at the edge of the hole. The local temperature at the laser spot can be estimated from the Raman spectrum. The temperature coefficients of the *G* and 2*D* bands for suspended graphene were measured recently by Chen *et al.* [4]. Since the 2*D* band is more sensitive to temperature than the *G* band, we used the 2*D* band for the estimate of the temperature. As the laser power increases, the 2*D* frequency redshifts due to increased heating.

In order to estimate the thermal conductivity, we used the heat diffusion equation ignoring the heat conduction to the ambient air. We considered heat conduction through suspended graphene and graphene on the substrate as well as between graphene and the substrate. The substrate is assumed to be a heat sink at the ambient temperature. From analyses with the heat diffusion equation, we estimated the thermal conductivity of suspended graphene. It decreases as the temperature increases: from ~2000 $Wm^{-1}K^{-1}$ near 300 K to ~690 $Wm^{-1}K^{-1}$ at 500 K.

References

[1] A. A. Balandin, S. Ghosh, W. Z. Bao, I. Calizo, D. Teweldebrhan, F. Miao, and C. N. Lau, Nano Lett. **8** (2008) 902.

[2] C. Faugeras, B. Faugeras, M. Orlita, M. Potemski, R. R. Nair, and A. K. Geim, ACS Nano **4** (2010) 1889.

[3] J. H. Seol, I. Jo, A. L. Moore, L. Lindsay, Z. H. Aitken, M. T. Pettes, X. S. Li, Z. Yao, R. Huang, D. Broido, N. Mingo, R. S. Ruoff, and L. Shi, Science **328** (2010) 213.

[4] S. Chen, A. L. Moore, W. Cai, J. W. Suk, J. An, C. Mishra, C. Amos, C. W. Magnuson, J. Kang, L. Shi and R. S. Ruoff, ACS Nano (2010) DOI: 10.1021/nn102915x.

[5] W. W. Cai, A. L. Moore, Y. W. Zhu, X. S. Li, S. S. Chen, L. Shi, and R. S. Ruoff, Nano Lett. **10** (2010) 1645.

[6] D. Yoon, H. Moon, Y. W. Son, J. S. Choi, B. H. Park, Y. H. Cha, Y. D. Kim, and H. Cheong, Phys. Rev. B **80** (2009) 125422.

[7] A. C. Ferrari, J. C. Meyer, V. Scardaci, C. Casiraghi, M. Lazzeri, F. Mauri, S. Piscanec, D. Jiang, K. S. Novoselov, S. Roth, and A. K. Geim, Phys. Rev. Lett. **97** (2006) 187401.

[8] D. Yoon, H. Moon, H. Cheong, J. S. Choi, J. A. Choi, and B. H. Park, J. Korean Phys. Soc. **55** (2009) 1299.

Figures
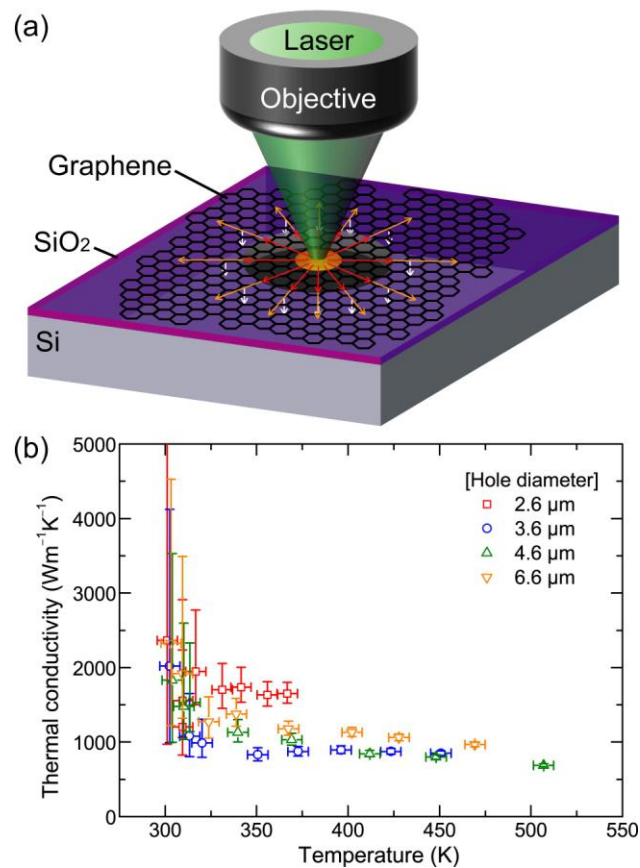
(a) Schematic diagram of experiment which measured the thermal conductivity of suspended pristine graphene. (b) Estimated the thermal conductivity of graphene as a function of temperature.

Interaction between Metal and Graphene: Dependence on the Layer Number of Graphene

Jisook Lee,[†] Konstantin S. Novoselov,[‡] and Hyeon Suk Shin[†,]*

[†]Interdisciplinary School of Green Energy, Ulsan National Institute of Science and Technology (UNIST), Banyeon-ri 100, Ulsan 689-805, Korea. [‡] School of Physics and Astronomy, University of Manchester, Oxford Road, Manchester, M13 9PL, UK

shin@unist.ac.kr

One of important themes in recent graphene-based research is to investigate changes in physicochemical properties of graphene as a function of the layer number.[1,2] In this presentation we show surface-enhanced Raman scattering (SERS) of graphene was investigated by depositing Au and Ag nanoparticles using thermal evaporation.[3,4] With increasing the number of graphene layers, the SERS enhancement factor of the G band decreased; 1L > 2L> 3L. Also, the interaction between graphene and metal was investigated by studying the G band splitting in SERS spectra of single-, bi-, and tri-layer graphene. In particular, the G band was split into two distinct peaks in the SERS spectrum of graphene. The extent of the G band splitting was 13.0 cm^{-1} for single-layer, 9.6 cm^{-1} for bi-layer and 9.4 cm^{-1} for tri-layer graphene, whereas the G band in the SERS spectrum of thick multi-layer was not split. These results indicate that there is a correlation between the SERS enhancement factor and the extent of the G band splitting, and the strongest interaction occurs between metal nanoparticles and single-layer graphene. Furthermore, the Ag and Au deposition on graphene can induce doping of graphene. The intensity ratio of 2D and G bands (I_{2D}/I_G) decreased after the metal nanoparticles deposition on graphene, indicating doping of graphene. From changes in positions of G and 2D bands after the metal deposition on graphene, the Ag deposition induced n-doping of graphene, whereas the Au deposition p-doping.

References
 [1] Jung, N. Kim, N. Jockusch, S. Turro, N. J. Kim, P. Brus, L. *Nano Lett.*, **9**, (2009), 4133.
[2] Pollak, E. Geng, B. Jeon, K.-J. Lucas, I. T. Richardson, T. J. Wang, F. Kostecki, R. *Nano Lett*. **10**, (2010), 3386.
[3] Lee, J. Shim, S. Kim, B. Shin, H. S. Chem. Eur. J., DOI: 10.1002/chem.201002027.
[4] Lee, J. Novoselov, K. S. Shin, S. H. ACS Nano., DOI: 10.1021/nn103004c

Figure
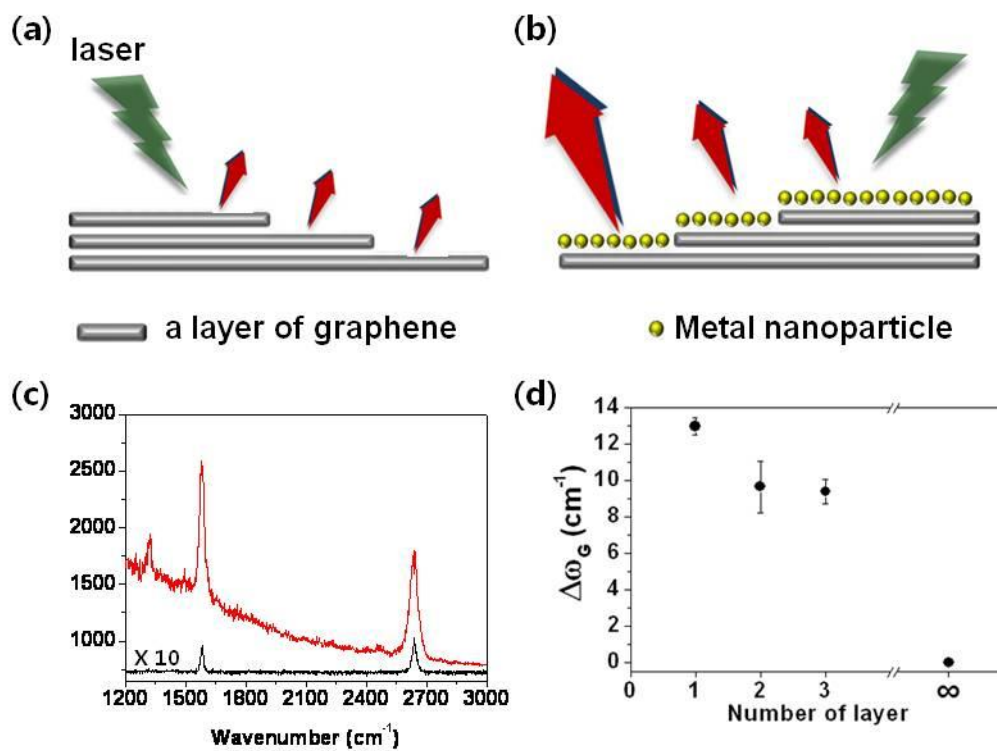
Figure 1. Schematic illustration of the interaction between metal and graphene depending on the number of the graphene layers (a) before and (b) after metal deposition. (c) SERS (red curve) and normal Raman (black curve) spectra of single layer graphene on which Au of 4 nm was deposited and (d) the extent of G band splitting after deposition of Ag nanoparticles depending on the graphene layers.

Nucleation and growth of magnetic nanoclusters on graphene moiré

Philipp Leicht[1], Muriel Sicot[1], Samuel Bouvron[1], Ole Zander[1], Thomas Tietze[2], Eberhard Goering[2], Yuriy Dedkov[3] and Mikhail Fonin[1]

[1]Fachbereich Physik, Universität Konstanz, Germany
[2]Max-Planck-Institut für Metallforschung, Stuttgart, Germany
[3]Fritz-Haber-Institut der Max-Planck Gesellschaft, Berlin, Germany

philipp.leicht@uni-konstanz.de

Arrays of magnetic nanoclusters can have important technological implications, such as magnetic recording media for the new generation high-density data storage applications. In a search for an appropriate non-magnetic template for cluster arrays, van-der-Waals surfaces are a promising alternative to the reconstructed noble-metal surfaces. Recently, a new two-dimensional form of boron-nitride was discovered [1]: highly regular structure of hexagonal boron nitride with a 3 nm periodicity and a 2 nm hole size can be formed by self-assembly on Rh(111). Graphene was also shown to form Moiré superstructures, with a periodicity of about 3 nm as a result of lattice mismatch, on Ir(111) [2] and Rh(111) [3] surfaces. This regular graphene nanostructure can serve as a template for the preparation of monodisperse nanocluster arrays [2], e.g., magnetic nanoclusters (NCs) [3]. On the other hand magnetic materials in contact with graphene are of interest for spintronic applications such as spin filter e.g. [4]. In this work, we use a graphene moiré grown on Rh(111) or Ir(111) as a template. Submonolayers of ferromagnetic metals including Ni, Fe and Co are deposited on the graphene moiré template at room temperature and at low temperature around 150 K and are investigated by scanning tunneling microscopy (STM) and by x-ray magnetic circular dichroism (XMCD). Additionally, we study the process of intercalation of ferromagnetic materials underneath the graphene layer.

In the first step a graphene layer is prepared on the metallic surface by thermal decomposition of hydrocarbons. Subsequently ferromagnetic metals are deposited on the graphene surface. Fig. 1 (a) shows STM topographs of a small amount of Ni deposited on graphene/Rh(111) at 150 K. Large terraces and steps of graphene/Rh(111) covered with Ni nanoclusters (NCs) can be clearly distinguished. The NCs show mostly hemispherical shapes with at least some cluster edges which appear to be oriented along the in-plane < 1-10 > direction. The apparent height of the clusters was measured to be 0.85 ± 0.1nm which roughly corresponds to four fcc (111) planes of Ni. The diameter distribution of the clusters is very narrow with the average cluster diameter being 3.1 nm. Most of the Ni clusters were found to be located on the regular grid showing a quite high unit cell occupation probability for the deposited amount. However, the nucleation of NCs obviously occurs at two different regions within the moiré unit cell (top-fcc and top-hcp). The randomized occupation can be attributed to the fact that the deposition temperature of 150 K is below the optimum temperature. Upon increasing Ni coverage no visible order of the cluster arrangement can be realized. At higher coverage Ni clusters exhibit a distinctly different size distribution compared with that at lower coverage. The lateral size of the clusters is more spread.

Ni deposited at room temperature exhibits a completely different growth mode compared with deposition at 150 K. Instead of small compact NCs, Ni forms triangular-shaped islands with their edges roughly aligned with the close packed < 1-10 > directions of the Rh(111) substrate as shown in Fig. 1 (b). The existence of large islands nucleated at terraces indicates that Ni atoms are highly mobile on the graphene surface at room temperature. On the other hand, it is remarkable that, in spite of the weak bonding strength between Ni and the graphene surface, the moiré structure imposes registration and orientation on the Ni nanostructures. The average apparent height of the islands is 1.8 nm and the size defined by the length of the edges is ranging from about 5 nm to about 18 nm.

Deposition on graphene on Rh(111) at room temperature shows significant differences in the growth mode for Ni compared to Fe and Co [compare Fig. 1 (b) and (c)]. Whereas Ni preferentially forms flat triangles with alignment to the moiré structure of the graphene template, the growth of Fe clusters shows only little faceting. In the case of Ni/Gr/Rh(111) the clusters are of order 20 nm in size and show

a broad size distribution. For Fe/Gr/Rh(111) the clusters are slightly smaller, around 8 nm. XMCD measurements on the Ni clusters are currently in progress to study the impacts of the different geometries on the spin and orbital moments and on magnetic anisotropies.

Partial intercalation of the room temperature grown Ni and Fe clusters can occur upon soft annealing and yields mono-atomically thick epitaxial islands incorporated between substrate and graphene layer. The moiré structure of the graphene layer is preserved on top of the intercalated clusters. In the intercalated state both materials show a strong alignment of the borders to the moiré structure.

References

[1] M. Corso et al., Science **303** (2004), 217
[2] A. T. N'Diaye et al., Phys. Rev. Lett. **97** (2006), 215501
[3] M. Sicot et al., Appl. Phys. Lett. **96** (2010), 093115
[4] V. M. Karpan et al., Phys. Rev. B **78** (2008), 195419

Figures
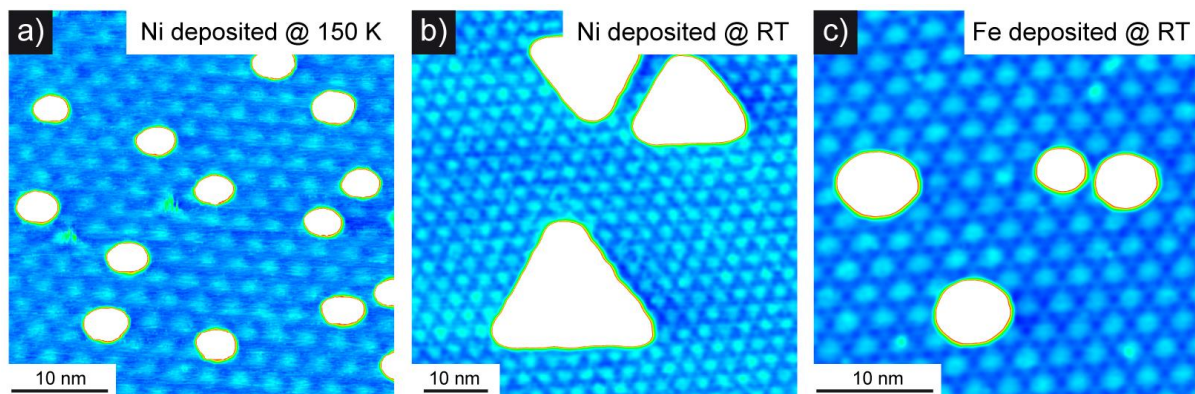
Fig. 1 *(a) STM topograph (40 nm x 40 nm; U=1.03 V; I=0.13 nA) of Ni nanoclusters deposited at 150 K on Gr/Rh(111)   (b) STM topograph (60 nm x 60 nm; U=1.54 V; I=1.14 nA) of Ni clusters deposited at room temperature on Gr/Rh(111)   (c) STM topograph (33 nm x 33 nm; U=1.11 V; I=0.49 nA) of Fe clusters deposited at room temperature on Gr/Rh(111)*

Exfoliation of graphene in solvent free conditions by ball-milling

V. León-Castellanos,[1] M. Quintana,[2] M. A. Herrero,[1] M. Prato,[*2] E. Vazquez[*1]

[1]Departamento de Química Orgánica-IRICA, Facultad de Química, Universidad de Castilla-La Mancha, 13071 Ciudad Real, Spain
[2]Dipartamento di Scienze Farmaceutiche, Università degli Studi di Trieste, Piazzale Europa 1, 34127 Trieste, Italy

Veronica.Leon@uclm.es

Graphene, a single thick perfectly two-dimensional lattice of sp^2 carbon atoms, has emerged in recent years as a novel class of nanomaterial with remarkable electronic and mechanical properties. However, a major obstacle of graphene materials is the preparation of a single-layer graphene and its inherent lack of solubility. These two handicaps make difficult the handling and manipulation during processing.

We present a scalable and easy technique for exfoliation of graphite flakes in the presence of melamine. This methodology permits the exfoliation of single- and few-layer graphene sheets by ball-milling processes under absence of solvent. Afterwards, the materials were suspended in a variety of aqueous solutions and organic solvents by means of soft sonication conditions. This procedure presents a powerful approach in order to form stable dispersions of single- and few-layer graphene sheets for several days. Layers of graphene were characterized by several techniques such as UV-vis spectrometry, Raman spectrometry, thermogravimetric analysis and transmission electron microscopy. This new approach opens the way to carry out different organic reaction on stable graphene sheets, in order to produce specific structures for several applications.
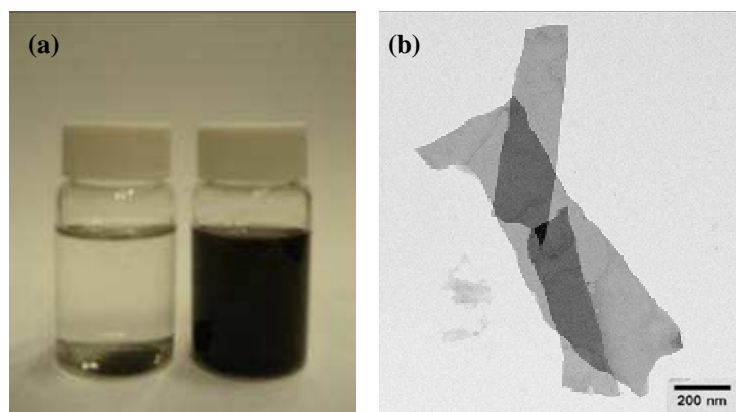
Figure: (a) Graphite in dimethylformamide (left) and graphene in dimethylformamide (right). (b) TEM image of graphene flakes.

Electronic Transport in Two-dimensional Graphene with Structural Defects.

Aurélien Lherbier[1,2], Simon M.-M. Dubois[1,3], Xavier Declerck[1,2],
Stephan Roche[4,5], Yann-Michel Niquet[6], and Jean-Christophe Charlier[1,2]

[1] Université Catholique de Louvain (UCL), Institute of Condensed Matter and Nanoscience (IMCN),
Place Croix du Sud 1 (NAPS-Boltzmann), 1348 Louvain-la-Neuve, Belgium
[2] European Theoretical Spectroscopy Facility (ETSF)
[3] University of Cambridge, Cavendish Laboratory, Theory of Condensed Matter group,
JJ Thomson Avenue, Cambridge CB3 0HE, United-Kingdom
[4] Institut Català de Nanotecnologia (ICN) and CIN2, UAB Campus, E-08193 Barcelona, Spain
[5] Institució Catalana de Recerca i Estudis Avançats (ICREA), 08010 Barcelona, Spain and
[6] CEA-UJF, INAC, SP2M/L_Sim, 17 rue des Martyrs, 38054 Grenoble Cedex 9, France

aurelien.lherbier@uclouvain.be

Graphene, a single carbon plane arranged on a honeycomb lattice, has sparked out a lot of activities both from experimental and theoretical point of view in the last few years. The striking physical properties of this recent material are due to a peculiar electronic structure which yields notably to room temperature quantum hall effect, large coherence length and a high electronic mobility.

Graphene is expected to become a material of choice for future nanoelectronics. Nevertheless, this requires the capability to fine control the electronic and transport properties of this material.

Graphene is also an excellent platform to investigate the fundamental aspects of the localization phenomena. The existence of pseudospin is expected to induce weak antilocalization.

Parametrized on ab initio calculations, a tight-binding model for graphene with structural defects is used to study its transport properties with an order-N real-space Kubo-Greenwood formalism [1,2]. It is shown that a **large plateau of minimum of conductivity** is developed for 1% of Stone-Wales and divacancies defects (Fig.1). The structural defects are characterized by **strong resonant scattering** energies [3,4,5] which yield to an enhanced contribution of quantum interferences leading to strong localization effects. Rather short localization lengths suggest that Anderson localization should be observable in two dimensional irradiated graphene containing such structural defects.

References

[1] S. Roche, D. Mayou, Phys. Rev. Lett. ,**79** (1997) 2518
[2] A. Lherbier, X. Blase, Y. M. Niquet, F. Triozon, S. Roche, Phys. Rev. Lett. ,**101** (2008) 036808
[3] T. O. Wehling, S. Yuan, A. I. Lichtenstein, A. K. Geim, M. I. Katsnelson, Phys. Rev. Lett. ,**105** (2010) 056802
[4] Y. V. Skrypnyk, V. M. Loktev, Phys. Rev. B , **82** (2010) 085436
[5] A. Lherbier, S.M.-M. Dubois, X. Declerck, S. Roche, Y.M. Niquet, J.-C. Charlier, submitted to Phys. Rev. Lett.

Figures
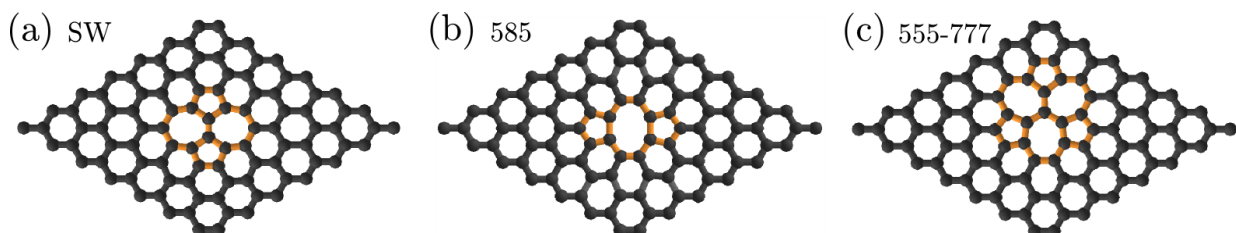
Figure 1: Three structural defects in graphene:
(a) Stone-Wales, (b) Divacancy 585, and (c) Divacancy 555-777

Topological origin of subgap conductance in insulating bilayer graphene

Jian Li,[1] Ivar Martin,[2] Markus Büttiker,[1] and Alberto F. Morpurgo[3]

1 Département de Physique Théorique, Université de Genève, CH-1211 Genève 4, Switzerland
2 Theoretical Division, Los Alamos National Laboratory, Los Alamos, New Mexico 87545, USA
3 DPMC and GAP, Université de Genève, CH-1211 Genève 4, Switzerland

Jian.Li@unige.ch

The edges of graphene-based systems possess unusual electronic properties, originating from the non-trivial topological structure associated to the pseudo-spinorial character of the electron wave-functions. These properties, which have no analogue for electrons described by the Schrodinger equation in conventional systems, have led to the prediction of many striking phenomena, such as gate-tunable ferromagnetism and valley-selective transport [1-3]. In most cases, however, the predicted phenomena are not expected to survive the influence of the strong structural and chemical disorder that unavoidably affects the edges of real graphene devices. Here, we present a theoretical investigation of the intrinsic low-energy states at the edges of electrostatically gapped bilayer graphene (BLG), and find that the contribution of edge modes to the linear conductance of realistic devices remains sizable even for highly imperfect edges (see Figure 1 below). This contribution can dominate over that of the bulk for sufficiently clean devices, such as those based on suspended BLG samples. Our results illustrate the robustness of phenomena whose origin is rooted in the topology of the electronic band-structure, even in the absence of specific protection mechanisms.

References

[1] Y. Son, M. L. Cohen, and S. G. Louie, Nature **444** (2006), 347–349.
[2] A. Rycerz, J. Tworzydlo, and C. W. J. Beenakker, Nature Phys. **3** (2007), 172–175.
[3] F. Guinea, M. I. Katsnelson, and A. K. Geim, Nature Phys. **6** (2010), 30–33.

Figures
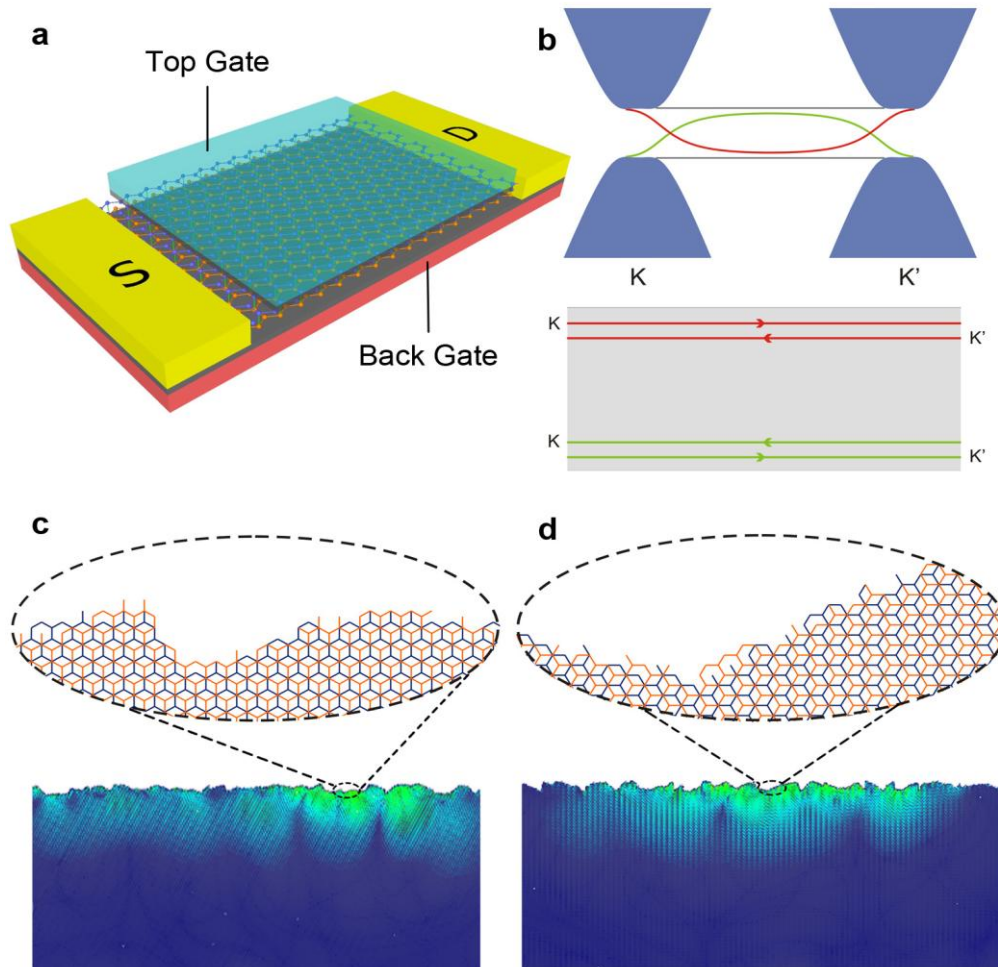
*Figure 1: **Edge states in gapped BLG.** Panel **a** shows a schematic view of the device. By controlling the gate voltages applied to the top and back gates separately, an energy gap in the bulk of BLG can be opened and tuned, while maintaining the Fermi energy in its center. Panel **b** shows the dispersion of the sub-gap edge states in gapped BLG at a zig-zag edge. At both edges, the states are helical with respect to the valley degree of freedom, with states in opposite valleys propagating in opposite directions. This conclusion holds for periodic edges of rather general shape (i.e. not only for zig-zag), but it does not hold for the ideal armchair edge, where two valleys (K and K') are fully coupled and no sub-gap edge states are present. Panels **c** and **d** show the typical probability density near zero energy for strongly disordered BLG zig-zag (**c**) or armchair (**d**) edges. In the presence of realistically strong disorder, the existence of such edge states -- and their long localization length -- is a universal property of gapped BLG (the panels correspond to a BLG that is approximately 100 nm long).*

Electronic and Magnetic Properties of Hybrid Graphene Nanoribbons

Yafei Li,[†] Zhen Zhou,[†,*]

Institute of New Energy Material Chemistry, Key Laboratory of Advanced Energy Materials Chemistry (Ministry of Education), Nankai University, Tianjin 300071, China

zhouzhen@nankai.edu.cn

Using spin-polarized first-principles computations, we have systematically studied the electronic and magnetic properties of a new class of infinitely long hybrid graphene nanoribbons (HGNRs), which are constructed on the basis of experimentally-observed zigzag/armchair graphene nanoribbon heterojunctions.[1] HGNRs are initially nonmagnetic semiconductors, and then covert to magnetic semiconductors with increasing the length of zigzag segments. Interestingly, although the edge states of two zigzag edges in HGNRs are antiferromagnetically coupled to each other, the magnetization on two edges is not equal. Further investigation demonstrates that the electronic properties of HGNRs are mainly controlled by the zigzag segment length and the ribbon width. The electronic properties of nonmagnetic HGNRs are rather robust to the external electronic field. In contrast, the electronic properties of magnetic HGNRs are rather sensitive to external electronic field, and intrinsic half metallictiy can be realized under a critical value of 0.8 V/Å.

References

[1] Jia, X.; Hofmann, M.; Meunier, V.; Sumpter, B. G.; Campos-Delgado, J.; Romo-Herrera, J. M.; Son, H.; Hsieh, Y. P.; Reina, A.; Kong, J.; Science, **323** (2009), 1701–1705.

Figures
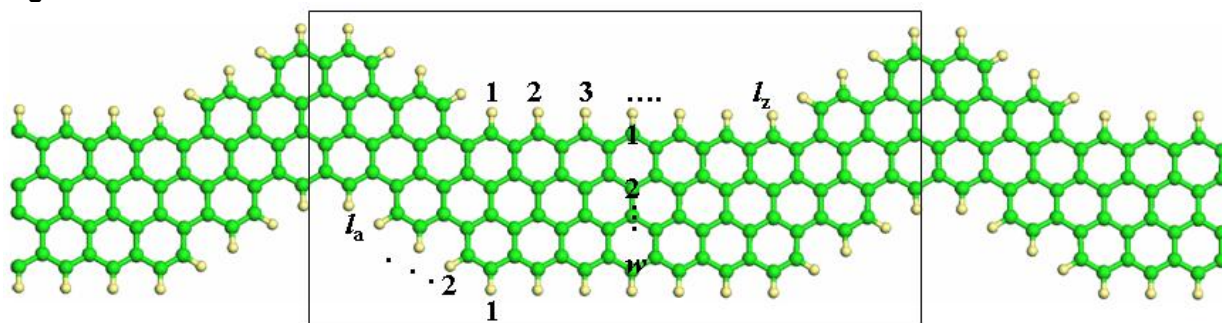
Atomic structure of HGNR (l_z,l_a,w). Carbon and hydrogen atoms are denoted with green and light yellow balls, respectively. The rectangle marks one-unit supercell in the ribbon axis direction.

Thermally-Limited Current Carrying Ability of Graphene Nanoribbons

Albert D. Liao[1], Justin Wu[2], Xinran Wang[2], Kristof Tahy[3], Debdeep Jena[3], Hongjie Dai[2], Eric Pop[1]

[1]*Dept. of Electrical & Computer Eng., Univ. Illinois at Urbana-Champaign, Urbana, IL 61801, USA*
[2]*Dept. of Chemistry & Lab for Advanced Materials, Stanford University, Stanford, CA 94305, USA*
[3]*Dept. of Electrical Engineering, University of Notre Dame, Notre Dame, IN 46556, USA*
aliao@illinois.edu

Graphene nanoribbons (GNRs) are essential building blocks of future graphene electronics [1], however many unknowns persist about their electrical and thermal properties. Among these, the maximum current density of GNRs and their behavior under high-field transport are of both fundamental and practical importance. Here, we measure current densities of GNRs up to ~3 mA/μm near breakdown, but ultimately find that heat dissipation is the key mechanism limiting transport and reliability. Finally, we extract the GNR thermal conductivity for the first time, k ~ 80 W/m/K or more than an order of magnitude lower than that of 2-D graphene [2-4], most likely limited by edge roughness scattering.

GNRs devices (predominantly bilayer) with two-terminal Pd contacts were prepared from multi-wall carbon nanotubes [1] on SiO_2(300 nm)/Si substrates (Fig. 1). High-field measurements were combined with breakdown thermometry analysis [5] used previously for carbon nanotubes. Breakdown was carried out by applying an increasing DC voltage between source and drain until the device breaks irreversibly from Joule heating and oxidation in air (Fig. 1B). The breakdown temperature of graphene and nanotubes in air is known, T_{BD} ~ 600 ^{o}C [5]. In addition, the gate voltage is set at V_G = -40 V to minimize hysteresis (Fig 1C). Similar devices of micron-sized 2-D exfoliated graphene (ex-G) were studied as well.

We find that the device breakdown power (P_{BD}) increases with the square root of the device surface area (Fig. 2A). To understand this trend, a self-heating model is used to predict the breakdown power, P_{BD} in our devices. The calculations take into account the Joule heat dissipated into the oxide, the contacts, as well as within the GNR itself. We note that our model is in good agreement with our data. Examining Fig. 2A, we note that data for GNRs < 0.3 μm varies more than that for graphene > 0.3 μm. The spread in the data can be described by varying the graphene thermal conductivity, k in the model, thus pointing out the increased role this parameter has on power dissipation at small dimensions.

In Fig. 2B we plot the breakdown current density (I_{BD}/W) vs. device width. The results show that the maximum current density scales inversely with width, and can reach >3 mA/μm for GNRs ~15 nm wide. To find the cause of this trend, we study how the total thermal conductance per unit area, G'' and the thermal conductance per unit area into the underlying substrate, h scale with width in Figs. 3A and 3B. From both figures, we observe a similar inverse scaling with width for both h and G'' as we did for the current density. Such dependence can be explained by Figs. 3C-E. Figure 3C diagrams how heat is dissipated both into the contacts and into the underlying substrate. In addition, we find that for larger 2-D graphene sheets >0.3 μm (Fig. 3D), dissipation occurs mainly 'vertically down' into the SiO_2. However for narrow GNRs (Fig. 3E), the lateral heat spreading into the SiO_2 becomes a significant contributor for dissipation, leading to an increase of G'', the total thermal conductance per unit area.

Likewise, heat dissipated in GNRs at high field depends on the thermal conductivity (k) and length (L) of each sample, as indicated by Figs. 3A and 3B. Here, GNR lengths were L = 0.2-0.7 μm. By fitting the measured breakdown power and current density with our thermal breakdown model, we extracted the GNR thermal conductivity for the first time. We found the range k = 63-450 W/m/K for our 15 GNR samples, with a median k ~130 W/m/K at T_{BD} ~ 600 ^{o}C, or k ~ 78 W/m/K at 20 ^{o}C, estimated from the T dependence of heat capacity [5]. The thermal conductivity of such GNRs is an order of magnitude lower than that of "large" 2-D graphene [2-4] on SiO_2 (Fig. 4). The reduction of k suggests a strong effect of edge scattering on high-field and thermal transport in narrow GNR transistors.

References

[1] L. Jiao *et al*, Nat. Nanotech., **5** (2010) 321.
[2] S. Ghosh *et al*, Nat. Mat., **9** (2010) 555.
[3] J. H. Seol *et al*, Science, **328** (2010) 213.
[4] W. W. Cai *et al*, Nano Letters, **10** (2010) 1645.
[5] A. Liao *et al*, Phys. Rev. B, **82** (2010) 205406.

Figures
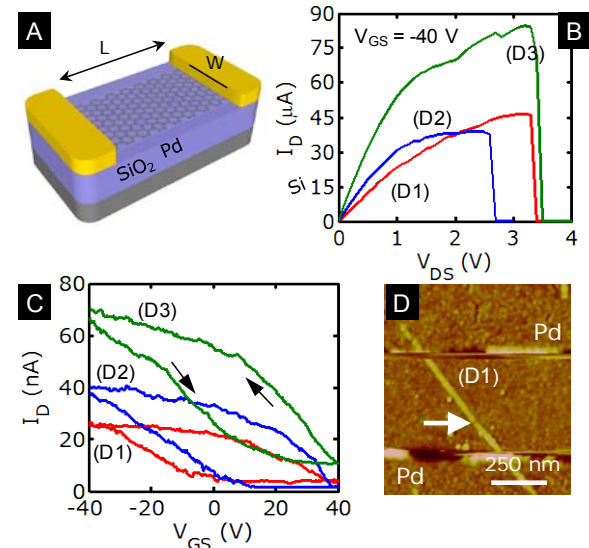
Fig. 1. (A) Schematic of typical graphene device used in this work. (B) Measured current-voltage (I_D-V_{DS}) up to breakdown of GNRs in air; dimensions are (D1) W = 20 nm, L = 510 nm, (D2) W = 16 nm, L = 590 nm, and (D3) W = 38 nm, L = 390 nm. (C) Corresponding I_D-V_{GS} transfer curves display typical hysteresis in air (arrows show sweep direction). Data in (B) were taken at V_{GS} = -40 V where hysteresis is minimal. (D) AFM image of GNR device D1 after high-current sweep; white arrow shows breakdown location.
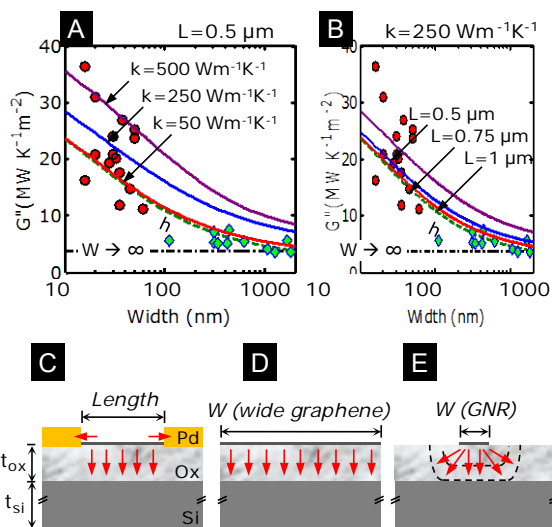
Fig. 3. Thermal conductance of device per unit area (G'') vs. width for graphene of varying (A) thermal conductivity and (B) length. Both parameters affect heat sinking along the device, as illustrated in (C), affecting sensitivity to in-plane k. Dashed lines show the modeled contribution from the graphene/SiO$_2$ thermal boundary conductance h; horizontal dash-dotted line is the limit for $W \to \infty$ which applies to the case shown in (D), only "vertical" heat sinking through oxide. The significance of lateral heat spreading from GNRs is shown in (E).
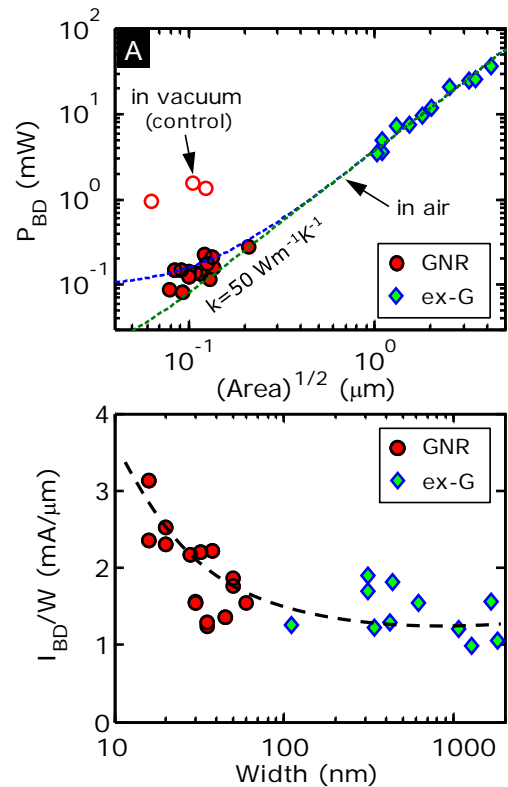
Fig. 2. (A) Scaling of breakdown power with square root of device footprint. Dashed lines are thermal model with k = 50 and 500 W/m/K. Lateral heat sinking and in-plane GNR thermal conductivity begin to play a role in devices < ~0.3 µm (also see Fig. 3). Heat sinking from larger 2-D exfoliated devices (ex-G) is entirely limited by the SiO$_2$. A few GNRs were broken in vacuum as a control group. (B) Scaling of maximum current vs. device width, demonstrating greater current density in narrower GNRs that benefit from 3-D heat spreading and lateral heat flow along the GNR (also see Fig. 3). Dashed line drawn to guide the eye.
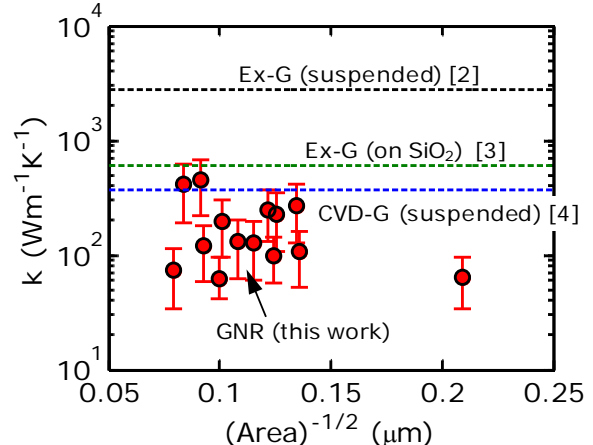
Fig. 4. Thermal conductivity of GNRs from this work, compared to large-area graphene measurements from literature [2-4]. The range obtained is 63–450 Wm^{-1}K^{-1} with a median of 130 W/m/K at the breakdown temperature (600 ^{o}C). The median value at room temperature is ~40% lower, or ~78 W/m/K, nearly an order of magnitude below that of large-sized exfoliated graphene on SiO$_2$ [3], illustrating the role of phonon-edge scattering.

Aharonov-Bohm effect in graphene having Aluminum mirrors

Niclas Lindvall[1*], Youngwoo Nam[2], Jai Seung Yoo[2], Yung Woo Park[2], Thilo Bauch[1], and August Yurgens[1]

[1]Department of Microtechnology and Nanoscience, Chalmers University of Technology, SE-412 96, Gothenburg, Sweden
[2]Department of Physics and Astronomy, Seoul National University, Seoul 151-747, Republic of Korea

niclas.lindvall@chalmers.se

We observe the Aharonov-Bohm (A-B) effect in graphene rings with aluminum (Al) mirrors. The Al pads acting as mirrors are deposited in two different configurations, either on the bias lines (L-mirrors) or in the perpendicular direction (T-mirrors). This is shown in Figure 1a and 1b. Graphene is fabricated using mechanical exfoliation of Kish graphite and patterned using e-beam lithography (ebl) and oxygen plasma. Electrodes and Al pads are also defined using ebl.

At temperatures down to 17 mK, we could observe up to the third harmonic of A-B oscillations in the case of L-mirrors and up to the second harmonic in the case of T-mirrors. This represents an enhancement of the visible phase coherence as compared to earlier A-B experiments on graphene[1]. A typical measurement of resistance with varying magnetic field at our base temperature is shown in Figure 1c. Small periodic oscillations are seen on top of the stronger aperiodic universal conductance fluctuations. In Figure 1d, the FFT spectrum for such measurements is shown for temperatures ranging from 17 mK to 1590 mK.

We observe the higher order harmonics at magnetic fields up to ~1 T which is lower than in previously reported experiments but still exceeds the superconducting critical field of Al. This indicates that it is not superconductivity which is responsible for the observed improved coherence. We believe instead that a large Fermi-energy mismatch between graphene and aluminum explains this. The Al pads act as mirrors, confining the electrons within the A-B ring making the higher number of revolutions more probable. From weak localization measurements we estimate the phase coherence length to be 1.1 μm and 1.4 μm for L- and T-mirrors, respectively.

Our measurements were performed at temperatures down to 17 mK which is lower than for previously reported A-B experiments on graphene. At such low temperature we also observe a small transport gap of less than 1 mV. Assuming Coulomb-blockade effects, the size of the gap can be reasonably explained.

References

[1] S. Russo, J. B. Oostinga, D. Wehenkel, H. B. Heersche, S. S. Sobhani, L. M. K. Vandersypen, and A. F. Morpurgo, Phys. Rev. B, **77** (2008) 085413.

Figures
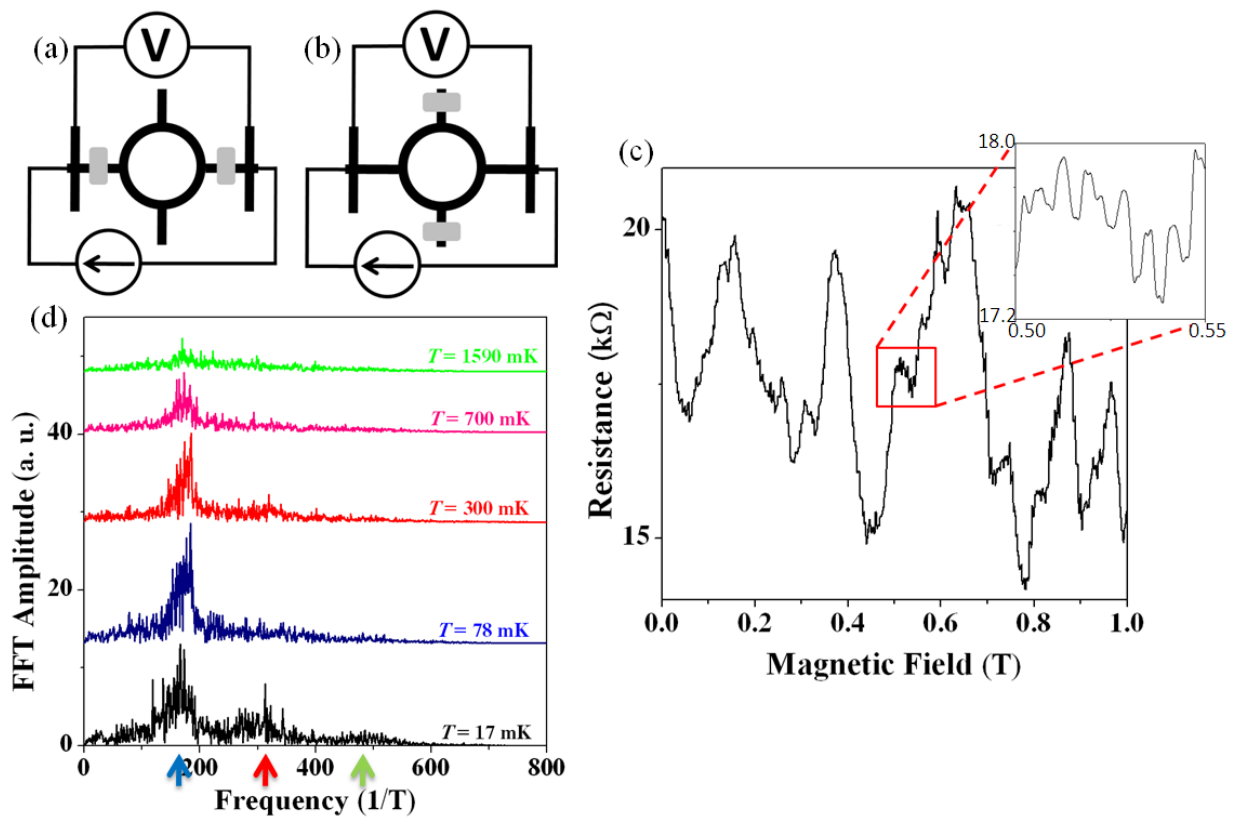
Figure 1: a), b) The graphene is shaped into a A-B ring with several electrodes connecting to it. The grey rectangles correspond to Al pads deposited on the bias lines (L-mirrors) or in the perpendicular direction (T-mirrors) as shown in a) and b), respectively. c) Resistance of a graphene structure with L-mirrors as a function of magnetic field at 17 mK. There are small periodic oscillations on top of the large aperiodic universal conductance fluctuations. d) FFT spectrum of traces such as that in c) for temperatures ranging from 17 mK to 1590 mK. At our base temperature of 17 mK, we can see up to the third harmonic and at 1590 mK the first harmonic is still visible. The blue, red and green arrows correspond to the first, second and third harmonic peak as estimated from the device geometry.

Quick purification of protein complexes for structural proteomics, using grpahene and single walled carbon nanotubes

Zunfeng Liu, Xiang Zhou, Elisabeth Meulenbroek, Willem-Jan Waterreus, Navraj Pannu, Jan Pieter Abrahams

Biophysical Structural Chemistry, Leiden University, Leiden, The Netherlands
liuz2@chem.leidenuniv.nl

In our postgenomic era, understanding of protein–protein interactions by characterizing the structure of the corresponding protein complex is becoming increasingly important. An important problem is that different protein complexes have different degrees of stability over time; many protein complexes have a half-life of only several or several tens of minutes. The typical purification methods for protein complexes, such as tandem affinity purification and multiple chromatographic separations, are time consuming and therefore are only suitable for stable protein complexes. Up till now, a quick and efficient protein complex purification method for 3D structure characterization has not been developed.

My new research-line aims at developing a quick and efficient method that is suitable for structural characterization of unstable protein complexes. In this project, single walled carbon nanotubes (SWNTs) and graphene oxide (GO) are used to 'fish' the target protein complex through affinity interaction by chemically binding affinity pairs on SWNTs and GO and the target protein complex respectively, as shown in Figure 1 A-E.

The protocol will be validated in single particle structure determination by cryo-EM, as shown in Figure 1 F-G. Any captured protein complex on a SWNT can be flash frozen and transferred into a cryo electron microscope (EM) for imaging without removal of the SWNTs, because SWNTs are compatible with EM characterization. The native structure of the protein complex can be kept intact during the whole process without any additional treatment.

We developed a novel method for preparing SWNT(GO)•streptavidin complexes via the biotin–streptavidin recognition.[1,2] Capturing biotinylated DNA, fluorophores, Au nanoparticles (NPs), and DNA/protein complexes on the SWNT (GO)•streptavidin complexes demonstrate their usefulness as a docking matrix, especially in our project, for purification of unstable protein complexes and structural characterization using cryo-electron microscopy.

References

Purification.

1. Zunfeng Liu, Linhua Jiang, Federica Galli, Igor Nederlof, René C. L. Olsthoorn, Gerda E. M. Lamers, Tjerk. H. Oosterkamp, Jan Pieter Abrahams.
   Adv. Funct. Mater. **2010**, 20, 2857.
2. Stable Single-Walled Carbon Nanotube−Streptavidin Complex for Biorecognition
   Zunfeng Liu, Federica Galli, Kjeld G. H. Janssen, Linhua Jiang, Heiko J. van der Linden, Daniel C. de Geus, Patrick Voskamp, Maxim E. Kuil, Rene C. L. Olsthoorn, Tjerk. H. Oosterkamp, Thomas Hankemeier and Jan Pieter Abrahams
   J. Phys. Chem. C **2010** 114 , 4345

Figures
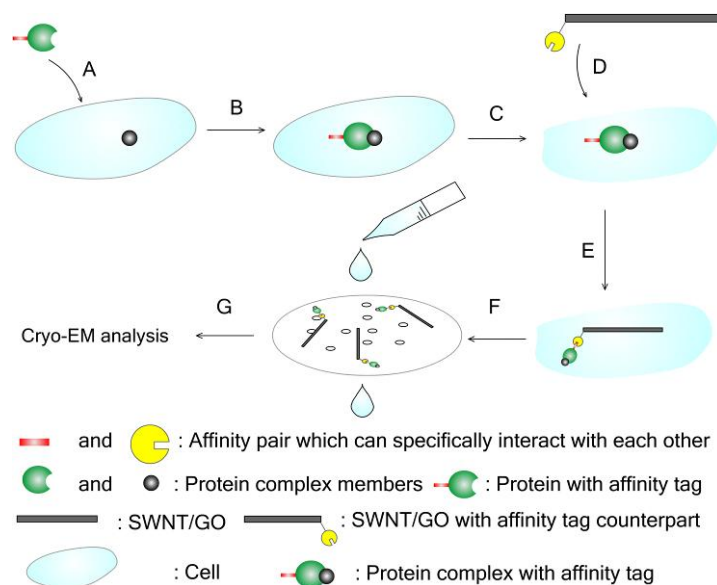
Figure 1 Schematic representation of capturing protein complex using SWNT and GO.

Hydrogen adsorption on palladium clusters deposited on graphene

María J.López[1], I.Cabria[1], S. Fraile[2], and J.A. Alonso[1]

[1] *Departamento de Física Teórica, Atómica y Óptica, University of Valladolid, Spain*

[2] *Departamento de Física Aplicada-LATUV, University of Valladolid, Spain*

maria.lopez@fta.uva.es

The Palladium might enhance hydrogen storage in porous carbons by surface reactions, especially by hydrogen spillover which consists in the dissociation-storage-recombination of hydrogen in the material. To gain some insight on the possible structures formed by palladium on nanoporous carbons, and on the role played by palladium in the storage of hydrogen, we have investigated the adsorption of palladium on a graphene surface and the adsorption and dissociation of molecular hydrogen on the Pd clusters. Density functional calculations show that, even at the earlier stages of Pd deposition on the graphene surface, the Pd atoms have a strong tendency to form clusters [1]. Three-dimensional clusters are more stable than planar clusters and the transition from planar to three-dimensional Pd clusters adsorbed on graphene occurs very early as a function of cluster size, at Pd_4. This tendency is a consequence of the strong Pd-Pd interaction. We have also investigated the adsorption and the dissociation of molecular hydrogen on the deposited Pd clusters as a function of cluster size. The mechanism for the activation of the hydrogen molecule and its possible subsequent dissociation is discussed. We also discuss the implications for the hydrogen storage capacity of Pd-doped nanoporous carbon materials.
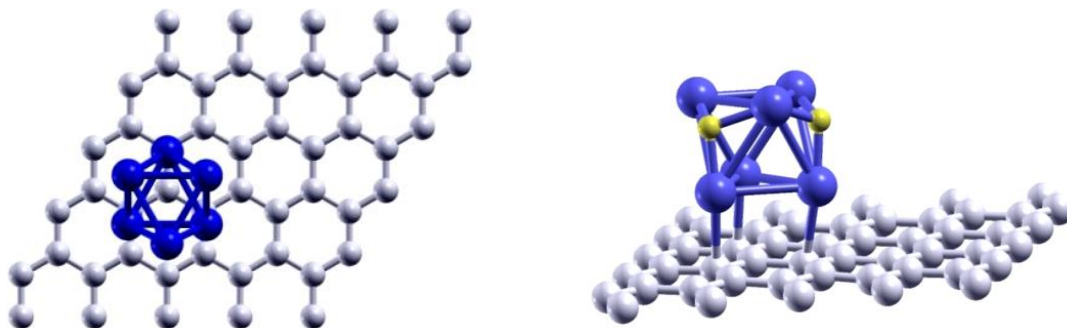
Figure 1: Pd_6 cluster deposited on graphene (left), and H_2 dissociated on the deposited Pd cluster (right).

References

[1] I. Cabria, M.J. López, and J.A. Alonso, Phys. Rev. B 81, 035403 (2010).

Harvesting energy from thermal noise through mechanical non-linearity of suspended graphene sheets

M. López-Suárez[1], R. Rurali[2], G.Abadal[1]

[1] Departament d'Enginyeria Electrònica, Universitat Autònoma de Barcelona (UAB), Bellaterra, 08193 Barcelona, Spain
miquel.lopez@uab.cat
[2] Institut de Ciència de Materials de Barcelona (ICMAB-CSIC),
Campus de Bellaterra, 08193 Bellaterra (Barcelona), Spain

It has been demonstrated that harvesting power from wide band noise energy sources can be more efficiently performed through non-linear bistable transducers [1]-[2], instead of using conventional linear micromechanical resonators. It is expected that the extrapolation of this concept to the energy extraction from thermomechanical noise [3]-[4] will need the small dimensions of a NEMS based transducer. In the present contribution a numerical model is proposed for the design of a bistable sheet of suspended graphene based on the analysis of its response to the thermomechanical noise driving force. As it is shown in Figure1, bistability behavior is obtained by the compression induced buckling of the suspended graphene layer. The mechanical characteristics of the grapheme sheet are defined by geometry, quality factor, Young modulus and density. The model allows solving numerically the motion equation of the bistable device when driven by the force associated to the thermomechanical noise (white and Gaussian).

A sweep of the compression parameter allows finding the maximum vibration amplitude (rms) of the grapheme sheet, which corresponds to the conditions of barrier height between potential wells that maximize the probability of the sheet to jump from one potential well to the other.

The shape of the potential energy, as a function of the out of plane displacement (z) of the sheet centre, is obtained from *ab initio* calculations. Figure 2 shows how this shape is modified depending on the intensity of the compression. With the appearance of the barrier, a bistable system is conformed, although the non compressed case is also nonlinear.

The motion equation to be solved numerically is the following:

$$m_{eff}\ddot{z} = -\frac{\partial V}{\partial z} - b\dot{z} + F_{noise}$$

Where $F_{noise} = \sqrt{\left(\frac{tw^2}{lQ}\right)\sqrt{16.7E\rho}(2k_BTB)}\xi(t)$ is the noise force where $\xi(t)$ represents a stochastic process, m_{eff} stands for the effective mass of the suspended sheet and b represents the mechanical damping of the system.

Figure 3 and 4 show the mechanical vibrational response to the noise force of such a system for different values of the compression. An evaluation of the vibration speed $\dot{z}_{rms}$ allows to determine the rms value of the mechanical power ($F_{rms} \cdot \dot{z}_{rms}$).

As it is shown in Figure 6, a local maximum of 6fW is harvested close to the optimal compression corresponding to the maximum vibration amplitud z_{rms}. However, an absolute maximum power around 7fW is obtained at 0% compression, which is consistent with the nonlinear shape of the potential energy in this conditions.

References

[1.] Cottone, F., Vocca, H., Gammaitoni, L., *Nonlinear energy harvesting.* Physical Review Letters, (2009). **102**, 080601.

[2.] Gammaitoni, L., Neri, I., and Vocca, H., *Nonlinear oscillators for vibration energy harvesting.* Applied Physics Letters, (2009). **94**: p. 164102.

[3.] Stowe, T., et al., *Attonewton force detection using ultrathin silicon cantilevers.* Applied Physics Letters, (1997). **71**(2): p. 288-290.

[4.] Cleland, A. and M. Roukes, *Noise processes in nanomechanical resonators.* Journal of Applied Physics, (2002). **92**: p. 2758.

Figures
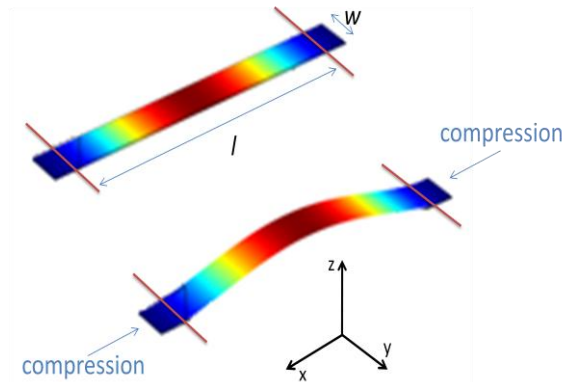
Figure 1: Non compressed and compressed suspended graphene sheet. Length l and width w.
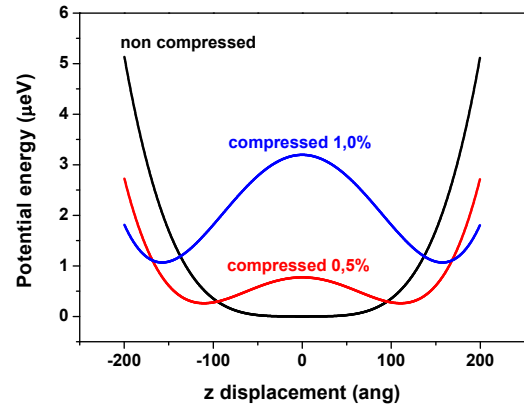
Figure 2: Potential energy vs. z displacement for different compression. l=300nm, w=0.25297nm
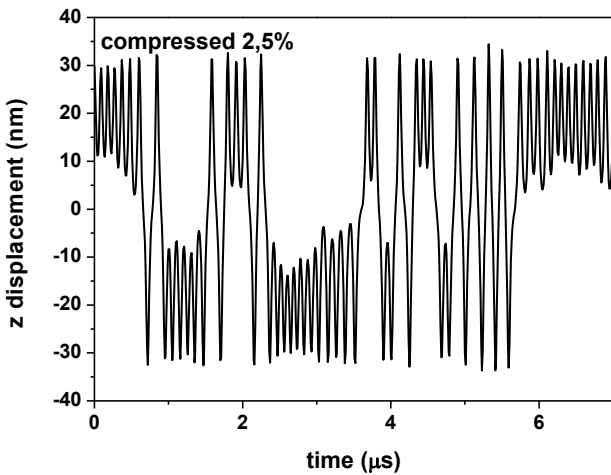
Figure 3: Time evolution of z displacement for a 2.5% compressed graphene. l=300nm, w=200nm
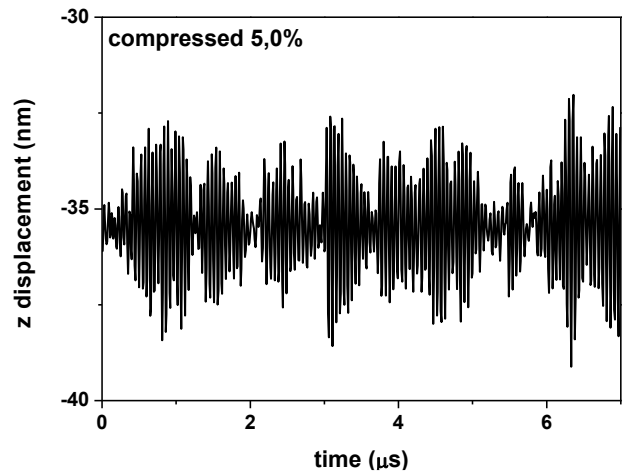
Figure 4: Time evolution of z displacement for a 5.0% compressed graphene. l=300nm, w=200nm
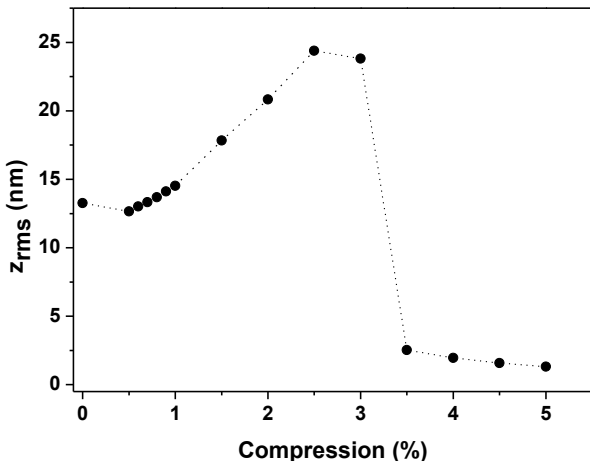
Figure 5: z displacement root mean square vs. compression. l=300nm, w=200nm

268
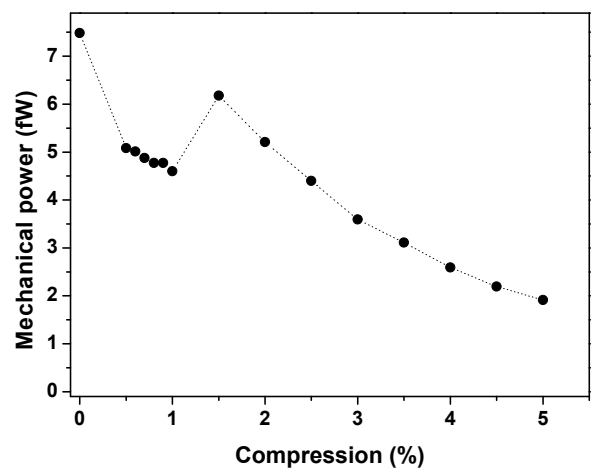
Figure 6: Mechanical power vs. compression. l=300nm, w=200nm

Temperature dependent interaction of graphene with thin TiO_2 and Al_2O_3 layers

G. Lupina[1], O. Seifarth[1], G. Lippert[1], J. Dabrowski[1], I. Costina[1], T. Schroeder[1]
C. C. Bof Bufon[2], O. G. Schmidt[2]

[1]IHP, Im Technologiepark 25, 15236 Frankfurt (Oder), Germany
[2]Institute for Integrative Nanosciences, IFW, Helmholtz Strasse 20, 01069 Dresden, Germany
lupina@ihp-microelectronics.com

In many graphene device concepts a single or few layer graphene is neighboring device elements composed of metals, dielectrics or semiconductors forming interfaces [1]. The properties of these interfaces and their evolution during technological processing are likely to have a big impact on the performance of graphene devices. In this work, using Raman spectroscopy, we investigate the interaction of thin TiO_2 and Al_2O_3 layers with single layer graphene during annealing treatment to shed some light on the interface reactivity and thermal stability in these material systems.

Graphene flakes were exfoliated from natural graphite and deposited onto 300 nm SiO_2/Si substrates. Subsequently the samples were covered with thin (5-15 nm) layers of TiO_2 (Al_2O_3) by atomic layer deposition at 200°C. Ti (IV) isopropoxide and TMA precursors were used for TiO_2 and Al_2O_3, respectively. For temperature Raman measurements, graphene flakes sandwiched between TiO_2 (Al_2O_3) and SiO_2 were heated up in flowing N_2 to the target temperature with a rate of 20°C/min (see Fig.1). Before starting the measurement samples were held at the chosen temperature for 30 min to minimize the drift of the laser spot along the surface. The laser beam (λ = 514nm) was focused using a 50x long-working-distance objective lens with NA=0.5. The laser power on the sample surface was ~ 0.3 mW.

Fig.2 (a) shows the evolution of the Raman G band of a graphene sample at various experiment stages. For the as-deposited graphene flake the G peak is located at 1585 cm^{-1} and is slightly up-shifted with respect to the intrinsic graphene samples (~1580 cm^{-1} [2]) indicating a hole-doping (n ~ 1 x 10^{12}/cm^2) possibly due to O_2 adsorbed on graphene [3]. TiO_2 deposition results in a further blue shift of the G peak to ~1591 cm^{-1}. This shift can be interpreted as either an increased hole-doping (n ~ 4 x 10^{12}/cm^2) [4] or a compressive biaxial strain of ~0.08% in the graphene sheet caused by the TiO_2 layer [5]. Increasing temperature results in a red shift of the G peak. Assuming a linear change of the temperature-induced Raman shift in the chosen range, a G peak temperature coefficient is estimated to be -0.36 cm^{-1}/°C [Fig. 2(b)]. This value is significantly higher than that obtained recently for uncovered graphene on SiO_2 in vacuum (-0.019cm^{-1}/°C) [6] and air ambient (-0.016cm^{-1}/°C) [7]. The disorder-induced Raman D band (~ 1350cm^{-1}) was not detected during annealing implying a negligible change in the sp^2 hybridization. This suggests that the SiO_2/graphene/TiO_2 stack is thermally stable at least up to 600°C and that the graphene sample is still of high quality after the thermal treatment [8].

Beside Raman signatures, we investigate the morphology and chemical composition of the oxide layers covering graphene before and after the thermal treatment and discuss the prospects of using them as barrier dielectrics in graphene high frequency tunneling devices.

References

[1] P. Avouris, Nano Lett., **10** (2010) 4285
[2] C. Casiraghi et al., Appl. Phys. Lett., **91** (2007) 233108
[3] S. Ryu et al., Nano Lett., (2010) DOI: 10.1021/nl1029607
[4] J. Yan et al., Phys. Rev. Lett., **98** (2007) 166802
[5] T.M.G. Mohiuddin et al., Phys. Rev. B, **79** (2009) 205433
[6] Z. H. Ni et al., J. Raman Spectroscopy, **41** (2010) 479
[7] I. Calizo et al., Nano Lett., **7** (2007) 2645
[8] M. S. Dresselhaus et al.,Phil. Trans. R. Soc. A **368** (2010) 5355

Figure1
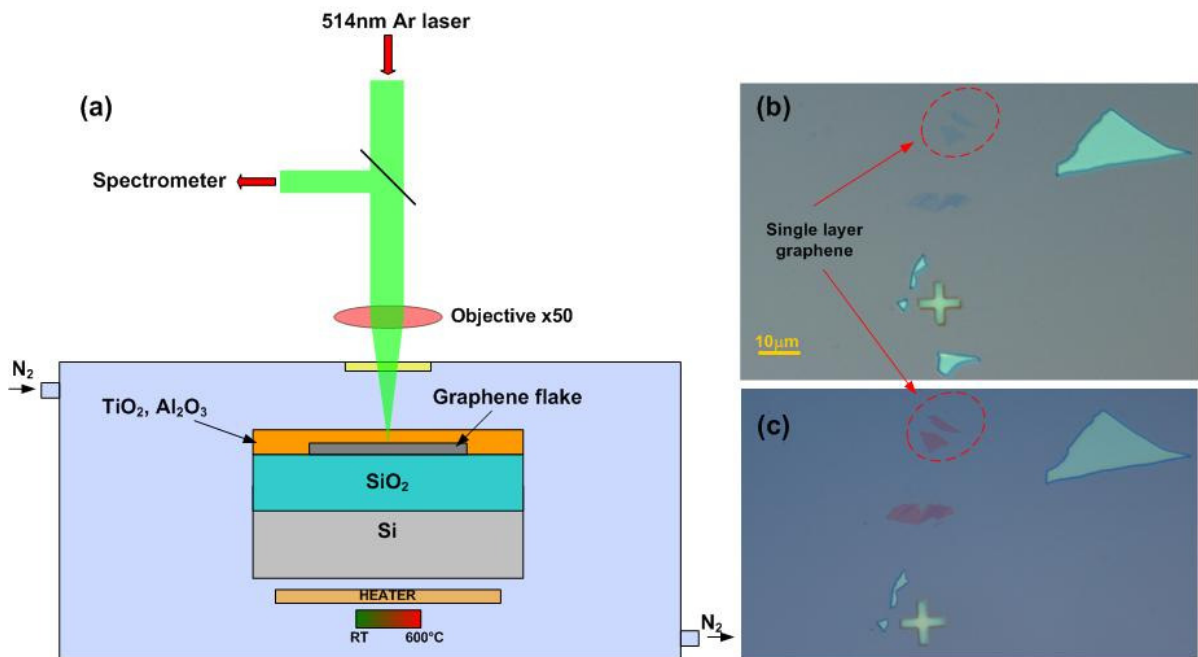
Fig.1. Schematic diagram of the experimental setup (a), optical image of single-layer graphene flakes before (b) and after deposition of ~ 5nm of TiO_2 (c).

Figure2
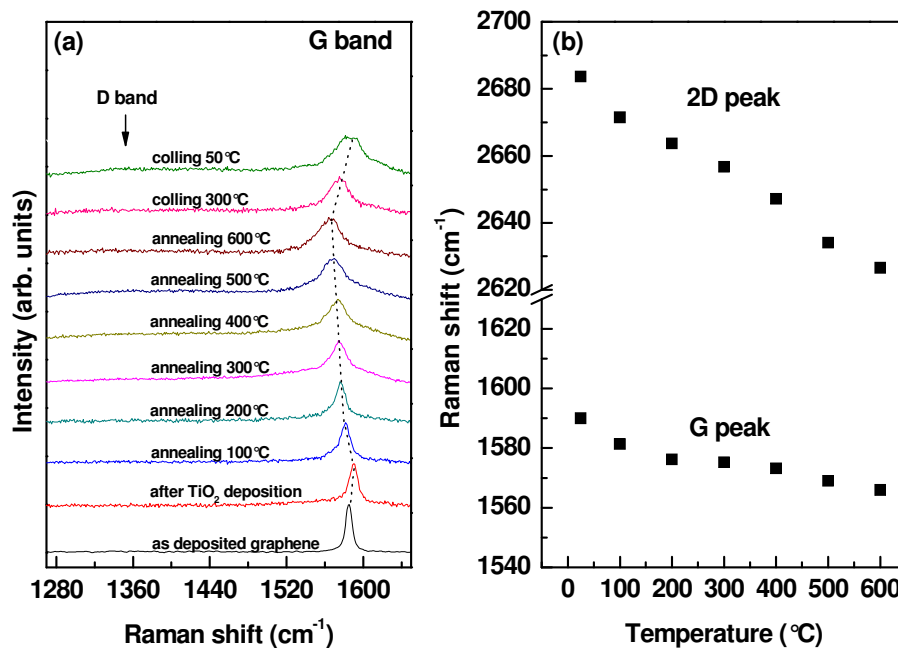
Fig.2. Raman spectra of graphene acquired after subsequent preparation steps (a). The dashed line is a guide to the eye. Variation of the G and 2D peak position as a function of the annealing temperature (b).

Substrate interactions of graphene directly grown on van-der Waals type insulators

O. Seifarth[1], M. Weser[2], G. Lippert[1], J. Dabrowski[1], Y. Dedkov[2], K. Horn[2], G. Lupina[1], W. Mehr[1]

[1] IHP, Im Technologiepark 25, 15236 Frankfurt (Oder), Germany
[2] Fritz-Haber-Institut, Faradayweg 4-6, 14195 Berlin, Germany
seifarth@ihp-microelectronics.com

A few ways to grow graphene are known today, among them the decomposition of SiC surfaces [1] and graphene catalysis on metals [2] are the most prospective for future applications in microelectronics. The first is rather expensive due to the costs of the SiC and requires high thermal budgets; the second needs a layer transfer to Silicon. A possible third way would be graphene growth directly on insulating materials, which allow device fabrication without layer transfer.

In this contribution, we present the direct growth of few layer graphene down to bilayers on an insulating van-der Waals substrate containing Si. We will address for the first time the interaction of the grown graphene with the insulating substrate by means of spectroscopic techniques like Raman and synchrotron-radiation based XPS.

A freshly cleaved sample of Muscovite with a stoichiometry of $KAl_2(AlSi_3O_{10})(F,OH)_2$ and 3T (trigonal) structure was annealed in UHV to 800-1000°C and exposed to a direct beam from a solid carbon source (source-substrate distance: 0.3 m). Muscovite is considered as one of the flattest materials available, similar to graphene, and both are van-der Waals systems. In addition, Muscovite is a good insulator due to its band gap of 7.8 eV.

The samples were analyzed with µ-Raman spectroscopy (Renishaw InVia) with a wavelength of 633 nm and a spot size of ~0.5 µm. The laser power at the sample surface was ~0.07 mW. X-ray photoelectron spectroscopy (XPS) was performed at BESSY II (Berlin/Germany) at beamline U56/2 PGM 2 with a SPECS / PHOIBOS 100 hemispherical electron analyzer. The beam diameter was 800 x 100 µm.

Figure 1 shows results of the Raman map. The bright areas (points 3 & 4) in the optical micrograph (panel a) turn out to be few layer graphene with good quality, grown via direct carbon deposition on a van-der Waals alumino silicate. These points exhibit 2 and 4 layers of graphene, respectively. The surrounding is composed of "highly reduced graphene oxide" HRGO (point 2) and of "SiC-like" species (point 1) several 100 µm apart. The spatial distribution of the D-line intensity (the strong intensity of the HRGO D-line was extracted and excluded by a fitting routine) monitors the quality of the grown graphene. The observed quality (small D-line, panel b) is highest for higher number of layers (here 4) (with low 2D/G intensity, panel d). A small shift of the G-line with respect to intrinsic graphene samples by ~3 cm^{-1} indicates an unintentional background doping [3], most probably due to interaction with the insulating substrate.

Spatial resolved XPS is presented in Fig.2. Here, the C 1s emission of the sample was detected when the sample was stepwise scanned by the synchrotron-radiation beam. Three distinct regions can be observed. One exhibits a brought emission in the energy range of carbides at 283 eV (blue) and a weak satellite at 288 eV (carbon-oxygen bonds), for simplicity labeled "SiC-like". The next spectrum (red) has one line at 284.7 eV (C-C bonds) [4]. The small width of this XPS emission and its asymmetric character are typical for highly conducting species like graphene / graphite. The black spectrum has a strong emission at 288 eV with contributions in the C-C bond and carbide region. In analogy to our Raman results we label this area HRGO; however the single XPS components do not fully reflect the characteristic spectrum of a graphene oxide.

In summary, we demonstrated the feasibility to grow graphene directly on an insulator. In contrast to the van-der Waals like nature of Muscovite and graphene we have clear evidence that an interaction stronger than van-der Waals forces appears which includes chemical bonds. This allows high quality graphene growth for higher numbers of layers but limits the quality of bilayers.

References

[1] C. Berger et al., J. Phys. Chem B **108** (2004) 19912
[2] S. Bae et al., Nature Nanotech. **5** (2010) 574
[3] C. Casiraghi et al., Appl. Phys. Lett., **91** (2007) 233108
[4] J.F.Moulder et al., *Handbook of X-ray Photoelectron Spectroscopy* , Perkin-Elmer (1992)

Figure 1
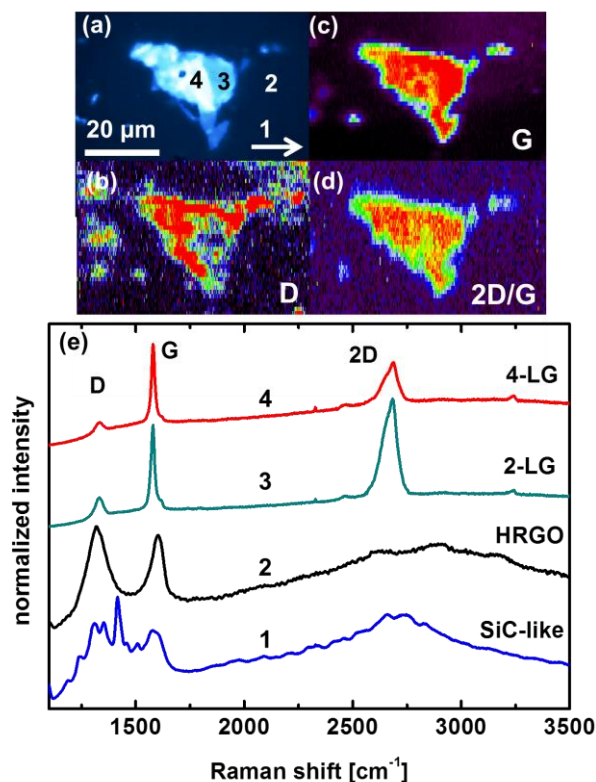
Fig.1. Raman spectroscopic investigation of few layer graphene grown on insulator. Optical micrograph (a), Raman intensity maps of the D and G line and the ratio 2D/G (b-d). The corresponding spectra recorded at the points 1-4 (e).

Figure 2
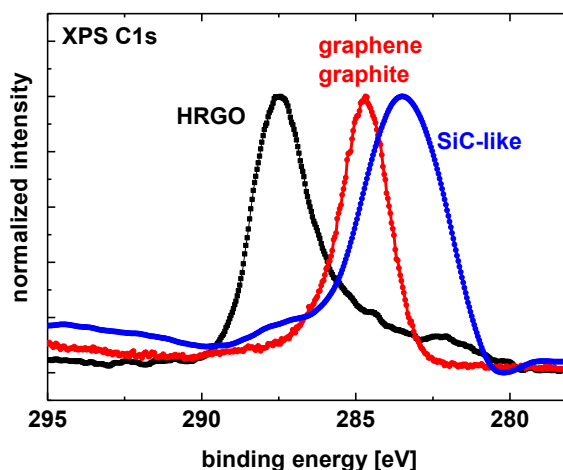
Fig.2. Synchrotron radiation based XPS of the C 1s line of few layer graphene grown on insulator. The spectra represent distinct regions on the substrate.

The piezoresistance effect in carbon nanotubes and graphene ribbons

O.S. Lyapkosova, N.G. Lebedev

Volgograd State University, University Avenue, 100, Volgograd, 400062 Russia
lyapkosovaolga@mail.ru

The piezoresistance effect is in the change of the electroconductivity of the semiconductors caused by the anisotropic deformation of a crystal [1]. The piezoresistance effect in single walled carbon nanotubes [2] of two geometry modifications "arm-chair" and "zigzag" has been investigated. The electronic structure of nanotubes has been simulated within the framework of π-electronic approach and Hubbard's model [3] taking into account only for the energy of electrons in carbon atoms and the energy of the transition between the neighbor lattice units. The band structure of carbon nanotubes is described by the dispersion relation for the graphite sheet [2]:

$$\varepsilon(k_x, k_y) = \pm\gamma_o \left\{ 1 + 4\cos\left(\frac{\sqrt{3}k_x R}{2}\right)\cos\left(\frac{k_y R}{2}\right) + 4\cos^2\left(\frac{k_y R}{2}\right) \right\}^{1/2}, \qquad (1)$$

where γ_0 is the transfer integral, k_x and k_y are the wave vector components, one of which is continuous along the tube axis and another is quantized along the tube circumference according to "arm-chair" or "zig-zag" geometry type, R is the interatomic distance, which has beendefined to be equal 1.44 A.

The bulk and linear deformations have been simulated by small changes of the bond length R. The band structure change caused by small deformation can be expressed within the framework of the linear approximation as following:

$$\varepsilon(k_x, k_y) \approx \varepsilon_0(k_x, k_y) + R\frac{\partial\varepsilon}{\partial R}\delta, \qquad (2)$$

where $\varepsilon_0(k_x, k_y)$ is band structure of the ideal carbon nanotube expressed by the formula (1), δ - relative change of carbon-carbon bond length.

The band structure changes, which influence on conducting properties of carbon nanotube and graphene and cause the piezoresistance effect, have been analyzed. The effect can be used for the identification of single walled carbon nanotubes and the development of electro-mechanical energy transformers.

References
[1] G.L. Bir, G.E. Pikus, Symmetry and deformation effects in semiconductors, Moskow, "Nauka", 1972, 584 p. [in Russian]
[2] P.J.F. Harris, Carbon nanotubes and relative structures. New materials of twenty-first century, (Cambridge University Press, 1999; 336).
[3] Yu.A. Izyumov, N.I. Chaschin, and D.S. Alekseev, Theory of Strongly Correlated Systems: Method of Generating Potential (Moscow, NITs "Regulyarnaya i Khaoticheskaya Dinamika," 2006) [in Russian].

Large Scale CVD Graphene Nanoribbon Transistors with High-κ Dielectrics and Top Gates

Austin S. Lyons[1,2], Edmond K. Chow[2], Vince E. Dorgan[1,2], Eric Pop[1,2]

[1]*Dept. of Electrical & Computer Eng., Univ. Illinois at Urbana-Champaign, Urbana, IL 61801, USA*
[2]*Micro and Nano Technology Laboratory, Univ. Illinois at Urbana-Champaign, Urbana, IL 61801, USA*
lyons24@illinois.edu

Graphene nanoribbon field-effect transistors (GNRFETs) are promising candidates for nanoelectronic applications. Researchers have demonstrated that one-of-a-kind GNRFETs can have mobility values >1,000 cm^{2}V^{-1}s^{-1} [1] and I_{on}/I_{off} ratios ~10^6 [2]. However, such one-of-a-kind GNRFETs use chemically derived or mechanically exfoliated graphene, neither of which are practical for large scale fabrication. On the other hand, synthesis of graphene by chemical vapor deposition (CVD) is a promising method [3] for creating wafer-scale transistors and circuits.

In this study we use a novel fabrication technique to demonstrate the first large scale arrays of top-gated GNRFETs using CVD graphene. This approach can be used to fabricate thousands of GNRFETs on a single test chip, enabling systematic and statistical characterization of device performance as a function of device dimension, material, and temperature. This method also paves the way toward realistic GNRFET-based circuits.

Our CVD graphene growth and transfer process is illustrated in Fig. 1. CVD growth on copper foil results in monolayer growth (Fig. 2) on both sides of the Cu foil [3]. After growth, one side of the foil is protected with poly-methyl methacrylate (PMMA), while the other side is exposed to an O_2 RIE plasma etch to remove the additional graphene film. The Cu foil is removed using $FeCl_3$ and the PMMA/graphene film is transferred to a deionized (DI) water bath. After rinsing, the film is transferred to SiO_2 (90 nm) on highly doped Si wafers. When the sample is dry, PMMA is removed using a 1:1 methylene chloride to methanol solution.

Figure 3 depicts our top-gated GNRFET fabrication process. Electron-beam evaporation is used to deposit source and drain Ti/Au (1 nm/50 nm) contacts. We introduce a novel technique for defining the nanoribbon while simultaneously providing a sticking layer for the high-κ dielectric. The narrow GNR channel is first patterned between the source and drain, and then 2 nm of Al is deposited. The sample is removed from vacuum, immediately oxidizing the thin layer of Al [4]. After PMMA liftoff, the 2 nm AlO_x film covering the GNR channel is used as an O_2 RIE plasma etch mask. Etching removes all exposed graphene, defining a nanoribbon between source and drain while electrically isolating all devices on the chip. The nanoribbon is completely covered with AlO_x, enabling the high-quality atomic layer deposition (ALD) of either Al_2O_3 or HfO_2 [4,5]. In this work we deposited 12 nm of Al_2O_3 over the surface of the sample after the O_2 etch. The top gate is patterned and Ti/Au (1 nm/50 nm) is evaporated onto the high-κ dielectric. We anneal the samples in vacuum at 200 ºC overnight, reducing contact resistance up to 25%.

We used relatively conservative dimensions in our initial proof-of-concept experiments. Nanoribbons were W = 50 nm wide, with channel lengths from L = 350-500 nm (Fig. 4). The top gate was kept narrow (L_G = 100 nm) to prevent overlap with source or drain from misalignment. Measurements were taken in vacuum (Fig. 5) and ambient (Fig. 6) at room temperature. Device yield was a respectable 63%, even for the initial fabrication runs, highlighting the large-scale utility of the novel GNR patterning approach. Extracted mobility values were μ_{GNR} ~ 100-200 cm^{2}V^{-1}s^{-1} across all samples, typical of narrow GNRs where edge scattering dominates [2]. It is important to point out that CVD-grown GNRs had not been evaluated before, but the mobilities estimated here are similar to GNRs obtained from exfoliated graphene. This may indicate that our GNRs are smaller than the CVD graphene grain size, and thus edge scattering dominates. Future work must better characterize such issues, improve the parasitics of these devices, and decrease their dimensions.

In summary, we have demonstrated (to our knowledge) the first large-scale CVD-graphene nanoribbon transistors with top gates and high-k dielectrics. We have also introduced a novel technique for defining the nanoribbon while simultaneously seeding the high-k dielectric. Combined, these approaches pave the way toward systematic and statistical characterization of GNRFETs, and toward the implementation of realistic GNRFET-based circuits.

References

[1] L. Jiao *et al*, Nature Nano, **5** (2010) 321
[2] X. Wang *et al*, PRL, **100** (2008) 206803
[3] X. Li *et al*, Science, **324** (2009) 1312
[4] S. Kim *et al*, APL, **94** (2009) 62107
[5] B. Fallahazad *et al*, APL, **97** (2010) 123105
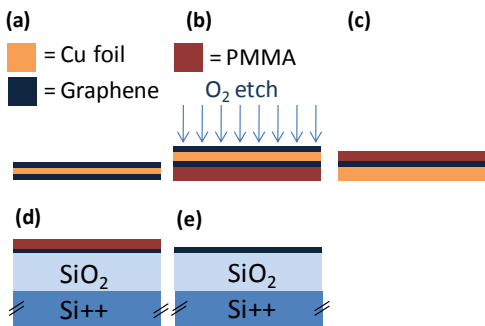
Fig. 1. (*A*) *Monolayer CVD grown graphene on both sides of a Cu foil. (B) PMMA is used to protect graphene on one side of the foil while the other is removed by O₂ etching. (C) PMMA and graphene on Cu foil before FeCl₃ etching. (D) PMMA/graphene film transferred to 90 nm SiO₂ on heavily doped Si. The substrate is used as the back gate in electrical measurements. (E) PMMA liftoff completes the CVD growth and transfer process.*
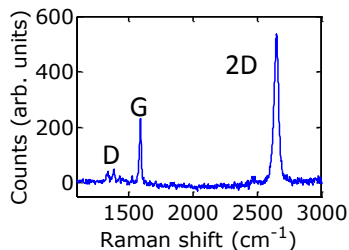
Fig 2. *Raman spectra of the monolayer graphene used in this experiment. The graphene has a 2D:G ratio of ~2.*
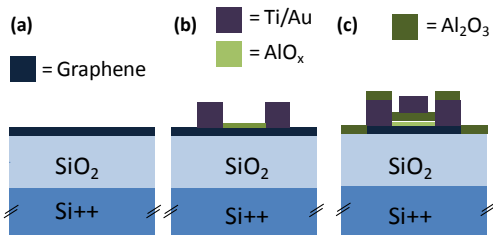
Fig. 3. (*A*) *Large scale GNRFET fabrication commences with CVD graphene transferred to an SiO₂/Si++ substrate. (B) E-beam evaporation is used to deposit Ti/Au (1 nm/50 nm) contacts. Al (2 nm) is deposited between source and drain to serve as an etch mask for defining the GNR and as a nucleation layer for high-κ oxide deposition. The Al instantly oxides into AlOₓ upon removal from vacuum. (C) An O₂ plasma etch defines the GNR and electrically isolates GNRFETs from each other. Al₂O₃ (12 nm) is grown by ALD. A Ti/Au (1 nm/50 nm) top gate completes the large scale CVD GNRFET fabrication process.*

276
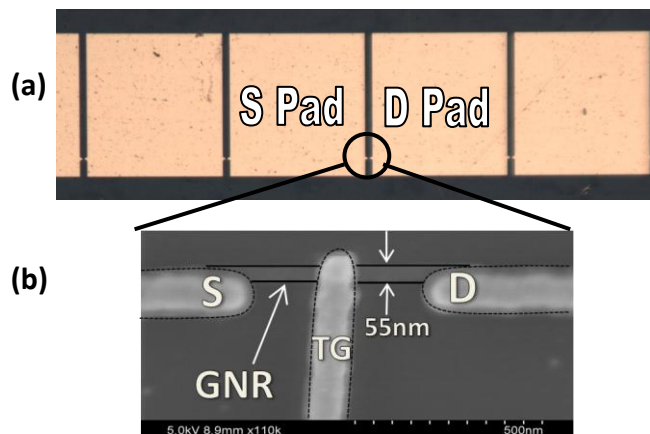
Fig. 4. (*A*) *A row of GNRFETs (B) An SEM image of a top-gated high-κ GNRFET on CVD graphene with channel W=55 nm L=450 nm and top gate W=100 nm.*
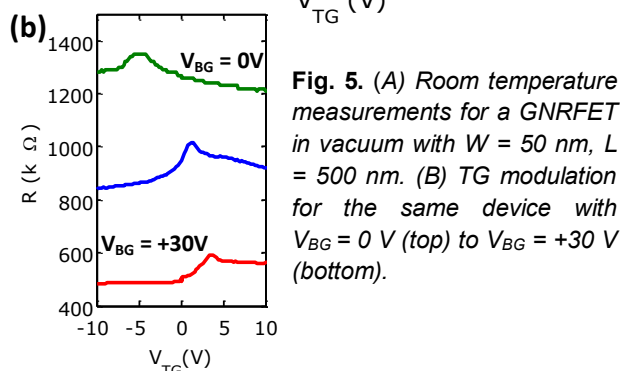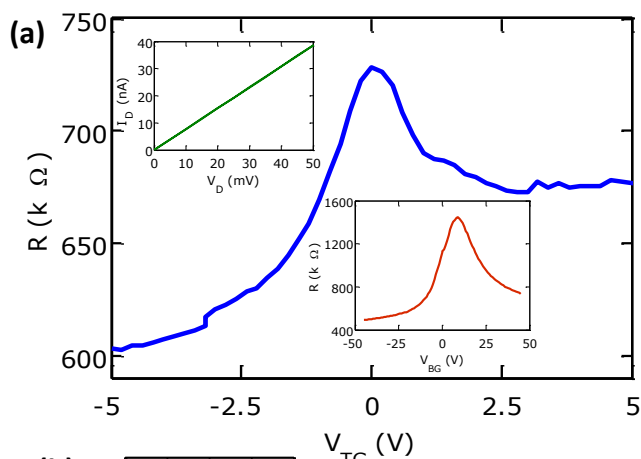
Fig. 5. (*A*) *Room temperature measurements for a GNRFET in vacuum with W = 50 nm, L = 500 nm. (B) TG modulation for the same device with V_{BG} = 0 V (top) to V_{BG} = +30 V (bottom).*
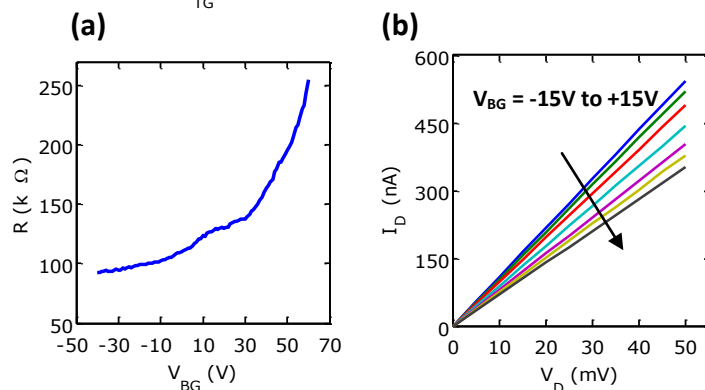
Fig. 6. (*A*) *Room temperature, ambient R-V_{BG} of a W = 50 nm, L = 400 nm device. (B) Id-Vd for the same device.*

Nitrogen-doped graphene for electrochemical oxygen reduction

Stephen M. Lyth, Y. Nabae, N. M. Islam, S. Kuroki, M. Kakimoto, S. Miyata

Tokyo Institute of Technology, Tokyo, Japan
stephenlyth@gmail.com

Fuel cells could offer an alternative to fossil fuels by using hydrogen generated from renewable sources. However, oxygen reduction in these devices is performed on a Pt catalyst which is extremely expensive. If cheap alternatives can be discovered, fuel cells may become serious contenders in the energy sector.

One candidate is nitrogen-doped carbon. Such catalysts have been extensively studied and are generally made via heat-treatment of Fe/C/N-containing materials. The performance of this class of catalysts is gradually improving.[1] The role of iron in these catalysts is debated, but recent evidence suggests that Fe-coordination to C and/or N atoms is not needed for efficient oxygen reduction.[2,3,4] However, the performance of these catalysts must improve if they are to rival platinum.

Graphene has recently taken the scientific world by storm. Among its many remarkable properties it is highly conductive, can support high current density, is chemically stable and has large surface area. Thus, graphene is an ideal material for use in fuel cells. There are relatively few reports of N-doped graphene (Figure 1a), but research in this field is growing, with various reported synthesis techniques (Figure 1b).[5,6,7,8,9,10]
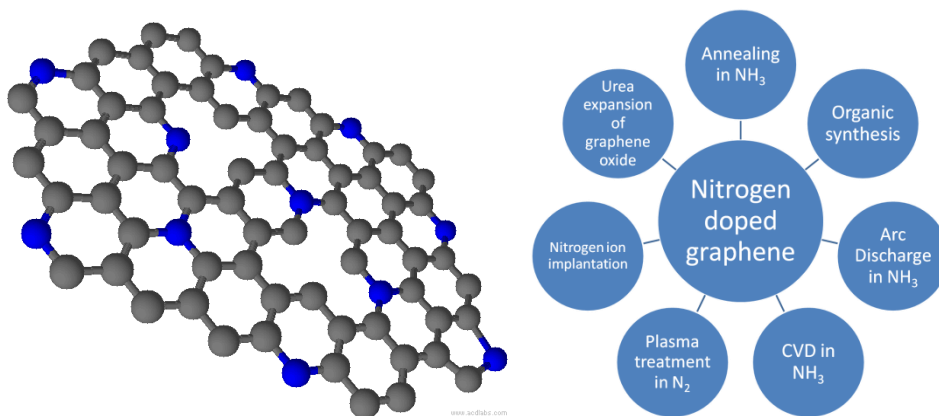
Figure 1: (a) Schematic of N-doped graphene, (b) Techniques used to produce N-doped graphene.

Using an organic synthesis protocol we have produced gram-quantities of graphene powder with extremely high N content, which can be varied by changing the chemical precursors, or by thermal treatment. This N-doped graphene is an ideal candidate for use as a catalyst for fuel cells. Figure 2(a) shows transmission electron microscopy of N-doped graphene sheets at least 10 μm in size. Various folds and crumples can be observed. Figure 1(b) shows the N1s region of the X-ray photoelectron spectum of N-doped graphene, with a large peak centered at ~400.5 eV attributed to quaternary bonded N, indicating that a significant amount of N in the basal plane. The smaller shoulder peak at ~398.5 eV is attributed to pyridinic-type N, which may indicate bonding at edges, or at vacancies in the graphene plane. Table 1 shows the N content measured by CHN analysis for N-doped graphene derived from diethanolamine, pyrolysed at various temperatures. The N content varies from 14.83 wt.% for as-produced N-doped graphene to 6.27 wt.% for N-doped graphene subjected to pyrolysis at 1000°C. This demonstrates the ability to tune the nitrogen content as desired for a particular application. Additionally, the nitrogen content remains high even after high temperature treatment, indicating the stability of N in this material.

Figure 2(c) shows linear sweep voltammograms for graphene and N-doped graphene catalysts. In these results, there is an improvement in the current density with increasing pyrolysis temperature for N-doped graphene, which is attributed to an increase in conductivity, or in the number of available active sites for oxygen reduction. There is also an increase in the onset potential (measured at 2 $\mu A/cm^2$) from 0.78 V for pristine graphene to 0.84 V for N-doped graphene pyrolysed at 1000°C.
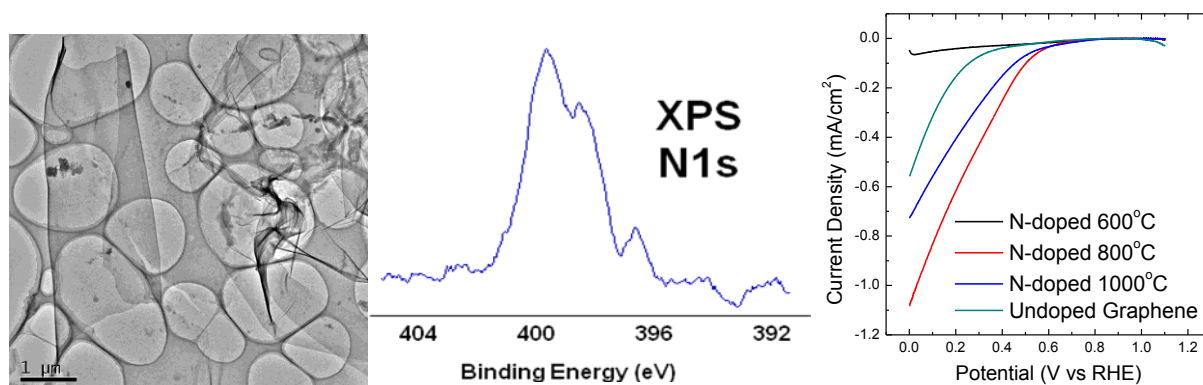
Figure 2. (a) TEM image of nitrogen-doped graphene. (b) XPS N1s signal for nitrogen-doped graphene. (c) Oxygen reduction voltammogram for N-doped graphene cathodes.

Precursor	Temperature (°C)	Nitrogen Content (wt.%)
Ethanol	600	0
Diethanolamine	600	14.83
Diethanolamine	800	10.11
Diethanolamine	1000	6.27

Table 1. CHN analysis of graphene and N-doped graphene pyrolysed at various temperatures.

These preliminary results indicate that N-doped graphene is a suitable candidate for use as an oxygen reduction catalyst in fuel cells and give some insight into the mechanism of oxygen reduction. This material is fabricated via a cheap and scalable organic synthesis method. However, this is a work in progress and efforts are being made to increase the surface area, N content and conductivity of the material to make N-doped graphene a viable catalyst for oxygen reduction in fuel cells.

References

[1] Y. Nabae, S. Moriya, K. Matsubayashi, S. M. Lyth, M. Malon et al. Carbon **48** (2010) 2613.
[2] S. M. Lyth, Y. Nabae, S. Moriya, S. Kuroki et al J. Phys. Chem. C **113** (2009) 20148.
[3] M. Chokai, M. Taniguchi, S. Moriya, K. Matsubayashi, et al., J. Power Sources **195** (2010) 5947.
[4] S. M. Lyth, Y. Nabae, N. M. Islam, S. Kuroki, et al., J. Electrochem. Soc. **58** (2011) B194.
[5] X. Li, et al., Journal of the American Chemical Society **131** (2009) 15939.
[6] X. Wang, et al., Science **324** (2009) 768.
[7] D. Long, W. Li, L. Ling, J. Miyawaki, I. Mochida, S-H. Yoon, Langmuir **26** (2010) 16096.
[8] X. Li, et al., Journal of the American Chemical Society **131** (2009) 15939.
[9] D. Wei, et al., Nano Letters **9** (2009)1752.
[10] S. Wakeland, R. Martinez, J. K. Grey, C. C. Luhrs, Carbon **48** (2010) 3463.

Molecular Beam Epitaxy Growth of Graphene and Ridge-Structure Network of Graphene Using Cracked Ethanol

Fumihiko Maeda, Hiroki Hibino

NTT Basic Research Laboratories, NTT Corporation, 3-1 Morinosato-Wakamiya, Atsugi-shi, Kanagawa 243-0198, Japan
fmaeda@will.brl.ntt.co.jp

While the excellent electrical performance of few-layer graphene (FLG) has been demonstrated for exfoliated FLG, the exfoliation process cannot form the basis of a large-scale manufacturing process. Hence, establishing alternative ways of forming wafer-scale FLG is of great interest from the viewpoint of large-scale integration, and some new alternative approaches have been proposed. Recently, we have proposed a new method based on gas-source molecular beam epitaxy (MBE), in which a cracked-ethanol source is employed [1]. In our previous study, although we showed the feasibility of this growth method, the quality of the graphene was not sufficient. To optimize this growth method to produce high-quality graphene, we examined the substrate temperature dependence of the growth in this study. In addition, we observed a ridge-structure network, consisting of FLG, on graphene after the growth.

As a substrate, we used graphene, whose layers were around 1.3 monolayers, formed on n-type SiC(0001) by annealing at 1800°C in Ar ambient at about 100 Torr. For the MBE growth, the substrate had been heated at temperatures between 600 and 915°C under the flow of cracked ethanol for four hours. Then, we transferred the samples to the analysis system equipped with a monochromatized Al Kα source (1486.6 eV) and a photoelectron analyzer via an ultra-high vacuum and performed *in situ* measurements. Further details are described in [2].

Figure 1 shows the substrate temperature dependence of growth thickness, estimated using the peaks of graphene and SiC substrate derived from the C 1s spectra by a fitting procedure. We found that the thickness decreased with increasing substrate temperature. This trend indicates that the substrate temperature is in a region where the rate-limiting factor is the mass transport, which is higher than the temperature region where the growth is kinematically limited [3]. The growth limited by the mass transport means that the growth rate dose not simply increase even when the supply of ethanol gas increased, which is consistent with the previous study [2]. We obtained a high-contrast transmission electron microscope (TEM) image of the MBE-grown graphene layer (Fig. 2, closed arrow) at 915°C, the highest growth temperature in this study. This layer is better than those in the previous study, in which there are vacancies and fluctuation in the graphene layers [1]. Thus, high-temperature growth improves the quality of the MBE-grown graphene layers, though the growth rate becomes too slow to be of practical use. Since the previous study [2] suggests that the rate-limiting factor may be etching reaction, we believe its suppression is key to increase the growth rate and to improve the graphene quality by the high-temperature growth.

Further, in the center of the TEM image in Fig. 2, we can see a ridge structure of FLG grown in out of plane direction. This structure would be formed by the collision between incommensurate domains of graphene at their interface. An atomic force microscope (AFM) image of the same sample (Fig. 3) indicates that this ridge structure forms a network on the graphene surface. If our assumption is correct, these structures indicate the domain boundaries of graphene and the domain size is estimated to be less than 100 nm.

References

[1] F. Maeda and H. Hibino, Phys. Stat. Solidi B, 247 (2010) 916.
[2] F. Maeda and H. Hibino, submitted to Jpn. J. Appl. Phys. (2011)
[3] D.W. Shaw, J. Cryst. Growth 31(1975) 130.

Figures
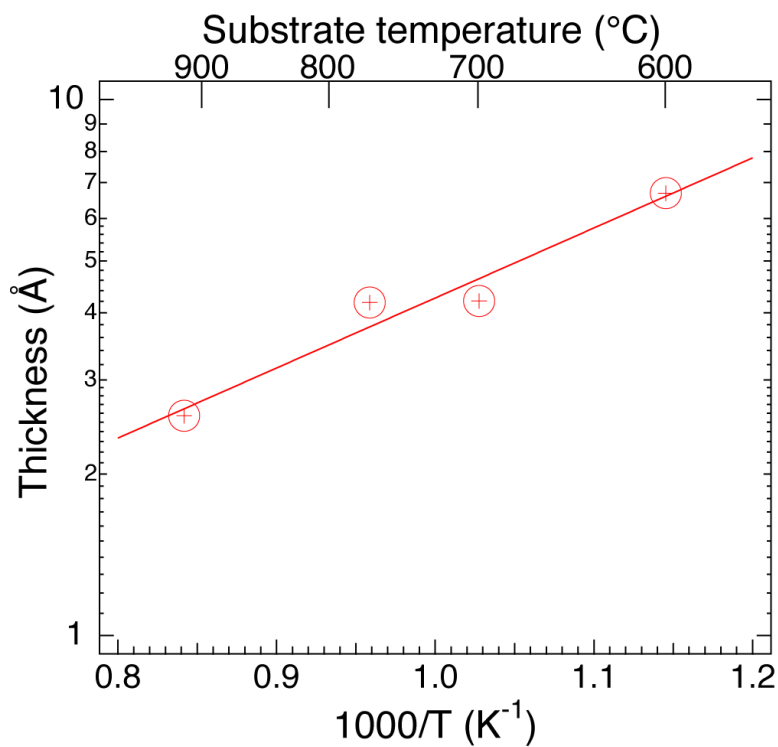
Fig. 1. Substrate temperature dependence of growth thickness.
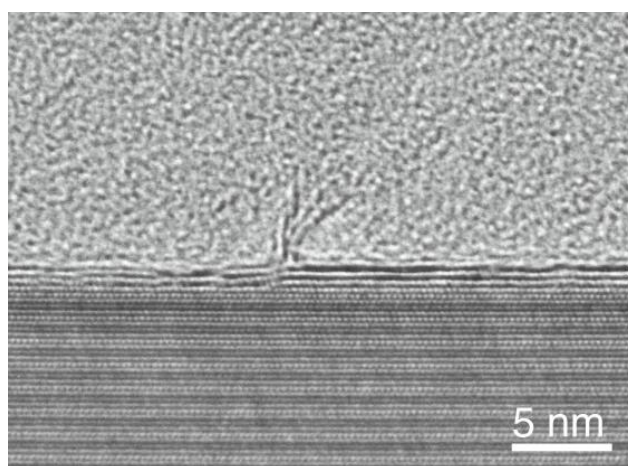
Fig. 2. Cross-section TEM image after MBE growth at 915 °C. The closed arrow points to the MBE-grown graphene layer and the open arrow points to the initial graphene formed by thermal decomposition of SiC.
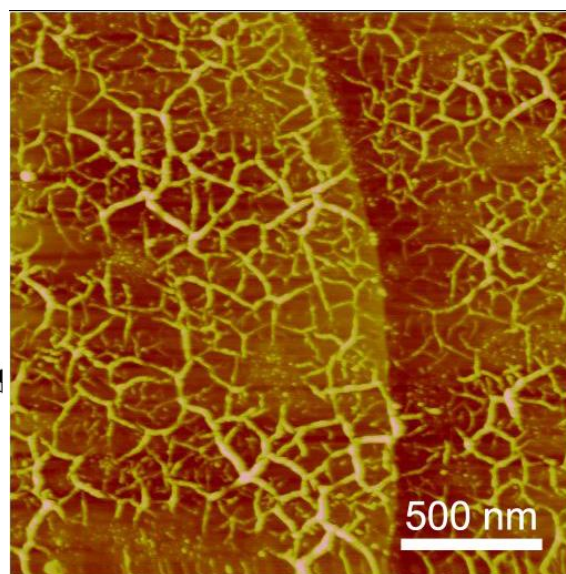
Fig. 3. AFM image after MBE growth at 915 °C

Chemically converted Graphene Nanosheets: Langmuir-Blodgett deposition

B. Martín-García[1], M.M. Velázquez[1], E. Diez[2], F. Rossella[3], V. Bellani[3], J.A. Pérez-Hernández[4] and J. Hernández-Toro[4]

[1]Dpto Química-Física, Universidad de Salamanca, Plaza de los Caídos s/n, 37008 Salamanca (Spain)
[2]Laboratorio de Bajas Temperaturas, Universidad de Salamanca, 37008 Salamanca (Spain)
[3]Dipartimento di Fisica "A. Volta", Università di Pavia, 27100 Pavia, (Italy)
[4]Centro de Láseres Pulsados Ultraintensos (CLPU), 37008 Salamanca (Spain)
beamagaiq@usal.es

Graphene has attracted much interest because of its superior physical, chemical and mechanical characteristics that make possible its use for thin-film transistors, solar cells, and sensor applications [1]. This material is a single layer of graphite with a perfect sp^2-hybridized 2D carbon structure. Graphene has been made by chemical vapor deposition, epitaxial growth or micromechanical exfoliation; nevertheless, the uniform growth of graphene monolayer is still a challenge. One of the most promising alternative options, developed in the last years, is the reduction of graphite oxide (GO) in colloid dispersions or in films adsorbed in solid substrates, however the low productivity of these methodologies make it unsuitable for large-scale applications [2]. Moreover, dispersions of graphene-sheets offer a great deal of flexibility in the creation of novel graphene-based nanocomposites with many others molecules and nanostructures [3]. According to it, the aim of this work is the preparation and characterization of graphene layers obtained from reduction of GO by different methodologies. In the first one, aqueous dispersions of GO were reduced by several reducing agents in the absence and presence of surfactants forming aqueous dispersions of graphene nanosheets. The chemically converted graphene, obtained by filtration and sonication, is a water-insoluble material suitable to form Langmuir monolayers. Thus, these graphene monolayers are transferred onto silicon wafers using the Langmuir-Blodgett (LB) technique. The third methodology explored in this work is to transfer GO onto silicon by LB technique and then chemically reduced.

The sheet morphology was observed by Atomic Force Microscopy (AFM) and shows that the LB technique offers us a great control over the orientation and placement of the sheets on the substrates. All routes lead to a few-layer graphene. The presence of surfactants in the reduction process of the GO aqueous dispersions produces lighter graphite flakes. Comparison between the Raman spectra of graphene sheets prepared by the different methodologies and the graphene obtained by micromechanical exfoliation (scotch tape) provides us useful information about the properties of the graphene materials sheets.

References

[1] K. S. Novoselov, A. K. Geim, S. V. Morozov, D. Jiang, M. I. Katsnelson, I. V. Grigorieva, S. V. Dubonos, A. A. Firsov, Nature **438** (2005) 197.

[2] S. Park, R.S. Ruoff, Nat Nanotechnol. **4** (2009) 4.

[3] D. Li, M.B. Müller, S. Gilje, R.B. Kaner, G.G. Wallace, Nat Nanotechnol. **3** (2008) 101.
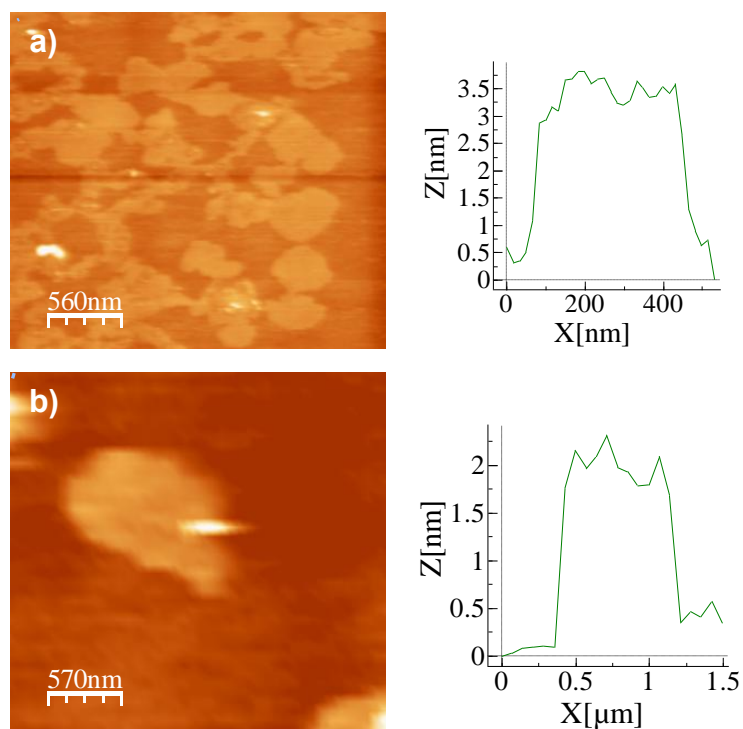
Figure 1. AFM images and line profiles for chemically reduced graphene nanosheets LB deposited onto silicon wafers. Reducing agents: hydrazine (a) and vitamin C (b).

Acknowledgements

CVD synthesis of a MWCNT-graphene composite

I. Martin-Fernandez[1], N. Mestres[2], P. Godignon[1]

[1]Instituto de Microelectrónica de Barcelona (IMB-CNM, CSIC), Campus UAB,
E-08193 Cerdanyola del Vallès, Spain
[2]Institut de Ciència de Materials de Barcelona (ICMAB, CSIC), Campus UAB,
E-08193 Cerdanyola del Vallès, Spain
inigo.martin@imb-cnm.csic.es

Carbon nanotubes (CNTs) and graphene have generated great interest for device applications due to their particular physicochemical properties and, thus, big efforts are being dedicated to the optimization of their synthesis. These efforts, however, are not only leading to solve their growth mechanism, but also to the finding of new material architectures aimed to possible new functionalities [1]. This way, for example, a new composite material based on multi-walled (MW) CNTs and multi-layer graphene was presented recently [2].

This contribution presents a CNT-graphene composite similar to that reported in [2] but where a single graphene layer is formed on top of the CNT array.

The CNT-graphene composite is formed by a vertically aligned array of nanotubes and by a top film that is formed during the same synthesis process. The synthesis of the composite is performed by thermal CVD and, first, a few nanometer thick layer of platinum (that is a non-conventional catalyst material for CNTs and graphene) needs to be deposited on the substrate to catalyze its growth [3]. The synthesis of the composite is performed at 800ºC and CH_4 is used as the carbon feeding gas.

The composite is dark colored. The vertically aligned CNTs are MW, analogous to those synthesized in previous works [3]. Their diameter is ~10 nm, and their walls are parallel and present low density of defects. The top film is smooth and flexible, and its roughness is related to the MWCNT array underneath. Cracks on the top film are only observed close to positions where the composite had been modified because of scratches or because of squashing. The SEM images in Figure 1 show (a) a shifted flake of the top film on top of the MWCNT array as a result of a scratch on the composite, and (b) a tilted view of the composite at a section that had been fabricated by FIB.

The composition of the composite was analyzed by EDX and micro-Raman spectroscopy. These analyses were performed at different positions of the sample to discriminate the different components of the composite The EDX analyses determined that the top layer is made of carbon. The Raman analysis was performed on the squashed composite area shown in Figure 2(a-b). The Raman spectra, A-F, in Figure 2(c) are related to the positions A-F in Figure 2(a). The low frequency region in these spectra (1200-1800 cm^{-1}) is dominated by the typical spectral features of MWCNTS. The large relative intensity of the G' peak in the spectra for positions A, E and F may only match that of graphene [4]. In particular, the Raman spectra could be attributed to a single layer graphene [5,6] or to a few layers graphene film where the layers are folded or arranged according to a disordered stacking [7].

References

[1] F.D. Novaes, ACS Nano **4** (12) 7596-7602

[2] D. Kondo, et al., Applied Physics Express **1** (2008) 0740031-0740033.

[3] I Martin-Fernandez, et al., Microelectronic Engineering **86** (2009) 806–808.

[4] M.S. Dresselhaus, et al., Nano Letters **10** (2010) 751-758.

[5] A.C. Ferrari, et al., Physical Review Letters **97** (2006), 187401;

[6] J.S. Park, et al., Carbon **47** (2009) 1303-1310.

[7] Z. Ni, et al., Physical Review B **77** (2008) 235403.

Figures
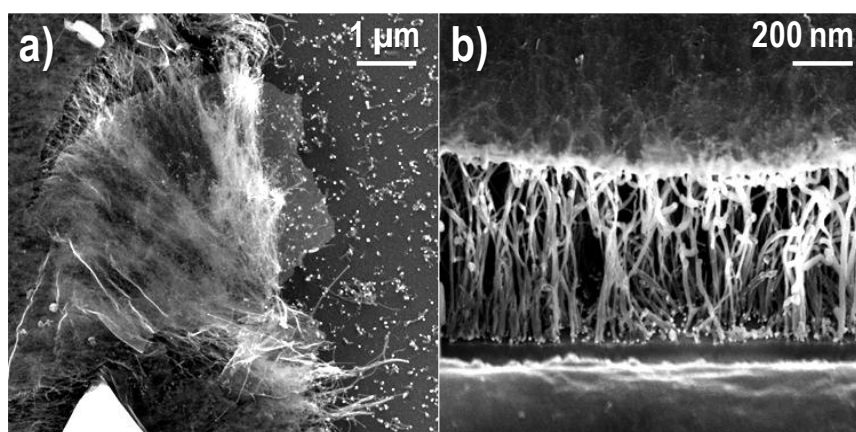
Figure 1: SEM images on the composite material. (a) Shifted top film flake on top of the CNT array. (b) Tilted view of the FIB made section of the composite.
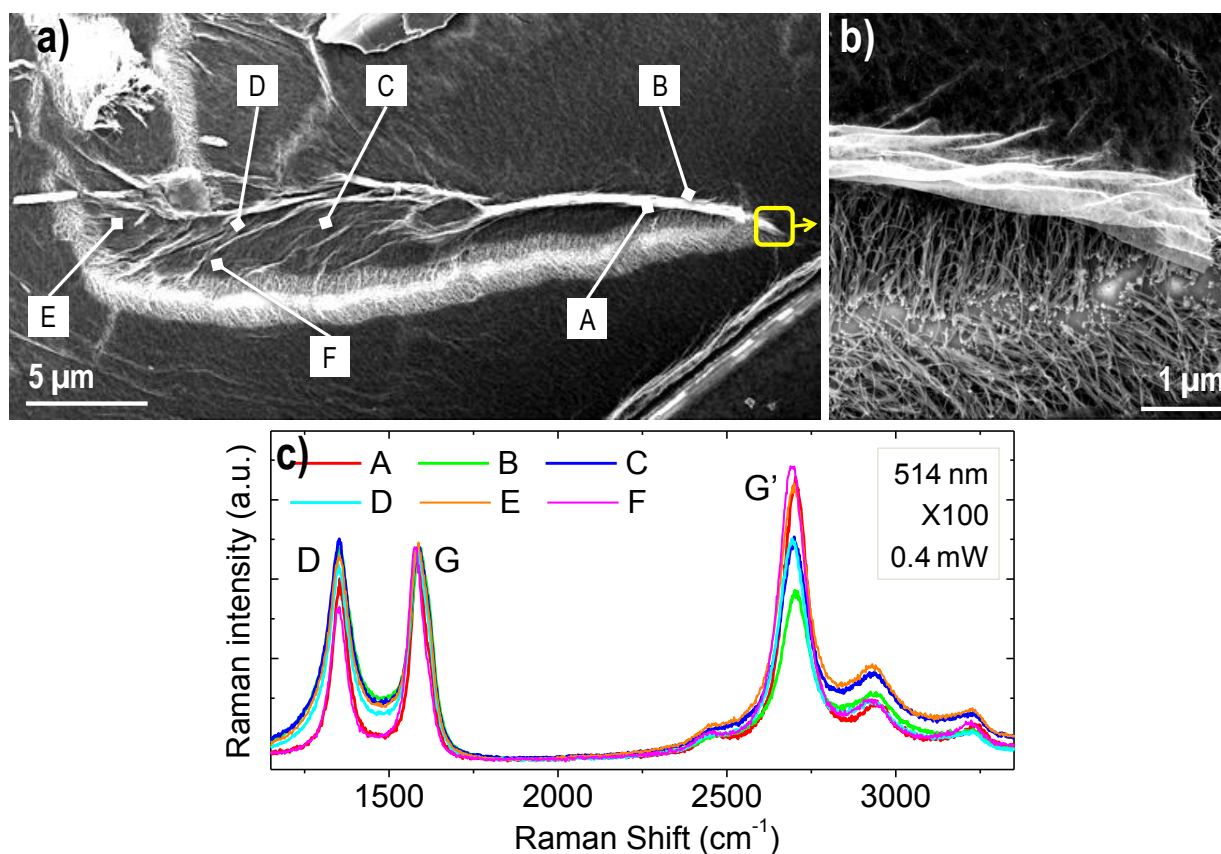
Figure 2: Raman analysis of the composite material at a squashed area. A-F in (a) denote the positions from which the Raman spectra A-F in (c) were obtained.(b)Detail of the folding of the top film.

Simultaneous Reduction of Graphene Oxide and Polyaniline:
Doping Assisted Formation of a Solid State Charge-Transfer Complex

Wolfgang K. Maser, Cristina Vallés, Pablo Jiménez, Edgar Muñoz, Ana M. Benito

Instituto de Carboquímica (CSIC), Department of Nanotechnology, 50018 Zaragoza, Spain
wmaser@Eicb.csic.es

Formation of a solid state charge-transfer complex is observed upon simultaneous reduction of a graphene oxide – polyaniline (GO-PANI) composite consisting of GO sheets coated by a thin layer of PANI. Controlling the reduction conditions and morphology of (GO-PANI) we synthesized a reduced R(GO-PANI) product, which exhibited an unprecedented donor-acceptor interaction between reduced graphene oxide (RGO) and PANI in the solid state [1]. Here RGO plays a dual role as electron acceptor of reduced PANI (leucoemeraldine, LE) and as stable counterion of the doped state of PANI (emeraldine salt, ES). Hence the doping assisted charge-transfer leads to a partial redox doping of PANI by RGO stabilizing PANI in an atypical intermediate oxidation state between LE and ES. In addition, charge-transfer in R(GO-PANI) is responsible for improved material properties including enhanced conductivity, superior thermal and redox stability, and a remarkably high water dispersibility. These results may enable opportunities for the development of novel functional materials based [2,3] on graphene and intrinsically conducting polymers through improved processing routes [4,5].

References

[1] W.K. Maser, C. Vallés, P. Jiménez, E. Muñoz, A.M. Benito, J. Phys. Chem C, submitted (2011).

[2] S. Stankovich, Nature, **442,** 282 (2006)

[3] M.D. Stoller, S.J. Park, Y.W. Zhu, J.H. An, R.S. Ruoff, Nano Lett., **8,** 3498 (2008)

[4] D. Li, R.B. J. Kaner, Chem. Commun., 3286 (2005)

[5] P. Jiménez, W.K. Maser, P.Castell, M.T. Martínez, A.M. Benito, Macromol. Rapid Commun. **48**, 487 (2010)

Figures
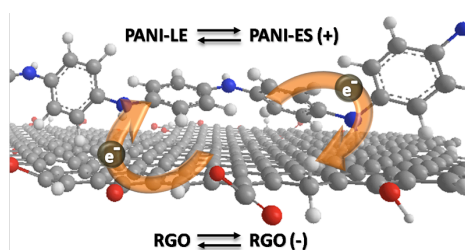
Donor-acceptor interactions in reduced (GO-PANI) charge transfer complex

Water soluble reduced (GO-PANI)

Atomic force microscope tip-induced local tunable oxidation of graphene

S. Masubuchi and T. Machida

[1] Institute of Industrial Science, University of Tokyo, 4-6-1 Komaba, Meguro-ku, Tokyo, 153-8505, Japan
[2] INQIE, University of Tokyo, 4-6-1 Komaba, Meguro-ku, Tokyo, 153-8505, Japan
[3] PRESTO-JST, 4-1-8 Honcho, Kawaguchi, Saitama, 332-0012, Japan
msatoru@iis.u-tokyo.ac.jp

Chemical functionalization of graphene is an attractive method for opening a transport gap in graphene because this method provides wide-range tunability of the transport gap. In this work, we report on a method for oxidizing graphene in nanometer scale region with variable extent of functionalization by using atomic force microscope (AFM) tip-induced local anodic oxidation (LAO) lithography.

The schematic setup for the LAO lithography is shown in Fig. 1. We used the contact-mode AFM in the enclosure box. The relative humidity was maintained at 75%. A negative bias voltage V_{tip} was applied to the conducting silicon cantilever with graphene and silicon substrate grounded in order to oxidize graphene. Fig. 2 shows the width of oxidized area w as a function of the scanning speed of AFM cantilever v_s from 5 to 200 nm/s and V_{tip} from 0 V to -9.0 V. The value of w depends systematically on v_s and V_{tip}. The minimum value of w was as small as 18 nm.

We fabricated graphene/graphene oxide/graphene (G/GO/G) junctions and conducted the transport measurements at T = 4.2 K. The current-voltage characteristic of the G/GO/G junction fabricated with the sufficiently large bias voltage V_{tip} = -8 V exhibits strong nonlinearity, which is qualitatively consistent with the results in metal/graphene oxide/metal junction. The size of the transport gap derived from the width of plateau in current-voltage curve is 2 eV. The size of transport gap in the junction is independent of the width of oxidized area w. The current-voltage characteristics are explained by the thermionic emission over Schottky barriers at G/GO interface.

When V_{tip} is increased from -8 V to -5.5 V so that the moderate oxidation takes place, the conductance of G/GO/G junction increases from 0.4 μS to 136 μS. The size of transport gap decreases from 2 eV to 0.1 meV. This result indicates that the transport gap of graphene/graphene oxide/graphene junction changes depending on the extent of oxidation in GO.

Thus the transport gap of G/GO/G junctions can be tuned by using LAO lithography using AFM. Since AFM lithography provides extremely fine oxidized patterns in graphene, one can form various sizes of transport gaps in graphene in nanometer scale region by using this technique. The results presented above indicate that LAO lithography using AFM is an attractive method for fabricating graphene-based nanoelectronic devices.

References
[1] S. Masubuchi, K. Suga, M. Ono, K. Kindo, T. Takeyama, and T. Machida, J. Phys. Soc. Jpn., **77** (2008) 113707.
[2] S. Masubuchi, M. Ono, K. Yoshida, K. Hirakawa, and T. Machida, Appl. Phys. Lett., **94** (2009) 082107.
[3] S. Masubuchi and T. Machida (in preparation).

Figures
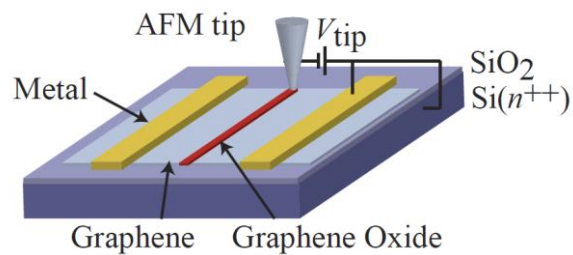
Figure 1 Schematic setup for the local anodic oxidation of graphene. A graphene flake is deposited on a SiO₂/Si substrate and is contacted by the metal electrodes. A negative bias voltage (V_tip) is applied to the conductive silicon cantilever with the graphene sheet and silicon substrate grounded.
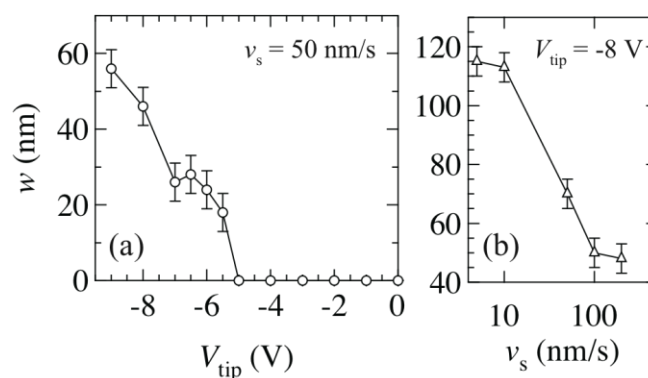
Figure 2 The width of oxidized area w as a function of (a) the bias voltage applied to AFM tip V_{tip} for vs = 50 nm/s and (b) the scanning speed of the AFM tip v_s for V_{tip} = -8 V.

Microscopic Correlation Between Chemical and Electronic States in Epitaxial Graphene Grown On SiC(000-1)

C. Mathieu[1], N. Barrett[2], J. Rault[2], Y. Mi[2], B. Zhang[3], W.A. de Heer[3], C. Berger[3], E. Conrad[3], O. Renault[1]

[1]CEA-LETI, MINATEC campus 17, rue des Martyrs – 34054 Grenoble Cedex 09, France
[2]IRAMIS/SPCSI/LENSIS, F-91191 Gif-sur-Yvette, France
[3]The Georgia Institute of Technology, Atlanta, Georgia 30332-0430, USA

claire.mathieu@cea.fr

The imaging of surfaces using X-ray PhotoElectron Emission Microscopy (XPEEM) has recently received considerable interest, mainly thanks to the use of high brilliance synchrotron radiation which facilitates the study of surface properties and chemical selectivity. The use of an energy filter permits to obtain chemical and work function mapping from real space imaging, which can be correlated, using reciprocal space imaging, to the complete band structure of a region of interest down to the micron scale.

We have studied spatial variations and correlations between the work function, chemical and electronic states of few layer graphene grown epitaxially on SiC(000-1), using full field, energy filtered XPEEM. Thanks to this technique, microscopic variations in the substrate/graphene interface are highlighted, depending on the graphene thickness (2-3 monolayers) and continuity. These variations would not be seen using area-averaged techniques, but are discernible on the length scale relevant for electronic devices. The full *k*-space band dispersion relations confirm the very high crystalline quality of the graphene layers and show a hitherto unobserved diffraction effect of the Dirac cones related to the registry between commensurately rotated graphene sheets. In the perspective of graphene for microelectronics, this underlines not only the importance of the sample preparation, but also the availability of spatially resolved spectroscopic tools to probe the local chemical and electronic structure.
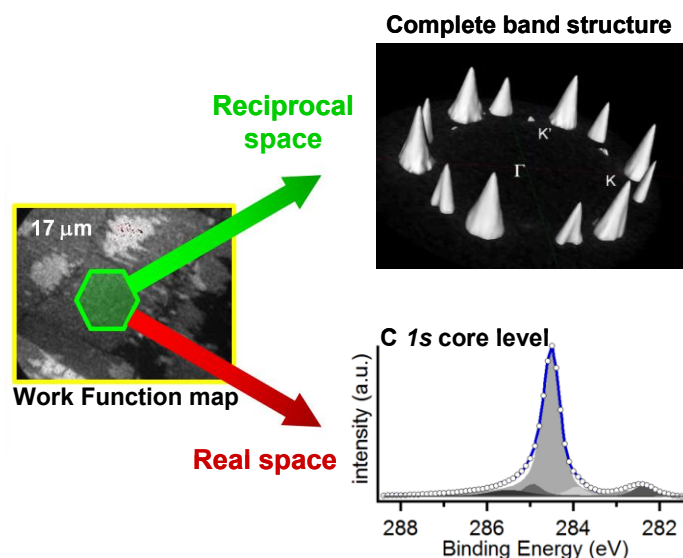
Figure 1: Work function map of a graphene sample epitaxially grown on a SiC(000-1) substrate. On a selected area, one can either image the real space, and obtain chemical information, or the reciprocal space and acquire the full band structure.

Optical Characterization of Single Layer and Few Layer Graphene

A. Matković[1,*]**, U. Ralević**[1,*], M. Jakovljević[1], G. Isić[1] and R. Gajić[1]

[1]Institute of Physics, University of Belgrade, Pregrevica 118, P.O. Box 68, 11080 Belgrade, Serbia
* Both authors contributed equally, amatkovic@ipb.ac.rs, uros@ipb.ac.rs

Graphene, a single layer of carbon atoms packed tightly into a honeycomb lattice, has been attracting wide attention due to its unique electrical, optical and mechanical characteristics. In order to fully understand this system and put in practical use remarkable effects that are manifested within, detailed characterization of its optical and electrical parameters is required. Here, we report on optical characterization of single layer and few layer graphene via infrared spectroscopy and spectroscopic ellipsometry. Micromechanically exfoliated graphene samples are prepared on SiO_2/Si substrate. Samples are then used for the characterization in NIR range by FT IR spectroscopy. Obtained reflectance is used for retrieving complex refraction index and conductivity of the sample in measured range. In the visible and UV range characterization is done by spectroscopic ellipsometry. Results are again used for retrieving complex refraction index and conductivity of the sample. In the measured ranges conductivity saturates to universal optical conductivity due to dominance of its interband component. Obtained results are in agreement with both theoretical and experimental data reported by other groups.

References

[1] K.S.Novoselov, D.Jiang, F.Schedin, T.J.Booth, V.V.Khotkevich, S.V.Morozov, A.K.Geim, Proc. Natl. Acad. Sci. U.S.A, **102** (2005) 10451.

[2] Z.Q.Li, E.A.Henriksen, Z. Jiang, Z.Hao, M.C.Martin, P.Kim, H.L.Stormer, D.N.Basov, Nat. Phys., **4** (2008) 532-535.

[3] K.F.Mak, M.Y.Sfeir, Y.Wu, C.H.Lui, J.A.Misewich, T. F.Heinz, PRL, **101** (2008) 196405

[4] V.G.Kravets, A.N.Grigorenko, R.R.Nair, P.Blake, S.Anissimova, K.S.Novoselov, A.K.Geim, Phys. Rev. B, **81** (2010) 155413.

[5] J.W.Weber, V.E.Calado, M.C.M van de Sanden, APL, **97** (2010) 091904

[6] H.Fujiwara, Spectroscopic Ellipsometry: Principles and Applications (Wiley, New York, 2007)

[7] G.W.Hanson, J.Appl. Phys., **103** (2008) 064302.

Figures
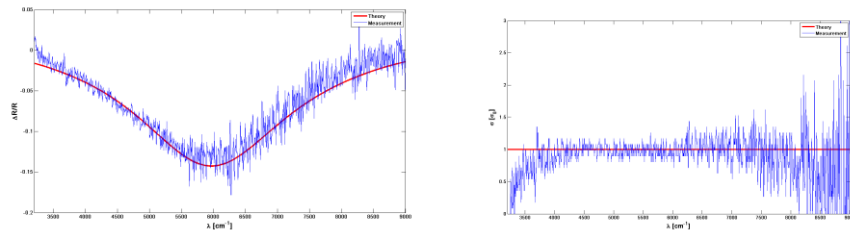
Figure1: NIR measured reflectance and calculated conductivity for single layer graphene sample.
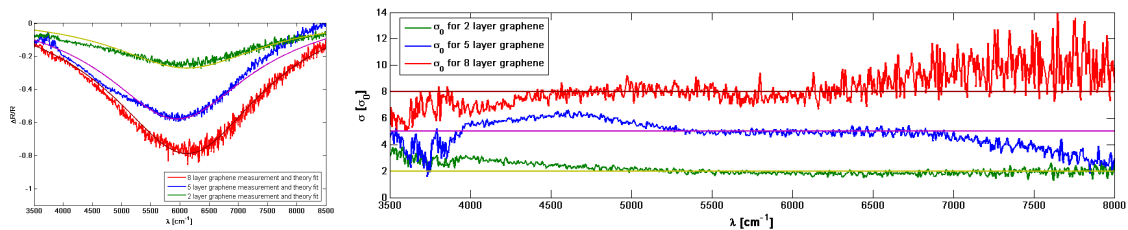
Figure2: NIR measured reflectance and calculated conductivity for different few layer graphene samples.
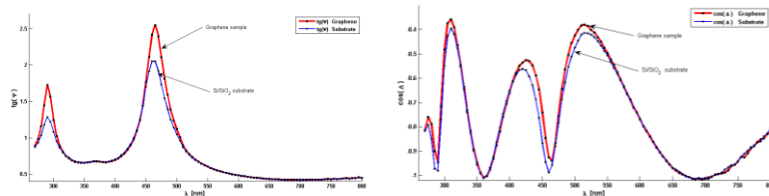
Figure3: Spectroscopic ellipsometry measurements of SLG sample (60º incidence angle).
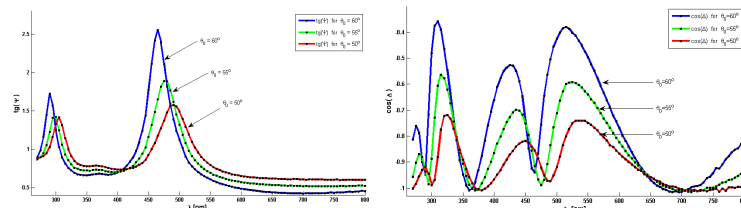
Figure4: Spectroscopic ellipsometry measurements of SLG sample (different incidence angles).
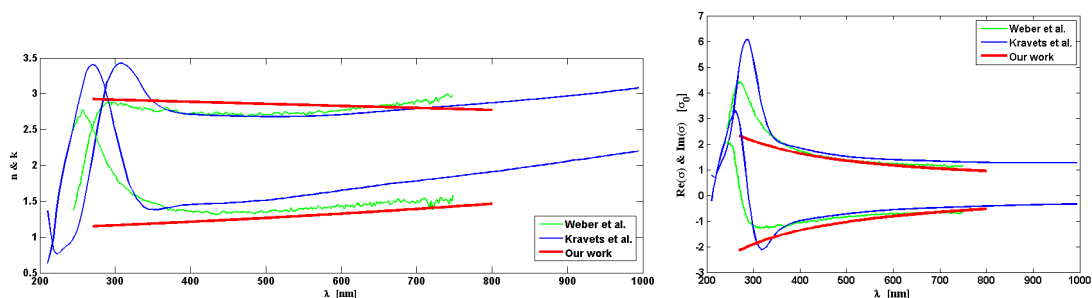
Figure5: Obtained complex refractive index and optical conductivity of SLG sample.

Chemical vapour deposition (CVD) growth of graphene on copper grains of different crystallographic orientations

Cecilia Mattevi[1], HoKwon Kim[1] and Manish Chhowalla[2]
[1] Department of Materials, Imperial College London, London, United Kingdom
[2] Department of Materials Science and Engineering, Rutgers, the State University of New Jersey, Piscataway, USA

c.mattevi@imperial.ac.uk

Large-scale production of high quality graphene thin films is necessary to integrate it into optoelectronic devices. Chemical vapor deposition (CVD) of graphene on copper is a scalable route for high quality deposition because copper is easy to etch, facilitating transfer onto insulating substrates [1] and it is inexpensive. In order to produce graphene films of high quality and variable thickness it is necessary to understand the mechanism of growth, which is dictated by the nature of graphene nucleation sites and their kinetics on the Cu surface. However the interrelated mechanisms of activation of graphene nucleation [2] and density of such sites as a function of the copper morphology, size and crystallographic orientation of grains, are not yet fully understood.

Here we demonstrate the thickness dependence of graphene on CH_4 (carbon precursor source) flow rate, growth pressure, different polycrystalline textures, morphologies and purity of Cu foils (Figure 1). We used different gas mixtures, namely CH_4 /H_2 and CH_4/H_2/Ar to grow graphene by low pressure (LP) CVD (0.03-0.5 Torr) and copper foils which underwent different manufacturing processes (Figure 1a).

Uniform graphene coverage (Figure 1b) was obtained at low CH_4 flow rate (0.5 sccm) on copper foils with uniform crystallographic orientations of the grains (Figure 1a). Higher growth pressure increased the graphene thickness only in specific areas that were higher in roughness. While applying the same growth conditions on Cu foils with random crystallographic orientation of the grains, the resulting film was composed of monolayers and 2-3 layers where the distribution of thicknesses reflects the underlying copper morphologies (Figure 1c). Finally, perceptible difference in the graphene nuclei growth directions and rate on different Cu orientations [(111) versus (100)] are reported (Figure 1d). Our results reveal that the graphene nucleation sites can be activated differently from the evolution dynamics of the Cu surface at high temperature, as well as from the CH_4 partial pressure. Hence, altering the copper texture and the feedstock could lead to control of the graphene thickness.

References

[1] X. Li, W. Cai, J. An, S. Kim, J. Nah, D. Yang, R. Piner, A. Velamakanni, I. Jung, E. Tutuc, S. K. Banerjee, L. Colombo, and R. S. Ruoff, Science **324**, (2009), 1312.
[2] J. M. Wofford, S. Nie, K. F. McCarty, N. C. Bartelt, and O. D. Dubon, Nano Lett. **10**, (2010), 4890.
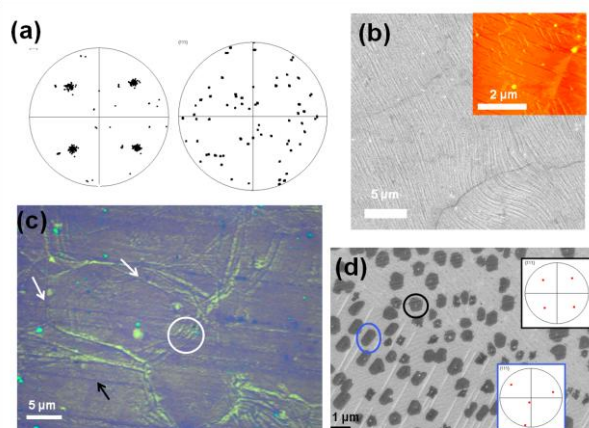
Figure 1. Electron Backscatter Diffraction (EBSD) pole figures display a strong texture of the Cu films in the first case (left) while a random crystallographic orientations of the Cu grains in the second case (right); (b) scanning electron microscope (SEM) image of single layer graphene grown on Cu film with preferential crystallographic orientations of the grains. Atomic force microscope (AFM) image of the copper morphology is reported in the inset; (c) optical image of transferred graphene on 300 nm SiO_2. The film thickness varies depending upon of the pre-existing copper morphologies. White arrows and circle indicate the profile of grooves while black arrow indicates areas of higher roughness; (d) SEM image of graphene nuclei grown on Cu grains of different crystallographic orientations. Nuclei with elongated shape are preferentially found on Cu (111) (blue circle), while nuclei with isotropic shape are preferentially found on Cu (100). EBSD pole figures display (111) and (100) orientation of the two adjacent Cu grains.

Enhancement of thermoelectric properties via resonant electronic transport in graphene nanoribbons

F. Mazzamuto, V. Hung Nguyen, J. Saint-Martin and P. Dollfus

Institut d'Electronique Fondamentale, CNRS-Univ. Paris-Sud, 91405 Orsay, France
Fulvio.mazzamuto@u-psud.fr

Besides the fascinating discoveries on graphene electronic properties [1, 2], much attention has been recently focused on thermal [3] and thermoelectric [4] properties of graphene structures. The promising results for two-dimensional graphene [5] have suggested also exploring thermoelectric properties of one-dimensional structures as the graphene nanoribbons (GNRs). Recently, it has been predicted that the thermoelectric figure of merit ZT can exceed unity in honeycomb chains of carbon atoms [6] and also in long rough edge GNRs [7]. However, detailed information on the potential of short GNRs to provide with a high factor of merit is still missing.

In this work a new way to enhance the figure of merit ZT in GNRs is proposed. The dependence of electronic and thermal transport on GNR edge orientation is explored and exploited to suggest a GNR structure with higher ZT values compared to the perfect armchair (AGNRs) and zigzag (ZGNRs) nanoribbons. The suggested structure is built by alternating different edge orientations in the ribbons (Mixed-GNR) as presented in Figure 1.a. In the figure are shown a perfect AGNR and a ZGNR with their elementary cells and a MGNR generated by alternating AGNR and ZGNR portions. The enhancement of thermoelectric properties in MGNR is connected to two main phenomena: the resonant tunneling of electrons and the reduction of thermal conductance.

In the analyzed ribbons, the figure of merit ZT, defined by the expression $T\, G_e\, S^2 / \kappa$ is evaluated by solving both the electron and phonon transport equations. The simulation of electron transport provides the thermopower S, the electronic conductance G_e and the electron contribution to the thermal conductance κ, while the simulation of phonon transport gives access to the phonon contribution to the thermal conductance. Charge transport simulations in the GNRs are developed on the basis of the non-equilibrium Green's functions (NEGF formamlism) and an atomistic tight-binding Hamiltonian is used to model the ribbons [8, 9]. In recent works the NEGF formalism has been successfully applied also to the phonon transport problem. In most of these works, a force constant model (FCM) limited to the fourth nearest-neighbors [10,7] was considered for phonons. Here, we use a similar method with a fifth nearest-neighbors FCM phonon Hamiltonian [11].

To present the enhancement of thermoelectric properties in MGNR the influence of GNR edge orientation on electronic, thermal and thermoelectric properties is investigated. We compare for instance 18-AGNR, 20-AGNR, 18-ZGNR and two 18-MGNRs with different elementary cells. The main simulation results may be summarized as follows: the electronic conductance, the thermal conductance, the thermopower and the figure of merit, calculated at room temperature, are shown in figure 1.b, 1.c, 1.d and 1.e respectively. Electron transport properties of the MGNR are strongly dependent on the fraction n of armchair edges and the fraction m of zigzag edges (MGNR (n,m)). As expected from an NNTB calculation, the ZGNRs have a metallic behavior and the AGNRs have a band gap strongly dependent on the number of dimmers in the elementary cell. In MGNR, the presence of armchair edges induces a band gap opening, and the presence of zigzag edges induces edge-localized electron states. So the armchair edge sections can be seen as barriers for the localized zigzag edge states. This interpretation is confirmed by the resonant oscillation of the electronic conductance and the positive values of the thermopower, which is a classical behavior of multi-barrier channels [12]. If the armchair edge section is narrow, MGNR (1, 1) for instance, the band gap is small and the resonant tunneling effect is not important. If the fraction of armchair edges over the zigzag ones is increased, as shown for an

MGNR (4,1), the width of the gap is enhanced and the resonant phenomenon becomes dominant. To explain this resonant tunneling effect, the atomic LDOS is plotted in Fig. 2 for the chemical potential of 0.3 eV. The figure shows clearly the regions of strong electron density localized at the zigzag edges separated by depleted armchair zones. In addition to this resonant tunneling effect, MGNRs exhibit very low thermal conductance compared to perfect AGNRs or ZGNRs. The phenomenon is probably due to the mismatch of phonon modes between AGNR and ZGNR portions. The resonant tunneling transport provides a rather high value of *S*, which induces a high *ZT* value of more than 0.1, boosted by the low thermal conductance. It is expected that further optimization of GNR structures with appropriate width may result in ZT values exceeding unity at room temperature.

References
[1]   A.K. Geim and K.S. Novoselov, Nature materials, **6** (2007) 183-191
[2]   A.H.C. Neto et al., Rev. Mod. Phys., **81** (2009) 109-162
[3]   A.A. Balandin et al. Nano Letters, **8** (2008) 902-907
[4]   Y.M. Zuev, W. Chang and P. Kim, Phys. Rev. Lett., **102** (2009) 096807
[5]   D. Dragoman and M. Dragoman, Appl. Phys. Lett., **91** (2007) 203116
[6]   X. Ni, G. Liang, J.S. Wang, and B. Li, Appl. Phys. Lett., **95** (2009) 192114
[7]   H. Sevinçli and G. Cuniberti, Phys. Rev. B, **81** (2010) 113401
[8]   G. Fiori and G. Iannaccone, Electron Device Letters, **28** (2007) 760-762
[9]   P. Zhao, J. Chauhan and J.Guo, Nano Letters, **9** (2009) 684-688
[10]   Y. Chen et al., J. Phys. Condens. Matter, **22** (2010) 372202
[11]   M. Mohr et al., Phys. Rev. B, American Physical Society, **76** (2007) 035439
[12]   G. D. Guttman, E. Ben-Jacob and D. J. Bergman, Phys. Rev. B, **51** (1995) 17758-17766
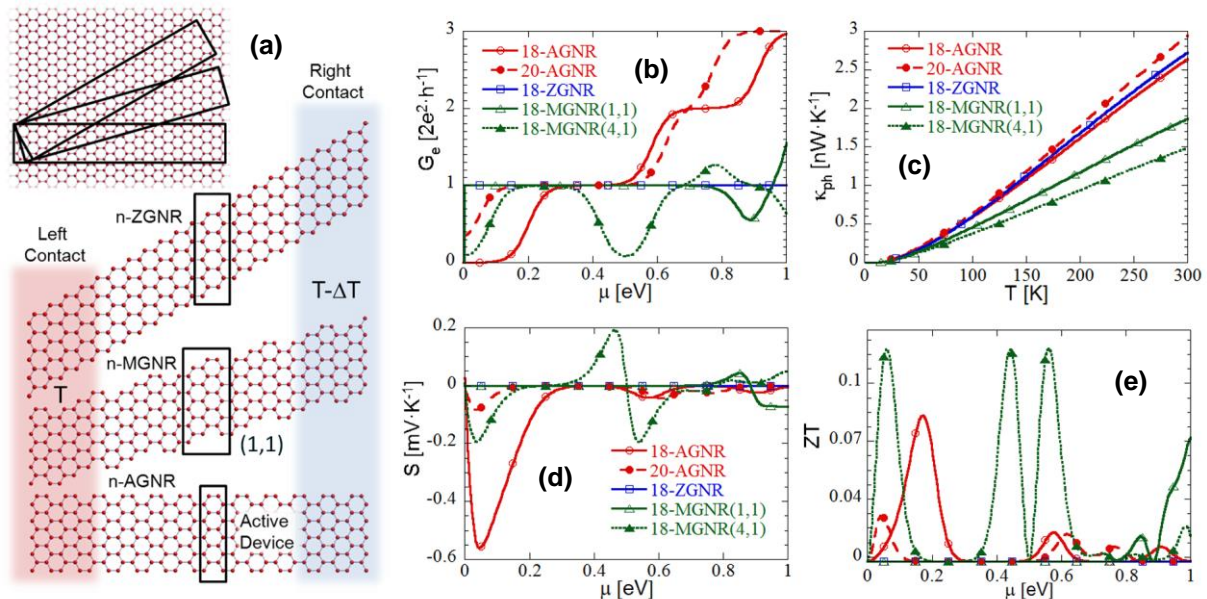
Figure 1. (a) Different edge orientations considered in simulations (b) Electronic conductance G_e as a function of the chemical potential μ, (c) phonon contribution to thermal conductance as a function of the temperature, (d) Seebeck coefficient and (e) factor of merit ZT as a function of chemical potential for a 18-AGNR, 20-AGNR, 18-ZGNR, 18-MGNR with chirality (1, 1) and 18-MGNR with chirality (4, 1).
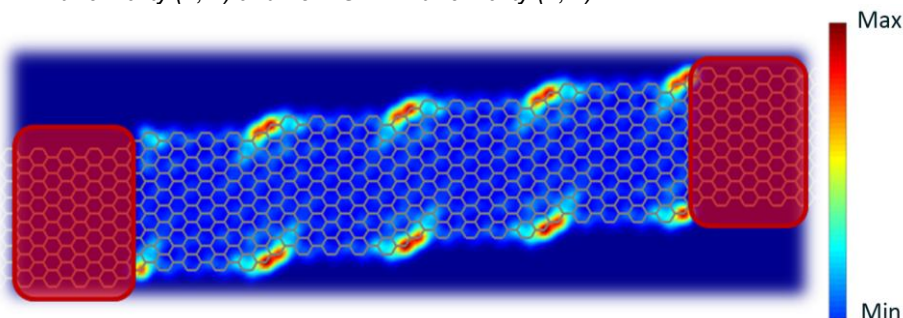
Figure 2. Atomic LDOS of the 18-MGNR with chirality (4,1) calculated at the chemical potential of 0.3 eV.

Graphene growth *via* electron beam

R. G. Mendes, A. Bachmatiuk, M. Knupfer, B. Büchner, M. H. Rümmeli

Leibniz Institute for Solid State and Materials Research Dresden, Helmholtzstrasse 20, 01069, Dresden, Germany

r.g.mendes@ifw-dresden.de

Since the first observation of graphene in 2004 by Geim and Novoselov [1], the research field of this new two-dimensional material has rapidly grown. Graphene has exciting physical properties such as high mechanical stiffness and excellent electronic transport properties [1,2]. These exceptional properties of graphene are thought to be used in a wide range of applications, from low-dimensional physics to drug delivery system in biomedicine [3]. One of the limitations to bring these applications to reality is our lack of understanding in graphene formation which ideally should be highly reproducible with atomic precision. Most of the techniques used for graphene production are time consuming and normally delivery material with many defects and impurities, which are not suitable for device fabrication.

Towards overcoming this problem we propose a new approach for the growth of graphene from fatty acids and polymers. Using these materials as a source of carbon and a TEM electron beam to drive the reaction we are able to coat oxide nanoparticles with graphene layers. In situ observations are presented and discussed. This approach might be an easy and inexpensive route for coating surfaces and nanoparticles with graphene.

References

[1]   Novoselov, K. S.; Geim, A. K.; Morozov, S. V.; Jiang, D.; Zhang, Y.; Dubonos, S. V.; Grigorieva, I. V.; Firsov, A. A. Electric field effect in atomically thin carbon films. *Science,* **306**(2004), 666 – 669.

[2]   Lee, C.; Wei, X.; Kysar, J. W.; Hone, J. Measurement of the elastic properties and intrinsic strength of monolayer graphene. Science, **321**(2008), 385–388.

[3]   Zhang, L.; Xia, J.; Zhao, Q.; Liu, L.; Zhang, Z. Functional graphene oxide as a nanocarrier for controlled loading and targeted delivery of mixed anticancer drugs. Small, **6(4)**, (2010), 537-544.

Electronic and transport properties of chemically functionalized nanographenes

Francesco Mercuri, Daniele Selli, Matteo Baldoni, Antonio Sgamellotti

ISTM-CNR, c/o Department of Chemistry – University of Perugia, 06123 Perugia, Italy
francesco.mercuri@cnr.it

Recent advancements in production techniques have allowed the synthesis and characterization of novel nanostructured materials based on graphene.[1] Particularly, recent research efforts have been targeted to the investigations of low-dimensional nanographenes, such as graphene quantum-dots (GQDs) and nanoribbons (GNRs). Here, the dimensional confinement at the nanoscale allows the tuning of the intrinsic electronic properties of graphene, which can potentially be exploited for the production of next-generation nanostructured electronic devices. Nevertheless, limitations in current experimental methodologies hinder both the controlled synthesis of nanographenes, with well-defined electronic properties, and large-scale production. To overcome these issues, the chemical modification of graphenes has been spotted as a viable route to produce materials with controlled and well-defined properties with potential use in applications. However, despite recent theoretical and experimental efforts,[2,3] a comprehensive understanding of the relationships between chemical structure and electronic properties in nanostructured graphenes is still missing. This concern is particularly critical in relation to the electron transport properties of chemically-modified graphenes, in view of their use in nanoelectronics.

In this work, we analyze, by means of density functional theory and non-equilibrium Green's function calculations, the electronic and transport properties of low-dimensional graphene nanostructures subjected to chemical functionalization. Our calculations concern models based on GQDs, GNRs and functionalized nanostructures thereof, targeting systems of interest in recent experiments, focused on oxidization and edge-functionalization of nanographenes.[4] In particular, we demonstrate how the remarkably versatile chemistry of sp^2 carbon and the use of traditional organic chemistry concepts[5,6] provide a reliable guide to rationalize the properties of chemically functionalized graphenes. The application of rigorous concepts in the definition of model systems and the use of high-performance computing platforms constitute crucial prerequisites for realistic simulations of low-dimensional carbon nanostructures aimed at the development of novel materials with potential application in nanoelectronics.

References

[1] Geim AK, Novoselov KS, Nature Materials, **6** (2007) 183.
[2] Allen MJ, Tung VC, Kaner RB, Chem. Rev., **110** (2010) 132.
[3] Castro Neto AH, Guinea F, Peres, NMR, Novoselov KS, Geim, AK, Rev. Mod. Phys., **81** (2009) 109.
[4] Ruoff R, Nature Nanotechnology, **3** (2008) 10.
[5] Baldoni M, Sgamellotti A, Mercuri F, Org. Lett., **9** (2007) 4267.
[6] Baldoni M, Sgamellotti A, Mercuri F, Chem. Phys. Lett., **464** (2008) 202.

Figures
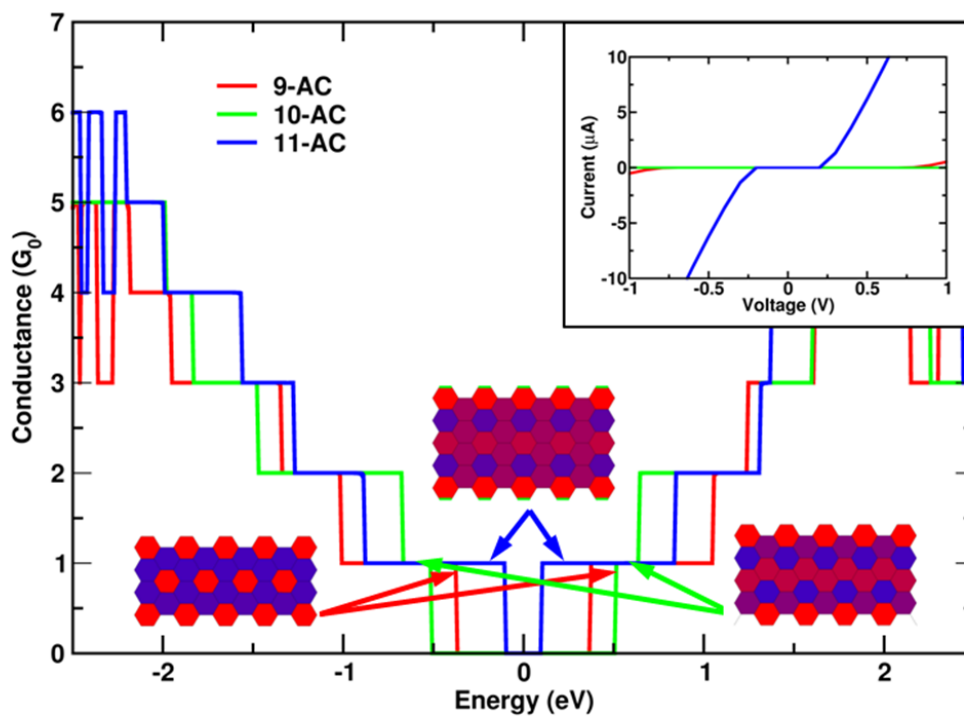
Transmission spectra and I(V) characteristics (inset) of armchair-edge 9-AC (red lines), 10-AC (green lines) and 11-AC (blue lines) GNRs. Optimized structures, color-coded according to their mean bond length (average of the six C-C bond lengths for each six-term ring), are also depicted above the corresponding transmission plateau.

Transport through quantum spin Hall insulator/metal junctions in graphene ribbons

Georgo Metalidis[1], Elsa Prada[2]

[1] Institut für Theoretische Festkörperphysik, Karlsruhe Institute of Technology (KIT), D-76128 Karlsruhe, Germany
[2] Instituto de Ciencia de Materiales de Madrid, (CSIC), Cantoblanco, 28049 Madrid, Spain

georgo.metalidis@kit.edu

Quantum spin Hall insulator/metal interfaces are naturally formed in graphene ribbons with intrinsic spin-orbit coupling by selectively doping two regions creating a potential step. For a clean graphene ribbon, the transmission of the topological edge states through a n-n or p-p junction is perfect irrespective of the ribbon termination, ribbon width and potential step parameters due to the orthogonality of incoming and outgoing edge channels. This is shown numerically for an arbitrary crystallographic orientation of the ribbon and proven analytically for zigzag and armchair boundary conditions. Perfect transmission is also present in n-p junctions for armchair and antizigzag terminations. In disordered ribbons, the orthogonality between left- and right-movers is in general destroyed and backscattering sets in. However, perfect transmission is restored by increasing the ribbon's width, even in the presence of strong edge roughness.

References

[1] G. Metalidis and E. Prada, arXiV:cond-mat/1012-4345.

Combined Focused-Electron-Beam-Induced-Deposition and Electron Beam Lithography for spin transport measurements in Graphene.

J. M. Michalik [a, b], J. Fan [a], L. Casado [a], S. Roddaro [c], M. R. Ibarra [a, b, d], J. M. De Teresa [b, d]

[a] Instituto de Nanociencia de Aragón, Universidad de Zaragoza, Zaragoza, 50018, Spain
[b] Departamento de Física de la Materia Condensada, Universidad de Zaragoza, Facultad de Ciencias, Zaragoza, 50009, Spain
[c] NEST, Istituto Nanoscienze-CNR and Scuola Normale Superiore, I56127 Pisa, Italy
[d] Instituto de Ciencia de Materiales de Aragón, Universidad de Zaragoza-CSIC, Facultad de Ciencias, Zaragoza, 50009, Spain

jmichali@unizar.es

Graphene – a single-layer hexagonal lattice of carbon atoms – has recently attracted a lot of attention in the scientific community, in particular after the observation of exotic transport phenomena such as the anomalous quantum Hall effect [1]. Moreover, a very high [2] and tunable conductivity at room temperature together with a spin polarized transport up to room temperature [3] makes graphene a promising material for applications in Spintronics. Investigation of the spin polarized transport in graphene becomes consequently of the key importance. This requires a clear distinction between charge and spin signals. In that sense, a "non-local" technique has been used by Tombros et al. [4] combined with the use of magnetic contacts.

The drawback of the commonly-used technique for fabricating electrical contacts (electron beam lithography, EBL) is that for the spin polarized transport measurement one needs an additional tunnel barrier between the contact and the sample in order to adjust their respective spin resistances. This increases the complexity of the lithography process and may possibly affect physical properties of graphene itself.

We have recently discussed [5] the influence of the FEBID on graphene. We showed that the deposition process, although up to some extent harmful for this material, is a good way of preparing complex graphene based devices. In our recent work (poster contribution by J. Fan et al.) we focus on the lithography (both Electron Beam and UV) processes.

Here, we present a complete procedure of fabrication of a fully operative graphene based device with magnetic electrodes, suitable for the investigation of spin transport. In our approach graphene flakes are obtained by mechanical exfoliation and deposited on thermally oxidized n-doped Silicon wafers (Au covered on the back-side for easy application of gate voltage). All the samples are first identified with optical microscope, and the most promising flakes are carefully checked by Raman spectroscopy. As a next step we perform EBL followed by Ti/Au evaporation and lift-off. In order to accomplish the device fabrication we put Cobalt electrodes by FEBID on top of graphene and connected to recently prepared connections. The Co electrodes have width varying from 100 nm to 1 μm assuring that the switching fields are different for each electrode thus allowing a study of spin polarized transport while sweeping applied magnetic field.

In Figure 1 we present the FEBID of Co that allows a very precise fabrication of magnetic electrodes on graphene flakes of size down to a few microns with well controlled dimensions.

Figure 2 presents a completed device optical image (left) and a close-up of the central part of the device, where the EBL and FEBID fabricated connections meet. Again one can appreciate a high accuracy of this two-step process allowing a nice combination of the two common nano- and microfabrication methods.

References

[1] K.S. Novoselov, A. K. Geim, S. V. Morozov, D. Jiang, M. I. Katsnelson, I.V. Grigorieva, S. V. Dubonos, A. A. Firsov, Nature London **438**,197 (2005)

[2] K. S. Novoselov, A. K. Geim, S. V. Morozov, D. Jiang, Y. Zhang, S. V.Dubonos, I. V. Grigorieva, and A. A. Firsov, Science **306**, 666 (2004); A. K. Geim and K. S. Novoselov, Nature Mater. **6**, 183 (2007).

[3] N. Tombros, C. Jozsa, M. Popinciuc, H. T. Jonkman , B. J. van Wees, Nature London **448**, 571 (2007)

[4] N. Tombros, S. Tanabe, A. Veligura, C. Jozsa, M. Popinciuc, H. T. Jonkman, B. J. van Wees, Phys. Rev Lett. **101,** 046601 (2008)

[5] J. M. Michalik, S. Roddaro, L. Casado, M. R. Ibarra and J. M. De Teresa, Accepted for publication in Microelectronic Engineering (available online; doi:10.1016/j.mee.2010.12.002)
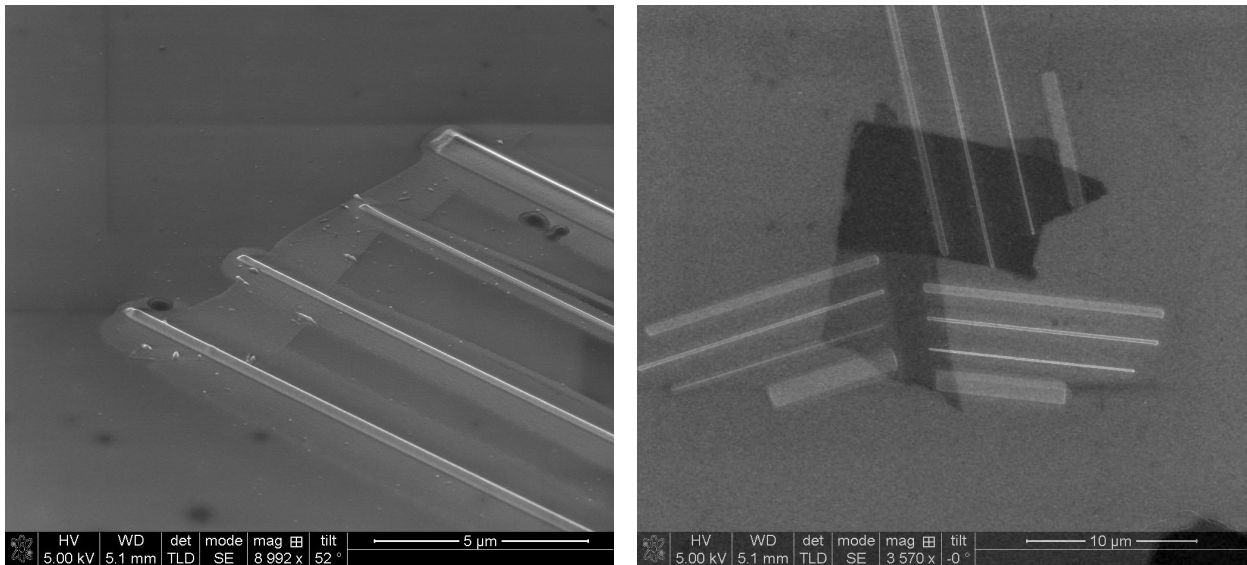
Figures

Figure 1. Left: SEM image of a graphene flake with FEBID deposited Co electrodes with different width for a non-local spin transport measurements (see text for details). Right: a proof of a high precision of the FEBID process – single layer, bilayer and multilayer graphene flake regions connected each with own set of four electrodes.
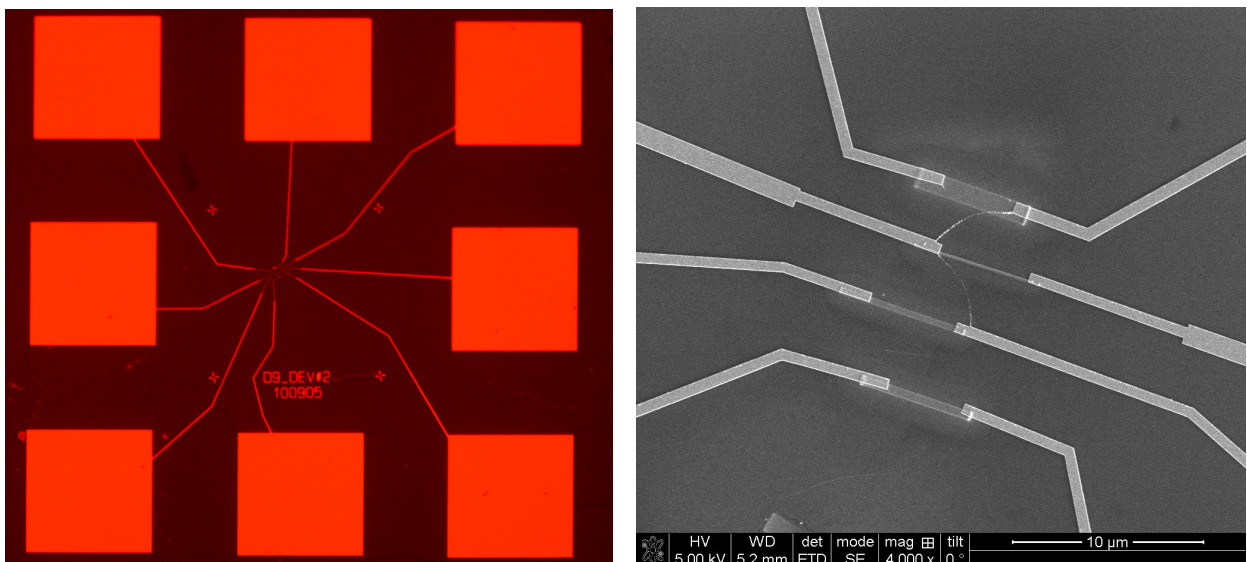
Figure 2. Left: optical microscope image of a complete graphene device for spin transport measurements. Central part of the device is presented in the SEM image on the right. Co FEBID electrodes are made on top of graphene flake (not visible in the photo). The rest of connections as well as large µWelding pads are fabricated with EBL and Ti/Au evaporation.

Frequency and damping of plasma waves in intrinsic graphene

S. A. Mikhailov

Institute of Physics, University of Augsburg, D-86135 Augsburg, Germany
sergey.mikhailov@physik.uni-augsburg.de

In contrast to conventional semiconductor materials the two-dimensional (2D) electrons and holes in graphene have not a parabolic but the linear energy dispersion near the Fermi level. This leads to many unusual electrical, mechanical, thermal and optical properties. In this work we theoretically study the electromagnetic response and plasma oscillations in *intrinsic* graphene, under the condition, when the chemical potential μ coincides with the Dirac points and the density of electrons and holes in the conduction and valence bands is determined by the finite temperature T (μ=0, T>0). In doped graphene ($|\mu|\neq0$, T=0) the plasma waves have been studied both within the Dirac model [1,2], when the electronic spectrum is described by two cones touching each other at the Dirac points, and within the full-band tight-binding approximation [3,4]. In intrinsic graphene the frequency of plasmons has been investigated only within the Dirac model in [5]. We calculate the electromagnetic properties of intrinsic graphene (the dielectric function and the polarization operator) within the self-consistent-field approach (equivalent to the random phase approximation) describing the spectrum of electrons and holes in full-band tight-binding approximation. We have found that the 2D plasmon frequency substantially differs from the result known in the literature [5]. We have also calculated the damping of the 2D plasmons and studied the influence of the wave-vector, temperature and the scattering rate of electrons on the plasmons damping. Nonlinear effects in the electromagnetic response of graphene have been also studied.

References

[1] B. Wunsch, T. Stauber, F. Sols, and F. Guinea, New J. Phys., **8** (2006) 318.
[2] E. H. Hwang and S. Das Sarma, Phys. Rev. B, **75** (2007) 205418.
[3] A. Hill, S. A. Mikhailov, and K. Ziegler, Europhys. Lett., **87** (2009) 27005.
[4] T. Tudorovskiy and S. A. Mikhailov, Phys. Rev. B, **82** (2010) 073411.
[5] O. Vafek, Phys. Rev. Lett., **97** (2006) 266406.

Substrate Dependent Raman D Band of Mechanically Exfoliated Graphene

Nobuhiko Mitoma, Ryo Nouchi, Xiao-Yan Fan, Katsumi Tanigaki

Tohoku University, 6-3 Aoba, Aramaki, Aoba-ku, Sendai, Japan
mitoma@sspns.phys.tohoku.ac.jp

Graphene is a rising star in recent condensed matter physics. It has been attracting lots of interests not only from the viewpoint of fundamental physics but also as an exciting potential candidate for future electronic devices. Here, we investigate the effect of substrates on the Raman D band of mechanically exfoliated graphene.

It is important to use graphene with high quality when we investigate its fundamental properties. There are several methods to obtain graphene such as chemical vapor deposition. We employ mechanically exfoliation in this study. This method is not suitable to application; however, graphene obtained from this method has less defects compared with graphene obtained from other methods.

We can get lots of information about graphene by using the Raman spectroscopy. Characteristic Raman spectra of graphene are named D($\sim$1350 cm^{-1}), G($\sim$1570 cm^{-1}), 2D($\sim$2680 cm^{-1}) bands. Among them the D band peak is thought to originate from defects in graphene. A recent paper[1] says that mechanically exfoliated graphene also shows very weak Raman D band and it originates from strongly-adsorbed atoms/molecules on the graphene surface.

We deposited graphene on various kinds of substrates and took Raman spectroscopy. Two of them are shown in Fig. 1. The blue curve is the data obtained from graphene on a pristine SiO$_2$ substrate, and the red one is from graphene on an O$_2$ plasma treated SiO$_2$ substrate. These curves are normalized with respect to the G band intensity and shifted for clarity. We can see peak shifts of the G and 2D bands. These are considered due to carrier doping effect as the O$_2$ plasma treated surface becomes hydrophilic and adsorbed H$_2$O molecules induce the doping effect. Magnified spectra around the D band is shown in Fig. 2. Weak but non-negligible D band has appeared with the sample on the pristine SiO$_2$ substrate. On the other hand, the peak was suppressed with the sample on the plasma treated substrate. If the adsorbates on the graphene surface induce the D band, both samples should display the D band. If the hydroxyl groups on the SiO$_2$ substrate enhance the D band, a larger peak should be observed in graphene on the O$_2$ plasma treated substrate. We propose an idea that the substrate surface roughness enhances the D band. We will discuss the origin of the substrate-dependent D band from the viewpoint of the curvature-induced D band[2].

References

[1] Z. H. Ni *et al*., Nano Lett., **10** (2010) 3868.
[2] A. K. Gupta *et al*., J. Phys.: Condens. Matter., **22** (2010) 334205.

Figures
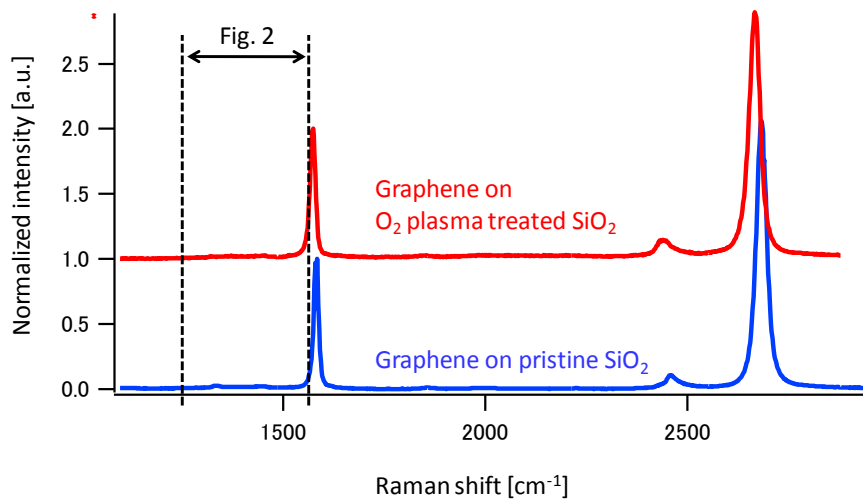
Fig. 1. Raman spectra of graphene on two kinds of substrates. The curves are normalized with respect to the G band intensity and shifted for clarity.
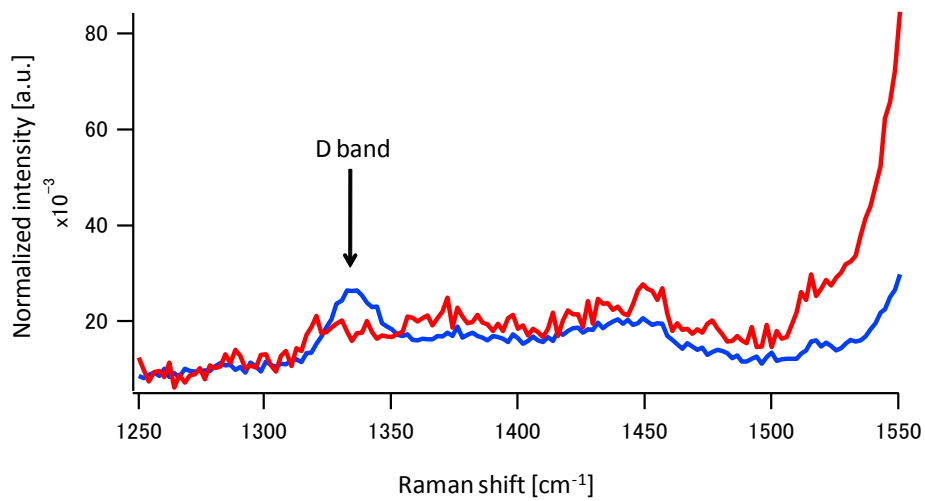
Fig. 2. Magnified Raman spectra around the graphene D band. The band is suppressed when graphene is on the O_2 plasma treated substrate.

Tunable transmission in a graphene photonic crystal in mid-infrared

Z. Moktadir, M. D. B. Charlton, M. E. Pollard, H. Mizuta and H. Rutt

Electronics and Computer Science, University of Southampton, Highfield, Southampton, SO17 1BJ, UK

zm@ecs.soton.ac.uk

Optical properties of Graphene have recently attracted enormous attention from investigators [1-5]. A significant amount of work is devoted to the calculation of optical conductivity σ(ω) with the aim of probing the interaction of light with this material. These calculations take the electronic band structure of graphene as their starting point and most of them are restricted to the low frequency range where the electronic dispersion is linear in energy i.e. $E(q) \propto q$ and optical properties are essentially captured by the Dirac Hamiltonian, which essentially describes two-dimensional massless Dirac fermions. At high frequency (energy), the electronic dispersion relation becomes non-linear and the optical conductivity is dominated by non-linear effects.

An expression for the real and the imaginary parts of the dynamic conductivity at low energies is given in reference[6] and reads:

$$Re(\sigma) = \sigma_0 \left(\frac{1}{2} + \frac{\hbar\omega^2}{72t^2} \right) \left(tanh \frac{\hbar\omega + 2\mu}{4k_BT} + tanh \frac{\hbar\omega - 2\mu}{4k_BT} \right)$$

$$Im(\sigma) = \frac{1}{\hbar\omega} \frac{4}{\pi} \sigma_0\mu - \frac{\sigma_0}{\pi} log \left| \frac{\hbar\omega + 2\mu}{\hbar\omega - 2\mu} \right| - \frac{\sigma_0}{36\pi} \left(\frac{\hbar\omega}{t} \right)^2 log \left| \frac{\hbar\omega + 2\pi}{\hbar\omega - 2\mu} \right|$$

In these equations: μ, ω and T are the chemical potential, angular frequency and the temperature respectively and $\sigma_0 = \pi e^2/2h$. The parameter $t \simeq 3\,eV$ is the hopping parameter linking nearest neighbours atoms in the graphene lattice.

In this work we investigate the mid-infrared transmission properties along the Γ-X direction of a square lattice graphene photonic crystal (GPhC). We show that transmission is widely tunable using the gate voltage as a tuning parameter. We also show that the transmission is less sensitive to temperature. The photonic crystal consists of an array of graphene discs patterned into a graphene sheet as shown in the inset to figure 1-a. The radius of each disc is 400 nm and the periodicity is set to 1 μm. Maxwell's equations for a TM-wave are solved by means of a 2D finite difference time domain method (FDTD). A broadband light pulse is launched from the left hand side of the structure and the transmission of the GPhC is monitored in the wavelength range [2 μm - 6 μm]. Periodic boundary conditions are implemented in the transverse direction. We write the refractive index as $n_r = \sqrt{1 + i\sigma(\omega)/\epsilon_0 d\omega}$, where $d \simeq 3.35\,\mathring{A}$ represents the graphite interlayer lattice constant [7]. The free parameters of the simulation are the temperature and the gate voltage.

The gate voltage V_g is related to the chemical potential by the relation $\mu = \sqrt{n\pi}\hbar v_0$ where $n = \epsilon_s\epsilon_0 V_g/e\Delta$, is the electron density, v_0 is the electron band velocity in graphene, Δ = 300 nm is the underlying oxide thickness and ϵ_s is the oxide relative permittivity.

 Figure 1-a shows transmission at *T* = 300 K and *Vg* = 80 *V*. We clearly see the collapse of the transmission at a cutoff frequency 9.0×10^{13} Hz. In figure 1-b we show the transmission spectrum for three different temperatures at a fixed gate voltage *Vg* = 80 *V*. We can see that, overall the temperature has little effect on the transmission of the GPhC. Figure 1-c shows the transmission spectrum for four different voltages V_g = 20, 40, 60 and 80 V, which clearly indicates that the transmission is modulated by varying the gate voltage. The drop in transmission from $V_g = 40$ V to $V_g = 80$V is about 25 dB. To identify a photonic bandgap in the structure we change the periodicity to 2 μm while the ratio of the radius of graphene discs to the period is set to 0.3. This is shown in figure 1-d where we can clearly identify two transmission gaps in the Γ-X direction.

This study shows that graphene can be used as an efficient light modulator in mid-infrared range of the spectrum, despite the fact that there are several practical challenges to overcome; mainly in-plane coupling of light to a two-dimensional graphene sheet.

References

[1] V. P. Gusynin, S. G. Sharapov, and J. P. Carbotte, Int. J. Mod. Phys. B 21, 4611 (2007)

[2] N. M. R. Peres, F. Guinea, and A. H. Castro Neto, Phys. Rev. B **73**, 125411 (2006).

[3] L. A. Falkovsky and A. A. Varlamov, Eur. Phys. J. B **56**, 281 (2007) .

[4] L. A. Falkovsky and S. S. Pershoguba, Phys. Rev. B **76**, 153410 (2007).

[5] A. B. Kuzmenko, E. van Heumen, F. Carbone, and D. van der Marel, Phys. Rev. Lett. **100**, 117401 (2008).

[6] T. Stauber, N. M. R. Peres, and A. K. Geim, Phys. Rev. B 78, 085432 (2008)

[7] T. G. Pedersen et al. Phys. Rev. B 77, 245431 (2008)
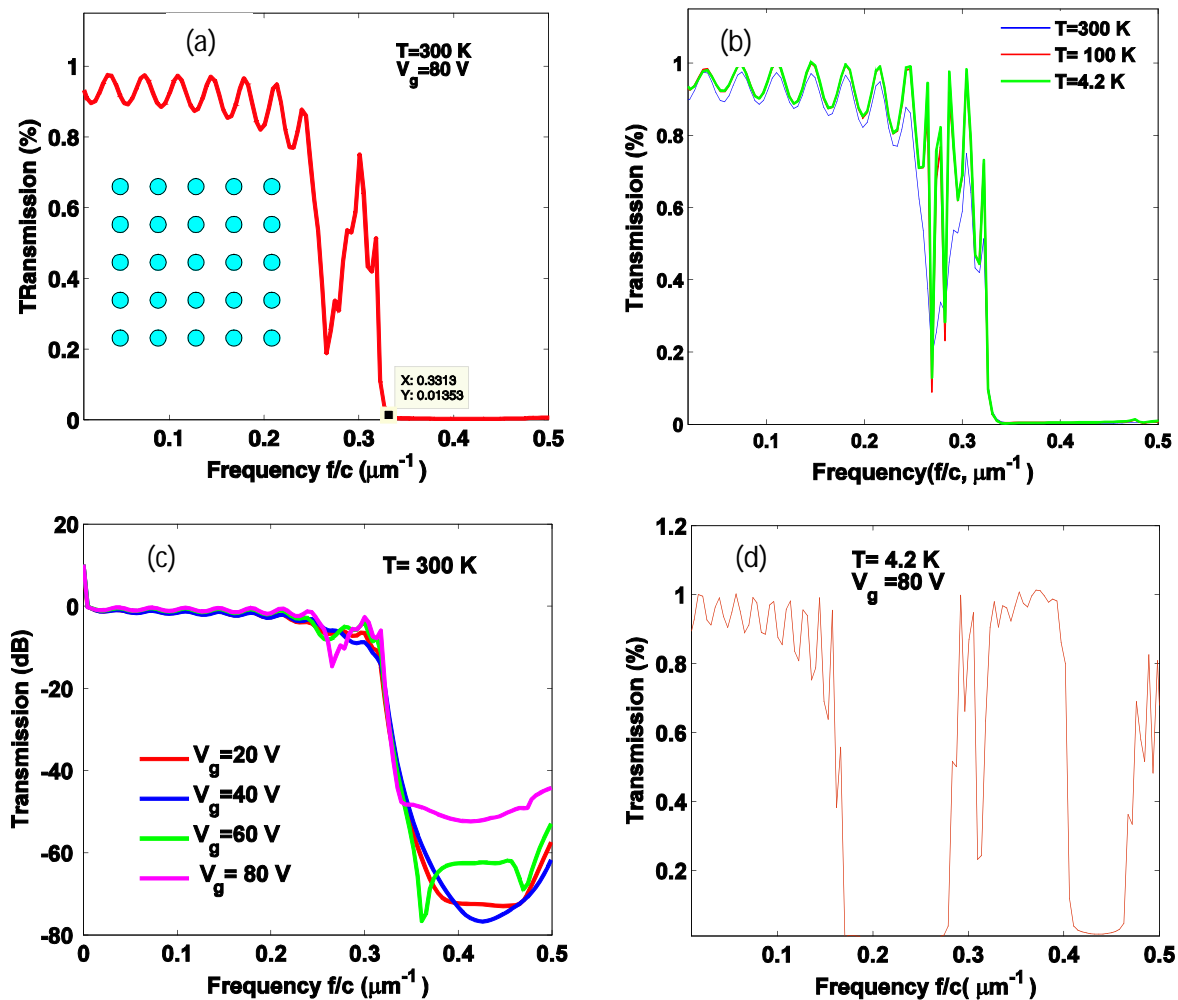
Figure 1: a) Transmission spectrum at V_g=80 V and T=300 K. The inset shows the GPhC structure, b) transmission at fixed voltage $V_g = 80$ V and at three different temperatures, c) transmission at fixed temperature T= 300 K and at values of V_g=20, 40, 60 , and 80 V, d) transmission of a GPhC with a period of 2 μm and a radius of the graphene discs of 600 nm, showing a photonic band gap.

Motion and merging of Dirac points in two-dimensional crystals

G. Montambaux, F. Piéchon, J.-N. Fuchs and M.-O. Goerbig

Laboratoire de Physique des Solides, CNRS, Université Paris-Sud, 91405-Orsay, France
montambaux@lps.u-psud.fr

We study under which general conditions a pair of Dirac points in the electronic spectrum of a two-dimensional crystal may merge into a single one. In the specific case of graphene, this situation is reached by a modification of one among the three hopping parameters between nearest neighbors. More generally, we consider the most general lattice Hamiltonian of a 2D crystal with two atoms or molecules per unit cell, and we show that Dirac points merge always at a symmetric point G/2 of the reciprocal space, where G is a reciprocal lattice vector.

The merging signals a topological transition between a semi-metallic phase and a band insulator. At the transition, the spectrum has the remarkable property to be linear in one direction and quadratic in the other direction. We derive a *universal Hamiltonian* that describes the vicinity of the transition, characterized by three parameters, a mass, a velocity and a driving parameter Δ whose values are related to the band parameters of any 2D crystal with time-reversal and inversion symmetries. This model describes *continuously* the coupling between valleys associated with the two Dirac points, when approaching the transition $\Delta=0$. We calculate thermodynamic quantities.

The spectrum in a magnetic field B is related to the resolution of a Schrödinger equation in an asymmetric double well potential. The Landau levels obey the general scaling law $\varepsilon_n \, \alpha \, B^{2/3} \, f_n(\Delta / \, B^{2/3})$ and evolve continuously from a $(n \, B)^{1/2}$ to a linear $(n+1/2)B$ dependence, with a $[(n+1/2)B]^{2/3}$ dependence at the transition. The spectrum in the vicinity of the topological transition is very well described by a semi-classical quantization rule.

The universal Hamiltonian is applied to the description of graphene-like structures. It reproduces analytically the low field part of the Rammal-Hofstadter spectrum for the honeycomb lattice, when one hopping integral is varied. We discuss the existence of such a merging of Dirac points in graphene-like structures, in the organic salt $(BEDT-TTF)_2 \, I_3$ and in optical lattices of cold atoms.

References

[1] P. Dietl, F. Piéchon and G. Montambaux, *New Magnetic Field Dependence of Landau Levels in a Graphenelike Structure,* Phys. Rev. Lett. **100** (2008) 236405

[2] G. Montambaux, F. Piéchon, J.-N. Fuchs, M. O. Goerbig*, Merging of Dirac points in a two-dimensional crystal,* Eur. Phys. J. B **72** (2009) 509

[3] G. Montambaux, F. Piéchon, J.-N. Fuchs and M.O. Goerbig*, A universal Hamiltonian for the motion and the merging of Dirac cones in a two-dimensional crystal*,   Phys. Rev. B **80** (2009) 153412

Evolution of the spectrum when the parameter Δ is varied and changes in sign at the topological transition. $\Delta \ll 0$ corresponds to the case of very weakly coupled valleys, like in graphene.

Spectrum of H

$$\varepsilon = \pm c\sqrt{2neB}$$

$$\varepsilon = \Delta + \sqrt{\frac{2mc^2}{\Delta}}\left(n+1/2\right)\omega_c$$

$$\varepsilon_n = A(mc^2)^{1/3}\left[(n+1/2)\hbar\omega_c\right]^{2/3}$$
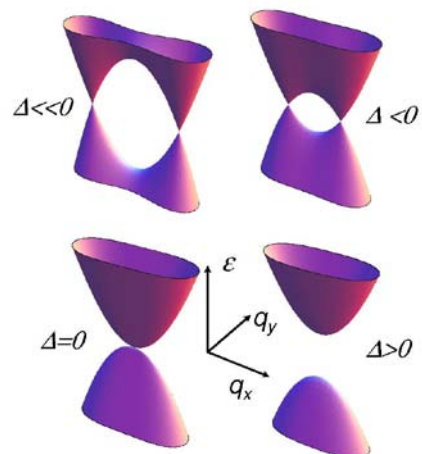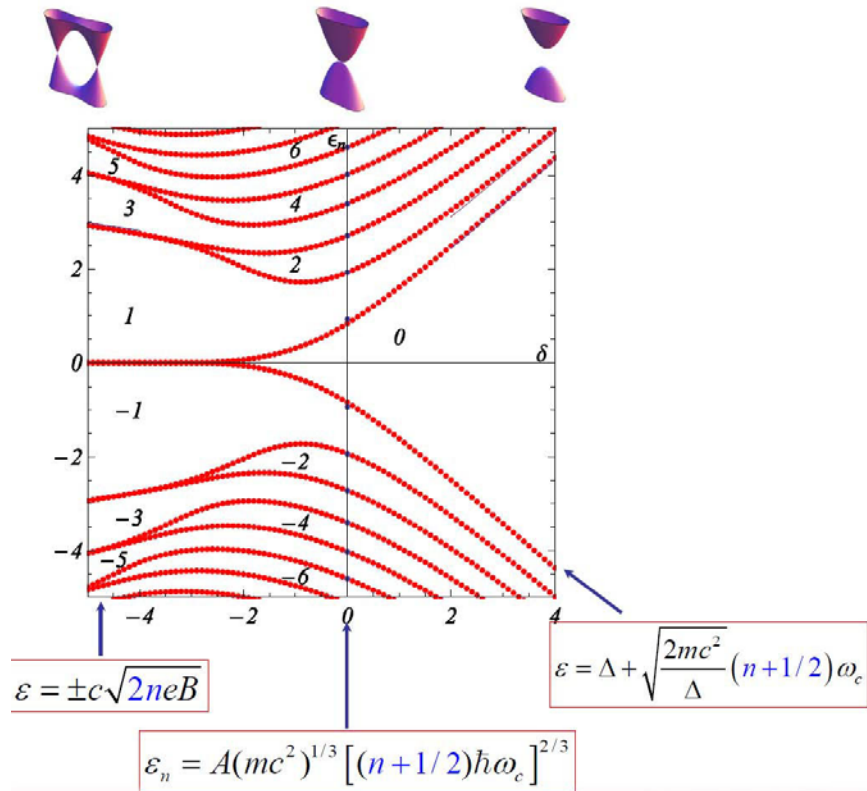
Evolution of the Landau levels spectrum as a function of Δ (δ in appropriate dimensionless units [3]). We describe the continuous evolution between the spectrum of two uncoupled valleys (graphene, left) to the usual Landau level spectrum (right), with a new power law at the topological transition ($\Delta=0$).

Towards graphene based quantum interference devices at nanoscale.

J. Munárriz, F. Domínguez-Adame, A. V. Malyshev

GISC, Departamento de Física de Materiales, Universidad Complutense, E-28040 Madrid, Spain
j.munarriz@fis.ucm.es

Graphene is a promising candidate for replacing semiconductors as basic material for the design of new nanodevices due to its truly two-dimensional geometry as well as large carrier mobility [1]. However, confining and controlling charge carriers in graphene can be a complicated task because of their very special tunneling properties [2]. Therefore, a significant amount of the efforts has been focused on graphene-based nanodevices that could enhance carrier confinement, such as *p-n* junctions [3, 4] and superlattices [5, 6, 7].

Interference effects of coherent electron transport through graphene nanorings open an alternative possibility to control quantum transport without relying on confinement. These interference effects were already observed as Aharonov-Bohm conductance oscillations in ring-shaped devices etched in graphene when a perpendicular magnetic field was applied [8]. In this contribution we introduce a new graphene interference device (GID) in which electron transport is controlled without applying a magnetic field. We demonstrate that charge carrier transport can be tuned instead by applying a lateral gate voltage across a graphene nanoring. We show that in this case the relative phase of the electron wavefunction in the two arms can also be varied, leading to a constructive or destructive interference at the output and, therefore, to current modulation and control.

It is well known that the type of the nanoribbon edges (zigzag or armchair) determine its electronic structure [1]. To avoid the impact of energy structure changes on the transport, we used the ring geometry with 60° turns, so that the type of edges remains the same for the whole sample. The results depicted in Fig. 1 correspond to samples having lead widths of 20 (left panel) and 21 (right panel) unit cells (4.9 and 5.1 nm contact widths respectively). The nearest-neighbor tight-binding Hamiltonian formalism and quantum transmission boundary method [9] were employed to calculate the transmission coefficient and current-voltage characteristics of the device for different source-drain, back-gate and lateral gate voltages.

For energies close to the Fermi energy (which can be controlled by the back gate), two types of behavior were obtained. Nanorings with armchair edges having an intrinsic energy gap manifested wide transmission bands (see Fig. 1, left panel), while resonance-like behavior characterized by very sharp peaks in the transmission were observed in the remaining cases (see Fig. 1, right panel). Such narrow transmission peaks can easily be affected by disorder or other perturbations resulting in low reliability of devices of these types. Contrary to that, the former case is much more promising. We demonstrate that the modulation of the wide transmission bands shown in Fig. 1 are due to the interference effects. Figure 2 displays density plots of the electron wavefunctions in the considered GID calculated for three lateral gate voltages corresponding to maxima/minima of the transmission (marked with red dots in the left panel of Fig. 1). For an electron incident from the left, a clear constructive interference at the output (at the right extreme of the device) can be seen for the voltages corresponding to transmission maxima while the destructive interference pattern is observed for the case of zero transmission resulting in vanishing current. We argue therefore that our proposed device design promises various applications, such as a graphene based quantum interference transistor with high on/off ratio.

References

[1] A. H. Castro Neto, F. Guinea, N. M. R. Peres, K. S. Novoselov and A. K. Geim, Rev. Mod. Phys, **81** (2009), 109.

[2] M. I. Kastnelson, K. S. Novoselov and A. K. Geim, Nat. Phys. **2** (2006), 620.

[3] J. R. Williams, L. DiCarlo and C. M. Marcus, Science, **317** (2007), 638.

[4] H.-Y. Chiu, V. Perebeinos, Y.-M. Lin and P. Avouris, Nano Lett. (in press) (2010).

[5] C. Bai and X. Zhang, Phys. Rev. B, **76** (2008), 075430.

[6] H. Sevinçli, M. Topsakal and S. Ciraci, Phys. Rev. B, **78** (2008), 245402.

[7] M. Yang, A. Nurbawono, C. Zhang, Y. P. Feng and Ariando, Appl. Phys. Lett, **96** (2010), 193115.

[8] S. Russo *et al*, Phys. Rev. B, **77** (2008), 085413.

[9] D. Z.-Y. Ting *et al*, Phys. Rev. B, **45** (1992) 3583.

Figures
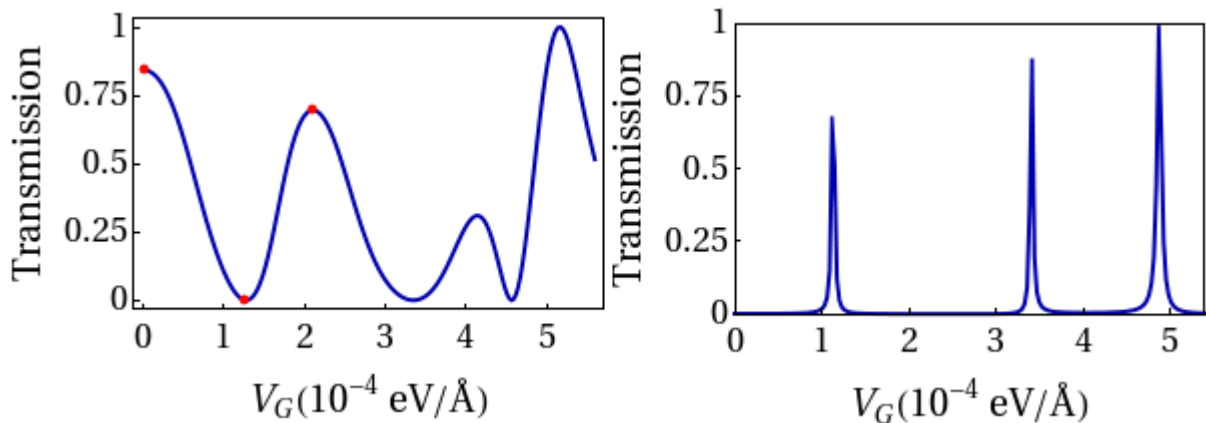
Figure 1: Transmission coefficient for two different nanorings at a given energy E=0.15 eV as a function of the applied lateral electric field. Left panel – all nanoribbons comprising the ring have widths of 20 unit cells (corresponding to a Dirac-like dispersion relation), right panel – sample with 21 unit cells wide branches (the parabolic dispersion case). The resonance-like behavior in the former case and the interference-like one in the latter case can be seen.
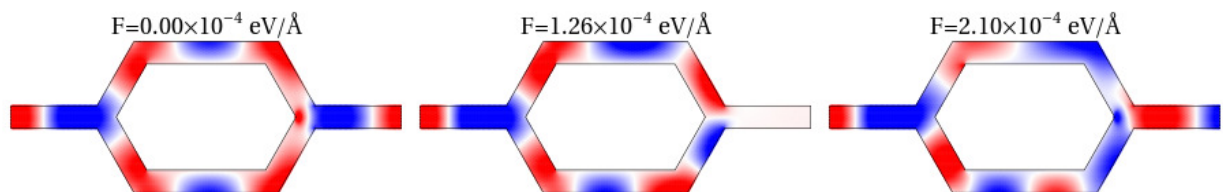
Figure 2: Density plot of the real part of the electron wavefunction for three lateral gate voltages (corresponding to red points in the left plot of Fig. 1). For the sake of clarity, only a regular sublattice of atoms (around ¼ of the total number of atoms) is plotted. Interference effects due to different number of nodes/antinodes of the wavefunction in the two branches can clearly be seen at the output (right extreme of the nanoring).

Hydrocarbon Sensing in Aqueous Solutions Using a Functionalized Graphene Chemiresistor

Matthew Myers[1,2], James Cooper[3], Bobby Pejcic[1], Murray Baker[2], Burkhard Raguse[3] and Lech Wieczorek[3]

[1]CSIRO, Earth Science and Resource Engineering, Kensington, WA 6151, Australia
[2]University of Western Australia, School of Biomedical, Biomolecular and Chemical Sciences, Crawley, WA 6009, Australia
[3]CSIRO, Material Science and Engineering, Wealth from Oceans Flagship, Lindfield, NSW 2070, Australia

matt.myers@csiro.au

Chemiresistor sensors based on carbon black/polymer composites, carbon nanotube/polymer composites and conductive polymers (e.g., polyaniline nanofibres and PEDOT-PSS) have been used extensively to detect a wide variety of analytes (e.g., benzene, aniline, chloroform) in the vapor phase [1, 2]. However, there is a need for direct detection of aromatic hydrocarbons (e.g., benzene and toluene) dissolved in water for environmental monitoring and oil exploration applications. Chemiresistors are particularly attractive due to their potentially very low per unit cost and are simple to operate. Most chemiresistor designs are not suitable for direct sensing in aqueous environments due to interfering conductive pathways through water. However, if micron sized electrodes are used, a very small double layer capacitance between the sensing film and the bulk water is formed [3]. This results in a large effective impedance through the conducting aqueous medium (e.g., deionized water or seawater) allowing for the conductivity of sensing film to be measured independently. This principal has been demonstrated using conducting films of hexanethiol functionalized gold nanoparticles to sense toluene dissolved in water with a 100 ppb detection limit [3]. The proposed response mechanism is based on the swelling of the nanoparticle film resulting in an increase in the effective distance between the individual nanoparticles leading to a decrease in the inter-particle tunneling current.

Recently, hydrazine reduced dispersions of graphene oxide have been used in to detect NO_2, NH_3 and 2,4-dinitrotoluene in a chemiresistor type platform [4]. The sensor response is based on a charge transfer mechanism in which the analyte affects the electronic states of the graphene causing a change in conductance [5]. In this study, we demonstrate that dispersions of octadecylamine functionalized graphene nanosheets [6], which have been drop cast onto interdigitated microelectrodes (5 μm wide and 5 μm separation) can be used for directly sensing aromatic hydrocarbons dissolved in water. The graphene nanosheets range from 0.5 to 3 μm in size which implies that there are only a few interconnects between the separate graphene nanosheets spanning the electrodes. The equilibrium response to varying concentrations of toluene in water is given in Figure 1. The detection limit for benzene, toluene, ethylbenzene, xylenes and cyclohexane ranges from 3 ppm to 10 ppm. The response time to analyte solutions is generally less than 60 seconds and restores to the baseline in less than 120 seconds when exposed to pure water (see Figure 2 for toluene responses). Based on the comparable responses to cyclohexane (response slope $\Delta R/R_0 \sim 19.1 \times 10^{-5}$ / ppm) vs. benzene (response slope $\Delta R/R_0 \sim 9.09 \times 10^{-5}$ / ppm), we deduce that the mechanism is most likely attributed to swelling and not chemical doping. If chemical doping contributed significantly to the sensing mechanism, the response to cyclohexane which cannot participate in pi-pi interaction would be diminished.

We are currently working on incorporating other functionalized graphene nanosheets and/or other chemiresistor materials (e.g., conducting polymers and carbon nanotubes) into sensor arrays for improved analyte differentiation.

References

[1] D. James, S. M. Scott, Z. Ali and W. T. O'Hare, Microchimica Acta, **1-2**, (2005), 1-17.

[2] A. D. Wilson and M. Baietto, Sensors, **7**, (2009), 5099-5148.

[3] B. Raguse, E. Chow, C. S. Barton and L. Wieczorek, Analytical Chemistry, **19**, (2007), 7333-7339.

[4] J. D. Fowler, M. J. Allen, V. C. Tung, Y. Yang, R. B. Kaner and B. H. Weiller, ACS Nano, **2**, (2009), 301-306.

[5] X. C. Dong, D. L. Fu, W. J. Fang, Y. M. Shi, P. Chen and L. J. Li, Small, **12**, (2009), 1422-1426.

[6] G. X. Wang, X. P. Shen, B. Wang, J. Yao and J. Park, Carbon, **5**, (2009), 1359-1364.

Figures
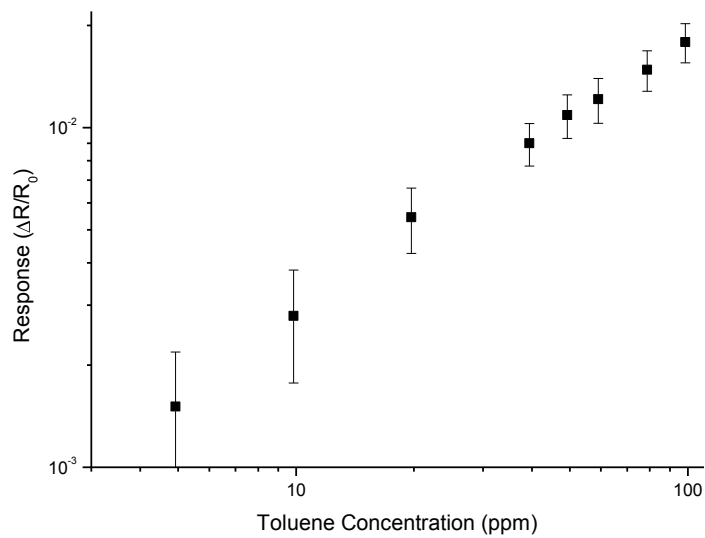
Figure 1. Equilibrium responses of ODA functionalized graphene chemiresistors to toluene (5 to 100 ppm)
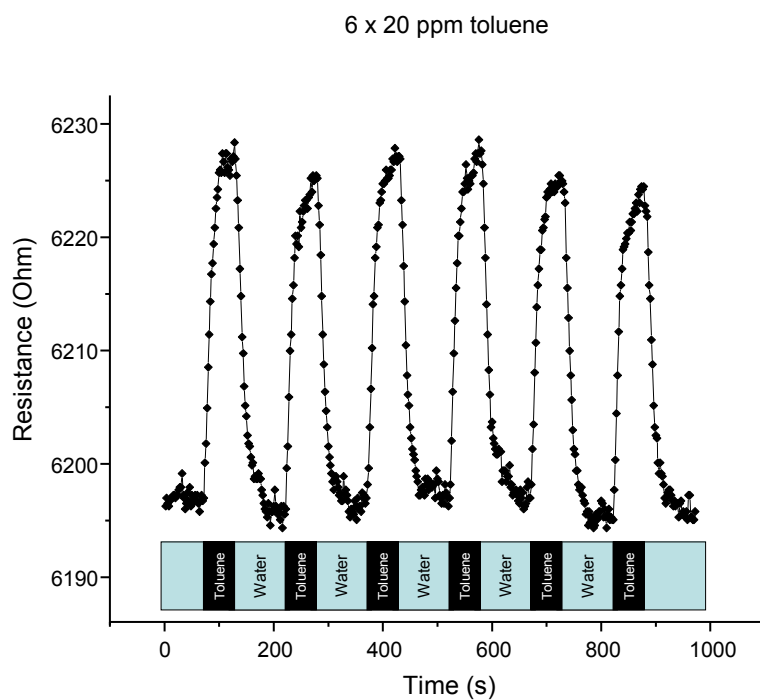
6 x 20 ppm toluene

Figure 2. Response to cycling of 20 ppm toluene in water (45 seconds) and de-ionized water (90 seconds)

316

Quantum Transport in a Graphene Waveguide with Smooth Edge Terminations by Magnetic Vector Potential

Nojoon Myoung[1], Gukhyung Ihm[1], and S. J. Lee[2]

[1]Department of Physics, Chungnam National University, Daejeon 305-764, Republic of Korea
[2]Quantum-functional Semiconductor Research Center, Dongguk University, Seoul 100-715, Republic of Korea
ghihm@cnu.ac.kr

Graphene is a single atomic layer of carbon atoms of which low-lying excitation provides quasi-particles obeying the linear dispersion relation near the specific point in the momentum space called the Dirac points. For the freestanding graphene, the equality of two Dirac points leads to the valley degeneracy in addition to the spin, and the quasi-particles, which are named as the Dirac fermions, are massless and chiral. Because of these properties, the Klein tunneling has been an obstacle to using graphene for nanoelectronics[1]. In order to overcome it, magnetic vector potential structures induced by inhomogeneous magnetic fields can be candidates for a way of fabricating graphene-based electronic devices. Actually, the Dirac fermions are reflected and confined by the magnetic vector potential structures which do the role of potential structures in a real sense[2,3,4]. This magnetic confinement also allows us to overcome another difficulty in realizing graphene nanoelectronic devices such as graphene nanoribbons, which comes from the edge nature of graphene. There are typically two kinds of edge-terminations in graphene nanostructures, armchair and zigzag, and the electronic states are very sensitively dependent on the edge nature[5,6]. However, it is difficult to prepare nano-sized graphene samples having clean edges with the atomic-scaled precision.

In this study, we show that the waveguide is produced by applying the delta-function-like profile of magnetic field to the graphene sheet, and also investigate quantum transport in the magnetically modulated graphene waveguide in which the magnetically induced scattering potential is introduced at the center. This profile of magnetic field can be generated experimentally by using ferromagnetic gates onto the graphene layer as depicted in Fig. 1. The magnetically modulated graphene waveguide is treated as a quantum-wire with the finite conducting channels. Similar to the typical quantum-wire, the number of the conducting channels depends on the Fermi energy. In results, the well-localized current density is observed in the unmodified waveguide, and the conductance is calculated by the Landauer-Buttiker formula, which exhibits the stepwise increase as a function of energy. The interesting situation occurs when the waveguide is modified by introducing a magnetic potential barrier as a scattering center in the sense that the backscattering and foregoing Dirac fermions experience effectively different potential structures. While the foregoing Dirac fermions are still confined, the backscattering fermions are no longer confined because the effective potential depends on the longitudinal momentum, q_x. For the modified waveguide, the conductance becomes oscillatory as shown in Fig. 2. The threshold energies to open the conducting channel are shifted because the scattering potential affects the transport properties. The results in the present study may provide the novel candidate for applications of graphene-based transport devices.

References

[1] M. I. Katsnelson, K. S. Novoselov, and A. K. Geim, Nature Phys., **2** (2006) 620.
[2] N. M. R. Peres, A. H. Castro Neto, and F. Guinea, Phys. Rev. B, **73** (2006) 241403(R).
[3] A. De Martino, L. Dell'Anna, and R. Egger, Phys. Rev. Lett., **98** (2007) 066802.
[4] N. Myoung, and G. Ihm, Physica E, **42** (2009) 70.
[5] L. Brey, and H. A. Fertig, Phys. Rev. B, **73** (2006) 235411.
[6] L. Yang, C. H. Park, Y. W. Son, M. L. Cohen, and S. G. Louie, Phys. Rev. Lett., **99** (2007) 186801.

Figures
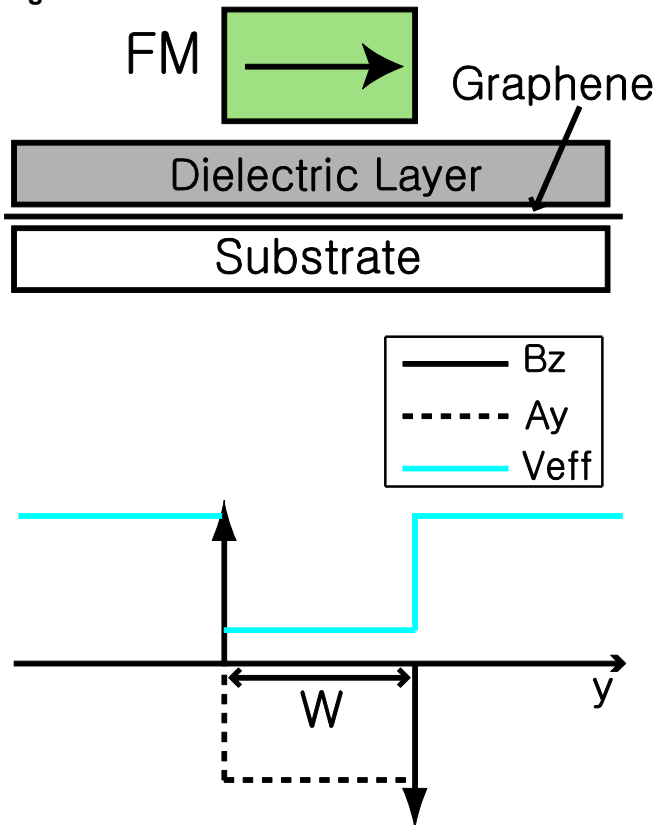
Figure 1
Schematic view of experimental setup and model.
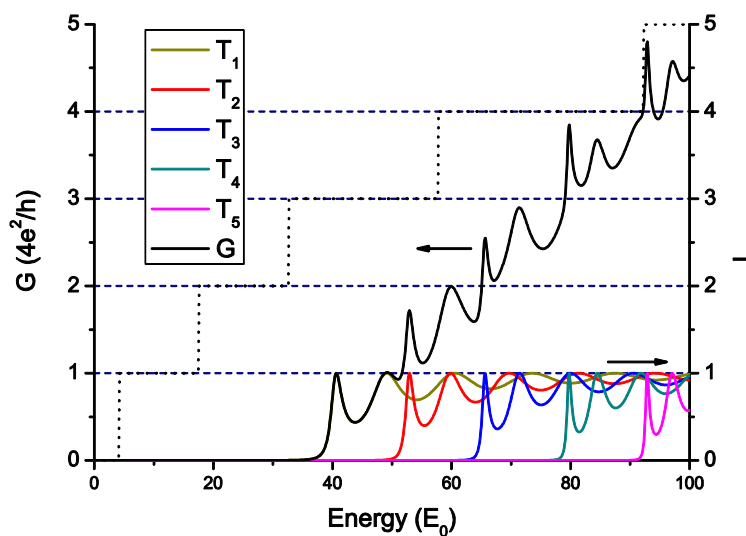
Figure 2
Conductance of the graphene waveguide and transmission probabilities for each channel.

Hybrid Graphene-Superconductor Devices

Matthew Newman, Gavin Burnell

E.C. Stoner Laboratory, School of Physics and Astronomy, University of Leeds, UK
pymn@leeds.ac.uk

An interesting consequence of the crystallographic structure of graphene is that its charge carriers are described as massless relativistic particles. The ability to isolate individual graphene layers therefore enables us to investigate relativistic phenomena in a solid state system. A particularly interesting method of probing this unusual electronic state is to interface graphene with superconducting materials whereby unique characteristics such as specular Andreev reflection are expected to be observed. While there is a wealth of theoretical work on superconducting graphene devices present within the literature there remains very little experimental work published to date. The vast majority of experimental work has so far concentrated on using Aluminium as the superconductor. We have investigated the use of Niobium which has a larger superconducting gap and allows for measurements at higher temperatures.

To further investigate the unique transport characteristics of graphene we are fabricating planar Josephson junctions using graphene as a barrier medium. Devices have been fabricated by mechanical exfoliation of graphite with single layer graphene flakes identified using Raman spectroscopy. Electron beam lithography was used to pattern contacts with separations of ~100nm which were subsequently sputter deposited with Pd/Nb using a DC magnetron. We present low temperature measurements taken on these devices showing evidence of Andreev reflection occurring at the graphene-superconductor interface. Andreev reflection is shown to be influenced by the application of a back gate voltage as well as being modified by low temperature current annealing.

Charge and spin transport in bilayer graphene nanostructures using non-equilibrium Green's function technique

V. Hung Nguyen[1,2], A. Bournel[1], and P. Dollfus[1]

1. Institut d'Electronique Fondamentale, UMR8622, CNRS, Univ. Paris Sud, 91405 Orsay, France.
2. Center for Computational Physics, Institute of Physics, VAST, PO Box 429 Bo Ho, Hanoi 10000, Vietnam.
Email: viet-hung.nguyen@u-psud.fr

Though it is unsuitable for standard digital applications, the gapless character of graphene with chiral massless Dirac carriers gives to this material unusual and attractive transport properties which deserve to be considered carefully [1]. Additionally, there are several ways of inducing bandgap in graphene, which still enlarge the possible fields of application. The first idea is to cut mono-layer graphene into nanoribbons to benefit from induced quantum confinement effect. Alternatively, the interaction with an SiC substrate can break the symmetry of the two sub-lattices forming the graphene crystal, which can open a bandgap of up to 0.26 eV [2]. A similar bandgap may be also induced in bi-layer graphene by applying a vertical electric field [3,4]. Finally, thanks to very weak spin-orbit interaction leading to spin flip length higher than 1.5 µm [5], graphene also offer a high potential for spintronics.

In this work, the non-equilibrium Green's function calculation developed in ref. [6] has been extended to treat the transport equation of chiral fermions in bilayer graphene nanostructures. The approach has been applied to investigate the transport properties of charges in typical structures, including a single potential barrier, a double gate or a ferromagnetic gate. In single barrier structures, the chiral resonant tunnelling effect and the resulting negative differential conductance is shown to be stronger than in monolayer graphene [7], as illustrated in Fig. 1. Especially, strong oscillation of transconductance with respect to the barrier height can be achieved. In double gate structures, our study shows the appearance of an electrical current gap and therefore demonstrates the possibility of switching the current by tuning the gate voltages [8]. Considering ferromagnetic gate structures, a significant improvement of spin polarization effect and tunnelling magneto-resistance is obtained in comparison with previous results predicted for monolayer graphene, which therefore demonstrates the high potentialo of bilayer graphene for spintronic applications. It is illustrated in Fig. 2 which shows the spin polarization as a function of gate barrier height in both monolayer and bilayer graphene structures. Our NEGF model provides a clear description of charge transport and may provide meaningful information for future development of many kinds of bilayer graphene electronic and spintronic devices.

References:

[1] A. K. Geim and K. S. Novoselov, "The rise of graphene", Nature Mater., vol. 6, pp. 183-191, 2007.
[2] S. Y. Zhou et al., "Substrate-induced bandgap opening in epitaxial graphene", Nature Mater., vol. 6, pp. 770-775, 2007.
[3] E. V. Castro et al., "Biased bilayer graphene: semiconductor with a gap tunable by the electric field effect", Phys. Rev. Lett., vol. 99, 216802, 2007.
[4] Y. Zhang et al., "Direct observation of a widely tunable bandgap in bilayer graphene", Nature, vol. 459, pp. 820-823, 2009.

[5] N. Tombros et al., "Electronic spin transport and spin precession in single graphene layers at room temperature", Nature, vol. 448, pp. 571-575, 2007.

[6] V. N. Do, V. H. Nguyen, P. Dollfus, and A. Bournel, J. Appl. Phys. **104**, 063708 (2008).

[7] V. H. Nguyen, A. Bournel, V. L. Nguyen, and P. Dollfus, Appl. Phys. Lett. **95**, 232115 (2009)

[8] V. H. Nguyen, A. Bournel, and P. Dollfus, J. Phys.: Condens. Matter **22**, 115304 (2010)
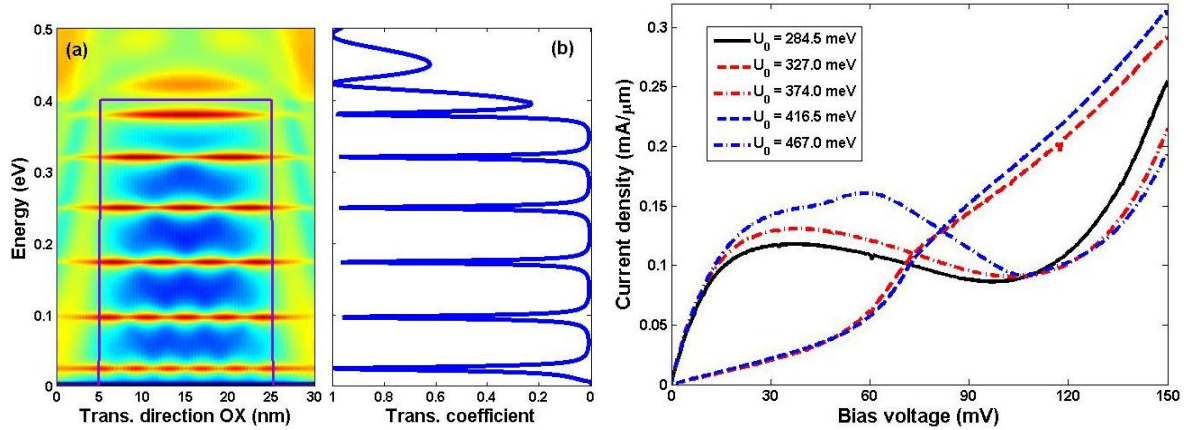
Fig. 1. (Left panel) LDOS and transmission coefficient in a single barrier bi-layer graphene structure under zero bias. Other parameters are $E_y = 50$ meV, $U_0 = 0.4$ eV, and $L = 20$ nm. (Right panel) Low temperature current as a function of bias voltage in a single barrier bi-layer graphene structure of barrier length $L = 20$ nm for different barrier heights.
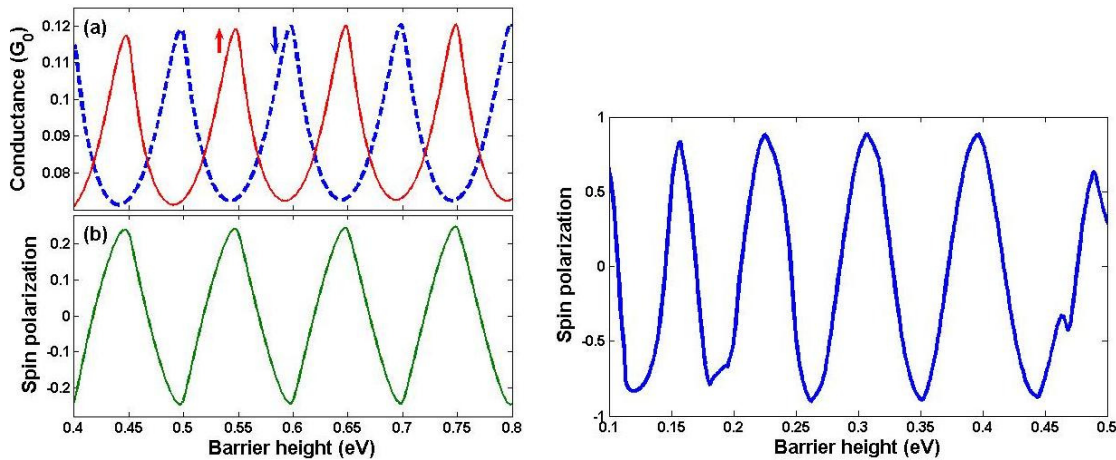
Fig. 2. (left panel) (a) Spin up and spin down conductance and (b) spin polarization in a single ferromagnetic gate monolayer graphene structure as a function of the gate barrier height, for $L = 20$ nm, $E_F = 100$ meV and exchange splitting energy $h = 25$ meV. (Right panel) Spin polarization in a single ferromagnetic gate bilayer graphene structure as a function of the gate barrier height, for L 20 nm, $E_F = 75$ meV and $h = 22.5$ meV.

Toward a real-time time STM simulation engine using Green's functions

Fabien Archambault[†], Stéphane Bedwani[*], Michaël Magoga[†] , Jorge I. Cerdá[‡] and Alain Rochefort[*]

[†] Nanotimes, 1 rue Saint Aubin, 31000 Toulouse, France
[*]Département de génie physique and Regroupement québécois sur les matériaux de pointe (RQMP),
École polytechnique de Montréal, Montréal, Québec H3C 3A7, Canada
[‡]Instituto de Ciencia de Materiales de Madrid (ICMM), CSIC, 28049 Madrid, Spain
fabien.archambault@nanotimes.fr
alain.rochefort@polymtl.ca

Within the framework of atomic resolution STM images, the understanding of relations between the surface, the tip, the adsorbate (if present) and the bulk materials is not always straightforward. Depending on the inherent quality of an experimental STM image, the nature of component within the entire system can be determined with a very limited certainty. In order to extirpate vital information from STM images, a strong coupling between experimental and theoretical analysis is always a source of success and should be strongly encouraged.

One common way to compare experimental images with theoretical one is to use the Tersoff-Hamann [1] model. Even if that model is very popular and effective, the absence of the tip contribution in the tip-surface interaction is nowadays a limiting factor. With the constant increase in computer power it is now feasible to simulate a part of the system from first principles --- for example using the density functional theory (DFT). Although DFT can address sophisticated systems with a very good accuracy, it cannot be reasonably used to perform large and non-periodic calculations where the computational time and the memory required become excessively demanding. Hence, a compromise between accuracy and time spent for atomistic calculations, such as for STM simulations, leads us to use a suitable approach such as tight-binding Hamiltonian in conjunction with Green's functions. Here, we followed the general computational approach developed by Cerdá *et al.* [2] that was implemented in the GREEN code. This code has been recently [3] improved with highly parallel subroutines. In addition, a more intimate coupling between GREEN and the quantum-mechanical software, SIESTA [4], allows a rapid and appropriate determination of atomic parameters needed for STM simulations. This opens perspectives for the development of new materials and a faster comprehension of STM images. We will show a few computing benchmarks with this package on large parallel machines showing its efficient scalability. We will also present a few representative test cases where a comparison to Tersoff-Hamann images was performed, and which were supported by density functional theory. A recent work [5] on multilayers of polythiphene on graphite and graphene (see Fig. 1) will emphasize the strength of our STM simulation approach to reveal properties related to charge transport and π-electron coupling.

References

[1] J. Tersoff and D. R. Hamann, Phys. Rev. B, **31** (1985) 805.
[2] J. Cerdá, M. A. Van Hove, P. Sautet, and M. Salmeron, Phys. Rev. B, 56 (1997) 15885.
[3] B. A. Janta-Polczynski, J. Cerdá, G. Éthier-Majcher, K. Piyakis, and A. Rochefort, J. Appl. Phys., **104** (2008) 023702.
[4] J. M. Soler, E. Artacho, J. D. Gale, A. García, J. Junquera, P. Ordejón, and D. Sánchez-Portal., J. Phys. Condens. Matter, **14** (2002) 2745.
[5] A. Rochefort, S. Bedwani and A. Lopez-Bezanilla, to be submitted.

Figures
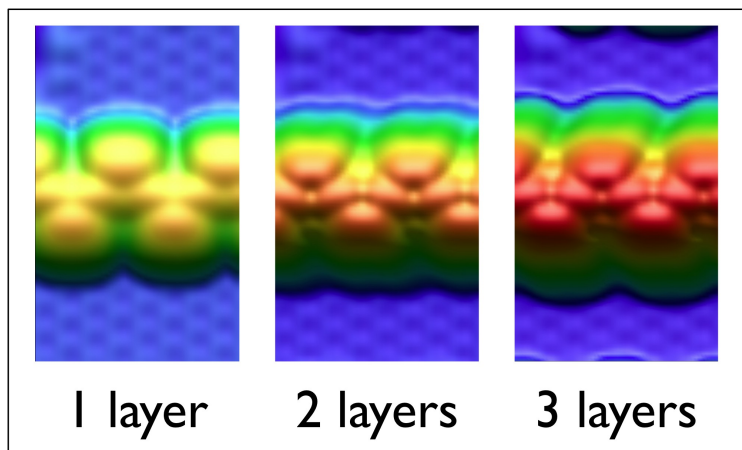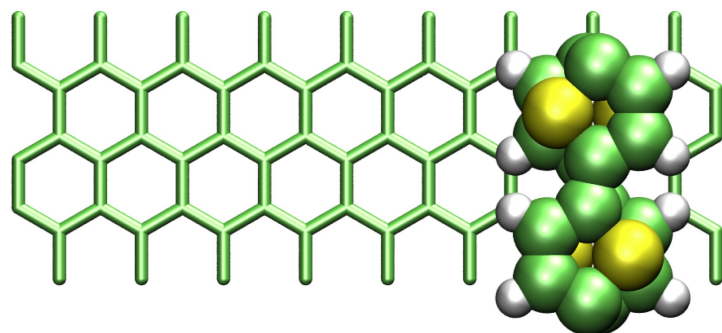
Molecular model of the unit cell considered for a polythiophene multilayer stack on graphite (upper panel) and resulting STM images calculated for one, two and three polythiophene layers on graphite (lower panel). (I = 0.1 nA, V = 1.5 V)

Towards graphene Plasmonics: electric dipole radiation in graphene

A. Yu. Nikitin[1], L. Martín-Moreno[1], F. J. García-Vidal[2]

[1]Instituto de Ciencia de Materiales de Aragón and Departamento de Física de la Materia Condensada, CSIC-Universidad de Zaragoza, E-50009, Zaragoza, Spain
[2]Departamento de Física Teórica de la Materia Condensada, Universidad Autónoma de Madrid, E-28049 Madrid, Spain

alexeynik@rambler.ru

While the electronic properties of graphene have recently been extensively studied [1], the photonic properties are much less known. In the present work, the interaction of a point electromagnetic emitter and a graphene sheet will be theoretically considered (see Fig. 1). This problem reduces to finding the Green's function corresponding to an electric dipole in graphene, which is fundamental for description of electromagnetic effects in graphene.

We describe the electromagnetic fields using Maxwell's equations, and the graphene is represented by a conductivity surface with the conductivity depending upon the temperature, chemical potential and frequency. Applying adequate mathematical techniques [2,3] we find an analytical representation of the electromagnetic propagator for the graphene sheet. We identify every term in the analytical solution and discuss its origin with respect to the peculiarities on the density of electromagnetic states. We find that an electric dipole can hardly couple to transverse electric surface modes, but at certain frequencies do strongly couples to transverse-magnetic ones (long-range surface plasmon-polariton modes) essentially increasing the amplitude of the field in the vicinity of the emitter. The field patterns are drastically different for different values of chemical potential and frequency ranges and orientations of the dipole.
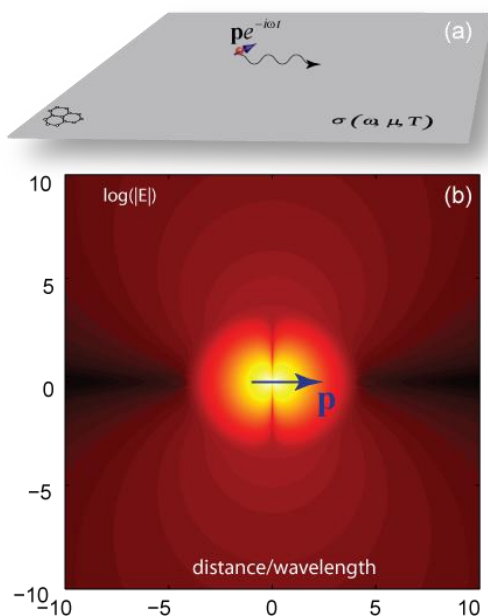
Figure 1. Schematic illustration of the system under study (a) and the distribution of the electric field modulus in the graphene plane (b) for T=300 K, μ=0.2 eV, ω=0.08 eV.

References

[1] A. H. Castro Neto, F. Guinea, N. M. R. Peres, K. S. Novoselov and A. K. Geim, Rev. Mod. Phys. 81, 109 (2009).
[2] L. P. Felsen and N. Marcuvitz, Radiation and Scattering of Waves (IEEE Press, Piscataway, NJ, 1994).
[3] A. Yu. Nikitin, F. J. García-Vidal, and L. Martín- Moreno, Phys. Rev. Lett. 105, 073902 (2010).

Features of graphene layers on SiC (000-1) revealed by transmission electron microscopy

W. Norimatsu, J. Takada, and M. Kusunoki

EcoTopia Science Institute, Nagoya University, Furo-cho, Chikusa-ku, Nagoya-shi, Japan
w_norimatsu@esi.nagoya-.ac.jp

Graphene is a one-atom-thick carbon material, having a hexagonal honeycomb lattice [1]. Graphene can be spontaneously formed by thermal decomposition of SiC [2,3]. Interestingly, structures and electronic properties of graphene formed on Si-terminated and C-terminated faces of the SiC substrate are different from each other. Graphene on C-terminated surface SiC (000-1) behaves like an isolated one, which is thought to be due to the rotational stacking faults. In addition, graphene on SiC (000-1) has higher mobility than that on SiC (0001). Then, it is quite important to fabricate homogeneous and large-area graphene layers on SiC (000-1). For the development of the mass production method, growth mechanism of graphene layers should be clarified in detail. In this study, we investigate the crystallographic features of graphene layers formed on SiC (000-1) mainly using high-resolution transmission electron microscopy (HRTEM), and propose the formation mechanism of them.

Graphene-on-SiC(000-1) samples were prepared by annealing SiC single-crystal in an Ar atmosphere. Specimens for transmission electron microscope (TEM) observation were prepared by an Ar-ion thinning method. Details of the preparation procedure are described in our previous papers [4]. Atomic force microscope observations were also carried out.

As a result of TEM observations, it was revealed that the decomposition of SiC was suppressed by increasing Ar-pressure. As for the growth mechanism, it is suggested that several layers of graphene were nucleated on SiC (000-1) surface, and then grows laterally over the terrace. Details of the crystallographic features of graphene layers on SiC (000-1), compared with those of graphene on SiC (0001) [4], will be discussed in the presentation.

References

[1] K. S. Novoselov, A. K. Geim, S. V. Morozov, D. Jiang, Y. Zhang, S. V. Dubonos, I. V. Grigorieva, and A. A. Firsov, Science, **306** (2004) 666.
[2] C. Berger, Z. Song, X. Li, X. Wu, N. Brown, C. Naud, D. Mayou, T. Li, J. Hass, A. N. Marchenkov, E. H. Conrad, P. N. First, and W. de Heer, Science, **312** (2006) 1191.
[3] M. Kusunoki, T. Suzuki, T. Hirayama, N. Shibata, and K. Kaneko, Appl. Phys. Lett., **77** (2000) 531.
[4] W. Norimatsu, and M. Kusunoki, Chem. Phys. Lett., **468** (2009), 52, Physica E, **42** (2010) 691, Phys. Rev. B, **81** (2010) 161410.

Negative Contact Resistances Apparently-Appeared at Graphene/Metal Contacts

Ryo Nouchi, Tatsuya Saito, Nobuhiko Mitoma, Katsumi Tanigaki

WPI-AIMR and Department of Physics, Tohoku University, 6-3 Aoba, Aramaki, Aoba-ku, Sendai, Japan
nouchi@sspns.phys.tohoku.ac.jp

Graphene, a single atomic layer of graphite, has been attracting incredible attention for its unique physical properties and for its applicability to future high-speed electronic devices. In order to investigate electrical properties of graphene and to construct graphene devices such as field-effect transistors (FETs; see Fig. 1a), metallic materials should make a contact with graphene. The metal contacts have been reported to affect the electronic property through charge transfer (CT) from the metals to graphene and charge-density pinning of graphene at the metal-graphene interfaces, where the gate voltage, V_G, cannot tune the charge density of graphene at the metal electrodes [1] (Figs. 1b, 1c). We have studied the effect of such metal contacts to transfer characteristics (V_G dependence of the drain current, I_D) of graphene FETs, and have reported that charge-density depinning can occur at easily-oxidizable metal contacts [2,3], which is contrary to what has been experimentally observed to date. In this presentation, we focus on metal contacts with charge-density pinning, and show that the metal-to-graphene CT is accountable for many intriguing features such as "negative" contact resistances.

The contact resistance, R_C, is one of the most important parameters to characterize metal contacts [4]. Figure 2a shows the V_G dependence of R_C, which is normalized by the contact width W, of graphene FETs with Ag contacts, where R_C was extracted by the commonly-used transfer length method (TLM; see Fig. 2b). Surprisingly, the extracted R_C becomes negative near the charge neutrality point, V_{NP} (V_G corresponding to the minimum I_D in transfer characteristics). Although there is one report on the apparently negative contact resistance at Ti contacts [5], the detailed investigation has not been performed so far.

Figure 2c displays the simulated result using a simple model which assumes that a total resistance of the graphene channel is obtained by integrating the local resistivity along the channel [3]. Although the simulation considers only the channel region, apparently R_C becomes finite and negative near V_{NP} if CT from metal contacts is taken into account. The TLM presumes a homogeneous channel, which is not applicable to the actual devices due to the charge-density inhomogeneity induced by the metal-to-graphene CT. The asymmetry of the R_C-V_G characteristics indicates hole doping from Ag contacts, which is in agreement with what can be derived from other features such as a V_{NP} shift with decreasing the channel length [6].

References

[1] T. Mueller, F. Xia, M. Freitag, J. Tsang and P. Avouris, Phys. Rev. B **79** (2009) 245430.
[2] R. Nouchi, M. Shiraishi and Y. Suzuki, Appl. Phys. Lett. **93** (2008) 152104.
[3] R. Nouchi and K. Tanigaki, Appl. Phys. Lett. **96** (2010) 253503.
[4] H. H. Berger, Solid-State Electron. **15** (1972) 145.
[5] P. Blake, R. Yang, S. V. Morozov, F. Schedin, L. A. Ponomarenko, A. A. Zhukov, R. R. Nair, I. V. Grigorieva, K. S. Novoselov and A. K. Geim, Solid State Commun. **149** (2009) 1068.
[6] R. Nouchi, T. Saito and K. Tanigaki, submitted.

Figures
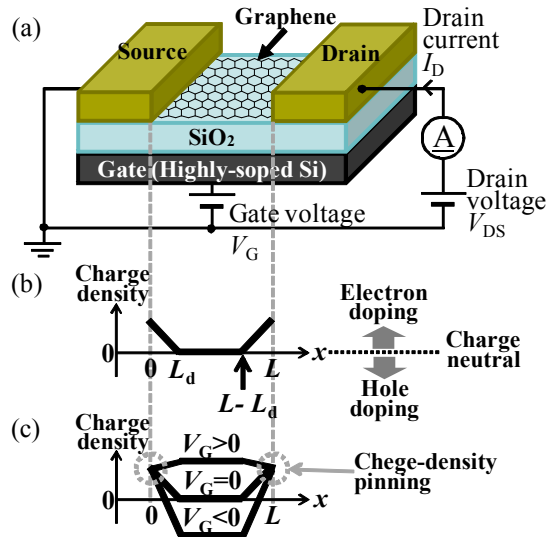
Figure 1. Metal-contact effect on graphene FETs. (a) Schematic diagram of a graphene FET. Simplified charge-density profiles including (b) the contact-doping effect and (c) the charge-density pinning at the contacts.
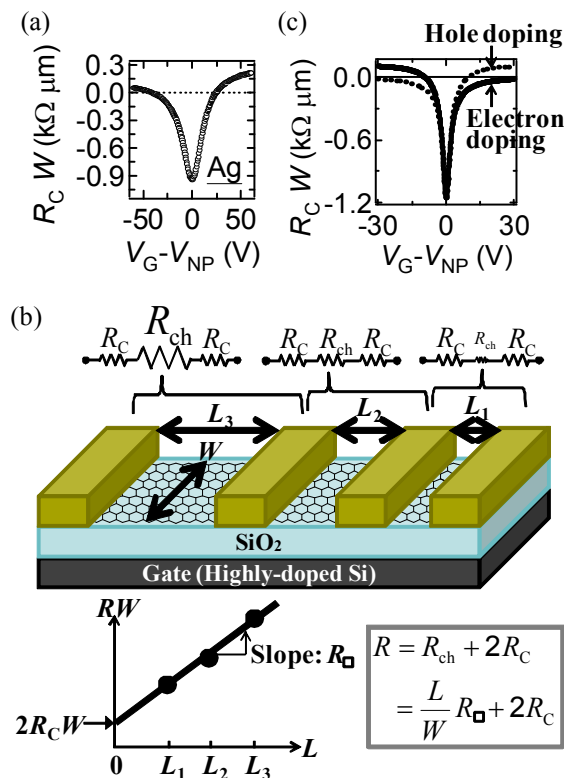
Figure 2. Extraction of R_C from the TLM analysis. (a) R_C-V_G characteristics of Ag contacts. (b) Schematic illustration of the TLM. (c) Simulated R_C-V_G characteristics of electron- (solid line) and hole-doped (dashed line) contacts.

Metal to semiconductor transition in graphene by oxygen plasma treatment: a building block for graphene-based electronics

A. Nourbakhsh,[a,b] M. Cantoro,[a,c] A. Klekachev, [a,c] M. H. van der Veen,[a] S. De Gendt,[a,d] and B. Sels[b]

[a] imec, Kapeldreef 75, B-3001 Leuven, Belgium

[b] Department of Microbial and Molecular Systems, K.U.Leuven, Kasteelpark Arenberg 23, B-3001 Leuven, Belgium

[c] Department of Physics and Astronomy, K.U.Leuven, Celestijnenlaan 200d, B-3001 Leuven, Belgium

[d] Department of Chemistry, K.U.Leuven, Celestijnenlaan 200f, B-3001 Leuven, Belgium

nourbakh@imec.be

Graphene is considered a promising material in both fundamental science and technology because of its unique electronic and chemical properties[1] In particular, single- and bi-layer graphene are being investigated to fabricate various devices such as field-effect transistors (FETs),[2] biosensors,[3] and photodetectors.[4]

In this work the results of experiments devoted to the modification of the pristine electronic properties of single-layer graphene by means of an oxygen plasma will be illustrated. Electrical characterization and photoluminescence measurements are carried out to investigate the opening of a bandgap in plasma-treated graphene. figure 1(a, b) show room-temperature output characteristics of a SLG FET collected in pristine conditions and after steps of O2 plasma treatment. The symmetric rectifying behavior observed in figure 1(b) can be explained by building an equivalent circuit of the plasma-treated metal/SLG/metal structure, comprising two identical Schottky diodes connected back-to-back.

The PL maps in figure 2(b) shows the emission from the two SLG areas of the flake in figure 2(a), while no emission is collected from the thicker graphene areas. A corresponding PL spectrum representative of the bright PL emission from the SLG areas is shown in figure 2(d). It shows a broad peak lying in the visible range and centered at ~620 nm, corresponding to a ~2 eV optical bandgap. After two steps of O2 plasma treatment, the graphene sample shows PL emission (figure 2(c)) from the regions previously indicated as bilayers in figure 2(a). The analysis of the evolution of the PL maps upon O2 plasma treatment suggests that: (a) the plasma progressively renders the SLG regions photoluminescent; (b) as the O2 plasma is believed to affect the entire graphene surface in a similar fashion, regardless of the thickness of the flake, the absence of PL from the plasma-treated FLG is indicative of an emission quenching of the topmost layer by subjacent untreated layers. The experimental results are explained in terms of a functionalization of the pristine sp^2 graphene lattice with chemisorbed epoxy groups.The effects of epoxidation on graphene optoelectronic properties are further investigated by *ab initio* calculations. Figure 3 shows electronic band structure and electronic density of states (DOS) calculated for different oxygen densities. They confirm that progressively larger bandgaps are introduced in graphene upon functionalization with increasing amount of oxygen.

Furthermore, we demonstrate the potential of metal-contacted plasma-treated graphene rectifying junctions to fabricate Schottky diodes with turn-on voltages below 0.5 V. The use of low- (Al, Yb) and high- (Pd) work function metals, directly in contact with modified graphene, allows for the modulation of the Schottky barrier height. Figure 4(a, b) illustarte the diagrams of the band alignment in the cases of a *p*–doped semiconductor (work function φ_s) contacted with (a) two identical metal electrodes ($\varphi_M < \varphi_S$), and (b) two metal electrodes M_1 and M_2 with different work functions ($\varphi_{M1} < \varphi_S < \varphi_{M2}$, $\varphi_S \sim \varphi_{M2}$). The Schottky barrier height φ_B is indicated. Figure 4(c) dispalys output characteristics of Al–SSLG–Pd and Yb–SSLG–Pd devices, whereby the rectifying behavior is visible. Our results suggest that an oxygen plasma treatment represents a valid approach to control graphene chemistry toward tunable-bandgap graphene-based electronics.

References
[1] Geim, A.K., et al., Science, **324**(2009) 1530-1534.
[2] Novoselov, K.S., et al., Science, **306**(2004) 666-669.
[3] Liu, Y., et al., Langmuir, **26**(2010) 6158-6160.
[4] Xia, F.N., et al., Nature Nanotechnology, **4**(2009)839-843.

Figures
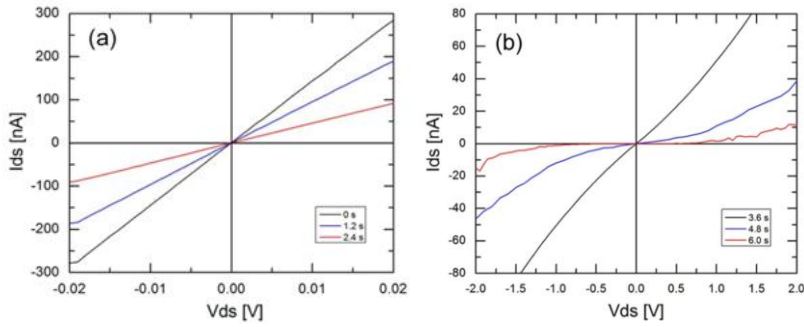
Figure 1: output characteristics of a SLG-FET collected in pristine conditions and after steps of O_2 plasma treatment (15 W, 1.2 s interval). The curves shown in (b) for longer O_2 plasma treatment times are indistinguishable from the X-axis in panel (a), measured in the cases of shorter O_2 plasma treatment times.
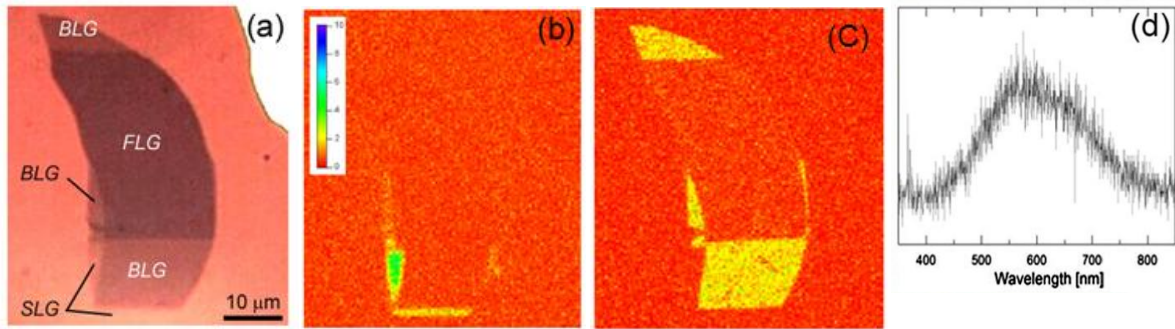
Figure 2: PL measurements on a graphene sample subjected to O_2 plasma for increasing time duration.
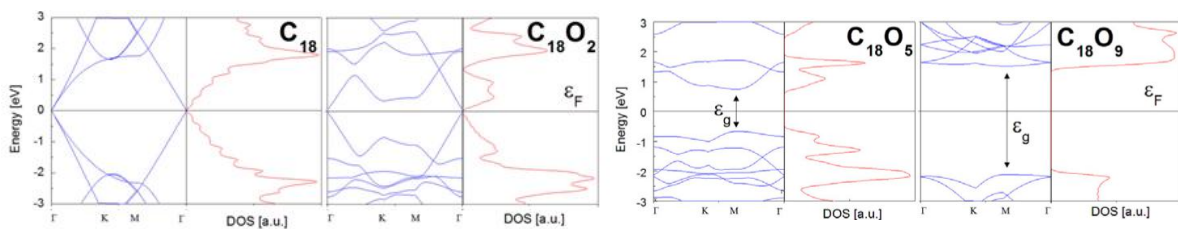
Figure 3: Electronic band structure and electronic density of states (DOS) calculated for different oxygen densities.
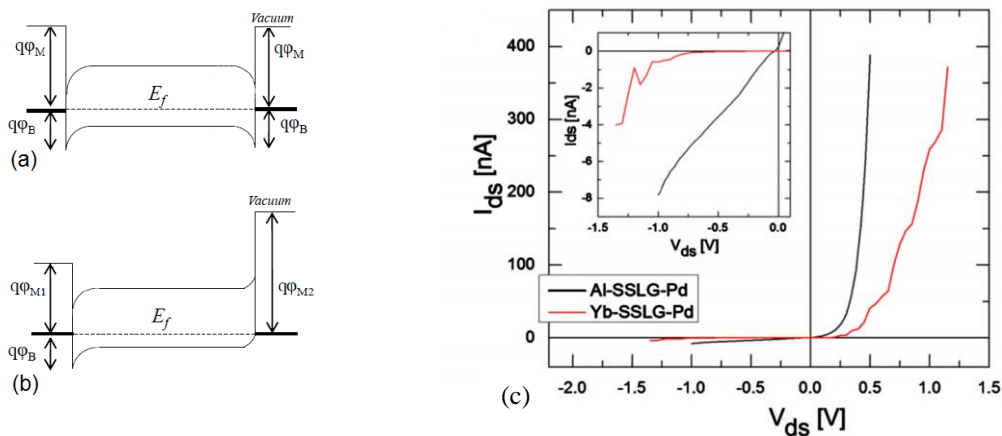
Figure 4: Diagrams of the band alignment in the cases of a p–doped semiconductor (work function φ_S) contacted with (a) two identical metal electrodes ($\varphi_M < \varphi_S$), and (b) two metal electrodes M_1 and M_2 with different work functions ($\varphi_{M1} < \varphi_S < \varphi_{M2}$, $\varphi_S \sim \varphi_{M2}$). The Schottky barrier height φ_B is indicated. (c) Comparison of the room-temperature, output characteristics of Al–SSLG–Pd and Yb–SSLG–Pd devices, whereby the rectifying behavior is visible. A detailed behavior of the two devices in reverse bias is shown in the inset.

Crystallographically Anisotropic Etching of Graphene

Florian Oberhuber, Dieter Weiss, and Jonathan Eroms

Institute for Experimental and Applied Physics, University of Regensburg,
D-93040 Regensburg, Germany

Florian.Oberhuber@physik.uni-regensburg.de

We report crystallographically anisotropic carbothermal etching of graphene on SiO_2 substrates in an argon gas flow at atmospheric pressure. The samples were prepatterned with antidot lattices by electron beam lithography and reactive ion etching. The hexagonal form of the antidots obtained by the carbothermal reaction

$$SiO_2(s) \; + \; C(s) \; \rightarrow \; SiO(g) \; + \; CO(g).$$
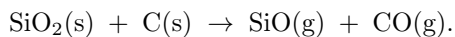
suggests the absence of armchair edges [1]. The anisotropic process could provide access to the highly interesting physical properties of zigzag-edged graphene structures. We further studied the dependence of the etching rate on the number of graphene layers. In all samples rates decreased with increasing layer thickness.

Furthermore we conducted electron transport measurements on a set of single- and bilayer samples patterned by lattices of hexagonal antidots. From temperature dependent investigation of the clearly resolved weak localization peak we deduce the phase coherence length as well as lengths for inter- and intravalley scattering. The samples exhibited good quality and phase coherence lengths of even 1µm at 1.7K despite the etching processes. Carrier mobilities up to $8000\text{cm}^2/\text{Vs}$ at 1.7K and Shubnikov de Haas oscillations were observed.

Reference

[1] P. Nemes-Incze, G. Magda, K. Kamarás, and L.P. Biró, Nano Research **3** (2010) 110-116

Figure
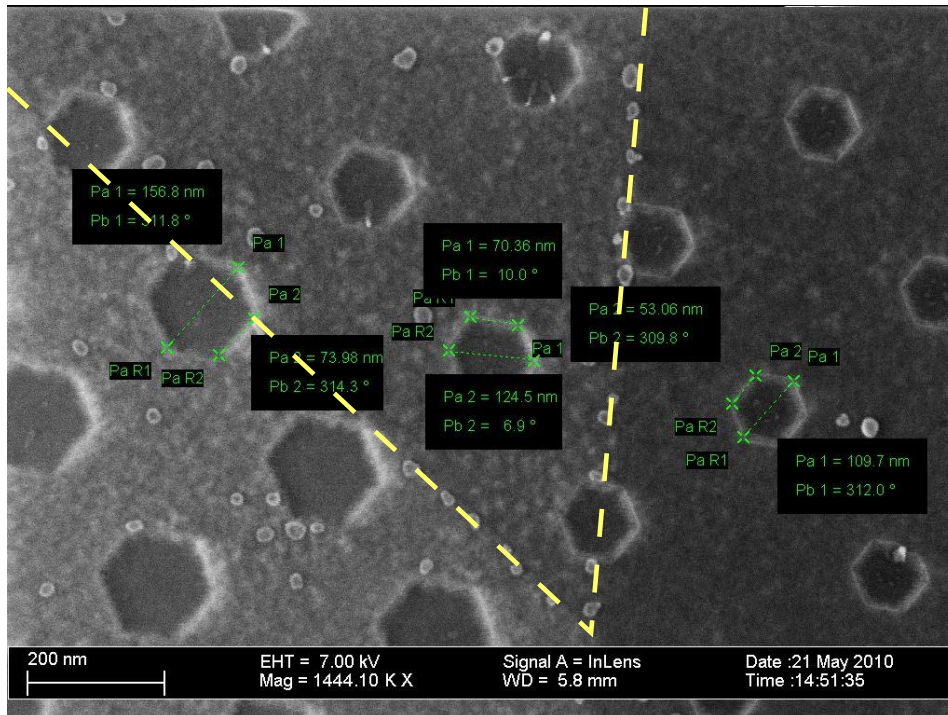
Typical appearance of antidot lattices in graphene samples after the crystallographically anisotropic carbothermal reaction. The left-hand side of the flake is bilayer graphene, the center part is four-layer and the right-hand side six layer. After prepatterning the antidots by reactive ion etching their diameter was about 45nm. The etching process grew the antidots to diameters of about 157nm, 125nm and 110nm in the two-, four- and six-layer system, respectively.

Spin-orbit coupling and spin relaxation times in *sp³*-like distorted graphene

H. Ochoa[1], F. Guinea[1], and A. H. Castro Neto[2]

[1] Instituto de Ciencia de Materiales de Madrid (CSIC), Sor Juana Inés de la Cruz 3 E-28049, Madrid, Spain
[2] Department of Physics, Boston University, 590 Commonwealth Ave., Boston MA 02215, USA
hector.ochoa@icmm.csic.es

Graphene is considered as a potential material for spintronics. The spin-orbit (SO) coupling in graphene is expected to be weak due to the low mass of the carbon atom. Besides this, the intrinsic SO coupling between flat graphene π electrons, which are the relevant ones in what concerns to transport properties, is a second order process since it involves virtual transitions into σ states [1]. However, the measured spin diffusion lengths [2] are much shorter than the expected ones [3].

Recently, longer spin lifetimes have been reported in monolayer and bilayer graphene spin valves [4]. The results of this work, which shows how the spin lifetime is longer in bilayer graphene than in monolayer, when the effective SO coupling between electrons is higher in the bilayer case due to the non-zero hoppings between π and σ orbitals in next-nearest neighbor atoms of different layers [5], suggest an extrinsic source of spin scattering, as impurities or other lattice defects.

In this work we analyze the enhancement of the SO coupling induced by a *sp³*-like distortion of the *sp²* graphene lattice. Such kind of distortion can be produced by adatoms as hydrogen [6]. This perturbation mixes π and σ states, so the SO coupling in this system is a first order process. The effect of such kind of defects in spin relaxation is investigated as due to the Elliot-Yafet mechanism produced by the enhancement of the SO coupling.

References

[1] D. Huertas-Hernando, F. Guinea, and A. Brataas, Phys. Rev. B, **74** (2006) 155426.
[2] N. Trombos, C. Jozsa, M. Popinciuc, H. T. Jonkman, and B. J. van Wees, Nature, **448** (2007) 571.
[3] D. Huertas-Hernando, F. Guinea, and A. Brataas, Phys. Rev. Lett., **103** (2009) 146801.
[4] W Hang and R. K. Kawakami, arXiv:1012.3435v1 [cond-mat.mtrl-sci] (2010).
[5] F. Guinea, New J. of Phys., **12** (2010) 083063.
[6] A. H. Castro-Neto and F. Guinea, Phys. Rev. Lett., **103** (2009) 026804.

Scanning Confocal Raman microscopy at low temperature and in high magnetic fields

Florian Otto, Martin Zech

attocube systems AG, Koeniginstrasse 11a (Rgb), 80539 Muenchen, Germany
florian.otto@attocube.com

The advent of Graphene has generated the need for a whole new set of characterization tools in order to tailor new electronic devices based on the outstanding material properties of this unique material. The attoRAMAN combines a high resolution, low temperature confocal microscope with ultra sensitive Raman optics. This innovative product enables state of the art confocal Raman measurements at cryogenic environments combined with magnetic fields of up to 15 T. The attoRAMAN is a ready-to-use system and is delivered with laser source, high throuput spectrometer including a peltier-cooled, back-illuminated CCD, and a state-of-the-art SPM/Raman controller & software package.

We show micro-Raman spectra on epitaxial as well as exfoliated Graphene and on GaAs based nanowires at 4 K and 9 T.

For further technical information concerning attocube systems' products, please visit our website www.attocube.com.

Figures
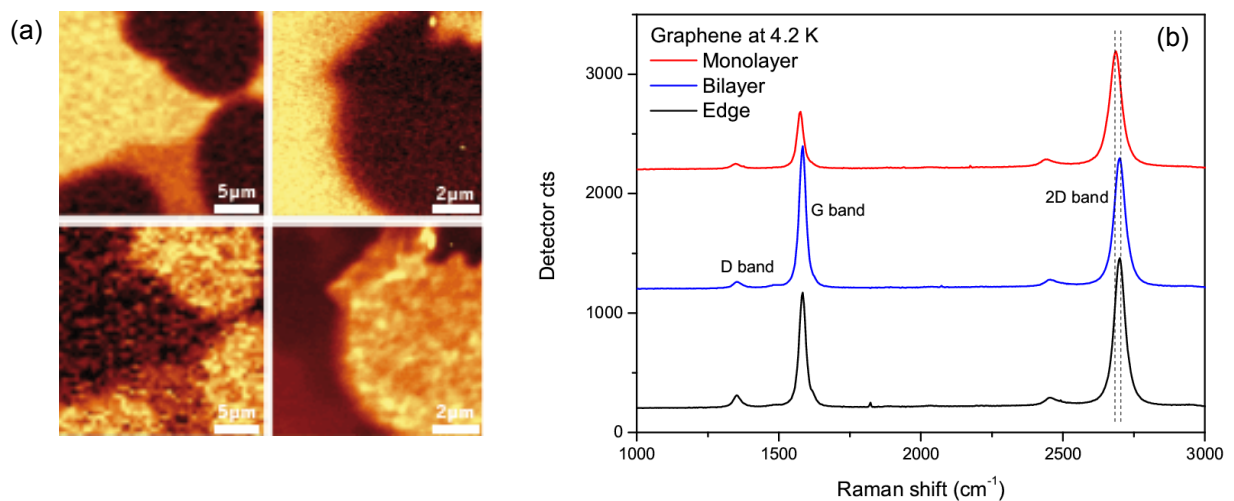
Figure caption: (a) Raman images of epitaxially grown Graphene layers, showing the SiC substrate (top) and the Graphene 2D band (bottom). Left images were recorded at 300 K, right images at 4.2 K. (b) Raman spectra recorded at 4.2 K, depicting (from top to bottom) monolayer and bilayer graphene, and the edge of the latter. The 2D band shifts by approximately 14 cm-1 at the transition from mono- to bilayer Graphene.

Transport properties of graphene heterostructures

M. Pacheco,[a] J.W. Gonzalez,[a] L. Rosales,[a] P.A. Orellana[b]

[a]Universidad Técnica Federico Santa María, Casilla 110 V, Valparaíso, Chile,
[b]Universidad Católica del Norte, Casilla 1280, Antofagasta, Chile.

monica.pacheco@usm.cl

Graphene nanoribbons (GNRs) are stripes of graphene [1] that can be obtained through high-resolution lithography, by controlled cutting processes or by unzipping multiwalled carbon nanotubes[2]. Different heterostructures (HST) based on patterned GNRs have been proposed and constructed in which the interference quantum effects are exceptionally strong and determine their electronic behavior. Here we present a theoretical study of transport properties HST formed by segments of GNR with different widths connected forming a double crossbar junction [3]. The systems are described by a single-band tight binding Hamiltonian and the Green's function formalism using real space renormalization techniques. We show calculations of the local density of states, linear conductance and I-V characteristics. Our results depict resonant behavior in these HST which can be controlled by changing the geometrical parameters. By applying gate voltages on determined regions of the structure it is possible to modulate the transport response of the system. We show that negative differential resistance (DR) is obtained as a function of the applied gate and bias voltage.

 An interesting feature of certain confined nanostructures is the presence of bound states in the continuum (BICs). The search of new systems which could be able to reveal the existence of BICs and with the capability of do measurements of these states is an important field of research. The great advances in the controlled manipulation and measurements reported in graphene based systems, and the feasibility of modified their electronic properties by apply external potentials, suggests that BICs could be observable in graphene HST [4]. In this work we discuss the mechanism of formation of these exotic states and the feasibility to observe them experimentally in symmetrical HST composed by segments of GNRs with different widths.

References

[1] K. S. Novoselov et al. Science **306** (2004) 666 ;C. Berger et. al. Science **312** (2006) 1191.
[2] L. Ci et. al. Nano Res **1** (2008)116 ; D. V. Kosynkin et al . Nature 458, 872 (2009); M. Terrones, Nature **458** (2009) 845.
[3] J. W. González, L. Rosales, M. Pacheco, Physica B: Cond. Matt. **404** (2009) 2773; Eur. Phys. Lett. **91** (2010) 66001.
[4] N. Moiseyev, Phys. Rev Lett. **102** (2009) 167404.

Indirect interaction research of the double layer impurity graphene in the framework of s-d model

A.V. Pak, M.B. Belonenko, N.G. Lebedev

Volgograd State University, The University avenue, 100, Volgograd, Russia

E-mail: pak.anastasia@gmail.com

Recently the big attention of researchers is concentrated on calculations of electronic, magnetic, conductive changes and other properties of graphene, caused by introduction of single atomic impurity on its surface [1 - 4]. From the data received at the analysis of substances properties with collectivized electrons, it is known, that at impurity introduction with *d-* or *f-* electrons strong updating of electronic or magnetic properties is possible. The most known fact is, apparently, Kondo effect is the change of conductive properties at impurity introduction with temperature change.

Therefore research of the collective effects connected with interaction of the impurity with a crystal lattice of graphene, i.e. RKKY (Ruderman-Kittel-Kasuya-Yosida) interaction [5 - 7] is very interesting.

In the given work in the framework of s-d model features of RKKY-interaction in double-layer impurity graphene have been calculated. Atomic hydrogen was considered as an impurity. Calculations have shown, that on small distances antiferromagnetic ordering of the impurity spins is preferable, and with distance increasing the ordering becomes ferromagnetic. Dependences of exchange interaction factor on parameters are shown.

Dispersion relation for the impurity graphene was obtained analitically by using the mathematical formalism of Green's functions. Then, using the Frohlich's method of calculating indirect interaction expression for the indirect coupling constant depending on the distance between the impurities was obtained. The dependence of the indirect interaction for different values of the external electrostatic potential is shown in Figure 1.

The increase of electric field intensity leads to the strongly oscillating dependence of indirect interaction of the impurity spins on the distance between impurities that can be connected with resonant transitions of the electrons between the split levels.

The increase of an external magnetic field also leads to non-uniform distribution of the impurity spins, formation of domain structures, alternation of areas of ferromagnetic and antiferromagnetic orderliness is actually observed.

Thus, it is quite probable, that graphene sheets, processed by hydrogen plasma, are useful for creation of spintronics devices, changing magnetic properties of a material by variation of external parameters.

The feature of the RKKY-interaction of adsorbed atoms on the surface of double-layer graphene, made in this paper is that it considered the exchange interaction on the basis of the total (including short-wave part) electron spectrum of the crystal lattice. The dispersion relation includes electrons pulses in the whole Brillouin zone.

Refrences:

[1] D. Henwood, J. David Carey, Phys. Rev. B. **75** (2007), 245413.
[2] Alejandro Lugo-Solis and Igor Vasiliev, Phys. Rev. B. **76** (2007), 235431.
[3] Rudro R. Biswas and Subir Sachdev.Phys. Rev. B. **76** (2007), 205122.
[4] M I. Katsnelson, Phys. Rev. B **74** (2006), 201401 (R).
[5] Annica M. Black-Schaffer. Phys. Rev. B **82,** (2010), 073409
[6] V. K. Dugaev, V. I. Litvinov, J. Barnas. Phys. Rev. B **74,** (2006), 224438.
[7] T. Stauber, N. M. R. Peres, F. Guinea, A. H. Castro Neto, Phys. Rev. B. **75** (2007), 115425.
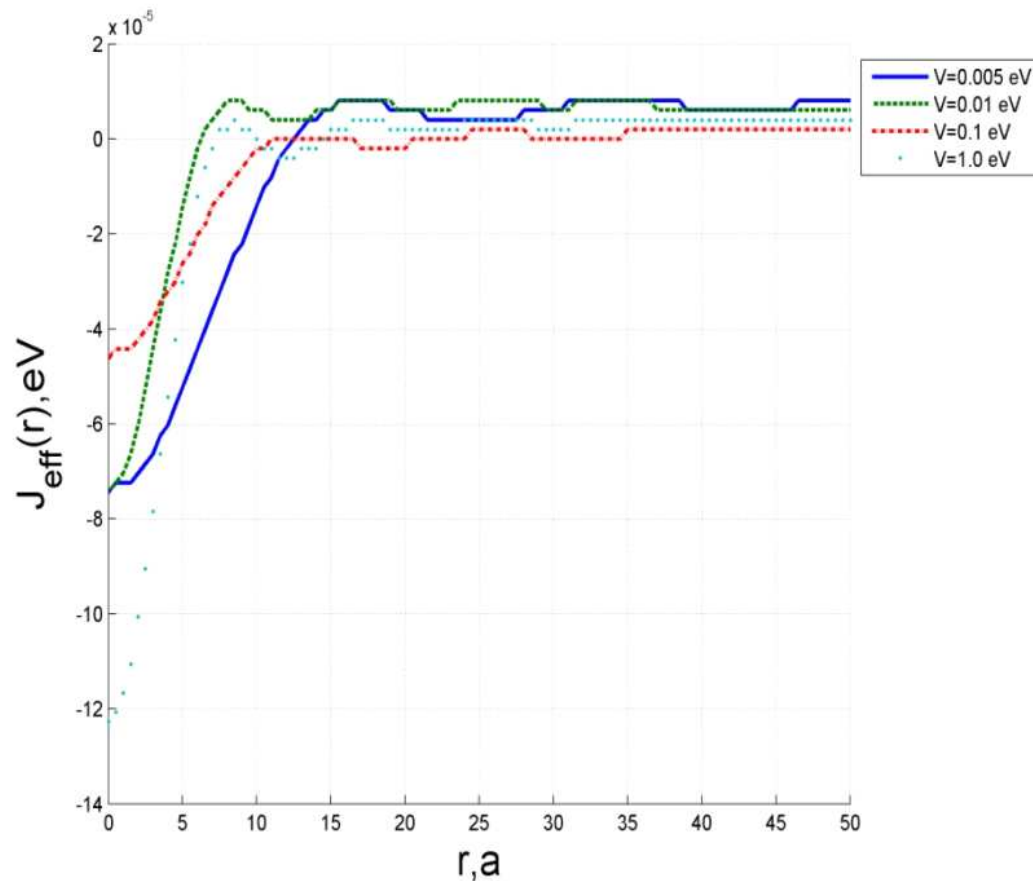
Figure 1. The d*ependence of exchange interaction distribution on the distance for various values of electrostatic potential. The distance is expressed in terms of a constant lattice, a=2.49 Å.*

Physical vapor deposition of metal nanoparticles on chemically modified graphene, and their application for hydrogen sensing

Priyanka A. Pandey[1], Jonathan P. Rourke[2], James A. Covington[3], Gavin R. Bell[1], Matthew Bates[1], Ana M. Sanchez[1], Jurgis Aleksandravicius[3], Mark Elkin[4], Bryan J. Hickey[4] and Neil R. Wilson[1]

[1]Department of Physics, University of Warwick, Coventry, CV4 7AL, UK
[2]Department of Chemistry, University of Warwick, Coventry, CV4 7AL, UK
[3]School of Engineering, University of Warwick, Coventry, CV4 7AL, UK
[4]School of Physics and Astronomy, University of Leeds, Leeds, LS2 9JT, UK
Priyanka.Pandey@warwick.ac.uk

The properties of graphene are known to be highly dependent on the substrate on which it is supported. It is equally true that the properties of graphene can be influenced by material deposited on top of it, and that additional functionality can be added by combining graphene with other materials. The interaction between metals and graphene are of particular importance; metal contacts are used to probe graphene's transport properties and to inject spin-polarized carriers, metal substrates are used for chemical vapor deposition growth of graphene, and metal nanoparticles are used on graphene for applications such as catalysis, energy storage and generation, and biosensing. Many such applications are likely to involve not graphene, which is still expensive and difficult to fabricate in bulk quantities, but instead chemically modified graphene (CMG).

Oxidation of graphite to graphite oxide and its subsequent exfoliation to water soluble graphene oxide (GO) has proved to be a convenient route to bulk quantities of graphene-like material [1]. Graphene oxide can also be used as the starting point for further functionalization to tailor desirable properties into the graphene-like sheets. Removal of the oxygen to return graphene oxide to graphene is also being heavily investigated. Although complete return to graphene from GO has so far proved impossible, the reduced graphene oxide (rGO) which has been produced has acceptable conductivities of up to ~ 10^2 S/cm [1] and mechanical strength within an order of magnitude of pristine graphene [2]. The comparatively low cost of these CMGs, combined with their ease of processing make them interesting materials for a range of applications. Understanding their properties and their interactions with other materials will be essential for developing and optimizing these applications.

Here we investigate metal-on-CMG, and in particular the growth morphology of metallic nanoparticles formed on CMG by physical vapor deposition (PVD). We have previously shown that single layer CMG support grids can be readily fabricated and enable high-contrast HR-TEM imaging of nanoparicles (e.g. ferritin) [3] and single molecules [4]. Here we use TEM to study the growth morphology of metals-on-CMG. We show that the morphology of the nanoparticles produced by PVD varies for different metals, from a uniform thin film for Ti to a droplet-like growth for Au. These differences in morphology can be understood and predicted by considering the strength of interaction between the CMG and metal adatoms. Fine control over the size (down to ~1.5 nm) and coverage (up to 5 ×10^4 μm^{-2}) of nanoparticles can be achieved, Figure 1. This control can be used to combine nanoparticles and CMG in rationally designed composite materials. We demonstrate the effectiveness of this approach through the fabrication of selective, highly sensitive (ppm), and practical hydrogen gas sensors, Figure 2.

References

[1] S. Park, and R. S. Ruoff, Nat. Nano. **4**, (2009). 217

[2] J. W. Suk *et al.*, ACS Nano **4**, (2010). 6557

[3] N. R. Wilson *et al.*, ACS Nano **3**, (2009). 2547

[4] J. Sloan *et al.*, Nano Lett. **10**, (2010). 4600
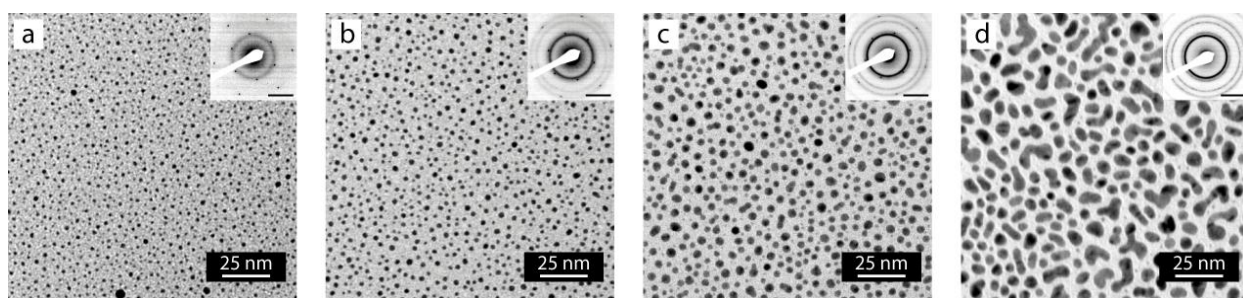
Figures

Figure 1. Brightfield TEM images of nominally (a) 0.15 nm, (b) 0.30 nm, (c) 0.75 nm, and (d) 1.5 nm thick Au films on graphene oxide. Inset top right in each image are the corresponding SAED patterns (scale bars correspond to 3 nm^{-1}).
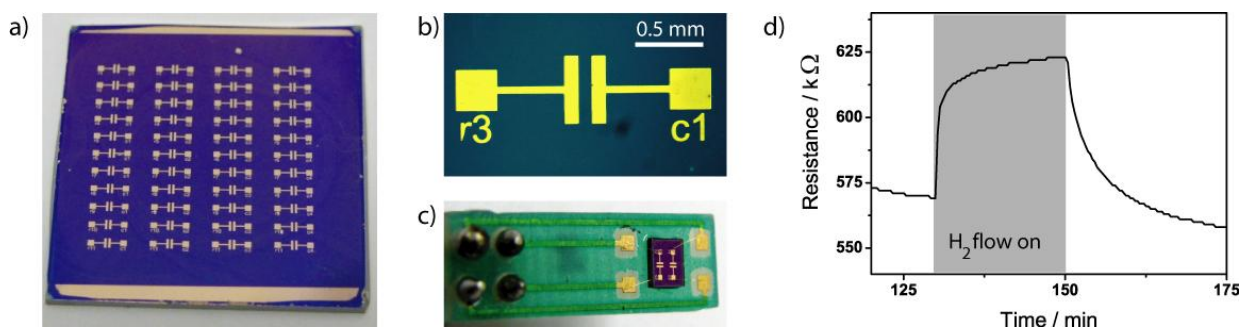
Figure 2. (a) Photograph of array of metal-on-rGO sensor devices, (b) photograph of one device, and (c) photograph of two devices mounted and bonded ready for testing. (b) Example response of one such device to hydrogen gas.

A unified Raman picture from nano-crystalline graphite to amorphous carbons: electron-phonon coupling and aromatic domain size

Cedric Pardanaud, Celine Martin, Pascale Roubin

Lab. PIIM (UMR 6633 CNRS-Universite de Provence) Saint-Jerome, F-13397 Marseille Cedex 20
cedric.pardanaud@univ-provence.fr

Raman microspectroscopy is routinely used for characterizing carbons. Structural information can be obtained thanks to previous works by coupling with other techniques. The shape of the Raman spectra depends on the excitation wavelength and, from IR to near UV, is sensitive to the sp_2 content of the material, the G and D band parameters being strongly dependent on their nanostructure. Raman analysis can give an estimation of how the material is disordered: sp^2/sp^3 ratio, %H… can be estimated. We focus here on several Raman parameters: the G band wavenumber σ_G, the G and D band widths Γ_G and Γ_D together with their relative intensities $R=H_D/H_G$. We extend some properties known for nanocrystalline graphite to amorphous carbons, such as the Raman diffusion cross-section dependence with the excitation wavelength, and also some properties known for amorphous carbons to nanocrystalline graphite, such as the cluster size estimation (L_a) using various excitation wavelengths. We also give evidence for the importance of the electron-phonon coupling on the D band width of a large range of disordered carbons.

To interpret Raman signals of a large variety of carbons (graphitic, nc-G, a-C:H, …) we have investigated carbonaceous samples from the plasma facing components of the Tore Supra tokamak (referred as TS samples), both the virgin C/C composite and the carbon deposits formed during plasma operation. Figure 1-a displays typical Raman spectra obtained for these samples with λ_L=514.5 nm. C/C samples are graphitic carbons. TS spectra are more heterogeneous: some are similar to a-C spectra with broad G and D bands while some either are similar to nc-G spectra with well separated G and D bands or look intermediate, between nc-G or a-C spectra. We have analyzed a great amount of data, focusing on relations between σ_G, Γ_G and Γ_D, and the D and G band relative intensity, R, and we have emphasized the similarity of nc-G and a-C properties revealed by the continuous clouds formed by Raman parameters, as shown for example for Γ_G in figure 1.b.

Data, recorded with λ_L=325.0, 514.5 and 785.0 nm, have been interpreted in the framework of laws linking Raman parameters together known from the literature. For nano-crystalline samples, these laws are the Tuinstra relation [1] and the λ_L dependence of R [2]. These studies have also shown that Γ_G could be approximated for such materials by a linear law with R. For a-C data, we have used the relations proposed by Ferrari and Robertson [3,4] for R and Γ_G for the green excitation wavelength.

Then, we have assumed first, a similar fourth power λ_L dependency for a-C than for nc-G and second, continuity between nc-G and a-C at $L_a = L_{a0}$. With these simple assumptions, and defining the scaled intensity ratio $R_\lambda = R \times (514.5/\lambda_L)^4$, we succeed in fitting a-C data for the three λ_L used in this study. Figure 1.b displays experimental (points) and fitted (lines) Raman parameters in the (R_λ, Γ_G) plot in the case of λ_L= 325 nm (blue) and 514.5 nm (green) data. The good fit obtained indicates that the λ_L dependency of R is shared by both a-C and nc-G.

Nevertheless a lot of green data are still not reproduced using this modeling and we divide TS samples in three groups: pure nc-G, pure a-C, and intermediate samples, these latter samples being those not correctly described by the previous laws (grey lines of figure 1.b). We propose to interpret these spectra as the sum of two sets of bands: one nc-G set composed of three bands, G, D and D', and one a-C set composed of two bands, G and D. The ratio between these two sets of bands. This choice is supported by the spectral decomposition usually made in the literature [5, 7]. Our method thus consists in first building simulated spectra by adding these two sets of bands using realistic parameters (with the "s" exponent, meaning "simulation") and second analyzing these simulated spectra with their raw Raman parameters exactly in the same way as the experimental spectra. The curve of figure 1.b at low Γ_G ($\Gamma_G <$ 80 cm^{-1}), referred to as simulation S1, is obtained by only taking into account the nc-G set of bands. For larger Γ_G, a deviation from the grey line appears which qualitatively reproduces the experimental trend. This origin of the deviation from a straight line is thus merely the apparent broadening of the G band due to the presence of the D' band. To reproduce the experimental trends at larger Γ_G, introducing the a-C set of bands is needed, as shown with simulation S2. Finally, to correctly simulate spectra with $\Gamma_G >$ 80 cm^{-1} an additional broadening Γ_{adds} is needed for the G and D bands of nc-G, (simulation S3).

Figure 2 displays Γ_D versus Γ_G (experimental and simulated data). Graphitic and pure nc-G, intermediate and a-C sample widths have been displayed for the green excitation wavelength. C/C data points are localized on the straight line corresponding to $\Gamma_D = 2 \Gamma_G$. All the TS data points are distributed around this straight line, S-shaped. According to [8] the natural broadening of the G band for graphene is proportional to $<D_\Gamma^2>_F$ which is called the electron-phonon coupling at the Γ point of the Brillouin zone (EPC, see [9]). These authors have also shown that $<D_K^2>_F/<D_\Gamma^2>_F = 2$ where $<D_K^2>_F$ is the electron phonon coupling at the K point of the Brillouin zone. As the phonons at this K point are involved in the existence of the D band of disordered carbons this is an indication that electron-phonon coupling plays a similar role for all types of carbon.

To conclude, we have shown that fundamental properties such as the λ_L dependency of the Raman cross-section and the electron-phonon induced broadening could be used to interpret nc-G as well as a-C data, indicating common trends and a continuum of properties among these types of carbons. We thus get a consistent description of the Raman properties of both types of carbon.

References

[1] F. Tuinstra, and J. L. Koenig, J. Chem. Phys. **53** (1970) 1126
[2] L. G. Cançado, A. Jorio, and M. A. Pimenta, Phys. Rev. B **76** (2007) 064304
[3] A. C. Ferrari, and J. Robertson, Phys. Rev. B **61** (2000) 14095
[4] A. C. Ferrari, and J. Robertson, Phil. Trans. R. Soc. Lond. A **362** (2004) 2477
[5] C. Beny-Bassez, and J. N. Rouzaud, Scanning electron microscopy **1** (1985) 119
[6] T. Jawhari, A. Roid, and J. Casado, Carbon **33** (1995) 1561
[7] A. Sadezky *et al.*, Carbon **43** (2005) 1731
[8] S. Piscanec *et al.*, Phys. rev. lett. **93** (2004) 185503
[9] M. Lazzeri *et al.*, Physical review B **73** (2006) 155426

Figures
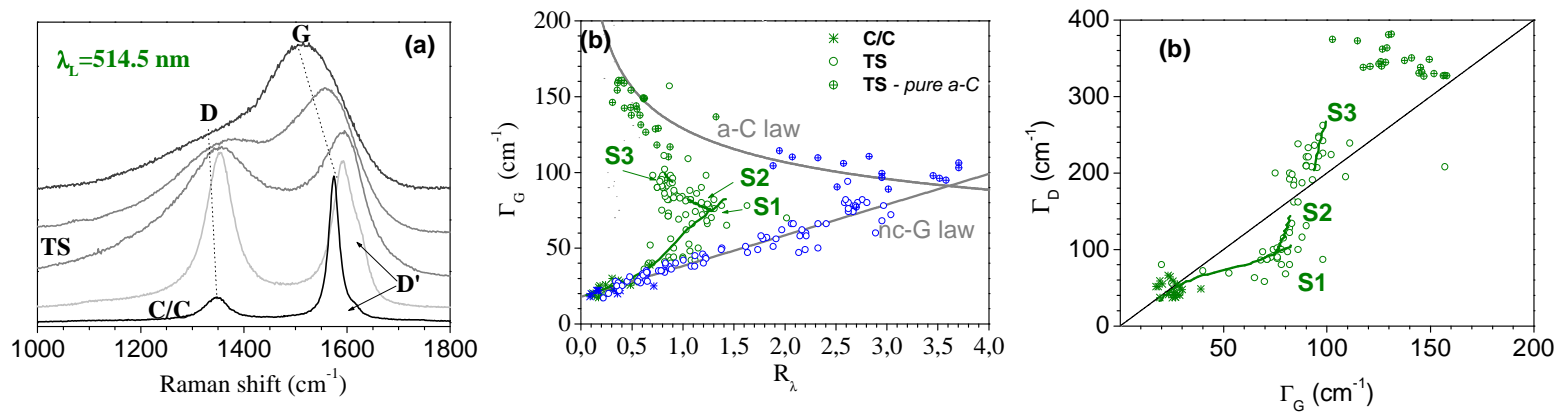
Figure 1. Raman data corresponding to C/C and Tore Supra samples (green for λ_L = 514.5 nm, blue for λ_L = 325.0 nm). (a) Typical Raman spectra of C/C and TS samples. (b) Raman parameters compared to simulations. Simulation S1 is obtained with a pure nc-G component. Simulations S2 is obtained by adding to a nc-G component an a-C component with the introduction of an additional broadening for S3 simulation. (c) is the same as (b) but in the (Γ_G,Γ_D) plot.

Ionic and non-ionic surfactants for the production of highly concentrated aqueous dispersions of pristine graphene

L. Guardia, M. J. Fernández-Merino, **J. I. Paredes**, P. Solís-Fernández, S. Villar-Rodil, A. Martínez-Alonso, and J. M. D. Tascón

Instituto Nacional del Carbón, CSIC, Apartado 73, 33080 Oviedo, Spain
paredes@incar.csic.es

Graphene dispersions are usually prepared through conversion of graphite to graphite oxide, subsequent exfoliation of the latter in aqueous or organic medium to yield graphene oxide sheets, and finally chemical reduction of the exfoliated dispersion [1-3]. Such procedure boasts the merit of affording single-layer sheets in very large quantities and has proved suitable toward some specific applications [4]. Still, the resulting graphenes bear a substantial amount of structural defects and residual oxygen inherited from the oxidation step [5]. This constitutes a serious drawback, as many of the unique properties of graphene are severely degraded by the presence of disorder. With a view to attaining dispersions of defect-free graphene, some recent research has concentrated on the liquid-phase exfoliation of more pristine forms of graphite, rather than graphite oxide [6, 7]. In particular, aqueous dispersions of relatively defect-free graphene stabilized by some ionic surfactants have been demonstrated [6]. However, the reported concentrations were typically on the order of 0.01 mg mL^{-1}, which are too low for many practical uses. Likewise, the availability of aqueous dispersions of high-quality graphene with surfactants of different types (e.g., non-ionic) could facilitate its use in a wider range of applications. To the best of our knowledge, these issues have not yet been addressed.

In this communication, we present the preparation of aqueous dispersions of high-quality graphene in a wide range of surfactants [8]. We compare the performance of non-ionic and ionic surfactants toward the ultrasound-assisted dispersion/exfoliation of pristine graphite in water. We find the former to be generally superior to the latter as regards the amount of exfoliated material that can be stably suspended. Concentrations of high-quality, single- and few-layer graphene as high as ~1 mg mL^{-1} can be attained with some specific surfactants (Figure 1). The potential utility of these highly concentrated dispersions is demonstrated by processing them into different materials, such as free-standing paper-like films and hydrogels (Figure 2).

Acknowledgements

References

[1] Park S, Ruoff RS. Nat Nanotechnol, **4** (2009) 217.
[2] Li D, Müller MB, Gilje S, Kaner RB, Wallace GG. Nat Nanotechnol, **3** (2008) 101.
[3] Villar-Rodil S, Paredes JI, Martínez-Alonso A, Tascón JMD. J Mater Chem **19** (2009) 3591.
[4] Dua V, Surwade SP, Ammu S, Agnihotra SR, Jain S, Roberts KE,et al. Angew Chem Int Ed, **49** (2010) 2154.
[5] Allen MJ, Tung VC, Kaner RB. Chem Rev, **110** (2010) 132.
[6] Lotya M, Hernandez Y, King PJ, Smith RJ, Nicolosi V, Karlsson LS, et al. J Am Chem Soc, **131** (2009) 3611.
[7] Vadukumpully S, Paul J, Valiyaveettil S. Carbon, **47** (2009) 3288.
[8] Guardia L, Fernández-Merino MJ, Paredes JI, Solís-Fernández P, Villar-Rodil S, Martínez-Alonso A, Tascón JMD. Carbon (2011), doi:10.1016/j.carbon.2010.12.049

Figures
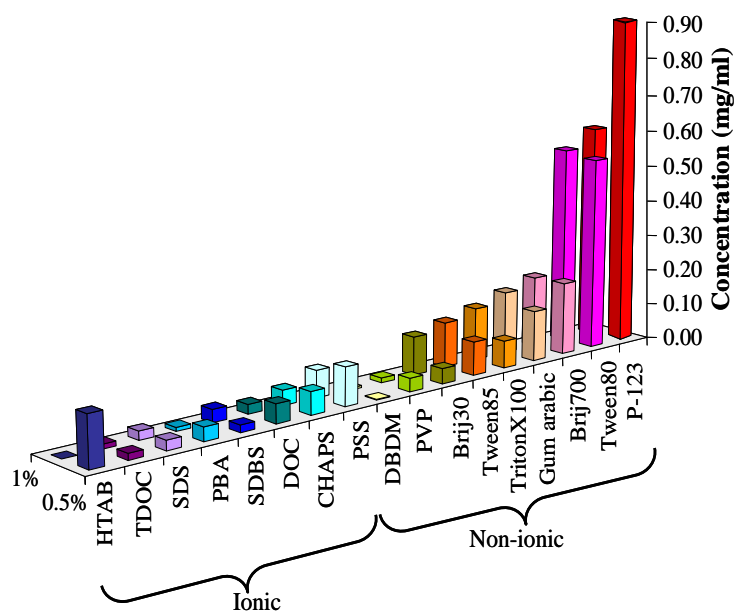
Figure 1. *Graphene concentration in aqueous dispersions achieved by using different surfactants, as estimated from UV–vis absorption measurements. Two surfactant concentrations are shown: 0.5% and 1.0% wt./vol.*
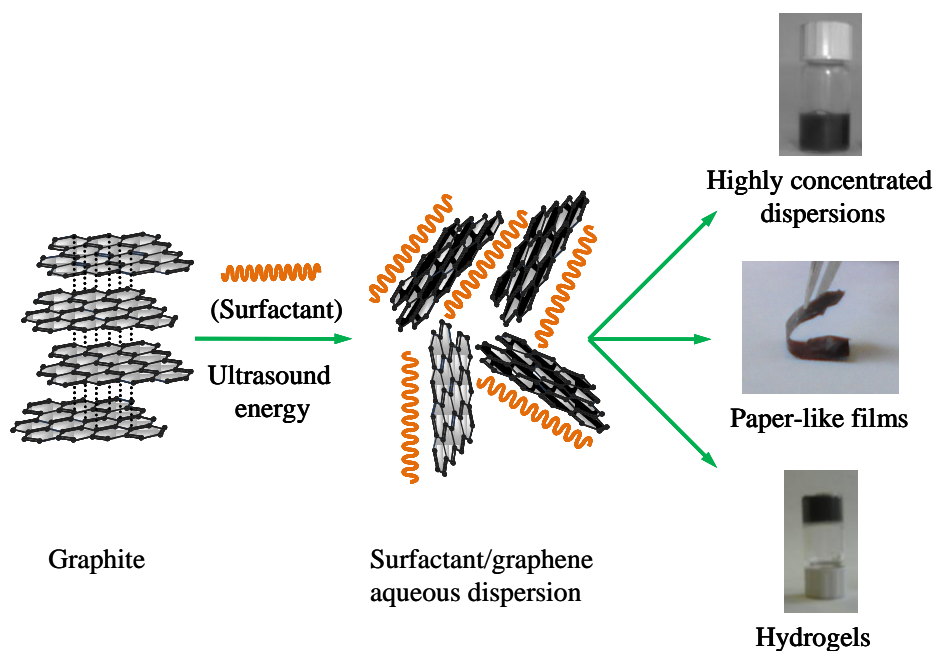
Figure 2. *Scheme for the production of aqueous dispersions of pristine grapheme, paper-like films and hydrogels.*

Work-function engineering of graphene electrodes by self-assembled monolayers for high-performance organic field-effect transistors

Jaesung Park,[1] Seon Ho Kim,[1] Sung Hyun Sim[2], Byung Hee Hong,[2] and Kwang S. Kim[1]

[1]Center for Superfunctional Materials, Department of Chemistry, Pohang University of Science and Technology, Pohang 790-784, Korea, [2]SKKU Advanced Institute of Nanotechnology (SAINT) and Center for Human Interface Nano Technology (HINT), Sungkyunkwan University, Suwon 440-746, Korea

Kim@postech.ac.kr

We have devised a method to optimize the performance of organic field-effect transistors (OFET) by controlling the work functions of graphene electrodes by functionalizing the surface of SiO_2 substrates with self-assembled monolayers (SAMs). The electron-donating NH_2-terminated SAMs induce strong n-doping in graphene, while the CH_3-terminated SAMs neutralize the p-doping induced by SiO_2 substrates, resulting in considerable changes in the work functions of graphene electrodes. This approach was successfully utilized to optimize electrical properties of graphene field-effect transistors and organic electronic devices using graphene electrodes. Considering the patternability and robustness of SAMs, this method would find numerous applications in graphene-based organic electronics and optoelectronic devices such as organic light emitting diodes and organic photovoltaic devices.

Strain effect on the electronic properties in graphene

F. M. D. Pellegrino [1,2,3,4], G. G. N. Angilella [1,2,4,3] and R. Pucci [1,3]

1 Dipartimento di Fisica e Astronomia, Università di Catania, Via S. Sofia, 64, I-95123 Catania, Italy
2 Scuola Superiore di Catania, Via S. Nullo, 5/i, I-95123 Catania, Italy
3 CNISM, UdR Catania, I-95123 Catania, Italy
4 INFN, Sez. Catania, I-95123 Catania, Italy

e-mail address of the corresponding author: fmd.pellegrino@gmail.com

Within the tight binding approximation, we study the dependence of the electronic band structure and of plasmonic spectra of a graphene single layer on the modulus and direction of applied uniaxial strain. While the Dirac cone approximation, albeit with a deformed cone, is robust for sufficiently small strain, band dispersion linearity breaks down along a given direction, corresponding to the development of anisotropic massive low-energy excitations. We recover a linear behavior of the low-energy density of states, as long as the cone approximation holds, while a band gap opens for sufficiently intense strain, for almost all, generic strain directions. Our calculation of the dielectric function is based on the random phase approximation (RPA), besides we consider local field effects (LFE), following the method developed by Hanke and Sham for the calculations of the dielectric response properties of crystalline systems. In this way we will take into account possible collective excitations of any wavelength as a function of the uniaxial strain.

References

[1] A. H. Castro Neto *et al.*, Rev. Mod. Phys. **81**, (2009) 109
[2] F. M. D. Pellegrino, G. G. N. Angilella and R. Pucci, Phys. Rev. B **80**, (2010) 094203
[3] S. M. Choi *et al.*, Phys. Rev. B **81**, (2010) 081407 (R)
[4] F. M. D. Pellegrino, G. G. N. Angilella and R. Pucci, Phys. Rev. B **81**, (2010) 035411
[5] W. Hanke and L. J. Sham, Phys. Rev. Lett. **33**, (1974) 582
[6] B. Wunch *et al.*, New J. Phys. **8**, (2006) 318
[7] E. H. Hwang and S. Das Sarma, Phys. Rev B **75**, (2007) 205418
[8] A. Hill *et al.*, EPL **87**, (2009) 27005
[9] M. H. Gass *et al.*, Nature Technology **3**, (2008) 676
[10] T. Eberlein *et al.*, Phys. Rev. B **77**, (2008) 233406
[11] C. Kramberger *et al.*, Phys. Rev. Lett. **100**, (2008) 196803
[12] F. Liu *et al.*, Phys. Rev. B **76**, (2007) 064120
[13] K. S. Kim *et al.*, Nature **457**, (2009) 706

Well-defined Nanographenes through Aryne Chemistry

Diego Peña, Dolores Pérez, Enrique Guitián

Centro de Investigación en Química Biolóxica e Materiais Moleculares (CIQUS)
Campus Vida, Universidade de Santiago de Compostela
15782-Santiago de Compostela, Spain
diego.pena@usc.es

Structurally, nanosized graphenes are nothing but large polycyclic aromatic hydrocarbons (PAHs). During the last century, organic synthesis has provided numerous methods to prepare large PAHs. These synthetic methodologies could enable the preparation of graphene fragments with well-defined edges, a crucial feature of these carbon-based material.[1]

In this contribution we described our efforts to obtain well-defined graphene nanoribbons through organic synthesis, in particular using aryne cycloaddition reactions. Figure 1 shows some examples of graphene fragments that have been synthesize in our labs by these bottom-up methodologies.

References

[1] Peña, D. (2010) Bottom-up Approaches to Nanographenes through Organic Synthesis, in Ideas in Chemistry and Molecular Sciences: Advances in Synthetic Chemistry (ed B. Pignataro), Wiley-VCH Verlag GmbH & Co., Weinheim, Germany. DOI: 10.1002/9783527630554. Ch11.
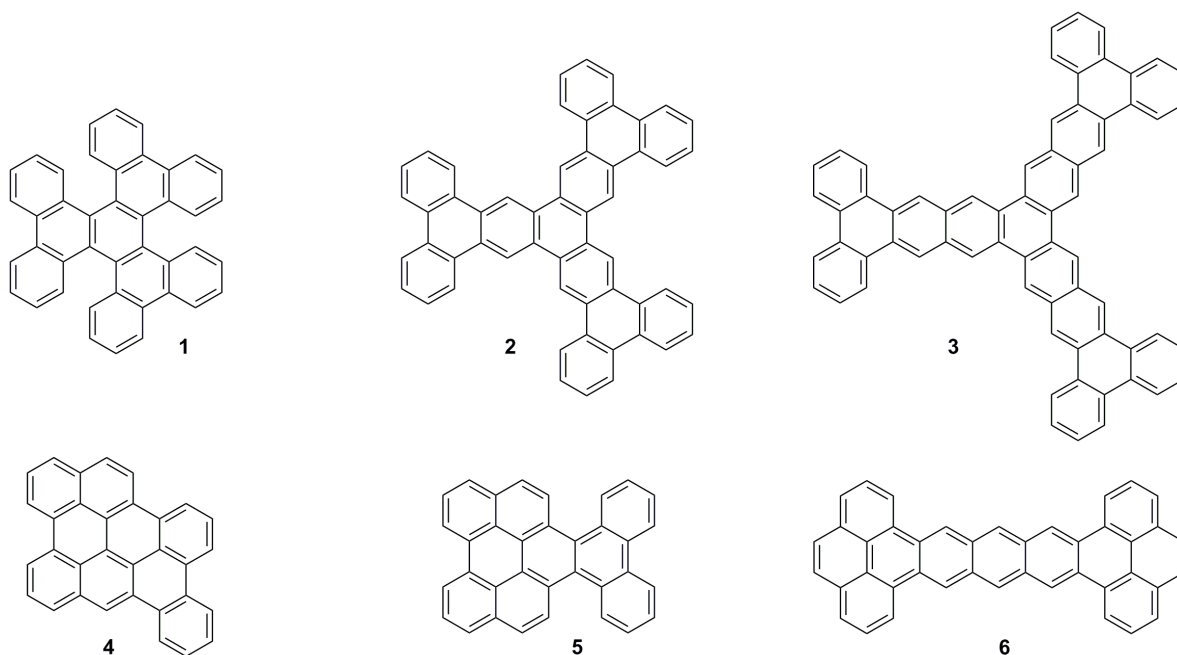
Figure 1

Dynamics of laser bullet propagation in carbon nanotube array with metal inhomogeneities

Alexander Popov[1], Mikhail Belonenko[2], Nicolay Lebedev[1]

[1]Department of Physics ant Telecommunication, Volgograd State University
400062, Prospect Universitetsky, 100, Volgograd, Russia
[2]Laboratory of Nanotechnologies, Volgograd Institute of Business
400048, Uzhno-ukrainskaya Street 2, Volgograd, Russia
A.Popov.VolSU@gmail.com

In constructed model of ultra-short optical pulse propagation in a 2D array of CNTs we assume that the electric field vector $\mathbf{E}(x, y, t)$ is directed along the tube axis, and electromagnetic wave propagates in the transverse direction (Fig. 1). We also assume the CNTs being ideal, so they have a zigzag modification and all of them are oriented in the space along about the same direction. The inhomogeneities of two-dimensional array of carbon nanotubes is simulated by two small diameter metal wires ($\Delta x, \Delta y \sim 32$ nm), which is placed into the array of CNTs. The axis of the wire coincides with the axes of nanotubes. To determine the electric current within the region occupied by wires, we assume the Ohm's law, $j = \sigma E = -\sigma \partial A / c \partial t$, where σ is the complex conductivity, which generally depends on the applied field frequency.

The electromagnetic field is considered on the basis of Maxwell equations, and the electronic system of carbon nanotubes is treated by the Boltzmann equation in relaxation time approximation.

As a result of mathematical transformations we finally come to the following resulting equation for the vector potential:

$$\frac{\partial^2 A_x}{\partial x^2} + \frac{\partial^2 A_z}{\partial y^2} - \frac{1}{c^2}\frac{\partial^2 A_z}{\partial t^2} + \frac{q}{\pi \hbar}\sum_m c_m \sin\left(\frac{maq}{c} A_z(t)\right) = 0$$

$$c_m = \sum_s a_{ms} b_{ms} \qquad b_{ms} = \int_{-q_0}^{q_0} dp_z \cos(map_z) F_0(\mathbf{p})$$

As was established by numerical simulation, during this evolution, an ultrashort pulse separates into two components with different amplitudes. Figure 2 shows the result of the numerical simulation of a laser bullet propagating in a 2D array of CNTs with two closely spaced metal wires. Calculations were performed for the metal inclusions situated at a distance of 570 nm from the initial pulse position and displaced each by 60 nm from the axis.

The results of simulation reveal a principally new effect that takes place upon the laser pulse scattering on two closely spaced wires, namely, the periodic separation of the intensity maximum into two components and their subsequent merging back into a single maximum. We believe that this phenomenon is closely analogous to the dynamics of internal soliton modes [3, 4] and consists in the excitation of intrinsic oscillation modes in the laser bullet upon its scattering on the system of defects, which leads to the appearance of periodically separating and merging maxima as a result of the interference between the scattered and primary pulse. The observed behavior allows us to suggest that boomeron analogs are also possible in other strongly nonlinear 2D systems.

Thus, the results of this investigation can by formulated as follows:

1) A model is proposed and an effective equation for the vector potential is obtained that describes the dynamics of propagation of an ultrashort laser pulse in an array of CNTs. Assumptions used for the model construction are formulated.

2) The results of numerical calculations according to the model show that stable nonlinear waves localized in two directions, which are analogous to the laser (light) bullets, are possible in the 2D case.

3) The scattering of the ultrashort laser pulse on a pair of closely spaced metal defects is accompanied by a periodic separation of the pulse maximum into two components followed by their merging.

References
[1] M. S. Dresselhaus, G. Dresselhaus, P. C. Eklund Science of Fullerenes and Carbon Nanotubes. Academic Press, Inc. (1996) 965 p.
[2] Belonenko M. B., Lebedev N. G., Popov A.S. // JETP. Vol. 91, **9** (2010) p. 506
[3] P. I. Krepostnov, V. O. Popov, and N. N. Rozanov // Opt. Spektrosk. **89**, (2000) 964
[4] A. B. Vittenberg P. I. Krepostnov, V. O. Popov, and N. N. Rozanov. // Opt. Spektrosk. **92**, (2002) 603

Figures
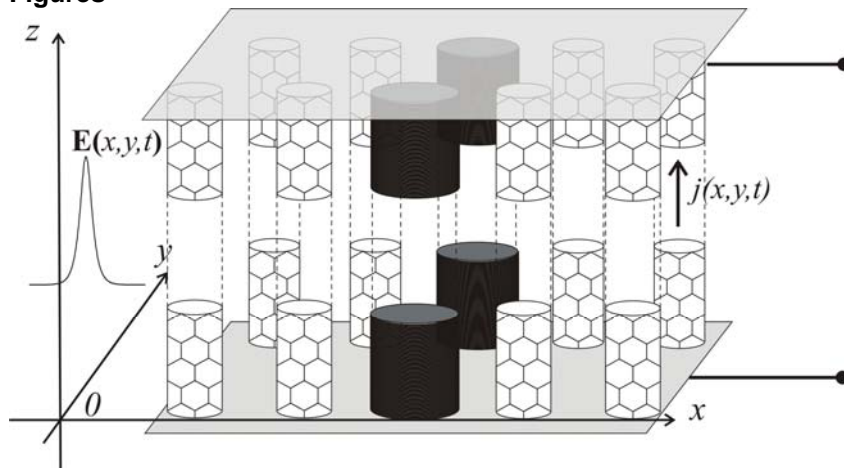
Fig. 1: Geometry of the problem.
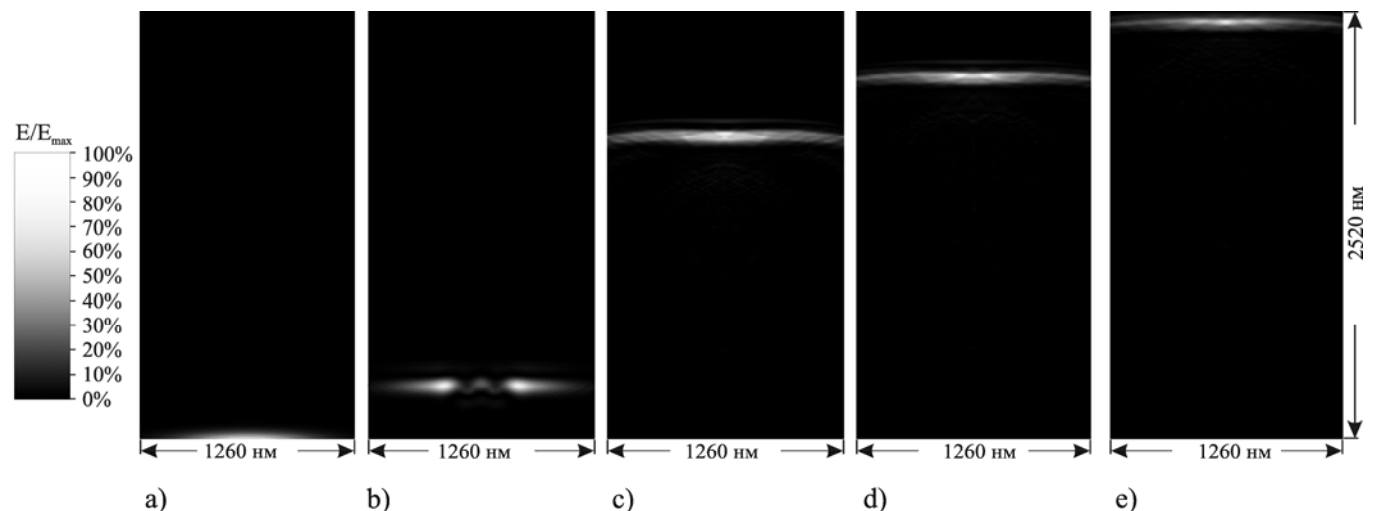
Fig. 2: Distribution of light bullet in an array of carbon nanotubes with two metallic irregularities for two-dimensional case. a) initial form of light bullet, b) $t=0.5 \cdot 10^{-12}$ s , c) $t=2.2 \cdot 10^{-12}$ s, d) $t=2.6 \cdot 10^{-12}$ s, e) $t=2.9 \cdot 10^{-12}$ s.

Structural and electrical investigations of graphene / 3C-SiC heterostructures elaborated by CVD on (111) and (100) silicon substrates

Marc PORTAIL[1,*], Adrien MICHON[1], Stéphane VEZIAN[1], Marcin ZIELINSKI[3], Thierry CHASSAGNE[3], Antoine TIBERJ[2], Jean CAMASSEL[2] and Yvon CORDIER[1]

[1]CNRS – CRHEA, Rue Bernard Gregory, 06560 VALBONNE, France
[2]CNRS - Laboratoire Charles Coulomb, Université Montpellier 2, France
[3]NOVASiC, Savoie Technolac, Arche Bat4, 73375, LE BOURGET DU LAC, France
*mpo@crhea.cnrs.fr

The past decade has seen the emergence of graphene as a promising material for developing high frequency electronic applications. But before the future graphene based devices can compete with the current Si technology major challenges must be overcome. Among them, the formation of nanoscale graphene domains, suitable for the realisation of ambipolar devices, puts light on the importance both of the elaboration method and the substrate on which graphene is obtained. If bulk hexagonal Silicon Carbide (α-SiC) substrates have demonstrated a high efficiency for obtaining tuneable graphene structures [1], their relatively high cost with respect to Silicon as well as their limited diameter size constitute major issues regarding a widespread dissemination of a graphene based technology. In this perspective, cubic-SiC (β-SiC or 3C-SiC) epilayers grown on silicon recently gained interest since the ability to produce graphene films on such templates has been demonstrated under ultra high vacuum environment [2-4].

In this way, this work aims to discuss the structural and electrical properties of graphene films elaborated on 3C-SiC/Si templates. Contrary to the previous cited works [2-4], graphene films under consideration in this contribution have been elaborated under Chemical Vapour Deposition (CVD) environment, using a derived approach from that we recently proposed to perform direct epitaxy of graphene on 6H-SiC [7]. It has been demonstrated that such a CVD environment is more efficient to produce high quality graphene but, to date, only using bulk h-SiC substrates [5-6].

For this work, 3C-SiC epilayers were previously grown on 2inches silicon substrates oriented along (111) and (100) crystalline directions. Deposition was done in a resistively heated hot wall Chemical Vapour Deposition chamber with classical two steps deposition process (carbonization / growth) using silane and propane as precursors diluted in hydrogen. After deposition, epilayers are released to air for characterization and, for some cases, polishing before graphitization process. This last is done in the same reactor used for 3C-SiC elaboration. The 3C-SiC epilayers are annealed at 1300°C under a mixture of argon and propane during 30-60min at a pressure ranging from 6 to 600mbar. After thermal annealing, structural properties of the graphene/graphite surface phase were investigated by means of Low Energy Electron Diffraction (LEED), Atomic Force Microscopy (AFM), X ray Photoemission Spectroscopy (XPS) and Raman Spectroscopy. Basic electrical properties of the surface after thermal treatment have been measured in a second time by using the circular-Transfer Length Method (c-TLM). For that purpose, Ti/Au (30/200nm) films have been deposited in an e-beam evaporator using standard lithography and lift off process to reveal c-TLM patterns. In order to benchmark the graphitization mechanism, the same graphitization processes have been applied to Si terminated 6H-SiC substrates.

In a first time, we briefly introduce the structural properties of the 3C-SiC/Si templates used for the study. So we discuss in details the formation of the surface graphitic phase, for both (100) and (111) crystalline orientations. That is attested by XPS and Raman where typical spectral features attributed to sp2 carbon linked network are observed after graphitization process. The intrinsic differences of the graphitization process applied to the two differently oriented 3C-SiC/Si templates are presented. Basing on XPS and Raman data, it is demonstrated that a more ordered graphitization mechanism, leading to

the formation of graphene films similarly to the Si terminated face of 6H-SiC substrates, is obtained on (111) faces. In case of (100) faces, the graphitic phase which is formed subsequently to graphitization process is more rapidly achieved than on (111) faces but is accompanied by a lower degree of organization (see Fig. 1). It is also shown that a good homogeneity of the graphene formation on the whole 2inches template is achieved. The case of polished 3C-SiC(111) epilayers is also discussed. Finally we present the electrical characterizations performed on both orientations. The influence of the 3C-SiC underlying film on the electrical properties obtained (specific contact resistance and sheet resistance, ρ_c and R_{sh}) is discussed and compared to that obtained with graphene on 6H-SiC substrates (see Fig. 2).

In summary, our contribution demonstrates the elaboration of graphene films on 2inches 3C-SiC/Si templates using a CVD approach. We show that structural differences exist between both crystalline orientations and are investigated. We also present some basic electrical measurements which reveal the ohmic character of the contact on graphitic phase / 3C-SiC and indication of a better conductivity of graphitic phase obtained on 3C-SiC(100) films despite a lower surface crystalline arrangement. This contribution allows to substantiate a low cost approach of graphene formation which could be suitable for integrating graphene within Si technology.

References

[1] M. Prinkle et al, Nature Nano. **5** (2010) 727
[2] A. Ouerghi et al, Appl. Phys. Lett. **96** (2010) 191910
[3] M. Suemitsu et al, J. Phys. D **43** (2010) 374012
[4] V. Aristov et al, Nano Lett. **10** (2010) 992
[5] K. Emstev et al, Nature Mat. **8** (2009) 203
[6] C. Virojanadara et al, Phys. Rev. B**78** (2008) 245403
[7] A. Michon et al, Appl. Phys. Lett. **97** (2010) 171909

Figures
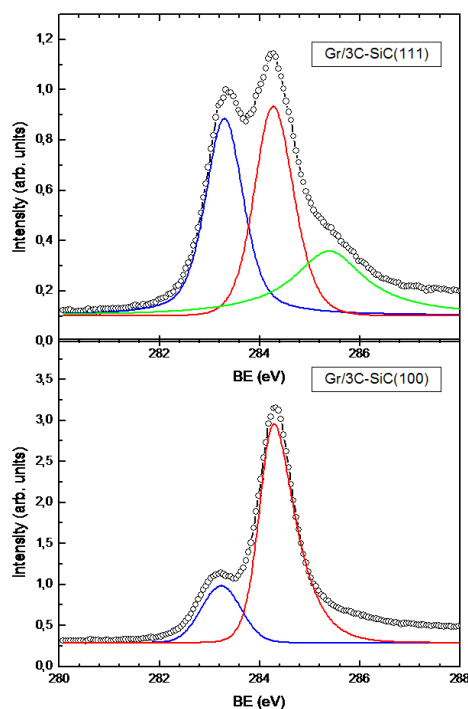
Fig 1 : XPS analysis of the CVD graphitization mechanism on 3C-SiC(111) and 3C-SiC(100) templates, under the same experimental conditions.
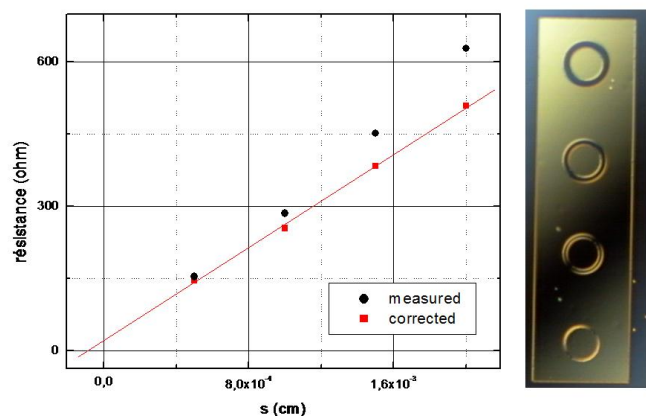
Fig 2: Determination of ρ_c and R_{sh} by c-TLM method. Left: experimental measures; right, c-TLM patterns

Electronic and magnetic properties of triangular graphene quantum rings

P. Potasz[1,2], A. D. Guclu[1], O. Voznyy[1], J. A. Folk[3] and P. Hawrylak[1]

[1]Institute for Microstructural Sciences, National Research Council Canada, *ON K1A 0R6,* Ottawa, Canada
[2]Institute of Physics, Wroclaw University of Technology, Wybrzeze Wyspianskiego 27, 50-370 Wroclaw, Poland
[3]Department of Physics and Astronomy, University of British Columbia, BC V6T 1Z4, Vancouver, Canada
pawel.potasz@pwr.wroc.pl

The graphene nanostructures allow the control of bandgaps and magnetic properties with size and shape[1-3]. In particular, the existence of a band of degenerate states near Fermi level of zigzag ribbons[4, 5] and triangular dots[6-8] was predicted by tight-binding model and confirmed by density functional theory calculations. In this work, electronic and magnetic properties of triangular graphene rings potentially fabricated using carbon nanotubes as masks (Fig. 1) are described as a function of their size and width. We show that many of the properties of triangular graphene quantum dots survive [7,8] and that new properties related to ring formation appear. The electronic properties of the charge neutral system are calculated using tight-binding method and interactions are treated using the mean-field Hubbard model. We show that for triangular quantum dots with a triangular hole, the magnetic properties are determined by the width of the ring, leading to ferromagnetic corners and antiferromagnetic sides. The electronic properties of graphene quantum dots as a function of additional number of electrons or holes are described by a combination of tight-binding, Hartree-Fock, and configuration interaction methods. The ground state of the outer edge is found to be maximally spin polarized for almost all filling factors. The evolution of the excitation gaps as a function of shell filling shows oscillations as a result of electronic correlations.

References

[1] A. H. Castro Neto, et. al., Rev. Mod. Phys. **81** (2009), 109.
[2] F. Xia et. al., Nature Nanotechnol. **4** (2009), 839.
[3] T. Mueller, et. al., Nature Photon. **4** (2010), 297.
[4] K. Nakada, et. al., Phys. Rev. B **54** (1996), 17954.
[5] Y. Son, et al., Nature (London) **444** (2006), 347.
[6] M. Ezawa, Phys. Rev. B **76** (2007), 245415.
[7] J. Fernandez-Rossier and J. J. Palacios, Phys. Rev. Lett. **99** (2007), 177204.
[8] A. D. Güçlü, et. al., Phys. Rev. Lett. **103** (2009), 246805.

Figure 1
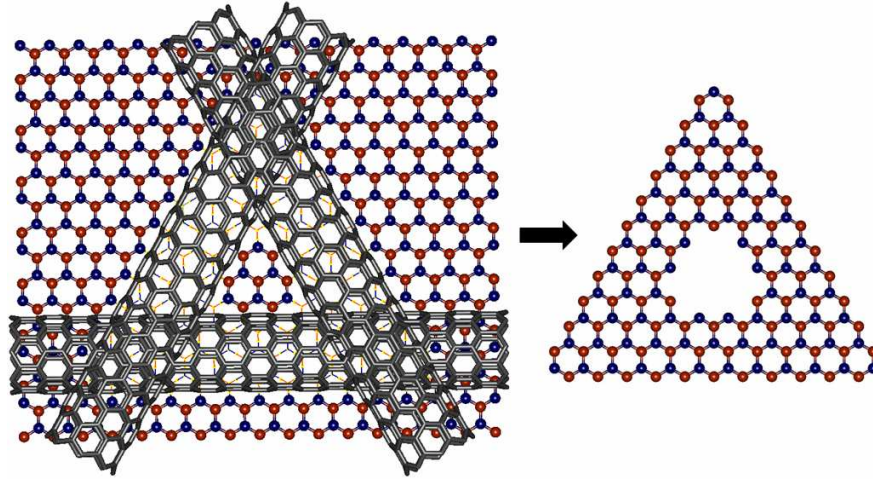
Figure 1: Experimental method for designing a TGQR. Three CNTs arranged in equilateral triangle along zigzag edges play the role of a mask. By using etching methods one can obtain TGQR with well defined edges. The circumference of CNT determines the width of TGQR. Red and blue colors distinguish between two sublattices in the honeycomb graphene lattice.

Nanostructuring epitaxial Graphene by Focused Ion Beam patterning

B. Prével, J-M. Benoit, L. Bardotti, P. Mélinon,

Laboratoire de Physique de la Matière Condensée et Nanostructures, Université Lyon 1, CNRS, UMR 5586, Domaine Scientifique de la Doua, F-69622 Villeurbanne, France

A. Ouerghi, D. Lucot, E. Bourhis, J. Gierak
Laboratoire de Photonique et Nanostructure – CNRS, Route de Nozay, 91460 Marcoussis, France

Contact : brigitte.prevel@univ-lyon1.fr

Since its discovery, graphene has attracted tremendous interest and their unusual properties make it a promising candidate for future electronic and optic applications [1. 2]. Along the view of designing graphene-based devices many efforts are devoted to the achievement of large scale graphene patterning in a reproducible way with controlled structural quality [3]. It is also of prior fundamental significance to further control the band gap. Recent theoretical studies demonstrated that antidot lattice can turn semimetalic graphene into a gapped semiconductor, where the size of the gap can be tuned via the geometry of the lattice [4]. The possibility to open band gaps by inducing artificial defects and the ability to control the conductivity by physical means is hence a crucial step in order to establish graphene as a competitive material for future nanoelectronics [5]. Further studies would be important to find a way to produce graphene with desired defects to modify electronic properties [6]. The functionalization is suitable way to detect imperfections in a graphene crystal lattice and to separate natural and arficial defects [7, 8].

We show in this presentation that ultra high resolution Focused ion beam (FIB) is a powerful technique for tailoring tunable defects by irradiation of a graphene sheet. FIB has the unique capability for rapid prototyping since it requires neither mask nor resist while processing [9]. Such direct writing does not require subsequent pattern transformation either. The sub-10 nm spot size achievable by the FIB method enables the patterning of diverse nanostructures at a very high resolution and offers the opportunity to functionalize surfaces with a periodic array of controlled identical extended nanodefects. nanometer scale arrays were fabricated via FIB technology in the low-current processing condition, which is promisingly useful in the construction of various templates using "Few Layer" graphene on 6H-SiC(0001). The topography of the graphene surface before and after fabrication of the patterned areas is characterized by atomic force microscopy in tapping mode. Raman spectroscopy is used to study graphene nanostructured with different ion doses. Several examples of patterned graphene will be presented.

References

[1] K. S. Novoselov, Z. Jiang, Y. Zhang, S. V. Morozov, H. L. Stormer, U. Zeitler, J. C. Maan, G. S. Boebinger, P. Kim, and A. K. Geim, Science **315** (2008), 1379

[2] K. S. Novoselov, et al. Science **306**, (2004) 666

[4] T. G. Pedersen, C. Flindt, J. Pedersen, N. Asger Mortensen, A. P. Jauho, K. Pedersen, Phys. Rev. Lett. **100** (2008), 136804

[5] Y. B. Zhang, Y. W. Tan, H. L. Stormer, P. Kim, Nature **438** (2005), 7065, 201

[6] J. O. Sofo, A. S. Chaudhari, G. D. Barber; Phys Rev B **75**, (2007) 153401

[7] Boukhvalov D, Katsnelson W, Phys. Rev. B **78** (2008) 085413

[8] Ribeiro R M, Peres N M, Coutinho R, Briddon J, Phys Rev B **78** (2008) 075442

[9] B. Prével, L. Bardotti, S. Fanget, A. Hannour, P. Mélinon, A. Perez, J. Gierak, G. Faini, E. Bourhis, D. Mailly, Appl. Surf. Sci. **226** (2004) 173

Figure
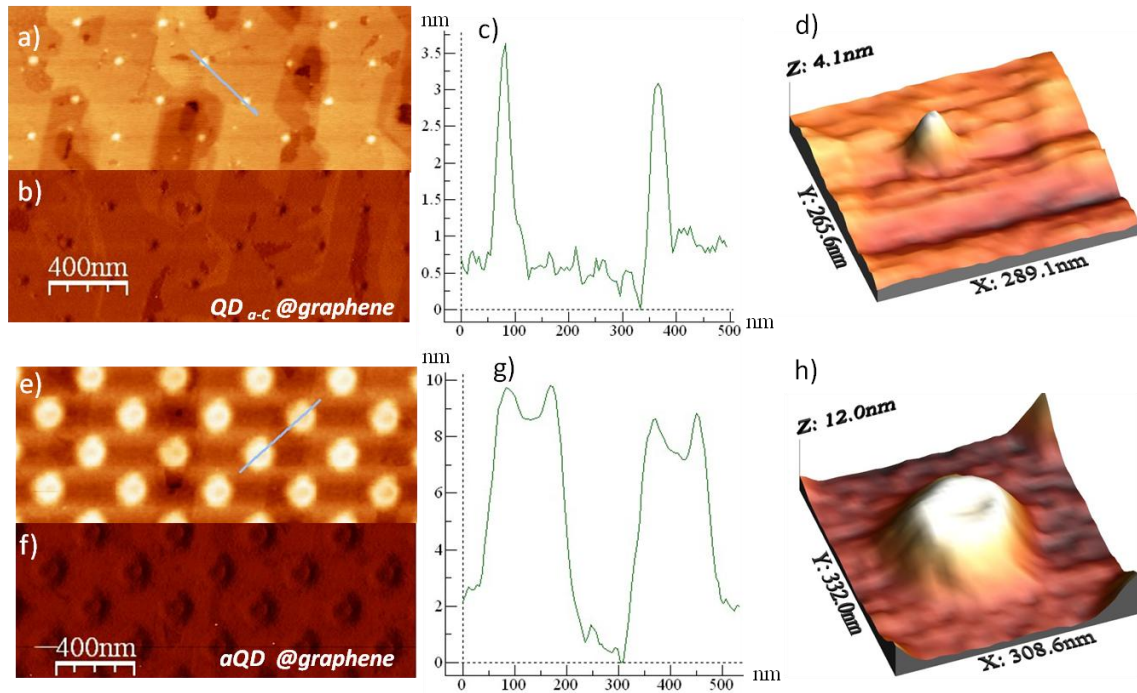
TMAFM topography image(a), (e); phase image (b), (f) and profiles (c), (g) of the morphologies of defects created by FIB on graphene for a 300 nm defect periodicity. (d), (h) represent 3D magnification of one randomly chosen defect. Top (a), (b), (c), (d) : moderate fluence 10^4 ions/dot (2×10^{16} ions cm^{-2}). Defect characteristics: bump shape, FWHM: 30 nm. Bottom (e), (f), (g), (h) : large fluence 10^6 ions/dot (2×10^{18} ions cm^{-2}). Defect characteristics: hollow pit shape, FWHM: 140 nm. The blue lines in figure 3a) and 3e) correspond to profiles given in figures 3c) and 3g)

Edge effects in graphene nanoislands on Co(0001) probed by STM measurements and first principles calculations

Deborah Prezzi[1,2], Daejin Eom[2], Kuang T. Rim[2], Hui Zhou[2], Michael Lefenfeld[2], Shengxiong Xiao[2], Colin Nuckolls[2], Mark S. Hybertsen[3], Tony F. Heinz[2], and George W. Flynn[2]

[1] CNR — Nanoscience Institute, S3 Center – via Campi 213/a, Modena, Italy
[2] NSEC — Columbia University – New York, 10027 NY, USA
[3] CFN – Brookhaven Natl. Lab., Upton, 11973 NY, USA

deborah.prezzi@unimore.it

We recently demonstrated the growth of regularly shaped, nanoscale islands of graphene on Co(0001) surfaces [1]. Here we combine low-temperature scanning tunneling microscopy (STM) measurements and DFT based calculations to study their edge properties [2]. These nanoislands reveal a well-ordered structure with predominant zigzag termination at the edges, as opposite to what is predicted to be the most stable configuration in isolated systems [3]. Moreover, STS tunneling spectra show prominent peaks at low bias, where the edges dominate the images. DFT calculations provide insights into the relative stability of different edge configurations and passivation conditions, as driven by interactions with Co. The coupling with the substrate results also in a dramatic modification of both electronic and magnetic properties at the edges. In order to study hybridization and size effects, we transform to localized Wannier states and develop a minimal model for the effective π states of these graphene nanostructures.

References

[1] D. Eom, D. Prezzi, K. T. Rim, H. Zhou, M. Lefenfeld, S. Xiao, C. Nuckolls, M. S. Hybertsen, T. F. Heinz, and G. W. Flynn, Nano Lett., **9** (2009) 2844.

[2] D. Prezzi et al., to be published (2011).

[3] T. Wassmann et al., Phys. Rev. Lett., **101** (2008) 096402.

Sedimentation-based and Isopycnic Separation of Liquid Phase Exfoliated Graphene Layers

G. Privitera[1], F. Bonaccorso[1], F. Torrisi[1], V. Nicolosi[2], T. Hasan[1], G. Savini[1], N. Pugno[3], A.C. Ferrari[1]

[1] Department of Engineering, University of Cambridge, Cambridge CB3 0FA, UK
[2] Department of Materials, Oxford University, Oxford OX1 3PH, UK
[3] Dept. of Structural Engineering, Corso Duca degli Abruzzi 24, 10129 Torino, Italy

gp332@cam.ac.uk

Ultracentrifugation is a well-established technique for Single Wall Carbon Nanotube (SWNT) purification [1,2,3]. It separates various particles into fractions on the basis of sedimentation rate in response to the centrifugal force acting on them. There are two main approaches to ultracentrifugation: sedimentation-based separation (SBS) and isopycnic separation, also known as Density Gradient Ultracentrifugation (DGU). The former discriminates particles by their difference in mass. The latter exploits subtle density differences between particles in a density gradient medium. Here we demonstrate high yield production of liquid phase exfoliated graphene [4] by mild-sonication of graphite in aqueous solution of sodium deoxycholate (SDC), followed by ultracentrifugation-based separation. In particular, we compare SBS and DGU to obtain dispersions highly enriched in monolayer and few layer graphene [5] .Transmission electron microscopy (TEM) and Raman spectroscopy show that ~65% of the flakes produced by SBS are monolayers with average size of ~$600nm^2$ [6,7]. DGU, besides sorting flakes by number of layers, allows us to obtain larger flakes with respect to SBS. The sorting strategy relies on the 'creation' of density differences between graphite flakes with different number of layers [8]. In addition to stabilizing the hydrophobic graphitic flakes in water, surfactants provide the variation of buoyant density dependent on the flake thickness (Fig. a). We show that sorting by number of layers is strongly affected by the flake surface/volume ratio and the coverage and clustering (aggregation properties) of the surfactant molecules (Fig. b). Bile salts and polymers provide better surface coverage compared to linear chain surfactants resulting in superior DGU separation. SDC bile salts show the best efficiency in exfoliation and sorting, with ~60% of the flakes in the topmost fraction being monolayers.

References

[1] O'Connell *et al.* Science 297, 593 (2002)
[2] M. S. Arnold *et al.*, Nat. Nano 1, 60 (2006)
[3] F. Bonaccorso *et al.*, Journal of Physical Chemistry C 114, 17267 (2010)
[4] Y. Hernandez *et al.* Nature Nano 3, 563 (2008)
[5] F. Bonaccorso *et al.*, submitted (2010)
[6] O.M. Marago' *et al.*, ACS Nano 4, 7515 (2010)
[7] F. Bonaccorso *et al.*, Nature Photonics 4, 611 (2010)
[8] A. A. Green *et al*, Nano Lett. 9, 4031 (2009)
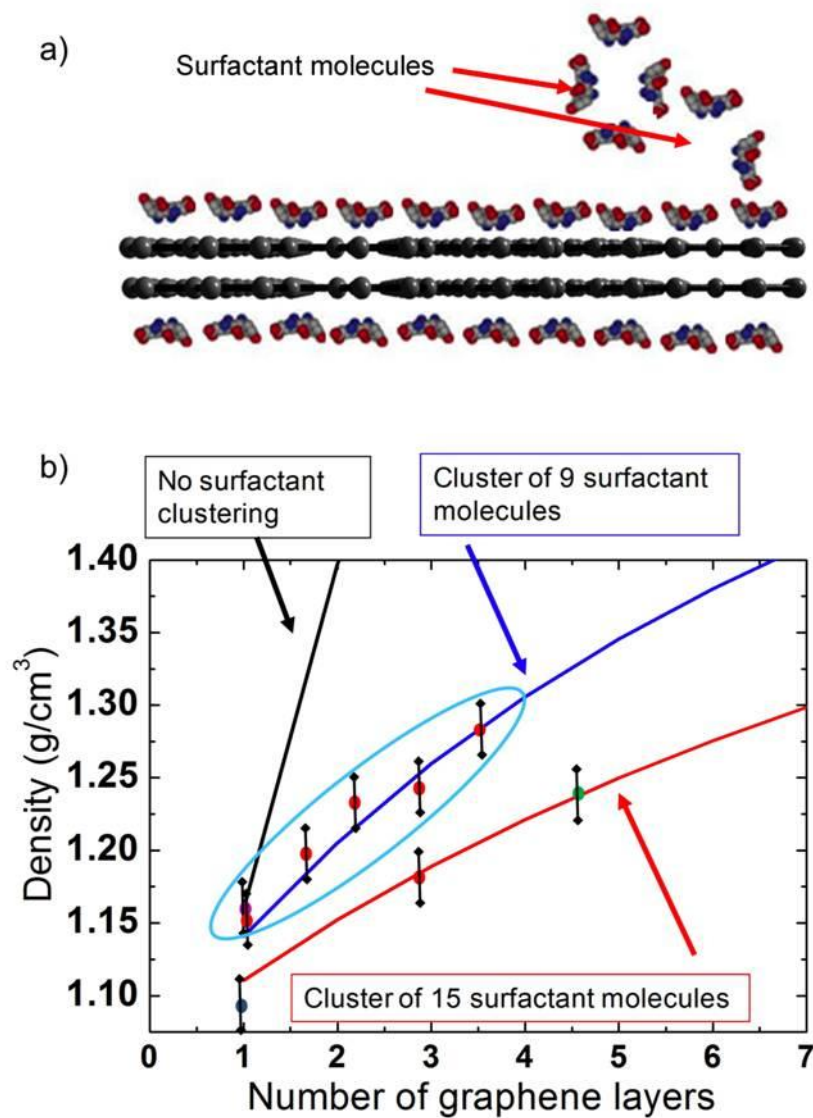
a) Schematic illustrating the ordering of surfactant molecules around a bilayer graphene flake and the formation of clusters. The aggregation properties of the surfactant molecules on the flake surface depend on the surfactant type and concentration b) Fit of the geometrical density model to the experimental data for different surfactants, showing how the aggregation properties of surfactant molecules adsorbed on the graphite flakes determine their buoyant density, influencing the sorting by number of layers. The cases of Sodium Cholate, SC (blue curve,) and Sodium Deoxycholate, SDC (red curve), are compared with the expected trend for no cluster formation (black curve). The experimental data for SC are taken from [8]. Large SDC aggregates tend to reduce the buoyant density of the graphene/surfactant complex, permitting the separation of flakes with a higher number of layers with respect to SC.

Roll to roll processable graphene-nanotube based hybrid transparent conductors for electrically switchable, flexible optical shutters

T. Hasan, A. Dyadyusha, Z. Sun, G. Privitera, F. Torrisi, T. Kulmala, W. Wu, F. Bonaccorso, O. Trushkevych, D. P. Chu, A. C. Ferrari

[1] Department of Engineering, University of Cambridge, Cambridge CB3 0FA, UK

th270@cam.ac.uk

Development of flexible, interactive electronic displays and devices has long been hindered due to the brittleness, processing limitations and fabrication costs of transparent conductive metal oxides like Indium Tin Oxide (ITO). Both Single Wall Carbon Nanotubes (SWNTs) and graphene offer ideal alternatives as flexible transparent conductors (FTC)[1]. A solution processable hybrid SWNT-graphene conducting film can be integrated into roll to roll manufacturing of devices requiring FTCs.

Polymer dispersed liquid crystal (PDLC) devices employ liquid crystal (LC) microdroplets embedded in a host polymer matrix, sandwiched between two transparent conducting electrodes[2]. In the absence of an external electric field, the LC director distribution (the average direction of the long molecular axis for uniaxial LC molecules) inside the LC microdroplets causes a refractive index mismatch between the LC and polymer matrix, resulting in strong forward scattering with a milky white or 'frosted' appearance and very low optical transmittance. Application of an electric field across the host polymer matrix embedding the LC microdroplets using the FTCs aligns the LC director distribution parallel to the field, making the device transparent. Figure 1(a) shows a schematic of flexible PDLC using SWNT-graphene FTCs.

Here, we demonstrate an up-scalable SWNT-graphene hybrid FTC for a PDLC based smart window. We employ wire-wound rod coating for the aqueous dispersions of SWNTs and graphene on a 125μm thick polyethylene terephthalate (PET) substrate. First, the SWNT dispersions are ultrasonicated and centrifuged to remove residual bundles. Graphene flakes are then exfoliated in water by mild sonication with sodium deoxycholate (SDC), also centrifuged to remove un-exfoliated flakes. The centrifuged dispersions are then characterized using optical absorption spectroscopy (OAS), Raman spectroscopy and Transmission Electron Microscopy (TEM). OAS shows a SWNT and graphene concentration of 0.4 and 0.2 gL^{-1}, respectively. TEM reveals the presence of ~65% mono and bi-layer in the graphene flakes of 300-600nm dimensions. Raman spectroscopy also confirm the presence of pristine graphene flakes without structural defects. Rod coating accompanied by washing in an alcohol-water mixture results in an optically homogeneous FTC. The SWNT-graphene coating itself has 94-97% transparency across the entire visible spectrum with <2% standard deviation in transmittance across a ~200cm^2 FTC sample. The FTC has ~1kΩ/□ sheet resistance with a standard deviation of ~80Ω/□. The FTCs exhibit ~15% change in resistance when bent to a radius of ~3.5mm in 10 cycles, far surpassing the ~25000% increase in a 60 Ω/□ ITO sample on 125μm PET (Sheldahl, Accentia 430300 ITO Coated Films).

A ~120cm^2 smart window is then fabricated by laminating a YM55 nematic LC and Norland Optical Adhesive 65 as the polymer host between two FTCs. The fabricated smart window exhibits excellent electric field induced light transmittance (~60%) under applied electric field (Figs. 1(b,c)). When OFF, the device transmits <0.25%, giving a >230 contrast ratio.

References

[1] F. Bonaccorso *et al.*, Nature Photonics 4, 611 (2010)
[2] J.L. Fergason, US Patent 4435047, (1984)
[3] C.M. Lampert, Sol. Energy Mater. Sol. Cells 52, 207 (1998)
[4] T. Hasan *et al.* Submitted (2010)

Figures
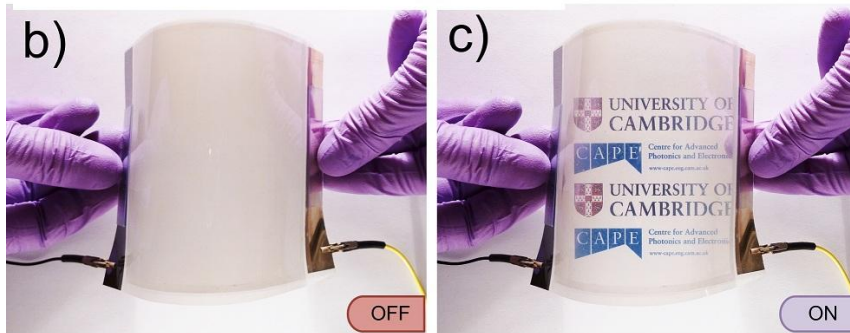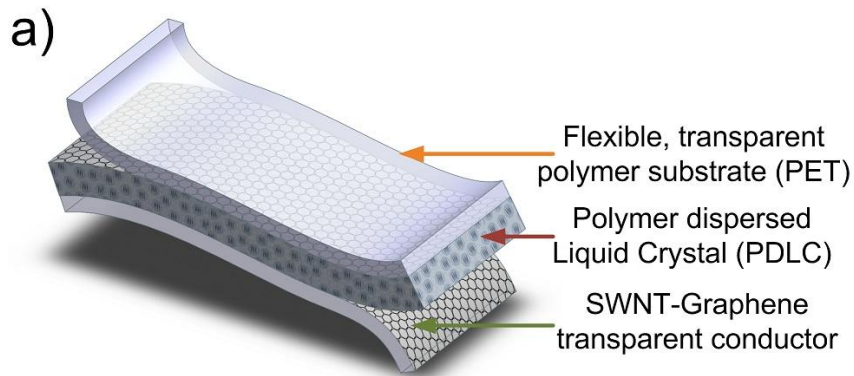
a) Schematic of a flexible smart window with SWNT-graphene based FTC. b) In the absence of an electric field, the LC microdroplets cause strong forward scattering, with complete loss of transparency c) under applied electric field, the director distributions of the LC mocrodroplets align, resulting in a transparent state.

Zigzag-edged interfaces between C and BN nanosheets

Miguel Pruneda

Centro de Investigación en Nanociencia y Nanotecnología (CIN2-CSIC), Campus UAB, Barcelona, Spain
miguel.pruneda@cin2.es

A number of new physical phenomena have been discovered in the last few years at the interfaces between very different materials. The electronic reconstruction induced at these boundaries can give rise to metallic states [1], magnetism [2], or even superconductivity [3], although the parent compounds were originally insulating oxides. But not only boundaries of bulk materials are important: in two dimensional graphene nanoribbons (GNR), edges have become relevant [4]. Here I will present new striking phenomena induced at the 1D interfaces of bidimensional heterostructures made of semimetallic graphene and insulating BN nanosheets that may become experimentally available soon [5]. First-principles density functional calculations of these hybrid C/BN systems show that the magnetic character of the edge states in zigzag shaped GNR and the polar BN edge team up to give a spin asymmetric screening that induces half-semimetallicity at the interface, with a gap of a few tenths of eV for one spin orientation and a tiny gap of hundredths of eV for the other [6]. It will be shown that these effects can also be observed in tubular geometries with zigzag edges between C and BN domains. The role of point defects close to the interface and the vibrational properties of these heterostructures will be discussed.

References

[1] A. Ohtomo and H. Y. Hwang, Nature, **427** (2004) 423.
[2] A. Brinkman, et. al. Nat. Materials, **6** (2007) 493.
[3] N. Reyren, et. al. Science **317** (2007) 1196.
[4] Y.-W. Son, M. L. Cohen, and S. G. Louie, Nature 444 (2006), 347.
[5] L. Ci, et. al. Nat. Materials **9** (2010) 430.
[6] J. M. Pruneda, Phys. Rev. B **81** (2010) 161409.

Figures
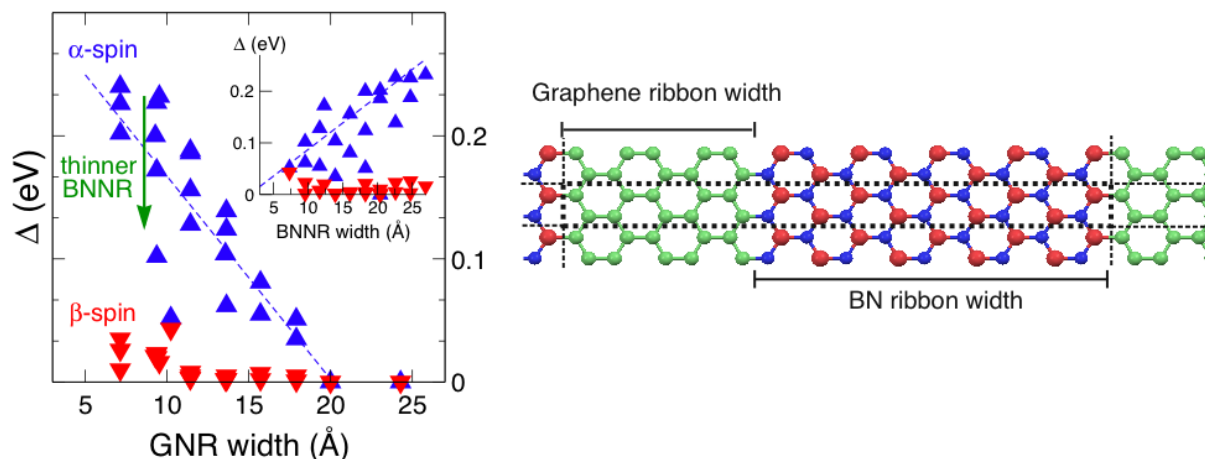
Atomic force microscope nanolithography of graphene: cuts, pseudo cuts and tip current measurements.

R. K. Puddy, P. Scard, D. Tyndall, C.G. Smith, G.A.C. Jones, M.R. Buitelaar
Cavendish Laboratory, University of Cambridge, Cambridge CB3 0HE, United Kingdom

Scanning probe microscopy (SPM), not only a powerful tool for imaging is also an established method for the manipulation and patterning of materials on the nanometre scale[1]. The atomic force microscope (AFM), part of the SPM family, now routinely used as a lithographic tool for Si and GaAs nano-scale device fabrication[2,3], shows significant potential for device fabrication in graphene[4], a material of great current interest due to its exceptional mechanical and electronic properties[5].

AFM lithography (AFML) on graphene, performed under ambient conditions, utilises the dissociation of water molecules, due to a tip induced electric field, and the subsequent oxidation of the graphene substrate to fabricate desired nano-structures. Most commonly electron beam lithography and subsequent plasma etching is used for the fabrication of nano-scale graphene devices[6,7] however AFML offers several advantages over this technique: it has nm scale resolution, can be performed under ambient conditions, eliminates the need for e-beam resists and associated contamination, allows in situ device measurement during lithography and allows further device modifications to be carried out easily and at any time. Many of the key parameters required for successful AFML are not yet well established and device fabrication is not yet routine. In addition there has as yet there not been any systematic study of the tip current during AFML of graphene.

In this work, we investigate in detail the cutting of the graphene lattice with an AFM tip. In particular, we measure the tip current, I_{tip}, during the cutting process. From these measurements we identify two distinct regimes (see Fig 1): finite and zero tip current lithography. We find that we cut graphene only when I_{tip}, drops to zero (within our noise floor) and that pseudo cuts appear when I_{tip}, is non-zero. These pseudo cuts, in which the electron system of graphene remains uninterrupted, cannot be distinguished from real cuts by AFM height imaging but become apparent using transport experiments and scanning electron microscopy (see Fig 2). Our results provide new insight into the oxidation mechanism of graphene and identify the parameter range for true cuts which is crucial for device fabrication.

Finally, we demonstrate device fabrication. Fig.3 (a) & (c) show AFM images of a quantum wire and quantum dot (QD), respectively, formed in a bi-layer flake by AFML. Fig.3 (b) shows conductance *vs* back gate voltage V_{bg} of the quantum wire at 4.2 K. The flexibility of AFML is illustrated by Fig.3 (d) which shows measurements of the QD conductance *vs* V_{bg} at 4.2 K both for the quantum dot as shown in Fig.3 (c) (blue line) as well as that of the same device but with the entrance barriers of the quantum dot narrowed from ~ 150 nm to ~ 50 nm in a subsequent AFML step shown by the blue arrows in Fig.3 (c). As expected the conductance is significantly lower in the post modification device with an increase in the gap observed[8]

In conclusion, we have studied the local oxidation of graphene by an AFM tip. We demonstrate that at low bias voltages the graphene is typically not cut even though clear depressions are observed in AFM height images. Our work demonstrates that a high tip current is not necessary for local oxidation of the graphene lattice. Only when the tip current vanishes is the graphene lattice cut. These conclusions are supported by scanning electron microscopy and transport experiments. The ability to distinguish between pseudo cuts and cuts as demonstrated here is important for graphene device fabrication by AFM nanolithography.

References

[1] A. A. Tseng, A. Notargiacomo, and T. P. Chen, j. Vac. Sci. Technol. **23**, (2005) 877.

[2] E. S. Snow and P. M. Campbell, Appl. Phys. Lett. **64**, (1994) 1932 .

[3] L. P. Rokhinson, D. C. Tsui, L. N. Pfeiffer, and K. W. West, Superlattices and Microstruct. **32,** (2002), 99

[4] A. J. M. Geisbers, U. Zeitler, S. Neubeck, K. S. Novoselov, and J. C. Maan, Solid State Communications, **147**, (2008), 366.

[5] A. K. Geim Science. **324,** (2009), 1530.

[6]C. Stampfer, E. Schurtengerger, F. Molitor, J. Guttinger, T. Ihn, and K. Ensslin, Nano. Lett. **8** (2008) 2378.

[7] L. A. Ponomarenko, *et al*, Science. **320**, (2008) 356.

[8] M. Y. Han, B. Ozyilmaz, Y, Zhang, and P. Kim, Phys. Rev. Lett. **98**, (2007) 206805.

Figures
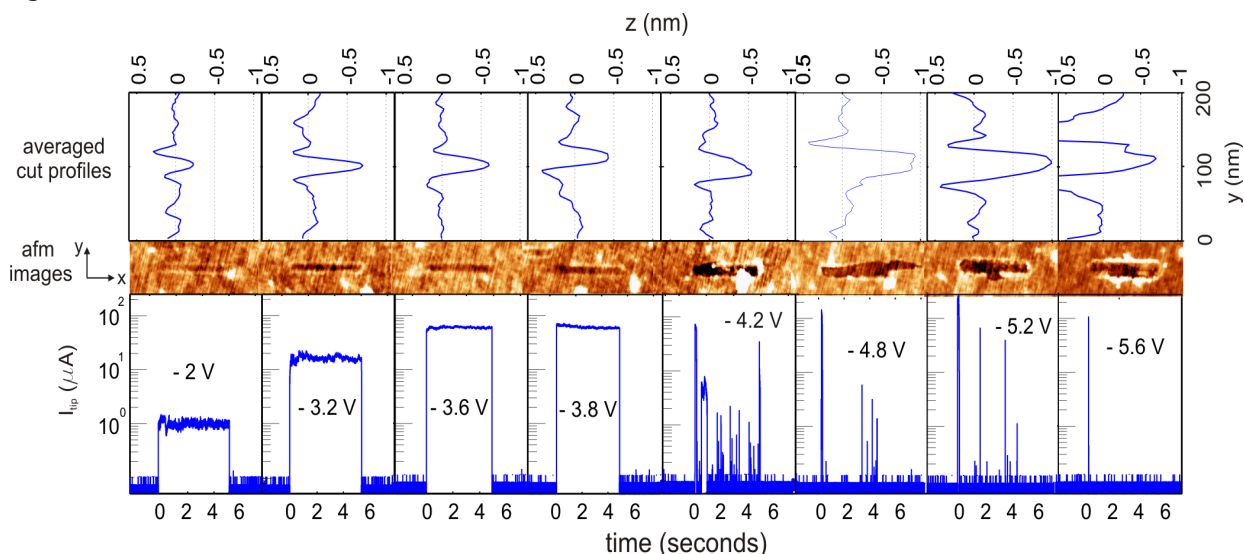
Figure 1. *A series of cuts in a monolayer graphene flake, made using an AFM tip at increasingly negative voltages relative to the grounded flake. Upper panels show averaged height profile cross-sections of the cuts, central panels show the corresponding AFM micrographs and the bottom panels show the current, I_{tip}, through the AFM tip as a function of time t, recorded during the cutting process where t = 0 is the start of tip contact. The series is performed using a single, non coated, doped silicon sensor tip.*
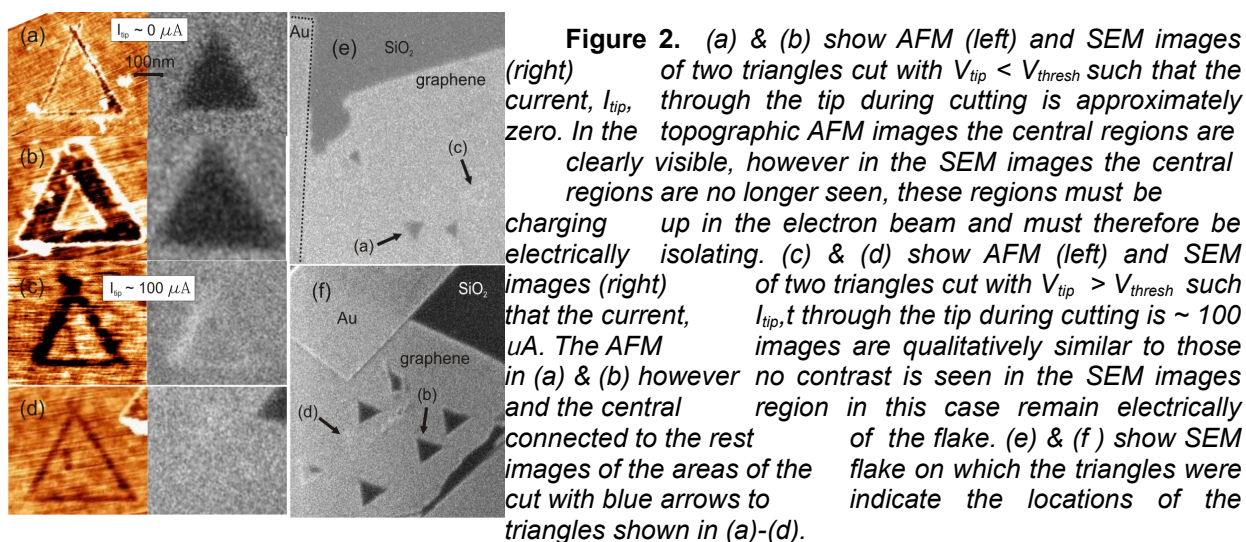
Figure 2. *(a) & (b) show AFM (left) and SEM images (right) of two triangles cut with $V_{tip} < V_{thresh}$ such that the current, I_{tip}, through the tip during cutting is approximately zero. In the topographic AFM images the central regions are clearly visible, however in the SEM images the central regions are no longer seen, these regions must be charging up in the electron beam and must therefore be electrically isolating. (c) & (d) show AFM (left) and SEM images (right) of two triangles cut with $V_{tip} > V_{thresh}$ such that the current, I_{tip},t through the tip during cutting is ~ 100 uA. The AFM images are qualitatively similar to those in (a) & (b) however no contrast is seen in the SEM images and the central region in this case remain electrically connected to the rest of the flake. (e) & (f) show SEM images of the areas of the flake on which the triangles were cut with blue arrows to indicate the locations of the triangles shown in (a)-(d).*
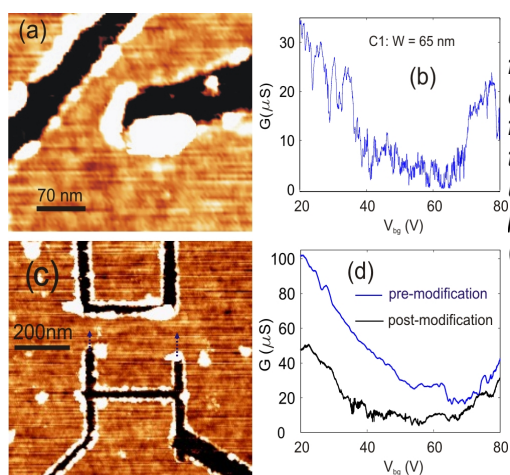
Figure 3. *(a) AFM image of a ~ 65nm constriction formed in a bilayer flake using AFML and (c), its conductance, G, vs V_{bg} at 4.2 K. (c) QD formed in a bilayer flake using AFML, the entrances are initially ~ 150 nm, these are then modified, as indicated by the blue arrows, using AFML to be ~50 nm. (d) G vs V_{bg} at 4.2 K of the dot pre-modification (blue curve) and post-modification (black curve).*

372

On the properties of new graphene nanoplatelet-silicon nitride composities consolidated by spark plasma sintering

C. Ramírez[1] , M.I. Osendi[1], P. Miranzo[1], C. Ocal[2]

[1] Instituto de Cerámica y Vidrio, CSIC, Cantoblanco. 28049 Madrid, Spain.
[2] Institut de Ciència de Materials de Barcelona, CSIC, Campus de la UAB. 08193-Bellaterra, Spain

cristina.ramirez@icv.csic.es

Silicon nitride (Si_3N_4) based materials are ceramics with a high potential for many applications owing to their interesting properties, such as the high hardness, the high temperature strengths, the good behavior under wearing conditions and the extraordinary toughness that can attain if convenient microstructures are developed [1]. Si_3N_4 is an electrical insulating material and regarding its thermal conductivity, a quite range of values can be achieved, again depending on the microstructure and the phases present in the material (α/β phase ratio) [2]. It would be valuable to explore how these properties may be altered by the addition of the new graphene nanostructures presently available in relatively large amounts. In this work we deal with the challenging preparation of silicon nitride – graphene nanoplatelets (GNPs) composites, taken special care in achieving dense materials with homogeneously dispersed GNPs. This was not an easy task and in fact some degree of platelets agglomeration was unavoidable.

To prepare the dense Si_3N_4-GNPs composites the spark plasma sintering (SPS) technique, in short a pressure assisted sintering furnace in which the heating is provided by a pulsed direct current supplied to the graphite die that contains the powdered mixture, was used because allows very high heating rates ($\sim$100 °C/min) and very short residence times at high temperatures. Composites with a range of GNP concentrations were equally processed (3-15 wt%). The preferential orientation of the platelets (less than 60 nm thickness, Fig 1 a-b) with the a-b graphene plane perpendicular to the sintering axis was favored by the applied pressure, generating certain degree of anisotropy in the properties of the composite.

Raman spectroscopy, used to control damage of the GNPs, allowed the observation of orientation by D peak integration and made possible the identification of few layer graphene stacks in the composites. Local electrical response was investigated by conducting scanning force microscopy showing differences in conductivity between the plane and cross section surfaces of the composites, signaling further the GNP orientation effect. Preliminary thermal conductivity studies also evidenced the role of the GNPs in this property and the orientation effect.

Mechanical properties of these composites has been determined by Vickers indentation tests, In general a decrease in hardness, elastic modulus and toughness was verified, but data need to be interpreted with precaution as residual stresses in the specimens were quite large as the spall off often revealed.
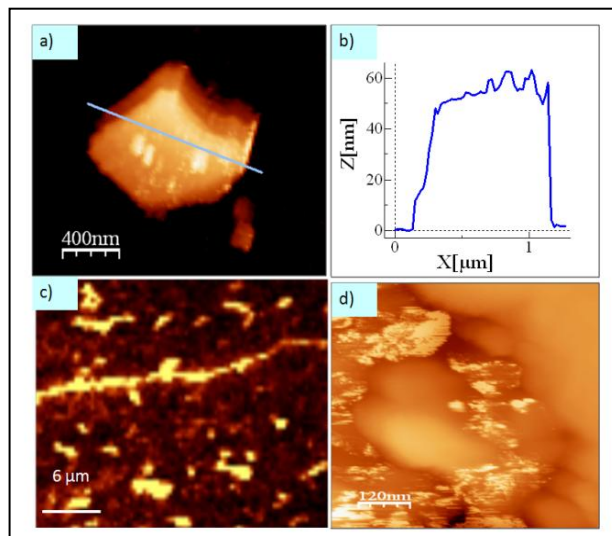
Figure 1.
a) Topography of graphene nanoplatelet and b) correspondent height profile, c) Confocal Raman image scan of a GNP-Si$_3$N$_4$ composite cross section showing platelet edges in bright color, d) Merged images of current map and topography of a Si3N4 grain surrounded by GNPs.

References

[1] I. W. Chen; A. Rosenflanz, Nature 389 (1997) 701.

[2] A. Pablos, M. I. Osendi, P.Miranzo, J. Amer. Ceram. Soc. 85 (2002) 200.

Gate Tuning of Optical Fabry-Perot Cavities with Suspended Multilayer Graphene Mirrors

Antoine Reserbat-Plantey, Laëtitia Marty, Nedjma Bendiab and Vincent Bouchiat

Institut Néel, CNRS-UJF-INP, BP 166, 38042 Grenoble cedex 9, France
antoine.reserbat-plantey@grenoble.cnrs.fr

Graphene based membranes provide ideal materials to implement semi transparent mirrors that can be electrostatically actuated [1, 2] and which motion can be optically detected [1]. We fabricate micron-scaled optical cavities composed of a multi-layer (MLG) graphene cantilevers free-standing over an oxidized silicon wafer. Reflectometry and Micro-Raman characterization is performed by scanning a laser probe over the cantilever. Thickness variations within the MLG/Silica gap induce equal spacing interference fringes in both the reflected and Raman scattered waves. Spatial variations within interference patterns allow to spatially split all Raman modes emitted by both MLG and Silicon substrate. The cavity finesse of the resulting Fabry-Pérot-like interferometer can reach about 6 and is in agreement with simulation involving graphite based semi-reflecting membrane of similar geometry. The MLG membrane is connected to a gold gate electrode that allow to apply an electric field within the cavity and tune the cavity thickness with nanometer precision. Intensity of the reflected light and Raman lines exhibit quadratic dependence upon the applied gate voltage while G and 2D Raman modes show a softening in frequency as well. We discuss the use of such devices for implementing devices that allow the measurement of Casimir force.

References

[1] J. Bunch, A. van der Zande, S. Verbridge, I. Frank, D. Tanenbaum, J. Parpia, H. Craighead, and P. McEuen. Electromechanical resonators from graphene sheets. Science, **15** (5811), 490, 2007.

[2] C. Chen, S. Rosenblatt, K. Bolotin, W. Kalb, P. Kim, I; Kymissis, H. Stormer, T. Heinz, and J. Hone. Performance of monolayer graphene nanomechanical resonators with electrical readout. Nature Nanotech, **4** (12) :861–867, 2009.

Figures
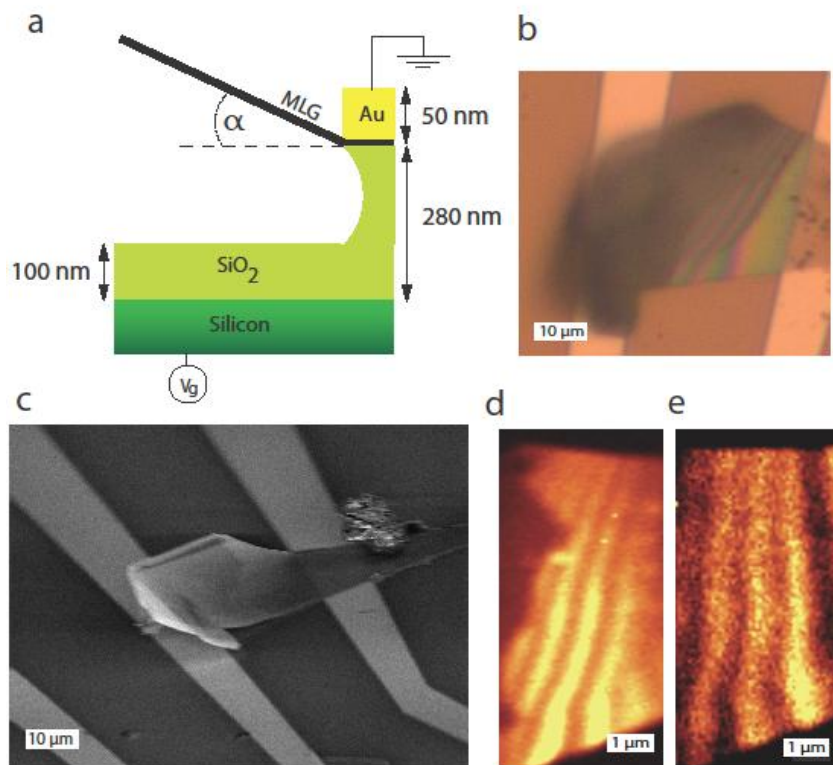
Figure 1 : (a) : Schematics cross-section of a MLG optical cavity showing the air-wedge obtained by partial underetch of silica. (b) : Optical micrograph acquired under white light irradiation of sample A showing iridescence effects. The left part of the flake sticks-up and thus show some blur due to off-focus. (c) : SEM micrograph of sample A. (d) : Raman map of MLG G mode intensity. (e) : Raman map of MLG 2D mode intensity
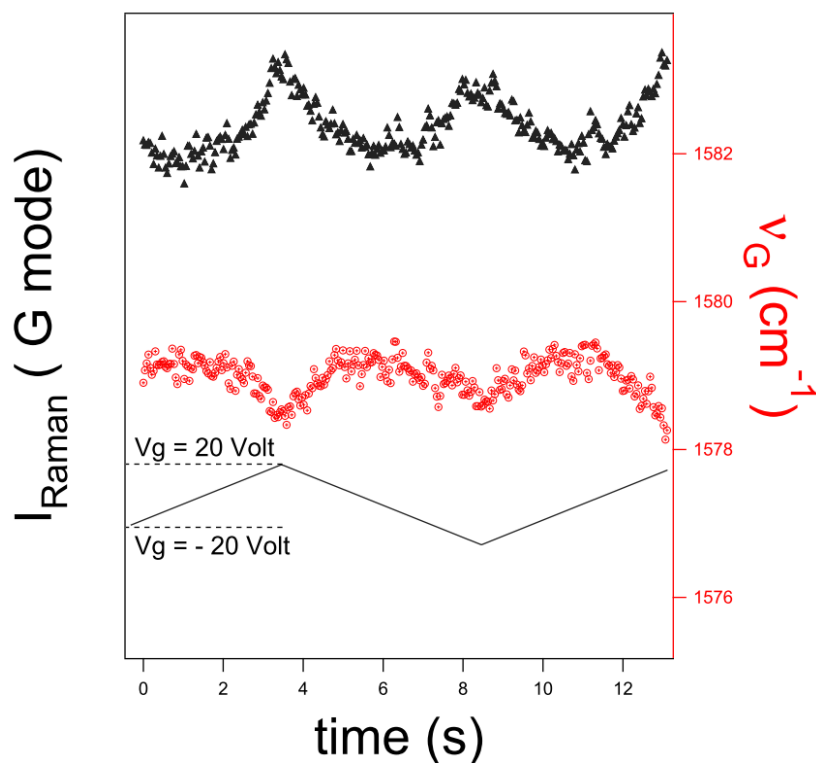
Figure 2 : dark triangles: Raman Intensity (left axis: arbitrary units) of E_{2G} phonon mode (G band) as a function of time. Red circles: E_{2G} phonon frequency (right axis: cm^{-1}) as a function of time. Plain dark line: Gate voltage applied as a function of time, triangular signal centered at zero.

Unveiling the Landau Levels Structure of Graphene Nanoribbons

R.L. Ribeiro[1], J.M. Poumirol[1], A. Cresti[2], W. Escoffier[1], J.M. Broto[1], S. Roche[3,4] and B. Raquet[1]

[1]Laboratoire National des Champs Magnétiques Intenses, INSA UPS CNRS,
UPR 3228, Université de Toulouse, 143 av. de Rangueil, 31400 Toulouse, France
[2]IMEP-LAHC, Grenoble-INP, Minatec 3 Parvis Louis Néel, BP 257 38016 Grenoble, France
[3]CIN2 (ICN-CSIC) and Universitat Autonoma de Barcelona, Catalan Institute of Nanotechnology,
Campus de la UAB, 08193 Bellaterra (Barcelona), Spain and
[4] ICREA, Institucio Catalana de Recerca i Estudis Avançats, 08010 Barcelona, Spain
rebeca.ribeiro@lncmi.cnrs.fr

In the present work we show the first experimental evidence of Hall quantization in graphene nanoribbons along with the impact of the 1-D confinement of Dirac fermions.

Carbon-based nanoelectronics is, in the actuality, one of the most promising subjects of nanotechnology. The challenging task for technologists is the achievement of clean devices with an engineered energy gap. The lateral confinement in graphene nanoribbons leads to a series of 1-D electronic sub-bands with a confinement gap. In presence of a large enough magnetic field, the band structure evolves to magneto-electric sub-bands and graphene-like Landau levels are expected to develop. The presence of these Landau levels makes itself evident with the appearance of Shubnikov-deHaas (SdH) oscillations and conductance quantization plateaus.

Up to now, Hall quantization in graphene nanoribbons (GNRs) remains puzzling since no experimental evidence has been found for widths smaller than 200 nm [1-4]. The absence of Hall quantization in GNRs has been attributed to disorder, which is suspected to crosslink the chiral edge currents and impede the conductance quantization.

Lithographically patterned GNRs of 100 and 70 nm widths are made using oxygen plasma etching and a PMMA etching mask. These GNR present a high conductance, a high field effect mobility and a weakly diffusive transport regime with presence of Fabry-Perot oscillations at low temperature. Magneto-resistance (MR) measurements show the first experimental evidence of Hall quantization in GNRs (Fig. 1) for filling factors v = 2 and 6. On the other hand, anomalies in the magneto-transport measurements are evidenced:

(i) At high electrostatic doping level SdH oscillations show a clear departure from the regular linear behaviour of the Landau index as a function of 1/B (Fig. 1(a) inset). This is a direct signature of the electronic confinement that starts to overcome the magnetic confinement.

(ii) The maxima of MR for all the ribbons, fingerprint of the Landau levels depopulation [5], present an up-shift of several Tesla compared to the theoretical value [6].

(iii) The narrower ribbons exhibit the expected $6G_0$ conductance maxima for a two-terminal measurement [5] but the $2G_0$ plateau is absent and the depopulation of the N=2 Landau level goes along with an unusual double peak of the resistance (Fig. 1(b)).

To unveil the origin of the singular Landau spectrum we performed numerical simulations of the GNR band structure as a function of the perpendicular magnetic field and self-consistent calculations of the carrier distribution under magnetic field. We directly compared the oscillatory behaviour of the magneto-resistance and the onset of the magneto-electric sub-bands (Fig. 2). The simulations give evidence of magneto-oscillations of the Fermi energy (blue line in Fig. 2) which consistently explains the broadening of the magneto-resistance peaks and their up-shift lo larger magnetic field. The presence of a second peak in the MR spectrum (Fig. 2 (b)) also finds a natural explanation: this is the clear signature of the orbital degeneracy lifting enhanced by the magnetic field and the pinning of the Fermi energy.

References

[1] C. Berger et al. Science, 312 (2006) 1191.
[2] F. Molitor et al. PRB 79 (2009) 075426.
[3] J. B. Oostinga et al. PRB, 81 (2010) 193408.
[4] J. M. Poumirol, et al. PRB, 82 (2010) 041413.
[5] J. R. Williams et al. PRB, 80 (2009) 045408.
[6] N. M. R. Peres et al. PRB, 73 (2006) 241403
[7] R. L. Ribeiro et al. (submitted).
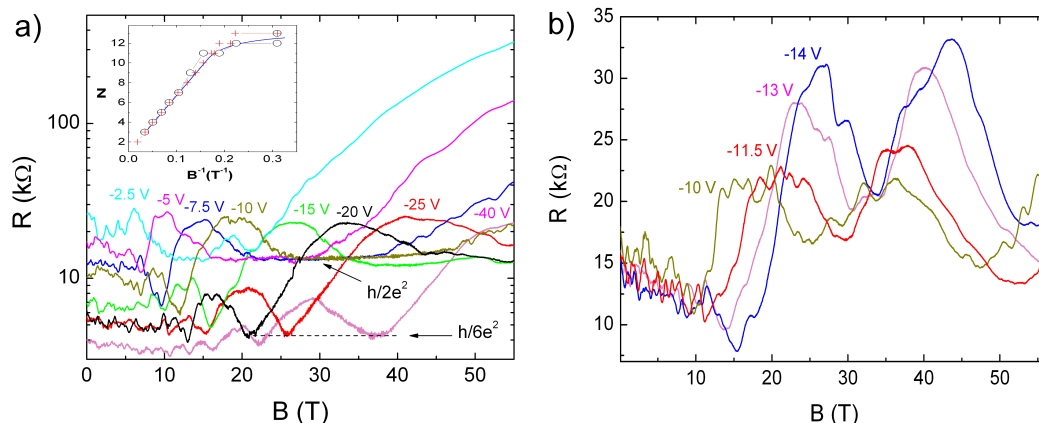
Fig 1. Two terminal magneto-resistance measurements in a) GNR of 100nm width exhibiting the $h/2e^2$ and $h/6e^2$ quantization Hall resistance. Inset: Landau level index as a function of 1/B from: experimental magneto-resistance (circles) at high electrostatic doping, band structure calculations (crosses) and calculations of occupied sub-bands in a hard-wall confinement.
b) Magneto-resistance of a GNR of 70nm width with the presence of a double resistance peak in the crossing of N=2 Landau level.
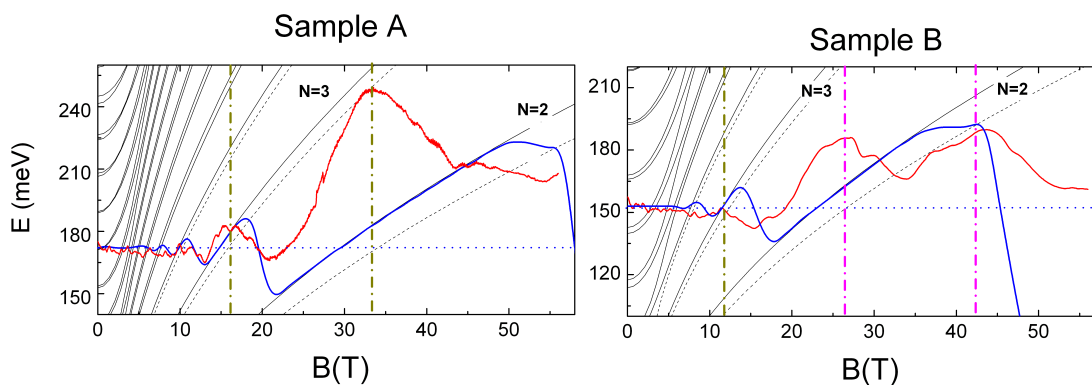
Fig 2. Numerical simulation of the band structure (black lines) in 814-aGNR (100 nm, Sample A) and 571-aGNR (70 nm, Sample B), self-consistent calculations of the Fermi energy under magnetic field (blue curve) and direct comparison with magneto-resistance measurements (red curve).

Catalytic-Free Synthesis of High Mobility Graphene on Sapphire

Mark A. Fanton, **Joshua A. Robinson,** Brian E. Weiland, Michael LaBella, Kathleen Trumbull, Richard Kasarda, Casey Howsare, Matthew Hollander, David W. Snyder

The Pennsylvania State University, University Park, PA, U.S.A
jrobinson@psu.edu

Recent success of graphene transistor operation in the GHz frequency range demonstrates the potential of this material for high speed electronics.[1,2,3] Methods such as spin deposition of reduced graphene oxide,[4] chemical vapor deposition (CVD) on metal substrates,[5,6] plasma assisted deposition,[7] and sublimation of Si from the surface of single crystal SiC semiconductor wafers[8] have all shown potential for large area synthesis routes. Of these techniques, the CVD process is likely the most attractive alternative to the "well established" silicon sublimation from SiC due to the inherent control over process chemistry and the flexibility in choosing precursors. To date, CVD of graphene has been limited to catalytic growth on Ni or Cu at temperatures near 1000°C.[9,10] However, the presence of a metal substrate induces challenges for the production of semiconductor devices. We present a novel CVD process for the growth of high quality monolayer graphene on sapphire *without* the presence of a metal catalyst.

We will discuss catalytic-free synthesis of graphene on standard 50 - 100 mm diameter c-plane sapphire wafers. Graphene films are synthesized via the decomposition of methane (CH_4) in hydrogen (H_2) using an argon (Ar) carrier gas. Growths are performed at 1425°C - 1700°C at pressures of 50 - 600 Torr. Highly uniform growth is achieved via this technique, with variation in sheet resistance across a 50mm wafer of <2% (Figure 1) – comparable to industry standards. Raman spectroscopy confirms the formation of monolayer and bilayer graphene, with improved structural quality as deposition temperature increases. Using the D/G ratio, we find that the domain size increases from an average low of 32 nm at 1425-1450°C (D/G = 0.42) to greater than 270 nm (D/G = 0.05) at 1575°C (Figure 2a and 2b). Additionally, we find that in all cases, the 2D/G ratio is greater than 1.5 with the 2D peak being fit to either one or four Lorentzians, indicating deposition of mono- or bi-layer graphene (Figure 2b and 2c) is achieved. In addition to high structural quality, CVD graphene on sapphire yields strain relieved films with minimal graphene/sapphire interaction, as indicated by a 2D peak position that ranges from 2685 – 2705cm^{-1} (Figure 2d), indicating minimal interaction between the graphene and sapphire. Additionally, according to XPS (Figure 2e), there is no evidence of an interfacial (buffer) layer between graphene and sapphire.

Importantly, we will also present data indicating that catalytic-free synthesis on sapphire produces graphene with superior transport properties compared to graphene on SiC(0001) and comparable to high quality catalytic-CVD graphene. Evident in Figure 4, the carrier mobility dramatically improves from <1000 cm^2/Vs to an average of 3200 cm^2/Vs as the growth temperature is increased to >1500°C. Additionally, we note that water vapor and other environmental conditions can significantly effect the charge carrier concentration and thus mobility. This is evident in Figure 4, where we find a mild anneal at 5x10^{-5} Torr for 3 hrs results in a 1.5x increase in carrier mobility, presumably the result of water desorption from the graphene. Finally, transport properties vary little with magnetic field and temperature (Fig.5).

References

[1]Moon, J.S.; Curtis, D.; Hu, M.; Wong, D.; McGuire, C.; Campbell, P.M.; Jernigan, G.; Tedesco, J.L.; VanMil, B.; Meyers-Ward, R.; Eddy, C.; Gaskill, D.K., *IEEE Elec. Dev. Lett,* **2009**, 30, 650-652.

[2] Lin, Y.M.; Dimitrakopoulos, C.; Jenkins, K.A.; Farmer, D.B.; Chiu, H.Y.; Grill, A.; Avouris, P., *Science* **2010,** 327, 662.

[3] Liao, L.; Bai, J.; Cheng, R.; Lin, Y.; Jiang, S.; Qu, Y.; Huang, Y.; Duan, X., *Nano Lett.,* **2010**, 10, 3952–3956.

[4] Nguyen, S.T.; Ruoff, R.S.; Stankovich, S.; Dikin, D.A.; Piner, R.D.; Kohlhaas, K.A.; Kleinhammes, A.; Yuanyuan, J.; Wu, Y., *Carbon* **2007**, 45, 1558-1565.

[5] Kim, K.S.; Zhao, .Y; Jang, H.; Lee,Y.S.; Kim, J.M.; Kim, K.S.; Ahn, J.H.; Kim, P.; Choi, J.; Hong, B.H., *Nature* **2009**, 457, 706-710.

[6] Xuesong Li; Weiwei Cai; Jinho An; Seyoung Kim; Junghyo Nah; Dongxing Yang; Piner, R.; Velamakanni, A.; Inhwa Jung; Tutuc, E.; Banerjee, S.K.; Colombo, L.; Ruoff, R.S., *Science,* **2009**, 324, 1312-1314.

[7] Malesevic, A.; Vitchev, R.; Schouteden, K.; Volodin, A.; Zhang, L.; Van Tendeloo, G.; Vanhulsel, A.; Van Haesendonck, C., *Nanotechnology*, **2008**, 19, 305604-305610.

[8] Berger, C.; Song, Z.; Li, X.; Wu, X.; Brown, N.; Naud, C.; Mayou, D.; Li, T.; Hass, J.; Marchenkov, A.N.; Conrad, E.H.; First, P.N.; de Heer, W.A., *Science* **2006**, 312, 1191-1196.

[9] Reina, A.; Jia, X.; Ho, J.; Nezich, D.; Son, H.; Bulovic, V.; Dresselhaus, M.S.; Kong, J., *Nano Lett*, **2009**, 9, 30-35.

[10] Li, X.; Cai, W.; An, J.; Kim, S.; Nah, J.; Yang, D.; Piner, R.; Velamakanni, A.; Jung, I.; Tutuc, E.; Banerjee, S.K.; Colombo, L.; Ruoff, R.S., *Science,* **2009**, 1312-1314.

Figures
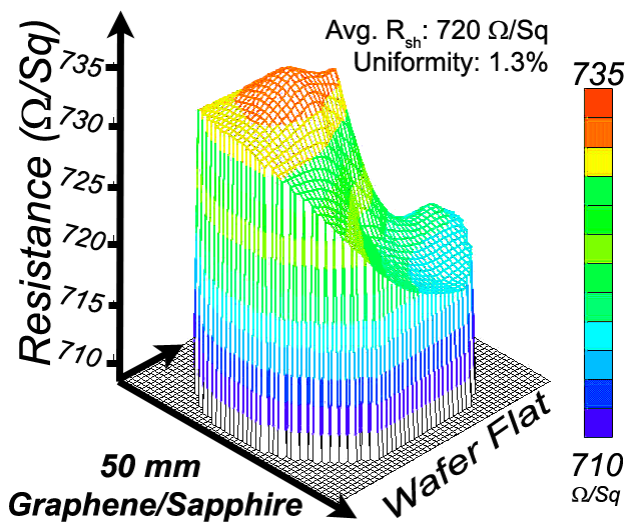
Figure 1: Sheet resistance map of a 50mm wafer of graphene on sapphire demonstrating a high level of uniformity.
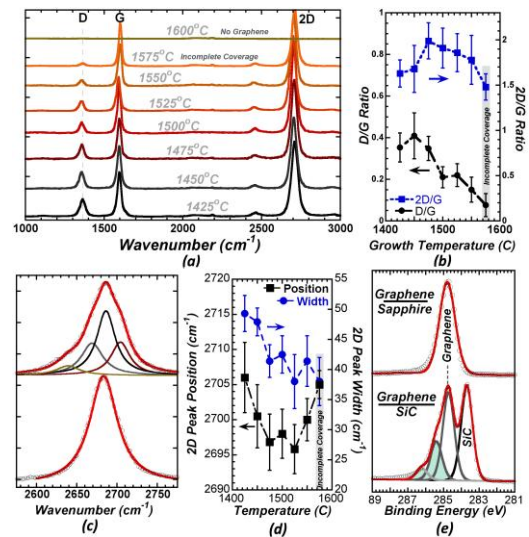
Figure 2: Raman spectroscopy (a-d) of graphene grown on sapphire demonstrating improved structural quality (a,b) with growth temperature, mono and bi-layer graphene (c), and XPS (e) indicating the lack of a buffer layer compared to graphene on SiC.
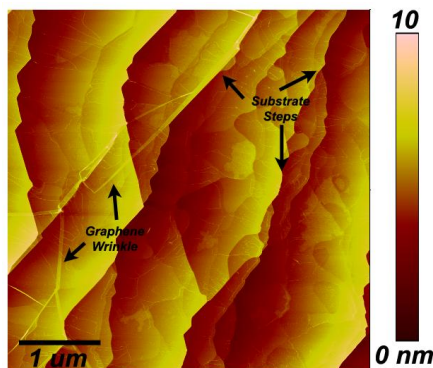
Figure 3: Atomic force micrograph of graphene on sapphire grown at 1500°C. Note the presence of steps in the sapphire substrate and small wrinkles (<1nm high) in the graphene film.
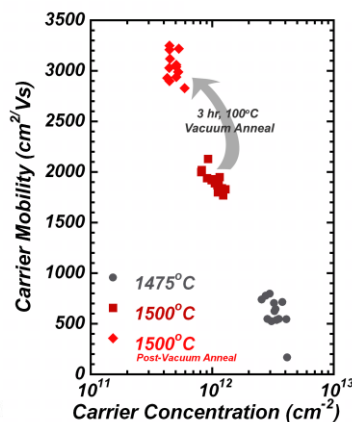
Figure 4: Carrier mobility and concentration of graphene/ sapphire as a function of temperature and measurement conditions.
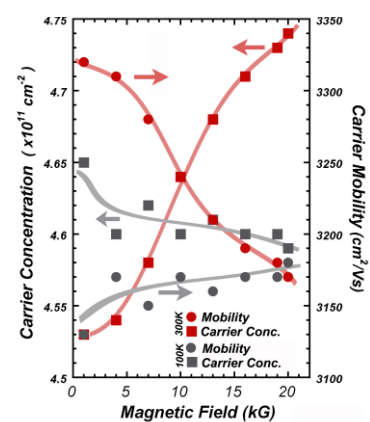
Figure 5: Carrier mobility and concentration of graphene / sapphire grown at 1500°C as a function of magnetic field at 300K and 100K.

In situ electron microscopy observations of graphene growth from metal films

Julio A. Rodríguez-Manzo and Florian Banhart

[1]Institut de Physique et Chimie des Matériaux, UMR 7504 CNRS, Université de Strasbourg, 23 rue du Loess, 67034 Strasbourg, France.
rodriguez@ipcms.u-strasbg.fr

Graphene can be obtained by different methods including mechanical exfoliation of graphite, surface decomposition of silicon carbide, chemical vapor deposition (CVD) of carbon-containing gases on suitable substrates, different chemical methods, or carbon segregation from solid solutions. For methods involving growth on metals, as in CVD and carbon segregation, the underlying principle implies the transformation of carbon from gas or solid solution to graphene. Therefore, in order to fully understand graphene growth we must consider how and under what conditions such transformations occur.

Here we show that single-and few layers graphene can be grown by annealing metal films supported on amorphous carbon films, the latter acting as the carbon source. The process involves the uptake of carbon by the metal films followed by graphene nucleation and growth on the metal surfaces. The process has been carried out in a Transmission Electron Microscope (TEM, JEOL 2100F) allowing for image acquisition with high spatial resolution during the growth process at high temperature [1].

Polycrystalline films with thicknesses and crystallite sizes of ~ 10 nm of Fe, Co or Ni were deposited over 20 nm thick amorphous carbon films in a cathodic sputtering chamber. The specimens where then heated in vacuum inside the TEM (~ 10^{-5} Pa) up to temperatures of 750°C while the induced transformations were observed. As the temperature was raised, ripening of the metal crystals occurred, leaving uncovered areas of the carbon film. Above ~ 600°C, the uncovered carbon film showed domains of single- and few layers graphene, proving that that the amorphous carbon had undergone a transformation to graphene which was catalyzed by the metal. A further increase of temperature led to ongoing ripening of the metal and areas of ~ 0.01-0.02 μm^2 of free-standing graphene were obtained (see figure, top).

During this work a second method to visualize the formation of graphene *in situ* has been developed. We have found (work in preparation) that by electron irradiation of the interfaces between the metal crystals and the amorphous carbon film at high temperature, it is possible to induce the migration of the metal atoms towards the amorphous carbon, and so to induce growth of a metal lamella on the carbon film. The inherent instability of such a thin lamella of ~ 20 nm width and tens of nanometers in length leads to a sudden retraction of the lamella towards the crystal from where it has grown after a certain length has been exceeded or after a further increase in temperature. Again, the uncovered area reveals graphene domains (see figure, bottom).

We put forward an experimental approach based on the solid-state transformation of amorphous carbon to graphene by a catalytically active metal. In addition, we show that it is possible to "pattern" graphene areas of 10-20 nm in width by making use of the interaction between metals and amorphous carbon under an electron beam. The process has been carried out in a Transmission Electron Microscope (TEM) which allows for *in situ* recordings of the complete growth process, involving the transformation of amorphous carbon into graphene via a catalytically active metal.

References

[1] Julio A. Rodríguez-Manzo, Cuong Pham-Huu and Florian Banhart, ACS Nano, (2011), accepted for publication.
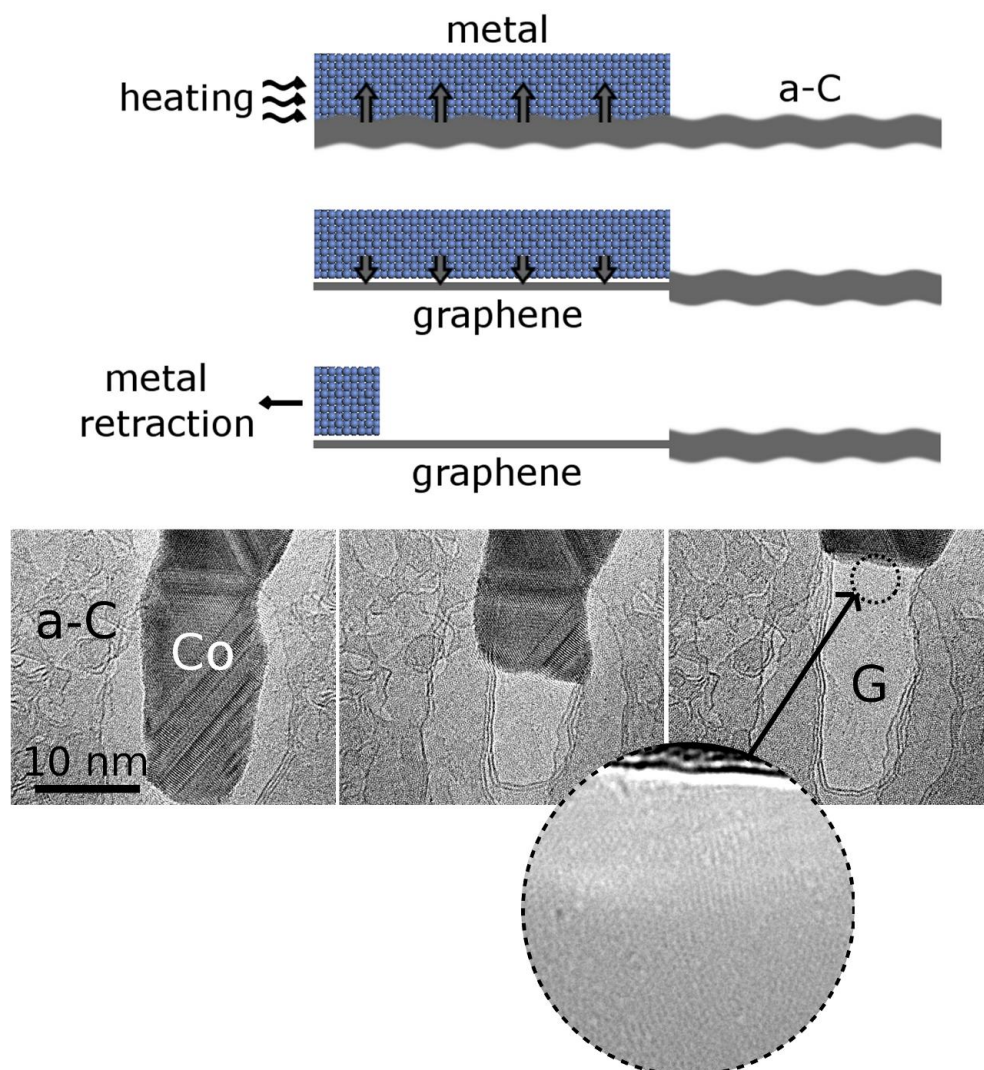
Figure 1: (Top) Scheme of graphene growth from a metal- carbon bilayer system. Carbon uptake in the metal is induced by an increase in temperature. This process is followed by graphene growth at the metal surface originally in contact with the amorphous carbon. Finally, metal retraction driven by ripening uncovers graphene domains. (Bottom, left to right) Top view of metal retraction from a graphene lamella. The inset shows how the amorphous carbon is graphitized next to the metal catalyst. Labels a-C, Co and G stand for amorphous-carbon, cobalt and graphene, respectively.

QUANTUM REVIVALS AND ZITTERBEWEGUNG IN GRAPHENE

ELVIRA ROMERA

Instituto Carlos I de Física Teórica y Computacional,
Universidad de Granada, Fuentenueva s/n, 18071 Granada, Spain.
 eromera@ugr.esl

Revivals of electric current in graphene in the presence of an external magnetic field are described. It is shown that when the electrons are prepared in the form of wave packets assuming a Gaussian population of only positive (or negative) energy Landau levels, the presence of the magnetic field induce revivals of the electron currents, besides the classical cyclotron motion. When the population comprises both positive and negative energy Landau levels, revivals of the electric current manifest simultaneously with zitterbewegung and the classical cyclotron motion. We relate the temporal scales of these three effects and discuss to what extent these results hold for real graphene samples.

Moreover, we study the time-evolution of localized wavepackets in graphene quantum dots under a perpendicular magnetic field, focusing on the quasiclassical and revival periodicities, for different values of the magnetic field intensities in a theoretical framework. We have considered contributions of the two inequivalent points in the Brillouin zone.   The revival time has been found as an observable that shown the break valley degeneracy.

References

[1] . E. Romera and F. de los Santos   Phys. Rev. B **80** 165416, (2009).
[2] J. J. Torres and E. Romera, Phys. Rev B **82**, 155489 (2010).

Adhesion of graphene on muscovite mica: an *ab initio* study

A.N. Rudenko[1], F.J. Keil[1], M.I. Katsnelson[2], and A.I. Lichtenstein[3]

[1]Institute of Chemical Reaction Engineering, Hamburg University of Technology,
Eißendorfer Str. 38, D-21073 Hamburg, Germany
[2]Institute for Molecules and Materials, Radboud University Nijmegen,
Heijendaalseweg 135, 6525 AJ Nijmegen, The Netherlands
[3]Institute of Theoretical Physics, University of Hamburg, Jungiusstraße 9, D-20355 Hamburg, Germany
rudenko@tu-harburg.de

Graphene is at the focus of many research activities worldwide. Its remarkable electronic properties make this material a promising candidate for a large variety of electronic applications. Although graphene is treated as a free-standing sheet, practically it is usually deposited on different substrates owing to the peculiarities of preparation techniques. The role of substrates and their effect on the electronic properties of graphene are actively debated, but are still not clearly understood.

Muscovite mica [$KAl_2(Si_3,Al)O_{10}(OH)_2$] is an appealing substrate for use in graphene-based devices owing to its relative atomic smoothness and good dielectric properties. Experimental studies show that graphene monolayers display an exceedingly flat structure being placed on mica, which is several times smoother than graphene on the most widely used dielectric (SiO_2) [1]. So far, the absence of theoretical investigations of this system was not allowing to establish unambiguously the nature of interfacial interactions between the mica surface and graphene.

In our work, we investigate the adhesion and electronic properties of graphene on a muscovite mica surface using the density functional theory (DFT) with van der Waals interactions taken into account. By assuming an atomic disorder on the mica surface we examine different possibilities for its surface structure: (i) electroneutral surface with uniform distribution of K^+ ions; (ii) electropositive structure with double K^+ coverage; and (iii) electronegative structure in the absence of K^+ ions (see Fig. 1).

We found that irregularities in the local structure of cleaved mica surface provide different mechanisms for the mica-graphene binding. By assuming electroneutrality for both surfaces, the binding is mainly of vdW nature, barely exceeding thermal energy per carbon atom at room temperature. In contrast, if potassium atoms are non uniformly distributed on mica, the different regions of the surface give rise to *n*- or *p*-type doping of graphene. In turn, an additional interaction arises between the surfaces, significantly increasing the adhesion. In Fig. 2 the densities of states (DOS) for all three considered cases are shown displaying the Fermi level shifts in the electropositive and electronegative cases.

A non uniform distribution of potassium atoms over the mica surface also provide a mechanism for variations of graphene height on mica. An estimation of maximum height variation shows an agreement with topographic date of atomic force microscopy (AFM) [1]. The upper limit of experimentally observed height variations corresponds to the calculated variations of the distance between graphene and the different types of mica surfaces (1.5 Å) with probability around 99%. This correspondence between theoretical results and experimental data allows us to conclude that the irregularity of potassium distribution on the substrate plays a major role in the formation of the graphene corrugations on mica.

In addition, it is important that the typical shape of a graphene electronic structure remains unchanged while graphene is deposited on mica (Fig. 2). This makes mica a potential candidate for its use as a substrate for graphene-based electronics, in spite of the fact that induced charge impurities may somewhat restrict the unique transport properties of graphene.

References

[1] C. H. Lui, L. Liu, K. F. Mak, G. W. Flynn, and T. F. Heinz, Nature, **462** (2009) 339.

Figures
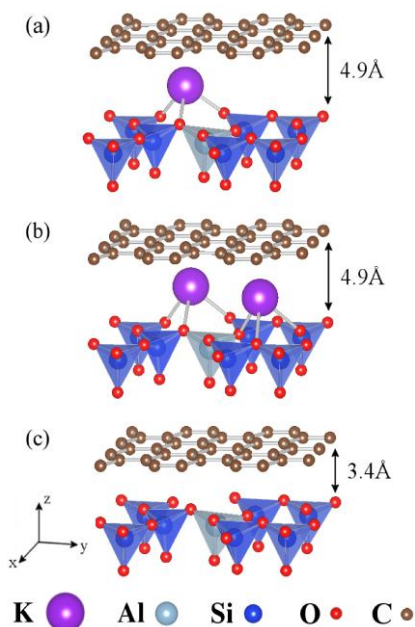
Fig. 1. Equilibrium structure of graphene supported on a (a) neutral mica surface, (b) positive mica surface, and (c) negative mica surface. Only the topmost tetrahedral layer of mica is shown.
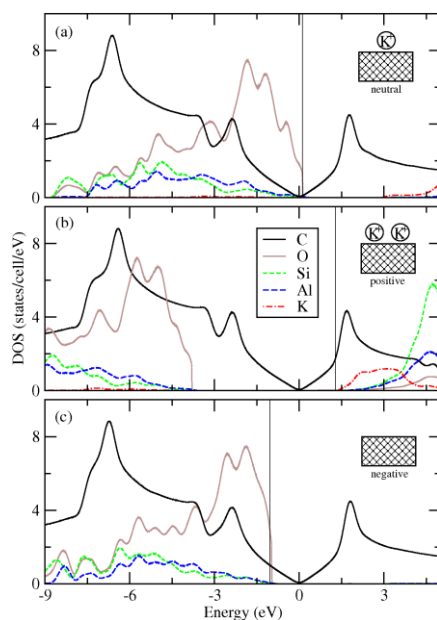
Fig. 2. Projected electronic density of states for graphene deposited on the (a) neutral mica surface, (b) positive mica surface, and (c) negative mica surface. Oxygen DOS is reduced by a factor of 5 for clarity. Zero energy corresponds to the Dirac point of graphene. The vertical line accentuates the Fermi level.

Magnetoconductance of the Corbino disk in graphene

Adam Rycerz[1,2]

[1]*Marian Smoluchowski Institute of Physics, Jagiellonian University,*
Reymonta 4, PL−30059 Kraków, Poland
[2]*Institut für Theoretische Physik, Universität Regensburg,*
D−93040 Regensburg, Germany

Electron transport through the Corbino disk in graphene is studied in the presence of uniform magnetic fields. At the Dirac point, we observe conductance oscillations with the flux piercing the disk area Φ_d, characterized by the period $\Phi_0 = (2h/e)\backslash\ln(R_o/R_i)$, where R_o (R_i) is the outer (inner) disk radius. The oscillations magnitude increase with the radii ratio and exceed 10% of the average conductance for $R_o/R_i \geq 5$ in the case of the normal Corbino setup, or for $R_o/R_i \geq 2.2$ in the case of the Andreev-Corbino setup. At a finite but weak doping, the oscillations still appear in a limited range of $|\Phi_d| \leq \Phi_d^{max}$, away from which the conductance is strongly suppressed. At large dopings and weak fields we identify the crossover to a normal ballistic transport regime.

[1] A. Rycerz, Phys. Rev. B **81**, 121404(R) (2010).

Simulation of hexagonal boron nitride substrates and realistic impurities on

graphene from first-principles

B. Sachs[1]**,** T. Wehling[1], M. Katsnelson[2], A. Lichtenstein[1]

[1] University of Hamburg, I. Institute for Theoretical Physics, Jungiusstr. 9, 20355 Hamburg, Germany
[2] Radboud University of Nijmegen, Institute for Molecules and Materials, Heijendaalseweg 135, 6525 Aj Nijmegen, The Netherlands
bsachs@physnet.uni-hamburg.de

A promising candidate to replace SiO_2 as a standard substrate material in graphene devices is hexagonal boron nitride (h-BN). Compared to graphite, it has a remarkably similar lattice structure (Fig. 1): weakly bound two-dimensional layers of strong sp^2 bonds within an honeycomb arrangement and a lattice constant which differs less than 2% from that of graphene. The electronic structure, however, exhibits clear differences: the chemically inequivalent occupation of the sublattices makes h-BN a wide band gap isolator. Experiments prove highly enhanced electron mobilities in graphene devices with h-BN substrates.

In this work, we present simulations of graphene adhesion on h-BN substrates based on first-principles methods. In detail, we calculate adhesion energies of different stacking configurations within the random phase approximation (RPA) in the framework of adiabatic connection fluctuation-dissipation theory (ACFDT). Comparing the results to local density approximation (LDA) and generalized gradient approximation (GGA) calculations, we show that a description of the weak adhesive forces with methods beyond standard density functional theory (DFT) is required to obtain accurate adhesion energies (Fig. 1). Analyzing the elastic properties of h-BN sheets, we discuss mechanisms leading to stacking disorder.

Another subject of our research is the simulation of realistic impurities on graphene with the focus on atomic and molecular adsorbates. Appearing either as undesired obstacles from the experimental environment or as controlled perturbations, these represent a frequent source of electron scattering. The mechanism delimiting the electron mobility of present graphene samples is still being controversially debated. Resonant impurities as well as charged impurities have been discussed as possible dominant scattering sources. Calculations relevant for both types of scattering will be presented in the following.

One part of this work is dedicated to the theoretical investigation of doping effects in graphene; in particular, monovalent adsorbates are considered. Extensive DFT calculations are presented to derive a theory of doping and charge redistributions in graphene and to identify simple models describing these effects realistically (Fig. 2). We concentrate on two issues: charge transfer as relevant for doping, i.e. changes in the number of mobile carriers, as well as charge transfer as relevant for Coulomb scattering. For hydrogen, fluorine, hydroxyl, chlorine and potassium adsorbates we determine the amount of the charge transfer by means of different electrostatic models and compare to band structure based methods. Furthermore, by means of a tight-binding model, impurities are illustrated to lead to long-range doping of graphene such that even ultra-low concentrations of contamination do affect the carrier concentration. We investigate the effects of long range Coulomb interaction in this context and show

that the Coulomb repulsion plays a minor role in the process of charge redistribution for realistic impurity concentrations.

Finally, we present a first-principles theory of resonant scatterers in graphene and show that a broad range of realistic impurities, such as various organic molecules, can limit electron transport in typical exfoliated graphene samples. In accordance with recent experiments, the conductivity of graphene contaminated with these impurities is obtained from Boltzmann transport theory as well as from a numerically exact Kubo formula approach with first-principles parameters.

References

[1] B. Sachs, T. Wehling, M. Katsnelson, A. Lichtenstein, accepted in Graphene, Theory, Research and Applications (InTech), **Theory of Doping: Monovalent Adsorbates** (2011).

[2] T. Wehling, S. Yuan, A. Lichtenstein, A. Geim, M. Katsnelson, Phys. Rev. Lett. **105, 056802** (2010)

Figures
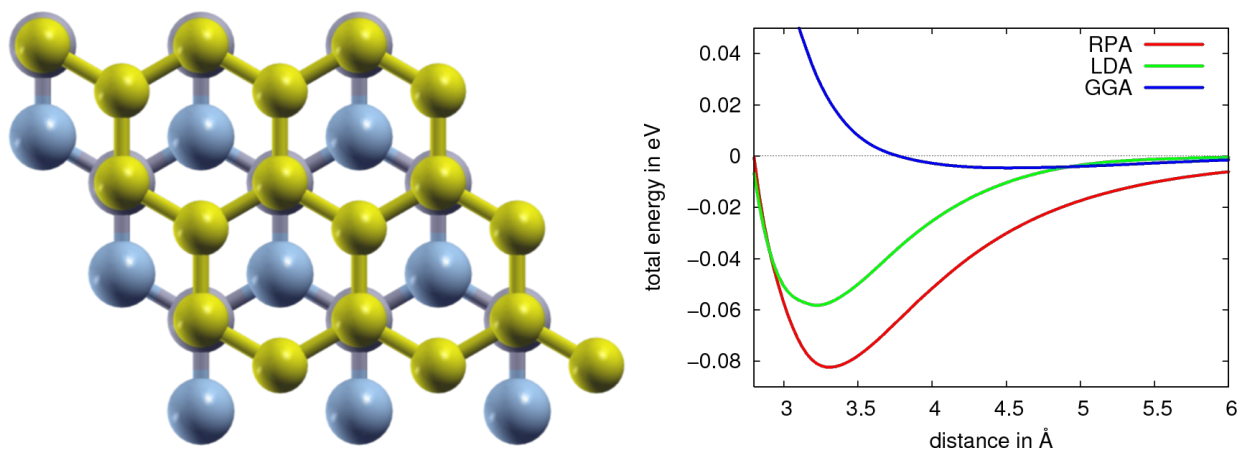
Figure 1. Left: Possible orientation of graphene on h-BN with the carbon atoms (yellow) sitting over the h-BN hollow site and on top of a boron atom (dark blue), while the nitrogen atoms (light blue) are uncovered. Right: Total energy calculations of the pictured stacking within RPA, LDA and GGA as a function of the distance between the graphene and the h-BN sheet.
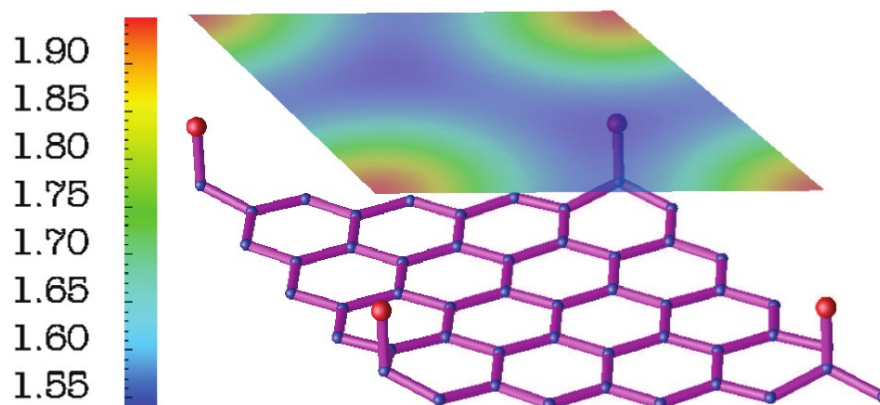
Figure 2. Graphene supercell with fluorine adatoms (red dots). The contour plot shows the electrostatic potential (in eV) in the vacuum at a height of 4.9 Å extracted from DFT simulations.

Click Chemistry Approach for the Covalent Modification of Graphene with Conjugated Poly(fluorene)

Horacio J. Salavagione,[1] Marta Castelaín,[1,2] José Luis Segura,[2] Gerardo Martínez[1]

[1] Dpto. de Física e Ingeniería de Polímeros. Instituto de Ciencia y Tecnología de Polímeros. Juan de la Cierva 3, 28006, Madrid. Spain
[2] Dpto. de Química Orgánica, Facultad de Química, Universidad Complutense de Madrid. Av. Complutense s/n, 28040, Madrid, Spain.
horacio@ictp.csic.es

Conjugated polymeric materials have been extensively investigated due to their potential commercial applications in molecular-scale electronics including light-emitting diodes, electrochromic displays, field-effect transistors, integrated circuits or solar cells [1]. In the last case the active layer of polymeric devices is a donor–acceptor bulk heterojunction composed of a conjugated donor polymer mixed with acceptor molecules or macromolecules [2].

The fascinating properties of Graphene, a one-atom-thick planar sheet of sp^2-bonded carbon atoms in a quasi-2-dimensional (2D) disposition have made it one of the most promising materials of the first decade of the 21st century [3]. Its electronic properties, particularly incredible electron mobility and large specific area render it a competitive alternative as electron-accepting material in photovoltaic device applications.

In order to prepare graphene/conjugated polymers we thought click chemistry to be the ideal tool because of its modular nature, high selectivity, reactivity and reliability. Here we describe the click reaction between alkyne-functionalized graphene (alqG) and Poly[(9,9-dihexylfluorene)-co-alt-(9,9-bis-(6-azidohexyl) fluorene)] (PFA). This is the first study of a broad work schedule planed in order to study the superior properties of graphene-reinforced composite obtained from click coupling between graphene and both conjugated and conventional polymers.

The alqG e was obtained by reduction of GO in alkaline aqueous medium followed by coupling reaction with 4-ethynylaniline at 80º C using isoamyl nitrite. The success of the reaction was confirmed by FTIR, Raman and HNMR spectroscopy. Subsequently, the click reaction was carried out by mixing the alq-G with the PFA using CuBr and PMDETA as catalytic system (Figure 1). The product was named PFA-click-alqG. The success of the click reaction was supported by FTIR, where the band around 2090 cm^{-1}, assigned to the azide group, markedly diminishes. The band did not completely disappear probably because the concentration of alkynes immobilized in graphene sheets is lower than that content of azide in the PFA. More studies are being undertaken in order to obtain the optimal reaction conditions.

Interesting results were obtained when the absorption/emission spectra were collected in a range of solvents with different polarities. For instance, in o-dichlorobenzene (o-DCB) the UV-visible and fluorescence spectra of the PFA-click-alqG resemble that obtained for the pure PFA suggesting no effect of the graphene on the electronic behaviour of the polymer. However, in a more polar solvent, dimethylformamide (DMF), the maximum absorption band blue shifted around 50 nm and the emission spectra of the polymer retained only a 10% of the original photoluminescence. This quenching may be originated by resonance energy transfer from the excited state of PFA to graphene.

The above results indicate that the PFA-click-alqG adopt different structures (with some degree of ordering) depending on the surrounding environment. In the first case, o-DCB it is a good solvent for graphene, keeping it away from the PFA chains; while in DMF, a poor solvent for graphene, graphene is folded polymer favouring the energy transfer and quenching.

These are preliminary results and more experiments are being conducted to confirm the above hypothesis.

References

[1] Handbook of Conducting Polymers, T.A. Skotheim, J. R. Reynolds, Eds.; CRC Press: Boca Raton, Florida (2007).

[2] (a) J. H. Burroughes, D. D. C. Bradley, A. R. Brown, R. N. Marks, K. Mackay, R. H. Friend, P. L. Burn and A. B. Holmes, Nature, **347** (1990) 539; (b) P. Schottland, K. Zong, C. L. Gaupp, B. C. Thompson, C. A. Thomas, I. Giurgiu, R. Hickman, K. A. Abboud and J. R. Reynolds, Macromolecules, **33** (2000) 7051.

[3] A. K. Geim, K. S. Novoselov, Nature Mater. **6** (2007)183

[4] Z. Liu, Q. Liu, Y. Huang, Y. Ma, S. Yin, X. Zhang, W. Sun, Y.Chen, Adv. Mater. **20** (2008) 3924

Figures
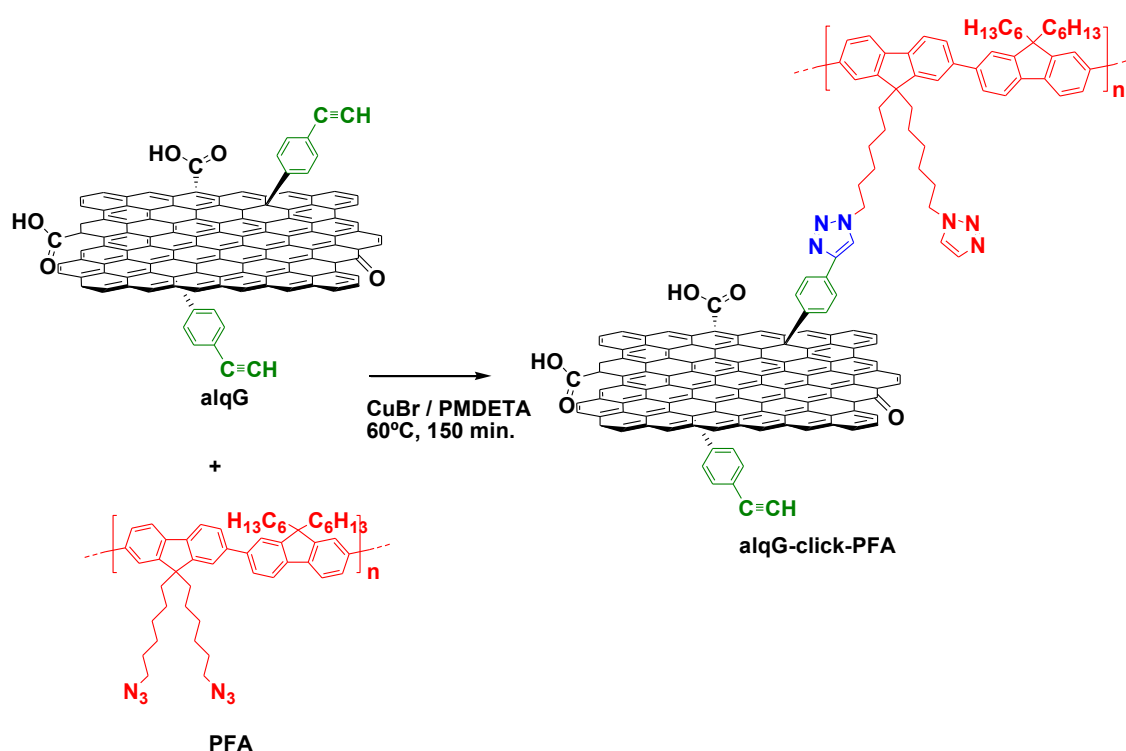
Figure 1. Draw representing the click coupling of graphene with PFA.

Quantum Hall Effect in trilayer graphene

E. Diez[1,*], C. Cobaleda[1], F. Rossella[2], V. Bellani[2], D. K. Maude[3]

[1]Laboratorio de Bajas Temperaturas, Universidad de Salamanca, E-37008, Salamanca, Spain.
[2]Dipartimento di Fisica "A. Volta", Università degli Studi di Pavia, I-27040 Pavia, Italy
[3]Laboratoire National de Champs Magnetiques Intenses, Grenoble, France
*enrisa@usal.es

We have carried out magnetotransport experiments in a trilayer graphene sample processed with Hall bar geometry. We have studied the temperature dependence of the Hall and longitudinal resistance in the temperature range 2-190 K and using as a driving parameter the magnetic field up to 22 T. We have observed the presence of the $\nu=6$ quantum hall (QH) plateau in our sample. To our knowledge this is the first report of a QH plateau in non-suspended trilayer graphene. This result is in agreement with the expected series for the QH plateaus in trilayer graphene: $\nu=\pm6,\pm10,...$ (see Refs. [1] and [2] and references therein).

We have also studied the symmetries of the four-terminal resistance configuration in the QH regime. We found an additional symmetry, $R_L^t(B)= R_L^b(-B)$ where the upper index denote the "top" and "bottom" pair of contacts as showed in Fig. 1. This symmetry does not emerge from a straight-forward application of the Büttiker multiprobe formula. It has been previously reported for mesoscopic samples prepared from InGaAs/InAlAs quantum wells [3] and it has been attributed [4] as a result of an interplay between chiral edge currents and the tunneling between the "top" and "bottom" edges of the Hall bar. We think our results could be of some interest to elucidate the role played by edge currents in the high-B regime in trilayer graphene.

References

[1] F. Guinea, A.H. Castro Neto, N.M.R. Peres, Phys. Rev. B **73,** (2007).
[2] M. Ezawa, Physica E **40**, 269 (2007).
[3] E. Peled, Y. Chen, E. Diez, D. C. Tsui, D. Shahar, D. L. Sivco, and A. Y. Cho, Phys. Rev. B **69,** 241305 (2004)
[4] C. Zhou and M. Berciu**,** Europhys. Lett., **69,** 602 (2005)

Figures

Figure 1: Geometry and contact labels for our trilayer graphene Hall bar.
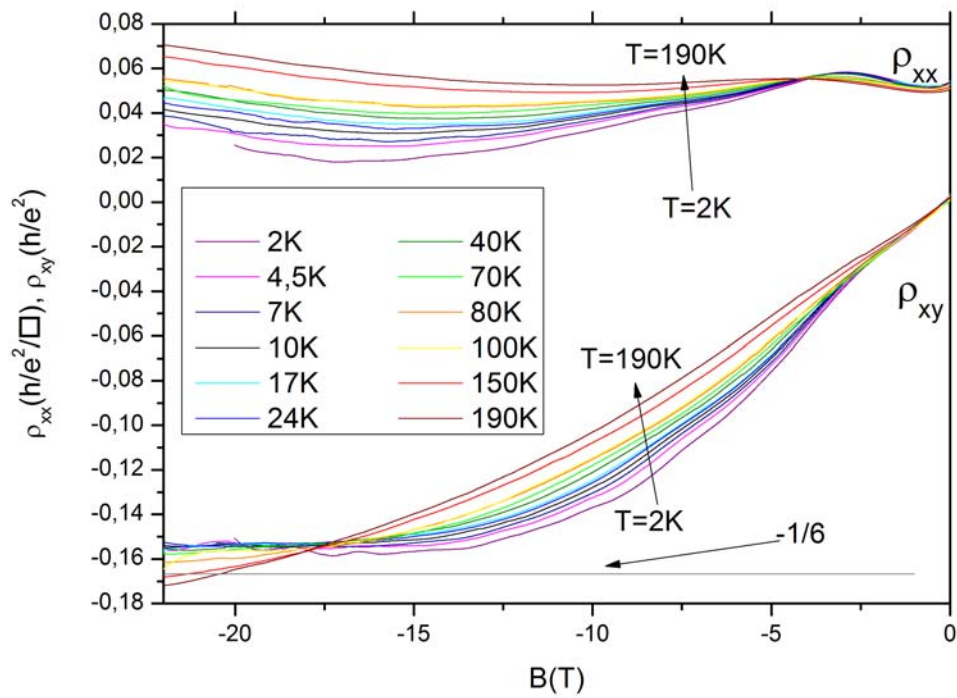
Figure 2: Longitudinal (ρ_{xx}) and Hall (ρ_{xy}) resistivities as a function of the magnetic field at temperatures from 2 K to 190 K.

Microelectronic devices in graphene

C. Cobaleda, E. Díez, M. Amado, V.Bellani, F. Rossella, D. López-Romero

Universidad de Salamanca, Dpto. Física Fundamental, Pza de la Merced S/N E-37008, Salamanca, Spain
ccobaleda@usal.es

Graphene is the thinnest electronic material, merely one atom thick, with very high carrier mobilities, and therefore it should enable transistors operating at very high frequencies. Here, we have explored several routes to graphene-based electronics.

We mainly used monolayer, bilayer and tri-layer graphene flakes obtained by peeling graphite onto a Si wafer with a 300 nm SiO2 top layer. We have processed several devices by using mainly e-beam nanolithography including Hall bars, FET and SET transistors and Quantum Rings.

To characterize the graphene quality we used micro-Raman and AFM studies previous to device processing. We first characterize our devices with quantum Hall effect (QHE) measurements to obtain density and mobilities as a function of the back gate.
We measured the concetration of carriers for different voltages and extract a rule for each device.
We made several tests to check the quality of our sample. The integer QHE appears both by varying the gate voltage and the magnetic field.

References

[1] J. Caridad, F. Rossella,V. Bellani, M. Grandi, and E. Diez, Journal of Raman Spectroscopy (*in press*)
[2] C. Faugeras, M. Amado et al. Phys. Rev. Lett. 103, 186803 (2009)
[3] M. Amado, E. Diez et al., New Journal of Physics **12,** 053004 (2010)

Figures
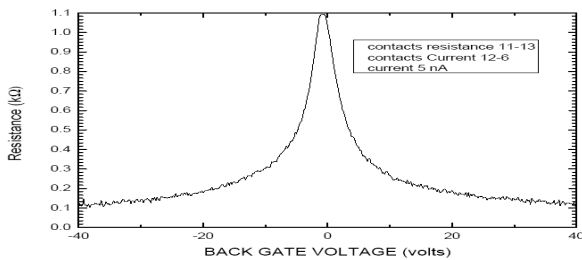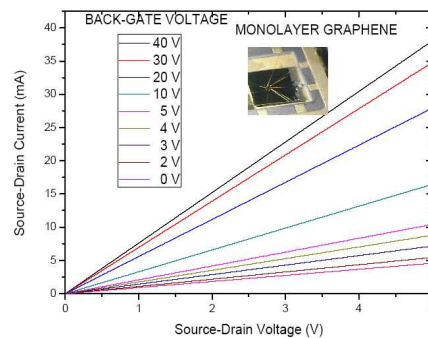
a)   *b)*

Figure 1: a)   The back gate allow us to change the carriers nature from hole (p) to electrons (n) changing the carrier density in several orders of magnitude. b) The output characteristics tuning the current with the back-gate contact. The back gate covers the whole device but this effect could be used in a more useful way creating top nano-gates allowing RF transistor working at very high frequencies
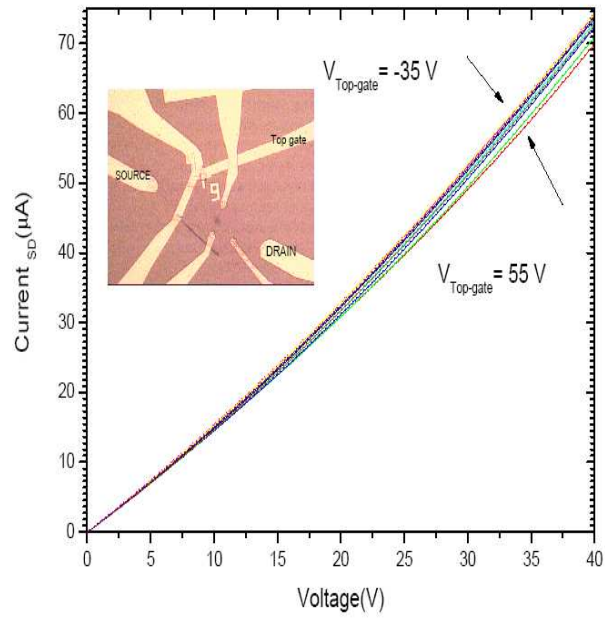
Figure 2: Output characteristics the transistor by applying different top gate voltages.

Magnetism of Graphene with Defects: Vacancies, Substitutional Metals and Covalent Functionalization

Elton J. G. Santos[1,2], S. Riikonen[3], D. Sánchez-Portal[1,2] and A. Ayuela[1,2]

[1]Donostia International Physics Center, Paseo Manuel de Lardizabal 4, 20018, San Sebastian, Spain.
[2]Centro de Física de Materiales CSIC-UPV/EHU, Paseo Manuel de Lardizabal 5, 20018, San Sebastian, Spain.
[3]Laboratory of Physical Chemistry, Department of Chemistry, University of Helsinki, P.O. Box 55, FI-00014, Finland.
eltonjose_gomes@ehu.es

Magnetic properties of graphenic nanostructures, relevant for future spintronics applications, depend crucially on doping and on the presence of defects. Here we present a theoretical study using density functional calculations of the structural, electronic and magnetic properties of defects such as: substitutional doping with transition metals[1, 2, 3], vacancies [6, 7], chemical functionalization with organic and inorganic molecules[4, 5], light atoms[4], and polymers[4]. We have found that such defects can be used to create and control magnetism in graphene-based materials. Our main results can be summarized as follows:

(i) Substitutional metallic impurities can be fully understood using a model based on the hybridization between the states of the metal atom, particularly the d electrons, and the defect levels associated with an unreconstructed D_{3h} carbon vacancy. We identify three different regimes associated with the occupation of the different electronic levels between hybridized graphene-metals which determines all the magnetic properties obtained by the doping;

(ii) In chemical functionalization, independently of the particular adsorbate, a spin moment of 1.0 Bohr is induced when a molecule chemisorbs on a graphene layer via a single C-C covalent bond. This effect is similar to H adsorption, which saturates one p_z orbitals creating an effect on the electronic structure that resembles a single vacancy in a π-tight-binding, however with universal character. The magnetic coupling between adsorbates was also studied and showed a key dependence on the sublattice adsorption site;

(iii) Monovacancies under isotropic strain display a rich phase diagram of spin solutions with the geometry configuration. Stretching increases the moment in different spin phases and compression reduces or even kills the magnetic moment. The transition to the non-magnetic solutions can be traced to changes in the local structure of graphene that are associated with the global rippling of the layer.

All these results provide key information about defects in the magnetism of graphene.

References

[1] Elton J. G. Santos, A. Ayuela and D. Sánchez-Portal, *New Journal of Physics*, **12** (2010) 053012.
[2] Elton J. G. Santos, D. Sánchez-Portal and A. Ayuela, *Phys. Rev. B*, **81** (2010) 125433.
[3] Elton J. G. Santos et al. *Phys. Rev. B*, **78** (2008) 195420.
[4] Elton J. G. Santos, A. Ayuela and D. Sánchez-Portal, *Submitted* (2011).
[5] Elton J. G. Santos, D. Sánchez-Portal and A. Ayuela, *Submitted* (2011).
[6] Elton J. G. Santos, S.Riikonen, D. Sánchez-Portal and A. Ayuela, *arXiv:1012.3304v1*.
[7] Elton J. G. Santos, S. Riikonen, A. Ayuela and D. Sánchez-Portal, *In preparation* (2011).

Figure: *Some of our models for: **A.** and **B.** Spin densities of a Co and Ni atoms at a substitutional site in graphene and a carbon nanotube, respectively; **C.** Exchange energy along zigzag direction of two Co atoms at the same or opposite graphene sublattice (e.g. AA or AB); **D.** Slater-Pauling-like plot for transition metal impurities saturating a monovacancy in graphene (substitutional site); **E.** Amplitudes of the rippling of a defective graphene monolayer under an moderate strain of 3.0%; **F.** Spin-strain phase diagram of a monovacancy in graphene; **G.** Geometry of a suspended graphene sheet with defects and strain.*
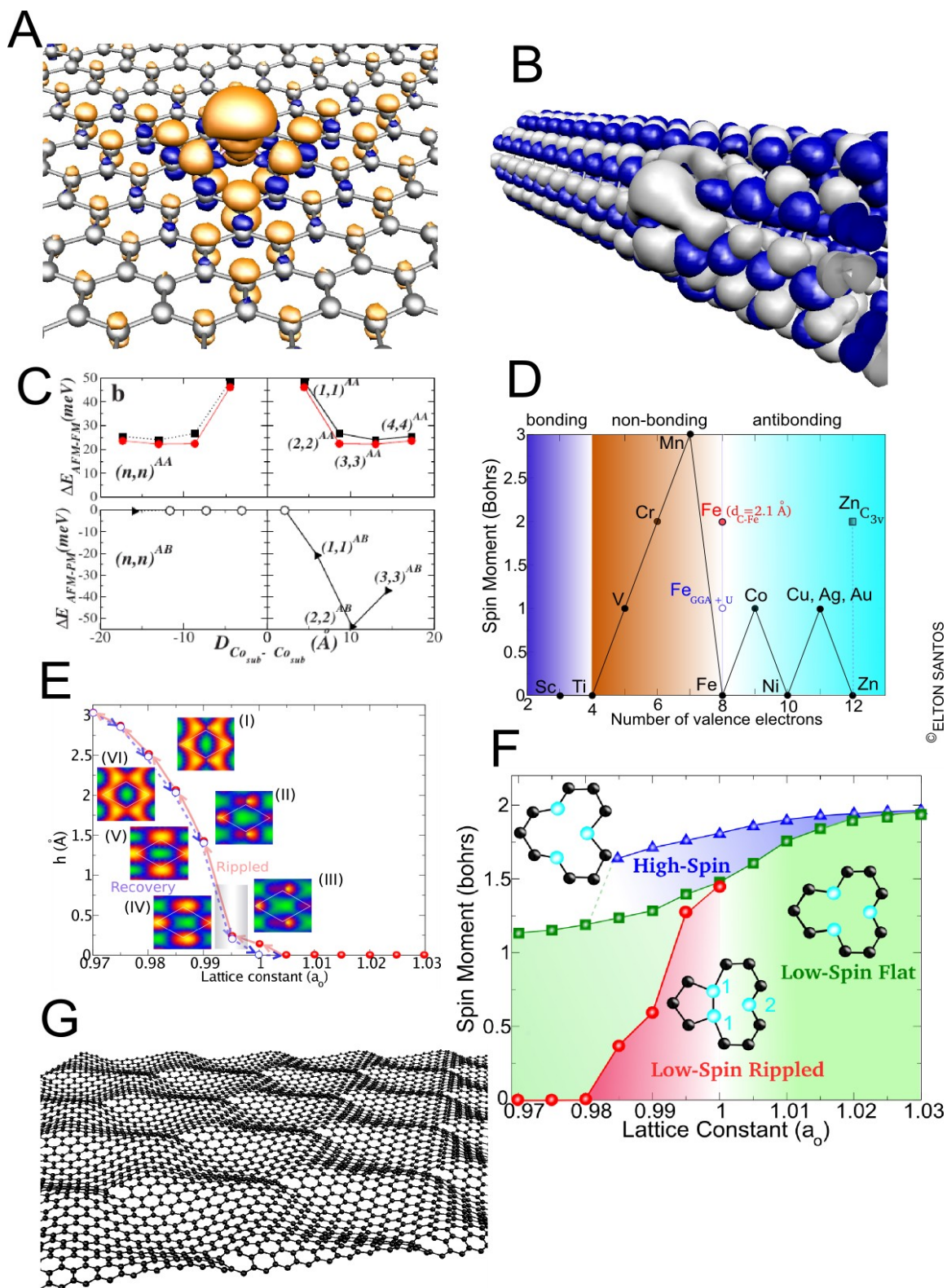
Stimulated Terahertz Emission from Optically Pumped Graphene and Its Threshold Behavior

Akira Satou[1,3], Stephane Boubanga-Tombet[1,3], Taiichi Otsuji[1,3], and Victor Ryzhii[2,3]

[1]Tohoku University, 2-1-1 Katahira, Aoba-ku, Sendai 980-8577, Japan
[2]University of Aizu, Tsuruga, Ikki-machi, Aizu-Wakamatsu 965-8580, Japan
[3]Japan Science and Technology Agency, Tokyo 107-0075, Japan
a-satou@riec.tohoku.ac.jp

Graphene has attracted much attention for wide variety of device applications due to its exceptional electronic and optical properties. Recently, we have proposed THz lasers using optically pumped graphene [1-3]. The negative dynamic conductivity can occur at THz frequency due to the population inversion and hence the lasing is possible (see Fig. 1(a)). In previous work, we measured the carrier relaxation and recombination dynamics in optically pumped epitaxial graphene on silicon [4] and exfoliated graphene [5] using THz time-domain spectroscopy based on an optical pump/THz&optical probe technique. A pulsed optical beam was impinged to a graphene sample and a CdTe crystal placed on it. The THz probe pulse generated from CdTe stimulates the THz emission from the sample. The comparison of emission spectra for sample spots with/without graphene indicated that the coherent THz probe pulse passing through graphene is amplified by the stimulated emission from optically pumped graphene. In this paper, we study both experimentally and theoretically the threshold behavior of the THz stimulated emission from graphene for pumping intensity.

An exfoliated monolayer-graphene/SiO2/Si sample is prepared. A 0.12-mm-thick (100)-oriented CdTe crystal is placed on the sample, acting as a THz probe pulse emitter as well as an electrooptic sensor. An 80-fs, 1550-nm fiber laser beam having 4-mW average power and 20-MHz repetition is split into two: one for optical pumping and generating the THz probe beam, and one for optical probing. The pumping laser is simultaneously focused at normal incidence from the back surface onto the graphene (for optical pumping) and to the CdTe (for generating THz prove pulse marked with "1" in Fig. 1(b)). This THz proves beam reflecting back in part stimulates the THz emission in graphene, which is electrooptically detected as a THz photon echo signal (the secondary pulse marked with "2" in Fig. 1(b)). We changed the spot size of the pumping beam by mechanically shifting a focal lens. Fig. 1 (c) shows the emission spectra and measured gain as a function of the pumping intensity. The gain was calculated by dividing the peak intensity of the stimulated emission from the sample spot with graphene by that of the emission from the spot without graphene. It can be seen in Fig. 1(c) that the threshold intensity is about 10^7 W/cm^2 and the gain increases linearly with the pulse intensity.

We also conducted numerical calculation based on the rate equations derived from the quasi-classical Boltzmann equation [3]. The carrier distribution (equivalent electron and hole distributions) is governed by the following equations for the total energy and concentration of carriers:

$$\frac{d\Sigma}{dt} = \frac{1}{\pi^2} \sum_{i=\Gamma,K} \int d\mathbf{k} \left[(1-f_{h\omega_i - v_w \hbar k})(1-f_{v_w \hbar k}) / \tau_{iO,\text{inter}}^{(+)} - f_{v_w \hbar k} f_{h\omega_i - v_w \hbar k} / \tau_{iO,\text{inter}}^{(-)} \right],$$

$$\frac{d\mathrm{E}}{dt} = \frac{1}{\pi^2} \sum_{i=\Gamma,K} \int d\mathbf{k}\, v_w \hbar k \left[(1-f_{h\omega_i - v_w \hbar k})(1-f_{v_w \hbar k}) / \tau_{iO,\text{inter}}^{(+)} - f_{v_w \hbar k} f_{h\omega_i - v_w \hbar k} / \tau_{iO,\text{inter}}^{(-)} \right]$$

$$+ \frac{1}{\pi^2} \sum_{i=\Gamma,K} \int d\mathbf{k}\, h\omega_i \left[f_{v_w \hbar k}(1-f_{v_w \hbar k + h\omega_i}) / \tau_{iO,\text{intra}}^{(+)} - f_{v_w \hbar k}(1-f_{v_w \hbar k - h\omega_i}) / \tau_{iO,\text{intra}}^{(-)} \right],$$

where Σ and E are the carrier concentration and energy density, f_ε is the quasi-Fermi distribution, $\tau_{iO,\text{inter}}^{(\pm)}$ and $\tau_{iO,\text{intra}}^{(\pm)}$ are the inverses of the scattering rates for inter and intraband OPs ($i = \Gamma$ for OPs near the Γ point with ω_Γ = 196 meV, i = K for OPs near the zone boundary with ω_K = 161 meV, + for

absorption, and – for emission). We calculated the time evolution of the quasi-Fermi energy ε_F and carrier temperature T_c, which characterize the carrier distribution, after the pulse excitation. We observed that the population inversion, i.e., positive quasi-Fermi energy, occurs after around 1 ps of the excitation with some threshold pulse intensity. Fig. 2 shows the normalized dynamic conductivity of optically pumped graphene after 3.5 ps of the pulse excitation, as a function of pumping intensity with signal frequency 2 THz and with different momentum relaxation time. We took t = 3.5 ps because it approximately corresponds to the duration of the THz emission from the CdTe coming to the graphene after the pulse excitation in our experiment. Comparing Figs. 1(b) and (c), one can see the qualitative agreement with experimental and theoretical results.

References

[1] V. Ryzhii, M. Ryzhii, and T. Otsuji, J. Appl. Phys. **101** (2007) 083114.
[2] V. Ryzhii, M. Ryzhii, A. Satou, T. Otsuji, A. A. Dubinov, and V. Ya Aleshkin, J. Appl. Phys. **106** (2009) 084507.
[3] A. Satou, T. Otsuji, and V. Ryzhii, Technical Digest of 2nd International Symposium on Graphene Devices: Technology, Physics, and Modeling, Sendai, Japan, 27-29 Oct. 2010.
[4] H. Karasawa, T. Komori, T. Watanabe, H. Fukidome, M. Suemitsu, V. Ryzhii, and T. Otsuji, J. Infrared Milli. Thrz. Waves onlin 2010. doi: 10.1007/s10762-010-9677-1.
[5] S. Boubanga-Tombet, S. Chan, A. Satou, T. Watanabe, V. Ryzhii, and T. Otsuji, European Optical Society Annual Meeting 2010, Paris, France, 26-29 Oct. 2010.

Figures

(a)	(b)	(c)
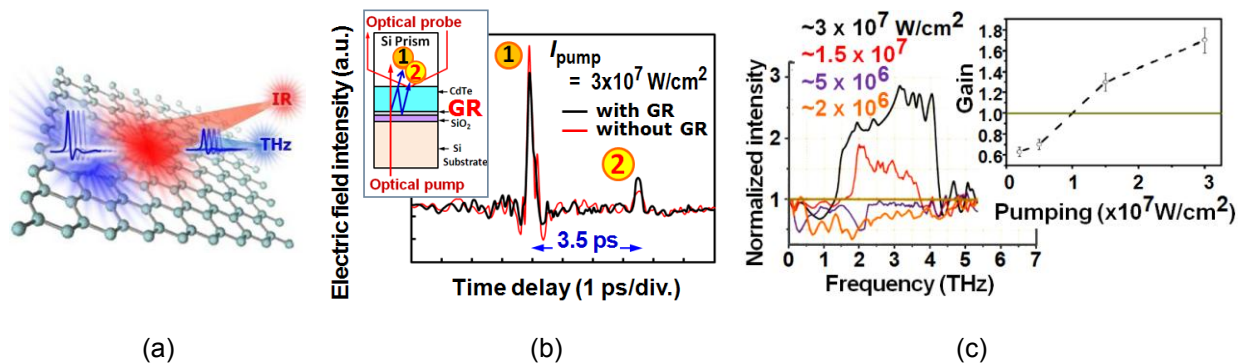
Figure 1: (a) Schematic view of the THz amplified stimulated emission from optically pumped graphene, (b) emission spectra and (c) pumping intensity dependence of measured gain of THz emission from optically pumped graphene.
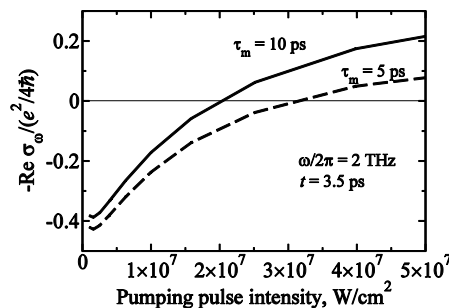
Figure 2: Normalized negative dynamic conductivity calculated theoretically.

Direct observation of sub-nanometer edge smoothness of catalytically etched suspended few layer graphene

Franziska Schäffel[1], Mark Wilson[2], Alicja Bachmatiuk[3], Mark H. Rümmeli[3,4], Ute Queitsch[3], Bernd Rellinghaus[3], G. Andrew D. Briggs[1], Jamie H. Warner[1]

[1] Department of Materials, University of Oxford, Parks Rd., Oxford OX1 3PH, United Kingdom
[2] Department of Chemistry, University of Oxford, South Parks Rd., Oxford OX1 3QZ, United Kingdom
[3] IFW Dresden, P.O. Box 270116, D-01171 Dresden, Germany
[4] University of Technology Dresden, 01062 Dresden, Germany
franziska.schaeffel@materials.ox.ac.uk

Due to the fact that truly two dimensional graphene is a half metal graphene width confinement through nanostructuring is needed to open a sufficient band gap for transistor operation at room temperature [1]. Further, it is imperative that the edges of such nanostructured graphenes are crystallographically well defined and, ideally, atomically smooth to reduce the negative impact of edge effects on electronic and thermal conductivity [1, 2].

Recently, catalytic etching of graphite or graphene by metallic and non-metallic nanoparticles has been suggested to be a key technology for the fabrication of graphene nanostructures and nanoribbons [3]. When exposed to hydrogen under elevated temperatures the catalytic particles act as knives and cut through the carbon they are in contact with, leaving pronounced etch tracks along specific crystallographic directions. This intrinsic crystallographic etching makes catalytic hydrogenation methods so popular in graphene nanostructuring.

Graphene edges have been extensively studied using low voltage high resolution transmission electron microscopy (LV-HRTEM) [4], scanning tunneling microscopy [5] and Raman spectroscopy [6]. However, not many studies can be found in literature on the edges of nanostructured graphenes. Here, quality control is mainly based on Raman spectroscopy. Low magnification microscopy has also been carried out, which may show smooth edges on a microscopic scale, but has not yet revealed the edge smoothness at the atomic level. Thorough characterization and evaluation of the atomic structure of nanoribbon edges with direct imaging techniques has not yet been accomplished.

Here, we present results from catalytic hydrogenation experiments catalyzed by gas-phase prepared cobalt nanoparticles. We successfully processed nanostructured graphenes and GNRs with clean edges ready for inspection using LV-HRTEM. In this way edges with sub-nanometer smoothness could be observed over a significant edge length (see figure 1). Further, we have employed rigid perforated Si$_3$N$_4$ membrane TEM grids to achieve compatibility of catalytic hydrogenation experiments with TEM. In this way the experimental steps of catalytic hydrogenation could be monitored throughout the process and the etching of suspended few layer graphene has been demonstrated. These results allow one to evaluate the degree of edge control that can be achieved by catalytic hydrogenation.

References

[1] X. Wang, Y. Ouyang, X. Li, H. Wang, J. Guo, H. Dai, Phys. Rev. Lett. **100** (2008) 206803.

[2] A. A. Balandin, S. Ghosh, W. Bao, I. Calizo, D. Teweldebrhan, F. Miao, C. N. Lau, Nano Lett. **8** (2008) 902.

[3] L. Ci, Z. Xu, L. Wang, W. Gao, F. Ding, K. F. Kelly, B. I. Yakobson, P. M. Ajayan, Nano Res. **1** (2008) 116; S. S. Datta, D. R. Strachan, S. M. Khamis, A. T. C. Johnson, Nano Lett. 8 (2008) 1912; F. Schäffel, J. H. Warner, A. Bachmatiuk, B. Rellinghaus, B. Büchner, L. Schultz, M. H. Rümmeli, Nano Res. **2** (2009) 695; L. Gao, W. Ren, B. Liu, Z.-S. Wu, C. Jiang, H.-M. Cheng, J. Am. Chem. Soc. **131** (2009) 13934.

[4] Ç. Ö. Girit, J. C. Meyer, R. Erni, M. D. Rossell, C. Kisielowski, L. Yang, C.-H. Park, M. F. Crommie, M. L. Cohen, S. G. Louie, A. Zettl, Science **323** (2009) 1705; Z. Liu, K. Suenaga, P. J. F. Harris, S. Iijima, Phys. Rev. Lett. **102** (2009) 015501.

[5] Y. Kobayashi, K.-I. Fukui, T. Enoki, K. Kusakabe, Phys. Rev. B **73** (2006) 125415; K. A. Ritter, J. W. Lyding, Nat. Materials **8** (2009) 235.

[6] C. Casiraghi, A. Hartschuh, H. Qian, S. Piscanec, C. Georgi, A. Fasoli, K. S. Novoselov, D. M. Basko, A. C. Ferrari, Nano Lett. **9** (2009) 1433; A. K. Gupta, T. J. Russin, H. R. Gutiérrez, P. C. Eklund, ACS Nano **3** (2009) 45.

Figures
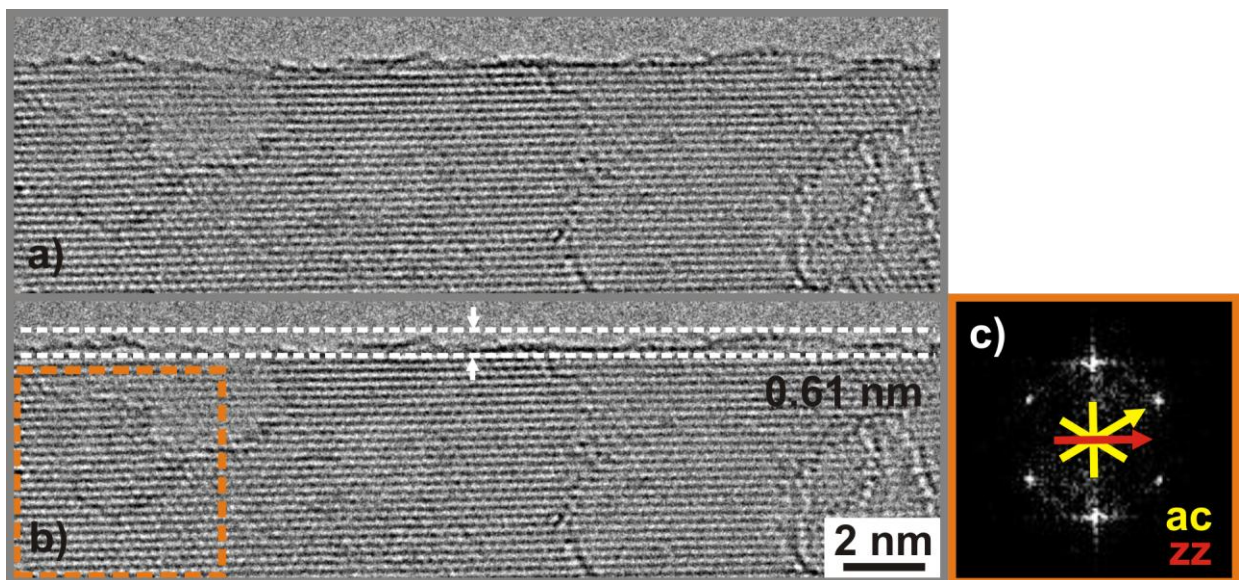
Figure1: a) LV-HRTEM micrograph of a sub-nanometer smooth edge of suspended catalytically etched few layer graphene; b) The same image as in a – here, the scale bar and the measurement marker from roughness determination have been included; c) Fast Fourier transformation of the area marked orange in b. The yellow lines represent armchair (ac) directions, the red line represents a zigzag (zz) direction of the graphene crystal lattice. From this the etching direction has been determined to be along a zigzag direction.

New techniques to improve the visibility of Graphene on multiple substrates

Peter Schellenberg [1], Michael Belsley [1], Hugo Gonçalves [1], Cacilda Moura [1], Tobias Stauber [2]

[1] Center of Physics, University of Minho, Campus de Gualtar, 4710-057 Braga, Portugal

[2] Department of Condensed Matter Physics, University Autónoma of Madrid,

Campus of Cantoblanco, E-28049Madrid, Spain

peter.schellenberg@fisica.uminho.pt

The mechanical exfoliation of natural graphite crystals is one of the foremost methods to gain high – quality graphene monolayer flakes, which are crucial for the investigation of its fundamental properties as well as for the development of electronic micro-circuits, nanophotonic assemblies and other microstructured graphene based devices. Although the visualization of the monolayer graphene is hampered by its low absorptivity, it is essential to develop techniques, which reliably and rapidly deliver images of graphene and graphene based structures.

A multitude of optical techniques have been investigated to this end, for example based on interference enhancement on specifically prepared substrates. Other imaging methods are based on Raman and Rayleigh scattering, or on fluorescence quenching of dyes by graphene layers. Generally these methods require relatively complex equipment or an optimized substrate coating. Here, we report on novel and easy to use techniques for the identification of potential graphene flakes.

The first method is long known as microdroplet condensation technique or breath condensation technique. It has previously been used in the context of visualizing hydrophobicity differences on patterned film structures such as self-assembled monolayers. Likewise, the hydrophobicity difference between the substrate and the carbon sheets produce a clearly visible condensation pattern, that singles out the graphene flakes. The effect can be seen on a wide variety of substrates without the need for any specific surface modification or preparation. It can be used on surfaces for which no other method is known such as plastics and uncoated metals. Similarly the contrast enhancement can also be observed in an optical transmission microscope, in which graphene flakes are notoriously difficult to observe.

The second method is based on contrast enhancement by refractive index matching. The graphene flake is immobilized on a dielectric substrate, and by using a refractive index matching liquid the reflection from the substrate is greatly diminished, thereby enhancing the contrast of the monolayer or few-layer graphene. An estimation of the number of layers also becomes possible.

References

[1] Hugo Gonçalves, Michael Belsley, Cacilda Moura, Tobias Stauber and Peter Schellenberg Appl. Phys. Lett., **97** (2010) 231905.

Phase coherent transport in graphene nanoribbons

Silvia Schmidmeier, Dieter Weiss and Jonathan Eroms

Institute of Experimental and Applied Physics, University of Regensburg,
D-93053 Regensburg, Germany
silvia.schmidmeier@physik.uni-regensburg.de

Phase coherent effects in graphene are determined by the combined action of several scattering mechanisms. In the past, extensive studies have been performed on those effects in bulk graphene [1], [2], [3]. Little attention, however, has been devoted to phase coherent behavior in graphene nanoribbons (GNRs) where lateral confinement creates a crossover from 2D to 1D behavior and additional scattering is introduced at the edges of the ribbons.

Here we study the magnetotransport of graphene nanoribbons at low temperatures, focusing on interference effects which lead to corrections to the resistance or conductance. In graphene weak localization is often suppressed and generally more complex than in diffusive metals [1 - 3]. In the case of graphene nanoribbons, however, edge scattering becomes the most important mechanism leading to the observation of weak localization. Another correction to the conductivity are universal conductance fluctuations (UCFs), which appear when the phase coherence length is comparable to the sample length. Both effects allow us to extract the phase coherence length L_Φ in an independent way.

Here we have studied the magnetoconductance of individual graphene nanoribbons and arrays of GNRs. Fig. 1 shows the magnetotransport data collected for a 40 nm wide GNR (Fig. 1a) and for an array of GNRs (Fig. 1b), respectively. Each ribbon of the array has a width of 40 nm and a spacing of 30 nm to the next. For all temperatures from T = 1.7 K to 48 K Fig. 1a displays clear weak localization for low field region (|B<1.5T|) and universal conductance oscillations. With decreasing temperature the amplitude of the oscillations increases. For lower temperatures large universal conductance fluctuations overlay the weak localization feature. Consequently the phase coherence length can no longer be determined by fitting the weak localization. In order to investigate weak localization also at low temperatures arrays of graphene nanoribbons were fabricated. As expected the parallel arrangement of the nanoribbons leads to a suppression of the universal conductance fluctuations via ensemble averaging, whereas weak localization is not suppressed (Fig. 1b). Thus the phase coherent effects can be separated. By extracting L_Φ from weak localization we can compare and verify results obtained from the amplitude of the UCFs and the autocorrelation function of UCFs for single GNRs.

References

[1]   F. V. Tikhonenko, A. A. Kozikov, A. K. Savchenko and R. V. Gorbachev, Phys. Rev. Lett, **103,** (2009), 226801

[2]   E. McCann, K. Kechedzhi, V. I. Fal´ko, H. Suzuura, T. Ando, B. L. Altshuler, Phys. Rev. Lett, **97,** (2006), 146805

[3]   F. V. Tikhonenko, D. W. Horsell, R. V. Gorbachev, A. K. Savchenko, Phys. Rev. Lett, **100,** (2008), 056802

Figures
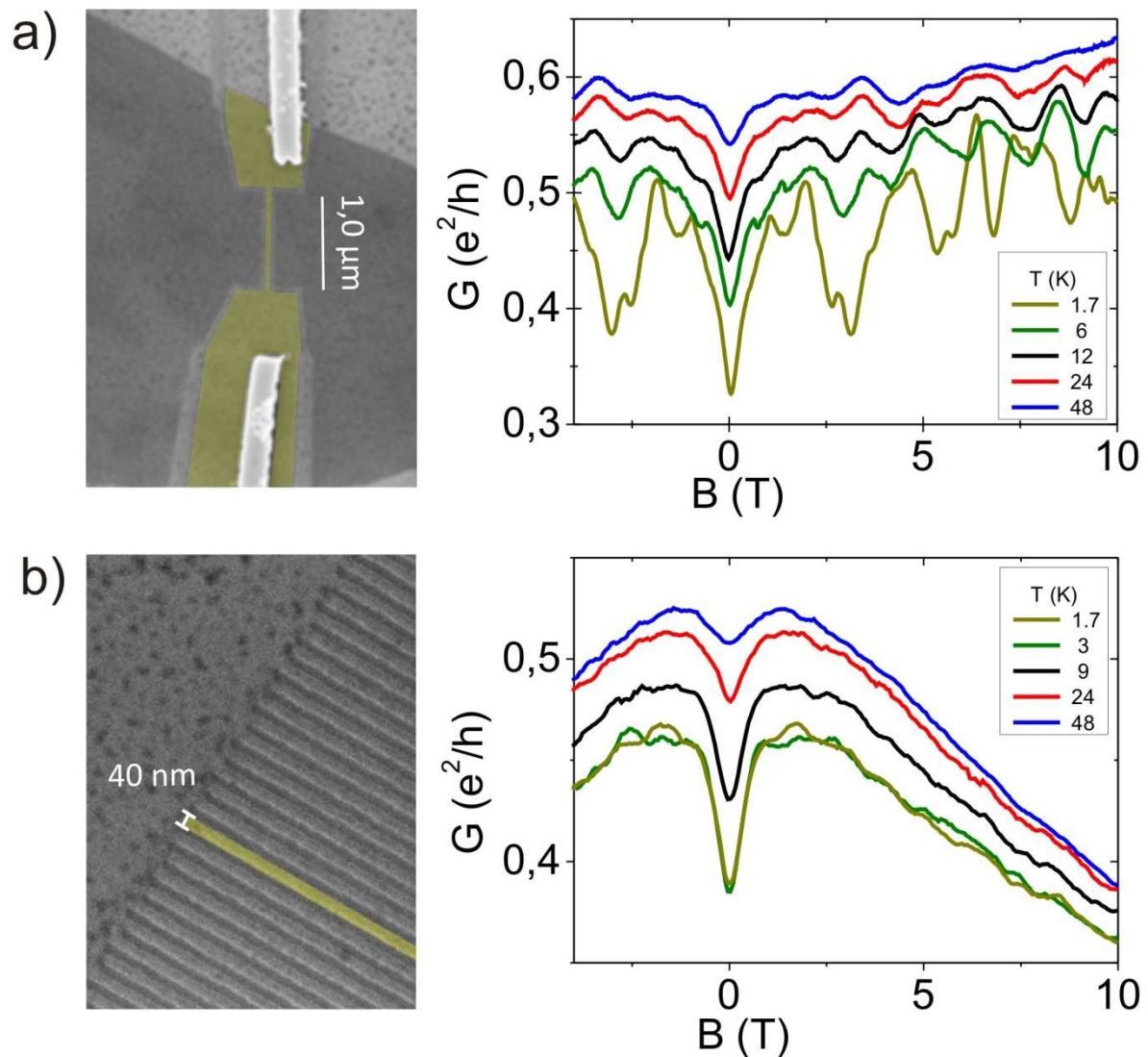
Fig.1 *(a) SEM image of a 40 nm wide and 1 µm long graphene nanoribbon (colored in yellow). The conductance G as a function of magnetic field B shows quantum interference phenomena like universal conductance fluctuations and weak localization for temperatures from T = 1.7 K to 48 K.*
(b) SEM image of a sector of a 3.2 µm wide array of 46 GNRs (one ribbon is colored in yellow). The ribbons of the array have a width of 40 nm and a length of 1µm, each with a spacing of 30 nm to the next ribbon. The magnetotransport data clearly shows a suppression of the universal conductance fluctuations for all temperatures, whereas the weak localization feature is not affected.

Fluorinated Graphene: A Stable Large-Gap Graphene Derivative Investigated by Scanning Tunneling Microscopy

Scott W. Schmucker[1,2], Joshua D. Wood[1,2], Richard T. Haasch[3], Joseph W. Lyding[1,2]

[1]University of Illinois at Urbana-Champaign, Department of Electrical and Computer Engineering, 1406 W. Green St., Urbana, Illinois, United States
[2]Beckman Institute, 405 N. Mathews Ave. MC-251, Urbana, Illinois, United States
[3]Frederick Seitz Materials Research Laboratory, 104 S. Goodwin Ave., Urbana, Illinois, United States
sschmuc2@illinois.edu

We present the first atomic-resolution microscopic and spectroscopic study of monolayer fluorinated graphene films. Graphene grown by chemical vapor deposition on polycrystalline copper foil is fluorinated by XeF_2 gas and characterized by x-ray photoelectron spectroscopy (XPS), Raman spectroscopy, scanning tunneling microscopy (STM), and scanning tunneling spectroscopy (STS). We directly measure the atomic and electronic structures of planar-sheet graphene fluoride, probe its stability under electron bombardment and thermal annealing, and elucidate interaction between the copper substrate and fluorinated graphene overlayer. We discover that fluorinated graphene C_6F retains a planar structure, exhibits a large band gap, and remains stable under electron bombardment and mild thermal annealing below 500°C.

While graphene has attracted a great deal of scientific interest, its inherent semi-metallic nature limits opportunities for this material in digital logic and microelectronics. In response, several techniques have been developed for modulation of the graphene band gap, including the patterning of nanometer-scale graphene ribbons and graphene hydrogenation. Fluorinated graphene offers unique advantages over these alternatives, as it lacks electronic edge states, and unlike hydrogenated graphene (graphane),[1] exhibits thermodynamic stability and high resistivity.[2,3,4]

Bulk fluorinated graphite exists in several forms and has been studied extensively. However, monolayer fluorinated graphene has been isolated only recently,[2,3,4] and very little is known of its structure, stability, and electronic properties, particularly in the case of planar-sheet graphene fluorides.

Like graphite fluoride, graphene fluorides exist in both planar-sheet and puckered-sheet configurations. In the puckered-sheet case, carbon atoms are fully sp^3 hybridized and covalently bound with fluorine, buckling the carbon skeleton, opening a large (>3 eV) energy gap, and leading to stable $(CF)_n$ or $(C_2F)_n$. This material can be exfoliated to produce few-layer and monolayer puckered-sheet graphene fluoride.[3,4] However, reduction is generally destructive to the graphene skeleton, undermining one important goal of graphene functionalization.[2] In contrast, planar-sheet graphite fluorides (C_xF), synthesized near room temperature, exhibit ionic (x>20) or semi-covalent (x≤4) bonding and preserve the planar graphitic structure, yet are found to have a sizable energy gap (0–3 eV) that depends on fluorine concentration.

In this work, planar-sheet graphene fluoride is synthesized from monolayer graphene films grown on copper foil.[5] Post-fluorination Raman spectroscopy of the D and D' bands shows increased sp^3 hybridization on the foil. As indicated by XPS (Figure 1) and STM, XeF_2 fluorination produces ~C_4F, which after a 10 min vacuum anneal at 500°C approaches ~C_6F (locally) to ~$C_{12}F$ (globally). The annealing process drives adsorbates and ionically-bound fluorine from the graphene, resulting in an energetically stable, atomically resolved fluorinated graphene lattice.

On high symmetry faces of polycrystalline copper the energy band structure (Figure 2) of fluorinated graphene is found to be consistent with theoretical predictions and spatially invariant across the graphene lattice. Although the observed band structure is predominantly that of fluorinated graphene, a copper surface state is often visible near –0.4 eV, an effect consistent with graphene on Cu(111).[6]

Structurally, the fluorine lattice is hexagonal with an inter-fluorine spacing of 6.0 Å (Figure 3). Despite semi-covalent C-F bonding the planarity of the graphene basal plane is preserved, following topographic modulation in the underlying copper substrate, and offering potential for future lithographic reduction of planar-sheet graphene fluoride.

References

[1] D.C. Elias, et al., Science, **323** (2009) 610; [2] J.T. Robinson, et al., Nano Lett., **10** (2010) 3001; [3] S.-H. Cheng, et al., Phys. Rev. B, **81** (2010) 205435; [4] R.R. Nair, et al., Small, **6** (2010) 2877; [5] X. Li, et al., Science, **324** (2009) 1312; [6] L. Gao, et al., Nano Lett, **10** (2010) 3512.

Figures
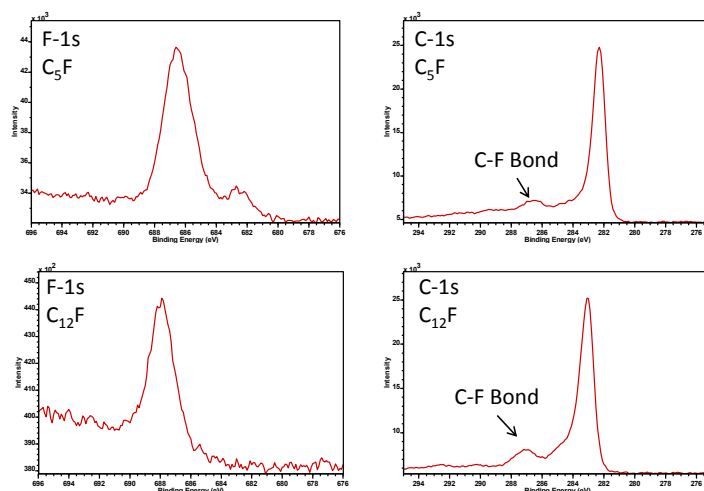
Figure 1: X-ray photoelectron spectroscopy of fluorinated graphene, consistent with semi-covalent carbon-fluorine bonding both before and after annealing. While XPS indicates a reduced fluorine concentration after anneal ($C_{12}F$ versus C_5F initially), the presence of a C-1s peak at 287 eV and F-1s peak at 688 eV suggest strong C-F bonding in both cases, indicating that remaining carbon-fluorine bonds are semi-covalent. (a) F-1s transition before annealing. (b) C-1s transition before annealing. (c) F-1s transition after annealing. (d) C-1s transition after annealing.
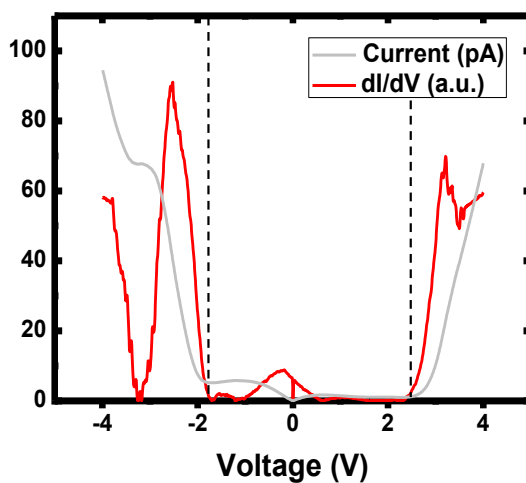
Figure 2: Scanning tunneling spectroscopy of fluorinated graphene on copper. Absolute value of current and dI/dV for graphene fluoride/copper system. Note the copper surface state near the Fermi level and the graphene fluoride band structure beyond ± 2V. Energy gap is larger than anticipated due to band bending resulting from charging in the graphene fluoride overlayer.
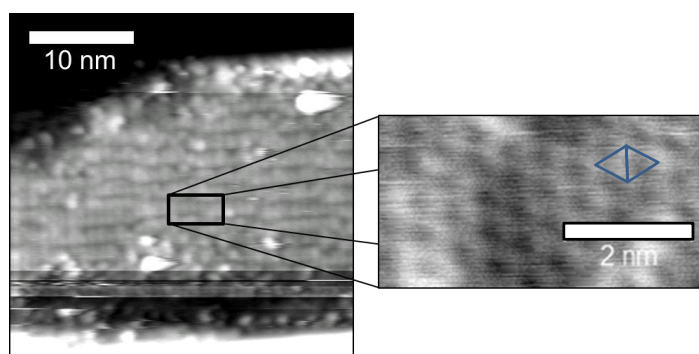
Figure 3: Atomic-resolution imaging of the graphene fluoride overlayer, exhibiting a hexagonal fluorine lattice with inter-fluorine spacing of 6.0Å. This spatial locality is further evidence for semi-covalent fluorine-carbon bonding.

Theoretical investigations on the transport properties of graphene nanoribbons

Daniele Selli, Matteo Baldoni, Gotthard Seifert, Mercuri Francesco

Institute for Chemistry and Electrochemistry, Technische Universität Dresden, 01062 Dresden, Germany
Daniele.Selli@chemie.tu-dresden.de

Recent advancements in the production techniques of novel materials based on graphene[1] allow us to envision next-generation electronic devices with active components based on nanostructured carbon. In particular, materials based on graphene nanoribbons (GNRs) are expected to play a crucial role in this sense due to the dimensional confinement which allows a fine-tuning of the electronic and, consequently, transport properties [2]. Although transport properties of GNRs have already been investigated in detail [3], a comprehensive understanding of the relationships between morphological features and quantum transport is still missing. Especially, this issue concerns the role of defects, edge terminations and structural details beyond high-symmetric morphologies. In this work we analyze and characterize, by means of density functional theory and non-equilibrium Green function calculations, the electronic and transport properties of defect-free, defected and functionalized graphene nanoribbons. Our methodology integrates valence bond (VB) concepts and Clar sextet theory [4,5] into electronic structure calculations by evaluating properties such as stability, band structure and molecular orbitals of the systems under investigation.

References

[1] Geim, AK, Novoselov KS, Nature Materials, **6** (2007) 183.
[2] Zhang, YB, Than YW, Stormer, HL, Kim P, Nature, **438** (2005) 201.
[3] Son, YW, Cohen, ML, Louie, SG, Phys. Rev. Lett., **97** (206) 216803.
[4] Baldoni, M; Sgamellotti, A; Mercuri, F, Org. Lett., **9** (2007) 4267.
[5] Baldoni, M; Sgamellotti, A; Mercuri, F, Chem Pyhs. Lett., **464** (2008) 202.
.

Figures
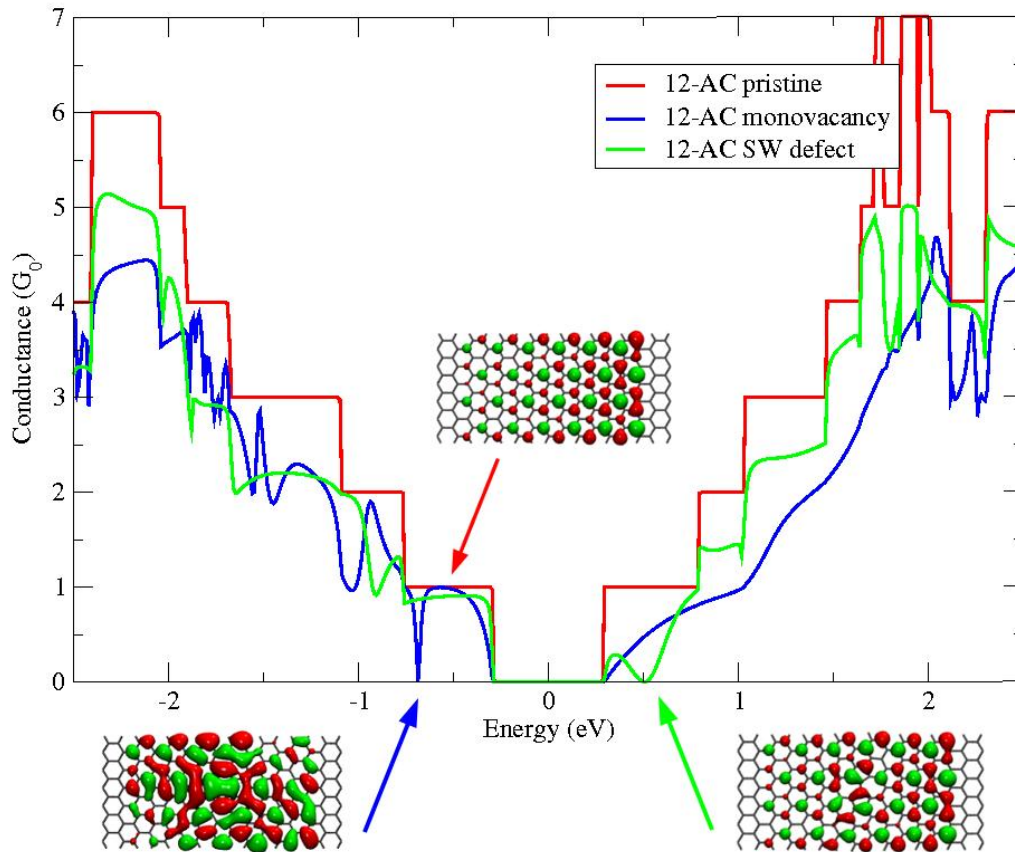
Transmission spectra of armchair-edge 12-AC pristine (red lines), with monovacancy defect (blue lines) and with Stone-Wales defect (green lines). Transmission eigenstates are also depicted above the correspondin transmission plateau.

Topography control over graphenes with single macromolecules

N. Severin[1], M. Dorn[1], A. Kalachev[2], B. Zhang[3], A.D. Schlüter[3], J.P. Rabe[1]

[1] Department of Physics, Humboldt-Universität zu Berlin, Newtonstr. 15, 12489 Berlin, Germany

[2] PlasmaChem GmbH, 12489 Berlin, Rudower Chaussee 29, Germany

[3] Institute for Polymer Chemistry, Department of Materials, ETH Hönggerberg, Wolfgang-Pauli-Strasse 10, CH-8093 Zürich, Switzerland

Precise control over the topography of graphenes on solid supports is of considerable interest, e.g., for strain engineered graphene electronics. Graphene may be exfoliated onto a pre-patterned surface, such that a strongly adhering graphene would replicate the substrate surface. Here we employed a mechanical exfoliation technique, which allowed to largely avoid the otherwise observed contaminations entrapped at the graphene-substrate interface, and which also affect the graphene topography. For example, contaminated graphenes exfoliated on freshly cleaved and atomically flat mica surface exhibit plateaus of a sub-nanometer height. The clean exfoliation, on the other hand, results in atomically flat graphenes over large areas. Exfoliated onto mica surfaces coated with vector DNA or dendronized polymers, they replicate the topography of the molecules with nanometer precision, as deduced from intermittent contact and contact mode scanning force microscopy images.
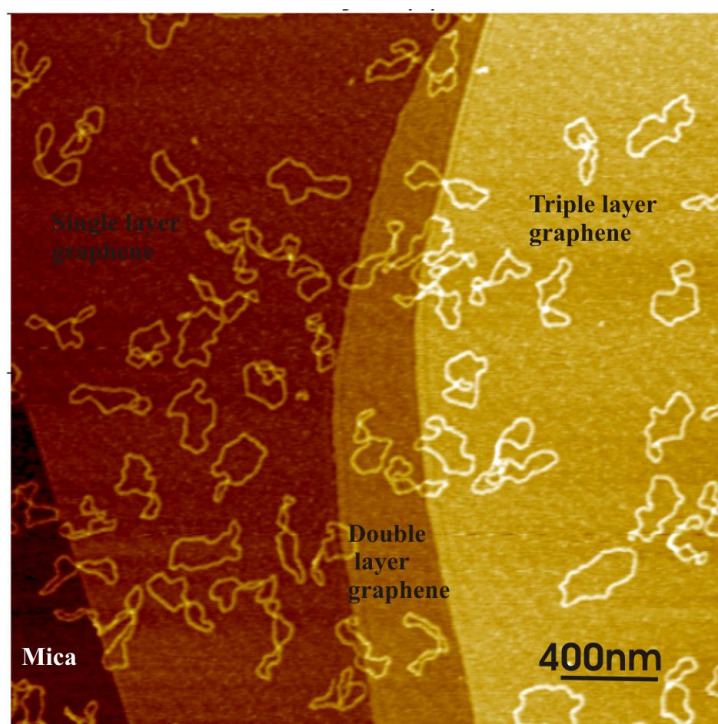
Figure: Topography of graphenes exfoliated onto mica surface covered with vector DNA molecules as imaged with a Scanning Force Microscope.

Finite frequency measurements and characteristic time scales in graphene devices.

Oleksii Shevtsov, Xavier Waintal

CEA/INAC/SPSMS/GT, 17 rue des Martyrs 38054 Grenoble, France
oleksii.shevtsov@cea.fr, xavier.waintal@cea.fr

Most numerical calculations that are performed with Recursive Green's Function (RGF) or similar techniques are concerned with DC transport. The AC case has been developed withing the Scattering formalism for some time [1-2], but has received little attention from the numerical community so far. To our knowledge, there have been not so many groups trying to do simulations for these types of questions [2-4]. A crucial point of physics at finite-frequency is that electron-electron interactions must be included, at least at the mean field level, in order to account for basic physical facts such as current conservation.

Finite-frequency physics makes it possible to consider a very large class of situations and questions. For instance, one could discuss the problematic of quantum pumping (making use of quantum interferences to pump a current in a device that would not work classically), quantum rectification or spin pumping (the spin analogue of quantum pumping which was observed in the line-width of ferro-magnetic resonances). Other examples include non-linear effects in the current-tension characteristic of a device ("Landauer dipoles"), AC conductance and quantum capacitances.

We perform numerical simulations of quantum transport in graphene based devices at finite (GHz - THz) frequencies. Our simulations are based on the Non Equilibrium Green Function (NEGF) approach that we extend in order to relate finite frequency quantities to Green function elements that can be calculated using standard recursive techniques. Our simulations show that characteristic time scales of the device (such as the transverse Thouless time from which the electronic speed can be extracted) can be obtained from the frequency dependance of the ac conductance. We also discuss the interplay between finite frequency and magnetic fields.

[1] M. Büttiker, Il Nuovo Cimento, B **110**, (1995) 509
[2] M. H. Pedersen and M. Büttiker, Phys. Rev. B, **58** (1998) 12993
[3] B. Wang, J. Wang, and H. Guo, Phys. Rev. Lett., **82** (1999) 398
[4] S. Kohler, J. Lehmann, P. Hänggi, Phys. Rep. , **406** (2005) 379

Graphene formation on GaN substrates and
electrical characteristics of metal/graphene/GaN structure

K. Tanaka[1], Y. Shimotsuji[1], S. Tanaka[2], A. Hashimoto[1], and K. Shiojima[1]

Graduate School of Electrical & Electronics Engineering, University of Fukui,
3-9-1 Bunkyo, Fukui, 910-8507, Japan[1]
Department of Applied Quantum Physics & Nuclear Engineering, Kyushu University,
Motooka 722, Nishi-ku, Fukuoka 819-0395, Japan[2]
shiojima@u-fukui.ac.jp

Excellent carrier and heat conduction of graphene has much attention for electronic device applications. Combination of graphene and wide-band-gap material, GaN is one of candidates to improve source resistance, surface passivation and thermal dissipation. From a material point of view, because GaN has a nature of crystal polarization, the device performance is surface sensitive. Investigation of graphene/GaN interfaces is important, and providing a new technique for surface potential control is possible. This paper reports successful transformation of epitaxial graphene layers on GaN crystals and current-voltage (I-V) characteristics of metal contacts inserting the graphene layers.

We used transfer process [1], which is that a graphene layer on a sublimated SiC surface is transferred onto another material. Firstly, SiC substrates were heated in vacuum to form epitaxial graphene on the surface. Then, Ti metal and poly-methil-methacrylate (PMMA) were deposited on the graphene, and the graphene layer was exfoliated from the SiC substrate. Finally, the PMMA/Ti/graphene layer was put on the GaN surface, and the PMMA and Ti were removed by using acetone and HCl, respectively. The n-GaN layer was grown on a sapphire substrate by metal organic chemical vapor deposition. The electron concentration was 4×10^{17} cm^{-3}.

Figure 1(a) shows a typical microscope image of the GaN surface before the Ti removing. Most of the Ti surface is covered with PMMA. After the HCl etching (Fig. 1 (b)), only small portions of the Ti layer without PMMA were etched away, and the graphene layer successfully remained on the GaN surface. A typical size of the graphene layer is around 50 μm.

Figure 2 shows typical Raman spectra from the transformed graphene on GaN, and GaN substrate. In the spectrum from the graphene on GaN, the peaks from GaN, G'-, D-, G-band can be seen. The FWHM of the G'-peak is 50 cm^{-1}, and the peak ratio (I(D) / I(G)) is about 0.5. Therefore, it can be considered that one- or two-mono-layer graphene was transferred.

In order to investigate I-V characteristics of metal/graphen/n-GaN structure, Ni electrodes (50-nm thick) were deposited by electron-beam evaporation method. After that, an Oxygen plasma treatment was conducted for the isolation between the electrodes. For the comparison, conventional Ni/n-GaN Schottky diodes were also prepared. Figure 3 shows the forward and reverse I-V characteristics for both samples. The diodes with a graphene layer showed rectifying characteristics. Comparing with the sample without graphene, the Schottky barrier height decreased. The effect of the graphene insertion was confirmed as the potential control.

Reference

[1] A. Hashimoto, H. Terasaki, K. Morita, H. Hibino and S. Tanaka. *International Conference on Silicon Carbide and Related Materials*, Tu-P-86, (2009).

Figures
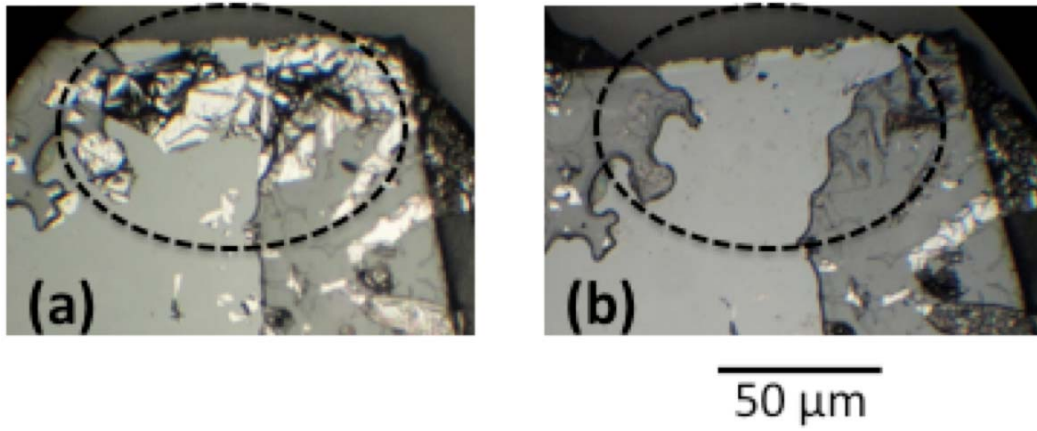
Fig. 1. Microscope images of the GaN surface (a) before and (b) after the Ti removing.
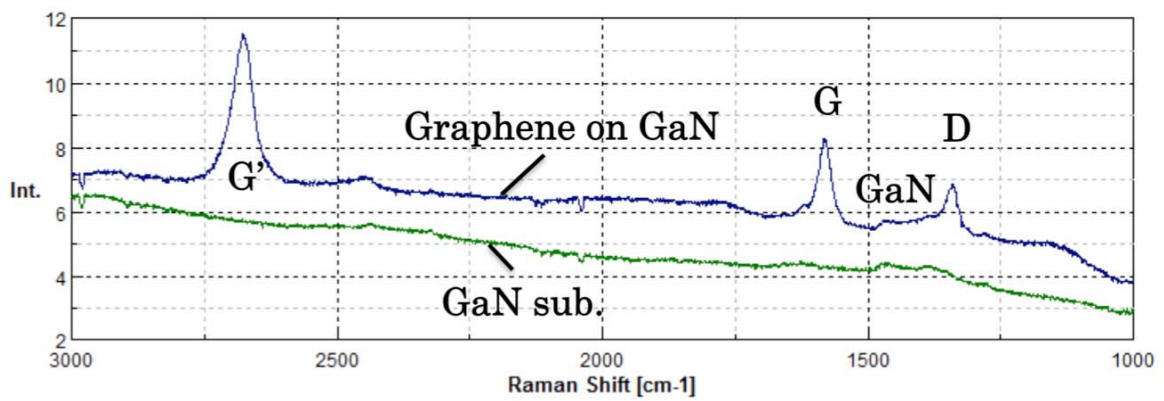
Fig. 2. Raman spectra from graphen/GaN and GaN.
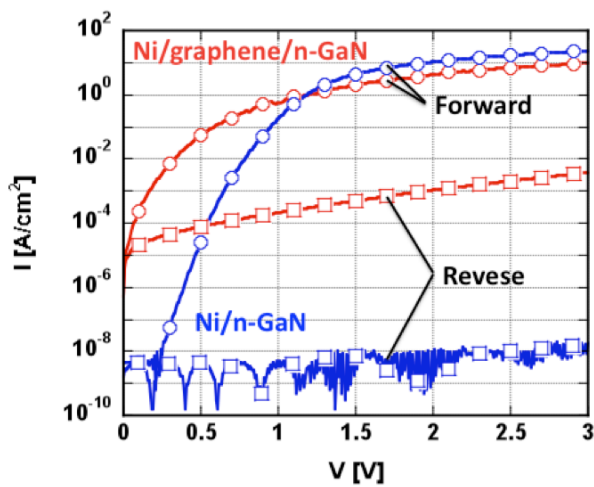
Fig. 3. I-V characteristics of Ni/graphen/n-GaN and Ni/n-GaN diodes.

Effect of electron interaction and spin in electronic and transport properties of graphene nanoribbons in the integer quantum Hall regime

Artsem Shylau, Igor Zozoulenko, Hengyi Xu and Thomas Heinzel

Solid State Electronics, ITN, Linkoping University, 601 74 Norrköping, Sweden
artsh@itn.liu.se

In the present work [1] we study a system consisting of a graphene nanoribbon (GNR) which is located on an insulating substrate and attached to semi-infinite leads acting as electron reservoirs. The system is subjected to a perpendicular magnetic field. The effects of electron interaction on the magnetoconductance are studied within the Hartree approximation. Self-consistent numerical calculations are based on the tight-binding p-orbital Hamiltonian. Local density of states and distribution of charge density are calculated using the Green's function technique.

We find that the perpendicular magnetic field leads to suppression instead of an expected improvement of the conductance quantization. This suppression is traced back to interaction-induced modifications of the band structure which is strongly modified in comparison to the single-particle case. The distortion of subbands leads to formation of compressible strips in the middle of GNRs. The compressible strips are partially filled and hence the system has a metallic character. As a result, the electron density can be easily redistributed in order to effectively screen the external potential. The detailed structure of propagating states of interacting electrons in GNRs shows that there are two types of states which have a different microscopic character. The first type corresponds to edge states propagating near the boundaries. These states have the same structure for interacting and noninteracting cases. The second type corresponds to states which form compressible strips in the center of the ribbon as discussed above. The most prominent feature of these states is that their direction of propagation is opposite to that one of the edge states residing in the same half of the GNR. This is in contrast to the noninteracting picture, where due to the presence of the magnetic field, forward and backward propagating states are localized at different boundaries by Lorentz forces. We demonstrate that the drastic modification of the GNR band structure by electron interaction leading, in particular, to the formation of compressible strips in the middle of the ribbon causes suppression instead of expected improvement of the conductance quantization. We predict that overlaps between forward and backward propagating states may significantly enhance backscattering in realistic GNRs.

We also discuss electronic and transport properties of GRNs in the lowest Landau level regime. The interaction between electrons with opposite spin orientation is described by the Hubbard term, and the conductance is calculated within the Landauer formalism by the recursive Green's function technique. Due to Zeeman interaction the self-consistent band structure is spin-split exhibiting two states of different spin orientation propagating in the opposite directions at the same edge. We study the effects of warping and short-range impurities on conductance of interacting electrons in GRNs. Our results show that these states are robust and the conductance near the Dirac point is almost unaffected. We therefore predict that the effect of increase of the magnetoresistance in the vicinity of the Dirac point commonly observed in bulk graphene samples, should be absent in confined geometry of GNRs.

[1] A. A. Shylau, I. V. Zozoulenko, Hengyi Xu, T. Heinzel, *Generic suppression of conductance quantization of interacting electrons in graphene nanoribbons in a perpendicular magnetic field*, Phys. Rev. B **82**, 121410(R) (2010).

Modeling of percolation in size distributed carbon nanostructures networks

Louis-Philippe Simoneau, Alain Rochefort

École Polytechnique de Montréal, Engineering Physics Department and Regroupement québécois sur les matériaux de pointe (RQMP), Montreal, Canada
louis-philippe-2.simoneau@polymtl.ca

Many photovoltaic and display devices rely on the use of transparent electrodes, which are generally rigid and brittle. Once a sufficient number of carbon nanotubes (CNTs) and graphene nanoribbon (GNRs) are connected to form a percolative network, their collective electronic and physical properties make these materials promising candidates for flexible transparent electrodes. The description of the underlying physics, along with an optimization of the characteristic of such nanostructures networks, can be efficiently addressed by computational means. Our understanding of the influence of the array structure on the final quality of the electrode can be improved by the modeling of charge transport in various networks, leading to a more selective optimization of their properties.

Models for charge transport have already been developed for percolation systems with high aspect ratio CNTs, but they typically consider a single parameter to describe the CNT-CNT junctions [1]. However, in such complex materials, the propagation of charge carriers is usually limited by contact resistance that is a strongly dependent characteristic of the multiple network properties [2].

We have developed Monte Carlo (MC) algorithms to study the charge transport in bidimensional networks of CNT and GNR networks by incorporating realistic distributions and descriptions of CNT-CNT (or GNR-GNR) junctions. Our MC algorithms generate random networks with many controlled parameters which can be tuned to represent CNT mats, GNR mats, or other rod-like networks. We then evaluate the total conductance of the generated networks on the basis of individual contacts conductance, which in turn depend on the local network properties. Our results show that the length, diameter, orientation and chirality distributions within the percolative network of the CNT and GNR networks have a great importance on the resulting electrical performances.

References

[1] J. Hicks *et al.*, Phy. Rev. E, **79**, (2009)

[2] P. N. Nirmalraj *et al.*, Nano Lett., **9**, (2009)

Figures
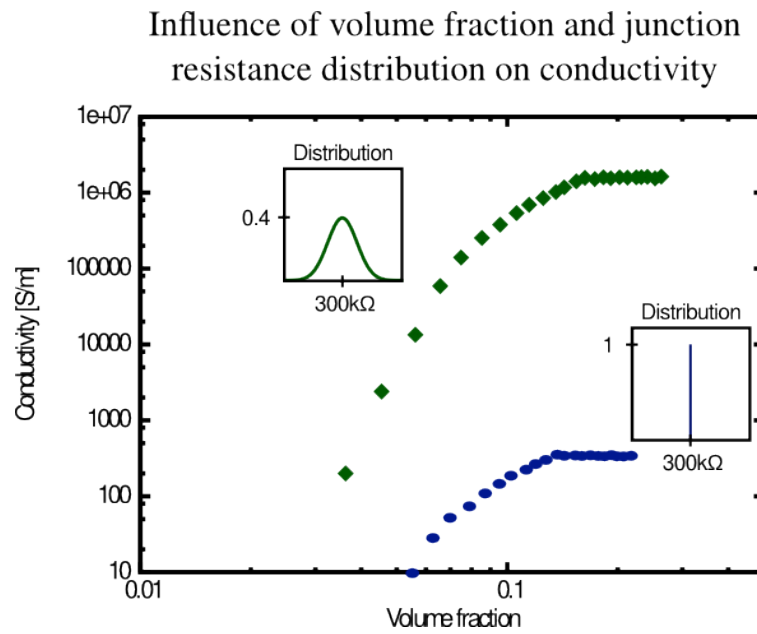
The distribution of the resistance values of the tube-tube junctions within a CNTs network has an important impact on the total conductivity of the system. A greater spread in the junction resistances lead in a higher conductivity.

Shaping Dirac fermions in graphene / h-BN layered systems

J. Slawinska[1], P. Dabrowski[2], I. Wlasny[2], I. Zasada[2], Z. Klusek[2]

[1] Theoretical Physics Department II, Pomorska 149/153, 90-236 Lodz, Poland
[2] Solid State Physics Department, Pomorska 149/153, 90-236 Lodz, Poland
jagoda.slawinska@uni.lodz.pl

Combining graphene and hexagonal boron nitride (h-BN) allows to construct multilayer structures [1] with amazing electronic properties, which are promising both for fundamental studies and novel applications. Since in most electronic devices the band gap is required, many approaches have been proposed to tailor the band structure of graphene for specific applications, especially to tune the energy gap in a controllable way, as in the Bernal stacked bilayer graphene (BLG). Recently, BLG transistors have been fabricated, but still graphene devices on SiO_2 substrate are highly disordered which limits the carrier mobility and suppresses the graphene unique properties. Moreover, in the unbiased bilayer graphene the low energy bands are parabolic, not cone-shaped, which leads to a finite value of the effective mass. The linear dispersion of pristine graphene can be preserved in one of the graphene/h-BN tunable systems, which offers new possibilities based on the properties of massless Dirac fermions.

It emerges in a natural way that structural similarities of graphene and h-BN layers allows to create heterostructures geometrically similar to pristine graphene multilayers with properties depending on number of layers, stacking order, configurations of boron, carbon and nitrogen atoms and on the lattice mismatch. By means of tight binding method and density functional theory, it is demonstrated that in graphene/h-BN analogue of AB bilayer graphene a substrate induced energy gap of about 50 meV should be opened in the spectrum [2, 3]. Using external electric field perpendicular to the layers, the band-gap can be continuously tuned up to 130 or 250 meV depending on the atomic configuration.

In contrast, in the unbiased ABC h-BN/graphene/h-BN sandwich the Dirac cones are exactly preserved in the band structure. It originates from the symmetry between A and B sublattices: it is not broken because both carbon atoms in the unit cell have identical neighbors (boron or nitrogen) either in the top or in the bottom layer. The external electric field breaks the structural symmetry and lifts the degeneracy of energy levels in the K/K' points, thus the band gap can be created in the biased system [4]. This unique mechanism of energy gap tuning in graphene-based systems seems to become useful in modern electronic devices.

Graphene is claimed to be a bridge between condensed matter physics and quantum electrodynamics (QED), in particular the Klein tunneling phenomenon provides the important knowledge of electron propagation through potential barriers [5, 6]. Since graphene/h-BN heterostructures are described in terms of tight binding Hamiltonians constructed in the same manner as for graphene layers, we will discuss the existence of massless or massive Dirac fermions, the chirality and charge conjugation symmetry. We will show that graphene/h-BN hybrids are interesting as complementary systems which should indicate features related to anomalies in Klein tunneling phenomenon.

References

[1] D. Usachov et al., Phys. Rev. B, **82** (2010) 075415.
[2] G. Giovannetti et al., Phys. Rev. B, **76** (2007) 073103.
[3] J. Slawinska, I. Zasada, Z. Klusek, Phys. Rev. B, **81** (2010) 155433.
[4] J. Slawinska, I. Zasada, P. Kosinski, Z. Klusek, Phys. Rev. B, **82** (2010) 085431.
[5] M. I. Katsnelson, K. S. Novoselov, A. K. Geim, Nature Physics, **2** (2006) 620-625.
[6] M. I. Katsnelson, K. S. Novoselov, Solid State Communications, **143** (2007) 3-13.

Figures
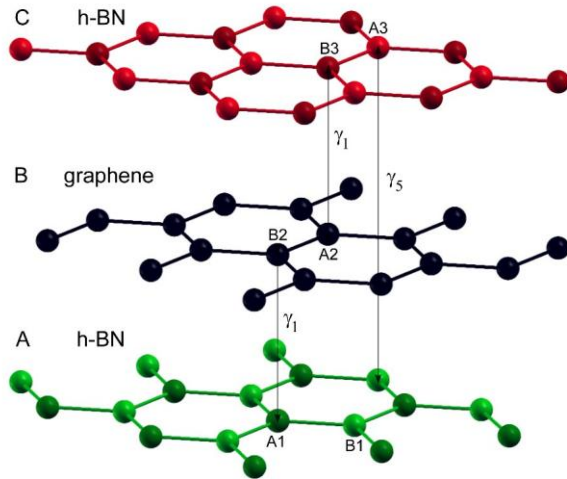
Fig. 1
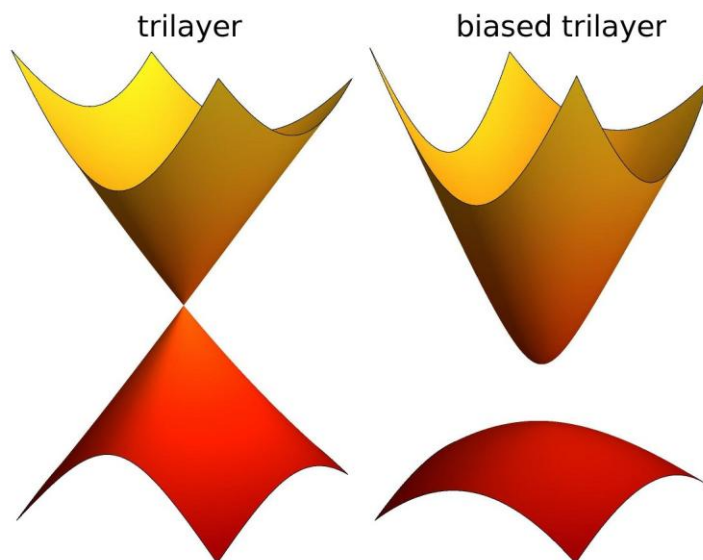
Fig. 2

Fig. 1 Geometry of ABC stacked h-BN/graphene/h-BN trilayer

Fig. 2 Energy gap tuning in ABC stacked h-BN/graphene/h-BN trilayer

Imaging the structure, symmetry and surface-inhibited rotation of polyoxometalate ions on graphene oxide

J. Sloan[1], Z. Liu[2], K. Suenaga[2], M. A. Dyson[1], N. R. Wilson[1], P. A. Pandey[1], L. M. Perkins[3], J. P. Rourke[4], and I. J. Shannon[3]

[1]Department of Physics, University of Warwick, Coventry, CV4 7AL, UK,
[2]National Institute for Advanced Industrial Science and Technology (AIST), Research Centre for Advanced Carbon Materials,Tsukuba, Ibaraki 3058565, Japan,
[3]Department of Chemistry, University of Birmingham, Edgbaston, Birmingham, B15 2TT, UK
[4] Department of Chemistry, University of Warwick, Coventry, CV4 7AL, UK
j.sloan@warwick.ac.uk

Extracting structural information routinely and dynamically from single molecules remains a significant challenge in spite of recent advances in this field. While it has been possible to produce atomically resolved images of static or moving molecules by either scanning tunneling microscopy (STM) or atomic force microscopy (AFM), the structural features produced are imprecise unless highly stringent experimental procedures are applied. Another approach has been to image molecules mounted within carbon nanotubes by low voltage, aberration corrected transmission electron microscopy (AC-TEM). For example, functional groups tethered to fullerenes and the structure of D_{5d} symmetry C_{80} or I_h symmetry $Er_3N@C_{80}$ molecules can be imaged at 80 keV using this approach. However this methodology is limited by the internal van der Waals surface of the host tubules, which restricts both the size of the molecules that can be imaged and also constrains their *in situ* motion. A new prospect is presented by the imaging of molecular-scale species on atomically thin 2D supports such as graphene or graphene oxide (GO).[1] These substrates do not exhibit the steric constraints of nanotubes and provides a periodic support that acts as both an *in situ* calibration and also a crystalline basis for tracking molecular motion.

In this presentation, we show how molecular-scale low-symmetry polyoxometalate anions can be imaged on GO by low-voltage AC-TEM, enabling static and dynamic imaging studies to be performed with precision. Imaging studies were performed on discrete C_{2v} $[\gamma\text{-}SiW_{10}O_{36}]^{8-}$ lacunary Keggin ions, a lower symmetry molecular species than the O_h symmetry $[W_6O_{19}]^{2-}$ ion previously imaged within carbon nanotubes.[2] Polyoxometalates (POMs) are a diverse family of compounds based on assemblies of metal oxide polyhedra with potential applications in medicine, catalysis, electrochemistry, nano-scale devices and as building blocks for more mesoscale superstructures. Lacunary Keggin ions differ from 'full' Keggin ions (e.g. $[\alpha\text{-}PMo_{12}O_{40}]^{3-}$) in that they have a reduced number of polyhedra per anion, exposing a reactive structural defect or 'lacuna' on the POM surface, and form lower symmetry structures that can exhibit greater catalytical activity and a tendency to align preferentially on electrode surfaces. Observing the behaviour of these ions on GO has revealed surface behaviour not previously reported for other ultra-thin TEM supports.

Atomic-resolution imaging of discrete $[\gamma\text{-}SiW_{10}O_{36}]^{8-}$ lacunary Keggin ions dispersed onto monolayer graphene oxide (GO) was achieved by 80kV aberration corrected transmission electron microscopy. Under low electron beam dose, individual anions remained stationary for long enough that a variety of projections of discrete C_{2v} symmetry $[\gamma\text{-}SiW_{10}O_{36}]^{8-}$ anions was observed and structural information extracted with ca. $\pm$ 0.03 nm precision. Unambiguous assignment of the orientation of individual ions with respect to the point symmetry elements was determined. The ion was imaged along its two-fold C_2 axis (Fig. 1(a)-(e)) or orthogonally with respect to one of two non-equivalent mirror planes (i.e. σ_v). Continued electron beam exposure of a second ion imaged orthogonal to σ_v (Fig. 2(a)) causes it to translate and/or rotate in an inhibited fashion so that the ion can be viewed in different relative orientations. The inhibited surface motion of the anion, which is in response to H-bonding-type interactions (Fig. 2(b)), reveals an important new property for GO in that it demonstrably interacts far more strongly with supported molecules than other ultrathin supports, including graphene. This behaviour indicates that GO has more in common with similar substrates used in imaging techniques such as AFM and STM and this feature also sets it apart from other support films used in transmission electron microscopy.

References

[1] N. R. Wilson, P. A. Pandey, R. Beanland, R. J. Young, I. A. Kinlock, L. Gong, Z. Liu, K. Suenaga, J. P. Rourke, S. York, J. Sloan, ACS Nano, **3**, (2009) 2547.

[2] J. Sloan, G. Matthewman, C. Dyer-Smith, A-Y. Sung, Z. Liu, K. Suenaga, A. I. Kirkland, E. Flahaut, ACS Nano **2**, (2008) 966.

[3] J. Sloan, Z. Liu, K. Suenaga, N. R. Wilson, P. A. Pandey, L. M. Perkins, J. P. Rourke, and Ian J. Shannon, Nano Lett. **10**, (2010) 4600.
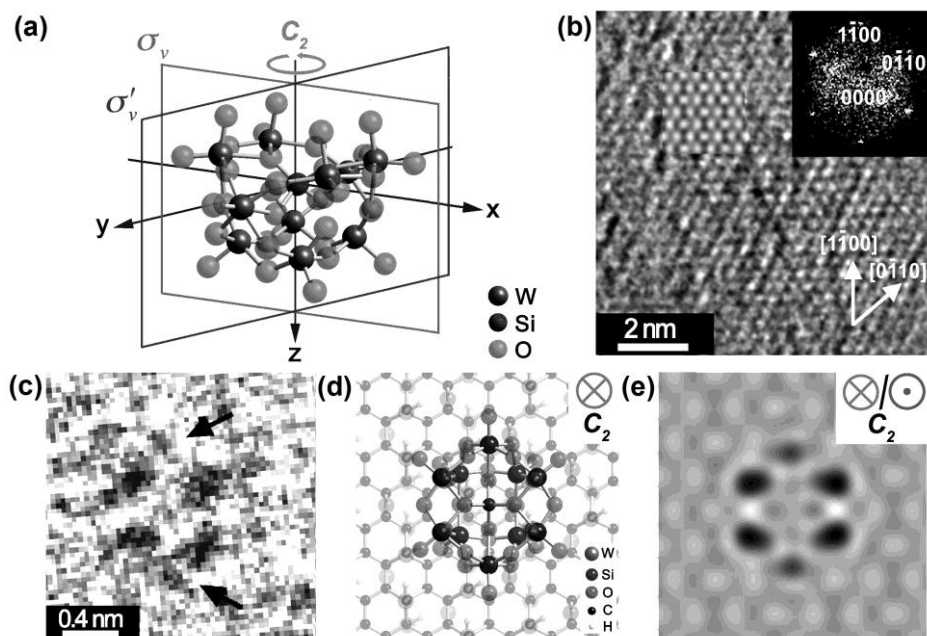
Figures

Figure 1. (a) Perspective view of the $[\gamma\text{-}SiW_{10}O_{36}]^{8-}$ ion with the C_2 axis and non-equivalent σ_v and σ_v' planes indicated. **(b)** HRTEM image of monolayer GO with indexed FFT and inset image simulation based on an ordered GO model[24]. The lattice vectors are indicated at the bottom right. **(c)** $[\gamma\text{-}SiW_{10}O_{36}]^{8-}$ ion imaged approximately along C_2. The two arrows indicate diffuse contrast due to the two single WO_6 octahedra on the periphery of the anion. **(d)** Structure model of a single $[\gamma\text{-}SiW_{10}O_{36}]^{8-}$ ion viewed along C_2 mounted on GO. **(e)** HRTEM image simulation produced from the model in **(d)**. The contrast is identical regardless of whether the anion is viewed along $\otimes$ or $\odot$ with respect to z or situated above or below the GO support.
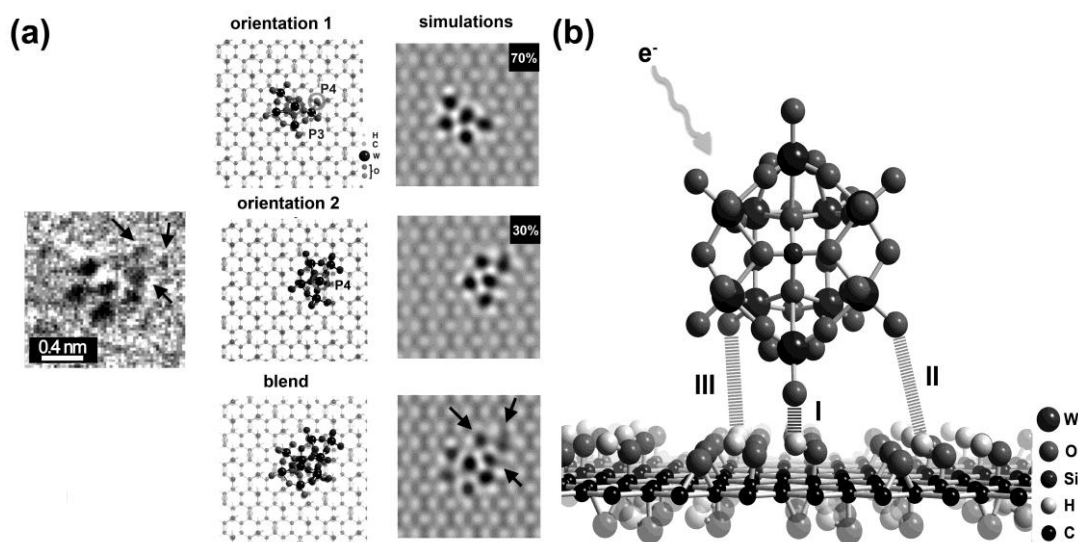
Figure 2(a) 0.8 s exposure HRTEM image (left) of a single $[\gamma\text{-}SiW_{10}O_{36}]^{8-}$ ion supported on monolayer GO. The main black spots correspond to strongly scattering W_2 atom columns. The indicated weaker spots correspond to a secondary orientational state of the anion captured during the exposure. The models (middle column) and simulations (right column) show how these two orientations are 'blended' to produce the final image. **(b)** Perspective schematic depiction of the proposed H-bonding interactions (**I-III**) which constrain the motion of the $[\gamma\text{-}SiW_{10}O_{36}]^{8-}$ ion on GO.

424

Cyclotron resonance of multi-layered epitaxial graphene under very high magnetic field

P. Y. Solane[1], N. Ubrig[1], S. George[1], P. Plochocka[2], M. Potemski[2], O. Portugall[1], C. Berger[3], W.A. De Heer[3]

[1]Laboratoire Nationale des Champs Magnétiques Intenses, 31400, Toulouse, France
[2]Laboratoire National des Champs Magnétiques Intenses, 38042, Grenoble, France
[3]Georgia Institute of Technology, Atlanta, 30328 Georgia, USA

pierre-yves.solane@lncmi-cnrs.fr

We have performed mid-infrared measurements on multi-layered epitaxial graphene probing the fundamental cyclotron resonance

Recent infrared spectroscopy measurements on epitaxial graphene have confirmed the square-root dependence of various intra- and interband transitions with respect to an external magnetic field. So far, these measurements have not included an extended study of the fundamental cylcotron resonance which is obscured by the opacity of the SiC substrate in the relevant energy range. Here we present first results obtained with a CO-laser while using semi-destructive magnetic fields up to 120 T generated with a single-turn-coil. A schematic drawing of the setup is shown in figure 1. Figure 2 shows experimental data which exhibit two prominent features :

1. The absorption peaks marked by black arrows correspond to the cyclotron resonance of graphene, the energy transition from the zeroth to the first Landau level. The position of absorption lines has a square-root dependance with the magnetic field. The measured Fermi velocity is in good agreement with previous measurements [1][2][3].

$$\Delta E_{(L_{-1(0)} \to L_{0(1)})} = v_f \sqrt{2\hbar eB}$$

2. One broad additional absorption line, marked by gray arrows, around 100 Tesla is observed. There is no theoretical predicted transition for single-layer graphene at this magnetic field and this energy excitation.

In this contribution, we present a detailed discussion of the temperature and radiation energy dependence of the observed transitions, which will be substantiated by further experiments.

References

[1] M.L. Sadowski and al, *Solid State Comm.* **143**, 123-125 (2007).
[2] P. Plochocka and al, Physical Review Letters, **100,** 087401 (2008)
[3] N. Ubrig and al (in progress)
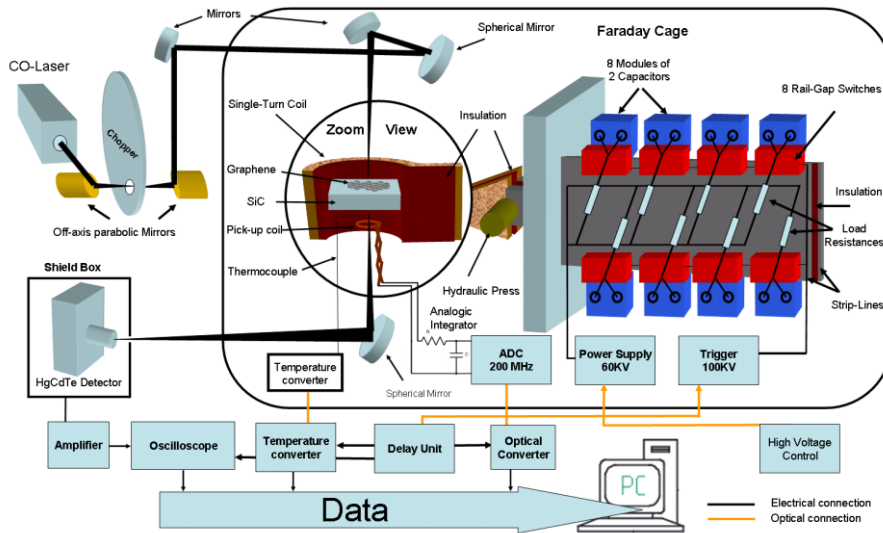
Figure 1 : **Experimental set-up for cyclotron resonance measurements.**
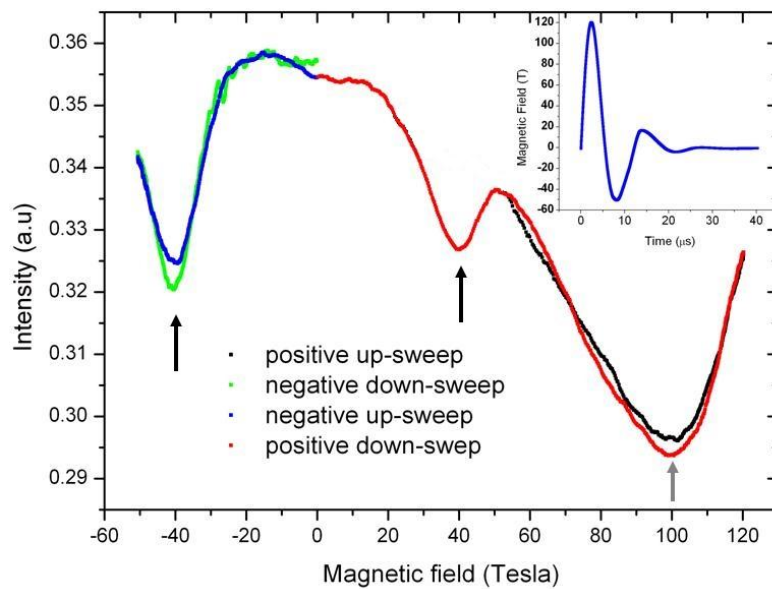
Figure 2 : **Transmission of multi-layered epitaxial graphene grown on Si-C. The incident energy is 229 meV. The magnetic field as a function of time is plotted in the inset. Black arrows are the absorption for the fundamental Landau level transition and gray arrows are an additional observed absorption.**

Precautions for the evaluation of thickness in chemically modified graphene sheets by scanning probe microscopy

P. Solís-Fernández, J. I. Paredes, S. Villar-Rodil, A. Martínez-Alonso, J. M. D. Tascón

Instituto Nacional del Carbón, CSIC, P.O. Box 73, 33080 Oviedo, Spain
pablo@incar.csic.es

Exfoliation and reduction of graphite oxide is one of the most promising ways to obtain processable graphene sheets at large scale in the near future. In order to characterize the properties of the obtained sheets, scanning probe microscopies (SPM) are widely employed. An accurate determination of the thickness is of crucial importance for graphene, due to the fact that its properties are heavily dependent on the number of layers. The common procedure to achieve this is measuring the height of the sheet relative to the employed substrate (sheet-to-substrate). Nonetheless, this method provides some contradictory results, for example in thickness measurements carried out before (GO) and after (rGO) the reduction, which do not show the expected thickness decrease following the reduction [1] due to the removal of oxygen functionalities. In order to clarify the validity of the obtained measures, we have evaluated in this work the effect of both, the nature of the substrate (HOPG, Si/SiO2, mica and borosilicate glass slide) and the specific SPM technique employed (STM, contact AFM and both attractive and repulsive Tapping AFM) in the measured thickness of both GO and rGO individual sheets. The results can be summarized in two general observations [2]:

1. Sheet-to-substrate apparent heights are dependant both on the employed substrate and the specific SPM technique (some examples can be seen in Figure 1).

2. On the other hand, results of sheet-to-sheet measurements (i.e., measuring the thickness of folded sheets, or the thickness in regions where different sheets overlap) provide constant apparent heights regardless of the substrate or the SPM mode (examples of this presented in Figure 1).

In view of these results, it becomes clear that the sheet-to-sheet approach leads to more realistic measurements, while the sheet-to-substrate measurements do not reflect the actual width of the sheets. Thus, measuring thickness over overlapped or bend sheets, provides height values of ~0.9-1.1 nm and ~0.5-0.7 nm for GO and rGO respectively. This decrease in the thickness is the expected behavior, as the reduction involves the removal of a large fraction of the oxygen functional groups that distort the graphitic skeleton. Even so, the thickness is not restored to the value expected for fresh graphene (0.34 nm), as a clear indication for the fact that a considerable proportion of oxygen remains in the sheets after reduction (as complementary XPS and Raman analyses confirm).

Sheet-to-substrate measurements are in general conditioned by differences in the interaction between the SPM tip and the different materials involved (sheet and substrate in the present case). Due to the inherent nature of data acquisition in SPM, those differences are translated into artificial height values. Although the induced error is quite small (a few to several tenths of nm [2]) to present a problem in other conditions, it proves to be crucial for atomically thin sheets, being of the same order as the measured magnitude. Thus, the actual width of the sheets becomes completely masked, providing inconsistent values. With this in mind, a sheet-to-sheet approach would be the convenient choice

whenever possible, thus eliminating the possible artifacts arising from material inhomogeneities and providing more accurate values.

Acknowledgements

References

[1] Paredes J.I., Villar-Rodil S., Solís-Fernández P., Martínez-Alonso A., Tascón J.M.D., Langmuir, **25** (2009) 5957.
[2] Solís-Fernández P., Paredes J.I., Villar-Rodil S., Martínez-Alonso A., Tascón J.M.D., Carbon **48** (2010) 2657.

Figures
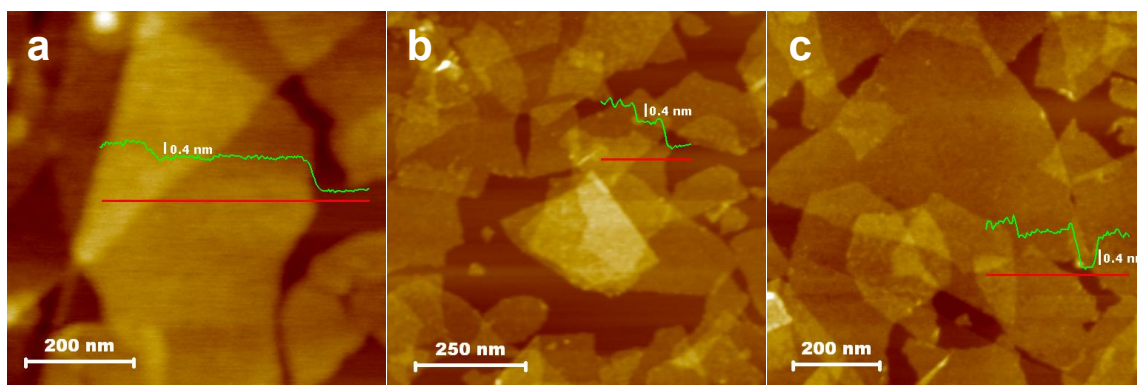
Figure 1. Contact AFM (a), repulsive (b) and attractive tapping (c) images of rGO deposited onto HOPG. Included line profiles show the apparent sheet-to-sheet and sheet-to-substrate heights.

Atomic-scale electron-beam sculpting of defect-free graphene nanostructures

Bo Song, Grégory F. Schneider, Qiang Xu, Grégory Pandraud, Cees Dekker, Henny Zandbergen

Kavli Institute of Nanoscience, Delft University of Technology, Lorentzweg 1, 2628 CJ Delft, The Netherlands

bo.song@tudelft.nl

First isolated in 2004,[1] graphene has received tremendous scientific attention due to its unique electronic properties.[2] Graphene also features edge dynamics[3] and mechanical properties,[4] opening up even more opportunities such as its use to sequence genomic DNA using nanopores.[5] In order to harvest the many promising properties of graphene in applications, a technique is required to cut, shape or sculpt the material on a nanoscale without damage to its atomic structure, as this drastically influences the electronic properties of the nanostructure. Here, we reveal a temperature-dependent self-repair mechanism allowing damage-free atomic-scale sculpting of graphene using a focused electron beam. Our technique allows reproducible fabrication and simultaneous imaging of single-crystalline free-standing nanoribbons, nanotubes, nanopores, and single carbon chains.

Temperature has a remarkable effect on the changes induced by 300 keV electrons (Figure 1). At room temperature (RT), a rapid amorphisation occurs, which prevents detailed high-resolution electron microscopy (HREM). At temperatures of 200 °C, we observe that electron beam irradiation leads to amorphisation with only short range order (Figure 1a). At 500 °C, the electron beam results in the formation of polycrystalline monolayers. The single crystalline graphene transforms into polycrystalline graphene with clear straight but short grain boundaries. At 700 °C, remarkably, graphene conserves its full crystallinity even under a very intense electron beam, as shown in Figure 1c. Figure 2 shows various graphene nanostructures made at 600°C~700°C. Carbon nanotubes can be made using elongated electron beams with a shape similar to the holes made (Figure 2a, inset). Figure 2(b) shows a flat single-walled nanotube (double layer graphene nanoribbon) made from few layers graphene. The inset gives the inferred tube shape with the HREM image averaged by translation, and the observed (red) and estimated (green) hexagon positions for a flat tube. Blue dots in the side view represent individual carbon atoms. Figure 2 (c) shows nanoribbon made from single layer graphene, where the monolayer was first made from few layers graphene. Note that the edges of the nanoribbon are armchair, as are most of the edges of the two holes. Inset shows the image simulation of two carbon ad-atoms attached to the graphene armchair edges and pointed out with red arrows. Figure 2 (d)-(e) showed a double carbon chain and a single carbon chain (formed from the double chain), respectively.

References
[1] K.S. Novoselov et al, Science, 306 (2004) 666.
[2] A.H. Castro Neto et al, Rev. Mod. Phys., 81 (2009) 109.
[3] C. O. Girit et al, Science, 323 (2009) 1705.
[4] C Lee et al, Science, 321 (2008) 385.
[5] G. F. Schneider et al, Nano Lett., 10 (2010) 1912.
[6] This work was supported by Nano-IMaging under Industrial Conditions (NIMIC) and funding from the European Union's Seventh Framework Programme (FP7/2007-2013) under grant agreement n° 201418 (READNA).

Figures
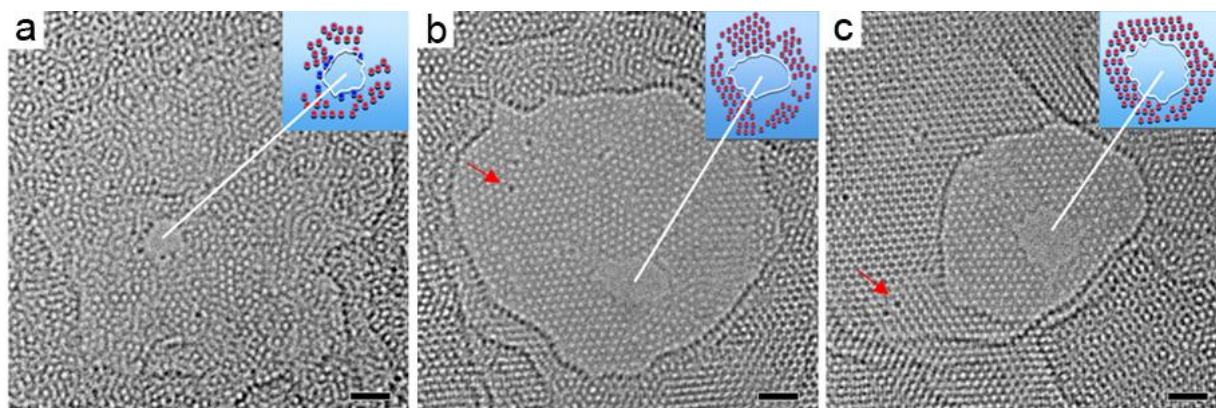
Figure 1. Influence of temperature on the sculpting of few-layer graphene by an electron beam. (a), at 200 °C. (b), at 500 °C. (c), at 700 °C. Red arrows indicate some of the C ad-atoms trapped at defects. The insets in (a)-(c) show the positions of the identifiable hexagons (red dots) and the estimated position of the edge (white line). The blue dots in the inset at 200 °C are ad-atoms. Scale bars, 1nm.
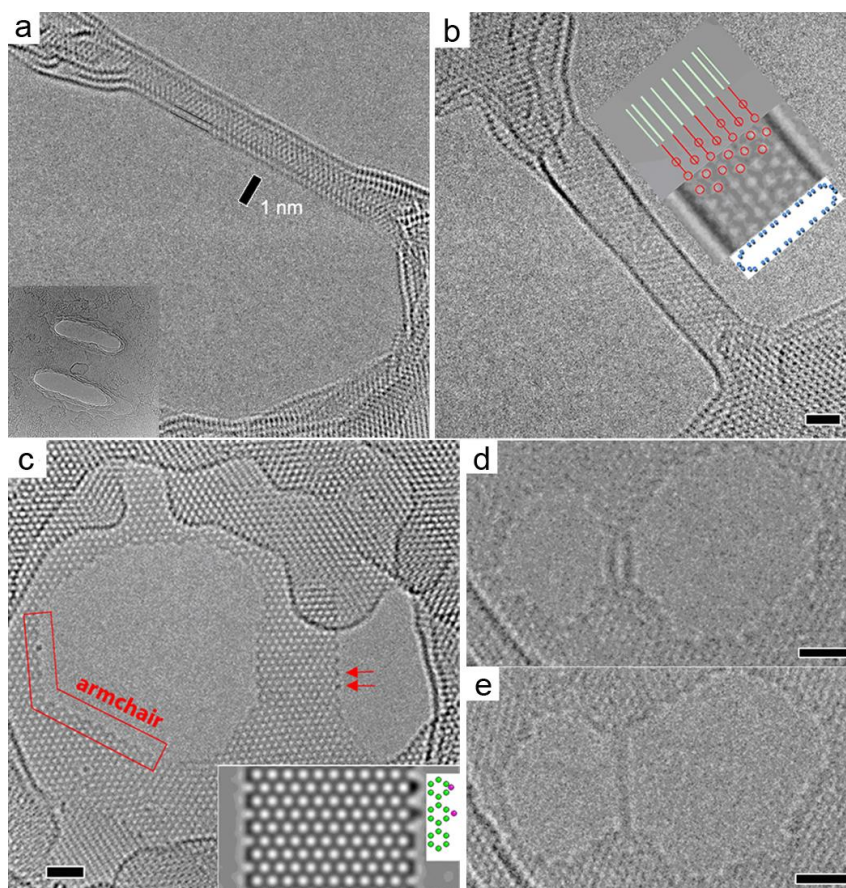
Figure 2. Variety of crystalline carbon nanostructures made with 300 kV electrons at 600-700 °C. (a) double wall carbon nanotube. (b) flat single wall carbon nanotube (double layer graphene nanoribbon). (c) armchair graphene nanoribbon. (d)-(e) carbon chains. Scale bars, 1nm.

Topologically protected edge-states in disordered graphene

David Soriano[1,2], D. Gosálbez-Martínez[1], Joaquín Fernández-Rossier[1] and Juan José Palacios[3]

[1] Dpto. de Física Aplicada, Universidad de Alicante, San Vicente del Raspeig, Spain
[2] Instituto de Ciencia de Materiales de Madrid (CSIC), Cantoblanco, Madrid, Spain
[3] Dpto. de Física de la Materia Condensada, Universidad Autónoma de Madrid, Cantoblanco, Spain
David.Soriano@ua.es

Since its discovery by A. K. Geim and K. Novoselov in 2004[1], Graphene has become one of the most important materials ever synthesized, mainly due to its amazing physical properties. This two-dimensional material, only composed by carbon atoms arranged in a honeycomb lattice, has a breaking strength much higher than steel and electrons can travel through it ballistically lengths close to the sub-micrometer scale. This unusual transport property of graphene is given by the massless Dirac-like behavior the electrons acquire as they move along the lattice.

In the last years, a lot of effort has been made in order to probe magnetism in graphene-based systems. This has opened a new branch in condensed-matter physics called carbon-based spintronics[2]. In this context, hydrogenated graphene[3, 4, 5] and graphene nanoribbons[6], together with zigzag graphene nanoribbons and nanoislands[7, 8] have become the best candidates to improve magnetism in graphene. The sp3-like defects, in the case of hydrogenated graphene samples, or zigzag-shaped edges, in the case of zigzag graphene nanoribbons, give rise to zero-energy states in the electronic structure which are localized around the defects and along the edges respectively. These zero-energy states tend to spin-polarize when the Coulomb interaction is taking into account giving rise to local magnetic moments.

In 2005, Kane and Mele[9,10], included the spin-orbit coupling in Graphene by using a model Hamiltonian containing a complex second-neighbor hopping term (very similar to that used by Haldane in 1988[11] to realize the quantum Hall effect in a honeycomb lattice in the absence of an external magnetic field). By including such interaction, Graphene evolves from a normal insulator to a spin Hall insulator with topologically protected edge states against disorder which preserves time-reversal symmetry. In this context, one can refer to graphene as a Topological Insulator[12]. In this novel phase, the edge states become spin-filtered in the sense that spin-up electrons goes forward in the upper edge and backward in the bottom edge, and inversely for spin-down electrons (Figure 1).

Here we address the electronic properties of a zigzag graphene nanoribbon when both Coulomb repulsion and spin-orbit coupling are considered within **(a)** a mean field Hubbard model with Kane-Mele spin-orbit interaction[13] and **(b)** a tight-binding model within the Slater-Koster approximation where the spin-orbit coupling is introduced by means of an intra-atomic potential[14]. We find that **(1)** spin-orbit interaction give rise to topologically protected edge states against different kind of disorder as Anderson-like or edge disorder (Figure 2a), **(2)** in the presence of spin-orbit coupling the ground state with counter-polarized ferromagnetic edges breaks valley symmetry and, above a critical spin-orbit strength, the gap closes in one valley only, resulting in a valley half-metal (Figure 2b), and **(3)** in the presence of spin-orbit coupling ferromagnetic edges give rise to charge currents in the edges reaching 0.4 nA without an applied magnetic field (Figure 2c).

References

[1] K. S. Novoselov, A. K. Geim, S. V. Morozov, D. Jiang, Y. Zhang, S. V. Dubonos, I. V. Grigorieva and A. A. Firsov , Science, **306** (2004) 666.

[2] O. V. Yazyev, Rep. Prog. Phys., **73** (2010) 056501.

[3] O. V. Yazyev and L. Helm, Phys. Rev. B, **75** (2007) 125408.

[4] D. C. Elias, R. R. Nair, T. M. G. Mohiuddin, S. V. Morozov, P. Blake, M. P. Halsall, A. C. Ferrari, D. W. Boukhvalov, M. I. Katsnelson, A. K. Geim and K. S. Novoselov, Science, **323** (2009) 610.

[5] S. Casolo, O. M. Løvvik, R. Martinazzo and G. F. Tantardini, J. Chem. Phys., **130** (2009) 054704.

[6] D. Soriano, F. Muñoz-Rojas, J. Fernández-Rossier and J. J. Palacios, Phys. Rev. B, **81** (2010) 165409.

[7] F. Muñoz-Rojas, J. Fernández-Rossier and J. J. Palacios, Phys. Rev. Lett., **102** (2009) 136810.

[8] J. Fernández-Rossier and J. J. Palacios, Phys. Rev. Lett., **99** (2007) 177204.

[9] C. L. Kane and E. J. Mele, Phys. Rev. Lett., **95** (2005) 226801.

[10] C. L. Kane and E. J. Mele, Phys. Rev. Lett., **95** (2005) 146802.

[11] F. D. M. Haldane, Phys. Rev. Lett., **61** (1988) 2015.

[12] B. A. Bernevig, T. L. Hughes and S. C. Zhang, Science, **314** (2006) 1757.

[13] D. Soriano and J. Fernández-Rossier, Phys. Rev. B, **81** (2010) 161302.

[14] D. Gosálbez-Martínez, J. J. Palacios and J. Fernández-Rossier, arXiv:1012.0228v1.

Figures
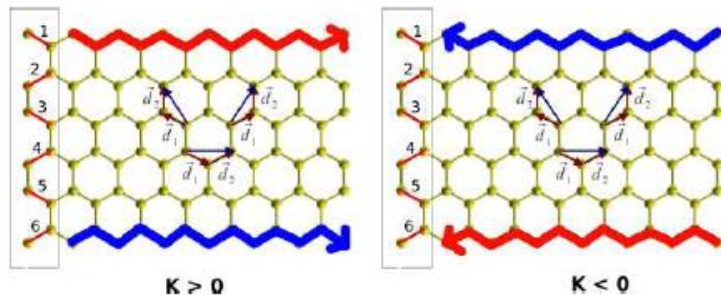
Figure 1. Pictorial description of the spin-orbit term of the Kane-Mele Hamiltonian where the second neighbors are connected along the two nearest neighbor bonds $\vec{d_1}$ and $\vec{d_2}$. It is also shown how electrons with opposite spins (blue and red arrows) propagate in opposite directions in each valley.
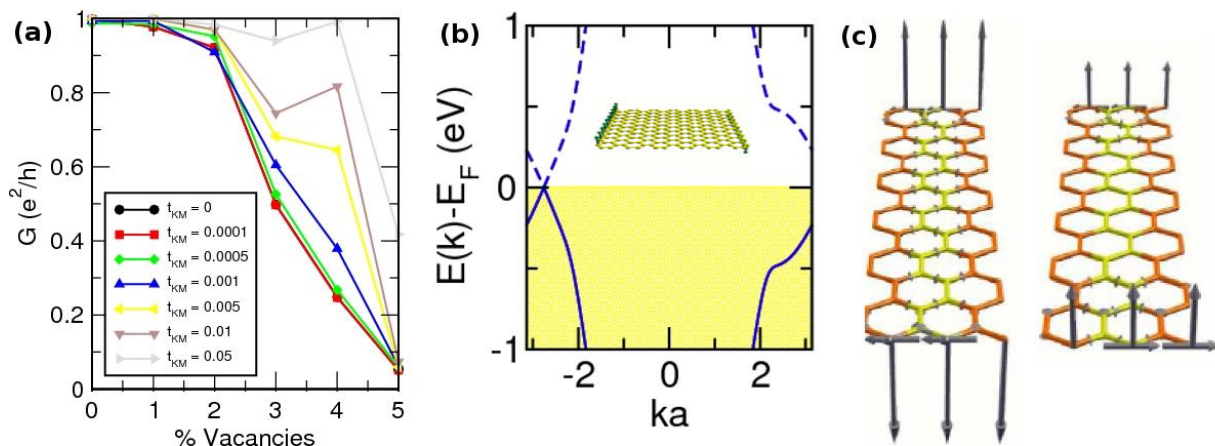
Figure 2. (a) The conductance decreases rapidly as the porcentage of vacancies is increased at the edges. Still, it is always possible to find a value of the spin-orbit coupling for which the edge states are preserved and the conductance approach 1 G_0. (b) For certain values of the spin-orbit coupling, the band structure of zigzag graphene nanoribbons with counterpolarized ferromagnetic edges breaks valley-symmetry giving rise to a valley half-metal. (c) Current and magnetization maps for antiferromagnetic and ferromagnetic zigzag ribbons computed using the Kane-Mele-Hubbard model. Charge currents in the edges approach 0.4 nA without an applied magnetic field.

Effect of Electrolysis Voltage on Graphene Structure Synthesized by One-step Electrolytic Exfoliation in PEDOT/PSS Solution

C. Sriprachuabwong, D. Phokharatkul, A. Wisitsoraat and A. Tuantranont*
National Electronics and Computer Technology Center (NECTEC), 112 Thailand Science Park, Phahon Yothin Rd., Klong 1, Klong Luang, Pathumthani, Thailand
*adisorn.tuantranont@nectec.or.th

Graphene has recently attracted great interest in a wide range of technological applications due to its extraordinary electronic, physical and chemical properties. Nevertheless, its local structures and characteristics are considerably dependant on synthesis method and process conditions. Several graphene production methods including micromechanical cleavage, epitaxial growth via ultra-high vacuum graphitation, chemical synthesis through oxidation of graphite, chemical vapor deposition (CVD), solvothermal synthesis and electrolytic exfoliation have been proposed [1-3]. Among these, electrolytic exfoliation is a relatively new organic solution-based route that is highly attractive due to its high-quality graphene production, low cost, low temperature processing and ease of large-scale production. In this work, we present a new electrolytic exfoliation of graphene in Poly (3,4ethylenedioxythiophene)/poly-styrene-sulfonic acid (PEDOT/PSS) conducting polymer and study the effect of electrolysis voltage on graphene formation.

Electrolytic exfoliation was conducted in an electrolysis cell filled with a commercial PEDOT: PSS solution and a constant voltage ranging from 3 to 12 V was applied between two graphite electrodes. The anode was corroding and a black precipitate was gradually formed in the reactor. The electrolysis time was varied from 5 to 40 hours to obtain stable graphene-PEDOT/PSS dispersion with different graphene concentrations. The dispersed product was centrifuged at 12000 rpm to separate large agglomerates and supernatant portion of the dispersion was decanted. The graphene concentration was estimated from weight loss of the graphite electrode.

The concentration of graphene in PEDOT/PSS solution estimated from weight loss of graphite electrode as a function of electrolytic voltage for various synthesis times are shown in Fig. 1. It can be seen that the concentration of graphene slowly increases as electrolytic voltage increases from 3 to 8 V and then rises more rapidly when the voltage increases further. For the effect of time, the concentration monotonically increases with time as expected. The detailed structure of graphene-PEDOT/PSS composites prepared at various electrolytic voltages for 40 hours are identified and characterized by TEM and selected area electron diffraction (SAED) as illustrated in Fig. 2. It can be seen that structures prepared at different voltages are polygon sheets with different shapes and morphologies. In addition, the size and thickness of graphene structure are increased as the electrolytic voltage increases and crystallinity is improved with the synthesized voltage of 8 V being a critical voltage that produces highly crystalline graphene structure.

Fig. 3 demonstrates Raman spectra from extracted graphene powder synthesized at various electrolytic voltages for 40 hours. It is evident that 2D/D peak ratio increases as the electrolytic voltage increases. This implies that the quality of graphene is improved as the synthesized voltage increases. In addition, 2D bands of all spectra are relatively broad compared to G band suggesting that all synthesized graphenes have multiple layers.

The functional groups of PEDOT/PSS, graphene-PEDOT/PSS and washed graphene powders are characterized by FTIR as illustrated in Fig. 4. It can be seen that the functional groups of graphene-PEDOT/PSS are almost exactly the same those of PEDOT/PSS and the FTIR spectrum of washed graphene confirms that the synthesized structures are graphene not graphene oxide, which typically

exhibits C-O and C=O peaks between 1600-1800 cm^{-1}. From the characterization results, 8 V is thus seen as an optimum electrolysis voltage that produces high-quality single crystal graphene structures in PEDOT/PSS solution.

References

[1] J. K. Wassei, R. B. Kaner, Mater. Today. **13** (2010) 52.

[2] M. Pumera, A. Ambrosi, A. Bonanni, E. K. Chng, H. L. Poh, Trac-Trend Anal. Chem. **29** (2010) 954.

[3] X. Wang, L. J. Zhi, K. Mullen, Nano Lett. **8** (2008) 323.
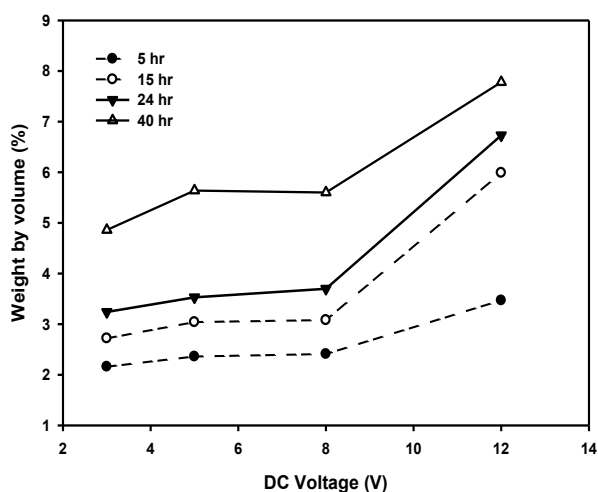
Figure 1. The concentration of graphene in PEDOT/PSS solution estimated from weight loss of graphite electrode as a function of electrolytic voltage for various synthesized times.
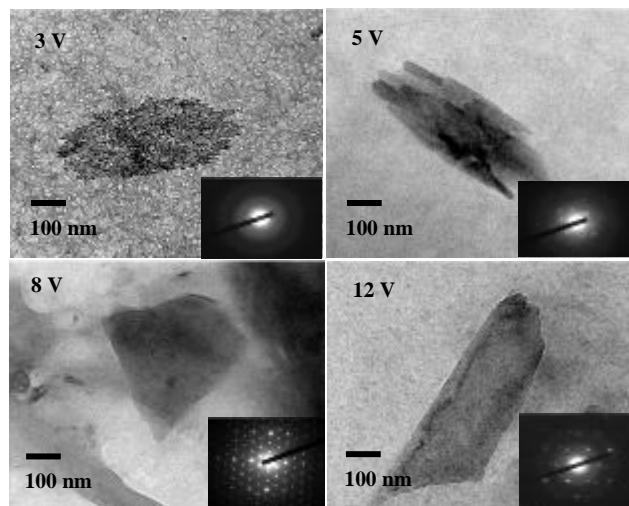
Figure 2. Bright field TEM images with SAED patterns of graphene-PEDOT/PSS composites synthesized at various electrolytic voltages for 40 hours.
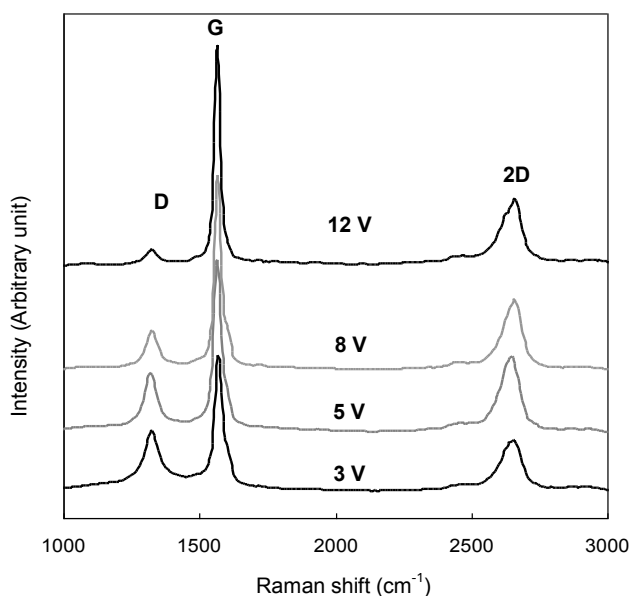
Figure 3. Raman spectra from graphene powders extracted from graphene-PEDOT/PSS composite synthesized at various electrolytic voltages for 40 hours.
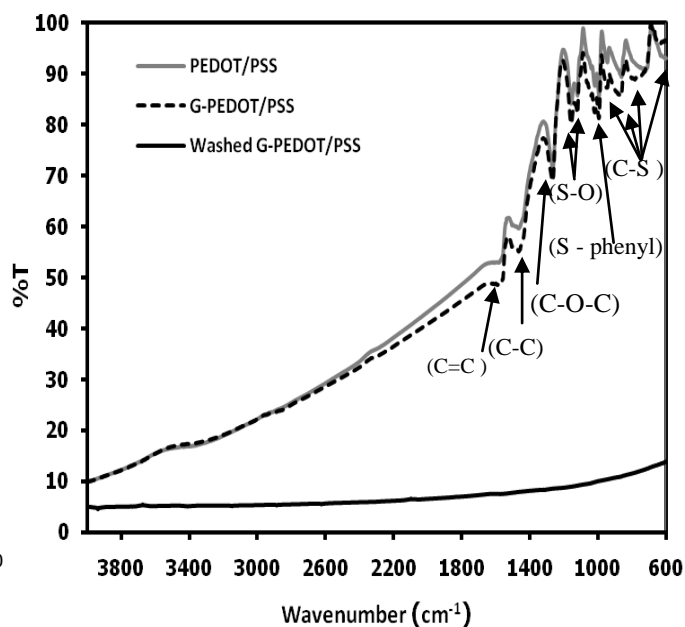
Figure 4. Typical FTIR spectra of PEDOT/PSS, graphene-PEDOT/PSS and washed graphene-PEDOT/PSS. Synthesized voltage and time are 8V and 40 hours, respectively.

Measurable lattice effects in graphene

T. Stauber and G. Gómez-Santos

Dep. de Física de la Materia Condensada, Universidad Autónoma de Madrid, E-28049 Madrid
tobias.stauber@uam.es

We calculate the magnetic susceptibility for the hexagonal tight-binding model [1] using a formalism initially introduced by Fukuyama [2] and find that lattice effects, up to now neglected in the ongoing discussion on the magnetic behavior in graphene, yield a relevant or even dominant contribution when compared to other sources (see figure) [3]. We also find new results for the much studied charge response of graphene and show that lattice effects restore the typical behavior of 2D-Friedel oscillations, observable for reasonably high doping levels [3]. We finally present analytical results for the dynamical polarizability of the hexagonal tight-binding model and discuss the van Hove singularity [4].

Acknowledgments

References

[1] T. Stauber and G. Gómez-Santos, Phys. Rev. B **82**, (2010) 155412.

[2] H. Fukuyama, Progr. Theor. Phys. **45**, (1971) 704.

[3] G. Gómez-Santos and T. Stauber, Phys. Rev. Lett. (in press).
[4] T. Stauber, Phys. Rev. B **82**, (2010) 201404(R).
[5] A. Principi, M. Polini, G. Vignale, and M. I. Katsnelson, Phys. Rev. Lett. **104** (2010) 225503.
[6] F. J. DiSalvo, S. A. Safran, R. C. Haddon, J. V. Waszczak and J. E. Fischer, Phys. Rev. B **20**, (1979) 4883.

Figure
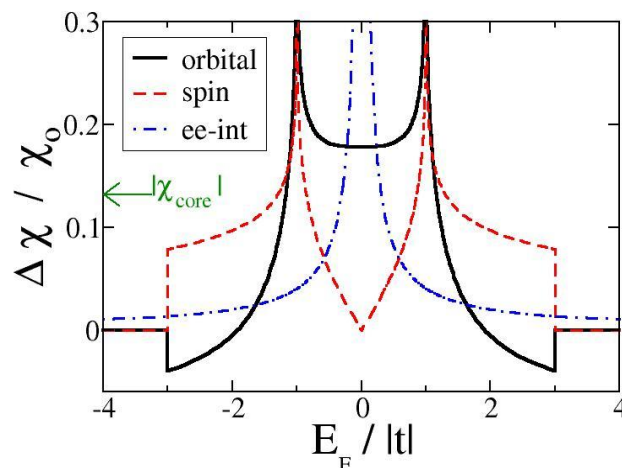
Figure caption: Continuous line: lattice contribution to the orbital magnetic susceptibility [3]. Dashed line: Pauli's spin paramagnetic contribution. Dashed-dotted line: contribution from electron-electron interaction to the orbital susceptibility [5]. The arrow marks an estimate of the absolute value of the diamagnetic contribution from core electrons [6].

Detection of modulated terahertz radiation
using combined plasma and mechanical resonances in torsion oscillating graphene nanoribbons

Y. Stebunov[1], A.V. Arsenin[1], V.G. Leiman[1] and V. Ryzhii[2]

[1]Department of General Physics, Moscow Institute of Physics and Technology,
Dolgoprudny 14170, Russia,
ystebunov@gmail.com
[2]Computational Nano-electronics Laboratory, University of Aizu, Aizu-Wakamatsu 965-8580, Japan

There is a strong need in effective detectors of terahertz (THz) radiation with high spectral selectivity. Recently [1], a resonant detector of modulated THz radiation in a micromachined high-electron mobility transistor (HEMT) with a microcantilever serving as the HEMT gate was proposed and evaluated. This detector utilizes the plasma resonance in the HEMT channel (with the frequency Ω in the THz range) at the carrier frequency of incoming THz radiation and the mechanical resonance (with the frequency Ω_m) at the radiation modulation frequency (usually in the MHz range). The combination of these resonances can lead to a huge response. To extend the THz radiation to the GHz range of modulation frequencies, the carbon nanotube or graphene nanoribbon mechanical oscillator might be used [2, 3].

We propose a novel detector of modulated THz radiation based on section two paralleled clamped elastic graphene nanoribbons (GNR) executing torsional oscillations and evaluate its performance using the developed device model. Device model is schematically shown in Fig. 1.

Symmetrical mode of mechanical oscillator and nonsymmetrical mode of plasma oscillation in two paralleled elastic GNRs are exited in proposed construction. Between these oscillators there is a parametric relation. Plasma oscillations are investigated by means of the transmission line model [3] that developed under satisfaction of quasi-one-dimensional requirement, which hold true for sufficiently narrow graphene ribbons. Mechanical oscillation are appeared due to the variation of electromagnetic energy stored in the system:

$$U = \int \frac{C_{\mathrm{E}} v^2}{2}\, dz,$$

where C_E is capacity of unit length, $v = v(z)$ is length distribution of voltage amplitude. Angular dependence of capacity of two GNR for typical dimensions of the system (length of ribbon 1 μm, their width 10 nm, distance between centers of GNRs 15 nm) is shown in Fig. 2. The output signal is associated with the variations of the displacement current, ΔJ, at the modulation frequency.
It was estimated that resonant frequency of such torsional oscillations is in GHz range [4,5]:

$$\omega_{\mathrm{tors}} = \sqrt{\frac{C}{I}} \approx 1\ \mathrm{GHz},$$

where C is torsional stiffness of clamped GNR and I is their moment of inertia.

So for typical dimensions of given system and bias voltage of 1V the responsivity in resonance can be estimated:

$$R = \frac{\Delta J}{P} \sim 10^{-4} \alpha Q^2 Q_{\mathrm{M}} \left[\frac{\mathrm{A}}{\mathrm{W}} \right],$$

where α is the modulation depth, Q_{M} and Q are the quality factors of the mechanical and plasma oscillations, and P is the power of THz radiation incident to the detector.

Poster

References

[1] V. Ryzhii, M. Ryzhii, Y. Hu, I. Hagiwara and M. S. Shur // *Appl. Phys. Lettl.* **90** (2007) 203503.

[2] V.G.. Leiman, M. Ryzhii, A. Satou, N. Ryabova, V. Ryzhii, T. Otsuji and M.S. Shur // *J. Appl. Phys* **104** (2008) 024514.

[3] V.G. Leiman, A.V. Arsenin, A.D. Gladun, V.L. Semenenko, Y.V. Stebunov, V. Ryzhii // The 2nd International Symposium on Graphene Devices: Technology, Physics, and Modeling, Oct. 27-29, 2010, Tohoku University, Sendai, Japan.

[4] A. Maffucci, G. Miano, F. Villone // *Int. J. Circ. Theor. Appl.* V. 36 (2008).

[5] A. Sakhaee-Pour et al // *Nanotechnology 19 (2008) 085702.*

[6] L.D. Landau and E.M. Lifshitz, Theory of Elasticity, 3rd ed. (Pergamon, Oxford, 1981).

Figures

(a)   (b)
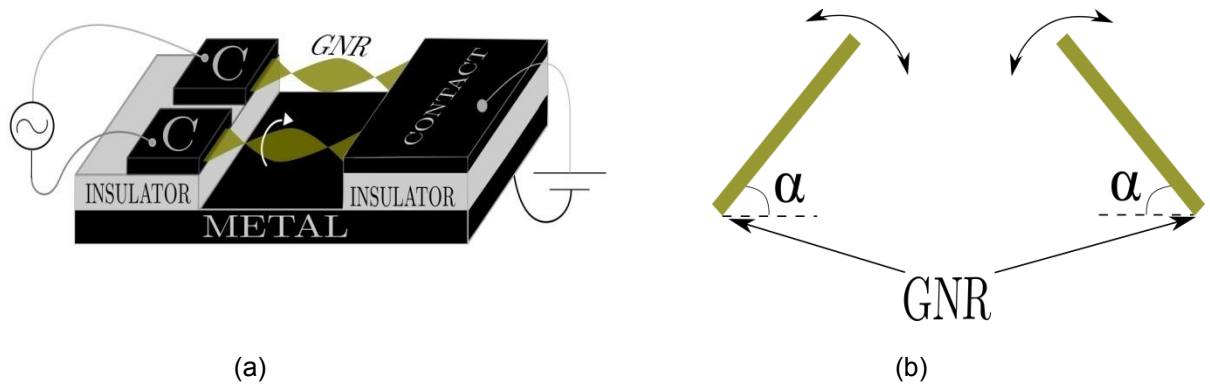
Figure 1. Device model: (a) schematic view of proposed detector and (b) capacitor based on two oscillating GNRs.
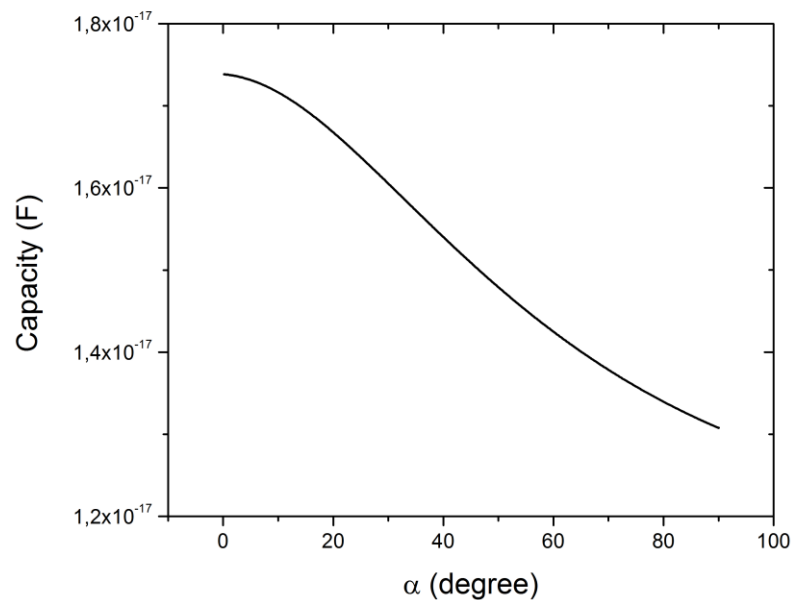
Figure 2. Angular dependence of capacity of two oscillating GNRs.

Fluorescence of laser-created electron-hole plasma in graphene

Rainer J. Stoehr, Roman Kolesov and Joerg Wrachtrup

University of Stuttgart, 3rd Physics Institut, Pfaffenwaldring 57, 70550 Stuttgart, Germany
r.stoehr@physik.uni-stuttgart.de

We present an experimental study of non-linear up- and down-converted luminescence of graphene subject to continuous-wave (cw), pico- and femotsecond laser excitation in the visible and the near infrared [1].

In case of cw visible excitation a spectrally broad down-converted fluorescence can be observed. We attribute this phenomenon to electron hole recombination after thermal equilibration with phonons. However, in the pulsed regime, graphene shows a non-linear luminescence which does not only extend to lower energies but which also reaches to energies higher than the laser excitation energy. This up- and down-converted luminescence originates from the recombination of a high density electron-hole plasma. Since excited charge carries can efficiently exchange energy due to scattering in momentum space the recombination of the resulting non-equilibrium electron-hole pairs yields the observed white light luminescence.

Furthermore, studying the luminescence intensity as a function of layer thickness gives additional insight into its nature and provides a new tool for substrate independent thickness determination of multilayer flakes.

Suspending graphene vertically (perpendicular to the substrate) and measuring the out-of-plane polarization dependence shows that this luminescence can only be excited with the laser beam electric field being parallel to the graphene plane. From this, the matrix elements for the electronic inter-band transitions can be determined.

References

[1] R.J. Stoehr, R. Kolesov, J. Pflaum and J. Wrachtrup, Phys. Rev. B, **82** (2010) 121408(R).
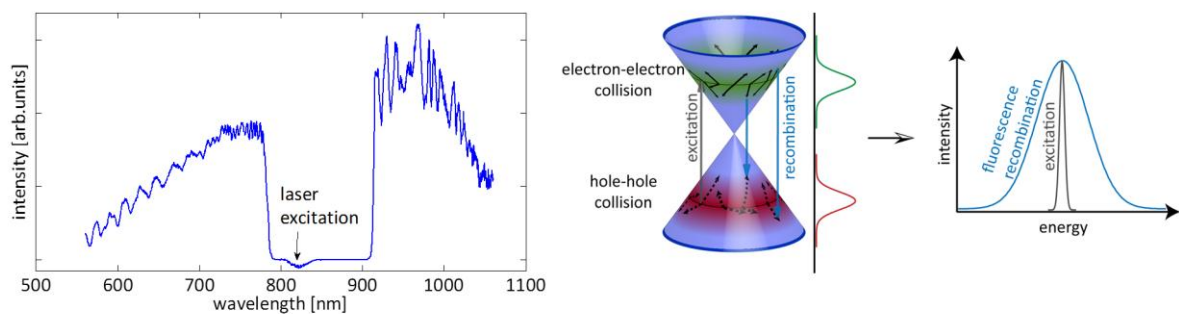
Left: Emission spectrum of a single graphene layer under picosecond excitation of 820 nm wavelength. Right: schematic representation of the 2D dispersion relation of graphene. The gray arrow shows the optical excitation of initially monoenergetic electron-hole pairs. Collisions lead to a broadening of the energy distribution as shown by the green and red curves. Recombination of shifted electron-hole pairs leads a broad fluorescence centered around the excitation energy.

Probing residual strain in epitaxial graphene layers grown on 4H-silicon carbide (000$\bar{1}$) with Raman Spectroscopy

A.J Strudwick, G.L Creeth, N.A.B Johansson & C.H Marrows

School of physics and Astronomy, University of Leeds, Leeds, UK, LS2 9JT
phy4ajs@leeds.ac.uk

Thermal decomposition of silicon carbide (SiC) in either UHV or inert gas atmospheres has shown promise as a process to allow the early exciting electrical properties [1,2] of graphene to be integrated into large scale electronics manufacturing . In this process, SiC is heated to temperatures ~1200°C or higher, at these high temperatures the Si preferentially evaporates away from the surface, thus leaving behind a carbon-rich surface that reconstructs to form a sp^2 bonded epitaxial graphene (EG) layer.[3]

Work here has concentrated on the carbon-terminated (000$\bar{1}$) face of 4H-SiC, EG grown on this face has been shown to provide higher carrier mobilities when compared to the silicon-terminated (0001) face [4]. EG grown on the (000$\bar{1}$) face has been proven to grow with rotational disorder between layers, rather than Bernal stacking, causing the graphene layers to be decoupled from each other and allowing multilayer films to maintain the electronic properties associated with single-layer graphene [5].

A series of techniques have been used to characterize our epitaxial graphene samples. In situ LEED measurements show the expected ring pattern associated with EG grown on SiC(000$\bar{1}$) at an onset temperature of around 1300°C with a full graphene film seen for 30 an anneal time of 30 minutes at this temperature. AFM shows a domain like structure with typical lateral grain size of 1µm for samples annealed at 1400°C which is an order of magnitude larger than the grain size observed in samples annealed at 1300°C. LEEM I-V measurements show areas with coherent response signals that are 2-3 µm in lateral size, suggesting a grouping together of the smaller domains seen in AFM micrographs. LEEM I-V measurements also show the samples to be around 2-3 monolayers thick, this measurement is consistent with recent preliminary TEM measurements.

The main focus of this work is the use of Raman microscopy to probe strains present in EG sheets on SiC (000$\bar{1}$) [6] formed at different anneal times (10-50 minutes) at a temperature of 1400°C in UHV (10^{-10} mbar). The strains where calculated by tracking the average 2D peak position deviation from a reference position measured in free-standing exfoliated graphene [7], then using a similar process to previous work on EG (0001) [8,9] strain values can be extracted by linking the Raman shifts to the strains via the Grüneisen parameter of graphene . A compressive strain is seen to increase with anneal time to a maximum value of -0.5% which is less than the -0.9% which would be expected if the strain was caused by differential contraction between the EG and SiC, a model which has fit well to work on EG on SiC(0001) [8,9]. This discrepancy has been attributed to the rotational disorder present during EG growth on SiC(000$\bar{1}$) which allows greater decoupling between graphene layers and therefore strain relief.[6] The understanding of the strains present within these epitaxial graphene films is off importance as they have been shown to affect electronic properties such as band gaps [10,11] and carrier mobilities.[8]

References
[1] K S. Novoselov et al, Science, **306** (2004) 666.
[2] N M R. Peres, Rev. Mod. Phys. **82** (2010) 2673.
[3] C. Berger et al, J. Phys. Chem. B. **108** (2004) 19912
[4] F. Schwierz, Nat Nano. **5** (2010) 487
[5] J. Hass et al, Phys. Rev. Lett. **100** (2008) 125504
[6] A J. Strudwick et al, APL, at press (2011)
[7] A C. Ferrari et al, Phys. Rev. Lett. **97** (2006) 187401
[8] J A. Robinson et al, Nano Lett. **9** (2009) 2873
[9] N. Mounet et al, Phys. Rev. B, **71** (2005) 205214
[10] Z H. Ni et al, ACS Nano, **2** (2008) 2301
[11] G. Cocco, Phys. Rev. B, **81** (2010) 241412

Figures
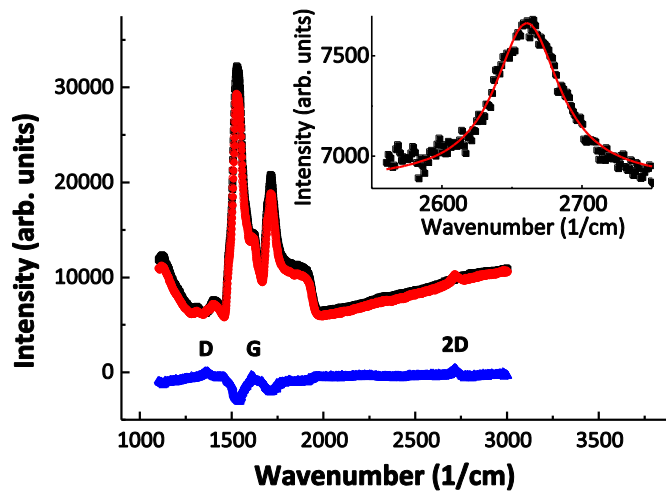
Fig. 1. Examples of Raman spectra of EG on SiC. Spectra are shown for the blank SiC (black squares) and for EG graphene after a 28 minute anneal at 1400°C (red circles). The results of subtracting the background are shown using the blue triangle data markers. The D,G, and 2D band peaks are marked. Only the latter is not obscured by features in the SiC spectrum. Inset: Example of a Lorentzian fit to determine the width and position of a 2D peak [6]
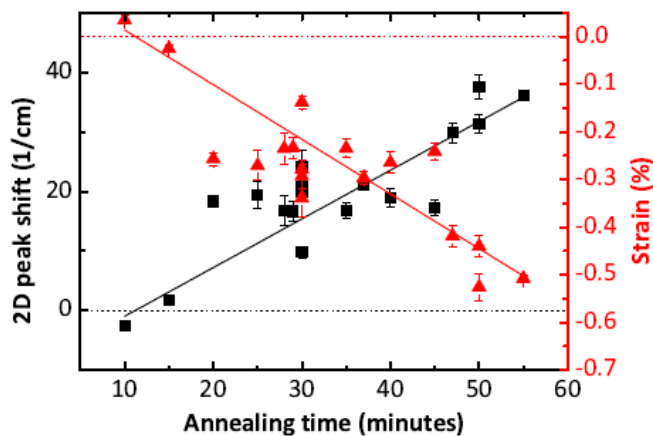
Fig. 2. Variation of 2D peak position shift from that for free-standing exfoliated graphene of 2642 cm^{-1} (squares) and calculated resulting strain values (triangles) as functions of UHV anneal times for an annealing temperature of 1400°C. The dotted lines are the zeroes of the two ordinate axes. The straight lines are linear fits to the data, and have a reduced R^2 value of 0.928.[6]

Graphene Epitaxy by Chemical Vapor Deposition on SiC

W.Strupinski[1], A.Grüneis[2], D.Haberer[2], T.Szkopek[3], K.Grodecki[1,4] and J.M.Baranowski[1,4]

[1]Institute of Electronic Materials Technology, Wolczynska 133, 01-919 Warsaw, Poland
[2]IFW Dresden, P.O. Box 270116, D-01171 Dresden, Germany
[3]Dept. of Electrical & Computer Engineering, McGill University, 3480 University Street, Montreal, H3A-2A7, Canada
[4]Faculty of Physics, University of Warsaw, Hoza 69, 00-681 Warsaw, Poland

wlodek.strupinski@itme.edu.pl

Graphene, a single sp^2-bonded carbon atomic sheet that is deposited on a SiC substrate has great potential for micro-electronics applications, including conventional components such as high frequency analog devices, and devices in emerging fields such as spintronics, terahertz oscillators, and single-molecule gas sensors. However, a major factor hindering the development of technology for the large-scale production of graphene-based nanoelectronic devices is the lack of access to high-quality uniform graphene layers grown on large SiC substrates. Graphene produced by sublimating Si from SiC heated to high temperatures (1200-2000°C) is sensitive to the surface quality of the SiC substrates. Concurrently, the CVD epitaxial growth of graphene on metal substrates has lately received much attention. Unfortunately, epitaxial growth on metals suffers from the disadvantage that electronic applications require graphene on an insulating substrate, and although wafer-scale transfer is possible, it is a difficult process. A fundamental question thus arises: how can one reduce the dependence of graphene growth on substrate quality and simultaneously improve graphene layer uniformity?

In this paper, we report the CVD of epitaxial graphene (CVD-EG) on SiC substrates using propane gas as the carbon precursor. Graphene layers were grown using a commercially available horizontal CVD hot-wall reactor (Aixtron VP508), which is inductively heated with an rf generator. The epitaxial CVD of graphene relies critically on the creation of dynamic flow conditions in the reactor that simultaneously stop Si sublimation and enable the mass transport of propane to the SiC substrate. Tuning the value of the Reynolds number Re enables the formation of optimized Ar boundary layer (BL). Propane that diffuses across the Ar BL to the SiC surface thermally decomposes, and the deposition of epitaxial graphene occurs on the SiC surface. The most critical step is to protect the SiC substrate against Si sublimation at conditions of high temperature ($T \approx 1600^o$C) and low Ar pressure (P). While protecting against Si sublimation, C deposition was enabled with one monolayer resolution by taking advantage of the high efficiency of kinetic processes at high T and low P. Additionally, the formation of FLG is possible on the Si-face SiC(0001) which, in comparison to max 2-3 ML of S-EG, creates greater research opportunities. The proposed method permits the growth rate of graphene on the C-face of SiC(000-1) to be considerably lowered enabling the growth of 1ML, which is extremely difficult in the case of S-EG.

Epitaxial carbon films were deposited predominantly on Si-faces of both semi-insulating and conductive on-axis 4H-SiC substrates. To prove high quality of CVD graphene the ARPES measurements have been performed. The results for layer grown on SiC(0001) are presented below. ARPES data clearly show the expected linear dispersion for relativistic electrons near Dirac point (fig.1). In addition, the samples were characterized by scanning tunneling microscopy (STM) and micro-Raman spectroscopy. The thickness of the graphene films were estimated by ellipsometry. The transport parameters of the graphene samples were measured with the van der Pauw method at room temperature. The electron density in several 1-2 ML graphene films grown in subsequent processes was typically $2\text{-}4\times10^{12}$ cm^{-2}, with a macroscopically averaged electron mobility in the range 1200-1800 cm^2/Vs, demonstrating the high electronic quality of the CVD-EG layers on the wafer scale.

The approach proposed here offers numerous potential benefits in comparison to S-EG (sublimated epitaxial graphene), including the application of well-developed commercial epi-systems for SiC epitaxy and the reduction of substrate surface influence on graphene thickness uniformity. Our proposed approach enables precise growth rate control by adjusting the mass transport of the carbon precursor in a similar way to the method used in MOCVD/CVD, as well as the passivation of the SiC substrate by any substances prior to graphene growth. Moreover, one can tune the reactor conditions to grow both CVD-EG and S-EG in the same system. This work is a significant step toward developing a graphene-on-SiC technology that is suitable for industrial scale production in commercial CVD reactors.
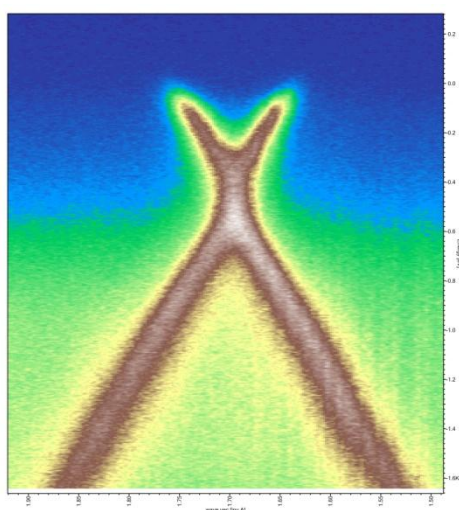
Fig.1 . ARPES spectrum of the CVD-EG grown on an on-axis 4H-SiC(0001) substrate.

A Graphene Nanoribbon Memory Cell

Eberhard Ulrich Stützel,[1] Marko Burghard,[1] Klaus Kern,[1,2] Floriano Traversi,[3] Fabrizio Nichele,[3] Roman Sordan[3]

[1] Max-Planck-Institut für Festkörperforschung, Heisenbergstr. 1, 70569 Stuttgart, Germany
[2] Institut de Physique de la Matière Condensée, Ecole Polytechnique Fédérale de Lausanne, 1015 Lausanne, Switzerland
[3] L-NESS, Department of Physics, Politecnico di Milano, Polo di Como, Via Anzani 42, 22100 Como, Italy
e.stuetzel@fkf.mpg.de

The past few years have witnessed a surge of interest in graphene, a recently isolated single sheet of graphite. Due to the absence of a bandgap in graphene and the formation of electron-hole puddles, graphene-based field-effect transistors cannot be turned off, thus limiting their application in electronic circuits. A strategy to increase the on/off ration relies upon patterning of graphene nanoribbons (GNRs), wherein quantum confinement opens a bandgap inversely proportional to the ribbon width.

Here, we demonstrate the operation of a digital memory cell consisting of a single GNR based on a nondestructive storage mechanism [1]. The devices are fabricated by patterning graphene into nanoribbons using V_2O_5 nanofibers as etching masks. A pronounced memory effect is observed under ambient conditions, which is attributed to charge traps in the vicinity of the GNRs. Gate voltage pulses of opposite polarity enable reliable switching between the distinct on- and off-states of the device for clock frequencies of up to 1 kHz and pulse durations as short as 500 ns for $> 10^7$ cycles. The durable and stable memory cell can be rendered nonvolatile upon exclusion of oxygen and humidity. Graphene nanoribbons thus emerge as promising components of highly integrated memory arrays.

References

[1] Eberhard Ulrich Stützel, Marko Burghard, Klaus Kern, Floriano Traversi, Fabrizio Nichele, Roman Sordan, *Small*, **6** (2010) 2822

Figures
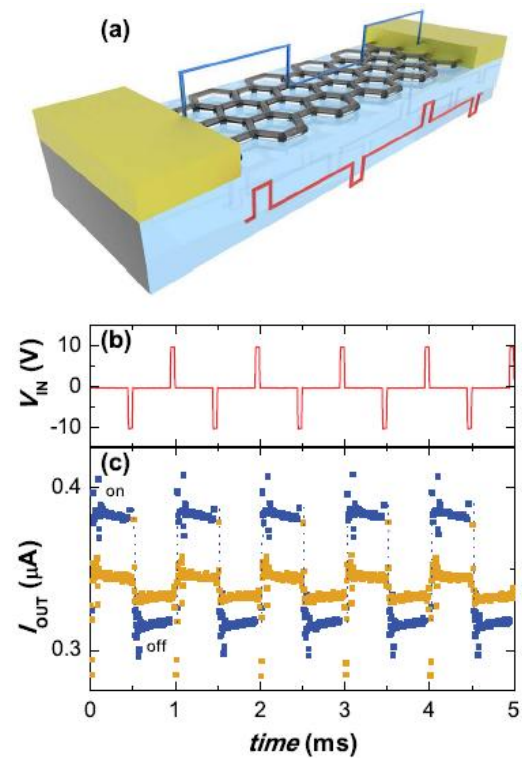
Figure 1: Digital waveforms gained from the GNR device under ambient conditions. (a): A schematic of the fabricated GNR memory device. The input trigger signal is the gate voltage (red) and the output signal is the drain current (blue). (b) Trigger signal at a frequency 1 kHz and a duty cycle of 10%. (c) Drain current at a drain bias of 1 V with an input signal frequency of 1 kHz. Two different duty cycles were used: 10 % (blue; pulse duration of 50 µs) and 0.1 % (gold; pulse duration of 500 ns).

Graphene Assemblies and Hybrids for Energy Conversion and Storage

Chengmeng Chen[1,2], Qiang Zhang[2], Xiaochen Zhao[2], Yonggang Yang[1], Quanhong Yang[1], Maozhang Wang[1], Robert Schlögl[2], **Dang Sheng Su**[2*]

1 Key Laboratory of Carbon Materials, Institute of Coal Chemistry, Chinese Academy of Sciences, 27 Taoyuan South Road, 030001 Taiyuan, China
2 Department of Inorganic Chemistry, Fritz Haber Institute of Max Planck Society, Faradayweg 4-6, 14195 Berlin, Germany

dangsheng@fhi-berlin.mpg.de

As a one-atom-thick two-dimensional crystal with unique electronic, mechanical, optical, and thermal properties, graphene has attracted great attention from scientific community. Graphite, a natural mineral compound formed after aeons of harsh geological process underground, is fundamentally composed of millions of graphene sheets stacking together. It is believed to be a low cost, easy accessible resource for scale-up graphene production, because functional graphene nanoplatates with single to several layers of graphene could be easily exfoliated from graphite oxide through mild ultrasonication or thermal expansion [1].

The chemically derived graphene sheets are often decorated by abundant intrinsic active sites, such as functional groups (mainly -OH, -COOH, -C=O, -C-O-C-), lattice defect (atom vacancy, distortion, dangling bonds) on the lateral surface and edge. On one hand, the introduction of functional groups increased the wettability and solvent compatibility of graphene, which offers an opportunity for macroscopic ordered assembly of graphene in solution based approach. On the other hand, the active sites could be further modified by surface reaction with heteroatoms such as nitrogen, boron, and phosphorus, so as to tune the acid/base property and electronic structure of graphene. These specific advantages provided tunable surface chemistry of graphene for advanced energy conversion and storage [2, 3].

The present research has been carried out following generally two mainlines including graphene assemblies from graphene oxide and graphene hybrids from reduced graphene oxide (as shown in Figure 1). The highlights of our work are as follows,

a) Graphite oxide was an element for graphene based advanced functional materials. Flexible, semi-transparent, and free-standing graphite oxide membranes (Figure 2a, 2b) could be fabricated at the liquid/air interface through a facile and efficient self-assemble method. Such macroscopic membranes are constructed from individual graphene oxide sheets by layer-by-layer stacking and show excellent mechanical and optical performance [4, 5].

b) To efficiently produce chemical-exfoliation-based production of graphene starting from graphite oxide, the preheated high-temperature environment is believed to be very critical. By introducing a high vacuum to the exfoliation process, high quality graphene sheet (Figure 2c) is available at a mild temperature, the exfoliated graphenes demonstrate an excellent energy storage performance, and the electrochemical capacitance is much higher than that of the high-temperature exfoliated ones. This vacuum exfoliation approach presents us with a possibility for a mass production of graphenes at low cost and great potentials in energy storage applications of graphene-based materials [6].

c) Graphene-based architectures have attracted much attention as a viable support material to improve the efficiency of various catalytic reactions, energy conversion and storage. The abundant functional groups, lattice defect provided tunable surface chemistry of graphene sheets. However, graphene sheets are always tending to form irreversible agglomerates through the van der Waals interaction. To demonstrate the extraordinary performance of the graphene, novel type hybrid

composites by combining nanomaterials with distinct structures and dimensions with unexpected properties and unique applications was a good solution. We proposed two strategies to fully demonstrate its potential for energy storage. The first route is introducing the secondary phase to separate graphene sheets. For instance, in present research, tin, which has a theoretical capacity of 992 mAhg^{-1}, has been proposed as one of the most promising anode materials for the coming decades and selected as the separator. A SnO$_2$/graphene hybrid was explored for energy storage application (Figure 2d). On the other hand, the graphene sheet was mediated by N, P, B doping. As an electron donor and acid-base adjuster, nitrogen modification has been proved to be a valid way to tune the chemical and electrical environment of carbon surface. The N modified nanocarbon materials often exhibits an exceptional property towards anchoring and nucleation of active species, such as metal ions, clusters and coordinated complex in solution based process. We expected that doped graphene was a novel platform for advanced graphene based materials for energy storage [7].

Through those efforts, graphene based assemblies and hybrids are expected to be a novel platform for advanced energy conversion and storage for sustainable society.

References

[1] Y. G. Yang et al., New Carbon Mater. 23 (2008) 193.
[2] M. Pumera, Chem. Soc. Rev. 39 (2010) 4146.
[3] D. S. Su et al., ChemSusChem 3 (2010) 169.
[4] C. M. Chen et al., Adv. Mater. 21 (2009) 3541.
[5] C. M. Chen et al., New Carbon Mater. 23 (2008) 345.
[6] W. Lv et al., ACS Nano 3 (2009) 3730.
[7] This research work was supported by the "Joint PHD Promotion Programme 2010" between Max Planck Society and Chinese Academy of Sciences.

Figures
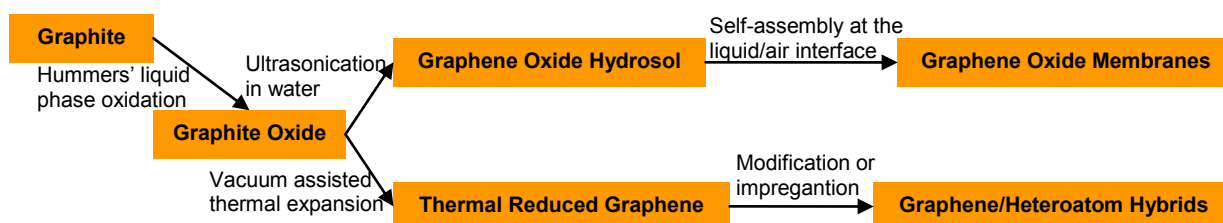
Figure 1. Route map of graphene based assemblies and hybrids for advanced energy conversion and storage
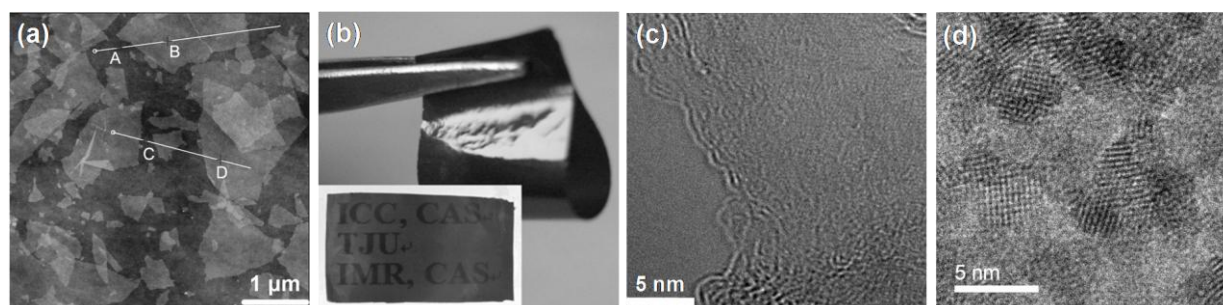
Figure 2. (a) AFM image of graphene oxide; (b) Self-assembled free-standing graphite oxide membrane; (c) HRTEM image of thermal reduced graphene oxide; (d) HRTEM image of SnO$_2$@RGO hybrids

Theoretical Design of High-Spin Polycyclic Hydrocarbon Materials

Nicolas Suaud, Georges Trinquier, Jean-Paul Malrieu, Nathalie Guihéry

Laboratoire de Chimie et Physique Quantiques, Université Paul Sabatier, 118 route de Narbonne, Toulouse, France
suaud@irsamc.ups-tlse.fr

This work addresses the conception of purely-organic magnetic materials. A first part is dedicated to the conception of high-spin organic building blocks obtained from fused polycyclic hydrocarbons by converting selected $HC(sp^2)$ sites into $H_2C(sp^3)$ ones, guided by Ovchinnikov's rule. Some molecules involving three to twelve fused six-member carbon rings are presented. Unrestricted DFT calculations, including geometry optimizations, confirm the high-spin multiplicity of ground states. Spin-density distributions and low-energy spectra are further studied through geometry-dependent Heisenberg–Hamiltonian diagonalizations and explicit correlated *ab initio* treatments (DDCI), which all agree on the high-spin character of the suggested structures, and locate the low-lying states at significantly higher energies. In particular, the lowest-lying state of lower multiplicity is always found to be higher than kT at room temperature (at least ten times higher).

The second part is focused on the conception of ferro-, ferri- and antiferromagnetic periodic bi-dimensional lattices. For this purpose, the nature and magnitude of magnetic coupling between the high-spin units are analyzed as functions of the topology of the connection. Simple rules to predict the preferred spin ordering between the units are established, resulting from the interplay between two main physical factors, namely (i) the spin-polarization of the bridge, and (ii) the M_s-spin component of the connecting carbons on each magnetic unit. The relevance of these rules is confirmed by UDFT calculations performed on bi-unit fragments.

References

[1] Georges Trinquier, Nicolas Suaud, Jean-Paul Malrieu, Chem. Euro. J, **29** (2010) 8762-8772.
[2] Georges Trinquier, Nicolas Suaud, Nathalie Guihéry, Jean-Paul Malrieu, to be submitted.

Figures

Smart

$S=0$ $S=3$
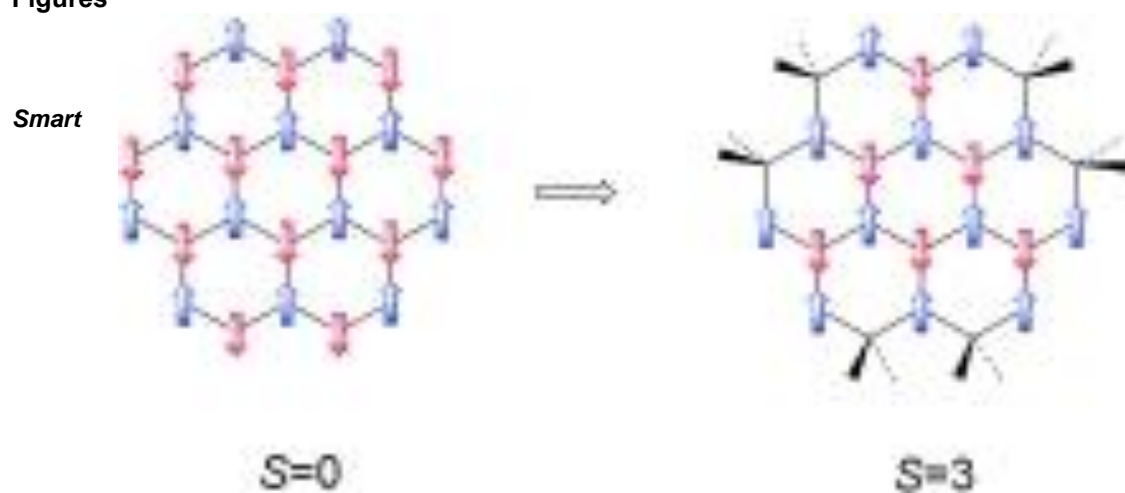
saturation: *Saturating properly chosen vertices of polycyclic conjugated hydrocarbons may lead to high-spin organic units*

Confined states and edge state on graphene nanoislands probed by scanning tunneling spectroscopy

D. Subramaniam[1,3], C. Pauly[1,3], V. Geringer[1,3], R. Reiter[2], M. Pratzer[1,3], M. Liebmann[1,3], C. Busse[4], Y. Li[1,3], R. Mazzarello[1,3], F. Libisch[2], T. Michely[4], and M. Morgenstern[1,3]

[1]II. Institute of Physics B, RWTH Aachen University, Otto-Blumenthal-Straße, 52074 Aachen, Germany
[2]Institut für theoretische Physik, Technische Universität Wien, Austria
[3]Jülich-Aachen Research Alliance: Fundamentals of Future Information Technology (JARA-FIT), Otto-Blumenthal-Straße, 52074 Aachen, Germany
[4]II. Physikalisches Institut, Universtität zu Köln, Germany

dinesh@physik.rwth-aachen.de

Epitaxial graphene islands are prepared by ethylene deposition on Ir(111) at room temperature and subsequent annealing to 1050°C. The lateral dimension of the islands varies from 5 nm to 40 nm. Using scanning tunneling spectroscopy we were able to visualize confined states within the islands. The state energies and corresponding local density of states patterns are in good agreement with third nearest neighbor tight-binding calculations for graphene. However, we had to include the potential of the moiré structure as well as a strongly absorbing character of the edge states. The width of the confined state energy peaks has been used to determine the lifetime of the Dirac electrons, which is inversely proportional to energy. Atomic resolution STM images show singly saturated zigzag edges which are predicted to feature a spin-polarized state. STS measurements at the graphene edge partly show a pronounced peak at the Fermi level. A similar peak with lower intensity at the Fermi level is measured on the iridium, which could be identified as a surface state. This suggests that the increase in intensity at the edge of the graphene is due to a coupling of the edge state to the iridium surface state which enhanced strongly the intensity of the peak. Spin-polarized STS has been performed using an antiferromagnetic chrome tip in order to analyze the magnetic character of the edge state.
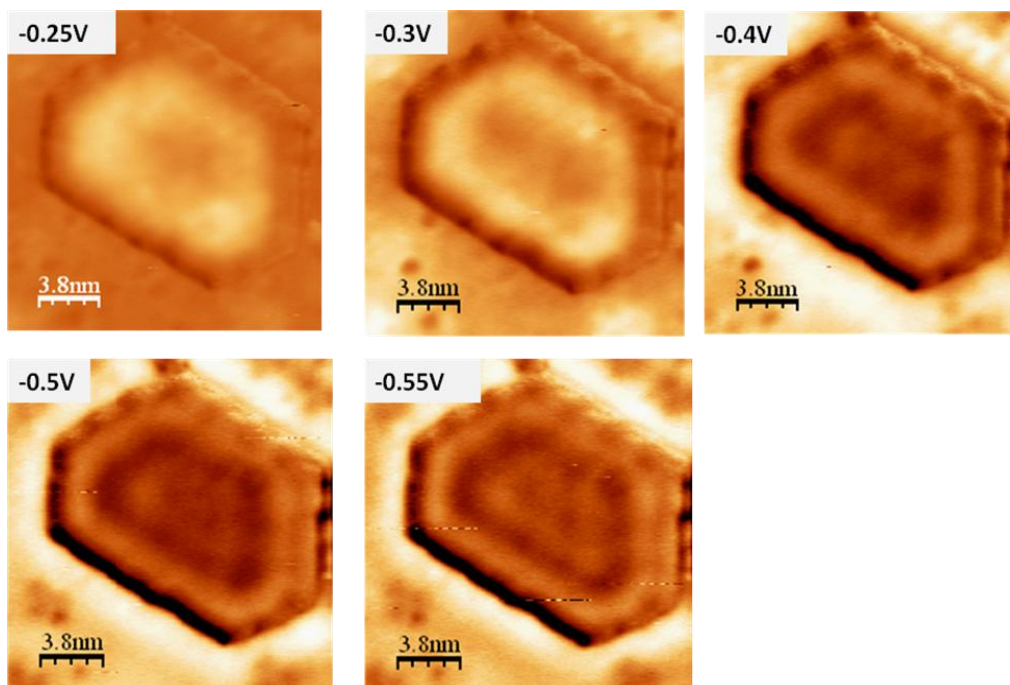
Fig. 1: dI/dV images at different sample voltage provide confined states on graphene island.

Graphene Oxides Dispersing Graphene Sheets: Unique Nanocomposites of Metal-Like Thermal Transport Performance and Beyond

Ya-Ping Sun

Department of Chemistry and Laboratory for Emerging Materials and Technology, Clemson University, Clemson, South Carolina 29634-0973, USA Tel: 864-656-5026, Fax: 864-656-6613, Email: syaping@clemson.edu

Graphene oxides (GOs), beyond their widely reported use as precursors for single-layer graphene sheets, are in fact excellent materials themselves. In the reported work we used aqueous GOs to effectively disperse few-layer graphene sheets (GNs) in suspension for facile wet-processing into nanocomposites of GNs embedded in GOs (as the polymeric matrix). The resulting light-weight and plastic-like nanocomposite materials remained mechanically flexible even at high loadings of GNs, and they were found to be highly efficient in thermal transport, with the experimentally determined thermal diffusivity competitive to those typically observed only in well-known thermal conductive metals such as aluminum and copper. As demonstrated, GOs apparently represent a unique class of two-dimensional polymeric materials for potentially "all-carbon" nanocomposites, among others, which may find technological applications independent of those widely proclaimed for graphene sheets.

Edge- and quantum confined states in atomically well-defined graphene quantum dots

Zhixiang Sun[1], Sampsa Hämäläinen[2], Mark Boneschanscher[1], Andreas Uppstu[2], Mari Ijäs[2], Ari Harju[2], Daniël Vanmaekelbergh[1], Peter Liljeroth[1,2]

[1] Condensed Matter and Interfaces, Debye Institute for Nanomaterials Science, Utrecht University, PO Box 80000, 3508 TA Utrecht, The Netherlands
[2] Department of Applied Physics, Aalto University School of Science, FI-00076 Aalto, Finland
z.sun@uu.nl

Despite the availability of good quality, large scale graphene layers, the realization of both the room-temperature graphene transistor as well as the more advanced theoretical ideas require well-defined samples, in particular in terms of the graphene edge structure. This level of control is currently not available through conventional lithographic techniques and there is a lack of experimental data on atomically well-defined graphene nanostructures. For example, opening a sufficient gap for room-temperature operation through quantum confinement requires structures in the size range of 10 nm. Furthermore, the electronic structure of graphene nanostructures is sensitive to the structure of the edges (e.g. zig-zag vs. armchair) [1]. There is a possibility of edge reconstructions and attachment of various functional groups, which further complicate the comparison between theory and experiment [2].

We use chemical vapour deposition (CVD) from ethylene on Ir(111) surface to grow small graphene flakes with well-defined edge structure [3]. We focus on the possible edge states and size-dependence of the quantum confined wavefunctions in these graphene quantum dots (GQDs) [4,5]. We explore the size-dependent electronic properties of the GQDs on Ir(111) using low-temperature, scanning tunneling microscopy (STM, Figure, top left). Graphene interacts only weakly with the underlying Ir(111) substrate and retains the electronic structure of isolated graphene [6].

The CVD growth yields a relatively broad distribution of different GQD sizes and shapes ranging from a couple of nanometers up to ca. 20 nm with a roughly hexagonal shape. All the flakes have edges in the zig-zag direction with a very small roughness (we see steps with a height of a single atomic row at the flake edges). We can readily access individual GQDs and measure their atomic structure using STM (Figure, top right). The local electronic properties can be probed by scanning tunneling spectroscopy (STS), which allows the measurement on the local density of states (LDOS, proportional to the dI/dV signal) with atomic spatial resolution. Figure (middle row) shows dI/dV maps (measured under constant-current STM feedback) at different bias voltages that show the presence of quantum confined states with different envelope wavefunction symmetries. We are able to reproduce the experimental results using tight-binding calculations of free-standing GQDs with the experimentally determined atomic structure (Figure, bottom row).

We have measured the size-dependence of the energy level spacing and the band gap of these GQDs. Our preliminary analysis shows that they both are approximately inversely dependent on the size of the GQD. In addition to these delocalized states, we are able to visualize edge states at energies close to the Dirac point. Our measurements show that CVD-grown graphene quantum dots form an ideal platform for a fundamental study of the electronic properties of atomically well-defined graphene nanostructures.

References

[1] A.H. Castro Neto et al., Rev. Mod. Phys. **81** (2009) 109.
[2] P. Koskinen, S. Malola, H. Häkkinen, Phys. Rev. Lett., **101** (2008) 115502.
[3] J. Coraux et al., New J. Phys., **11** (2009) 023006.
[4] L. A. Ponomarenko et al., Science, **320** (2008) 356.
[5] J.H. Bardarson, M. Titov, P.W. Brouwer, Phys. Rev. Lett. **102** (2009) 226803.
[6] I. Pletikosic et al., Phys. Rev. Lett., **102** (2009) 056808.

Figures
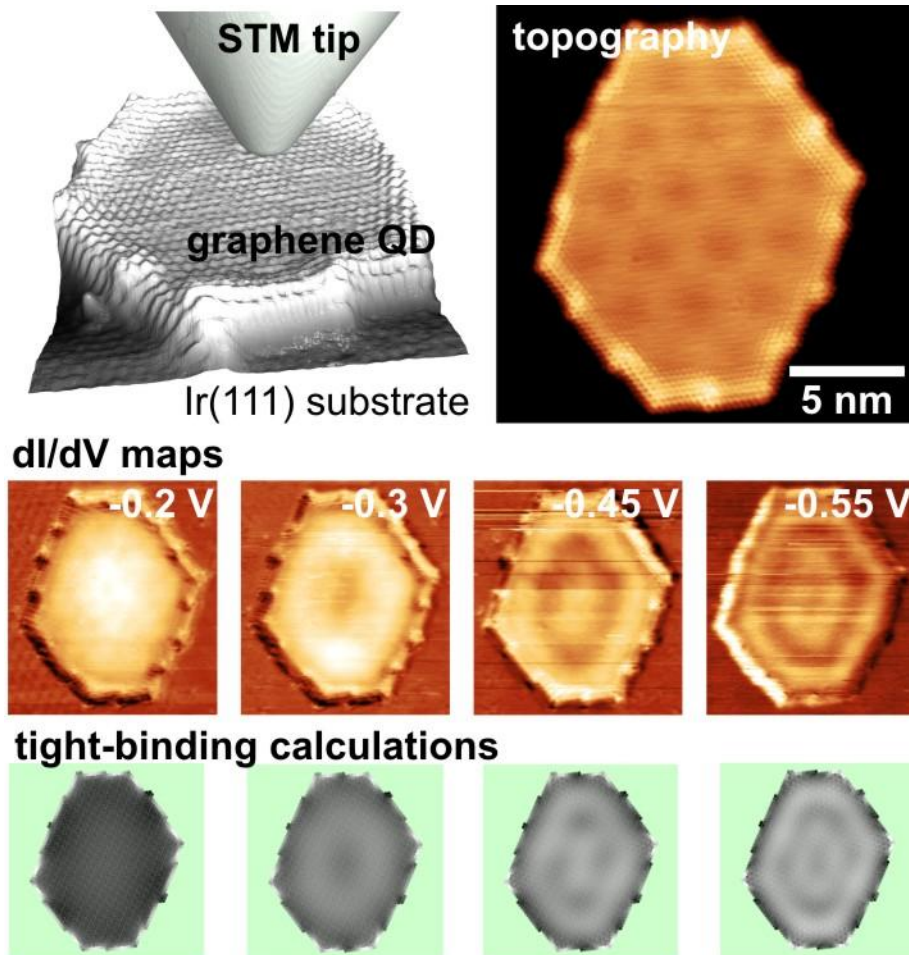
Top left: Schematic of the experimental setup. Graphene quantum dots with well-defined edges are grown epitaxially on Ir(111) and investigated by low-temperature STM. Top right: Typical atomically resolved STM image acquired at 0.5V / 100 pA. Middle row: dI/dV maps (proportional to local density of states) acquired under STM feedback at the bias voltages indicated in the figure. Bottom row: Local density of states at the energies corresponding to the experimental dI/dV images based on tight-binding calculations on a GQD with the experimentally determined atomic structure.

High on-off ratios in bilayer graphene field effect transistors realized by surface dopants

B.N. Szafranek, D. Schall, M. Otto, D. Neumaier, H. Kurz

Advanced Microelectronic Center Aachen (AMICA), AMO GmbH,
Otto-Blumenthal-Strasse 25, 52074 Aachen, Germany
szafranek@amo.de

For the application of graphene in logic switches transistors with a high on-off ratio are necessary to provide two discrete states. One method to increase the on-off ratio in graphene is the application of a perpendicular field to bilayer graphene. This can be realized with a double gate structure with a bottom and top gate fabricated around the bilayer. In this work we investigate a method to replace one of the gates by surface doping.

We fabricated back gated bilayer graphene field effect transistors (GFETs), where the graphene's top side was freely accessible for surface doping. We used highly p-doped Si covered with 90 nm thermally grown SiO_2 as a substrate. Prior to the graphene deposition the substrate was coated with HMDS in a chemical vapor deposition process [1]. A careful preparation of the samples was crucial for the observation of the discussed effects. The graphene was exfoliated with an adhesive tape from a natural graphite crystal and deposited on the substrate. After graphene deposition the contact electrodes were fabricated by optical lithography, sputter deposition of 40 nm nickel and subsequent lift-off. A schematic of the GFET's device stack is depicted in the inset of Fig. 1.

The doping of the upper graphene plane was achieved by two different approaches: The exposure of the device to ambient atmosphere for several hours led to a p-doping of the graphene. Although this method is not suited for device fabrication because of its experimental character, it is rather simple to perform and allows a stepwise removal of the dopants by annealing and therefore a quasi continuous tuning of the doping level. The second approach is based on the evaporation of a 1 nm thin aluminum layer that oxidizes immediately when exposed to ambient atmosphere. Aluminum causes a strong n-type doping in graphene [2]. The sheet resistance ρ_{SQ} as a function of the applied back gate voltage U_{BG} of two freshly fabricated bilayer graphene devices with n-type (aluminum) and p-type (atmospheric) doping are depicted in Fig. 1 together with the characteristics of an undoped device at room temperature. We observed that due to the doping not only the charge neutrality point (CNP) of the graphene is shifted to larger values (-42 V for n-type doping and +32 V for p-type doping), but also the resistance at the CNP and the on-off ratio increased. Previous investigations on double-gated bilayer GFETs [3,4] showed a similar behavior and in ARPES studies of doped bilayer graphene the opening of a band gap due to symmetry breaking was observed [5].

For an application oriented evaluation the on-off ratio of a GFET is defined as a figure of merit, governed by the ratio of the resistance at the CNP and the resistance at a carrier concentration of 10^{13} cm^{-2}, which corresponds to a back gate voltage of ±40 V. In Fig. 2 the on-off ratios $R_{CNP}/R_{CNP±40V}$ of all investigated devices are plotted as a function of their respective back gate voltage at the CNP. In the n-type regime for negative back gate voltages from -20 to -42 V the on-off ratio reached values between 18 and 43. In the case of atmospheric doping the on-off ratios were between 7 and 40 with the CNP voltages ranging from 10 to 60 V. After annealing at 200°C in nitrogen the GFETs had lost most of their doping as evidenced by the shift of the CNP voltage into the range of -5 to 5 V. As a consequence the on-off ratio was reduced to values between 6 and 10.

The method presented here for increasing the on-off ratio in bilayer graphene by surface doping has the potential to bias a bilayer GFET at an optimal working point and then control the channel by a single gate electrode.

References

[1] M. Lafkioti, B. Krauss, T. Lohmann, U. Zschieschang, H. Klauk, K. v. Klitzing, and J. H. Smet, Nano Lett. **10** (2010) 1149.

[2] G. Giovannetti, P. A. Khomyakov, G. Brocks, V. M. Karpan, J. van den Brink, and P. J. Kelly, Phys. Rev. Lett. **101** (2008) 026803.

[3] F. Xia, T. Mueller, Y. Lin, A. Valdes-Garcia, and P. Avouris, Nature Nanotech. **4** (2009) 839.

[4] B.N. Szafranek, D. Schall, M. Otto, D. Neumaier, and H. Kurz, Appl. Phys. Lett. **96** (2010) 112103.

[5] T. Ohta, A. Bostwick, T. Seyller, K. Horn, and E. Rotenberg, Science **313** (2006) 951.

Figures
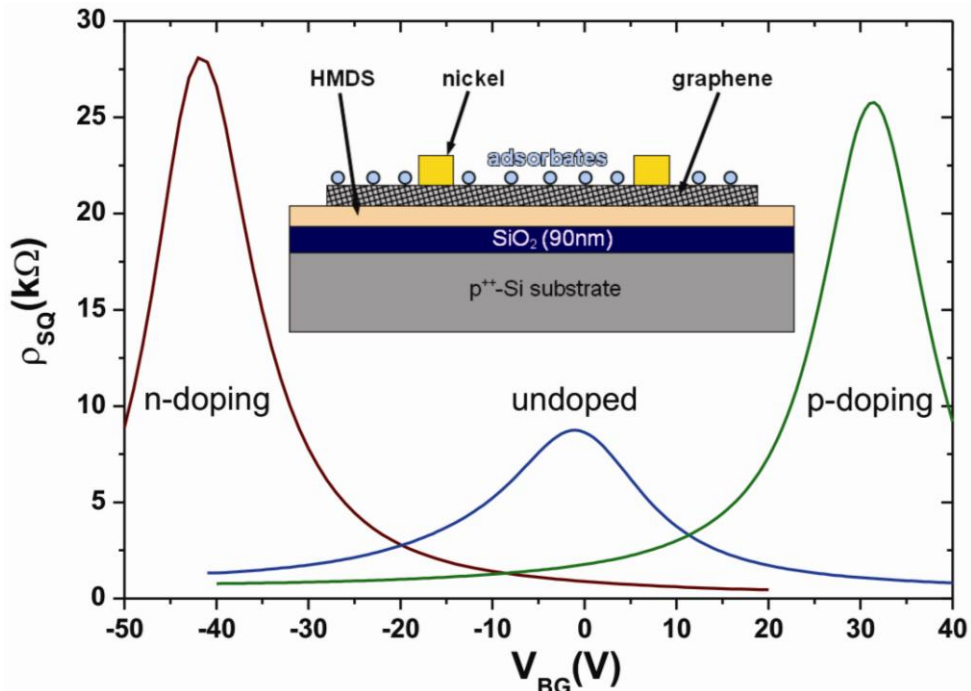
Fig. 1: Sheet resistance of n-type, p-type and an undoped bilayer GFET as a function of the applied back gate voltage at room temperature. The inset shows a schematic of the fabricated GFETs. The doping by adsorbates is indicated.
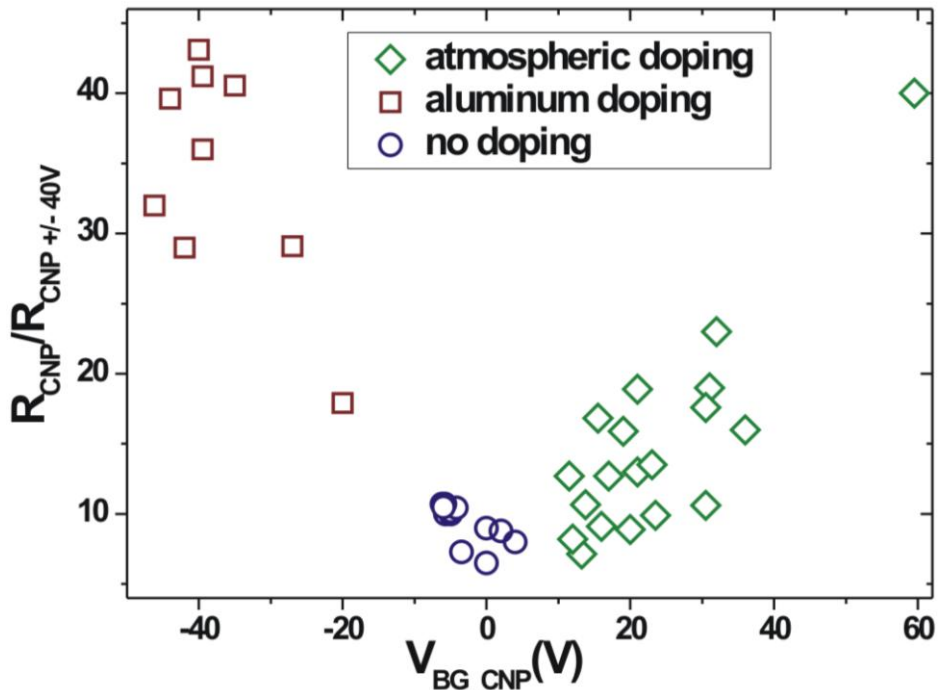
Fig. 2: On/off ratio vs. position of charge neutrality point V_{BG_CNP} of several devices. All measurements have been performed in nitrogen atmosphere and at room temperature.

Control of the Unintentional Doping in Epitaxial Graphene FETs

K. Tahy[1], W. S. Hwang[1], J.L. Tedesco[2], R.L. Myers-Ward[2], P.M. Campbell[2], C.R. Eddy[2] Jr.,
D.K. Gaskill[2], H. Xing[1], A. C. Seabaugh[1], and D. Jena[1]

[1]Department of Electrical Engineering, University of Notre Dame, Notre Dame, IN 46556, USA
[2]U.S. Naval Research Laboratory, Washington, DC 20375, USA
ktahy@nd.edu

The transport properties of graphene with saturation currents as high as 2.0 A/mm and electron mobilities of 15 000 cm^2/Vs [1] place this material in the limelight as an attractive candidate of next-generation nanoelectronic devices. The widely observed high carrier mobility naturally focuses our attention towards high frequency performance of graphene based devices. Gigahertz operation of exfoliated [2] and epitaxial [3] graphene FETs has been reported showing cut-off frequency up to 170 GHz [4]. A common trend [3] for these top gated epitaxial graphene FETs that they are highly n-type doped so switching them off is a difficulty. While it is not necessary a problem for analog applications, graphene could offer mixed analog/digital integration with an ease, and for digital transistors a low leakage off state is a necessity. For that purpose devices with close to intrinsic doping have to be fabricated. Here we present the study of the effect of different high-κ oxides and gate metals on the doping level of epitaxially grown graphene on SiC substrates.

Epitaxial graphene was grown on Si-face 6H-SiC. The epitaxial film may consist of double layer parts especially where the underlying SiC substrate has steps. According to AFM characterization and Raman measurements the graphene thickness is 1-2 layers in average over the wafer. A recent study has shown [5] that while double-layer graphene may be present in the immediate vicinity of the steps, it represents only a small perturbation to the normal linear dispersion relationship expected for single-layer graphene. To form FETs we patterned the graphene by e-beam lithography using HSQ and etched it in O_2 plasma. In terms of the gate oxide we fabricated two samples for comparison one with ~20 nm spin-on HSQ and another without it. Both got a 20 nm thick atomic-layer-deposited Al_2O_3 film. E-beam evaporated Cr/Au contacts were lastly deposited to form field-effect transistors (FETs). Hall measurements reveal μ ~ 500 – 600 cm^2/Vs throughout the sample, showing smooth variation and better performance in the middle of the wafer. The DC output characteristics of the devices were linear up to 5 V and slightly sub-linear at higher biases. The drain current had relatively weak (~ 1.5x - 3x) gate dependence as we swept the gate voltage between +/- 10 V. We performed a broader study to characterize the effect of the oxides and for that we used a more simple structure: 1x1 cm samples with metal contacts in the corners. Our conjecture was that a component of the high n-type doping are the states on the graphene/oxide interface. To test this we tried several materials (SiO2, HSQ, Al2O3, HfO2) deposited by different methods (e-beam evaporation, ALD, spin-coat). Another reason for the doping can be the polar nature of the oxide, what we tested by deposited a second layer of highly polar oxide after the surface layer.

We find that all the tested oxides introduced n-type doping. The quantity of the doping shows correlation to the dielectric constant of the oxides. By removing the oxide the initial doping can be restored. In case if we deposited a high-κ oxide on the top of the low-k oxide the n-type doping increased further. High temperature annealing can increase crystallinity of the oxide therefore decrease trapped charge density. We experienced some improvement in case of 600 °C rapid thermal annealing (RTA) but the quick thermal expansion introduced cracks in the oxide.

Our experiment showed that the unwanted doping effect can be minimized by utilizing certain oxide stacks, but intrinsic or p-type doping was not achieved. Growing on lightly p-doped SiC wafer or the use of a polymer surface layer can be a solution and it will be the subject of our further investigation.

References
[1] A. K. Geim *et al,* Nat. Mat., **6** (2007)183-191.
[2] Y-M. Lin *et al,* Nano Lett. **9** (2009) 422–426.
[3] J. S. Moon *et al,* IEEE EDL, **30** (2009) 650.
[4] Ph. Avouris *et al,* IEEE IEDM (2010) 552.
[5] J. M. B. Lopes dos Santos, *et al,* Phys. Rev. Lett. **99** (2007) 256802.

Figures
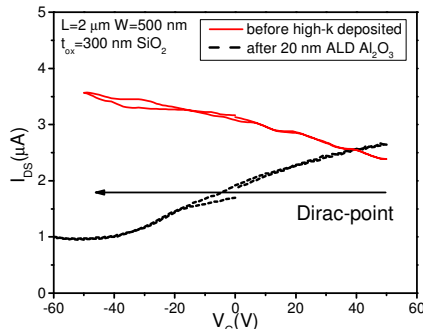
Figure 1. Doping effect of the high-κ top gate dielectric deposition in case of an exfoliated graphene FET on SiO₂. The FET has heavy p-type doping before high-κ deposition, the Dirac point is at some voltage higher than +50 V. After 20 nm ALD Al2O3 deposition the position of the Dirac point decreased by more than 100 V. It corresponds to more than $-7 \cdot 10^{12}$ cm^{-2} change in the carrier concentration at a given bias.
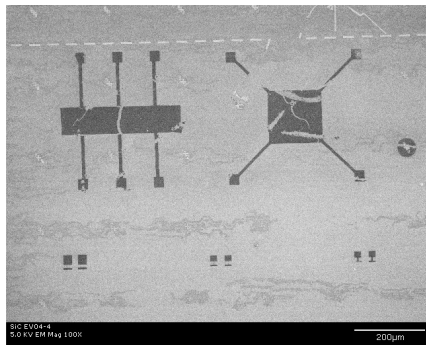
Figure 2. SEM micrograph of graphene on SiC. The cracks on the graphene are caused by the 600 ℃ rapid thermal annealing of the HSQ mask. Even though RTA can be beneficial to handle the unintentional doping of graphene the structural failure of the oxide excludes it as a useful tool in processing.
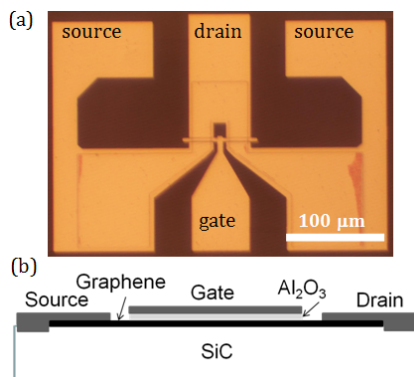
Figure 3. Optical image (a) and schematic cross-section (b) of a processed graphene FET on SiC optimized for RF amplification.
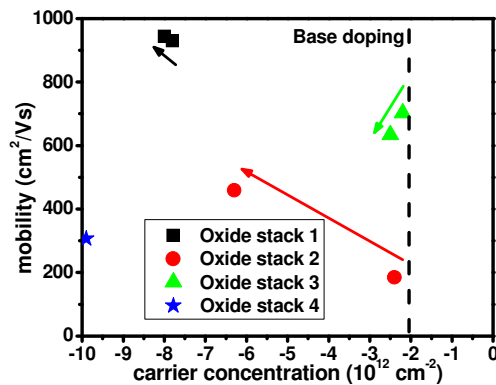
	R_s (kOhm/□)	μ (cm^2/Vs)	doping (10^{12} cm$^-$)
Base value	1.0	1040	-2.1
Oxide stack 1			
5 nm ebeam evaporated	0.86	930	-7.8
+10 nm ALD Al₂O₃	0.82	944	-8
Oxide stack 2			
5 nm ebeam evaporated	13.7	185	-2.4
+10 nm ALD Al₂O₃	2.1	459	-6.3
Oxide stack 3			
HSQ coating (not exposed)	3.9	702	-2.2
+10 nm ALD Al₂O₃	3.9	634	-2.5
Oxide stack 4			
HMDS		N/A	
+ 5 nm ALD Al₂O₃	2.0	307	-9.9

Figure 4. Change of the carrier concentration in case of different oxide stacks. The dashed line shows the initial doping of the sample. None of them provide lower n-type doping concentration than the original doping of the sample. Further high-κ oxide deposition added extra doping. The table shows the data in detail corresponding to the different oxide stacks.
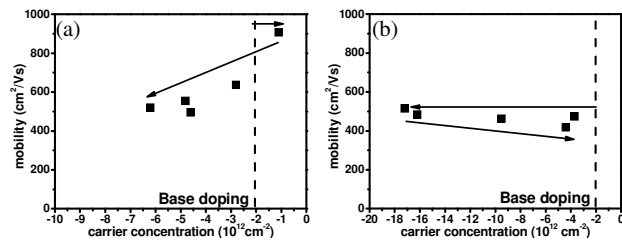
(a)	R_s (kOhm/□)	μ (cm^2/Vs)	doping (10^{12} cm$^-$)
HSQ coating (not exposed)	6.2	907	-1.1
+20 nm ALD Al₂O₃	3.4	636	-2.8
RTA, 400 ℃, 1 min	2.3	555	-4.8
RTA, 500 ℃, 1 min	1.9	520	-6.2
RTA, 600 ℃, 1 min	2.7	495	-4.6

(b)	R_s (kOhm/□)	μ (cm^2/Vs)	doping (10^{12} cm$^-$)
HSQ coating (not exposed)	3.5	474	-3.7
+20 nm ALD HfO₂	0.7	515	-17.2
RTA, 400 ℃, 1 min	0.8	483	-16.2
RTA, 500 ℃, 1 min	1.4	462	-9.5
RTA, 600 ℃, 1 min	3.3	418	-4.4

Figure 5. Change of the carrier concentration in case of HSQ + high-κ oxide stacks and the effect of RTA. The dashed line shows the initial doping of the sample. (a) HSQ + Al₂O₃ oxide stack. The RTA continuously increases the doping. (b) HSQ + HfO₂ oxide stack. The highly polar HfO₂ heavily increases the n-type doping but the RTA continuously decreases it. The tables are showing the details of the process.

460

Carbonaceous field effect transistor with graphene and diamondlike carbon

Susumu Takabayashi[1,2], Shuichi Ogawa[3], Yuji Takakuwa[3], Hyun-Chul Kang[1], Ryota Takahashi[1], Hirokazu Fukidome[1,2], Maki Suemitsu[1,2], Tetsuya Suemitsu[1,2], Taiichi Otsuji[1,2]

[1] Research Institute of Electrical Communication, Tohoku University,
2-1-1 Katahira, Aoba-ku, Sendai 980-8577, Japan
[2] JST-CREST, 5 Sanban-cho, Chiyoda-ku, Tokyo 102-0075, Japan
[3] Institute of Multidisciplinary Research for Advanced Materials, Tohoku University,
2-1-1 Katahira, Aoba-ku, Sendai 980-8577, Japan
stak@riec.tohoku.ac.jp

Selection of the gate dielectric is a critical issue for fabrication of topgate graphene field effect transistors (G-FETs).[1] Well-known oxide gate dielectrics are not applicable due to the oxidative destruction of the π-system of graphene during the deposition process.

Diamondlike carbon (DLC) is a carbonaceous material with an amorphous structure composed of sp^2 carbon, sp^3 carbon, and hydrogen.[2] DLC behaves widely in electrical characteristics as from a conductor to a dielectric by controlling the amount of hydrogen incorporated.[3] So far, dielectric DLC films have been challenged as topgate dielectrics of Si FETs, but have not become popular because the production accompanies carbon waste and resultant contamination so that it may not be suited for the clean-room fabrication process. On the other hand, in graphene devices, DLC may be applicable because of the affinity in material chemistry between graphene and DLC. In this work we have fabricated a topgate G-FET with a DLC film as a gate dielectric (DLC-gated G-FET).

Figure 1 shows the schematic cross section of the DLC-gated G-FET. Graphene used here is prepared on a 6H-SiC substrate by annealing.[4, 5] Pt was selected as the source and drain ohmic-contact metal because of its better adhesion and affinity to graphene.[6, 7] The channel width (W_C), channel length (L_C), and gate length (L_G) were 11, 6, and 5 μm, respectively. The DLC gate was prepared by photoemission-assisted plasma enhanced chemical vapor deposition (PA-PECVD).[8, 9] This consists of dc plasma triggered by UV-photoemission from the sample, giving much smaller output power to minimize the plasma damage to graphene. The thickness of the present DLC gate was 100 nm. The dielectric constant was 5.1 and the equivalent oxide thickness (EOT) was estimated to be 76 nm.

Figures 2 and 3 show the I_{DS}-V_{DS} and I_{DS}-V_{GS} characteristics, respectively. For both cases V_{GS} scans from (a) -12 and (b) +12 V, respectively. No drain current saturation is observed in the I_{DS}-V_{DS} characteristics (Figs. 2(a) and (b)), reflecting non-Bernal stacked gapless graphene formation. When V_{GS} scans from -12 V (Figs. 2(a) and 3(a)), the device operates in the ambipolar mode and the Dirac voltage (V_{Dirac}) is observed in the far positive region. On the other hand, when V_{GS} scans from +12 V (Figs. 2(b) and 3(b)), the ambipolar mode is also observed, but V_{Dirac} is observed in the far negative region. This hysteresis may be the difference of the hole or electron doping induced by V_{GS}. Theoretically in the ambipolar mode V_{Dirac} shifts with V_{DS} at the level of 1/2 V_{DS} where the concentration of electrons and holes are in equilibrium; however, the observed ones are much higher (lower) when V_{GS} scans from negative (positive), suggesting that the graphene channel is still p- (n-) doped.

Figure 4 shows the transconductance (g_m)-($V_{GS} - V_{Dirac}$) characteristics obtained from Fig. 3(a). The maximum absolute g_m's in n- and p-channel modes of the ambipolar performance are 6.3 and 2.8 mS/mm, respectively. Considering that g_m is in proportion to the reciprocals of L_G and EOT, $|g_m|$ = 2-3 S/mm, which is an extremely high value, is expected when L_G = 100 nm and EOT = 10 nm.

Consequently, although the hysteresis is a critical issue to be solved, DLC can be a promising material as a gate dielectric of a topgate G-FET.

References

[1]   ITRS, Emerging Research Materials 2009 ed. (2009).
[2]   J. Robertson, Mater. Sci. Eng. R **37** (2002) 129.
[3]   S. Takabayashi et al., Jpn. J. Appl. Phys. **47** (2008) 3376.
[4]   C. Berger, et al., J. Phys. Chem. B **108** (2004) 19912.
[5]   W. A. de Heer, et al., Solid State Commun. **143** (2007) 92.
[6]   A. Dinger, C. Lutterloh, J. Biener, J. Küppers, Surf. Sci. **421** (1999) 17.
[7]   G. Gupta et al., J. Phys. Chem. C **114** (2010) 10796.
[8]   T. Takami et al., e-J. Surf. Sci. Nanotech. **7** (2009) 882.
[9]   H. Sumi et al., Jpn. J. Appl. Phys. **49** (2010) 076201.

Figures

Figure 1 Schematic cross-section of the DLC-gated G-FET. The scale of each block is shown in nm.

Figure 2 (left) I_{DS}-V_{DS} characteristics of the DLC-gated G-FET at different V_{GS}'s. V_{GS} was stepped by (a) +4 V from -12 and (b) -4 V from +12 V. V_{GS} applied at each curve is distinguished in color and line-shape (solid for positive and broken for negative signs), as explained in the figure.

Figure 3 (right) I_{DS}-V_{GS} characteristics of the DLC-gated G-FET at different V_{DS}'s corresponding to Figs. 2(a) and (b) V_{GS} scanned from (a) -12 and (b) +12 V with a V_{DS} step of +0.2 V from -1.0 to 1.0 V. V_{DS} applied at each curve is distinguished in color and line-shape (solid for positive and broken for negative signs), as explained in the figure. Black circle and square indicate V_{Dirac} and 1/2 V_{DS}, respectively.

Figure 4 g_m curve in the ambipolar mode as a function of $V_{GS} - V_{Dirac}$ derived from Fig. 3(a). V_{DS} applied at each curve is distinguished in color and line-shape (solid for positive and broken for negative signs), as explained in the figure. $|g_{mn}|_{max}$ and $|g_{mp}|_{max}$ are indicated.

Influence of dispersion state of graphene on percolation threshold of conductive graphene/polymer nanocomposites.

Evgeniy Tkalya[a] , Marcos Ghislandi[b], Ronald Otten[c], Mustafa Lotya[d], Alexander Alekseev[b], Paul van der Schoot[c], Jonathan Coleman[d], Cor Koning[a].

[a] Department of Polymer Chemistry, Technische Universiteit Eindhoven, P.O.Box 513, 5600 MB Eindhoven, The Netherlands.
[b] Laboratory of Materials and Interface Chemistry, Technische Universiteit Eindhoven, P.O. Box 513, 5600 MB Eindhoven, The Netherlands.
[c] Theory of Polymers and Soft Matter and Eindhoven Polymer Laboratories, Technische Universiteit Eindhoven, P.O. Box 513, 5600 MB Eindhoven, The Netherlands.
[d] School of Physics, Centre for Research on Adaptive Nanostructures & Nanodevices (CRANN), Trinity College Dublin, Dublin 2, Ireland.

e.e.tkalya@tue.nl

The large variation in the reported percolation threshold values of graphene-based nanocomposites which ranges from 0.1 to greater than 2 wt% indicates that the dispersion states and other properties of graphene affected by processing conditions are important in determining the electrical properties of graphene/polymer nanocomposites. For nanofiller/polymer nanocomposites dispersion state of a nanofiller was recognized as one of the critical factors governing conductivity of composites as well as physical properties. It is generally accepted that a good filler dispersion within the polymer matrix enhances the physical properties of the composite. However, a few studies done on carbon nanotubes/polymer nanocomposites suggest that agglomeration of the nanotubes could favor the formation of a percolating network [1,2]. In this work dispersion state of graphene as parameter having influence on percolation threshold of corresponding composites prepared with latex technology [3] is discussed.

Graphene dispersions of different degree of exfoliation and stability were prepared with the aid of sonication. The dispersion process was monitored by measuring UV–Vis absorption. Quality of the nanofiller was characterized by Raman spectroscopy. The conductivities of the final composites were measured by a four-point method. The organization of graphene sheets in nanocomposites and their conductivity distribution was analyzed with nanometer resolution by means of conductive atomic force microscopy (C-AFM). The results indicate that agglomeration of graphene sheets and clustering formation can significantly decrease a percolation threshold of the nanocomposites.

References

[1] Li J., Ma P. C., Chow W. S., To C. K., Tang B. Z., Kim J-K., Advanced Functional Materials, **17** (2007), 3207–3215.
[2] Martin C. A., Sandler J. K. W., Shaffer M. S. P., Schwarz M-K., Bauhofer W., Schulte K., Windle A. H., Composites Science and Technology, **64** (2004), 2309–2316.
[3] Tkalya E., Ghislandi M., Alekseev A., Koning C., Loos J., Journal of Materials Chemistry, **20** (2010), 3035-3039.
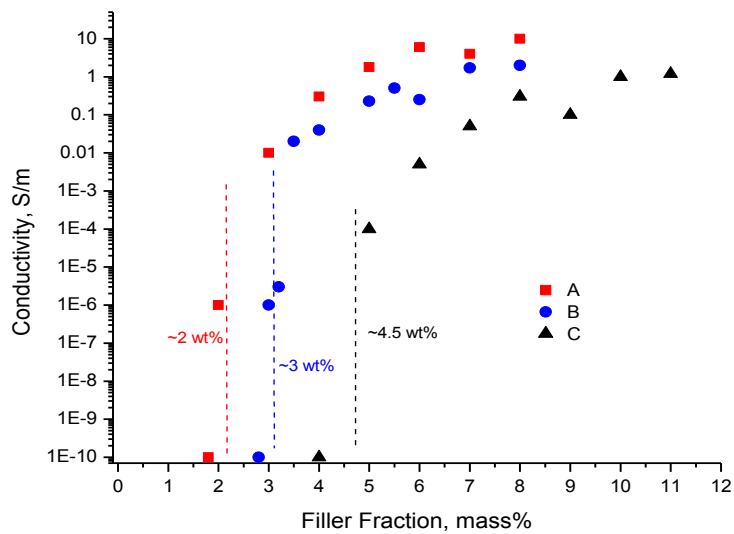
Figure 1. *Conductivity profile for composites prepared with graphene dispersions of different stability. Stability of the dispersions is increasing in the range A<B<C.*
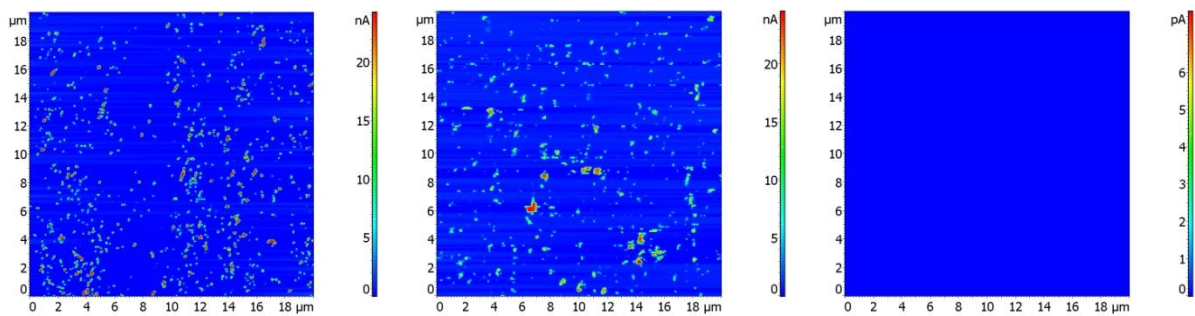
Figure 2. *C-AFM images of graphene/polymer nanocomposites containing 4 wt% of graphene prepared with dispersions A, B and C respectively.*

Ink-Jet printed graphene electronics

F. Torrisi, T. Hasan, W. Wu, Z. Sun, A. Lombardo, T. Kulmala, G. W. Hshieh, F. Bonaccorso, P. J. Paul, D. P. Chu, A. C. Ferrari

University of Cambridge, 9 J.J. Thomson Avenue CB3 0FA, Cambridge, United Kingdom
ft242@cam.ac.uk

Ink-jet printing is one of the most promising techniques for inexpensive large area fabrication of flexible plastic electronics[1], due to its versatility, the limited number of process steps[2], the ease of mass fabrication[2]. Despite much progress, ink-jet printed organic Thin Film Transistor (TFT) still show poor air stability, limited lifetime, mobility ($\mu < 0.5$ cm^2 V^{-1} s^{-1}) [3], and ON/OFF ratios($<10^5$). The use of carbon nanotubes (CNT) ink [4,5] allowed to increase μ by at least one order of magnitude[3,4].

Graphene is at the centre of an ever expanding research area [6]. Near-ballistic transport and high mobility make it an ideal material for nanoelectronics, especially for high frequency applications. Furthermore, its optical and mechanical properties are ideal for thin-film transistors and transparent and conductive electrodes[7]. Here we exploit the extraordinary properties of graphene to fabricate graphene-based ink-jet printed transparent and conductive electrodes and TFTs. Liquid phase exfoliation (LPE) is ideal to produce printable graphene-based inks.

High quality graphite flakes are dispersed in organic solvents by ultrasonication (~9 hours) followed by ultracentrifugation to remove large graphite fragments that are likely to clog the nozzle of the ink-jet printer. We investigate N,N-dimethylacetamide, Ethyl Acetate, 1-Methyl-2-pyrrolidone (NMP), Dimethylformamide as organic solvents. By Optical Absorption Spectroscopy (OAS), Transmission electron microscopy (TEM) and Raman spectroscopy we find that NMP gives the highest yield of monolayer graphene [8].

Graphene-ink stripes are then ink-jet printed on Si/SiO$_2$ modified by Self-Assembled Monolayers (SAM), which reduce the wettability of the substrate and allow uniform printing of graphene electrodes. AFM shows that a ~20 nm thick conductive stripe is obtained with a uniform distribution of graphene flakes. Its optical and electrical properties are studied respectively by OAS and electrical four-point probe measurements at room temperature. The ink-jet printed graphene-ink stripes are then utilized to fabricate graphene-based TFTs achieving mobility up to 95cm^{2}V^{-1}s^{-1} and ON/OFF ratio of ~10^4-10^5. The electrical and optical performances observed in our devices, demonstrate the viability of graphene-ink to fabricate electronic devices, paving the way to graphene ink-jet printed electronics [9].

References

[1] H. Sirringhaus et al. Science, **290** (2000) 2123.
[2] B. J. DeGans et al. Adv. Mater. **16** (2004) 203.
[3] M. Singh et al. Adv. Mater. **22** (2010) 673.
[4] M. Ha et al. ACS Nano **4** (2010) 4388.
[5] P. Beecher et al. J. Appl. Phys. **102** (2007) 043710.
[6] A. K. Geim et al. Nat. Mater. **6** (2007) 183.
[7] F. Bonaccorso et al. Nat. Photon. **4** (2010) 611.
[8] Y. Hernandez et al. Nat. Nanotechnol. **3** (2008) 563
[9] F. Torrisi et al., submitted, (2011).

Figures
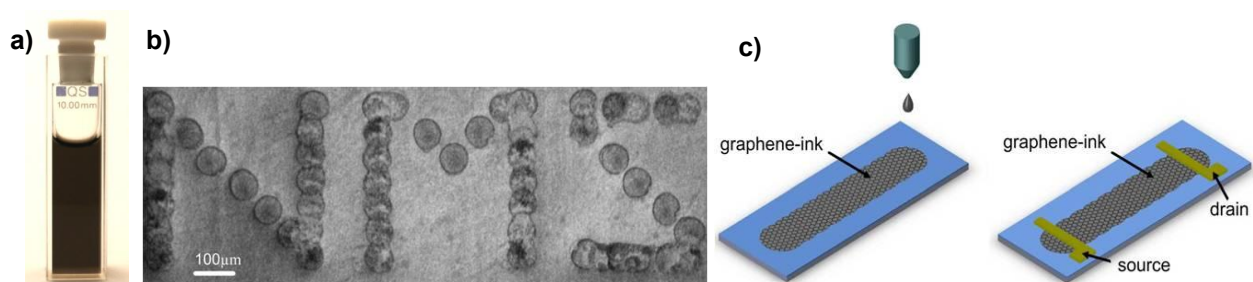
Figure: a) Graphene-ink. b) Example of graphene ink-jet printed pattern. c) Graphene TFT fabrication steps: graphene-ink is printed on Si/SiO$_2$ substrate, gold pads define source and drain.

Anisotropic photoconductivity in graphene

Maxim Trushin, John Schliemann

Institute for Theoretical Physics, University of Regensburg, D-93040 Regensburg, Germany
maxim.trushin@physik.uni-regensburg.de

We investigate the photoconductivity of graphene within the relaxation time approximation. In presence of the inter-band transitions induced by the linearly polarized light the photoconductivity turns out to be highly anisotropic due to the pseudospin selection rule for Dirac-like carriers. The possible observations and applications of this phenomenon are discussed.

One of the most unusual properties of carriers in graphene is the additional quantum degree of freedom which is dubbed as a pseudospin but, in fact, is connected with the sublattice index and has nothing to do with the real spin. Nevertheless, in some cases it turns out to be possible to deal with the pseudospin in a similar way as with the real electron spin. The experiment proposed below involves the optical excitation of the valence electrons to the conduction band in the intrinsic (or undoped) graphene. The idea is that the Hamiltonian describing the interaction between the electromagnetic wave and charge carriers inherits the pseudospin-momentum entangled structure from the effective Dirac-like Hamiltonian relevant for the electron pi-system of the single layer graphene near half filling. Assuming the normal incidence of a linear polarized electromagnetic wave one can arrive at the electron generation rate which strongly depends on the relative orientation between the electron momentum and the linear polarization plane, see Fig. 1. As consequence the photoconductivity parallel to the light polarization plane is 3 times smaller than the perpendicular one, i. e. the photoconductivity turns out to be highly anisotropic. Thus, changing the linear polarization angle from 0 to 2-Pi one can observe two minima (and two maxima) in the current flow, as depicted in the inset of Fig. 1. These double extrema can be seen as a signature of the effect proposed.

To evaluate the plausibility of the photoconductivity response proposed above one has to compare the residual carrier concentration due to the unintentional doping with the number of the photo-excited carriers. Assuming the CH3OH laser [1] operating at the wavelength 0.118 nm with the power 20 mW we find that the concentration of the photo-induced electrons is of the order of the residual carrier concentration in graphene after annealing. Thus, to observe the effect, we suggest utilizing the undoped suspended graphene samples which allow the laser beam to excite the substantial number of photo-carriers from the valence band. The cleaner samples are expected to demonstrate the better results. They can be used as the polarized light detectors.

References

[1] J. Karch *et al*., ArXiv:1002.1047
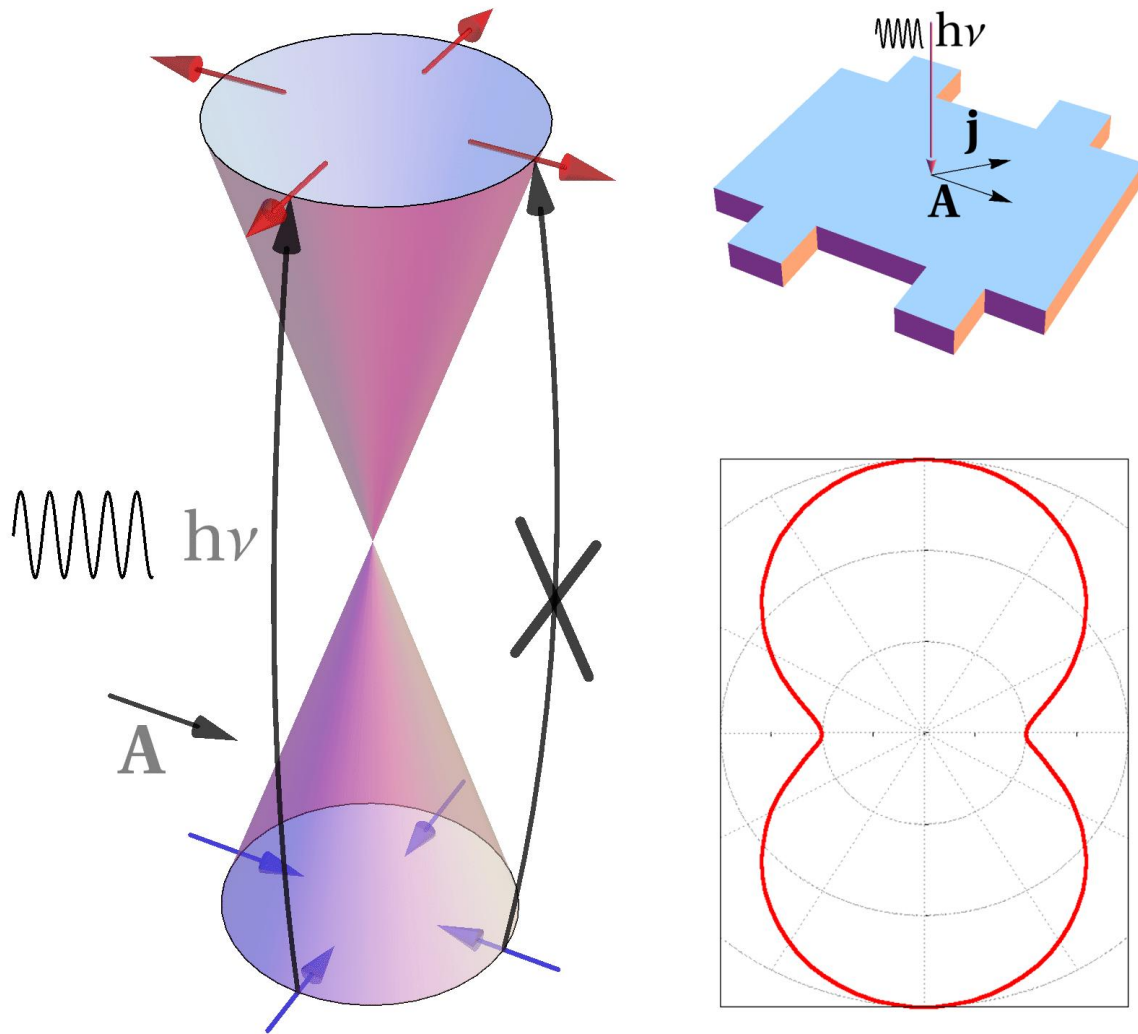
Fig. 1: The sample represents a Hall bar made of graphene which is irradiated by the linearly polarized electromagnetic wave characterized by the vector potential **A**. Applying the bias voltage one can observe the electrical current **j** which depends on the photo-induced carrier concentration. The carriers in graphene described by Dirac Hamiltonian with the cone-shaped dispersion law acquire additional degree of freedom known as pseudospin whose orientation entangled with the particle momentum is shown by arrows. The electrons in the valence band absorbing the photon energy are excited to the conduction band producing the photoconductivity response. The electron-hole excitation rate is zero if the light is polarized along the pseudospins of the excited particles. In contrast, the excitation rate is maximal if the vector potential and pseudospin are perpendicular to each other. Since the pseudospin orientation is coupled with the particle's momentum the resulting photoconductivity depends on the angle between **A** and **j**, as shown in the inset.

Suspended bilayer graphene in high magnetic fields

H.J. van Elferen[1], A. Veligura[2], N. Tombros[2], B.J. van Wees[2], J.C. Maan[1], U. Zeitler[1]

[1]High Field Magnet Laboratory, Radboud University Nijmegen, Toernooiveld 7, Nijmegen, The Netherlands
[2]Physics of nanodevices, Rijksuniversiteit Groningen, Nijenborgh 3, Groningen, The Netherlands

helferen@science.ru.nl

We have measured the two-terminal magnetoresistance in high-mobility suspended bilayer graphene at low temperatures down to 0.3 K and in high magnetic fields up to 30 T. We observe the field-induced appearance of an insulating phase at the charge neutrality point (CNP), a splitting of the lowest Landau level into eight distinct sub-levels, and, for the highest magnetic fields ($B > 20$ T), we demonstrate evidence for the development of a fractional quantum Hall effect (FQHE) in bilayer graphene

The mobility of standard graphene transistors is limited by the interaction with the SiO_2 substrate and chemisorbed impurities. Making suspended graphene eliminates the interaction with the substrate and allows removing impurities by local current annealing [1]. The most common technique for underetching the graphene is directly etching the SiO_2 with buffered HF. For our samples, the graphene is placed on an organic polymer on top of the SiO_2 [2]. This technique allows an underetching with inert solvents which make the devices much mechanically more stable. After processing the samples, we clean up the suspended graphene by using in-situ current annealing at cryogenic temperatures and obtain high mobilities up to 200.000 cm^2 $V^{-1}s^{-1}$.

In fig. 1a we show how the integer quantum Hall effect in one of our suspended bilayer samples becomes fully pronounce at 1 T. Additionally, we find a gap-opening at the CNP, visible as a strongly diverging resistance, $R \propto \exp(-\Delta/2\,k_B\,T)$. Plotting the gap as function of the magnetic field we obtain a square-root dependence (see fig. 1b) and thus tentatively attribute this behavior to a ferromagnetic origin which is in contrast to previous reported data in suspended bilayers with a linear field dependence of the gap proposing due to many body effects [3]. Owing the existence of inhomogeneities leading to electron and hole puddles, the Coulomb potential is disordered, which might be the reason for the observation of quantum Hall ferromagnetism in our device [4].

High magnetic fields break the complete eight-fold degenerated lowest Landau level in bilayer graphene, illustrated in fig. 1c. In addition the possible appearance of a FQHE in the lowest Landau level is illustrated in Fig. 1d where we plotted the conductance as function of filling factor v. When approaching the CNP, we can identify a FQHE at filling factors $v = 1/3$ and $v = 2/3$. Additional plateaus with an N-shaped features also appear for $v < 1/3$ as well as a relatively wide plateau between $v = 1/3$ and $v = 2/3$.

In conclusion we show the latest results on two-terminal measurements on bilayer graphene suspended on an organic polymer in high magnetic fields. Our experiments demonstrate experimental evidence for a FQHE in suspended bilayer graphene. So far, we can tentatively identify fractional filling factors with denominator three.

References

[1] J. Moser, A. Barreiro and A. Bachtold, Appl. Phys. Lett. **91** (2007) 163513

[2] N. Tombros, A. Veligura, J. Junesch, J. J. van den Berg, P. J. Zomer, M. Wojtaszek, I. J. Vera-Marun, H. T. Jonkman, B. J. van Wees, arXiv:1009.4213 (2010)

[3] B. E. Feldman, J. Martin and A. Yacoby, Nat. Phys. **5** (2009) 889

[4] D.V. Khveshchenko, Phys. Rev. Lett. **87** (2001) 206401

Figures
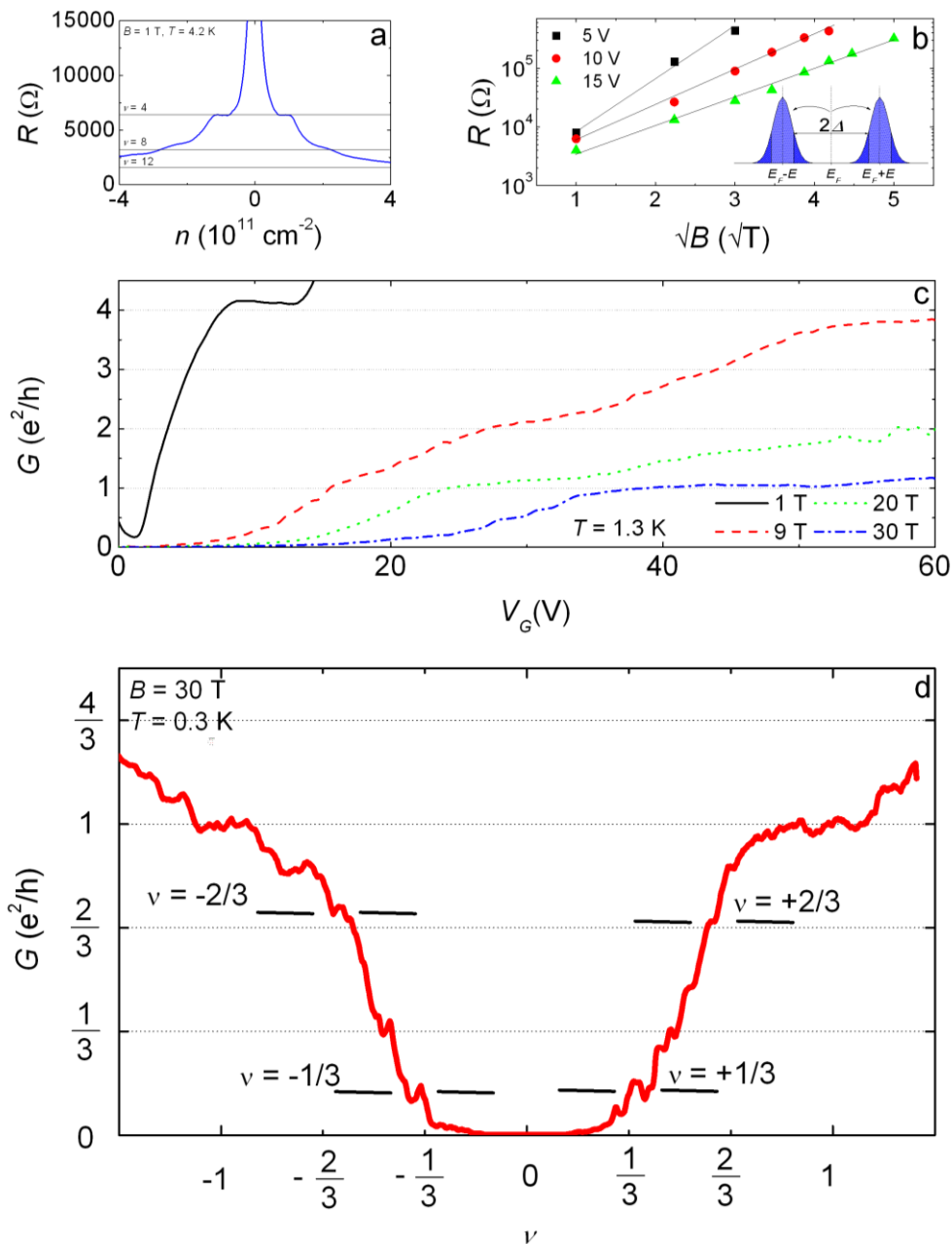
a) Two-terminal resistance of suspended bilayer graphene around the CNP. The integer quantum Hall effect with quantized plateaus at filling factors ν = 4 and 8 is already visible and the divergence of the resistance at the CNP indicates the opening of a gap.
b) Gaps extracted from the temperature dependent resistance around the CNP. The scaling $\sqrt{B}$ points towards a quantum Hall ferromagnetic behaviour.
c) Splitting of the eight-fold degenerated lowest Landau level in bilayer graphene.
d) High-field two-terminal conductance in the lowest Landau level at B = 30 T and T = 0.3K. Features appearing around ν = 1/3 and ν = 2/3 propose the appearance of a FQHE.

Tuning graphene's electronic structure via unbalanced disordered sublattices and defect superlattices

Francois Varchon, Aurélien Lherbier, Jean-Christophe Charlier

Université catholique de Louvain, IMCN/NAPS, Croix-du-sud 1, Louvain-la-Neuve, Belgium
francois.varchon@uclouvain.be

Graphene, a single carbon plane arranged on a honeycomb lattice, has received a lot of attention in the last few years due to its very appealing physical properties as the room temperature quantum hall effect, a large coherence length or a high electronic mobility [1]. These basic properties hold a high application potential for graphene in nanoelectronics. Nevertheless the future of this field strongly depends on the possibility to control the electronic properties of this material.

On the basis of extensive tight-binding and ab initio calculations, we demonstrate the possibility to tune graphene's electronic structure via realistic atomic defects (epoxide and hydroxyl groups chemisorbed on graphene).

For example we report on the bandgap opening in graphene monolayer induced by unbalanced disordered sublattices. Our findings show that the bandgap width depends on the nature, the concentration and the distribution (random, semi-random, periodic) of the impurities. We also perform an indepth study about the special case of periodic distribution of atomic defects. We demonstrate the existence of three different families of defect superlattices which conduct to specific band structures and therefore could lead to different electronic and transport properties [2].

References

[1] A.H. Castro Neto, F. Guinea, N.M.R. Peres, K.S. Novoselov, A.K. Geim*, Rev. Modern Phys., 81,* 109, (2009)

[2] A. Lherbier, F. Varchon, J.-C. Charlier (in preparation)

Mechanical behavior of high crystalline graphene oxide nanoplatelets in a thermoplastic polymer matrix

I. Rodriguez-Pastor[1], **H. Varela-Rizo[1]**, C. Merino[2], I. Martin-Gullon[1]

[1]Chemical Engineering Dept, University of Alicante, Ctra. de San Vicente s/n 03690 Alicante, Spain
[2]GRAnPH Nanotech, Ctra. Madrid-Irún, km. 244.8, 09007 Burgos, Spain
helena.varela@ua.es

The discovering of graphene with its impressive properties has involved the development of large-scale production methods, which is still challenging. Some techniques have been reported in the literature [1]: lithographic, chemical vapor deposition, chemical exfoliation, even methods that unzip carbon nanotubes into graphene layers or nanoplatelets. One of the most feasible, nowadays, is the chemical exfoliation [2]. This technique, traditionally performed from graphite [3], has been recently updated using CNTs as starting material [4], and consists of the intercalation and oxidation of graphene layers in graphite or CNTs to space them into separate graphene. The oxidation is followed by mechanical or thermal exfoliation, improving the yield of the separation into single layers. As innovation, in this work, we propose the use of helical-ribbon carbon nanofibers (HR-CNF), economical alternative of CNTs, as starting material for graphene synthesis by chemical exfoliation. High quality graphene oxide nanoplatelets (GONP) were produced [5].

This new material was introduced in a PMMA thermoplastic polymer matrix. Dispersion, tensile properties and fatigue of GONP/PMMA nanocomposites were studied and compared with PMMA nanocomposites containing pristine HR-CNFs and functionalized HR-CNFs with oxygen and nitrogen groups. GONP are easily exfoliated and more homogeneous dispersion is achieved compared to HR-CNFs (Figure 1 A and B). Furthermore, they provide better mechanical properties, with improvements never seen before with HR-CNFs (Figure 1 C), suggesting high potential of GONPS as reinforcement materials.

References

[1] Geim AK. Science 2009; 324 (5934): 1530-4.

[2] Marcano DC, Kosynkin DV, Berlin JM, Sinitskii A, Sun Z, Slesarev A, Alemany LB, Lu W, Tour JM. ACS Nano 4 (8): 4806-14.

[3] Stankovich S, Dikin DA, Piner RD, Kohlhaas KA, Kleinhammes A, Jia Y, Wu Y, Nguyen ST, Ruoff RS. Carbon 2007; 45 (7): 1558-65.

[4] Kosynkin DV, Higginbotham AL, Sinitskii A, Lomeda JR, Dimiev A, Price BK, Tour JM. Nature 2009; 458 (7240): 872-6.

[5] Varela-Rizo, H, Rodriguez-Pastor I, Merino C, Martin-Gullon I. Carbon 2010; 48(12): 3640-3643.

Figures
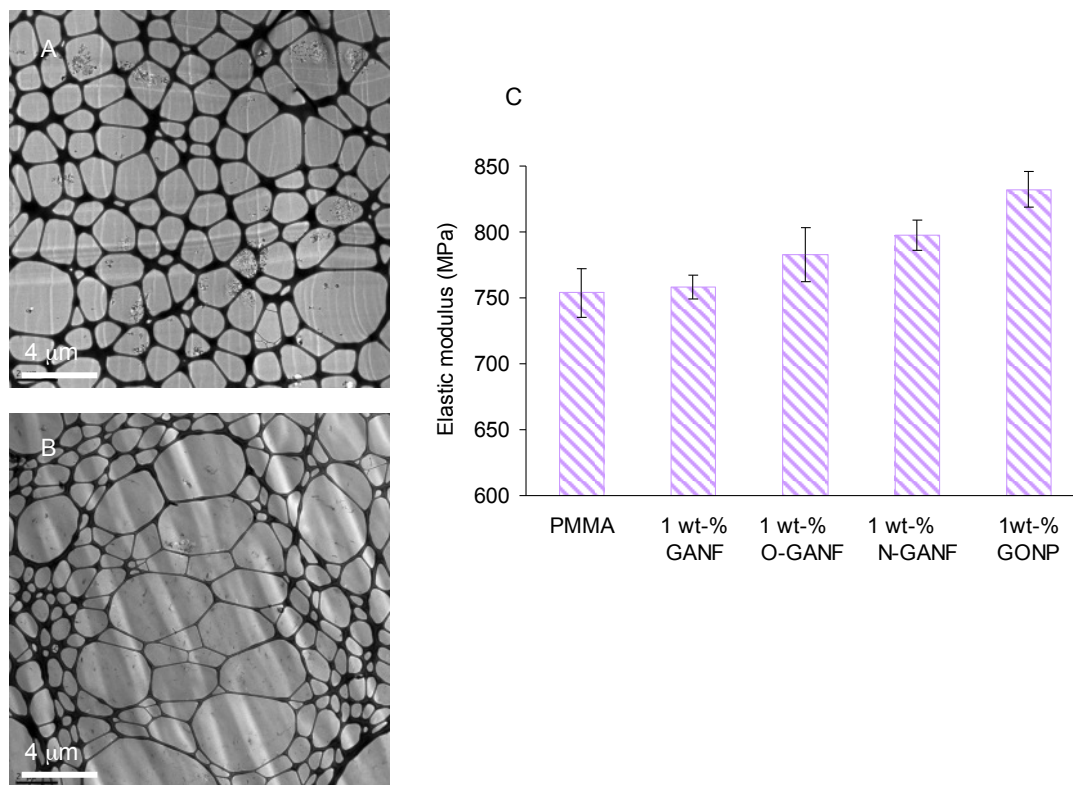
Figure 1. Comparison of GONP/PMMA and HR-CNFs/PMMA nanocomposites: A) Dispersion of HR-CNF/PMMA; B) Dispersion of GONP/PMMA; C) Elastic modulus of pristine and functionalized HR-CNF/PMMA and GONP/PMMA

Dual Gating of Suspended Graphene Devices via Contactless Gates

Jairo Velasco Jr., Lei Jing, Gang Liu, Philip Kratz, Yongjin Lee, Wenzhong Bao, Jeanie Lau
Department of Physics and Astronomy, University of California, Riverside
900 University Ave, Riverside Ca, USA
jvela004@ucr.edu

Monolayer and Bilayer graphene devices with local electrostatic gates present a rich platform for both academic and application driven inquiry. Realization of the veselago lensing effect and band gap engineering are a few of the most dazzling and promising physical phenomena that these systems are predicted to host. However, a major roadblock in this quest is the strict requirement for exceedingly clean samples. We have developed a method to fabricate suspended top gates above a suspended graphene flake to address this challenge. Using this technique we demonstrate dual gating of a suspended graphene flake. We will discuss the latest experimental progress towards the electrical transport of such a device in the zero-magnetic field regime, as well as in the quantum Hall regime.

Evaluation of the microwave frequency multiplication effects in microstrip gaps with graphene layers exfoliated from graphites with a different angular spread of the crystallite c-axes.

S. Ver Hoeye[1], F. Rodríguez[2], R. Menéndez[3], P. Álvarez[3], G. Hotopan[1], R. Camblor[1], C. Vázquez[1], M. Fernández[1], F. Las Heras[1]

[1]University of Oviedo, Campus Universitario de Gijón, Gijón, Spain
[2]Universidad de Alicante, Departamento de Química Inorgánica, Alicante, Spain
[3]Instituto Nacional del Carbón-CSIC,Oviedo, Spain
sverhoeye@tsc.uniovi.es

In this work, the frequency multiplication effect predicted in [1-2] is analyzed in a microwave microstrip gap covered with graphene layers exfoliated from graphites showing optically flat basal plane surfaces with different values for the angular spread of the crystallite c-axes. Three graphite samples have been used, two samples with a respective angular spread of the crystallite c-axes of 2.6º and 3.2º, and a third sample of less oriented graphite. The used microwave structure consists of two microstrip lines with tapered tips towards a gap of 0.15 mm that is covered with the exfoliated graphene layer (Fig. 1). The nonlinear behavior of the graphene layer is evaluated by applying on one side of the circuit an input signal at the fundamental frequency f_0 and measuring on the other side the third harmonic component that is generated at $3f_0$. The output power P_{out} of the third harmonic component at $3f_0$ (30 MHz to 10 GHz) has been measured when varying of the input frequency f_0 from 10 MHz to 3.33 GHz, and for different values of the input power P_{in} between 1 dBm and 10 dBm. The resulting ratio between the obtained output power $P_{out}(3f_0)$ and the input power $P_{in}(f_0)$ is shown in Fig. 2. With the used microstrip circuit, higher values for the output power have been obtained when using graphene layers exfoliated from less oriented graphites. From Fig. 2, it can also been observed that for higher values of P_{in} the output power slightly saturates. The measured third harmonic power has an almost flat frequency response along the whole frequency range.

References

[1] S.A. Mikhailov, K. Ziegler, "Nonlinear electromagnetic response of graphene: frequency multiplication and the self-consistent-field effects", Journal of Physics: Condensed Matter, 20 (2008) 384204.
[2] S.A. Mikhailov, "Electromagnetic response of electrons in graphene: Non-linear effects", Physica, E40 (2008), 2626-2629.

Figures
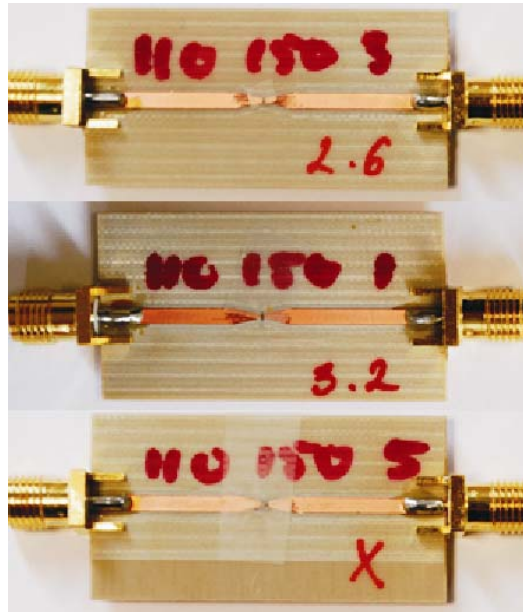
Fig. 1. Tapered microstrip line structures with a 0.15 mm gap covered with exfoliated graphene layers.
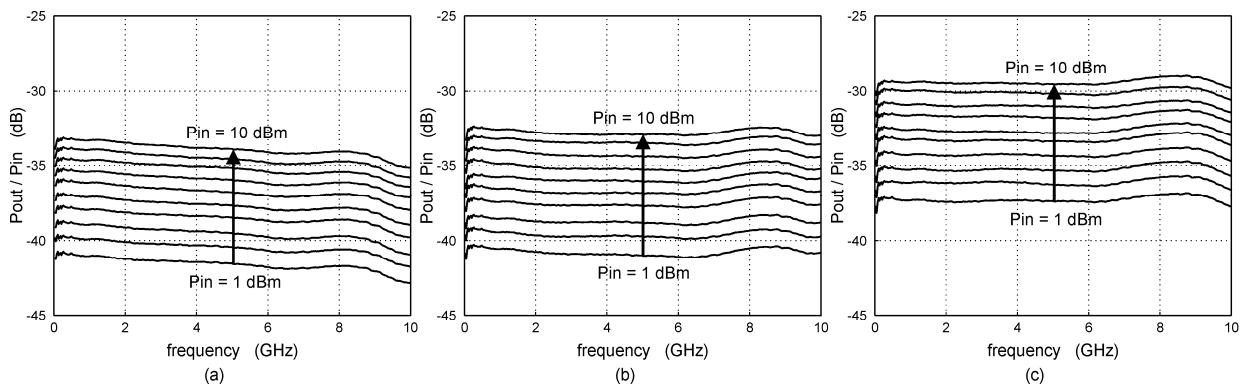
Fig. 2. Relation between the provided input power Pin at the fundamental frequency f_0 and the measured output power Pout at the third harmonic component at $3f_0$, for three types of graphites with corresponding angular spread of the crystallite c-axes: (a) 2.6º, (b) 3.2º, and (c) less oriented graphite.

Carbon nanowalls functionalization for controlling the metallic nanoparticles attachment

Sorin Vizireanu[1], Silviu Daniel Stoica[1], Bogdana Mitu[1], Catalin Romeo Luculescu[1], Leona Nistor[2]
Gheorghe Dinescu[1]

1 National Institute for Laser, Plasma and Radiation Physics, Magurele, 077125, Romania
2 National Institute for Materials Physics, Magurele-Bucharest, 077125, Romania
s_vizi@infim.ro

Carbon nanowalls, described as two-dimensional lamellar nanostructures assembled from few layers of graphene sheets, might be ideal hosts for supporting metallic nanoparticles because they have a large specific area related to their volume and present a nano-porous network. CNW decorated with metal nanoparticles can provide some of the most interesting nanocomposites materials, with applications in nano-sensors, catalysis and fuel cells. Important issues that need to be considered for development of nano-sensors are the attaching and integration of the nanoparticles on/in the nanostructures walls, their homogeneous dispersion/distribution, and their size. In general, the particle attachment to surfaces under controlled conditions is difficult. Promising results are obtained in case of functionalization (using for example plasma) of the nanostructured architecture support prior to the nanoparticles attaching.

The present contribution focuses on the CNW plasma functionalization processing for the promotion and control of nanoparticles attachment by activation and incorporation of functional groups. The functionalization with metal nanoparticles was achieved by sputtering of metal targets (Ni, Pt, Ag) using the magnetron technique implemented in the same deposition chamber in which the CNWs are synthesized. Magnetron sputtering deposition of metallic nanoparticles was done for different exposure times, on as –synthesized and plasma treated CNWs in hydrogen, oxygen and ammonia gases. The characteristics of the obtained nanoparticles/CNW materials were investigated by SEM, AFM, XRD, TEM, Raman Spectroscopy techniques.

WAVE PACKET DYNAMICS IN A MONOLAYER GRAPHENE AT THE PRESENCE OF ELECTRIC FIELD

V. Ya. Demikhovskii, **A. V. Volkov**

Nizhny Novgorod State University,
Gagarin Ave., 23, Nizhny Novgorod 603950, Russian Federation
on_ton@mail.ru

In this work we study the space-time evolution of electron wave packet moving in monolayer graphene placed in potential field, potential barrier, and wells. In particular, we describe and visualize the effect of additional splitting and interference in the process of Klein tunneling [1]. The Klein tunneling is one of the most important manifestations of the relativistic Dirac spectrum in graphene [2]. In this process an electron crosses a gap between two bands, which is a classically forbidden area, and transforms from an electron to a hole, or vise versa. At first time the effect of Klein tunneling on conductance in a graphene sheet in the ballistic regime was investigated in a series of works [2],[3].

Graphene is a single layer of carbon atom densely packed in a honeycomb lattice. The two-dimensional Hamiltonian describing its band structure has the form [4]

$$\hat{H} = \hat{H}_0 + \hat{I}U(x,y) = v_F\left(\hat{p}_y\hat{\sigma}_x + \hat{p}_x\hat{\sigma}_y\right) + \hat{I}U(x,y), \tag{1}$$

where v_F is the Fermi velocity, $\widehat{\vec{p}}$ is the momentum operator defined with respect to the centre of the valley centered at the corner of the Brillouin zone, $U(x,y)$ is the potential energy, $\hat{I}$ is a unit matrix. Here Pauli matrices $\hat{\sigma}_i$ operate in the space of the electron amplitude on two sites (A and B) in the unit cell of a hexagonal crystal, the internal degree of freedom playing a role of a pseudospin.

We represent the initial electron wave function by Gaussian wave packet having the width d and nonvanishing average momentum $p_{0x} = \hbar\, k_{0x}$,

$$\psi(\vec{r},0) = \frac{1}{d\sqrt{\pi(|c_1|^2+|c_2|^2)}}\exp\left(-\frac{r^2}{2d^2} + ik_{0x}x\right)\begin{pmatrix}c_1\\c_2\end{pmatrix}, \tag{2}$$

where coefficients c_1 and c_2 determine the initial pseudospin polarization, the packet width d is much greater than the lattice period and consequently $\psi(\vec{r},0)$ is smooth enveloping function. We suppose that Fermi level is located in the valence band and consider the problem in a one electron approximation.

For a numerical solution of the equation

$$i\hbar\frac{\partial}{\partial t}\begin{pmatrix}\psi_1\\\psi_2\end{pmatrix} = \hat{H}\begin{pmatrix}\psi_1\\\psi_2\end{pmatrix} \tag{3}$$

we adapt here a finite difference method described in [4] for solution of the two-dimensional massless Dirac equation. We use Crank-Nicholson scheme with Caley transformation of evolution operator.

Below we discuss the simple case when the initially localized wave packet Eq.(2) moves in a uniform electric field with potential $V(x) = -e\mathcal{E}x$. The results of numerical calculations for electron probability density (see Fig. (a)) and pseudospin density (see Fig. (b)) are presented below for the initial wave packet (2) with polarization $c_1 = 1$ and $c_2 = 1$ and average momentum k_{ox}. One can show that this initial wave packet can be considered as mainly a superposition of positive energy states of the Hamiltonian $\hat{H}_0$. As one can see from Fig. (a) the packet moving in the direction of vector $\vec{\mathcal{E}}$ parallel to x axis splits into parts. The splitting takes place at the point x_c where $k_x = 0$. At this point one part which is a superposition of the states with small k_y demonstrates Klein-like tunneling from the conduction band to the valence band. The right and left reflected parts are the superposition of the states with $k_y > 0$, $k_y < 0$ correspondingly. In Fig. (b) we illustrate the evolution of the component of the pseudospin density: $s_x(x,y,t) = 2Re(\psi_1^*\psi_2)$. If at $t = 0$ this component had the positive sign then at moment $t = 90$ *(in the units of d/u)* the reflected and transmitted parts get opposite pseudospin polarization. This is a result of that the reflected and transmitted part are superpositions of states with different chirality. If should be noted that the wave packet with the same initial average momentum k_{0x} and polarization $c_1 = 1$ and $c_2 = -1$ which is a superposition of negative energy states in a uniform

electric field propagates in opposite direction, and the tunneling takes place from the band E^- to the band E^+.

For the arbitrary pseudospin polarization when the wave packet can be considered as a superposition of the positive- and negative- energy states of Hamiltonian $\hat{H}_0$, the wave packet evolution is directly related to the Klein tunneling between two bands. In this case the reflected parts of the wave packet moving in opposite directions interfere that result in the new type of Zitterbewegung oscillation of the average packet coordinates and pseudospin polarization at the presence of electric field.

In our presentation we shall consider also the wave packet tunneling thought the potentials barriers and wells.

References

[1] O. Klein, Z. Phys. **53** (1929), 157.
[2] M. I. Katsnelson, K. S. Novoselov & A. K. Geim, Nature Phys. **2** (2006), 620.
[3] E. B. Sonin, Phys. Rev. B **79** (2009), 195438.
[4] J. C. Slonczewski and P. R. Weiss, Phys. Rev. **109** (1958), 272.
[5] G. M. Maksimova, V. Ya. Demikhovskii, and E. V. Frolova, Phys. Rev. B **78** (2008), 235321.
[6] T. Iitaca, Phys Rev. E **49** (1994), 4684.

Figure
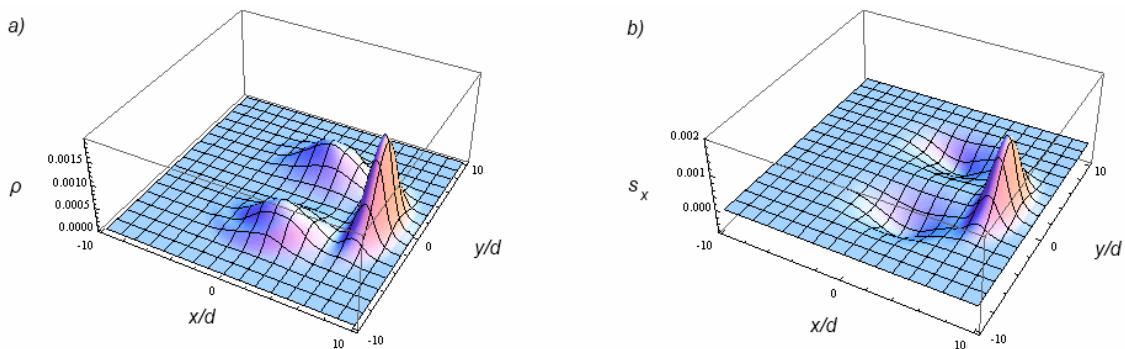
Figure caption

The electron probability density $\rho(x,y,t)) = |\psi_1|^2 + |\psi_2|^2$ (a) and pseudospin density $s_z(x,y,t)$ (b) for initial wave packet Eq.(2) with $c1 = 1$ and $c2 = 1$ for $k_{0x}d = 2$, at time $t = 90$ (in units of d/u). The calculation was performed for $d = 20\,nm$ and for electric field $E_x = u\hbar/3ed^2$ which corresponds to the amplitude $E_x = mV/cm$.

DFT calculation of spin-dependent transport properties of Z-shaped graphene nanoribbons

Jan Voves

Czech Technical University in Prague, Faculty of Electrical Engineering,
Technicka 2, CZ-16627 Prague 6, Czech Republic

voves@fel.cvut.cz

The recent fabrication of single layer graphene has promoted huge expectations in the field of all-carbon nanoelectronics and spintronics. The possibility to pattern graphene nanoribbons (GNRs) with widths of few tens of nm, has enabled band-gap engineering and the development of efficient GNRs-based spin filters. The lateral confinement of the 2DEG in GNR induces finite bandgap in semi-metallic graphene. It has been predicted that the electrical properties of GNR can be tuned from perfectly metallic, for zig-zag edge ribbons, to semiconducting behaviour, for armchair ribbons. In this later case, the gap varies with the ribbon width, length and topology [1] .

We performed density-functional theory (DFT) based calculations to obtain electronic structure of armchair/zig-zag/armchair Z-shaped GNRs [2] with a large variation of geometrical parameters. The spin-dependent exchange-correlation potential is approximated within the generalized gradient approximation (GGA) using the QuantumWise toolkit ATK, which employs local numerical double-zeta polarized basis orbitals. The spin-dependent transport properties of the electrode-device-electrode geometry were calculated by means of non-equilibrium Green's function formalism as implemented in ATK [3].

The GNR lateral asymmetry produces strong spin-dependent behavior resulting in a large spin polarisation effect. It is shown by analyzing the GNR trasmissivities. Our results endorse that for the generation of spin-polarized currents, formation of spin-ordered edge-localized states along the zigzag edges is the key mechanism [4, 5]. In the case of antiferromagnetic spin orientation at the opposite GNR edges spin dependent transmissivities appear when zigzag edges are long enough (Fig. 1). We analyzed the influence of the GNR width and of the lengths of arm-chair and zig-zag parts (Fig. 2). The first calculations of gate electrode influence is performed as well (Figs3, 4). Since GNRs have long spin-correlation lengths and good ballistic transport characteristics they can be considered as a promising active material of spintronic devices without the need of ferromagnetic electrodes or other magnetic entities [6]. The spin filtering structure could be prepared by the nanolithography of GNR.

References

[1] A.H.C. Neto, F. Guinea, N.M.R. Peres, K.S. Novoselov, A.K. Geim, Rev. Mod. Phys. **81** (2009) 109

[2] H. Ren, Q.X. Li, Q.W. Shi, J.L. Yang, Chin. J. Chem. Phys. **20** (2007) 489

[3] M. Brandbyge, J.L. Mozos, P. Ordejón, J. Taylor, K. Stokbro, Phys. Rev. **B 65** (2002) 165401

[4] T. Enoki, K. Takai, Solid. St. Comm. **149** (2009) 1144

[5] K. Nakada, M. Fujita, G. Dresselhaus, M.S. Dresselhaus, Phys. Rev. **B 54** (1996) 17954

[6] Y.T. Zhang, H. Jiang, Q. Sun, X.C. Xie, Phys Rev **B 81** (2010) 165404
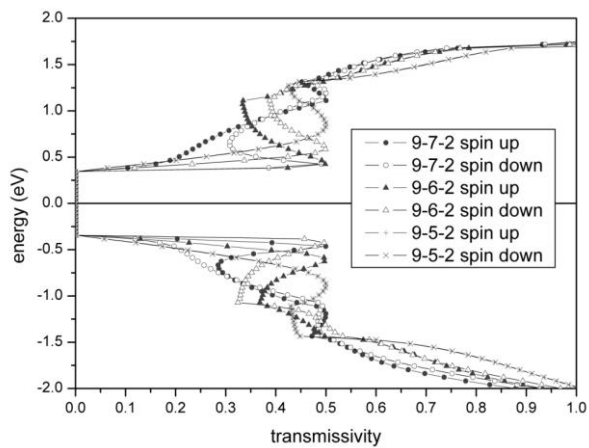
Fig 1.

Transmissivities of Z-shaped GNR with the width of 9 carbon atoms, two arm-chair segments with length of 2 carbon atoms and middle zig-zag part with length of 7, 6, and 5 carbon atoms for electrons with spin up and spin downorientations. No spin polarisation appears for the GNR with the shortest arm-chair part.
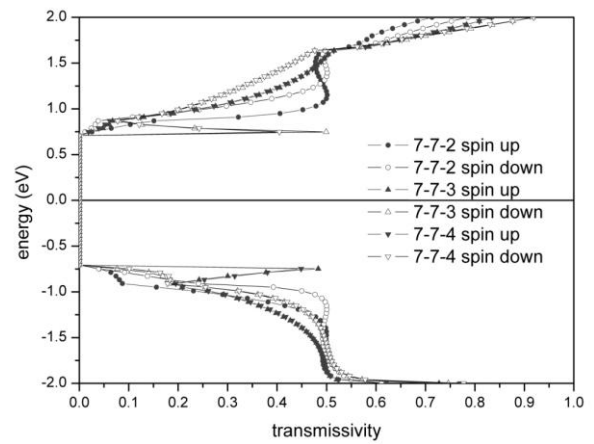
Fig. 2

Transmissivities for spin up and spin down of Z-shaped GNR with the width of 7 carbon atoms, two arm-chair segments with length of 2, 3 and 4 carbon atoms and middle zig-zag part with length of 7 carbon atoms. The GNRs with 3 and 4 carbon atoms in arm-chair segments show almost the same behavior.arm-chair part.
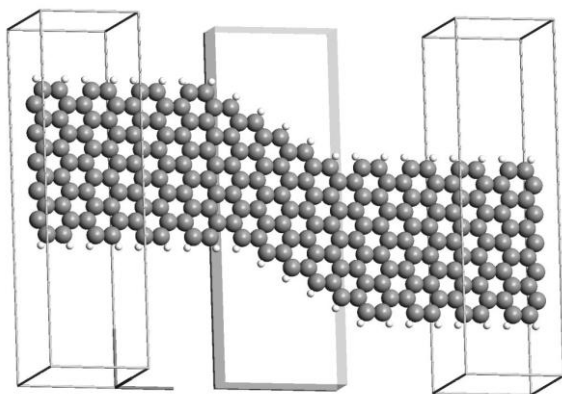
Fig. 3

Structure of Z-shaped GNR with the width of 11 carbon atoms, two arm-chair segments with length of 2 carbon atoms and middle zig-zag part with length of 7 carbon atoms and the gate beneath the zig-zag part.
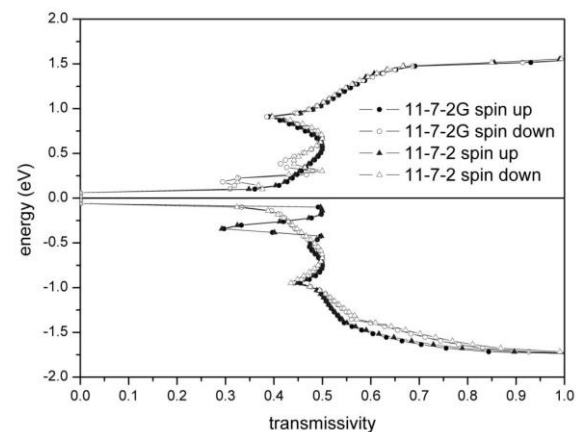
Fig. 4

Transmissivities for spin up and spin down of Z-shaped GNRs from Fig. 3 with (G) and without the gate beneath the zig-zag part. The gate potential is the same as at the both electrodes. The transmissivities are almost the same for this gate potential.

Chemical edge engineering of Graphene Nano Ribbons: a DFT study

Ph. Wagner[1]**,** A. Pateau[1], A. López-Bezanilla[2], S. Roche[3,4]**,** P. R. Briddon[5], C. P. Ewels[1]

[1] Institute of Materials, CNRS, Université de Nantes, BP32229, 44322 Nantes, France
[2] Oak Ridge National Laboratory, PO Box 2008, Oak Ridge, TN 37831, U.S.A.
[3] CIN2 (ICN-CSIC) and Universitat Autonoma de Barcelona, Catalan Institute
of Nanotechnology, Campus de la UAB, 08193 Bellaterra (Barcelona), Spain
[4] ICREA, Institució Catalana de Recerca i Estudis Avançats, 08010 Barcelona, Spain
[5] Department of Electrical Engineering, Newcastle University, Newcastle Upon Tyne, U.K.
philipp.wagner@cnrs-imn.fr

Although graphene displays a large number of extraordinary properties, there is still a need to modify some of these for graphene based devices. Notably for transistor design it is necessary to create and engineer an electronic gap in graphene. One way to introduce such a gap is by cutting graphene into graphene nanoribbons (GNRs). Previous studies have shown that ribbon gaps decrease exponentially with increasing width [1]. However less attention has been paid to other ways of controlling the band gap of ribbons. In particular, structure and chemical design of edge states are beginning to receive attention [2]. First experiments have shown that the most stable configurations of GNRs with chemically functionalised edges are mostly either zigzag or armchair edges [3]. The simplest chemical edge termination of GNRs is hydrogen termination, which is used almost exclusively in theoretical modeling [4,5]. In experiments however edges will be commonly terminated by a range of species including N, O, etc. Depending on the functional group both the electronic structure and the surface topology can change, as recently proposed in calculations of twisted F-terminated GNRs [6].

We present here the result of theoretical DFT studies of OH-terminated armchair and zigzag GNRs, and show first evidence of the stability of 3D-rippled edges as compared to flat OH-terminated ribbons. GNR result in a significant change of the GNR band gap as compared to equivalent hydrogen terminated ribbons. Hydrogen bonding occurs between neighbouring edge functional groups. We discuss resultant mobility and transport properties and the possibility for band gap and transport engineering through chemical control of edge site terminations.

References

[1] V. Barone, O. Hod, G. E. Scuseria, Nano Lett. **6** (12), (2006) 2748

[2] C. K. Gan and D. J. Srolovitz, Phys. Rev. B, **81**, (2010) 125445

[3] T. Wassmann, A. Seitsonen, A. Saitta, M. Lazzeri, F. Mauri, Phys. Rev. Lett., **101**, (2008) 096402

[4] Y. Kobayashi, K. Fukui, T. Enoki, K. Kusakabe, and Y. Kaburagi, Phys. Rev. B, **71**, (2005) 193406

[5] K. Nakada, M. Fujita, G. Dresselhaus, and M. S. Dresselhaus, Phys. Rev. B, **54**, (1996) 17954

[6] D. Gunlycke, J. Li, J. W. Mintmire, and C. T. White, Nano Lett., **10**, (2010) 3638

A complimentary approach to the chemical and structural characterisation graphene with Raman and X-ray photoelectron spectroscopy

M. Wall**, Kirill Bolotin****,T. S. Nunney*, R. G. White*, H. M. Meyer III***

* Thermo Fisher Scientific, The Birches, Imberhorne Lane, East Grinstead, West Sussex, RH19 1UB, UK.
** Thermo Fisher Scientific, 5225 Verona Rd, Madison, WI 53711, USA.
*** Materials Science and Technology Division, Oak Ridge National Laboratory, 1 Bethel Valley Road, Oak Ridge, TN, 37831-6064
**** Department of Physics, Vanderbilt University, Nashville, TN 37235
Mark.wall@thermofisher.com

The application potential of graphene is currently being extensively explored by the materials science commuinity. Its immediate potential as a transparent conductive electrode for the microelectronics industry is already being exploited and it is speculated that the unique combination of electronic, chemical and structural properties exhibited by graphene will imapct the development of thin film transistor development. Further applications for the development of graphene based molecular sensors are underway. In all stages of application development there is a requirement for materials characterization and analysis; from the initial research stages, through to testing of the finished devices. Most materials need to be analyzed for compositional homogeneity across the sample surface and thickness through the sample. It is rare that a single technique can achieve these testing requirements, and therefore a complementary approach involving several techniques is often required.

In this presentation we will discuss how a multi-technique approach using Raman and XPS can address the problems associated with the analysis of ultra thin film materials. This approach will be illustrated by examples from graphene and other carbon nanomaterials, comparing and contrasting the complementary chemical and structural information offered by each technique.

Raman microscopy is an analytical technique that is well suited for the characterization of graphene. Raman microscopy is a vibrational technique that that is very sensitive to small changes in a molecule's geometric structure and or its environment. This sensitivity allows Raman to be used as a probe for a number of properties important to a specific graphene samples. These properties include but are not limited to the determination layer thickness, the presence or absence of defects and for measuring local strain on a sample. Results from Raman investigations will be presented which will demonstrate Raman microscopy's usefulness in graphene and graphene based device characterization.

X-ray photoelectron spectroscopy (XPS) is ideally suited to the determination of the surface chemistry and the way in which that chemistry changes in the surface and near-surface region. The technique provides quantitative elemental and chemical information with extremely high surface specificity and is ideal for comprehensively and quantitatively characterising the elemental composition and chemical bonding states at surfaces and interfaces.

Anisotropic honeycomb lattice in the Hubbard

Guangquan Wang

National University of Singapore – (Singapore)

We explore the phase diagram of an anisotropic honeycomb lattice with in the frame work of the Hubbard Model. Other than the usual semi-metal, band-insulator and anti-ferromagnet, a new spin-liquid phase is identied, which can be understood in terms of strongly dimerized states. In the isotropic limit, in contrast to a recent Quantum Monte Carlo calculation, in addition to a gapped spin liquid, a gapless one is also found, which could possibly be eliminated by considering dierent dimer covering schemes.

Adsorption and Separation of Carbon-Monoxide on Metal-decorated Graphene Oxide

Lu Wang[1], Jijun Zhao[1]*, Yiyang Sun[2], Shengbai Zhang[2]

[1]Key Laboratory of Materials Modification by Laser, Ion and Electron Beams (Dalian University of Technology), Ministry of Education, Dalian 116024, P. R. China
[2]Department of Physics, Applied Physics, and Astronomy, Rensselaer Polytechnic Institute, Troy, New York 12180, USA
*Corresponding author: zhaojj@dlut.edu.cn

As the superstar in current nanoscience, graphene and related nanomaterials have attracted continuous interests in the past years, and have many applications in a variety of fields. Among these graphene related nanomaterials, graphene oxide (GO) has attracted resurgent attentions in recent years, though graphite oxide has been synthesized for more than 150 years. In our previous works, we have systematically investigated the structural stability of GO phases [1] and predicted that transition metal (e.g., Ti) anchored on GO can absorb molecular hydrogen at the room temperature avoiding metal clustering [2]. Here we will explore the potential applications of GO in the environmental field.

Release of toxic and exhaust gases into environment is a growing national concern and effective capture of these gases is an urgent issue to the environment protection. Finding the ideal sorbents for gas capture and separation is of great importance, and previous efforts have been focused on zeolites and metal-organic frameworks (MOF) materials due to their thermal stability, structural porosity, and high adsorption capacity. Separation and removal carbon monoxide (CO) from natural gas is one of the industrially significant separation processes and is an important issue in fuel cell technology. As the gas sorbents, GO has light mass with large surface area, very low cost and can be easily chemical modified. Here we will propose metal-decorated GO as an ideal sorbent for CO adsorption and separation from the natural gas (e.g., N_2) or the other gas mixtures (e.g., CH_4). The adsorption capacity and selectivity of different toxic and exhaust gases on the metal-decorated GO surface has been comprehensively studied using first-principles calculations and Grand Canonical Monte Carlo simulations. In addition to understand the binding strength and electronic effects of the gas adsorbed on the metal-decorated GO substrate, we further explore the possibility of selection/separation of gas mixture. Moreover, different decorated metals exhibit different adsorption capacities for gases.

References

[1] L. Wang, Y. Y. Sun, K. Lee, D. West, Z. F. Chen, J. J. Zhao, and S. B. Zhang, Phys. Rev. B **82** (2010) 161406.
[2] L. Wang, K. Lee, Y. Y. Sun, M. Lucking, Z. F. Chen, J. J. Zhao, and S. B. Zhang, ACS Nano, **3** (2009) 2995.

Figures

(a)   (b)
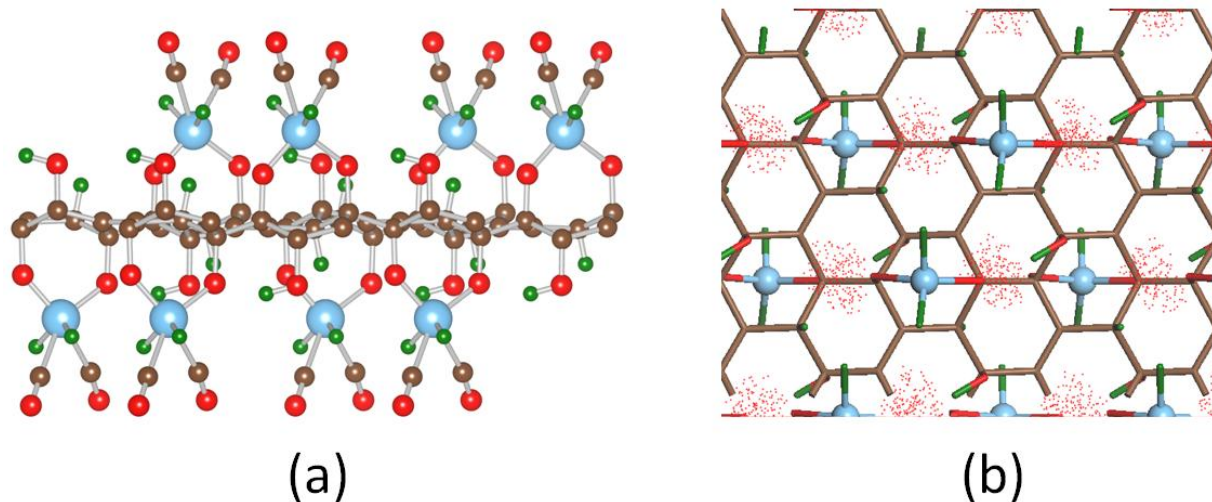
(a) Optimized structures of Ti-decorated GO with fully loaded CO adsorption from first-principles calculations, brown balls denote carbon atoms, red balls for oxygen atoms, green balls for hydrogen atoms and light blue for titanium atoms; (b) Density distributions for CO molecules on the Ti-decorated GO at the condition of 298 K and 10 Bar using the Grand Canonical Monte Carlo simulations, and the red points are the centers-of-mass of the adsorbed CO molecules.

Plasmons in graphene nanostructures

Weihua Wang, Peter Apell and Jari Kinaret

Department of Applied Physics, Chalmers University of Technology, Gothenburg, Sweden
Weihua.Wang@chalmers.se

We study plasmon excitations in nanoscale graphene disks and edge plasmons in semi-infinite sheets and compare to the corresponding results for 2D metals within a random phase approximation.. Our results indicate that the unusual dispersion relation of graphene gives rise to interesting deviations from the usual nanoparticle plasmons and surface and edge plasmons seen in conventional metals.

A finite doped graphene sheet, with Fermi level away from the Dirac point, shows metallic properties including the plasmon excitation also at zero temperature. The density dependence of the plasma frequency is $\omega \propto n^{1/4}$, while it is $\propto n^{1/2}$ for the 2D electron system. Taking into account that the electron density of a finite doped graphene is much smaller than that of usual metals results in a plasma frequency of doped graphene which is much lower than that of metals. This special feature makes the doped graphene a good candidate for studying the intrinsic THz plasmon excitation and inspiring THz applications such as THz sensor.

References

[1] E.H.Hwang and S.Das Sarma, Phys.Rew.B, **75** (2007) 205418.
[2] Marinko Jablan, Hrvoje Buljan and Marin Soljacic, Phys. Rew.B, **80** (2009) 245435.

In situ studies of graphene growth during realistic CVD conditions

Robert S. Weatherup[1], Bernhard C. Bayer[1], Raoul Blume[2], Carsten Baehtz[3], Robert Schloegl[2], Stephan Hofmann[1]

[1] Engineering Department, University of Cambridge, Cambridge, CB3 0FA, United Kingdom
[2] Fritz-Haber-Institut, 14195 Berlin, Germany
[3] Forschungszentrum Rossendorf, Germany & ROBL-CRG, France
rsw31@cam.ac.uk

Scalable, economic growth is a key requirement to utilise the unique properties of mono- and few-layer graphene (FLG) for device applications. The most promising and versatile growth technique for graphene is catalytic chemical vapour deposition (CVD), in which catalyst surfaces are exposed to a gaseous carbon precursor at elevated temperatures.[1] This offers a low-cost method of producing graphene across large areas, but at present the growth mechanism(s) are not well understood. Elucidation of the growth processes is needed to enable the control and optimisation of CVD graphene growth beyond the empirical calibrations of C dose and the process temperature profile. In particular, improvements in the domain size and the control of layer number are needed before CVD graphene becomes suitable for a wide range of applications.

We compare (few-layer) graphene growth based on a solid C source to graphene CVD based on low hydrocarbon exposures on thick (>300 nm), poly-crystalline transition metal films. We investigate a range of different solid and gaseous carbon precursors to understand the effect of C source on the growth. We focus on graphene nucleation and graphene domain size in relation to the catalyst grain size distribution and the C chemical potential.

We perform in-situ high-pressure X-ray photoelectron spectroscopy (XPS) and in-situ X-ray diffraction (XRD) during graphene growth at temperatures between ~300-700C, and during subsequent cooling. In situ XPS is carried out at the BESSY II synchrotron at the ISISS end station of the FHI-MPG and in-situ XRD at ESRF at the Rossendorf Beamline. Time- and depth- resolved, high-pressure XPS[2] is used to obtain a detailed record of transient C/metal core level signatures prior to and during graphene formation for the different experimental conditions. Whereas XPS provides compositional data for the catalyst surface and near-surface (<1nm) region, we complement this technique with in-situ XRD which allows characterisation of the bulk crystalline phases present during growth. This allows determination of the catalyst microstructure, phase composition, and how this evolves during graphene nucleation and growth. Based on this combination of in-situ techniques, we model the growth processes involved in catalytic graphene growth.

Ex-situ characterisation is used to assess the uniformity and domain sizes of as-grown and transferred graphitic layers by optical/scanning electron microscopy, Raman spectroscopy, and transmission electron microscopy (TEM). The graphene film properties are then compared with the in-situ data to aid and corroborate the interpretation of the in-situ XPS and XRD results.

References

[1] Oshima et al., J. Phys.: Condens. Matter, **9** (1997) 1

[2] Hofmann et al., J. Phys. Chem. C, **113** (2009) 1648

Graphene Oxide: a novel support for Transmission Electron Microscopy of Polymers

Ana M. Sanchez[1], Neil R. Wilson[1], Jonathan P. Rourke[2], Priyanka A. Pandey[1], Joseph P. Patterson [2] and Rachel K. O'Reilly[2]

[1]Department of Physics, University of Warwick, Coventry, CV4 7AL, U.K.
[2]Department of Chemistry, University of Warwick, Coventry, CV4 7AL, U.K.

a.m.sanchez@warwick.ac.uk

The design and synthesis of self-assembled block amphiphilic copolymers are of interest for the preparation of multifunctional polymeric nanostructures. By tuning the hydrophilic/hydrophobic balance of these polymers a range of morphologies can be accessed, including spherical micelles, cylinders and vesicles. These materials are of potential interest in applications such as nanoreactors or delivery vehicles [1,2]. However, accurate nanometre scale measurement of morphology is essential in order to give control and optimize these systems. Although transmission electron microscopy (TEM) and associated analytical techniques can supply information about morphology and chemical composition at sub-nanometre levels, scattering from light elements is weak. This leads to very low contrast when this type of specimen is examined upon a conventional support film such as amorphous carbon or formvar. The most common approach to overcome this problem is to stain the specimen with a heavy element (e.g. using OsO_4, or Phosphotungstic Acid PTA) to increase contrast, allowing morphology and the polymer phases in the system to be visualized. Nevertheless, staining is an invasive technique which may affect the morphology, can lead to significant and misleading artifacts, and make compositional analysis difficult or impossible. Analysis of polymer systems without staining would represent a major step forward.

Graphene is a highly electron-transparent material, as it consists of a single sheet of carbon atoms. It has found applications in recent years as a support film for nanoparticle analysis [3], but has the disadvantage that manufacture of graphene coated grids is both time-consuming and expensive and that graphene itself is hydrophobic. Graphene oxide (GO), however, is hydrophilic and water soluble, and large areas of single-sheet GO for use as TEM support films are extremely easy to prepare by drop casting methods. Furthermore, the chemical manufacture of GO is also simple and is a very low-cost process in comparison with graphene. GO retains the hexagonal symmetry of the unmodified graphene without any ordering in the functional groups [4]. It has been also demonstrated by TEM that GO is highly electron transparent and stable under the electron beam. The electron transparency of GO is close to that of graphene itself, and its hydrophilicity makes it easy to deposit samples directly from solution, and consequently it is an ideal support film for self-assembled diblock copolymer nanostructures. Furthermore, the chemistry of the GO surface can be tailored by further functionalisation, opening up the possibility of new fields of experimentation.

In this work, we show how diblock copolymer systems can be imaged on GO allowing morphological and compositional analysis to be carried out without staining. GO support films were prepared by drop casting from a 0.25 mg ml^{-1}GO aqueous suspension onto a lacy carbon TEM grid. The diblock co aggregates, consisting of Polylactide (aka Polylactic acid, PLA) (Hydrophobic) and Poly acrylic acid (PAA) (hydrophilic), were deposited directly onto this support and examined in a JEOL 2100 LaB$_6$ TEM operating at 200 kV. A typical image is shown in Fig. 1. The contrast in this TEM image arises from both mass-thickness and phase contrast mechanisms. To enhance the phase contrast, the image was recorded in under-focus conditions, i.e. inducing a phase shift of the scattered electrons. It is evident from the structural characterization of the unstained diblock copolymer on GO is that there is a wall

thickness of ~ 2 nm which could not be observed in the stained specimen Fig. 2. Additionally, the stained specimen does not reveal the presence of both open and closed cylinder nanostructures as can be observed in the specimen prepared directly on the GO support. The mottled background is contamination arising from the diblock copolymer deposition, its removal will enable further advances in resolution and detailed analysis of these self-assembled nanostructures.

References

[1] G Riess, *Prog. Polym. Sci.* **28**, (2003) 1107

[2] A. Blanazs, S. P. Armes, and A. J. Ryan, *Macromol. Rapid Commun* **30,** (2009) 267

[3] W. J. Huang, R. Sun, J. Tao, L. D. Menard, R. G. Nuzzo & J. M. Zuo, *Nat. Mat.* 7 (2008) 308

[4] N. R. Wilson, P. A. Pandey, R. Beanland, R. J. Young, I. A. Kinloch, L. Gong, Z. Liu, K. Suenaga, J. P. Rourke, S. J. York, and Jeremy Sloan, *ACS Nano* **3**, (2009) 2547.
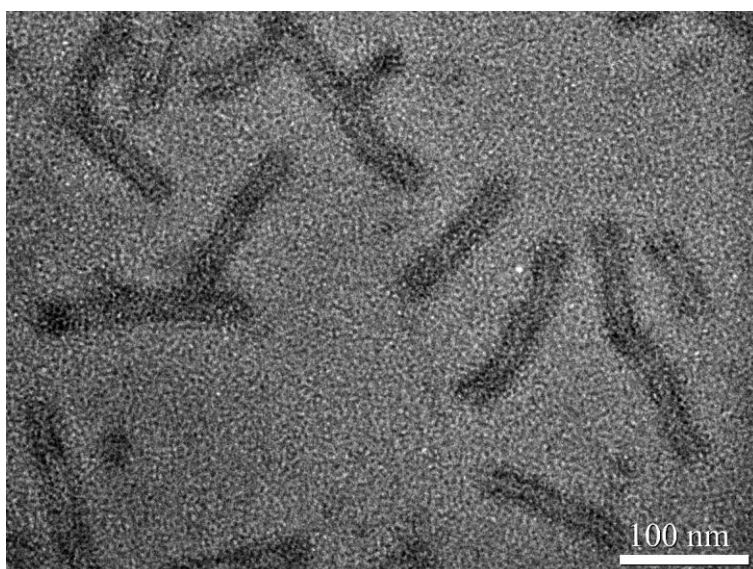
Figures

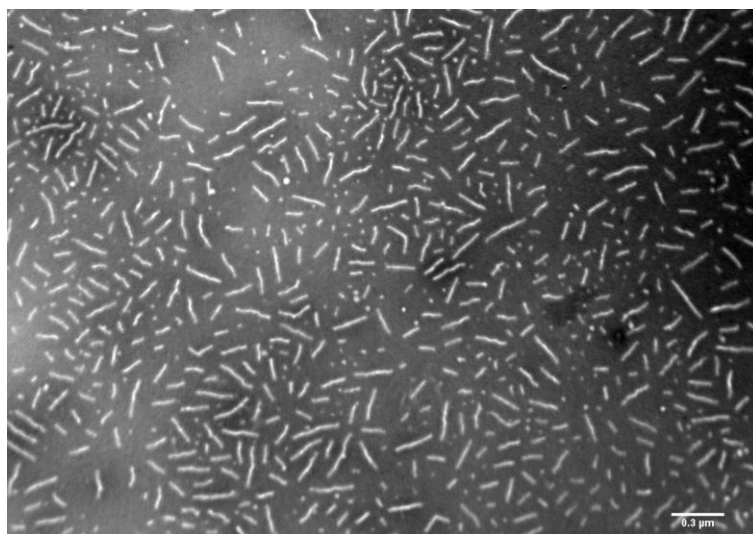*Figure 1. TEM image of the copolymer deposited directly on the GO support film.*

Figure 2. TEM image of the PTA-stained copolymer on a carbon support film.

The real graphene oxide revealed: stripping the oxidative debris from the graphene-like sheets

Neil R. Wilson[1], Priyanka A. Pandey[1], Joseph J. Lea[2], Matthew Bates[1], Ian A. Kinloch[3], Robert J. Young[3], and Jonathan P. Rourke[2]

[1]Department of Physics, University of Warwick, Coventry, CV4 7AL, UK
[2]Department of Chemistry, University of Warwick, Coventry, CV4 7AL, UK
[3]School of Materials, The University of Manchester, Grosvenor Street, Manchester, M1 7HS, UK
Neil.Wilson@warwick.ac.uk

Graphene oxide (GO) provides a potential route to large quantities of graphene, is cheap to make in bulk and easy to process.[1, 2] It is also a starting point for further functionalisation to create chemically modified graphenes (CMGs) e.g. for use in composites, light-harvesting, or as sensors. Understanding the chemical and physical structure of GO is a necessary step towards its controllable functionalisation for CMGs and potential complete reduction back to graphene.

Here we will provide compelling evidence that GO, as produced by the Hummers' method, is composed of functionalized graphene sheets decorated by strongly bound oxidative debris, which acts as a surfactant to stabilize aqueous GO suspensions. We will also show that the physical and chemical properties of the as-produced GO are strongly influenced by this oxidative debris.[3]

Upon the addition of NaOH as-produced graphene oxide (aGO) rapidly separated into a black aggregation and an essentially colorless supernatant, Figure 1. The black aggregate was separated and analysed; TEM and AFM showed it to contain graphene-like single sheets (we subsequently refer to it as base-washed GO, or bwGO). The supernatant was also dried and analysed; it showed a similar FTIR spectrum to aGO but contained no graphene-like sheets. We will show that this material contains oxidative debris, and refer to it as OD. Careful and independent measurement of the masses revealed that 64 ± 2 % of the mass of aGO can be attributed to bwGO, and 30 ± 9 % to OD. We conclude that base-washing separates aGO into two-parts, bwGO and OD, and that by mass they are present in a ratio of roughly 2:1. XPS analysis showed the C:O ratio increased from 2:1 for aGO to 4:1 for bwGO, with no discernible change in the Raman spectra, Figure 2. It was not possible to resuspend the bwGO in water. bwGO is conducting with a conductivity of order 10^0-10^1 S m^{-1}.

These results strongly suggest that the as-produced GO consists of functionalized graphene-like sheets to which oxidative debris is strongly adhered. The graphene-like sheets are oxidized, but at a much lower level than current models for GO suggest, Figure 3. This OD-bwGO complex appears to be indefinitely stable in water, but the removal of the oxidative debris can simply be effected with a base wash, whereupon the more highly functionalized debris dissolves fully into water, leaving a suspension of functionalized sheets. The importance of the oxidative debris is demonstrated by the change in properties of aGO after its removal: unlike as-produced GO, the resultant base-washed graphene oxide is not easily suspended in water and is conducting.

Our results suggest that models for the structure of graphene oxide need revisiting. The oxidative debris non-covalently attached to as-produced GO has important implications for the synthesis and application of CMGs, particularly where direct covalent functionalisation of the graphene lattice is required.

.

References

[1] S. Park, and R. S. Ruoff, Nat. Nano. **4**, (2009). 217
[2] D. R. Dreyer *et al.*, Chem. Soc. Rev. **39**, (2010). 228
[3] J. P. Rourke *et al.*, Angew. Chem. Int. Ed. **accepted for publication**, (2011)

Figures
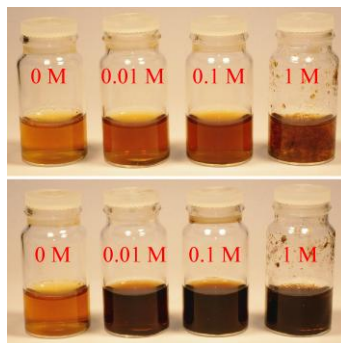
Figure 1. Photograph of 0.5 mg ml-1 aGO suspension in NaOH (concentrations as marked) within 30 s of addition of the NaOH (top), and after three hours (bottom).
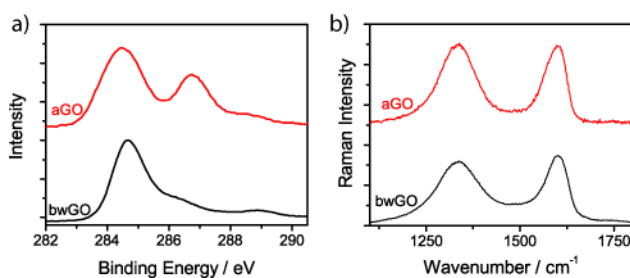
Figure 2. a) C 1s XPS spectra of as-produced GO (aGO) and base-washed GO (bwGO). b) Raman spectroscopy of aGO and bwGO using 633 nm laser excitation.
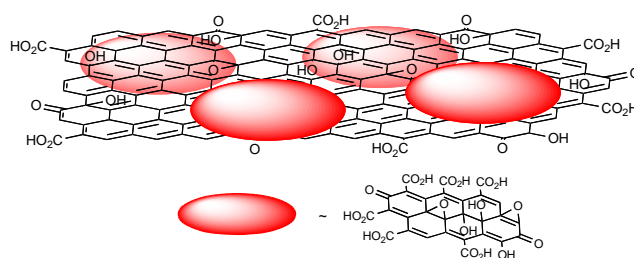
Figure 3. A diagrammatic representation of aGO; large oxidatively functionalized graphene-like sheets with surface bound debris. Note that the graphene-like sheets extend further than depicted.

Multiplication of photo-excited carriers in graphene

Torben Winzer, Andreas Knorr, and Ermin Malic

Technische Universitaet Berlin, Hardenbergstrasse 36, 10623 Berlin, Germany
t.winzer@mailbox.tu-berlin.de

We present microscopic calculations of the relaxation dynamics of photo-excited carriers in graphene. Our approach includes the major relaxation channels, i.e. carrier-carrier as well as carrier-phonon scattering, and considers the coupled ultrafast dynamics of carrier population, coherence, and phonon population resolved in time and momentum. In agreement with several differential transmission experiments, we observe a redistribution of the excited carriers to energetically lower states resulting in a hot Fermi-Dirac distribution on a hundred femtosecond timescale followed by phonon-induced cooling in the range of a few picoseconds [1-4].

Due to its zero-bandgap and the linear bandstructure of graphene, Auger-type relaxation channels become efficient, which are negligible in conventional semiconductors. In contrast to any other Coulomb-induced channels, these scattering processes modify the total carrier density by bridging the valence and conduction band. Two competing processes are important: Auger recombination (AR) annihilates an electron and a hole, whereas impact ionization (II) creates both (cp. fig. a). Here, we evaluate both Auger-type processes and find a significant influence on the relaxation dynamics in the form of ultrafast carrier multiplication (CM), a process where multiple charge carriers are generated from the absorption of a single photon [5].

The temporal evolution of the total carrier density during and after a 10 fs pulse (800 nm) is shown in figure b. To study the influence of Auger-processes, we compare two situations: First, only the excitation is simulated to obtain the number of optically excited carriers (blue line). In a second calculation we include the full Coulomb scattering resulting in a significant increase of the carrier density after the pulse (red line). This nonequilibrium effect is caused by an asymmetry between AR and II during the equilibration in favor of II. We note that the CM depends on the strength of the pulse, for higher excitations the CM is reduced. Including the carrier-(optical)phonon scattering we also estimate the efficiency of the CM under realistic conditions. As expected, we observe a phonon induced carrier recombination and temporal decay of the carrier density on a picosecond timescale. Thus, the carrier multiplication remains efficient up to a few picoseconds confirming the potential of graphene as a new material for photodevices.

References

[1] D. Sun, *et al.*, Phys. Rev. Lett., **101** (2008) 157402.
[2] J. M. Dawlaty, *et al.*, Appl. Phys. Lett. **92** (2008) 042116.
[3] H. Wang, *et al.*, Appl. Phys. Lett. **96** (2010) 081917.
[4] J. Shang, *et al.*, Appl. Phys. Lett. **97** (2010) 163103.
[5] T. Winzer, *et al.*, Nano Lett. **10** (2010) 4839-4843.
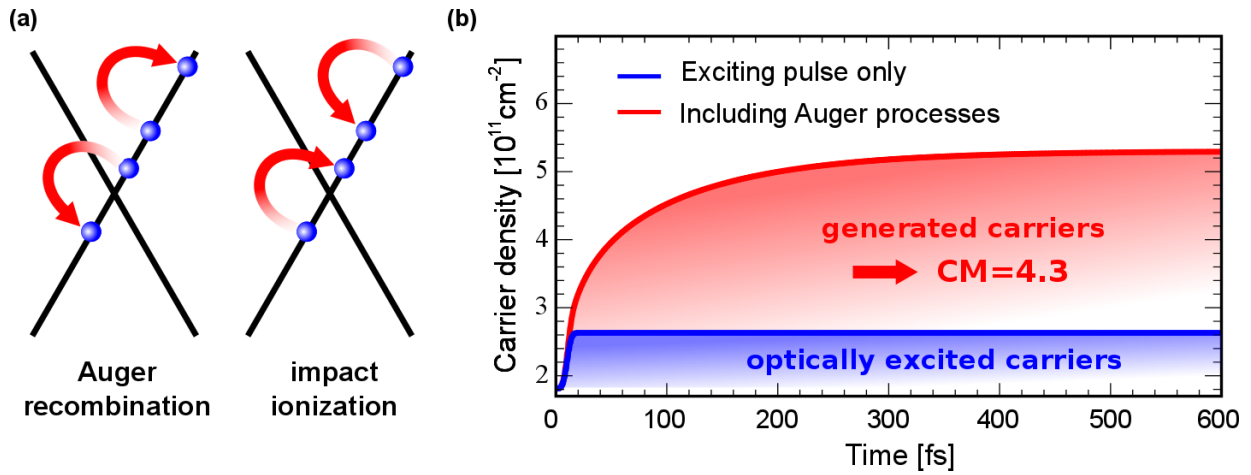
Figure: (a) Scattering scheme of Auger recombination and impact ionization. Both processes fulfill momentum and energy conservation. (b) Temporal evolution of the charge carrier density considering the exciting pulse (blue) and carrier-carrier scattering (red). The preference of II results in a significant increase of the carrier density during the equilibration.

Graphene-PEDOT:PSS modified Screen Printed Carbon Electrode for Electrochemical Sensing

A. Wisitsoraat, C. Karuwan, C. Sriprachuabwong, D. Phokharatkul, P. Sritongkham, A. Tuantranont

Nanoelectronics and MEMS Laboratory, National Electronics and Computer Technology Center, 112 Thailand Science Park, Phahon Yothin Rd., Klong 1, Klong Luang, Pathumthani 12120, Thailand
adisorn.tuantranont@nectec.or.th

Graphene is an ideal material for electrochemistry because of its very large two-dimensional electrical conductivity, excellent electron transfer rate, huge specific surface area and low cost. In addition, it is considered a more practical electrode material than carbon nanotubes (CNTs) counterpart because it can be cheaply produced from low cost graphite with no metallic impurity [1-2].

In this work, a electrochemically synthesized graphene-PEDOT:PSS (GP-PEDOT:PSS) is presented as a new electroactive material that is utilized for the first time to modify screen printed carbon paste electrode (SPCE) by inkjet printing technique. The electrochemical characteristics of the inkjet printed SPCE electrode is characterized by cyclic voltammetry (CV) for detection of salbutamol.

Two graphite rods were placed in an electrolysis cell filled with the PEDOT:PSS electrolyte and a constant potential of 8 V was applied between electrodes for 5 hours to obtain stable GP-PEDOT:PSS dispersion with intended graphene concentrations. The dispersed product was centrifuged at 1200 rpm to separate large agglomerates and supernatant portion of the dispersion was then decanted. The GP-PEDOT:PSS solution was used as an ink for inkjet printing on SPCE by the commercial Dimatrix material inkjet printer. Five layers of GP-PEDOT:PSS material were coated over 3×5 mm^2 electrode area. The surface morphologies of fabricated electrochemical electrodes were examined by SEM (Fig. 1). It is seen that uncoated SPCE electrode has rough surface with large grain size of several microns and surface becomes smoothen after inkjet printing with PEDOT:PSS or GP-PEDOT:PSS.

Cyclic voltammetric response of GP-PEDOT:PSS modified SPCE electrode in 1 mM salbutamol solution was compared to those of PEDOT:PSS modified and unmodified SPCE electrodes as shown in Fig. 2. It is found that the oxidation peak amplitudes of PEDOT:PSS modified and GP-PEDOT:PSS modified SPCE electrodes are approximately 30 and 150 times higher than that of unmodified SPCE electrode, respectively. The dramatic enhancement can be attributed to huge reactive surface area, high electronic conductivity and excellent electron transfer rate of graphene and PEDOT:PSS. Cyclic voltammetric responses of electrodes with different numbers of inkjet printing GP-PEDOT:PSS layers are shown Fig. 3 (a). It can be seen that the oxidation peak of salbutamol is considerably affected by the number of inkjet printing layers. The oxidation peak amplitude is then plotted as a function of number of inkjet printing layers as shown in Fig. 3 (b). It is evident that the current amplitude initially increases as the number of layers increases from 1 to 4 and then begins to decrease. Hence, the optimal number of printing layers is 4. From concentration depedent study, good analytical features with wide dynamic working range of more than 500 µM and low detection limit (3S/N) of 1.25 µM are obtained. Therefore, electrode based on inkjet printed GP-PEDOT:PSS layer is a promising candidate for advanced electrochemical sensing applications.

References

[1] Alwarappan, S.; Erdem, A.; Liu, C.; Li, C.-Z. J. Phys. Chem. C 2009, 113, 8853

[2] Pumera, M.; Ambrosi, A.; Bonanni, A.; Chng, E.L.K. Poh, H. L., Trends. Anal. Chem. 2010, 29, 954.

Figures
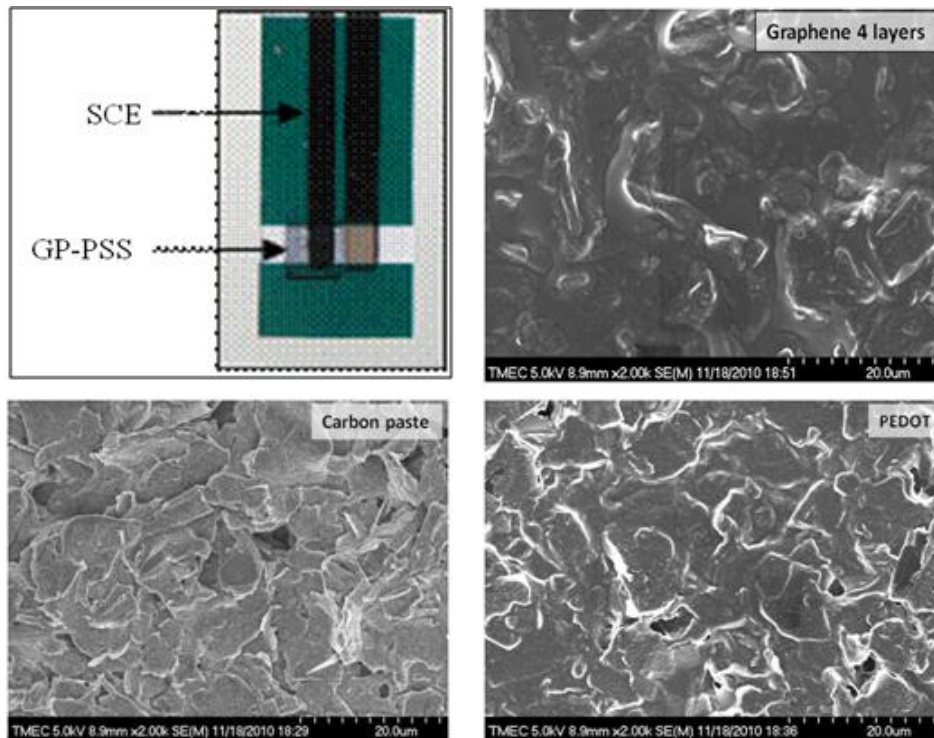
Fig. 1 Photograph of fabricated electrode and SEM micrographs of SPCE electrode, inkjet printed PEDOT:PSS on SPCE electrode and printed GP-PEDOT:PSS on SPCE electrode.
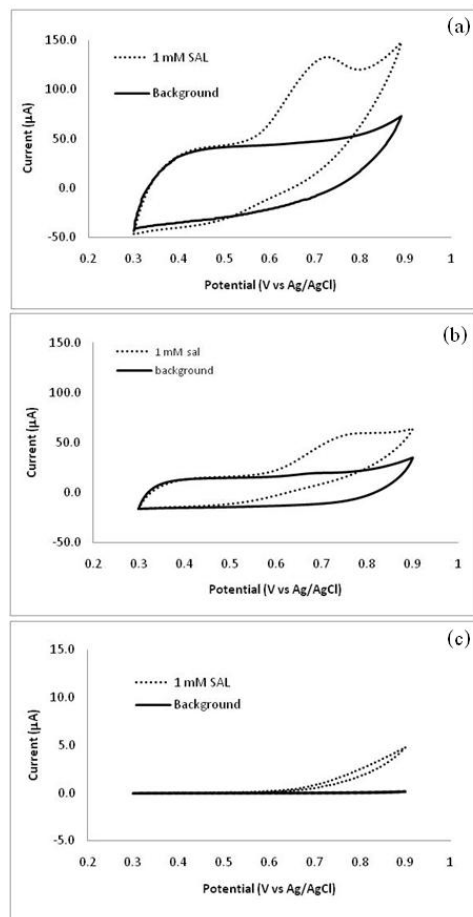
Fig. 2 The oxidation of 1 mM salbutamol on (a) GP-PEDOT:PSS and (b) PEDOT electrode and (c) SPCE electrode. Scan rate was 100mVs−1. 50 mM PBS: pH 7.0.
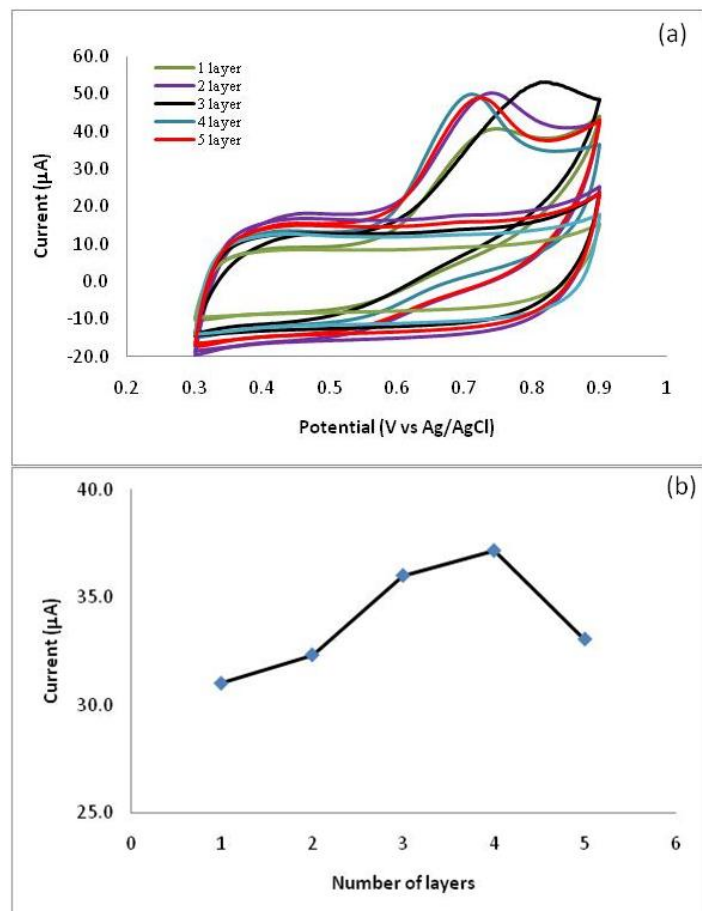
Fig. 3 (a) Cyclic voltammograms obtained at various number of printed GP-PEDOT:PSS layers on SPCE electrode. (b) Relationship between current response and number of GP-PEDOT:PSS layers. Scan rate was 100mVs−1. 50 mM PBS: pH 7.0.

Bandgap opening in hydrogenated graphene studied by electronic transport and STM

M. Wojtaszek, A. Castellanos-Gomez, Arramel, N. Tombros and B.J. van Wees

Physics of Nanodevices Group, Zernike Institute for Advanced Materials,
University of Groningen, Nijenborgh 4, Groningen, The Netherlands
M.Wojtaszek@rug.nl

Most electronic logic applications require material with a bandgap. Although graphene is a gapless conductor a gap can be created by chemical modification, e.g. hydrogenation [1], in which adsorbed H changes the orbital hybridization of carbon from sp2 to sp3. Depending on the degree of hydrogenation one can tune the graphene's transport properties from zero-gap semiconductor to insulator. In experiment we hydrogenate graphene by RF plasma with a gas mixture of Ar/H_2 (85:15). Here, the introduced defects like hydrogen adsorbates or argon induced vacancies, can be characterized by the ratio of the D and G band in Raman spectrum [2]. We present the systematic studies of electronic transport in graphene depending on plasma exposure time and report the influence of the amount of defects on graphene carrier mobilities and mean free path.

Additionally, we have explored the change in the electronic properties of CVD graphene and graphite after hydrogenation by scanning tunneling microscopy (STM). STM topography images reveal a non-uniform hydrogen chemisorption on the surface, forming islands, which cover roughly 20% of the surface. From the statistical analysis of scanning tunneling spectroscopy (STS) traces we have observed a hydrogen induced bandgap opening, with an average value of 0.6 eV. Further, we have studied the electronic and structural changes of the samples after a moderate thermal annealing which should de-hydrogenate the surface. Remarkably, it has been found that even though topographic changes are not fully reversible after annealing, the bandgap is closed. The full cycle of hydrogenation/de-hydrogenation can be repeated with similar results.

References

[1] Elias, D.C. et al. *Science (2009), 323*, 610-613
[2] Lucchese, M.M. et al. *Carbon 48 (2010)*, 1592-1597

Figures
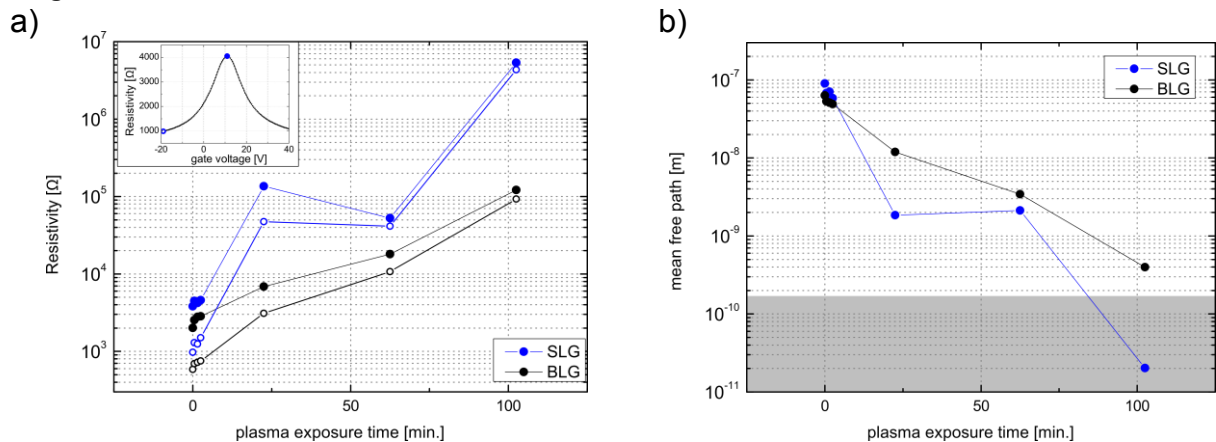
Figure 1. (a) Resistivity of single (blue) and double layer graphene (black) after several exposures to hydrogen plasma. Filled circles represent the resistivity at the Dirac point, open circles represent the resistivity in metallic regime (at $2 \cdot 10^{12}$ cm^{-2} carrier density). The inset present the single resistivity curve for SLG. (b) Mean free path of charge carriers in graphene after the exposures. The gray area indicates the values below the length of C-C bond, where the calculations of the mean free path are no longer valid.
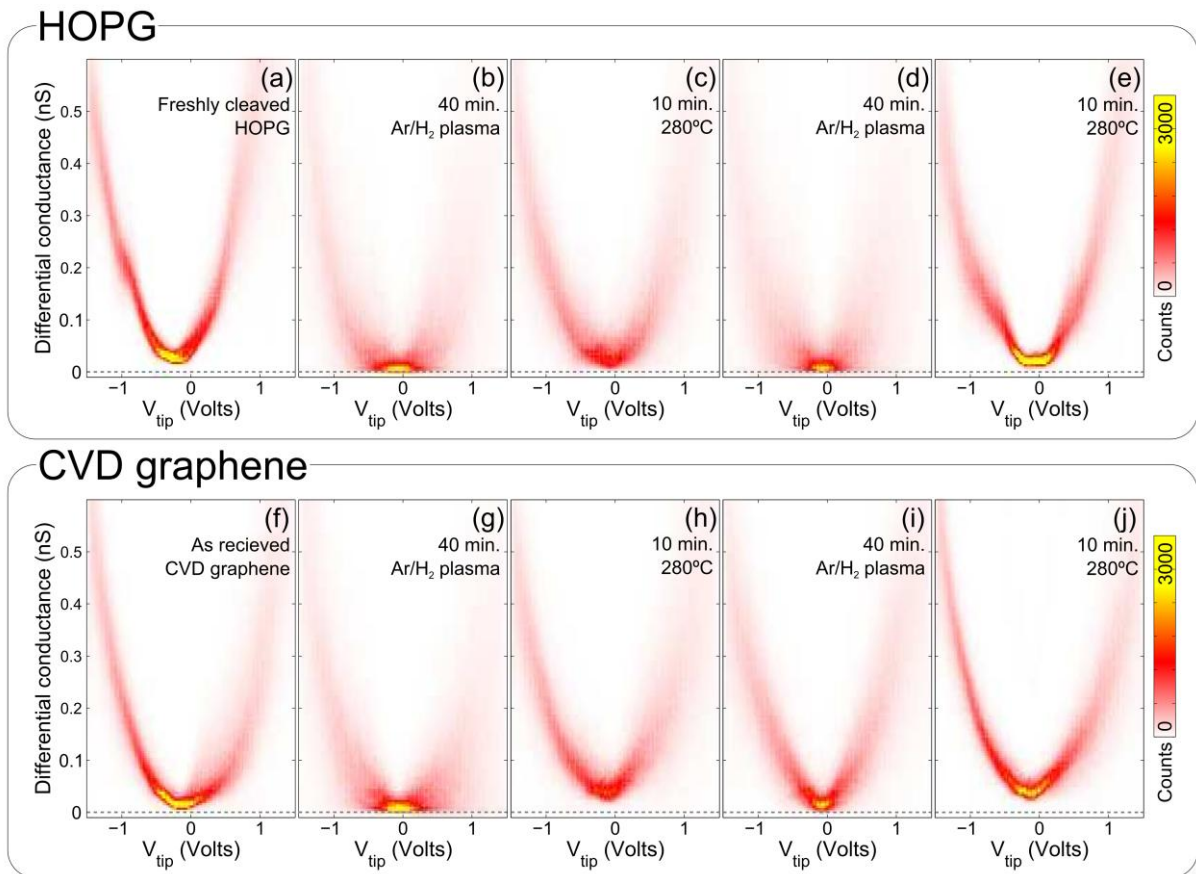
Figure 2. A set of 2D histogram of STM spectroscopic dI/dV traces acquired for two different samples: HOPG graphite and CVD graphene on Ni at different processing stages. In each histogram 2000 traces are collected at random STM tip locations on the sample. Initially both samples show metallic behaviour (dI/dV>0) (a, f), while after hydrogenation (b,g) the semiconducting behaviour, with the bandgap above 0.6 eV is present. Annealing recovers the metallic behaviour (c,h). The procedure of hydrogenation and annealing can be repeated (d,e,i,j)leading to similar properties.

Functionalization of few-layered graphene with MnO$_2$ for Li battery performance

Malgorzata Wojtoniszak, Ryszard J. Kalenczuk, Xuecheng Chen, Ewa Borowiak-Palen

Westpomeranian University of Technology in Szczecin, Department of Nanotechnology, Pulaskiego 10
70-322 Szczecin, Poland
mwojtoniszak@zut.edu.pl

Carsten Jähne, Rüdiger Klingeler,
University of Heidelberg, INF 227, 69221 Heidelberg, Germany

2D graphene due to its electrical properties has been investigated for nanoelectronic applications, including lithium ion batteries. It was proved that it exhibits an enhanced lithium storage capacity as anodes in lithium-ion cells and good cyclic performance [1-3]. Moreover, MnO$_2$/Graphene composite displays almost three times higher capacitance compared to the pristine graphene [4]. Here, we present a synthesis method of MnO$_2$/Graphene composite, where MnO$_2$ nanocrystals are deposited on few-layered graphene. The crystal formation is a result of redox reaction of KmnO$_4$ and oleic acid at the oleic acid/water interface at room temperature, according to the method of Yan et al. [5].The material was characterized by means of high resolution transmission electron microscopy (HR-TEM) and EDX as its mode, Raman spectroscopy, XRD and TGA. Electrochemical properties of the material are currently under investigation.

References

[1] Guoxiu Wang, Xiaoping Shen, Jane Yao, Jinsoo Park. Carbon 4 7, **8** (2009) 2 0 4 9
[2] Minghui Liang, Linjie Zhi. J. Mater. Chem. 19, **33** (2009) 5871
[3] Caiyun Wang, Dan Li, Chee O. Too, Gordon G. Wallace. Chem. Mater. 21, **13** (2009) 2604
[4] Jun Yan, Zhuangjun Fan, Tong Wei, Weizhong Qian, Milin Zhang, Fei Wei. Carbon 4 8, **13** (2010) 3825
[5] Hongmin Chen, Junhui He, Changbin Zhang, Hong He. J.Pphys. Chem. C. 111, **49 (**2007) 18033

Effects of Polycrystalline Cu Substrate on Graphene Growth by Chemical Vapor Deposition

J. D. Wood, S. W. Schmucker, J. C. Koepke, A. S. Lyons, E. Pop, and J. W. Lyding

Beckman Institute, Micro and Nanotechnology Laboratory, and Dept. of Electrical and Computer Engineering, Univ. of Illinois at Urbana-Champaign, 405 N. Mathews Ave., Urbana, IL 61801, USA
jwood2@illinois.edu

Previous experiments have shown that graphene chemical vapor deposition (CVD) on copper can form large monolayer sheets that can be transferred to a target substrate [1]. Nevertheless, graphene's lack of epitaxy with the underlying Cu causes issues with the as-grown material quality. Typical CVD growths employ polycrystalline Cu substrates, whose surfaces possess multiple polycrystalline facets, grain boundaries, annealing twins, and rough nucleation sites. Understanding how these surface structures affect graphene is critical for high quality, reproducible graphene growth.

In this work, we determine that Cu surface structures interact strongly with graphene, contrary to previous study [2]. Non-primary Cu crystal facets promote the growth of dendritic graphene lobes, causing irregular grain boundaries with other patchwork grains. We also find that graphene growth is not favored on both Cu annealing twins and non-primary crystal facets.

We grow graphene by CVD using 99.9% pure Cu foils in all of our experiments in a low pressure CVD process (~0.5 torr growth pressure). Fig. 1(a) and 1(c) are SEM and AFM images, respectively, of partially nucleated graphene, showing multi-lobed graphene "flowers" similar to those seen previously [1,2]. Around ~1000ºC, the average Cu surface energy decreases, becoming comparable to the Cu(111) surface energy, the lowest energy Cu surface [3]. In this case, small changes in surface energy from polycrystalline Cu facets [e.g. Cu(311), Cu(221)] drastically alter the Cu growth front, leading to bizarre, anisotropic lobed shapes in the Wulff construction, shown in Fig. 1(d). Combining the Cu and graphene growth fronts gives the multiple lobes seen in fig. 1(a) and in graphene dendrites [4]. Fig. 1(c) shows some of these graphene grains coalescing, bringing about irregular armchair and zigzag grain boundaries. To address this problem, one must lower the growth temperature to suppress the surface energy and limit Cu atomic diffusion; doing so gives hexagonal graphene grains with regular edges and grain boundaries, given in fig. 1(b).

To further characterize the effects of polycrystalline Cu on graphene growth, we grow a full graphene monolayer on patterned Cu registration mesas, with optical images in Fig. 2(a) and (b). Further, in fig. 2(c), we gather electron-backscatter diffraction (EBSD) data on the Cu mesa, showing that mesa is predominantly Cu(110). However, the mesa has many annealing twins present and non-primary (362), (441) facets, displaying crystallographic diversity. We correlate the EBSD data with spatial Raman maps of the typical G', G, and D bands found in graphene in fig. 3. Fig. 3(c-e) denote sparse or nonexistent graphene growth on annealing twins and non-primary crystal facets like Cu(441) and Cu(362). From fig. 3(b), the graphene distorts along Cu grain boundaries, and it is mainly monolayer on the Cu(110) surface. The Cu(232) and Cu(100) twins do not grow graphene from full width at half-maximum (FWHM) analysis. Additionally, it is possible that the twinning regions or non-primary facets have higher roughness, affecting nucleation site density [5]. Therefore, we perform AFM measurements on the mesa's facets, but find no dependence for the G' FWHM, $I_{G'}/I_G$ (signifying monolayer coverage), or I_D/I_G (signifying defect coverage) on RMS roughness. Thus, the graphene growth mechanism appears to be crystallographically dominated, based on the surface energy and diffusion of the underlying Cu substrate's crystal structure.

Once one has high quality graphene on Cu, one needs an effective technique to transfer to it to a choice substrate. We developed a process using multiple layers of PMMA (polymethyl methacrylate) with differing molecular weights. From Raman analysis with the Tuinstra-Koenig relation [7], it appears this transfer procedure does not introduce significant defects, transfers several inch wide monolayer graphene sheets, and allows the creation of unique graphene superstructures.

Our study elucidates the high graphene-Cu substrate interaction. To grow monolayer graphene with large, hexagonal grains, one must grow at temperatures <900ºC and employ dominant Cu facets such as Cu(110), Cu(100), and Cu(111), consistent with other results [2,6]. Additionally, low growth gas flow rates should be used to lower pressure, force surface catalysis [1], and eliminate multilayer dendritic formation [4].

References

[1] Li *et al.*, Science, **324** (2009) 1312.
[2] Wofford *et al.*, Nano Letters, **10** (2010) 4890.
[3] Chatain *et al.*, Interface Science, **12** (2004) 7.
[4] Bhaviripudi *et al.*, Nano Letters, **10** (2010) 4128.

[5] Pehrsson *et al.*, Thin Solid Films, **212** (1992) 81.
[6] Gao *et al.*, Nano Letters, **10** (2010) 3512.
[7] Dresselhaus *et al.,* Phil. Trans. R. Soc. A., **368** (2010) 5355.

Figures
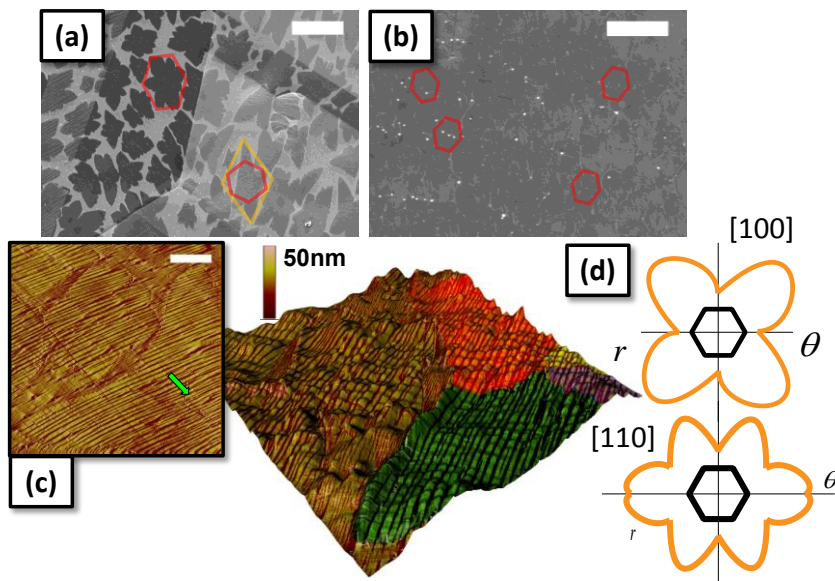
Figure 1. *(a) SEM of partial graphene coverage on 5 mil Cu (3 min, 1000°C, 200 sccm CH$_4$). The graphene flowers possess more than four lobes due to underlying polycrystalline Cu facets. Yellow diamond indicates a primary Cu facet, giving four lobed graphene, and scale bar is 20 µm. (b) SEM of partial graphene on 5 mil Cu (5 min, 900°C, 20 sccm C$_2$H$_4$). The lower temperature suppresses the Cu growth rate anisotropy. Perfect hexagons given in red, and scale bar is 5 µm. (c) False-color 3D rendering of an AFM image (inset) of coalescing graphene grains (green, purple, yellow, and red). (d) Wulff constructions for the [100] and [110] Cu zones (orange), showing asymmetric lobes for the Cu growth front (graphene growth front isotropic). For highly faceted surfaces, these lobes become more anisotropic, leading to dendritic graphene.*
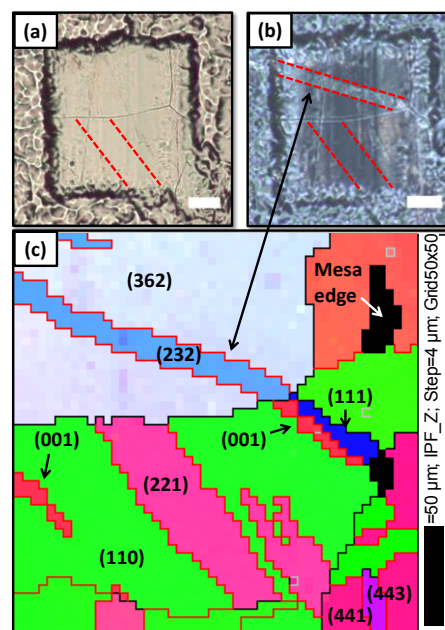
Figure 2. *Optical (a) and differential interference contrast (b) images of graphene on a Cu mesa, with Cu annealing twins in red. (c) Electron-backscatter diffraction (EBSD) data showing the different polycrystalline Cu facets, grain boundaries (black lines), and twins. Scale bar 50 µm.*
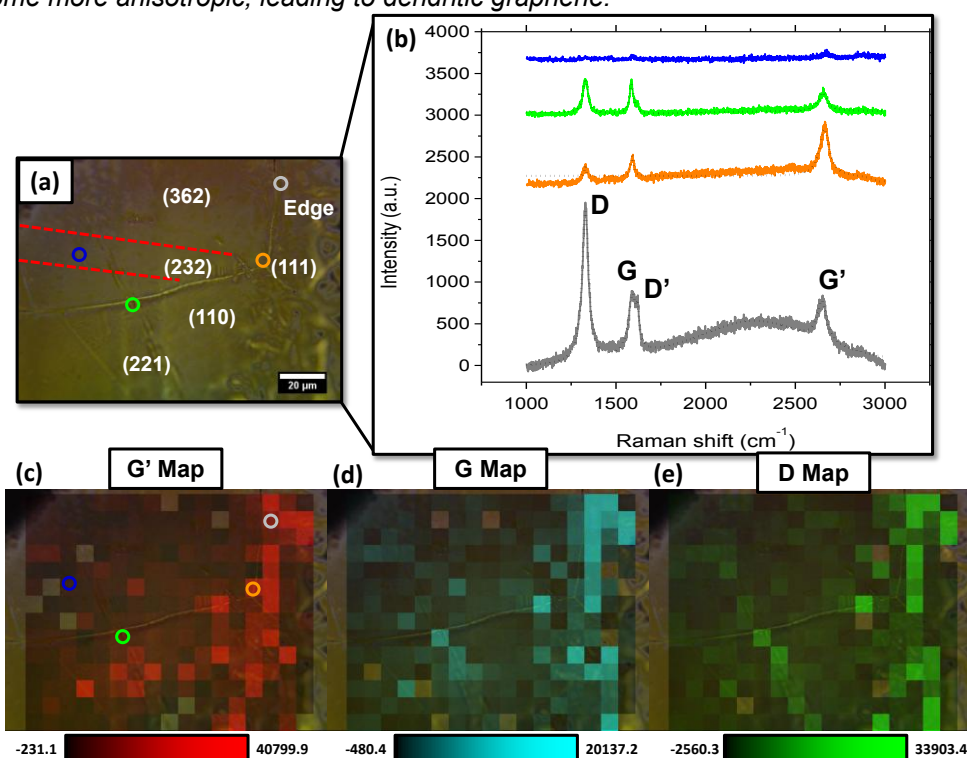
Figure 3. *(a) Mesa optical image, with Cu crystal facets identified. Raman spectra taken at the colored spots. (b) Raman spectroscopy of selected spots, with D, G, D', and G' bands present. The mesa edge shows defective graphene, and the Cu(232) twinning region has no graphene. Spatial maps for the G' band (c), G band (d), and D band (e), respectively. Highly faceted regions such as Cu(362) have lower G' and G intensities, indicating sparser graphene coverage. Raman pixel size is 7.5 µm.*

Edge Effects in Graphene Nanostructures - Spectral and Transport Properties

Juergen Wurm, Inanc Adagideli, Klaus Richter

Universitaet Regensburg, Universitaetsstrasse 31 93053, Regensburg, Germany
Juergen.Wurm@Physik.Uni-Regensburg.de

In this work we study edge specific effects on spectral and transport properties of nanostructured graphene. In particular, we focus on the different types of edges and show how they affect the spectrum and the conductance. Previously we have investigated the effects of edges on the transport and spectral properties of graphene quantum dots, as well as on the conductance of graphene nanoribbons numerically [1,2]. Some edges can lead to effective (e.g. zigzag and infinite mass edges) or real (magnetic edges) time reversal symmetry breaking, others are effective intervalley scatterers (e.g. armchair edges).

Here we describe the quasiparticle dynamics in graphene analytically using the effective 2D Dirac Hamiltonian and imposing appropriate boundary conditions that depend on the specific structure of the graphene edges. Starting from the multiple reflection expansion for the exact Green function, we develop a theory that naturally incorporates the influence of the edges.

We then use our formalism to study the density of states (DOS) of closed graphene billiards and the conductance of open cavities. For the DOS we derive the Weyl expansion for the smoothed DOS, where we find that the surface contribution is exclusively due to the zigzag edges. That allows us to relate the DOS directly to the total number of zigzag edges. Furthermore, we derive trace formulae that connect the oscillating part of the DOS with the periodic classical orbits of the system. The correlations of the spectrum are found to depend on the structure of the edges, especially on the amount of intervalley scattering boundary parts. The reason is that the effective symmetry classes are changed depending on the ratio of the different time scales of the system.

Related effects are found also in the average conductance and the universal conductance fluctuations of open systems. By means of a semiclassical theory we show that a finite weak localization correction relies on the existence of armchair edges. Furthermore we obtain the size of both the weak localization and the universal conductance fluctuations as a function of the relevant time scales.

References

[1] J.Wurm, A.Rycerz, I.Adagideli, M.Wimmer, K.Richter and H.U.Baranger.
Phys. Rev. Lett. **102** (2009) 056806

[2] J.Wurm, M.Wimmer, I.Adagideli, K.Richter and H.U.Baranger.
New J. Phys. **11** (2009) 095022

High quality multi-layer graphene grown by low-temperature plasma CVD for future nano-carbon LSI interconnects

Yuichi Yamazaki[1], Ryosuke Sawabe[2], Makoto Wada[1], Masayuki Katagiri[1], Naoshi Sakuma[1], Tatsuro Saito[1], Atsunobu Isobayashi[1], Mariko Suzuki[1], Akihiro Kajita[1], Yuji Awano[2], Tadashi Sakai[1]

[1]Low-power Electronics Association & Project (LEAP) , 1, Komukai-Toshiba, Saiwai, Kawasaki 212-8582, Japan.
[2]Keio University, 3-14-1 Hiyoshi, Kohoku-ku, Yokohama 223-8522, Japan.
y-yamazaki@leap.or.jp

Graphene has various superior properties over Cu such as high current tolerance, ballistic transport and high thermal conductivity, and therefore, is one of the most promising material for interconnect like carbon nantube (CNT). According to theoretical study[1], graphene shows lower resistivity compared with Cu in the form of ultrafine, less than 10 nm in width, interconnect. High-quality graphene growth at low temperature and on a large-area substrate is indispensable for realizing application for interconnect. In general, a plasma-based chemical vapor deposition (CVD) technique has the advantage of low-temperature thin film growth because it can supply a plasma-decomposed radicals and ions on a substrate. We have reported extremely high-density CNT growth at the growth temperature as low as 450 °C[2], which indicates that a plasma-based CVD is suitable for growing carbonaceous materials at low temperature. Since graphene is one of carbon allotropes, high-quality graphene growth at low temperature is expected by using a plasma-based CVD. In this study, we investigated the dependence of crystalline quality of graphene on major parameters of plasma, plasma power density and distance between a substrate and plasma, in low-temperature graphene growth by a plasma-based CVD.

Co was used as a catalytic thin layer in order to obtain multi-layer graphene. The thickness of which was 30 nm. Plasma power density was widely controlled to the range of 0.01-25 W/cm^2. Growth temperature was ranged 500-600°C. We employed a two-step growth method. Firstly, plasma pretreatment was carried out for reduction of Co film and subsequent step was graphene growth. Plasma pretreatment was performed at lower temperature, 25-350 °C, than that for growth temperature. Crystalline quality of graphene was evaluated by Raman spectroscopy and transmission electron microscope.

Figure 1 shows a typical Raman spectrum. The G/D ratio, ratio of G peak at ~1580 cm^{-1} to D peak at ~1360 cm^{-1}, which is used as an index of crystalline quality of graphene was calculated to be about 12. This was considerably high taking account of growth temperature of 580 °C. TEM image of graphene was shown in Fig. 2. Layers of graphene were clearly seen. It was observed that higher plasma power density leads to higher G/D ratio. Concerning plasma pretreatment, gas species have more influence on G/D ratio compared with plasma power density.

References

[1] A. Naeemi et al. IEEE EDL **28** (2007) 428.
[2] Y. Yamazaki *et al*. Appl. Phys. Express **3** (2010) 055002.
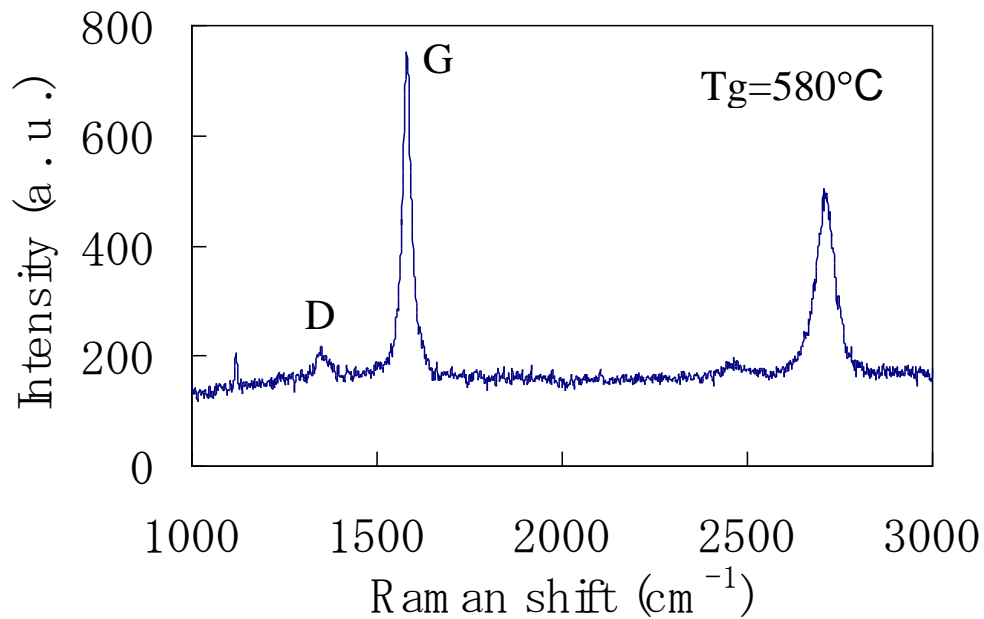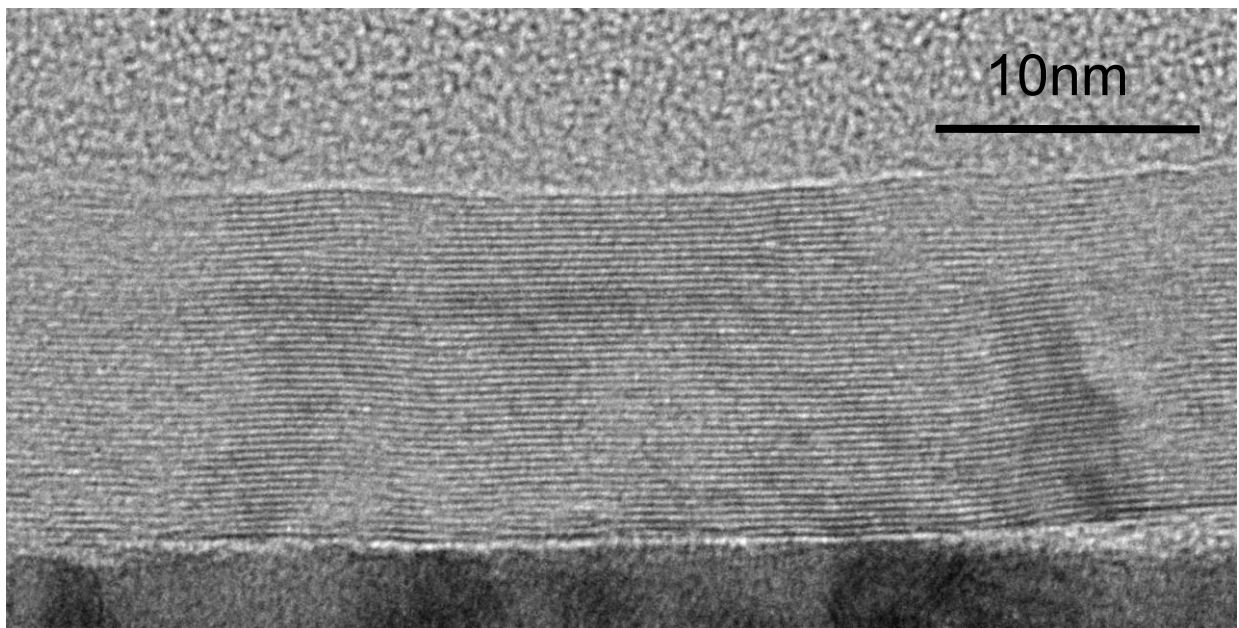
Figures

Fig. 1

Fig. 2

Figure caption
Fig. 1 Raman spectrum. The G/D ratio was calculated to be about 12.
Fig. 2 TEM image. Number of layers of graphene was typically 30-40.

The Optoelectronic Property of Single CdSe Nanowire/monolayer Graphene Heterojunctions

Yuan Yan, Yangbo Zhou, Xuewen Fu, Yazhou Wang, Zhimin Liao, Dapeng Yu.

State Key Laboratory for Mesoscopic Physics,Department of Physics,Peking University,
Beijing 100871, (P. R. China)
E-mail: liaozm@pku.edu.cn

Graphene has attracted wide atterntions since first discover in 2004[1] [2] and then awarded Nobel Prize in 2010 , because of its exceptionally high crystal and electronic quality[3]. However, as a strictly two-dimensional material with zero-gap, its optoelectronic property is not good enough. Considering the excellent luminescent material CdSe whose badgap is 1.74eV at 300K[4] [5], we constructed heterojunction structure based on a single CdSe nanowire and a monolayer graphene.

Here, graphene have been synthesized via a simple chemical vapor deposition method on Cu chip[6], and then transferred to a clean silicon substrate with 300nm oxide layer. The CdSe nanowires have also been synthesized via a simple chemical vapor deposition method at 0.5Mpa in a horizontal quartz tube furnace[7]. After the electrodes on graphene were done, the CdSe nanowire was transferred from silicon substrate to across on the graphene directly by glass fiber under an optical microscope.

Under wavelength-635nm, power-10mV red laser irradiated, the device should show some interesting phenomenons[8] [9] [10]. However, a similar phenomenon in our experiment did not be found. At the same time, this device just has a weak backgate modulation.

We will put much more attentions on the performance of the device, more and better results can be expected.

References

[1] Novoselov, K. S. et al. Electric field effect in atomically thin carbon films. **Science**(2004) 666-669.

[2] Novoselov, K. S. et al. Two-dimensional atomic crystals. **Proc. Natl Acad. Sci. USA**(2005)10451-10453.

[3] A. K. Geim and K. S. Novoselov. The rise of graphene. **Nature Materials**(2007) 183-191 .

[4] Sheng-Chin Kung, et al. 20 μs Photocurrent Response from Lithographically Patterned Nanocrystalline Cadmium Selenide Nanowires. **Nano Lett** (2010) 1481-1485.

[5] Muhammad Iqbal Bakti Utama, et al. Vertically Aligned Cadmium Chalcogenide Nanowire Arrays on Muscovite Mica: A Demonstration of Epitaxial Growth Strategy. **Nano Lett** (2010).

[6] Xuesong Li, et al. Large-Area Synthesis of High-Quality and Uniform Graphene Films on Copper Foils. **Science**(2009)1312-1314.

[7] Christopher Ma and Zhonglin Wang. Road Map for the Controlled Synthesis of CdSe Nanowires, Nanobelts, and Nanosaws—A Step Towards Nanomanufacturing. **Adv. Mater**. (2005) 2635-2639

[8] Yue Lin, et al. Dramatically Enhanced Photoresponse of Reduced Graphene Oxide with Linker-Free Anchored CdSe Nanoparticles. **ACSNANO**(2010) 3033-3038.

[9] Zheyuan Chen, et al. Energy Transfer from Individual Semiconductor Nanocrystals to Graphene. **ACSNANO**(2010) 2964-2968.

[10]Abdallah F. Zedan, et al. Ligand-Controlled Microwave Synthesis of Cubic and Hexagonal CdSe Nanocrystals Supported on Graphene. Photoluminescence Quenching by Graphene. **J. Phys. Chem. C** (2010) 19920–19927.

Figures
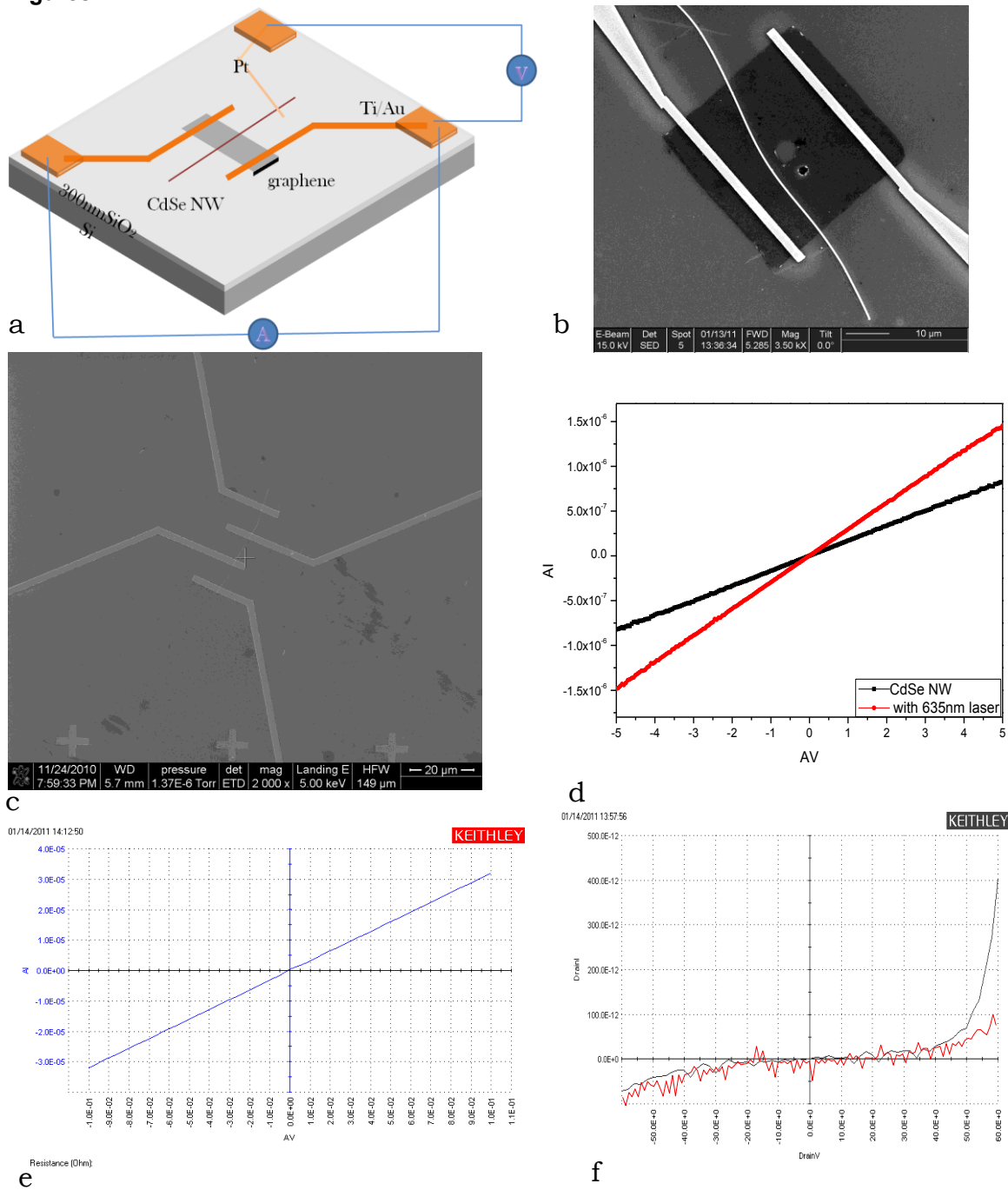
(a) Schematic picture of the heterojunctions and the schematic test circuit; (b) SEM image of the heterojunctions; (c) SEM image of the CdSe nanowire device; (d) I/V curves of CdSe nanowires device; (e) I/V curve of graphene; (f) I/V curves of CdSe Nanowire/Graphene heterojunction with backgate, red-0V, black-80V.

Shape induced Magnetic Moment in Graphene Nanomesh from First-Principles

H. X. Yang[1], M. Chshiev[1], X. Waintal[2], S. Roche[3,4]

[1]SPINTEC, UMR-8191 CEA/CNRS/UJF, 17 rue des Martyrs, 38054 Grenoble, France
[2]SPSMS-INAC-CEA, 17 rue des Martyrs, 38054 Grenoble, France
[4]SP2M-INAC-CEA, 17 rue des Martyrs, 38054 Grenoble, France
[3]CIN2 (CSIC-ICN) Barcelona, Campus UAB, E-08193 Bellaterra, Spain
mair.chshiev@cea.fr

Unique electronic properties arising from confinement of electrons in two dimensions leading to very large charge mobility make graphene to be extremely promising material for "beyond CMOS" nanoelectronics developments [1]. Furthermore, the inherently weak spin-orbit coupling allows long spin coherence times for carriers [2] making graphene also primary candidate for spin electronics (spintronics) [3]. Recent reports on possibility of inducing localized spin polarization and magnetic moments at one-dimensional zigzag edges in graphene nanoribbons open the way to novel concepts of building nanoscale spintronic devices [4]. Magnetic states in graphene can be also induced by single defects and disorder [5]. On another hand, recent reports on possibility of experimental fabrication of graphene nanomesh (GNM) gave rise to possibility of introducing of large scale patterned defects into graphene [6].

Motivated by recent reports on successful fabrication of GNM, on the one hand, and possibility of edge and defect induced spin polarization, on the other hand, we performed first-principles investigations of electronic and magnetic properties of pure and hydrogen terminated graphene nanomesh. Calculations were performed using Vienna Ab-Initio Simulation Package (VASP) which is based on density functional theory with generalized gradient approximation, for the exchange correlation potential and projector augmented wave based pseudopotentials [7]. Full structural relaxations in shape and volume have been performed to ensure the Hellman-Feynman forces acting on carbon atoms to be less than 10^{-3} eV/Å.

For pure GNM, non-spin-polarized states are found stable in armchair-type edges while antiferromagnetic states are found stable for balanced zigzag edge structures. Furthermore, an unbalanced edge structure shows stable ferrimagnetic state giving rise to a net magnetic moment up to 4 uB per 6 x 6 unit cell. We also found the gap opening in the balanced zigzag edge GNMs which may reach up to 0.40 eV. For hydrogen terminated GNM, we found that the ground state strongly depend both on the hole size and shape. For instance, a large net magnetic moment (~$2.15\mu_B$) is induced in the ground state for GNM with pentagon and trianglular shaped holes shown in Fig. 1(a) and (d), respectively. At the same time, the ground state is found to be paramagnetic for GNM with rhombic and 6-ring shaped holes represented in Fig. 1(b) and (e). Interestingly, the net magnetic moment for GNM with intermediate between trianglular and rhombic shaped holes is equal to $1.04\mu_B$ (Fig. 1(c)) providing that it scales between two end case values of $2.15\mu_B$ and $0\mu_B$, respectively. The magnetization is found to depend strongly on GNM hole size. Such behavior can be explained in the framework of Lieb's theorem [8].

References

[1] A. K. Geim and K. S. Novoselov, Nature Materials, **6** (2007) 183.
[2] D. Huertas-Hernando et al, Eur. Phys. J. Special Topics, **148** (2007) 177.
[3] A. Fert et al, *Mat. Sci. Eng. B,* **84** (2001) 1; S. A. Wolf et al, Science*,* **294** (2001) 1488.
[4] Y.-W. Son et al, Nature, **444** (2006) 347; O. Yazyev et al, Phys. Rev. Lett., **100** (2008) 047209.
[5] O. Yazyev et al, Reports on Progress in Physics, **73** (2010) 053501.
[6] J. Bai et al, Nature Nanotechnology, **5** (2010) 190.
[7] G. Kresse and J. Hafner, Phys. Rev. B, **47** (1993) 558; P. E. Blöchl, Phys. Rev. B **50** (1994) 17953;
G. Kresse and J. Joubert, *ibid.* **59** (1999) 1758.
[8] E. H. Lieb, Phys. Rev. Lett., **62** (1989) 1201.

Figures

Fig.1. Total magnetic moment in the ground state for geometries for (a) pentagon, (b) rhombic, (c) triangle-to-rhomb intermediate, (d) triangle and (e) 3-ring H-terminated GNMs.

rGO-Wrapped Fullerene (C$_{60}$) Wires

Jieun Yang, Mihee Heo, Jin Young Kim, Hyeon Suk Shin*

Interdisciplinary School of Green Energy, Ulsan National Institute of Science and Technology (UNIST), Banyeon-ri 100, Ulsan 689-805, Korea
shin@unist.ac.kr

The assembly of reduced graphene oxide (rGO) and fullerene (C$_{60}$) into hybrid wires were successfully performed by employing the liquid-liquid interfacial precipitation (LLIP) method.[1] C$_{60}$ wires are first formed and then rGO sheets are coated on surfaces of them. The structural characterization of the rGO/C$_{60}$ wires was carried out by using UV-Visible spectroscopy and Scanning Electron Microscope.[2],[3] FET devices with rGO/C$_{60}$ wires were prepared to investigate their electrical properties. The I-V$_g$ curve of the hybrid wires exhibited p-type semiconducting behavior, indicating the hole transport through rGO as a shell layer, whereas pure C$_{60}$ wires showed n-type behavior in vacuum.[4] In this presentation, furthermore, we show interesting applications using the hybrid wires like photocurrent generation and a photovoltaic device. The hybrid wires showed a significant enhancement of short circuit current (J_{SC}) when compared with pure rGO and evaporated C$_{60}$ devices. This improvement can be interpreted that the photocurrent by efficient exciton dissociation is generated between the rGO donor and C$_{60}$ acceptor.

References

[1] K. Ogawa, T. Kato, A. Ikegami, H. Tsuji, N. Aoki, Y. Ochiai, and J. P. Bird, Appl.Phys.Lett., **88** (2006) 112109.
[2] E. V. Chubarovaa and E. Yu. Melenevskayaa, Fullerenes, Nanotubes and Carbon Nanostructures, **16** (2008) 640.
[3] R. V. Bemasson, E. Bienvenue, M. Dellinger, S. Leach and P. Seta, J. Phys. Chem., **98** (1994) 3492.
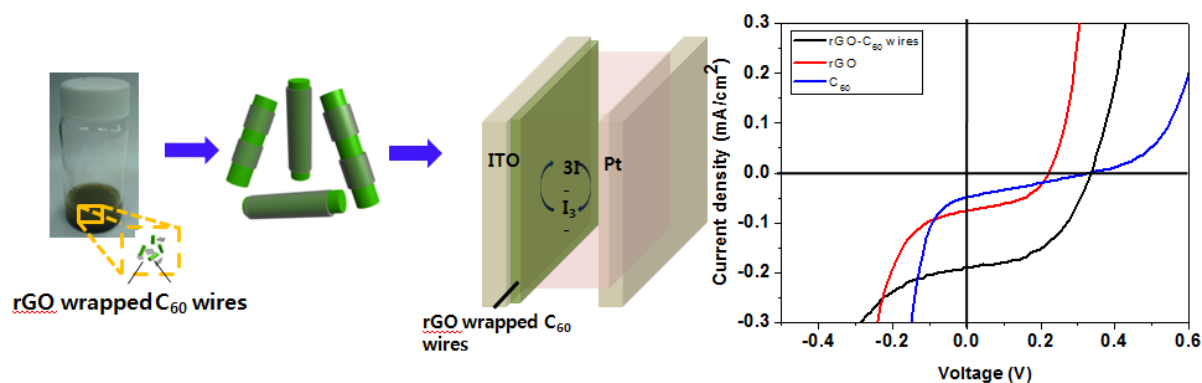[4] T. Matsushima, M. Yahiro and C. Adachi, Appl.Phys.Lett., **91** (2007) 103505.

Figure

Figure 1. Photovoltaic device of rGO- wrapped fullerene wires.

Breakdown of Quantum Hall Effect in Graphene

Cenk Yanik, Anil Gunay Demirkol, Cem Celebi, and Ismet I. Kaya

Quantum Transport and Nanoelectronics Laboratory,
Faculty of Engineering and Natural Sciences, Sabanci University, Istanbul 34956, Turkey

cenkyanik@sabanciuniv.edu

The breakdown of the quantum Hall effect, which is observed as an abrupt change in the longitudinal resistance by several orders of magnitude with an associated loss in quantization of Hall voltage is the major obstacle against improving the resistance standard which is currently based on this effect. Graphene is inherently a 2D material and in comparison with GaAs based 2DEG and has an unsual band structure that allows the quantization of the Hall resistance even at room temperature[1]. These unique properties of graphene make it a good candidate for being used as a high precision metrological characterization tool for the quantum Hall resistance. A relative uncertainty of 1 ppb in the resistance quantization can be achieved by quantum Hall effect GaAs based 2DEG. The uncertainty in the Quantum Hall resistance in graphene has been rapidly improving in the last couple of years, from 15 ppm in exfoliated graphene[2] to 3 pbb in epitaxial graphene[3]. Sufficiently high breakdown currents and low contact resistances are needed to obtain such high accuracy in determining the resistance quantum.

In this work, we report experimental results on the breakdown of quantum Hall effect in graphene. The Hall devices were fabricated on mechanically exfoliated graphene. Single layer, bilayer and a few layer graphene sheets are transferred onto SiO_x substrate where Raman spectroscopy is used to identify the number of graphene layers. Devices are patterned by optical and electron beam lithography. Measurements are done in a temperature range of 1.4 –300 K. Some samples exhibit immediate onset of the breakdown in the longitudinal resitance even at very small currents [Fig.1]. This behavior could be attributed to relatively mobility of the samples (~5.000 cm^2/V.s). However, in the same measurement we observe that the Hall plateaus [Fig.2] can endure to much higher currents. We elaborate on the physical phenomena underlying this behavior in the breakdown of the quantum Hall effect and its possible implications on the improvement of the accurate determination of the plateau levels.

References

[1] K.S.Novoselov, *et al.* Science 315, 1379 (2007).
[2] Giesbers A. J. M. *et al.* Appl. Phys. Lett. 93, 222109 (2008).
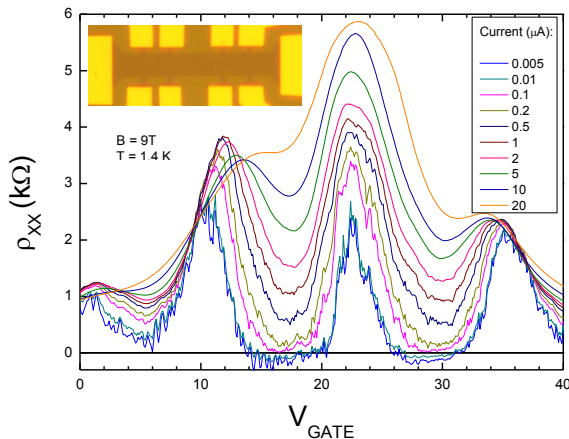[3] Tzalenchuk, A. *et al.* Nature Nanotech. 5, 186–189 (2010).

Figures

Fig.1

Fig.2
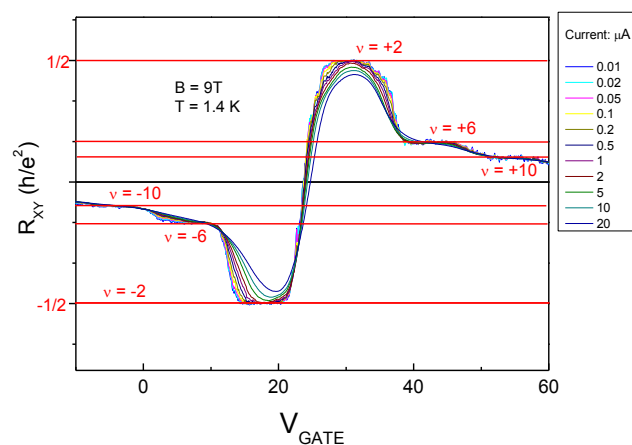
Figure captions

Fig.1. Longitidunal resistance vanishes below 100 nA even for $\nu = \pm 2$ and it rapidly increases for higher applied current values.These nonzero resistance values implies the breakdown of quantum Hall effect. Inset shows the optic microscope image of the graphene hallbar with the contact configuraiton.

Fig.2. The plateaues of Hall resistances at filling vactors $(\nu = \pm 2,6,10)$ due to the unsual band structure of graphene determines the anomalous quantum Hall effect in monolayer graphene. Quantized Hall plateaues at $\nu = \pm 2$ are clearly visible up to 1 μA.

Solitons in a system of coupled graphene waveguides

Yanyushkina N., Belonenko M., Lebedev N.

Volgograd State University, University Avenue 100, Volgograd, Russia
yana_nn@inbox.ru

We consider a propagation of ultra-short optical pulses, which can be represented as discrete solitons in the graphene waveguides. The effective equation, which has the form of an analog of the classical sine-Gordon equation was obtained. And the effects observed when changing the width of initial momentum were.

The unique properties of graphene [1-2], largely related to the periodical dispersion law, and also works on ultrashort optical pulses amplification in nanotubes and graphene [3] give additional incentive to study the problem of the propagation of electromagnetic pulses through a system consisting of several graphene sheets.

We consider Hamiltonian of the electron system in the Hubbard model. It should be noted taking into account the energy of the Coulomb repulsion between electrons located at one site leads to a change in the spectrum of elementary excitations of the model. Now we consider the propagation of electromagnetic pulse in geometry where the wave vector along a graphene layer and the polarization vector lies in a graphene plane.

Maxwell's equations taking into account dielectric and magnetic properties of the system [4] with Coulomb calibration can be written in the following form:

$$\frac{\partial^2 \vec{A}_k}{\partial x^2} - \frac{1}{c^2}\frac{\partial^2 \vec{A}_k}{\partial t^2} + \frac{4\pi}{c}\vec{j}_k - \frac{4\pi}{c}\frac{\partial \vec{P}_k}{\partial t} = 0$$

here $\vec{A}_k = (0,0,A_k(x,t))$ is the vector-potential which corresponds to electromagnetic field in the k-th layer of graphene. $\vec{j}_k$ is the current in k-th layer of graphene, and $\vec{P}_k$ is the polarization induced in the k-th layer of the electromagnetic field and currents of the neighboring graphene layers. Further we consider the simple model, where $\vec{P}_k = \alpha(\vec{E}_{k-1} + \vec{E}_{k+1})$, here α is the coupling coefficient, and $\vec{E}_{k\pm1}$ are the magnitudes of electric field in the neighboring graphene layers.

After the expansion rate of the carrier in a Fourier series, we obtain an effective equation which has the form of an analog of the classical sine-Gordon equation. The equations were solved numerically by using a direct difference scheme of the cross type. The initial condition was selected in the form of a Gauss curve:

$$R(t,N) = A \cdot e^{-(t-t_0)^2} \cdot e^{-\beta(N-N_c)^2}$$

where A is the pulse amplitude, N_c is the number of central waveguide (N_c=5), β is the parameter that determines the pulse wide, N is the number of waveguide, t_0 is the initial time.

Studying the dynamics of the momentum carried in the nine parallel graphene planes. The dependence of electric field on waveguide number is presented in Figure 1. The dependences suggest a significant effect of the pulse width β on the energy distribution between the waveguides. And the pulses evolution is shown in Figure 2. An inversion signal was observed starting from a certain time (t = 150), the amplitude of the inverted signal is almost identical to the amplitude of the original signal.

References

[1] Novoselov K. S., Geim A. K., Morozov S. V., Jiang D., Zhang Y., Dubonos S. V., Grigorieva I. V., Firsov A. A., Science, **306** (2004) 666.
[2] Novoselov K. S, Geim A. K., Morozov S. V., Jiang D., Katsnelson M. I., Grigorieva I. V., Firsov A. A., Nature, **438** (2005) 197.
[3] Yanyushkina N.N., Belonenko M.B., Lebedev N.G., Optics and Spectroscopy, **108** (2010) 618.
[4] Landau L.D., Lifshitz E.M., Theoretical physics. Theory of field. Moscow: Nauka, (1988) 512.
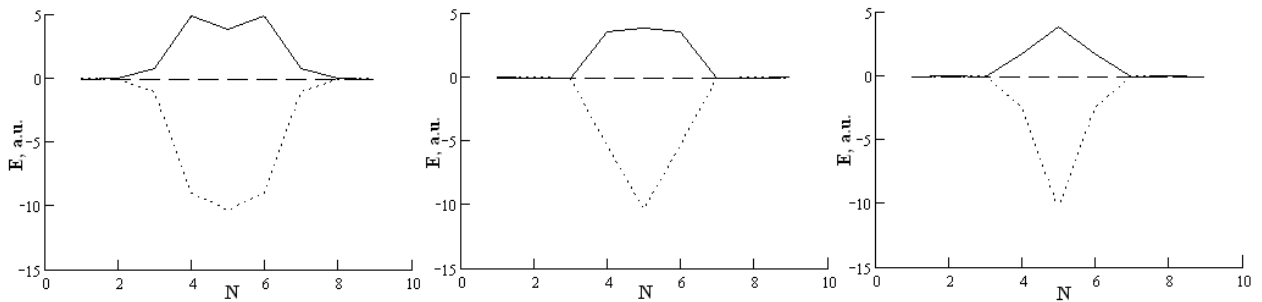
Figures

Figure 1. Dependence of the electric field on the waveguide number. All magnitudes are in the non-dimensionless units. For the solid curve the time is t=130, for the dotted curve t=200, for the dashed curve t=250: a) β=1; b) β=2; c) β=3.
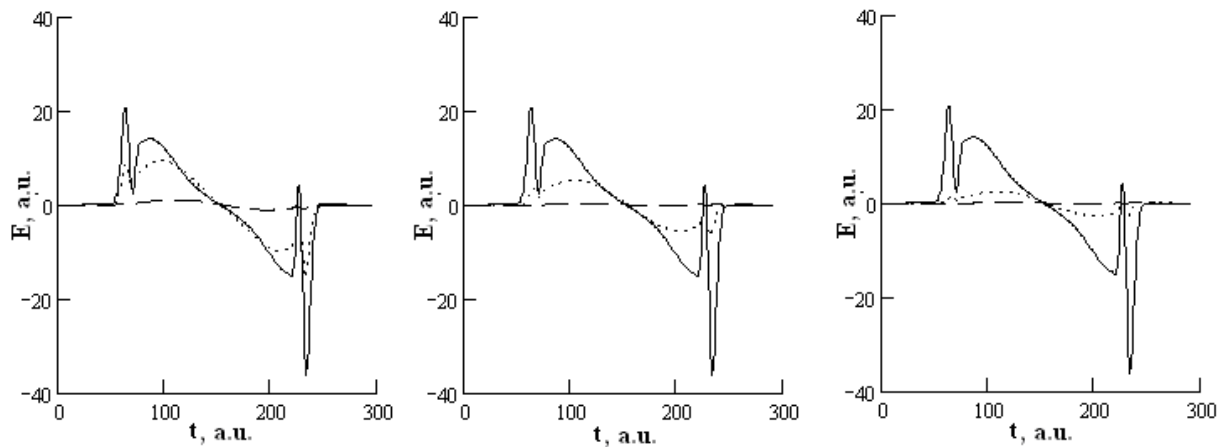

Figure 2. Dependence of the electric field on the time. All magnitudes are in the non-dimensionless units. For the solid curve the waveguide is N=5, for the dotted curve N=6, for the dashed curve N=7: a) β=1; b) β=2; c) β=3.

Acknowledgments

524

Local strains and gap formation in graphene

M. Yaro, Xavier Cartoixà

Departament d'Enginyeria Electrònica, Universitat Autònoma de Barcelona, Bellaterra, Spain
SimeonMoisesYaroMedina@uab.cat

Graphene is a novel two-dimensional material [1,2] that, due to its exceptional mechanical and electronic properties, has attracted a great deal of attention in the last year. Despite having an extremely high carrier mobility [3], its straightforward use in the electronics industry is precluded, among other factors, by its semimetallic character. Thus, great efforts have been made in order to open a gap in graphene and render it a semiconductor. These include adding an extra dimension of confinement, obtaining graphene nanoribbons (GNRs) [4], electrostatic patterning [5], chemical decoration [6], etc.

Band crossings, such as the one present at the graphene charge neutrality point (CNP), typically reflect an underlying lattice symmetry that forbids the coupling of the different participating states. Therefore, a common route for introducing such couplings is to apply a uniaxial strain to the system, thereby reducing the crystal symmetry. This approach has been followed by Zhong *et al.* and Farjam *et al.* [7,8], who have observed that, in isolated graphene, the application of a uniaxial strain is not sufficient to induce the opening of a gap. However, in that study the strain was applied uniformly, whereas, in some experimental situations, such as bent graphene [9], strain might be applied only to a limited region of the material.

Thus, we have investigated the band structure of graphene under several types of local strain that aim to isolate the different strain components that can be present when undergoing an experiment where graphene is strained in a limited region.

First we have studied the effect of a pure torsion of graphene (Fig. 1.a), while keeping all bond distances intact. We have observed that, no matter the width *w* of resulting "pseudoribbons" and the crystallographic direction (zigzag vs. armchair) along which the bending is applied, the band crossing remains at the CNP (Fig. 1.b).

We have also studied the effect of stretching one or two lines of bonds along an armchair direction, simulating the local stretching that can take place in the region with finite curvature when a graphene sheet is bent. For one stretched line of bonds, when account is taken of the periodic boundary conditions needed for ab-initio calculations, the resulting structure resembles an array of laterally coupled armchair GNRs (aGNRs) (Fig. 2.a). There are well known rules that determine the semimetallic or semiconductor character of isolated aGNRs, and we find that these rules are not modified by the introduction of the lateral coupling (Figs. 2.b and 2.c). Finally, we extend the area of application of the local strain by allowing two bond lines to stretch (Fig. 3.a). We observe that, now, electrons propagating along the *y* axis observe a gap, but those moving along *x* are still subject to a band crossing (Fig. 3.b). However, if the bond stretching occurs asymmetrically, as would be the case for a non-uniform strain, a gap does appear over the whole Brillouin zone.

References

[1] A. K. Geim and K. S. Novoselov. Nature Materials (2007), 6:183 – 191
[2] Novoselov, K. S. et al. Science (2002), 306:666 – 669
[3] X. Du, et al. Nature Nanotechnology (2008), 3:491 - 495
[4] L. Brey and H. A. Fertig, Phys. Rev. B (2006) 73:235411
[5] J. B. Oostinga et al. Nature Materials (2007) 7:151 – 157
[6] X. Dong et al. Phys. Rev. Lett. (2009) 102:135501
[7] Gui Gui et al. Phys. Rev. B (2008) 78:075435
[8] M. Farjam and H. Rafii-Tabar, Phys. Rev. B (2009) 80:167401
[9] Benjamin D. Briggs et al. Appl. Phys. Lett. (2010) 97:223102

Figure 1.
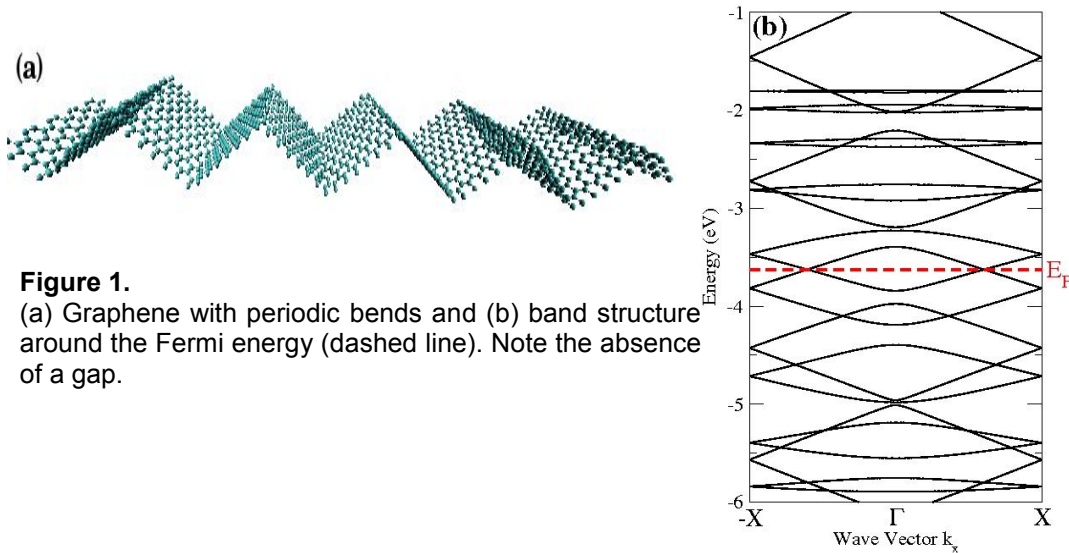(a) Graphene with periodic bends and (b) band structure around the Fermi energy (dashed line). Note the absence of a gap.

Figure 2.
(a) Graphene with local stretching (orange bond), obtaining transversal aGNRs. (b) Band structure of metallic and (c) semiconducting stretched graphene sheets.
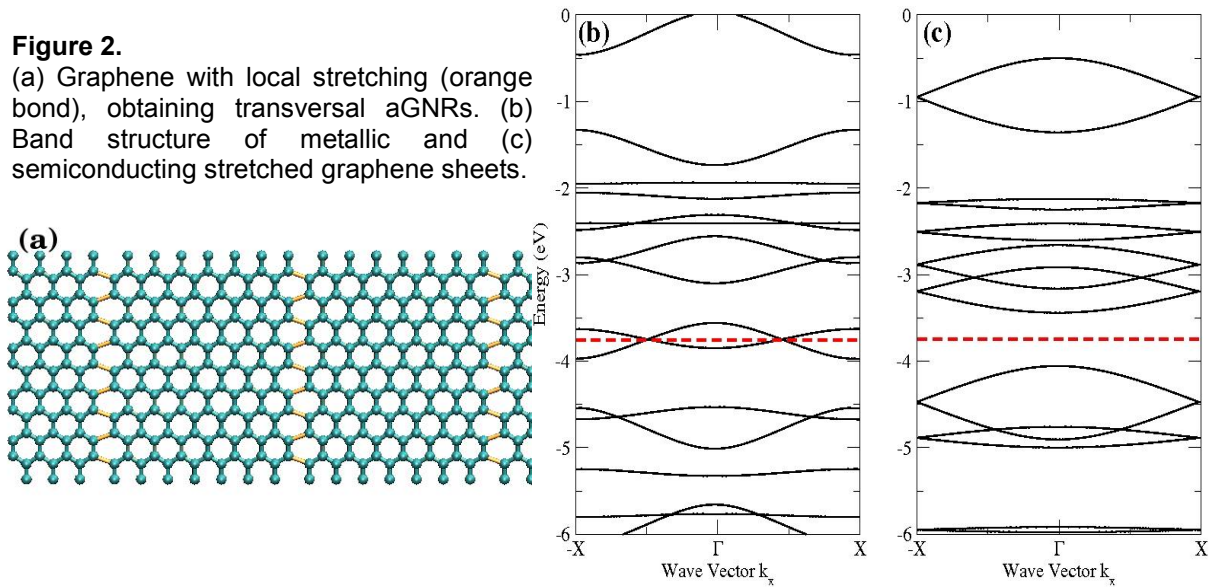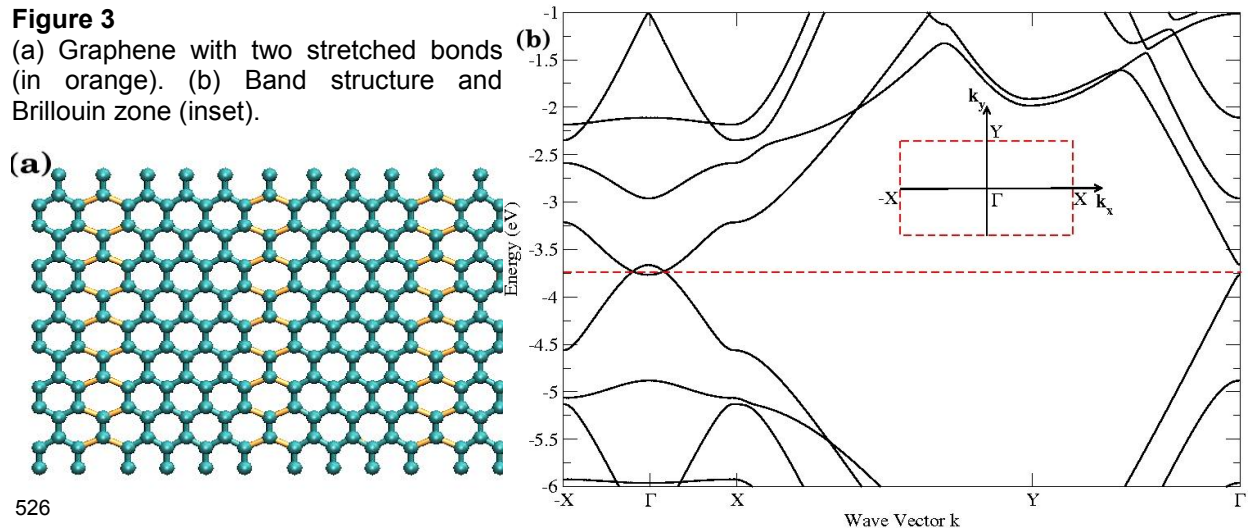

Figure 3
(a) Graphene with two stretched bonds (in orange). (b) Band structure and Brillouin zone (inset).

Thermal expansion coefficient of single-layer graphene measured by Raman spectroscopy

Duhee Yoon,[1] Young-Woo Son,[2] and Hyeonsik Cheong[1,*]

[1]*Department of Physics, Sogang University, Seoul 121-742, Korea,*
[2]*School of Computational Sciences, Korea Institute for Advanced Study, Seoul 130-722, Korea.*
hcheong@sogang.ac.kr

Graphene is attracting much interest due to potential application as next generation electronic material as well as its unique physical properties. In particular, its superior thermal and mechanical properties, including high thermal conductivity and extremely high mechanical strength that exceeds 100 GPa, make it a prime candidate material for heat control in high-density, high-speed integrated electronic devices. For such applications, knowledge of the thermal expansion coefficient (TEC) as a function of temperature is crucial, but so far few reliable measurements on the TEC have been reported [1]. Several authors have calculated the TEC using various models [2-6]. Mounet *et al*. estimated the TEC of graphene as a function of temperature by using a first-principles calculation and predicted that graphene has a negative TEC at least up to 2500 K [6]. Bao *et al*. experimentally estimated the thermal coefficient in the temperature range of 300 – 400 K by monitoring the miniscule change in the sagging of a graphene piece suspended over a trench and found that it is negative only up to ~350 K [1]. It is not yet clear whether this discrepancy between theory and experimental data is caused by uncertainties in the accuracy of the experimental measurements or limitations in the theoretical calculation. Since precise knowledge of the TEC in the temperature range around room temperature is crucial in designing graphene-based devices and heat management systems, more precise measurements are needed. In this work, we analyze the temperature-dependent shift of the Raman *G* band of monolayer graphene on SiO_2 to estimate the TEC of graphene. We find that the data can be explained in the temperature range of 200 – 400 K with the help of the calculated temperature dependence of the Raman *G* band of free standing graphene.

When the temperature of a graphene sample fabricated on a SiO_2/Si substrate is raised, two effects should be considered: the temperature dependence of the phonon frequencies and the modification of the phonon dispersion due to strain caused by mismatch of the TEC'ss of the substrate and graphene. The Raman frequency shift of the *G* band of free standing graphene as a function of temperature has been estimated by first-principles calculations [7]. Since most graphene samples are fabricated on SiO_2 substrates or over a trench held at the edges, the pure effect of temperature change on the Raman spectrum cannot be measured directly and compared with the theory. The discrepancy between the experimentally measured Raman frequency shift and the theoretical prediction can be reconciled by accounting for the TEC mismatch between the substrate and graphene.

Graphene samples used in this work were prepared on silicon substrates covered with a 300-nm-thick SiO_2 layer by mechanical exfoliation of natural graphite flakes. The number of graphene layers was determined by inspecting the line shape of the Raman 2*D* band. Temperature-dependent Raman spectra of graphene and graphite were obtained while cooling and heating the samples in a microscope cryostat where the temperature could be controlled between 4.2 K and 475 K. The 514.5-nm line of an Ar ion laser was used as the excitation source, and low power (< 0.3 mW) was used to avoid unintentional heating. A long-working-distance microscope objective (40x, 0.6 N.A.) was used to focus the laser beam onto the sample and collect the scattered light. The Raman scattered light signal was dispersed by a Jobin-Yvon Triax 550 spectrometer (1800 grooves/mm) and detected with a liquid-nitrogen-cooled CCD detector. The spectral resolution was ~0.7 cm^{-1}.

Figure (a) shows the frequency shifts of the Raman *G* band of single-layer graphene (SLG), bilayer graphene (BLG), and graphite samples as functions of temperature. The Raman peaks redshift as temperature rises and blueshift as temperature falls from room temperature. The Raman peak shift of SLG as a function of temperature is largest. Temperature-dependent Raman shift is commonly attributed to thermal expansion of the lattice and an anharmonic effect which changes the phonon self-energy. As the temperature rises, the SiO_2 layer expands whereas the graphene sheet contracts. This TEC mismatch would induce a biaxial tensile strain on the graphene sample. When the sample is cooled, a compressive strain is induced instead. In order to interpret our data correctly, we should consider the effect of stain on graphene induced by the TEC mismatch between the SiO_2 layer and the graphene sheet.

We estimated the TEC by fitting our data to the theoretical prediction [7] of temperature dependence of the Raman *G* band of *free standing* graphene. Figure (b) shows the temperature dependent TEC obtained from the fitting. TEC at room temperature is estimated to be -9×10^{-6} K^{-1}, which is similar to the previous experimental value of -7×10^{-6} K^{-1} [1].

References

[1]   W. Z. Bao *et al.*, Nat. Nanotechnol. **4** (2009) 562.

[2]   P. K. Schelling, and R. Keblinski, Phys. Rev. B **68** (2003) 035425.

[3]   Y. K. Kwon, S. Berber, and D. Tomanek, Phys. Rev. Lett. **92** (2004) 015901.

[4]   K. V. Zakharchenko, M. I. Katsnelson, and A. Fasolino, Phys. Rev. Lett. **102** (2009) 046808.

[5]   J. W. Jiang, J. S. Wang, and B. W. Li, Phys. Rev. B **80** (2009) 205429.

[6]   N. Mounet, and N. Marzari, Phys. Rev. B **71** (2005) 205214.

[7]   N. Bonini, M. Lazzeri, N. Marzari, and F. Mauri, Phys. Rev. Lett. **99** (2007) 176802.

Figures
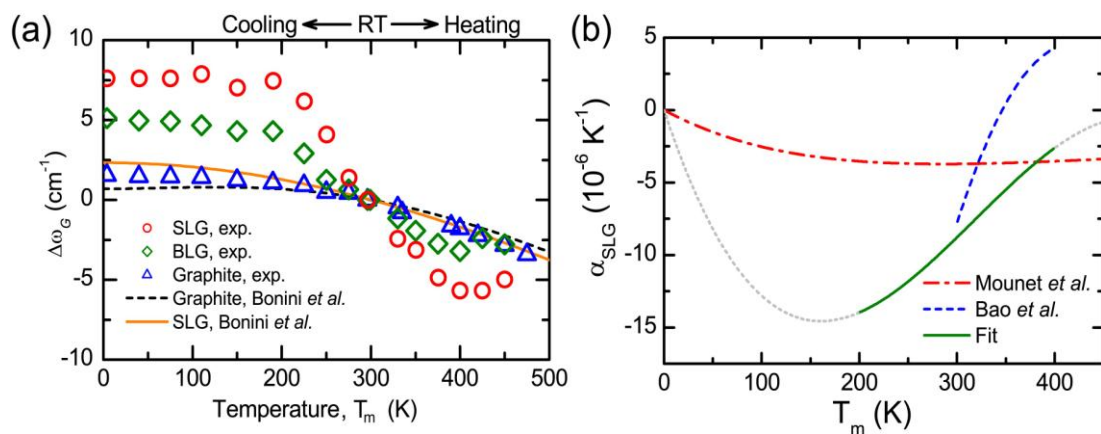
(a) Raman frequency shifts of graphene and graphite as functions of temperature. (b) Thermal expansion coefficient of single layer graphene that gives the best fit between data and theoretical estimate.

Carrier-optical phonon scattering and quasiparticle lifetime in CVD-grown graphene

*Ting Yu,[1, 2 *] Jingzhi Shang,[1] Gagik G. Gurzadyan[1, 3]*

[1]Division of Physics and Applied Physics, School of Physical and Mathematical Sciences, Nanyang Technological University, Singapore 637371, Singapore
[2]Department of Physics, Faculty of Science, National University of Singapore, Singapore 117542, Singapore
[3]Department Chemie, Technische Universität München, Garching 85748, Germany
Contact Email: Yuting@ntu.edu.sg

Ultrafast carrier dynamics in graphene grown by chemical vapor deposition (CVD) has been investigated by UV pump/white-light probe spectroscopy. Transient differential transmission spectra of monolayer and stacked graphene films are observed in the visible range from 380 (3.3 eV) to 670 nm (1.9 eV). After photoexcitation, the intraband carrier equilibration by carrier-carrier scattering occurs within 60 fs. The subsequent carrier relaxation process is governed by carrier-optical phonon (c-op) scattering. As extending the probe ranges from visible to infrared wavelengths, we find the evolution of carrier relaxation channels from monoexponential c-op scattering to double exponential decay including c-op and optical phonon-acoustic phonon scattering. Moreover, quasiparticle lifetimes of these graphene samples are continuously obtained for the probe photon energies from 1.9 to 2.3 eV. With the increase of the number of graphene layers, the dependence of quasiparticle decay rate on the probe photon energy becomes obvious and exhibits a clear linear feature for 10-layer stacked graphene films. From the linear fit, a dimensionless coupling constant *W* [1] is derived, which characterizes the scattering strength of quasiparticles by lattice points in graphene. The origin of this dependence is attributed to the dominant c-op intervally scattering and the linear density of states in the probed electronic band of graphene.

Reference:

[1]. T. Ando, Zero-mode anomalies of massless Dirac electron in graphene, Proceedings of 30th International Conference on the Physics of Semiconductors (2010).

Phonon dispersion and Raman spectra of graphene and graphene layers on gold substrate

I. Zasada [a], P. Dąbrowski [a], J. Sławińska [b], I. Własny [a], M. Wojtaniszak [c], E. Borowiak-Paleń [c], Z. Klusek [a]

[a] Solid State Physics Department, University of Lodz, Pomorska 149/153, 90-236 Lodz, Poland
[b] Theoretical Physics Department II, University of Lodz, Pomorska 149/153, 90-236 Lodz, Poland
[c] Centre of Knowledge Based Nanomaterials and Technologies, Institute of Chemical and Environment Engineering, West Pomeranian University of Technology, Pulaskiego 10, 70-322 Szczecin, Poland
izasada@wfis.uni.lodz.pl

The phonon dispersion of graphene displays two strong Kohn anomalies in the highest optical branch at the high-symmetry points Γ and K [1]. This phenomenon is related to the electron-phonon coupling with the graphene π bands and has a strong influence on Raman scattering. The interaction between graphene and metallic substrate can significantly modify the electron-phonon coupling thus the Raman spectra can be used to identify the type of doping together with determination of number of graphene layers and their electronic structure [2, 3]. In this work, we analyze the influence of gold substrate on the phonon dispersion of the graphene and graphene multilayer calculated with DFT-LDA and Van der Waals density functional. The simultaneous analyzes of the Raman spectra, e.g. the changes in shapes, widths and positions of D, G and 2D peaks, allows to identify first of all the number of graphene layers, next substrate influence on their electronic properties as well as the nature of doping and its probable source.

In Fig.1 we present the schematic view of the sample used in the Raman experiment. Measured Raman spectra with laser line 514 nm for different places of the sample are shown in Fig. 2. The layer number of graphene has been identified by analyzing the shape of 2D band. We could indicate 4 regions: monolayer, bilayer, trilayer and few layers. The simultaneous up-shifts of the G and 2D band positions confirm [4] the p-doping in the graphene/Au system. The accurate DFT calculations analyzed together with the computed phonon frequencies lead to the determination of the electron-phonon coupling which allows to understand and explain the observed p-doping.

References

[1] S. Piscanec, M. Lazzeri, F. Mauri, A. C. Ferrari, and J. Robertson, Phys. Rev. Lett., **93** (2004) 185503.
[2] A. Allard, and L. Wirtz, Nano Letters, **10** (2010) 4335.
[3] J. Lee, K. S. Novoselov, and H. Suk Shin, ACS Nano, **doi: 10.1021/nn103004c**.
[4] Z. Klusek, P. Dąbrowski, P. Kowalczyk, W. Kozłowski, W. Olejniczak, P. Blake, M. Szybowicz, and T. Runka, Appl. Phys. Lett. **95** (2009) 113114.
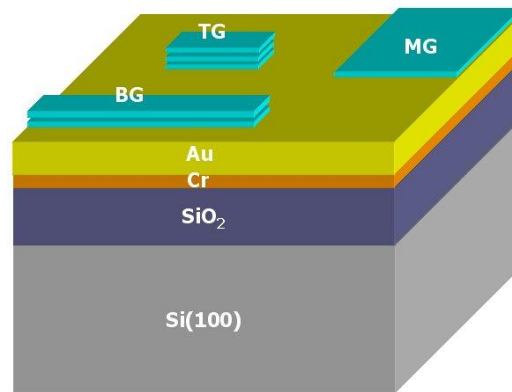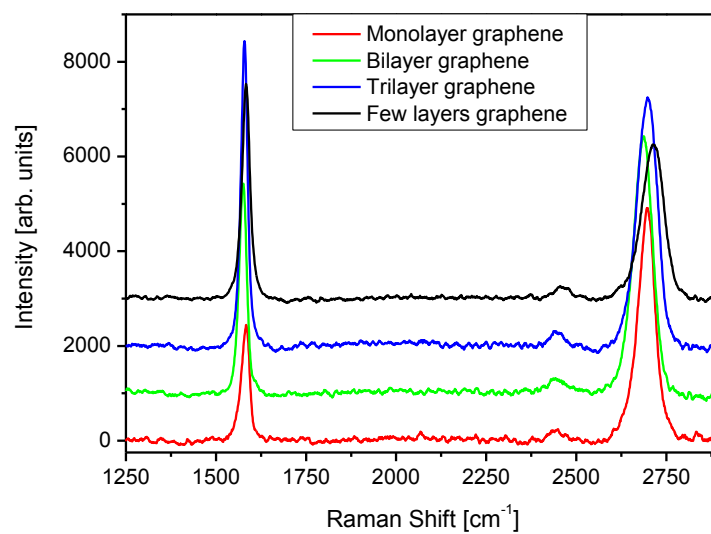
Figures

Fig. 1

Fig. 2

Fig. 1 Schematic view of a sample

Fig. 2 Raman spectra of mono-, bi-, tri-, and few layers graphene deposited on Au substrate.

Electronic structure of fully intercalated few-layer graphene probed by Raman spectroscopy

Da Zhan, Li Sun, Zhenhua Ni, Lei Liu, Xiaofeng Fan, Yanan Xu, Jiaxu Yan and Zexiang Shen*

Division of Physics and Applied Physics, Nanyang Technological University, 637371, Singapore
zexiang@ntu.edu.sg

Huge progress on graphene researches has been achieved in recent years including: Various methods for graphene fabrication; Discovery of its unique electronic, thermal and mechanical properties; Successful fabrication of prototype graphene-based devices. However, much of the unique properties of graphene are accorded to that of single layer graphene (SLG). It would be very desirable to modify few-layer graphene (FLG) samples so that they have similar properties as that of SLG. Graphite intercalation compounds (GICs) are complex materials that formed by insertion of atomic or molecular layers of different chemical species between graphite interlayer space.[1] The interlayer distance of graphite is dramatically increased due to presence of intercalants, which would strongly affect the electronic coupling between graphene layers, hence changes its properties. Thus, graphene based intercalation compounds would be an efficient method to modify the properties of FLG. [1-3] Until now, there are no experimental reports on few-layer graphene intercalation compounds (FLGIC) except the most recent report on Br_2 and I_2 intercalated FLG by Jung et al.,[4] however, the FLG is still not fully intercalated according to their Raman spectra and the structural model.[4]

In this presentation, we will report the fully intercalated $FeCl_3$-FLGIC which fabricated by two-zone vapor transport method. This is the first report on full intercalation for graphene samples. Fig. 1 shows the schematic crystal structure of FLGIC. The distance between adjacent graphene layers enlarged dramatically due to the insertion of $FeCl_3$. Furthermore, as $FeCl_3$ is an acceptor type intercalant, it gives rise to the strong charge transfer induced hole doping effect on graphene. The detailed information for FLGIC is investigated by Raman spectroscopy and mapping. For FLG, Raman G band properties are very sensitive to doping, while the 2D band properties quite dependent on the electronic band structure. Thus analyzing the evolution of G and 2D bands features from pristine FLG to FLGIC can give us a lot of information for probing the properties modification of FLGIC, such as Fermi level shift and band structure evolution. Fig. 2 shows the Raman spectra for graphenes (1 layer (1L) to 4 layers (4L)) after intercalation, which present obviously different Raman features compare with that of the pristine FLG. The features of the Raman G peak of such FLGIC are in good agreement with their full intercalation structures. The FLGIC presents single Lorentzian 2D peak, similar to that of single layer graphene, indicating the loss of electronic coupling between adjacent graphene layers. First principle calculations further reveals that the band structure of FLGIC is similar to single layer graphene but with strong doping effect due to the charge transfer from graphene to $FeCl_3$. Furthermore, the distribution of density states of FLGIC in k-space is strongly influenced because of the coupling with adjacent intercalant layer based on the observation of resonant Raman scattering for G peak.

FLGIC not only changes the physical structure from its precursor FLG, but also effectively modifies its properties, such as electronic structure and density of states. Therefore, the successful fabrication of FLGIC opens a new way to modify properties of FLG for fundamental studies and future applications.

References

[1] M. S. Dresselhaus, G. Dresselhaus, Adv. Phys. **51** (2002) 1.

[2] T. E. Weller, M. Ellerby, S. S. Saxena, R. P. Smith, N. T. Skipper, Nat. Phys. **1**(2005) 39.

[3] N. Emery, C. Herold, M. d'Astuto, V. Garcia, C. Bellin, J. F. Mareche, P. Lagrange, G. Loupias, Phys. Rev. Lett. **95** (2005) 087003.

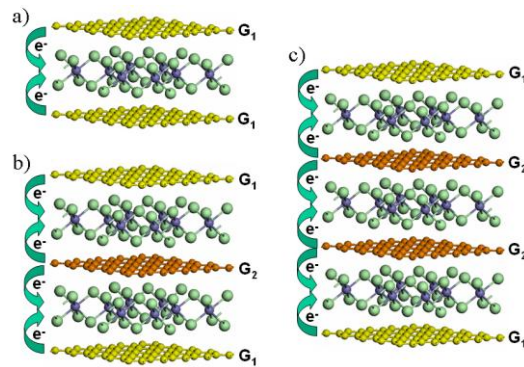[4] N. Jung, N. Kim, S. Jockusch, N. J. Turro, P. Kim, L. Brus, Nano Lett. **9** (2009) 4133.
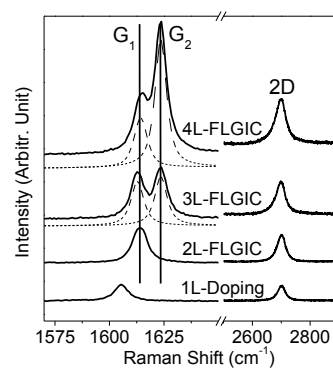
Figures

Figure 1

Figure 2

Figure caption

Figure 1. Schematic crystal structure of 2L- to 4L-FLGIC.

Figure 2. The Raman specta of 1L doped graphene and 2L-to 4L-FLGIC.

One Pot Functionalization of Graphene with Porphyrin using Cycloaddition Reactions

Xiaoyan Zhang,[a,b] Lili Hou,[a] Arjen Cnossen,[a] Anthony C. Coleman,[b] Bart J. van Wees,[b] Wesley R. Browne,[a] and Ben L. Feringa[a]

[a]Stratingh Institute for Chemistry, University of Groningen, Nijenborgh 4, 9747 AG Groningen, The Netherlands
[b]Physics of Nanodevices, Zernike Institute for Advanced Materials, University of Groningen, The Netherlands
xiaoyan.zhang@rug.nl

Two types of graphene based hybrid materials, graphene-TPP (TPP: tetraphenylporphyrin) and graphene-PdTPP (PdTPP: palladium tetraphenylporphyrin) were prepared directly from pristine graphene using one pot cycloaddition reactions. The hybrid materials were characterized by TGA, UV/Vis, FTIR, TEM, Raman, luminescence spectroscopy and fluorescence/phosphorescence lifetime measurements. The covalent linkage between graphene and porphyrin was confirmed by FTIR, Raman spectroscopy and further supported by control experiments. The presence of TPP (or PdTPP) in the hybrid material was demonstrated by UV/Vis spectroscopy, and TGA results indicate that graphene-TPP and graphene-PdTPP hybrid materials contain approximately 18% TPP and 20% PdTPP, respectively. The quenching of fluorescence (or phosphorescence) and decreased lifetime suggests excited state energy/electron transfer between graphene and the covalently attached TPP (or PdTPP) molecules. Considering the unique properties of both graphene and porphyrin, these two hybrid materials may have potential applications in a number of areas, such as solar cells, catalysts, sensors.

References

(1) A. K. Geim and K. S. Novoselov, Nat. Mater., **6** (2007), 183.
(2) X. Y. Zhang, A. C. Coleman, N. Katsonis, W. R. Browne, B. J. van Wees, B. L. Feringa, Chem. Commun., **46** (2010), 7539.
(3) V. Georgakilas, A. B. Bourlinos, R. Zboril, T. A. Steriotis, P. Dallas, A. K. Stubos and C. Trapalis, Chem. Commun., **46** (2010), 1766.
(4) M. Quintana, K. Spyrou, M. Grzelczak, W. R. Browne, P. Rudolf and M. Prato, ACS Nano, **4** (2010), 3527.
(5) D. Guldi, A. Rahman, V. Sgobba and C. Ehli, Chem. Soc. Rev., **35** (2006), 471.
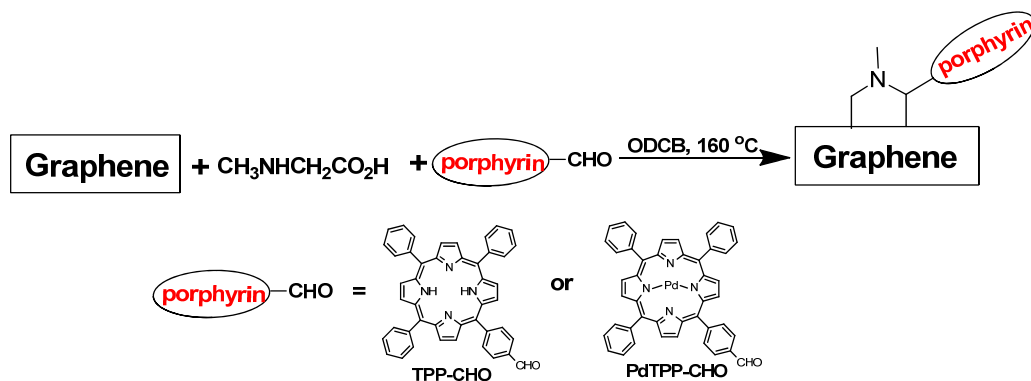
Scheme 1. Synthesis scheme of graphene-TPP and graphene-PdTPP hybrid materials.

Controllable Transfer and High Quality Nano Devices of CVD Growth Graphene Flakes with Variable Size and Shape

Yangbo Zhou, Yaqing Bie, Zhimin Liao, Dapeng Yu
State Key Laboratory for Mesoscopic Physics, Department of Physics, Peking University,
Beijing 100871, China
Email:pkubobo@gmail.com, yudp@pku.edu.cn

We developed a special graphene transfer technology based on traditional graphene transfer process. The technology used PMMA film as a transfer template, and electron beam lithography to make patterns of different size and shape of small graphene flakes all grown on one Cu substrate by CVD process. We could transfer specific graphene flakes onto specific locations of various kinds of substrates. The transfer process resulted tiny damage to graphene itself, and remained its high quality. Quantum Hall Effect was also observed in the so-transferred graphene flake.

The technology could make electrode-deposition-free graphene devices with good electrical behavior. It could also be used to "repair" breaks and damage in graphene-based "full carbon" circuits, and pointed out a new way of "bottom up" process to manipulate graphene as building blocks in nano devices.

References

[1] Liying Jiao, Xiaojun Xian, Zhongyun Wu, Jin Zhang, and Zhongfan Liu. Nano Letters, Vol.9, No.1 (2009), 205-205
[2] Xuesong Li, Weiwei Cai, Jinho An, Seyoung Kim, Junghyo Nah, Dongxing Yang, Richard Piner, Aruna Velamakanni, Inhwa Jung, Emanuel Tutuc, Sanjay K. Banerjee, Luigi Colombo, and Rodney S. Ruoff.Science. Vol.324, No.5932 (2009), 1312-1314
[3] C. R. Dean1, A. F. Young, I.Meric1, C. Lee, L. Wang, S. Sorgenfrei, K. Watanabe, T. Taniguchi, P. Kim, K. L. Shepard1 and J. Hone. Nature Nanotechnology, Vol 5(2010), 722-726

Figures
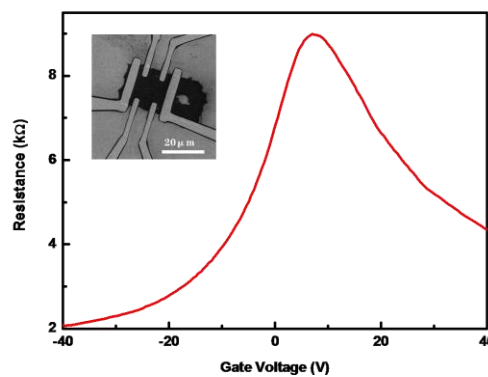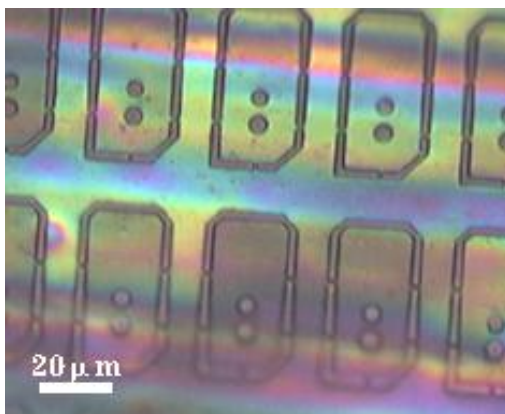
Magneto-transport through a side-gated graphene constriction

P. J. Zomer, M. H. D. Guimarães, N. Tombros and B. J. van Wees
Zernike Institute for Advanced Materials, Nijenborgh 4, 9747 AG, Groningen, The Netherlands
p.j.zomer@rug.nl

The electronic band structure of graphene allows for continuous tuning between electron and hole transport, making it an interesting candidate for pnp-type devices. Using reactive ion etching we pattern graphene flakes into various geometries, including side-gated constrictions, quantum dots and ribbons. Side-gating of graphene devices has the advantage that the graphene etched side-gate can easily be very close to the device, 20 nm for our devices. Furthermore, no additional fabrication steps are needed to locally gate etched graphene devices, compared to etched top-gated devices.

In this work we study magneto-transport in the quantum Hall regime through a side-gated graphene constriction. The quantum Hall effect was already measured in both two- and multi-terminal top-gated pnp-junctions [1,2]. To study magneto-transport through a side-gated graphene constriction we etched a Hall bar shaped device with a 100 nm wide constriction in the central region. By back- and side-gating we tune both the global and local charge carrier densities in our device, creating a pnp-junction. This way we control the chirality and number of edge states separately in the constriction and the rest of the device. The Landauer-Büttiker formalism is used to calculate the expected quantized conductance through the junction [2,3]. In the pp'p regime we find good agreement with theory, but in the pnp regime the conductance is lower than expected. This can be explained by a reduction of equilibration along the pn interfaces.

References

[1] B. Özyilmaz, P. Jarillo-Herrero, D. Efetov, D.A. Abanin, L.S. Levitov, P. Kim, PRL, **99** (2007) 166804.
[2] D.K. Ki, H.J. Lee, Phys. Rev. B, **79** (2009) 195327.
[3] M. Büttiker, Phys. Rev. B, **38** (1988) 9375.

Figures
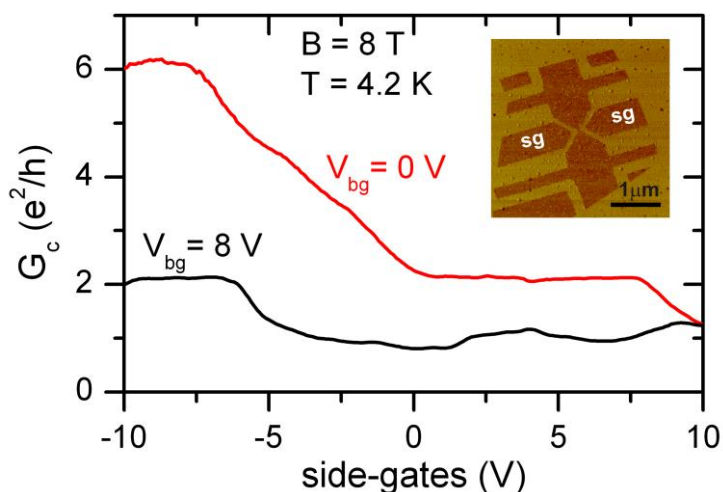
Quantized conductance through the constriction as function of side-gate voltage for two different back-gate voltages. In the pp'p regime we observe levels at $2e^2/h$ and $6e^2/h$. The inset shows an AFM phase image of the device. The dark areas are graphene, the light areas are SiO_2. The 100 nm wide constriction is in the center between two side-gates, labeled sg.

The origin of scattering mechanisms in single- and bilayer graphene

I. V. Zozoulenko

Solid State Electronics, ITN, Linkoping University, 601 74 Norrköping, Sweden

igor.zozoulenko@itn.liu.se

J. W. Kłos

Surface Physics Division, Faculty of Physics, Adam Mickiewicz University, Poznañ, Poland

Hengyi Xu and T. Heinzel

Condensed Matter Physics Laboratory, Heinrich-Heine-Universität, Düsseldorf, Germany

One of the central issues in graphene research is to identify scatterers that dominate the conductivity σ. This is not only a fundamental question, but also the prerequisite for progress regarding the quality of graphene-based devices for electronics and optoelectronics. Since the character of the scatterers (i.e. long- or short range) manifests itself directly in the dependence of the conductivity *σ* on the electron density *n*, this function plays a key role in the corresponding experimental and theoretical investigations.

In most experimental studies the conductivitiy of single layer graphene (SLG) and bilayer graphene (BLG) exhibit similar linear dependences $\sigma \sim n$. The experimental results are commonly analyzed on the basis of the standard Boltzmann approach within the Born approximation. This approach leads to qualitatively different predictions for the short- and long-range scatterers in respectively the SLG and the BLG. This, in its turn, leads to the conclusion that scattering mechanisms has to be different for the SGL and the BLG. This is a rather surprizing conclusion because these mechanisms in both systems are expected to be the same as both the SLG and the BLG are produced by the same manufacturing technique with the same substrate used in the measurements.

Because the conclusions on the nature of scattering mechanisms in graphene rely essentially on the predictions of the Boltzmann approach, it is of the utmost importance to establish the limits of its validity for the SLG and the BLG. In the present study we first derive analytical expressions for the conductivity of the SLG and the BLG within the standard Boltzmann approach for the Gaussian disorder and then compare them with the exact numerical tigth-binding (TB) Landauer-type calculations.

(a) SLG [1]. We demonstrate that for the SLG the TB calculations give the same linear density dependence of the conductivity, $\sigma^{TB} \sim n$, for short- and long-range Gaussian scatterers. In the case of short-range scattering the TB calculations are in agreement with the predictions of the Boltzmann theory going beyond the Born approximation but in qualitative and quantitative disagreement with the standard Boltzmann approach within the Born approximation predicting $\sigma^{Boltz} \sim$ const. Even for the long-range Gaussian potential the standard Boltzmann predictions are in quantitative and qualitative disagreement with the TB results in a parameter range corresponding to realistic systems, $\pi n \xi^2 << 1$ (with ξ being the effective screening length of the Gaussian potential). This questions the validity of the standard Boltzmann approach within the Born approximation, commonly used for the interpretation of the results of experimental studies of the conductivity in the SLG [1].

(b) BLG [2]. For the case of BLG we demonstrate that, as for the case of SLG, the standard Boltzmann approach and the TB calculations agree qualitatively and quantitatively in the regime of $\pi n \xi^2 >> 1$ (corresponding to high densities/smooth potential). This regime however is not achieved in realistic devices. In the opposite regime $\pi n \xi^2 << 1$ appropriate to all experiments, our findings are strikingly different from those for the case of SLG where the Boltzmann approach is not valid. We find that for the

BLG the Boltzmann approach is consistent with the corresponding TB calculations for the range of electron densities where the BLG dispersion is parabolic. In this regime the Boltzmann theory predicts σ ~ *n* regardless of the potential range *ξ* (i.e. for both short- and long-range Gaussian potential), which is confirmed by the TB calculations in the parameter range of *ξ* explored in our study. For higher electron densities when the BLG dispersion is linear, the Boltzmann and the TB calculations disagree.

References

[1] J. W. Klos and I.V. Zozoulenko, *Effect of short- and long-range scattering in the conductivity of graphene: Boltzmann approach vs tight-binding calculations*, Phys. Rev. B **82**, 081414(R) (2010).

[2] Hengyi Xu, T. Heinzel, and I. V. Zozoulenko, *The origin of scattering mechanisms in bilayer graphene*, submitted.

For the single-layer graphene predicting qualitative different
results for short- and long-range impurity scattering9–13
  = const   short-range scattering ,   1a
     n   long-range scattering   ,

[1] A. A. Shylau, I. V. Zozoulenko, Hengyi Xu, T. Heinzel, *Generic suppression of conductance quantization of interacting electrons in graphene nanoribbons in a perpendicular magnetic field*, Phys. Rev. B **82**, 121410(R) (2010).